frontiers | Research Topics

Harnessing natural plant extracts and probiotics to enhance host-gut microbiome interactions

Edited by
Chuanshe Zhou, Jie Yin, Kang Xu and Gabriele Brecchia

Coordinated by
Kaijun Wang

Published in
Frontiers in Microbiology
Frontiers in Marine Science

ISSN 1664-8714
ISBN 978-2-8325-6331-1
DOI 10.3389/978-2-8325-6331-1

About Frontiers

Frontiers is more than just an open access publisher of scholarly articles: it is a pioneering approach to the world of academia, radically improving the way scholarly research is managed. The grand vision of Frontiers is a world where all people have an equal opportunity to seek, share and generate knowledge. Frontiers provides immediate and permanent online open access to all its publications, but this alone is not enough to realize our grand goals.

Frontiers journal series

The Frontiers journal series is a multi-tier and interdisciplinary set of open-access, online journals, promising a paradigm shift from the current review, selection and dissemination processes in academic publishing. All Frontiers journals are driven by researchers for researchers; therefore, they constitute a service to the scholarly community. At the same time, the *Frontiers journal series* operates on a revolutionary invention, the tiered publishing system, initially addressing specific communities of scholars, and gradually climbing up to broader public understanding, thus serving the interests of the lay society, too.

Dedication to quality

Each Frontiers article is a landmark of the highest quality, thanks to genuinely collaborative interactions between authors and review editors, who include some of the world's best academicians. Research must be certified by peers before entering a stream of knowledge that may eventually reach the public - and shape society; therefore, Frontiers only applies the most rigorous and unbiased reviews. Frontiers revolutionizes research publishing by freely delivering the most outstanding research, evaluated with no bias from both the academic and social point of view. By applying the most advanced information technologies, Frontiers is catapulting scholarly publishing into a new generation.

What are Frontiers Research Topics?

Frontiers Research Topics are very popular trademarks of the *Frontiers journals series*: they are collections of at least ten articles, all centered on a particular subject. With their unique mix of varied contributions from Original Research to Review Articles, Frontiers Research Topics unify the most influential researchers, the latest key findings and historical advances in a hot research area.

Find out more on how to host your own Frontiers Research Topic or contribute to one as an author by contacting the Frontiers editorial office: frontiersin.org/about/contact

Harnessing natural plant extracts and probiotics to enhance host-gut microbiome interactions

Topic editors

Chuanshe Zhou — Chinese Academy of Sciences (CAS), China

Jie Yin — Hunan Agricultural University, China

Kang Xu — Institute of Subtropical Agriculture, Chinese Academy of Sciences (CAS), China

Gabriele Brecchia — University of Milan, Italy

Topic coordinator

Kaijun Wang — Hunan Agricultural University, China

Citation

Zhou, C., Yin, J., Xu, K., Brecchia, G., Wang, K., eds. (2025). *Harnessing natural plant extracts and probiotics to enhance host-gut microbiome interactions*. Lausanne: Frontiers Media SA. doi: 10.3389/978-2-8325-6331-1

Table of contents

frontiers | Frontiers in Microbiology

TYPE Editorial
PUBLISHED 28 April 2025
DOI 10.3389/fmicb.2025.1607339

OPEN ACCESS

EDITED AND REVIEWED BY
Zhiyong Li,
Shanghai Jiao Tong University, China

*CORRESPONDENCE
Jie Yin
✉ yinjie@hunau.edu.cn

RECEIVED 07 April 2025
ACCEPTED 14 April 2025
PUBLISHED 28 April 2025

CITATION
Wang K, Zhou C, Xu K and Yin J (2025) Editorial: Harnessing natural plant extracts and probiotics to enhance host-gut microbiome interactions. *Front. Microbiol.* 16:1607339. doi: 10.3389/fmicb.2025.1607339

Editorial: Harnessing natural plant extracts and probiotics to enhance host-gut microbiome interactions

Kaijun Wang[1,2], Chuanshe Zhou[3], Kang Xu[3] and Jie Yin[4]*

[1]College of Veterinary Medicine, Hunan Agricultural University, Changsha, Hunan, China, [2]Chinese Medicinal Materials Breeding Innovation Center of Yuelushan Laboratory, Changsha, Hunan, China, [3]Institute of Subtropical Agriculture, Chinese Academy of Sciences, Changsha, China, [4]Animal Nutritional Genome and Germplasm Innovation Research Center, College of Animal Science and Technology, Hunan Agricultural University, Changsha, Hunan, China

KEYWORDS

natural plant extracts, probiotics, gut microbiome, host-microbiome interactions, metabolic health

Editorial on the Research Topic
Harnessing natural plant extracts and probiotics to enhance host-gut microbiome interactions

Introduction

The intricate relationship between the gut microbiome and host health has emerged as a cornerstone of modern biomedical research. In recent years, natural plant extracts and probiotics have received considerable attention for their potential to modulate gut microbial communities and thereby promote host wellbeing. This Research Topic, "*Harnessing Natural Plant Extracts and Probiotics to Enhance Host-Gut Microbiome Interactions*" brings together 13 cutting-edge studies that collectively advance our understanding of how these interventions can shape host-microbiome dynamics. By exploring mechanisms ranging from immune modulation to metabolic regulation, these contributions underscore the promise of natural compounds in addressing pressing challenges in health and agriculture.

The gut microbiome as a therapeutic target

The gut microbiome plays a pivotal role in digestion, immune function, and metabolic homeostasis. Dysbiosis—an imbalance in microbial composition—has been linked to diseases such as obesity, inflammatory bowel disease (IBD), and even mental health disorders. Natural plant extracts and probiotics offer a sustainable approach to restoring microbial balance as they often act as prebiotics, antioxidants, or immunomodulators.

In this collection, several studies highlighted the role of plant-derived polysaccharides. For instance, Wen et al. demonstrated that *Atractylodes macrocephala* polysaccharide (AMP) improves growth performance and intestinal health in largemouth bass by enhancing beneficial bacterial taxa such as *Firmicutes* and *Bacteroidota*. Similarly, Zheng Y. et al. showed that grape seed proanthocyanidins (GSP) reduce oxidative stress and promote

growth in pigs by increasing the abundance of *Lactobacillus*. These findings align with the growing recognition that dietary polyphenols can act as prebiotics, fostering the growth of health-promoting microbes.

Immunomodulatory and antioxidant effects

A recurring theme in the contributions is the dual role of natural compounds in reducing inflammation and oxidative stress. For example, Tang et al. revealed that *Rosa roxburghii* polyphenol (RRTP) alleviates acute lung injury (ALI) in mice by enhancing short-chain fatty acid (SCFA) production and increasing *Akkermansia muciniphila,* a bacterium associated with gut barrier integrity. Cheng et al. further emphasized the protective effects of Mulberry leaf polysaccharide (MLP) against cyclophosphamide-induced immunosuppression in chicks, demonstrating improved antioxidant enzyme activity and tight junction protein expression. These results highlight the potential of plant extracts to mitigate oxidative damage and enhance mucosal immunity.

Metabolic health and disease management

Several studies have explored the impact of natural compounds on metabolic disorders. Freitas et al. investigated the nutraceutical supplement Slim, which reshapes the gut microbiota and reduces *Mucispirillum schaedleri* in obese mice, thereby improving lipid metabolism. Meanwhile, Zheng W. et al. discussed the aryl hydrocarbon receptor (AhR) pathway as a critical mediator of lipid metabolism, linking gut microbial metabolites to host inflammatory responses. These findings underscore the role of the gut microbiome in the metabolic syndrome and suggest that targeted interventions may offer novel therapeutic strategies.

Probiotics and microbial diversity

Probiotics, live microorganisms with health benefits, are another focus of this collection. For example, Wang et al. demonstrated that supplementation with *Bacillus amyloliquefaciens* alleviates LPS-induced intestinal inflammation in pigs by activating the AhR/STAT3 pathway (Wang et al., 2024). Similarly, studies by Ferrarezi et al. (2024) and Lin et al. (2024) highlighted the potential of probiotics to modulate gut microbial diversity in aquaculture, thereby enhancing disease resistance in fish. These findings emphasize the importance of probiotics in restoring microbial resilience and optimizing host health across species.

Challenges and future directions

While the studies in this collection provide compelling evidence for the efficacy of natural plant extracts and probiotics, several challenges remain. For instance, the precise mechanisms underlying microbial interactions with host signaling pathways (e.g., AhR, TLR4) require further elucidation. Additionally, standardization of extraction methods and dosage optimization are critical for translating these findings into clinical or agricultural applications. Future research should also explore the long-term effects of these interventions and their scalability across diverse populations.

Conclusion

This Research Topic consolidates groundbreaking contributions that advance our understanding of how natural plant extracts and probiotics can enhance host-gut microbiome interactions. By addressing inflammation, oxidative stress, and metabolic dysfunction, these studies pave the way for innovative therapies in human and veterinary medicine. As we continue to harness the power of nature, interdisciplinary approaches combining microbiology, immunology, and metabolomics will be key to unlocking the full potential of these interventions.

Author contributions

KW: Writing – original draft. CZ: Writing – review & editing. KX: Writing – review & editing. JY: Writing – review & editing.

Funding

The author(s) declare that financial support was received for the research and/or publication of this article. This work was supported by the Yuelushan Laboratory Joint Talent Introduction Project (2024RC2045).

Acknowledgments

All authors who contributed to this Research Topic are gratefully acknowledged.

Conflict of interest

The authors declare that the research was conducted in the absence of any commercial or financial relationships that could be construed as a potential conflict of interest.

Publisher's note

References

Ferrarezi, J. V. S., Owatari, M. S., Martins, M. A., de Souza, S. L., Dutra, S. A. P., de Oliveira, H. M., et al. (2024). Effects of a multi-strain Bacillus probiotic on the intestinal microbiome, haemato-immunology, and growth performance of Nile tilapia. *Vet. Res. Commun.* 48, 2357–2368. doi: 10.1007/s11259-024-10412-1

Lin, Y. T., Hung, Y. C., Chen, L. H., Lee, K. T., and Han, Y. S. (2024). Effects of adding Bacillus subtilis natto NTU-18 in paste feed on growth, intestinal morphology, gastrointestinal microbiota diversity, immunity, and disease resistance of Anguilla japonica glass eels. *Fish Shellfish Immunol.* 149:109556. doi: 10.1016/j.fsi.2024.109556

Wang, Q., Wang, F., Zhou, Y., Li, X., Xu, S., Jin, Q., et al. (2024). *Bacillus amyloliquefaciens* SC06 Relieving Intestinal Inflammation by Modulating Intestinal Stem Cells Proliferation and Differentiation via AhR/STAT3 Pathway in LPS-Challenged Piglets. *J. Agric. Food Chem.* 72, 6096–6109. doi: 10.1021/acs.jafc.3c05956

frontiers | Frontiers in Microbiology

TYPE Original Research
PUBLISHED 11 January 2024
DOI 10.3389/fmicb.2024.1351295

OPEN ACCESS

EDITED BY
Kang Xu,
Chinese Academy of Sciences (CAS), China

REVIEWED BY
Joseph Atia Ayariga,
Alabama State University, United States
Youyou Lu,
Huazhong Agricultural University, China

*CORRESPONDENCE
Xiuli Gao
✉ gaoxl@gmc.edu.cn

RECEIVED 06 December 2023
ACCEPTED 03 January 2024
PUBLISHED 11 January 2024

CITATION
Tang L, Zhang S, Zhang M, Wang P, Liang G, Gan Z and Gao X (2024) Unlocking the potential of *Rosa roxburghii* Tratt polyphenol: a novel approach to treating acute lung injury from a perspective of the lung-gut axis. *Front. Microbiol.* 15:1351295. doi: 10.3389/fmicb.2024.1351295

Unlocking the potential of *Rosa roxburghii* Tratt polyphenol: a novel approach to treating acute lung injury from a perspective of the lung-gut axis

Li Tang[1,2,3], Shuo Zhang[1,2], Min Zhang[1,2], Pengjiao Wang[1,2], Guiyou Liang[1,4], Zhitong Gan[1] and Xiuli Gao[1,2,4]*

[1]State Key Laboratory of Functions and Applications of Medicinal Plants, School of Pharmaceutical Sciences, Guizhou Medical University, Guiyang, China, [2]Microbiology and Biochemical Pharmaceutical Engineering Research Center of Guizhou Provincial Department of Education, Guizhou Medical University, Guiyang, China, [3]School of Chinese Ethnic Medicine, Guizhou Minzu University, Guiyang, China, [4]Translational Medicine Research Center, Guizhou Medical University, Guiyang, China

Introduction: Acute lung injury (ALI) is a serious respiratory disease characterized by progressive respiratory failure with high morbidity and mortality. It is becoming increasingly important to develop functional foods from polyphenol-rich medicinal and dietary plants in order to prevent or alleviate ALI by regulating intestinal microflora. Rosa roxburghii Tratt polyphenol (RRTP) has significant preventive and therapeutic effects on lipopolysaccharide-induced ALI mice, but its regulatory effects on gut homeostasis in ALI mice remains unclear.

Methods: This study aims to systematically evaluate the ameliorative effects of RRTP from the perspective of "lung-gut axis" on ALI mice by intestine histopathological assessment, oxidative stress indicators detection and short-chain fatty acids (SCFAs) production, and then explore the modulatory mechanisms of RRTP on intestinal homeostasis by metabolomics and gut microbiomics of cecal contents.

Results: The results showed that RRTP can synergistically exert anti-ALI efficacy by significantly ameliorating intestinal tissue damage, inhibiting oxidative stress, increasing SCFAs in cecal contents, regulating the composition and structure of intestinal flora, increasing Akkermansia muciniphila and modulating disordered intestinal endogenous metabolites.

Discussion: This study demonstrated that RRTP has significant advantages in adjuvant therapy of ALI, and systematically clarified its comprehensive improvement mechanism from a new perspective of "lung-gut axis", which provides a breakthrough for the food and healthcare industries to develop products from botanical functional herbs and foods to prevent or alleviate ALI by regulating intestinal flora.

KEYWORDS

Rosa roxburghii* Tratt polyphenol, acute lung injury, gut homeostasis, short-chain fatty acids, *Akkermansia muciniphila

1 Introduction

Acute lung injury (ALI) is a serious respiratory disease characterized by progressive respiratory failure with high morbidity and mortality. Currently, in addition to respiratory support, ALI lacks effective medication (Gorman et al., 2022). Oxidative stress, a crucial factor in the pathological progress of ALI, is pivotal for maintenance of tissue homeostasis and protection against infections (Ornatowski et al., 2020). A high level of reactive oxygen species (ROS) could damage microvascular barriers and aggravate pulmonary edema by exceeding the body's scavenging capacity (Meng et al., 2022).

Intestinal microbiota and their metabolites affect antibacterial action, immunoregulation and nutrient metabolism of human body (Huang et al., 2019; Iddrisu et al., 2022). Gut microecological imbalance, related to pulmonary disease, can disrupt the integrity of the intestinal barrier, activate the systemic immune system, and aggravate immune damage to the lung. This interaction between the lung and gut is called the "lung-gut axis" (Wedgwood et al., 2020). Therefore, maintaining intestinal homeostasis is essential to ameliorating lung disease. Short-chain fatty acids (SCFAs) are generated by symbiotic intestinal flora. As a vital energy source for intestinal epithelial cells, they play a significant role in maintaining microecological homeostasis of intestine and immune balance of host, and modulating gut pH value, and are "star" molecules which regarded as potential novel targets for ALI therapy (de Vos et al., 2022; Hou et al., 2022; Huang et al., 2022).

Functional foods, including flavonoids, polyphenols, terpenoids and other natural active ingredients, have the properties of regulating oxidative stress, protecting lung and ameliorating the disturbance of intestinal flora (He et al., 2021). Consequently, the food and healthcare industries are increasingly focusing on developing products to prevent or alleviate ALI by regulating intestinal flora from the plant-based functional herbal medicine and foods.

Rosa roxburghii Tratt (RRT) is an underutilized nutritional crop from the Rosaceae family with high medicinal properties and primarily distributed in the mountainous areas in southwest China. Phytochemical analyses confirmed that RRT contains organic acids, flavonoids, polyphenols and other natural active ingredients, with functional activities incomparable to other fruits (Wang et al., 2021). RRT exhibits a diversity of biological characteristics against immune disorder, inflammatory disease and tumors, and can also regulate gut microbiota dysfunction caused by hyperlipidemia and diabetes (Wang et al., 2020; Ji et al., 2022). RRT polyphenol (RRTP), including phenolic acids, coumarins, lignans, tannins, and flavonoids, is one of the most important active components of RRT. In our previous study, we confirmed that RRTP has a significant preventive and therapeutic effect on ALI mice induced by lipopolysaccharide (LPS) (Tang et al., 2022, 2023), and it is a functional food resource with great potential for adjuvant therapy of ALI. In addition, the intestinal flora of ALI mice has been found to be dysfunctional (Tang et al., 2021), and plant-based foods containing polyphenol have also been shown to alleviate inflammatory diseases by regulating intestinal homeostasis (Wu et al., 2021).

Accordingly, in order to further reveal the amelioration mechanism of RRTP on ALI, we hypothesized that RRTP had an intervention effect on intestinal microflora of LPS-treated ALI mice in this study. This intervention effect may shed light on adjuvant and complementary therapy development for ALI. To validate this hypothesis, we systematically estimated the effects of RRTP on intestinal tissues of ALI mice through intestine histopathological assessment, oxidative stress indicators detection and SCFAs production, and then explored the modulatory mechanisms of RRTP on intestinal homeostasis by metabolomics and *gut microbiome* of cecal contents.

2 Materials and methods

2.1 Reagents and chemicals

According to our previous research (Tang et al., 2022), RRTP is extracted from RRT fruit and preserved in microbiology and biochemical pharmaceutical engineering research center of Guizhou Medical University. Lipopolysaccharide (LPS, *Escherichia coli serotype* 055:B5) was purchased from Sigma-Aldrich. Acetonitrile and methanol (UPLC-grade) were collected from Merck.

2.2 Animals and drug administration

All animal experiments were performed in accordance with the Animal Care and Use Guidelines of Guizhou Medical University, and the protocols were reviewed and approved by the Animal Ethics Committee of institution (License No. SYXK (Qian) 2018-0001). Specific pathogen-free (SPF) male BALB/c mice were obtained from Changsha Tianqin Biotechnology Co., Ltd. (License No. SCXK (Xiang) 2019-0013, Hunan, China), and acclimatized in a standard mice laboratory with free access to water and food for 7 days. Animals were performed daily administration of physiological saline or RRTP. RRTP extracts dissolved in physiological saline gavage for 7 days at 10 mL/kg/d. Thirty minutes after the last administration, mice were anesthetized by intraperitoneal injection (10% chloral hydrate), and LPS (2 mg/kg) was administered by oropharyngeal instillation to establish ALI mice. Instead of LPS, physiological saline was given to the normal group. After the addition of LPS, the mice were sacrificed 24 h later, and gut tissues and cecal contents were collected and stored at −80°C for further analysis. The schematic of animal experiment protocols was depicted in Figure 1A.

2.3 Histopathological assessment

The gut tissues were washed with PBS, fixed with 4% paraformaldehyde, dehydrated with ethanol, embedded with paraffin wax and cut into 4 μm thick sections. After successive staining with hematoxylin-eosin (H&E), histopathological alteration was evaluated with an optical microscope.

2.4 Determination of oxidative stress indicators

A supernatant was obtained for biochemical measurement of intestinal tissues after homogenization and centrifugation in cold PBS, and its protein concentration was detected according to the manufacturer's

10.3389/fmicb.2024.1351295

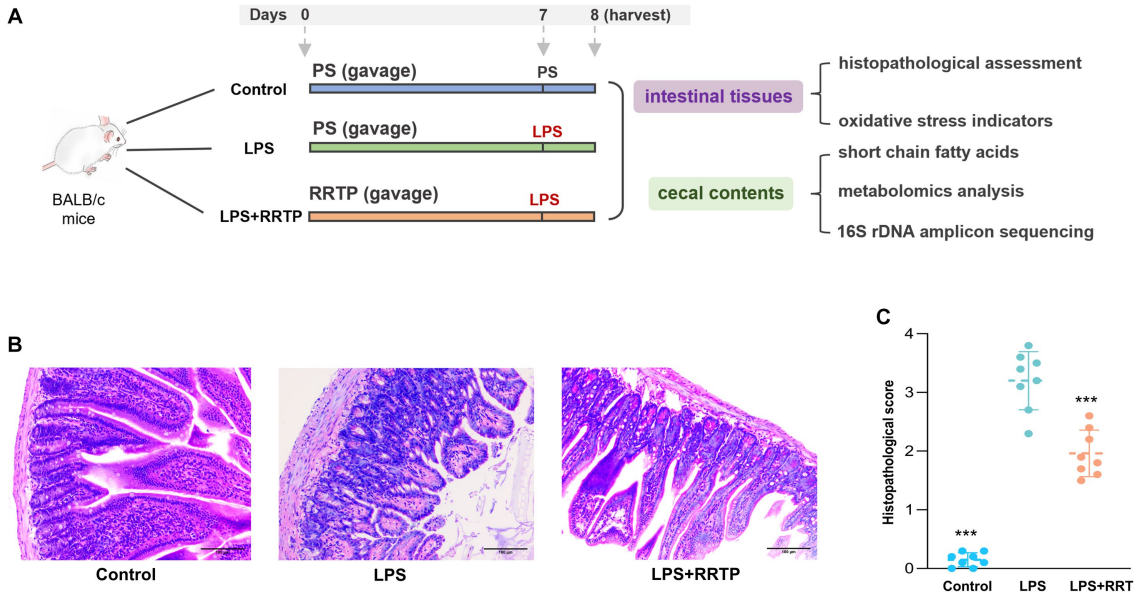

FIGURE 1
Comprehensive evaluation of RRTP on intestinal homeostasis in ALI mice. **(A)** Schematic of animal experiment protocols. PS: physiological saline. LPS: lipopolysaccharide. **(B)** Representative micrographs of histological sections of the gut tissues in LPS-induced ALI mice. (H&E staining, original magnification ×200). **(C)** Pathological score of histological sections. *Compared with the model group, ***$P < 0.001$.

instructions. The activity of glutathione (GSH), myeloperoxidase (MPO), superoxide dismutase (SOD) and malondialdehyde (MDA) in gut tissues were measured to evaluate the degree of oxidative stress damage in ALI mice. Oxidative stress detection kits were purchased from Nanjing Jiancheng Bioengineering Institute (Nanjing, China).

2.5 Measurement of short chain fatty acids

SCFAs were extracted from cecal contents with 1 mL aqueous solution. After centrifugation at 10,000 rpm for 10 min, the supernatant was collected, and SCFAs were extracted from the supernatant with 1 mL diethyl ether. Finally, the diethyl ether solution was detected by gas chromatography (GC).

The separation of SCFAs was carried out with GC system (7890B, Agilent) equipped with a DB-WAX capillary column (30 × 0.53 mm, 1 μm, Agilent). The temperature of injection port and detector were 270°C and 280°C, respectively. Injection volume was 2 μL. The initial temperature of the capillary column was set at 100°C for 1 min and then increased to 150°C at a rate of 5°C per minute for 7 min. The quantification of acetic acid, propionic acid and butyric acid was conducted by comparison with chemical standards.

2.6 Cecal contents metabolomics analysis

Endogenous metabolites in cecal contents were detected by UHPLC-Q-Exactive Plus Orbitrap-MS (Thermo Fisher Scientific). Briefly, 50 mg cecal contents was extracted with the precooled mixture of acetonitrile, methanol and aqueous solution (2:2:1). After homogenization, vortex and centrifugation at 4°C for 20 min, the supernatant was filtered through 0.22 μm membrane for metabolomics analysis.

The separation of metabolites was conducted on a 1.8 μm C_{18} column (2.1 × 100 mm, ZORBAX Eclipse Plus, Agilent, United States) with flow rate was 0.3 mL/min. The optimized gradient elution procedure (phase A: 0.1% formic acid H_2O; phase B: 0.1% formic acid acetonitrile) was as follows: 0–2.5 min, 2–2% B; 2.5–5 min, 2–40% B; 5–12 min, 40–100% B; 12–16 min, 100–100% B; 16–16.1 min, 100–2% B; 16.1–19 min, 2–2% B. Temperature of capillary and aux gas heater were 320°C and 350°C, respectively. Ion spray voltage was 3.5/2.8 kV (+/−), S-lens RF level was 50, dynamic exclusion was 3 s, and the data was analyzed in both negative and positive modes from 100 to 1,500 *m/z*. Compound Discoverer 3.2 was used to pretreat MS data, including retention time correction, peak matching and peak recognition. Primary and secondary mass spectrum fragment information from KEGG and HMDB databases was used to identify metabolites. In addition, components were validated by MS^2 spectroscopy using an internal metabolite spectrum library. An analysis of intestine-related metabolic pathways implicated in ALI after RRTP preventive treatment was carried out using MetabolAnalyst 5.0. Metabolic pathways with an impact value greater than 0.1 were considered significant.

2.7 16S rDNA amplicon sequencing

A CTAB method was used to extract genome DNA from cecal contents samples and 1% agarose gels were used to verify DNA purity and concentration. Bacterial 16S rDNA gene was amplified by PCR using specific primers. All PCR reactions were carried out with DNA template (10 ng), forward and reverse primers (2 μM) and Phusion® High -Fidelity PCR Master Mix (15 μL, New England Biolabs). During thermal cycling, initial denaturation was carried out at 98°C for 1 min, followed by 30 cycles of denaturation for 10 s, annealing for 30 s, and elongation for 30 s. PCR products were purified with Gel Extraction

Kit (Qiagen, Germany). The sequencing libraries were prepared following the manufacturer's instructions using TruSeq® DNA PCR-Free Sample Preparation Kit (Illumina, United States) and index codes were also added to the libraries. Finally, Illlumina NovaSeq platform was used to sequence the library and generate 250 bp paired-end reads.

2.8 Statistical analysis

A statistical analysis was carried out using GraphPad Prism 9.0 and SPSS 23.0. For metabolomics analysis, ANOVA and student's *t*-test were used to evaluate differences, with $p < 0.05$ considered significant. R packages (2.15.3) and QIIME were used for 16S rDNA amplicon sequencing analysis. Alpha diversity, including ACE (Abundance-based Coverage Estimator), observed-species, Chao1, and PD_whole_tree, were evaluated using OTU table in QIIME. PCA analysis in beta diversity was performed using the ade4 package and ggplot2 package in R to reduce the dimension of the original variables.

3 Results and discussion

3.1 RRTP alleviated pathological injury of intestinal tissues

Intestinal tissues were evaluated using H&E for morphological and histological changes. After physiological saline inhalation, the intestinal tissues of normal mice showed no significant histological changes (Figure 1B). Interestingly, in LPS-treated ALI mice, the gut tissues showed significant inflammatory zinfiltration, congestion as well as gut villus damage in the model group. It should be noted that after early intervention with RRTP, histopathological score of gut tissues in ALI mice was significantly decreased (Figure 1C), and the severity of pathological changes was significantly attenuated. Therefore, RRTP-mediated intestine-protection may be essential for maintaining intestinal tissues morphology.

3.2 RRTP attenuated oxidative stress damage of intestinal tissues

Excess ROS can cause the peroxidation of unsaturated fatty acid in the lipid layer of cell membranes, which stimulates neighboring epithelial or endothelial cells and amplifies tissue damage (Wang et al., 2020). Therefore, uncontrolled and prolonged oxidative stress response increases the risk of tissue injury in multiple organs, a characteristic feature of several inflammation-related lung diseases (Kawanishi et al., 2017). Accordingly, quantitative measurement of representative oxidation-related indicators of SOD, MPO, MDA and GSH in intestine samples is helpful to reveal whether RRTP can maintain intestinal homeostasis by alleviating oxidative stress response in intestinal tissues to achieve the prevention and treatment of ALI. The levels of oxidative stress indicators in the model group and the normal group were significantly different, indicating that the oxidative stress response was disturbed in the intestinal tissues of ALI mice. Notably, the increase of MPO and MDA and the decrease of SOD and GSH were remarkably restrained in ALI mice after early intervention with RRTP (Figures 2A–D), suggesting that RRTP played a direct role in the ALI therapy by inhibiting over-activated oxidative damage to maintain intestinal homeostasis.

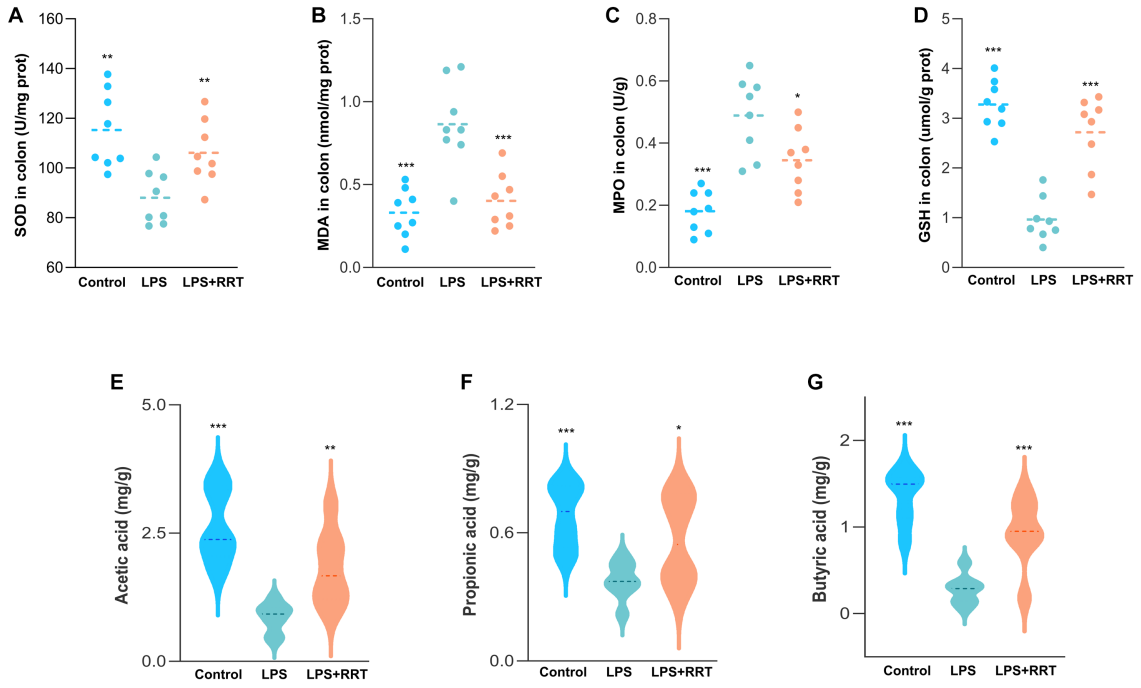

FIGURE 2
Comprehensive evaluation of RRTP on oxidative stress and SCFAs in ALI mice. **(A-D)** The levels of SOD, MDA, MPO and GSH. **(E-G)** Analysis of SCFAs in the cecal contents of the ALI mice. *Compared with the model group, *$P < 0.05$, **$P < 0.01$, ***$P < 0.001$.

3.3 RRTP strengthened the intestinal barrier by regulating SCFAs

SCFAs, one of the most important metabolites produced by intestinal flora, are a class of organic fatty acids with no more than 6 carbon atoms, mainly including acetic acid, propionic acid and butyric acid. Many studies have confirmed that SCFAs, particularly butyric acid, can maintain intestinal homeostasis and the dynamic balance of oxidation-antioxidant response, enhance intestinal barrier (Wang et al., 2022), and they can also reduce inflammation by activating immune cells and epithelial cell receptors after entering lung tissue through blood circulation (Dang et al., 2019; Yoo et al., 2020). Consequently, we detected the SCFAs concentration in the cecum of ALI mice to investigate whether the mitigatory effects of RRTP on ALI was connected with the production of SCFAs. Our results manifested that the SCFAs concentration in cecal contents of LPS-treated ALI mice was lower than that of the normal mice, and after early intervention with RRTP, the cecal SCFAs contents of ALI mice was significantly increased (Figures 2E–G). These results revealed that RRTP strengthened the intestinal barrier by increasing the contents of intestinal SCFAs to achieve a palliative effect of RRTP on ALI.

3.4 RRTP improved cecal contents metabolic disorders

Metabolic profiling data were analyzed without grouping using PCA to determine cecal contents samples distribution and the model's reliability. Compared with the model group, RRTP metabolomics data showed good separation without molecule selection, suggesting that RRTP have significant intervention effects on cecal contents metabolic disorders in ALI mice (Figure 3A). Supervisory pattern OPLS-DA was applied to identify differences in metabolic profiling between the two groups (Supplementary Figure S1), and its degree of reliability and fit was determined by 200 permutations. The results showed that Q^2 and R^2 were less than the original value, and the intersection of the vertical axis with Q^2 regression line was also less than 0 (Supplementary Figure S2). In general, the pattern was reliable, stable, and not overfit, making it suitable for metabolites prediction. Differentially expressed metabolites (DEMs) were defined as variables that significantly contributed to grouping ($p < 0.05$, VIP >1) (Figure 3B). According to the metabolomics of cecal contents, RRTP reversed 40 endogenous metabolites, of which 30 were upregulated and 10 were downregulated (Figure 3C). Among these biomarkers, more than 50% were indoles and their derivatives, amino acids and lipids (Figures 4A–J), and the endogenous metabolites were markedly enriched in five metabolic pathways, including riboflavin metabolism, histidine metabolism, arachidonic acid metabolism, arginine biosynthesis and nicotinate and nicotinamide metabolism (Figure 4K). The results indicated that RRTP modulated the abnormal amino acid metabolism and lipid metabolism of intestine in ALI mice.

3.5 RRTP alleviated the disturbance of gut microbiota

In recent years, the imbalance of intestinal flora has highlighted its role as a pivotal factor of a variety of acute and chronic pulmonary inflammatory diseases, and the disorder of gut microbiota can induce or promote the development of pulmonary inflammation (Frati et al., 2018). The holistic structural alteration of intestinal flora in response to RRTP were illustrated by analysis of the 16S rDNA gene sequencing of microorganic samples isolated from the cecal contents of the normal, model and RRTP mice.

To estimate the differences in bacterial diversity between the three groups, sequences were aligned to evaluate alpha diversity and beta diversity. There are differences in ACE, Chao1, PD_whole_tree and observed species among the three groups of samples (Figure 5A). Both weighted and unweighted PCoA analysis of beta diversity demonstrated a degree of separation of the three groups on the basis of first two PCoA (Figure 5B). These results indicated that RRTP consumption improved the species richness and community diversity of intestinal microflora in ALI mice.

Microbial taxon classification was used to determine the relative proportions of the phylum-level of dominant taxa. We noticed considerable variation in intestinal flora of samples in each group. *Firmicutes* (46.68% versus 14.98%), *Bacteroidota* (36.76% versus 56.16%), *Proteobacteria* (0.49% versus 21.96%), and *Verrucomicrobiota* (5.71% versus 2.52%) were enriched in the normal group compared to the model group (Figure 5C). Intriguingly, after early intervention with RRTP, the proportions of *Bacteroidota* and *Proteobacteria* in ALI mice were significantly reduced, while *Firmicutes* and *Verrucomicrobiota* were significantly increased, and this reversal trend was close to the normal group (Figure 5D). Notably, *Verrucomicrobiota* was the most predominant phylum in the RRTP group. This finding attracted the great attention of our team members, and further analysis of microflora composition at genus level and species level is helpful to reveal the intervention effects of RRTP on gut microbiota of ALI mice. The results showed that *Akkermansia* and *Akkermansia muciniphila* (*A. muciniphila*) were dominant in the RRTP group at the genus and species level, respectively (Figures 5E–G).

3.6 Correlation analysis

Association analysis of SCFAs with *A. muciniphila*, pathological score of the gut tissues, oxidative stress indicators and the representative DEMs was performed to better understand the comprehensive amelioration mechanism of RRTP on intestinal homeostasis in ALI mice (Figure 6). SCFAs, especially propionic acid and butyric acid, were closely related to the pathological score, oxidative stress indicators and intestinal endogenous metabolites (including indole and its derivatives, fatty acids) of ALI mice, suggesting that SCFAs as an effective messenger may be involved in the role of RRTP in maintaining intestinal homeostasis by alleviating intestinal tissue pathological damage, attenuating oxidative stress response and improving metabolic disorders. Conspicuously, butyric acid production was also associated with *A. muciniphila*, the most prominent dominant bacterium of the RRTP group, and this result accurately elucidated that butyric acid and *A. muciniphila* may play a synergistic role in the complex mechanism of RRTP. In addition, we also noted that *A. muciniphila* was negatively correlated with histopathological score, the concentration of MPO and MDA, and positively correlated with the concentration of SOD, GSH and endogenous metabolites indole derivatives. It is suggested that *A. muciniphila* may inhibit excessive oxidative stress response, reduce intestinal tissue injury and increase intestinal indole derivatives to promote intestinal homeostasis.

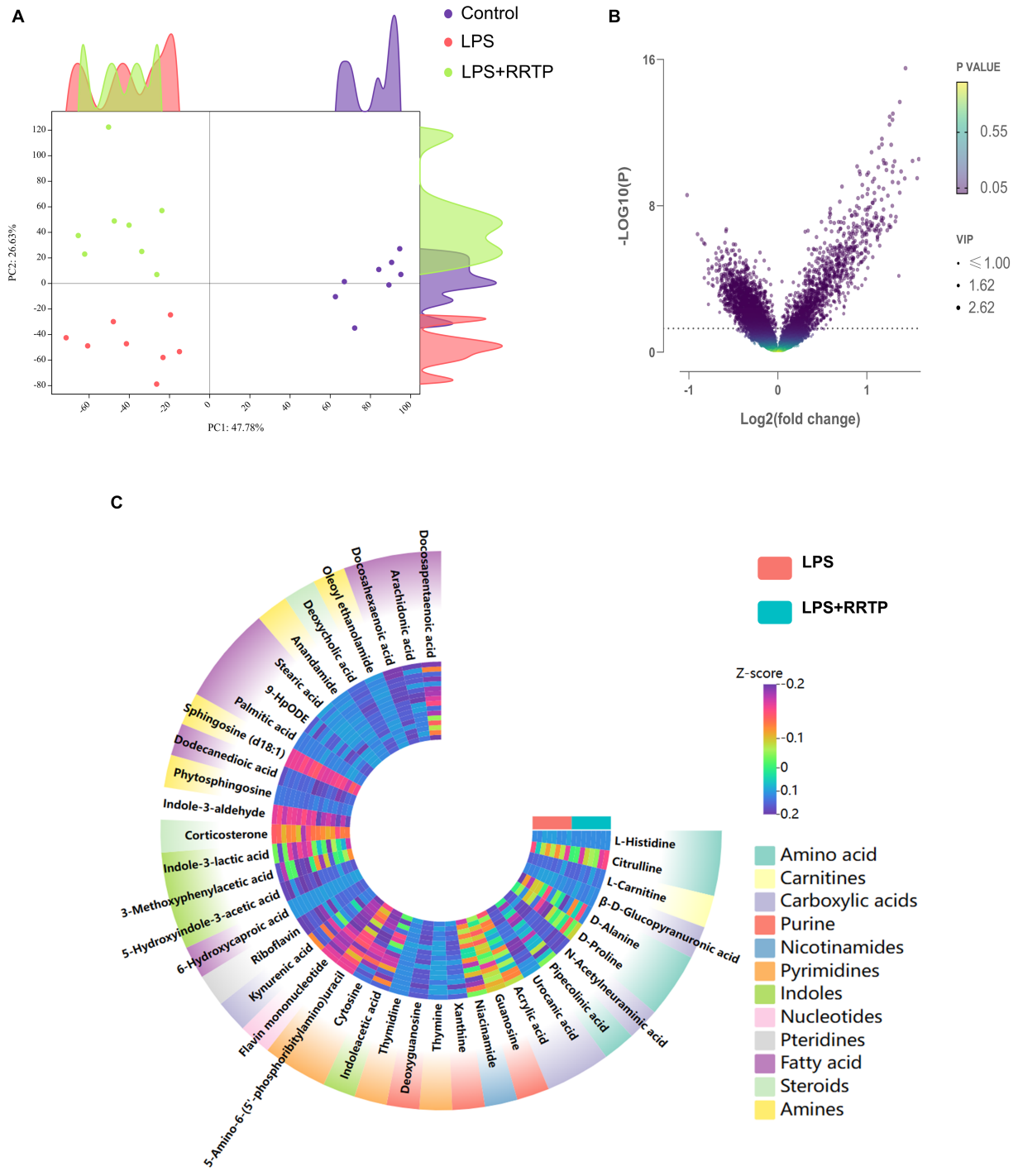

FIGURE 3
Metabolomics analysis of RRTP on the cecal contents in ALI mice. **(A)** PCA of metabolomics data in the three groups. **(B)** Volcano plot of endogenous metabolites in the model group and the RRTP group. **(C)** Heatmap of 40 differentially expressed metabolites (DEMs).

3.7 Comprehensive regulation of RRTP on intestinal homeostasis in ALI mice

3.7.1 Suppression of oxidative stress response

Lung tissue damage can easily cause hypoxia in local and adjacent tissues, causing the accumulation of reactive oxygen species, leading to oxidative stress, which in turn leads to the occurrence and aggravation of ALI (Kellner et al., 2017). MDA, a lipid peroxidation product, is a common marker of oxidative damage, while MPO is an accurate evaluative indicator of neutrophil infiltration and aggregation in inflammatory diseases, involved in the development of ALI and lipid peroxidation (Wang et al., 2020). GSH can catalyze the reduced glutathione to scavenge ROS, thereby alleviating tissue damage caused by lipid peroxides (such as MDA) (Day, 2009). SOD can relieve tissue

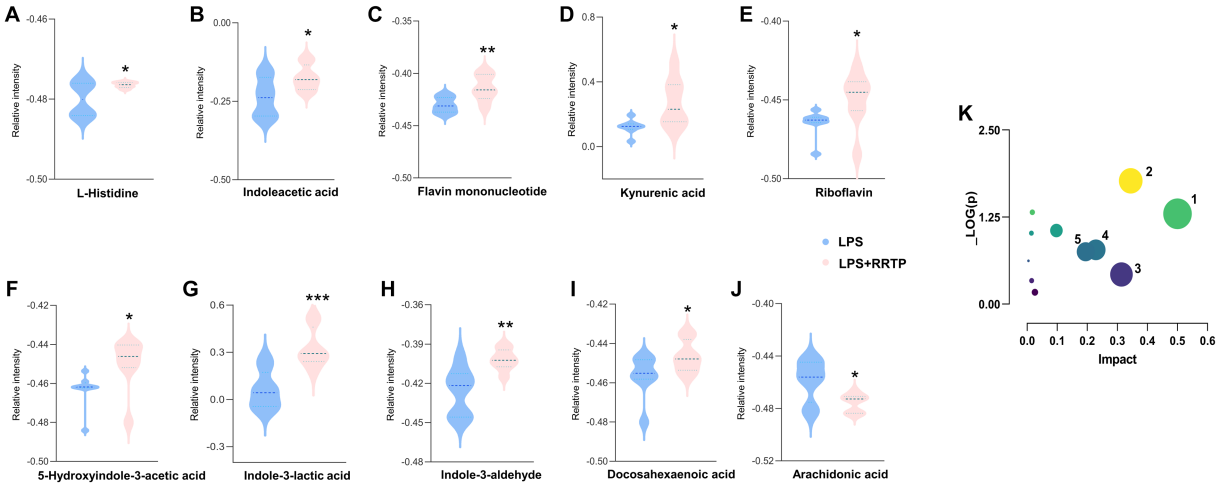

FIGURE 4
Metabolomics analysis of RRTP on the cecal contents in ALI mice. **(A-J)** The expression level of ten representative metabolites with significant difference between the model group and the RRTP group. **(K)** Metabolic pathways analyzed by MetaboAnalyst. 1: Riboflavin metabolism; 2: Histidine metabolism; 3: Arachidonic acid metabolism; 4: Arginine biosynthesis; 5: Nicotinate and nicotinamide metabolism. *$P < 0.05$, **$P < 0.01$, ***$P < 0.001$.

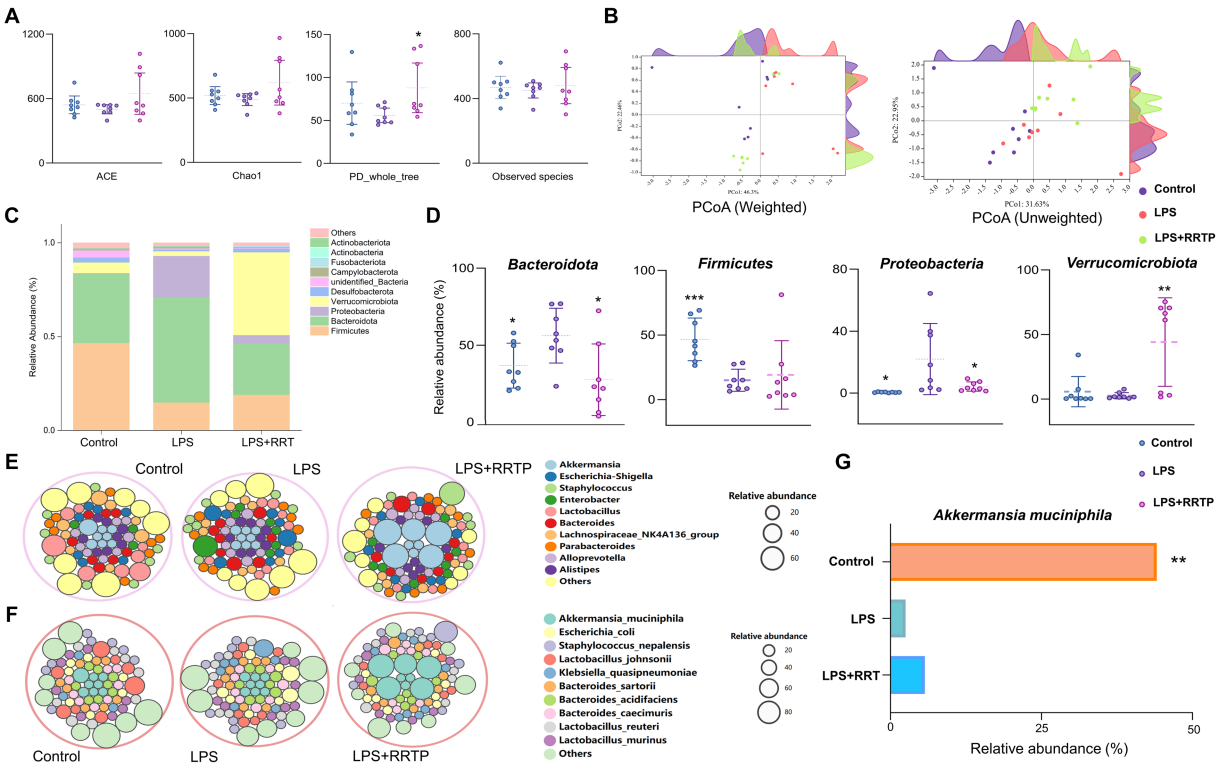

FIGURE 5
Systematic assessment of RRTP on gut microbiome diversity and structure in ALI mice. **(A)** Alpha diversity differences were estimated by the ACE, Chao1, PD_whole_tree, and observed species indices. **(B)** PCoA plot base of the relative abundance of OTUs showing bacterial structural clustering. Weighted UniFrac PCoA plots. Unweighted UniFrac PCoA plots. **(C)** Component proportion of bacterial phylum in each group. **(D)** Four representative bacteria significantly changed at the phylum level. **(E)** Circle packing diagram of bacteria at the genus level in each group. **(F)** Circle packing diagram of bacteria at the species level in each group. **(G)** The relative abundance of Akkermansia_muciniphila in the three groups. *Compared with the model group, *$P < 0.05$, **$P < 0.01$, ***$P < 0.001$.

damage by removing metabolic byproducts produced by oxidative injury (Miao and St. Clair, 2009). In this study, we found that the activities of MDA and MPO were significantly increased, while SOD and GSH were remarkably decreased in the model group ALI mice. Intriguingly, after early intervention with RRTP, MDA and MPO decreased significantly, while SOD and GSH increased significantly. The RRTP-regulated lipid and amino acid differential metabolites, including docosahexaenoic

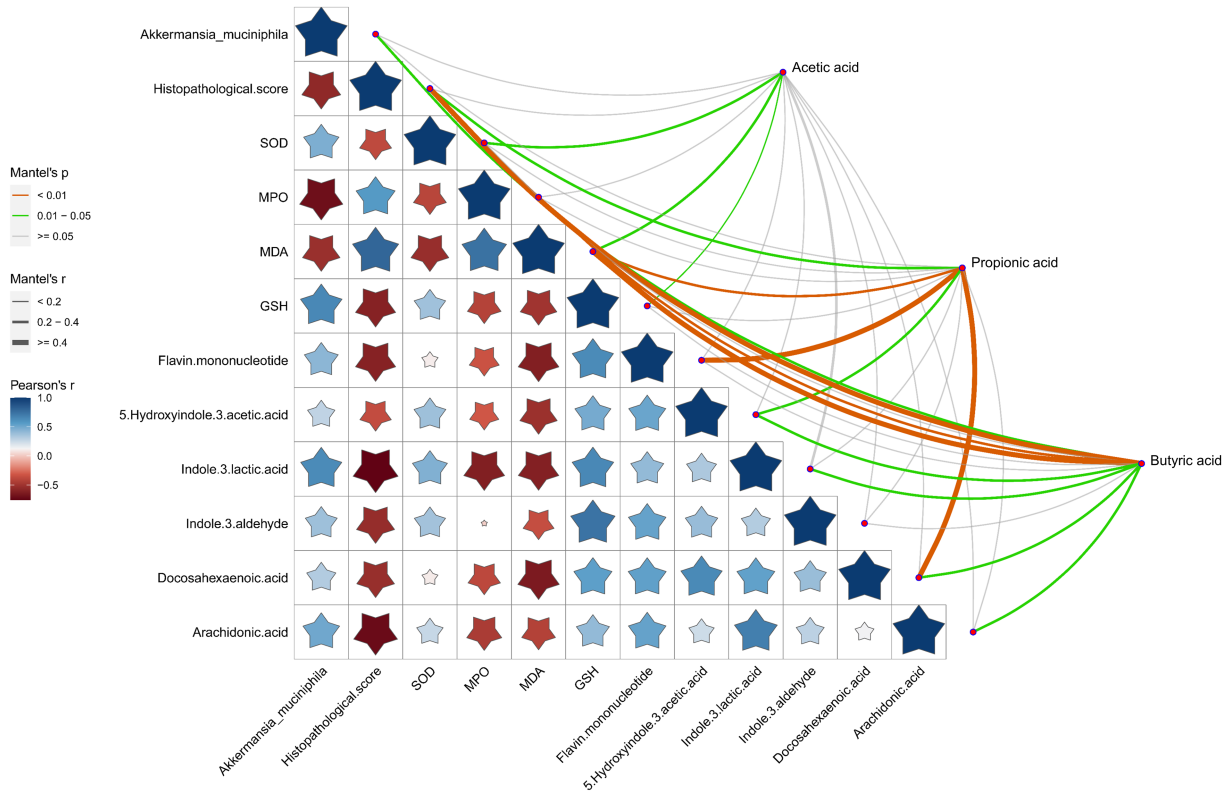

FIGURE 6
Correlation analysis of SCFAs with Akkermansia muciniphila, pathological score of the gut tissues, oxidative stress indicators and the representative DEMs. The orange color curve indicated the significant correlation, the green color curve indicated the statistical difference, and the gray curve indicated no significant correlation. The thickness of the curve and the size of the pentagram represent the size of the correlation coefficient. The thicker the curve (or the larger the pentagram), the greater the correlation coefficient.

acid (Tatsumi et al., 2022; Younes et al., 2022), docosapentaenoic acid (Wang et al., 2019) and histidine (Thalacker-Mercer and Gheller, 2020), identified in our metabolomics study, have effects on reducing inflammation and alleviating oxidative stress. Furthermore, *Bacteroidota* is one of the most aerobically tolerant anaerobic bacteria, and its relative abundance increases significantly under ascending levels of oxidative stress in the organism (Zafar and Saier, 2021). It is also involved in the release of toxic products in the process of protein decomposition, aggravating the inflammatory response of the body (Jandhyala et al., 2015). RRTP significantly decreased the relative abundance of *Bacteroidetes* at the phylum level in this study. Accordingly, our results suggested that oxidative stress response of RRTP on intestinal tissues of ALI mice may be achieved through effective modulation of endogenous metabolites and the composition of intestinal flora.

3.7.2 Promotion of *Akkermansia muciniphila* production

A. muciniphila, a "sentinel of the gut," has emerged as a promising candidate probiotic colonizing in the mucous layer. It plays an important role in promoting host metabolic function, repairing intestinal barrier, maintaining intestinal homeostasis to reduce tissue inflammation and oxidative stress (Zhang et al., 2019; Ouyang et al., 2020). Excitingly, we found that *A. muciniphila* was the most significant dominant bacteria in the RRTP group in this study, with a proportion of nearly 50%, indicating that RRTP could maintain intestinal homeostasis by improving the production of *A. muciniphila*. Given that the production of *A. muciniphila* is related to multiple improvements in intestinal functions, it comes as no surprise that early RRTP intervention induced *A. muciniphila* adequacy would provide protection against intestinal tissue injury.

3.7.3 Enhancement of SCFAs concentration

A variety of bacteria under *Firmicutes* belong to probiotics, which are the dominant bacteria producing SCFAs in intestinal flora and can maintain the homeostasis of gut microbiota (Markowiak-Kopeć and Śliżewska, 2020). In addition, it has been confirmed that *A. muciniphila* also produce SCFAs, and that the production of SCFAs, especially butyric acid, increases intestinal barrier integrity, restrains intestinal inflammatory and oxidative stress responses and minimizes bacterial translocation (Wang et al., 2022). RRTP significantly increased the relative abundance of *Firmicutes* at the phylum level in this study. Consequently, our results manifested that RRTP may enhance the production of SCFAs by regulating the composition and structure of gut flora in order to maintain intestinal homeostasis.

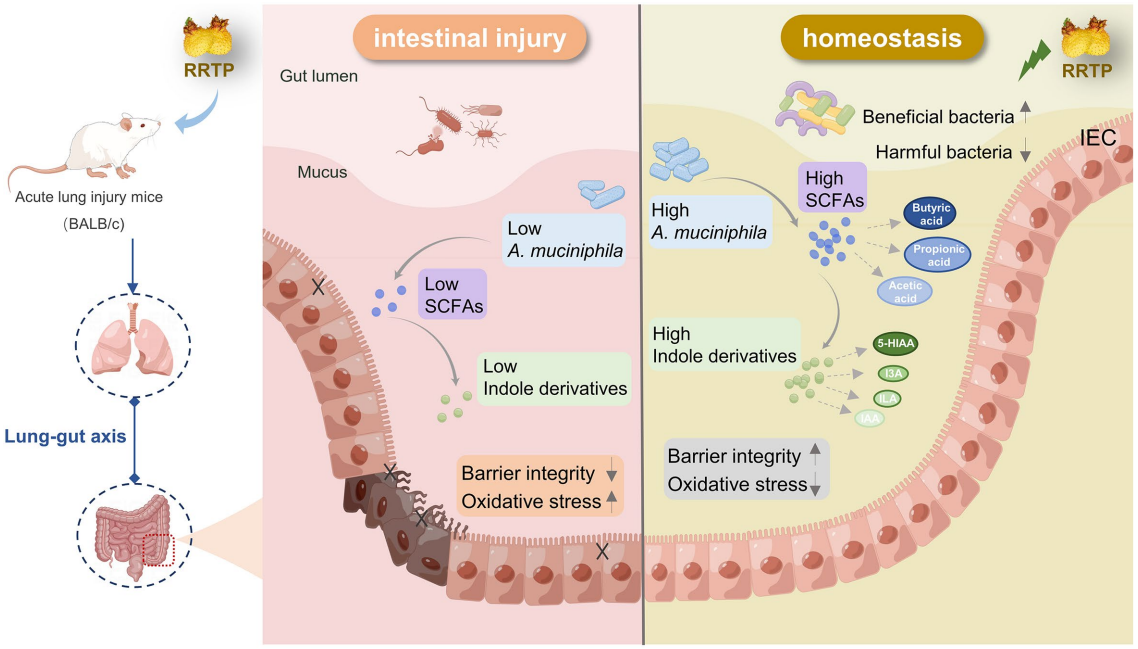

FIGURE 7
Schematic diagram representing the amelioration mechanism of RRTP improving intestinal homeostasis in LPS-induced ALI mice.

3.7.4 Regulation of indole derivatives

Tryptophan metabolites, including indoleacetic acid (IAA), 5-hydroxyindole-3-acetic acid (5-HIAA), indole-3-aldehyde (I3A), indole-3-lactic acid (ILA), and kynurenic acid, can be produced by gut microbiota through tryptophan or kynurenine transformation pathways. These intestinal microbiota-derived tryptophan metabolites play a vital role in maintaining gut homeostasis, as well as attenuating inflammatory-related diseases (Su et al., 2022). I3A can restore mucosal integrity and inhibit inflammation by regulating intestinal microbiome (D'Onofrio et al., 2021; Zhuang et al., 2022). ILA significantly reduced LPS-induced macrophage inflammatory response and oxidative stress response, and is elevated in infant feces, showing protective effect on intestinal epithelial cells (Ehrlich et al., 2020; Meng et al., 2020). In addition, butyrate supplements have been shown to reduce the severity of inflammation in arthritis mice by increasing levels of 5-HIAA (Rosser et al., 2020). In this study, we found the disordered indoles and their derivatives in ALI mice in the metabolomic analysis of cecal contents, and RRTP reversed this disturbance. Characteristically, RRTP significantly increased the intestinal microbiota-derived tryptophan metabolites described above, suggesting that RRTP can promote the remission of lung tissue injury by improving dysregulated metabolism in ALI mice through regulation of intestinal flora.

Cumulatively, RRTP is the active components of a promising underutilized functional food source that can synergistically exert anti-ALI efficacy by significantly ameliorating intestinal tissue damage, inhibiting oxidative stress, increasing SCFAs in cecal contents, regulating the composition and structure of intestinal flora, increasing *A. muciniphila* and modulating disordered intestinal endogenous metabolites (Figure 7).

4 Conclusion

This study showed that RRTP has significant advantages in adjuvant therapy of ALI, and systematically clarified its comprehensive improvement mechanism from a new perspective of "lung-gut axis," which provides a breakthrough for the food and healthcare industries to develop products from botanical functional herbs and foods to prevent or alleviate ALI by regulating intestinal flora.

Data availability statement

The original contributions presented in the study are included in the article/Supplementary material, further inquiries can be directed to the corresponding author.

Ethics statement

Ethical approval was not required for the studies on animals in accordance with the local legislation and institutional requirements because only commercially available established cell lines were used.

Author contributions

LT: Data curation, Validation, Writing – original draft, Writing – review & editing. SZ: Conceptualization, Writing – original draft. MZ: Formal analysis, Data curation, Writing – review & editing. PW: Supervision, Writing – review & editing. GL: Software, Writing – review & editing. ZG: Conceptualization, Writing – original draft. XG: Funding acquisition, Project administration, Writing – review & editing.

Funding

The author(s) declare financial support was received for the research, authorship, and/or publication of this article. This work was financially supported by Social Development Project of Guizhou Department of Science and Technology [(No. 2020)4Y214]; Guizhou Provincial Health Commission Project [(2021)141]; Scientific Research Project of Major Agricultural Industry of Guizhou Province [KY(2019)009].

Conflict of interest

The authors declare that the research was conducted in the absence of any commercial or financial relationships that could be construed as a potential conflict of interest.

Publisher's note

All claims expressed in this article are solely those of the authors and do not necessarily represent those of their affiliated organizations, or those of the publisher, the editors and the reviewers. Any product that may be evaluated in this article, or claim that may be made by its manufacturer, is not guaranteed or endorsed by the publisher.

Supplementary material

The Supplementary material for this article can be found online at: https://www.frontiersin.org/articles/10.3389/fmicb.2024.1351295/full#supplementary-material

References

Dang, A. T., and Marsland, B. J.. (2019). Microbes, metabolites, and the gut-lung axis. *Mucosal Immunology* 12:843–850. doi: 10.1038/s41385-019-0160-6

D'Onofrio, F., Renga, G., Puccetti, M., Pariano, M., Bellet, M. M., Santarelli, I., et al. (2021). Indole-3-carboxaldehyde restores gut mucosal integrity and protects from liver fibrosis in murine sclerosing cholangitis. *Cells* 10:1622. doi: 10.3390/cells10071622

Day, B. J. (2009). Catalase and glutathione peroxidase mimics. *Biochem. Pharmacol.* 77, 285–296. doi: 10.1016/j.bcp.2008.09.029

de Vos, W. M., Tilg, H., Van Hul, M., and Cani, P. D. (2022). Gut microbiome and health: mechanistic insights. *Gut* 71, 1020–1032. doi: 10.1136/gutjnl-2021-326789

Ehrlich, A. M., Pacheco, A. R., Henrick, B. M., Taft, D., Xu, G., Huda, M. N., et al. (2020). Indole-3-lactic acid associated with *Bifidobacterium*-dominated microbiota significantly decreases inflammation in intestinal epithelial cells. *BMC Microbiol.* 20:357. doi: 10.1186/s12866-020-02023-y

Frati, F., Salvatori, C., Incorvaia, C., Bellucci, A., Di Cara, G., Marcucci, F., et al. (2018). The role of the microbiome in asthma: the gut-lung axis. *Int. J. Mol. Sci.* 20:123. doi: 10.3390/ijms20010123

Gorman, E. A., O'kane, C. M., and Mcauley, D. F. (2022). Acute respiratory distress syndrome in adults: diagnosis, outcomes, long-term sequelae, and management. *Lancet* 400, 1157–1170. doi: 10.1016/S0140-6736(22)01439-8

He, Y.-Q., Zhou, C.-C., Yu, L.-Y., Wang, L., Deng, J.-L., Tao, Y.-L., et al. (2021). Natural product derived phytochemicals in managing acute lung injury by multiple mechanisms. *Pharmacol. Res.* 163:105224. doi: 10.1016/j.phrs.2020.105224

Hou, H., Chen, D., Zhang, K., Zhang, W., Liu, T., Wang, S., et al. (2022). Gut microbiota-derived short-chain fatty acids and colorectal cancer: ready for clinical translation? *Cancer Lett.* 526, 225–235. doi: 10.1016/j.canlet.2021.11.027

Huang, C., Du, W., Ni, Y., Lan, G., and Shi, G. (2022). The effect of short-chain fatty acids on M2 macrophages polarization *in vitro* and *in vivo*. *Clin. Exp. Immunol.* 207, 53–64. doi: 10.1093/cei/uxab028

Huang, X., Fan, X., Ying, J., and Chen, S. (2019). Emerging trends and research foci in gastrointestinal microbiome. *J. Transl. Med.* 17:67. doi: 10.1186/s12967-019-1810-x

Iddrisu, I., Soumyakrishnan, S., Joseph, A. A., Xu, J., Boakai, R., Sreepriya, M., et al. (2022). Modulatory effect of gut microbiota on the gut-brain, gut-bone axes, and the impact of cannabinoids. *Metabolites* 12:1247. doi: 10.3390/metabo12121247

Jandhyala, S. M., Talukdar, R., Subramanyam, C., Vuyyuru, H., Sasikala, M., and Nageshwar Reddy, D. (2015). Role of the normal gut microbiota. *World J. Gastroenterol.* 21, 8787–8803. doi: 10.3748/wjg.v21.i29.8787

Ji, J., Zhang, S., Yuan, M., Zhang, M., Tang, L., Wang, P., et al. (2022). Fermented *Rosa roxburghii* Tratt juice alleviates high-fat diet-induced hyperlipidemia in rats by modulating gut microbiota and metabolites. *Front. Pharmacol.* 13:883629. doi: 10.3389/fphar.2022.883629

Kawanishi, S., Ohnishi, S., Ma, N., Hiraku, Y., Oikawa, S., and Murata, M. (2017). Nitrative and oxidative DNA damage in infection-related carcinogenesis in relation to cancer stem cells. *Genes Environ.* 38:26. doi: 10.1186/s41021-016-0055-7

Kellner, M., Noonepalle, S., Lu, Q., Srivastava, A., Zemskov, E., and Black, S. M. (2017). ROS signaling in the pathogenesis of acute lung injury (ALI) and acute respiratory distress syndrome (ARDS). *Adv. Exp. Med. Biol.* 967, 105–137. doi: 10.1007/978-3-319-63245-2_8

Markowiak-Kopeć, P., and Śliżewska, K. (2020). The effect of probiotics on the production of short-chain fatty acids by human intestinal microbiome. *Nutrients* 12:1107. doi: 10.3390/nu12041107

Meng, M. M., Jia, Y. K., Shuang, J., Yuan, Y. W., Si, L. W., Jing, J. Y., et al. (2022). Melatonin suppresses macrophage M1 polarization and ROS-mediated pyroptosis via activating ApoE/LDLR pathway in influenza A-induced acute lung injury. *Oxidative Med. Cell. Longev.* 2022:2520348. doi: 10.1155/2022/2520348

Meng, D., Sommella, E., Salviati, E., Campiglia, P., Ganguli, K., Djebali, K., et al. (2020). Indole-3-lactic acid, a metabolite of tryptophan, secreted by *Bifidobacterium longum* subspecies infantis is anti-inflammatory in the immature intestine. *Pediatr. Res.* 88, 209–217. doi: 10.1038/s41390-019-0740-x

Miao, L., and St. Clair, D. K. (2009). Regulation of superoxide dismutase genes: implications in disease. *Free Radic. Biol. Med.* 47, 344–356. doi: 10.1016/j.freeradbiomed.2009.05.018

Ornatowski, W., Lu, Q., Yegambaram, M., Garcia, A. E., Zemskov, E. A., Maltepe, E., et al. (2020). Complex interplay between autophagy and oxidative stress in the development of pulmonary disease. *Redox Biol.* 36:101679. doi: 10.1016/j.redox.2020.101679

Ouyang, J., Lin, J., Isnard, S., Fombuena, B., Peng, X., Marette, A., et al. (2020). The bacterium *Akkermansia muciniphila*: a sentinel for gut permeability and its relevance to HIV-related inflammation. *Front. Immunol.* 11:645. doi: 10.3389/fimmu.2020.00645

Rosser, E. C., Piper, C. J. M., Matei, D. E., Blair, P. A., Rendeiro, A. F., Orford, M., et al. (2020). Microbiota-derived metabolites suppress arthritis by amplifying aryl-hydrocarbon receptor activation in regulatory B cells. *Cell Metab.* 31, 837–851.e10. doi: 10.1016/j.cmet.2020.03.003

Su, X., Gao, Y., and Yang, R. (2022). Gut microbiota-derived tryptophan metabolites maintain gut and systemic homeostasis. *Cells* 11:2296. doi: 10.3390/cells11152296

Tang, J., Xu, L., Zeng, Y., and Gong, F. (2021). Effect of gut microbiota on LPS-induced acute lung injury by regulating the TLR4/NF-kB signaling pathway. *Int. Immunopharmacol.* 91:107272. doi: 10.1016/j.intimp.2020.107272

Tang, L., Zhang, S., Zhang, M., Wang, P. J., Liang, G. Y., and Gao, X. L. (2022). Analysis of protective effects of *Rosa roxburghii* Tratt fruit polyphenols on lipopolysaccharide-induced acute lung injury through network pharmacology and metabolomics. *Food Sci. Nutr.* 10, 4258–4269. doi: 10.1002/fsn3.3019

Tang, L., Zhang, S., Zhang, M., Wang, P. J., Liang, G. Y., and Gao, X. L. (2023). Integrated proteomics and metabolomics analysis to explore the amelioration mechanisms of *Rosa roxburghii* Tratt fruit polyphenols on lipopolysaccharide-induced acute lung injury mice. *J. Agric. Food Chem.* 71, 3079–3092. doi: 10.1021/acs.jafc.2c04344

Tatsumi, Y., Kato, A., Niimi, N., Yako, H., Himeno, T., Kondo, M., et al. (2022). Docosahexaenoic acid suppresses oxidative stress-induced autophagy and cell death via the AMPK-dependent signaling pathway in immortalized Fischer rat Schwann cells 1. *Int. J. Mol. Sci.* 23:4405. doi: 10.3390/ijms23084405

Thalacker-Mercer, A. E., and Gheller, M. E. (2020). Benefits and adverse effects of histidine supplementation. *J. Nutr.* 150, 2588S–2592S. doi: 10.1093/jn/nxaa229

Wang, L., Li, C., Huang, Q., and Fu, X. (2020). Polysaccharide from *Rosa roxburghii* Tratt fruit attenuates hyperglycemia and hyperlipidemia and regulates colon microbiota in diabetic db/db mice. *J. Agric. Food Chem.* 68, 147–159. doi: 10.1021/acs.jafc.9b06247

Wang, T., Lin, S., Liu, R., Li, H., Liu, Z., Zhang, X., et al. (2020). Metabolomic profile perturbations of serum, lung, bronchoalveolar lavage fluid, spleen and feces in LPS-induced acute lung injury rats based on HPLC-ESI-QTOF-MS. *Anal. Bioanal. Chem.* 412, 1215–1234. doi: 10.1007/s00216-019-02357-1

Wang, Z., Liu, J., Li, F., Luo, Y., Ge, P., Zhang, Y., et al. (2022). The gut-lung axis in severe acute pancreatitis-associated lung injury: the protection by the gut microbiota through short-chain fatty acids. *Pharmacol. Res.* 182:106321. doi: 10.1016/j.phrs.2022.106321

Wang, L. T., Lv, M. J., An, J. Y., Fan, X. H., Dong, M. Z., Zhang, S. D., et al. (2021). Botanical characteristics, phytochemistry and related biological activities of *Rosa roxburghii* Tratt fruit, and its potential use in functional foods: a review. *Food Funct.* 12, 1432–1451. doi: 10.1039/d0fo02603d

Wang, M., Ma, L.-J., Yang, Y., Xiao, Z., and Wan, J.-B. (2019). n-3 Polyunsaturated fatty acids for the management of alcoholic liver disease: a critical review. *Crit. Rev. Food Sci. Nutr.* 59, S116–S129. doi: 10.1080/10408398.2018.1544542

Wedgwood, S., Gerard, K., Halloran, K., Hanhauser, A., Monacelli, S., Warford, C., et al. (2020). Intestinal dysbiosis and the developing lung: the role of toll-like receptor 4 in the gut-lung axis. *Front. Immunol.* 11:357. doi: 10.3389/fimmu.2020.00357

Wu, Z., Huang, S., Li, T., Li, N., Han, D., Zhang, B., et al. (2021). Gut microbiota from green tea polyphenol-dosed mice improves intestinal epithelial homeostasis and ameliorates experimental colitis. *Microbiome* 9:184. doi: 10.1186/s40168-021-01115-9

Yoo, J. Y., Groer, M., Dutra, S. V., Sarkar, A., and McSkimming, D. I. (2020). Gut microbiota and immune system interactions. *Microorganisms* 8:1587. doi: 10.3390/microorganisms8101587

Younes, N. B., Mohamed, O. A., and Rizk, N. M. (2022). Docosahexaenoic acid counteracts the hypoxic-induced inflammatory and metabolic alterations in 3T3-L1 adipocytes. *Nutrients* 14:4600. doi: 10.3390/nu14214600

Zafar, H., and Saier, M. H. Jr. (2021). Gut *Bacteroides* species in health and disease. *Gut Microbes* 13, 1–20. doi: 10.1080/19490976.2020.1848158

Zhang, T., Li, Q., Cheng, L., Buch, H., and Zhang, F. (2019). *Akkermansia muciniphila* is a promising probiotic. *Microb. Biotechnol.* 12, 1109–1125. doi: 10.1111/1751-7915.13410

Zhuang, H., Li, B., Xie, T., Xu, C., Ren, X., Jiang, F., et al. (2022). Indole-3-aldehyde alleviates chondrocytes inflammation through the AhR-NF-κB signalling pathway. *Int. Immunopharmacol.* 113:109314. doi: 10.1016/j.intimp.2022.109314

frontiers | Frontiers in Microbiology

TYPE Original Research
PUBLISHED 21 March 2024
DOI 10.3389/fmicb.2024.1382639

OPEN ACCESS

EDITED BY
Jie Yin,
Hunan Agricultural University, China

REVIEWED BY
Xiaofeng Shan,
Jilin Agricultural University, China
Yuying Li,
Institute of Bast Fiber Crops and Center for Southern Economic Crops, Chinese Academy of Agricultural Sciences, China

*CORRESPONDENCE
Hongbin Si
shb2009@gxu.edu.cn
Jiang Li
lijiangll@126.com

†These authors have contributed equally to this work and share first authorship

RECEIVED 06 February 2024
ACCEPTED 05 March 2024
PUBLISHED 21 March 2024

CITATION
Cheng M, Shi Y, Cheng Y, Hu H, Liu S, Xu Y, He L, Hu S, Lu Y, Chen F, Li J and Si H (2024) Mulberry leaf polysaccharide improves cyclophosphamide-induced growth inhibition and intestinal damage in chicks by modulating intestinal flora, enhancing immune regulation and antioxidant capacity. *Front. Microbiol.* 15:1382639. doi: 10.3389/fmicb.2024.1382639

Mulberry leaf polysaccharide improves cyclophosphamide-induced growth inhibition and intestinal damage in chicks by modulating intestinal flora, enhancing immune regulation and antioxidant capacity

Ming Cheng[1†], Yongbin Shi[1†], Yumeng Cheng[1], Hongjie Hu[1], Song Liu[1], Yanping Xu[1], Lingzhi He[1], Shanshan Hu[1], Yujie Lu[1], Fengmin Chen[2], Jiang Li[1*] and Hongbin Si[1*]

[1]College of Animal Science and Technology, Guangxi Key Laboratory of Animal Breeding, Disease Control and Prevention, Guangxi University, Nanning, China, [2]Hunan Provincial Key Laboratory of the TCM Agricultural Biogenomics, Changsha Medical University, Changsha, China

Polysaccharides are generally considered to have immune enhancing functions, and mulberry leaf polysaccharide is the main active substance in mulberry leaves, while there are few studies on whether mulberry leaf polysaccharide (MLP) has an effect on immunosuppression and intestinal damage caused by cyclophosphamide (CTX), we investigated whether MLP has an ameliorative effect on intestinal damage caused by CTX. A total of 210 1-day-old Mahuang cocks were selected for this experiment. Were equally divided into six groups and used to evaluate the immune effect of MLP. Our results showed that MLP significantly enhanced the growth performance of chicks and significantly elevated the secretion of cytokines (IL-1β, IL-10, IL-6, TNF-α, and IFN-γ), immunoglobulins and antioxidant enzymes in the serum of immunosuppressed chicks. It attenuated jejunal damage and elevated the expression of jejunal tight junction proteins Claudin1, Zo-1 and MUC2, which protected intestinal health. MLP activated TLR4-MyD88-NF-κB pathway and enhanced the expression of TLR4, MyD88 and NF-κB, which served to protect the intestine. 16S rDNA gene high-throughput sequencing showed that MLP increased species richness, restored CTX-induced gut microbiome imbalance, and enhanced the abundance of probiotic bacteria in the gut. MLP improves cyclophosphamide-induced growth inhibition and intestinal damage in chicks by modulating intestinal flora and enhancing immune regulation and antioxidant capacity. In conclusion, this study provides a scientific basis for MLP as an immune enhancer to regulate chick intestinal flora and protect chick intestinal mucosal damage.

KEYWORDS

mulberry leaf polysaccharide, oxidative stress, immunosuppression, intestinal damage, growth performance, intestinal flora

1 Introduction

Poultry are raised intensively, and chicks are often affected by stressful conditions, viral infections, nutritional deficiencies, infectious diseases, and other conditions that can cause immunosuppressive diseases (Shini et al., 2010). It not only affects the immune function of chicks, but also causes symptoms such as intestinal damage and intestinal oxidative stress, which also reduces the conversion rate of chick feed and affect the feed-to-meat ratio (Fussell, 1998; Jahanian and Rasouli, 2015). In the state of immunosuppression, the body loses the ability to resist pathogens, leading to a sharp increase in morbidity and mortality among chicks, which causes substantial losses in the farming industry (Hoerr, 2010).

Cyclophosphamide (CTX), the broad-spectrum chemotherapeutic utilized to treat cancer, kills cancer cells primarily through the genotoxicity and cytotoxicity of drug (Emadi et al., 2009). However, the excessive use of CTX can also cause body immunosuppression and oxidative stress, liver damage, and intestinal injury caused by intestinal mucosal barrier disruption (Duncan and Grant, 2003; Ahlmann and Hempel, 2016; Zheng et al., 2017). The intestine is the largest digestive organ of the body and also the greatest immune organ, while the intestinal barrier and mucosal immune system represent a key system to maintain body health against external pathogens (Walker et al., 2014). Therefore, in the case of declined immune function, the intestinal barrier and intestinal mucosal immune system are destroyed, the disease resistance of the body will be decreased and the risk of disease will be increased (Schoultz and Keita, 2019). In addition, under normal circumstances, the intestinal tract of the body is rich in flora to maintain the dynamic balance of the intestine, but is highly susceptible to the influence of the external environment, causing diarrhea and intestinal inflammation (Jang et al., 2019). Therefore, it is necessary to develop natural pharmaceutical feed additives that can increase organism immunity and improve intestinal flora and function (Wu et al., 2017; Wang et al., 2019).

Polysaccharides, as a type of high molecular weight long-chain carbohydrates, are widely present in plants, animals, and microorganisms (Kong et al., 2004). It has functions such as enhancing immunity and antioxidant and anti-inflammatory properties (Yu et al., 2018). Meanwhile, a large number of experiments have also proven that polysaccharides have the effect of improving the growth performance of livestock and enhancing immunity (Shu et al., 2021; Zhang et al., 2021). Mulberry leaf polysaccharide (MLP) is a natural polymer extracted from mulberry leaves and has been proven to have good antioxidant activity (Yuan et al., 2015). Mulberry leaf polysaccharide can also antagonize diabetes (Zhang et al., 2014). Meanwhile, Zhao demonstrated that MLP can improve the metabolism and immune function of weaned piglets (Zhao et al., 2019). However, the role of MLP in regulating intestinal injury and immune performance in immunosuppressive chicks is not clear. Therefore, this experiment established a CTX-induced immunosuppressive model in chicks to study the effects of MLP on the growth performance, immune performance, antioxidant performance, and intestinal injury of CTX-induced immunosuppressive chicks.

2 Materials and methods

2.1 Materials

We obtained mulberry leaf samples in the mulberry leaf garden in Nanning, Guangxi, China.

2.2 Preparation of MLP

After collection, fresh mulberry leaf samples were subjected to shade drying, crushing, and passing through 60 mesh sieve, after which they were soaked in 85% of ethanol for more than 7 days and then dried at 50°C. According to the 34 mL/g material–liquid ratio, at a 92°C extraction temperature, a 3.5-h extraction time, and after 2 extractions, the filtrate was combined by filtration and centrifugation, concentrated under reduced pressure at 70°C, the concentrate was centrifuged to remove the residue, anhydrous ethanol at 4-fold volume was introduced for concentration and left for 13 h, then the precipitate was collected by centrifugation, the precipitate was washed using anhydrous ethanol at 3-fold volume and collected by centrifugation again, and finally freeze-dried to obtain mulberry leaf polysaccharide. The content of sugar was 51.02% by phenol–sulfuric acid method.

2.3 Determination of physicochemical properties of the polysaccharide

Using the Shimadzu LC-10A system containing the BRT105-104-102 column (8 × 300 mm, Borui Saccharide) and the parallax detector, Mw of MLP was analyzed with high-performance gel permeation chromatography (HPGPC). Calibration curves were also drawn to determine molecular weight. Fourier transform infrared spectroscopy (FT-IR) was then conducted to analyze organic functional groups within MLP. Later, dried polysaccharides were blended with KBr powder, followed by pressing the mixture to sheets to record using the Fourier transform infrared spectrometer FT-IR650 within 4,000–400 cm^{-1}.

2.4 Preparation of MLE

Weigh a certain amount of dried mulberry leaves, add 20 times the weight of distilled water, soak for 2 hours, heat to boiling, and then keep boiling for 2 hours. Then filter the extract to remove the filter residue, centrifuge to remove impurities, use a rotary evaporator to concentrate the extract into 1 mL of liquid, equivalent to 1 g of the original drug, and then freeze dry it into powder using a freeze-drying machine. After drying, seal and store it.

2.5 Animal experiment

The Experimental Animal Ethics Committee of Guangxi University (GXU-2023-0013) approved our animal experimental protocols. In total, 210 1-day-old Mahuang cocks were chosen for the experiments. They were kept within wired cages with lighting and good ventilation at 50–55% relative humidity. For 1–14-day-olds, a 24-h light period was provided for the chicken house, followed by a gradual decline into 20 h every day. At 1–7-day-old, chicken house temperature was maintained under 32–34°C, followed by a gradual decline to 26°C. In this experimental process, chickens could eat and drink freely. After the chicks finished acclimatization, the chicks were evenly classified into 6 groups based on body weight at 7 days of age, with 7 chicks for every replicate, and 5 replicates for every group, specifically into blank control group (NC), cyclophosphamide model group (MC), mulberry leaf polysaccharide immunosuppression group (MLP + CTX), mulberry leaf aqueous extract immunosuppression

group (MLE + CTX), normal mulberry leaf polysaccharide group (MLP), and normal mulberry leaf aqueous extract group (MLE), and the experimental days were 35 days. During this period, NC and MC groups were given the basal diet, the MLP + CTX and MLP groups added 0.25% MLP to the basal diet, and the MLE + CTX and MLE groups added 0.25% MLE to the basal diet. On days 29, 31, and 33, the MC, MLP + CTX, and MLE + CTX groups were given injections of 80 mg/kg of CTX into the thoracic muscle, and the NC, MLP, and MLE groups were given injections of normal saline at an equivalent volume. On days 14, 21, 28, and 35, feed intake and body weight were determined to calculate the meat and feed ratio. At 35 days, we obtained blood, thymus, spleen, bursa, jejunum, and cecum contents from the chicks for subsequent analysis ($n = 6$). Table 1 displays diet information.

2.6 Growth performance and index of spleen, thymus, and bursa of Fabricius determination

Through this experiment, we measured body weight and feed consumption of chicken every day, acquired their spleen, thymus, and BF, and recorded the weights at the end of this experiment. The index of the spleen, thymus, and BF was determined as follows:

Index (g/kg) = immune organ weight/body weight.

2.7 Measurements of cytokines and immunoglobulins

Blood samples were obtained into the sterile tube, followed by 10-min natural coagulation under ambient temperature (Yin et al., 2020) and an additional 20-min centrifugation (3,000 rpm under 4°C) to obtain the serum. At last, the ELISA kits (Nanjing Boyan Biotech Co) were utilized for detecting IL-1β, IL-6, IL-10, IFN-γ, TNF-α, and IgG levels.

2.8 Determination of serum antioxidant enzyme activity

The serum collection method is consistent with 2.7. Serum samples were obtained from superoxide dismutase (SOD), catalase (CAT), glutathione peroxidase (GPx), total antioxidant capacity (T-AOC), and malondialdehyde (MDA) levels using an ELISA kit (Nanjing Boyan Biotech Co).

2.9 Histopathological staining

Chick jejunal and ileal samples were subjected to overnight fixation using 10% neutral formaldehyde, followed by dehydration, pruning, embedding, sectioning, staining, and tablet sealing for

TABLE 1 Basic diet information (%).

Items	Days 1–14	Days 15–28	Days 29–42
Ingredients			
Corn	56.80	57.36	58.88
Soybean meal	36.48	34.57	33.01
Soybean oil	1.63	3.42	3.89
NaCl	0.53	0.53	0.53
Limestone	1.40	1.22	1.05
CaHPO4	2.10	1.99	1.85
L-Lys·HCl	0.30	0.15	0.06
DL-Met	0.26	0.26	0.23
Choline chloride	0.10	0.10	0.10
Premix[1]	0.40	0.40	0.40
Total	100.00	100.00	100.00
Nutrient levels[2]			
AME, MJ/kg	12.89	13.50	13.94
Crude protein	21.00	20.00	20.00
Calcium	1.01	1.00	0.95
Available phosphorus	0.62	0.60	0.57
Lysine	1.04	0.91	0.88
Methionine	0.41	0.40	0.38
Threonine	0.74	0.70	0.70
Tryptophan	0.22	0.19	0.18

[1]The premix is provided per kilogram of ration: VA 10000 IU; VD 5200 IU, VE 40 IU; VK 8 IU; VB1 5 IU; VB2 8 IU; VB6 12 IU; VB12 2 IU; biotin 0.2 mg; nicotinic acid 45 mg; folic acid 0.8 mg; Fe 100 mg, Cu 8 mg, Zn 100 mg, Mn 120 mg, I 0.3 mg, Se 0.7 mg. [2]Nutrient levels were calculated values. AME, apparent metabolizable energy.

microscopic examination (Deng et al., 2021). Later, the digital trim camera microscope (BA210 Digital, Motic) was utilized for section observation; meanwhile, the image analysis software (Motic Images Advanced 3.2) was employed for measuring and analyzing villus length, crypt depth, and intestinal wall of jejunal and ileal samples. The tissue of 4 chicks in each group was selected as slices, three fields of view were selected from each tissue section, and 10 villus heights and 10 crypt depths were measured in each field with Image-Pro Plus 6.0. The villus length-to-crypt depth ratio was determined to be an index for evaluating the degree of intestinal injury.

2.10 RNA isolation and RT-PCR assay

Frozen jejunal samples (50–100 mg) were ground within liquid nitrogen; later, the TRIGene total RNA extraction reagent was utilized for RNA extraction. cDNA was synthesized using StarScript II First-Strand cDNA Synthesis Mix (GenStar) with gDNA remover. By adopting RealStar Green Fast Mixture, PCR was carried out using the LightCycler 96 System (Roche). RT-PCR was then conducted to detect TLR4, MyD88, NF-κB, Occludin, MUC2, ZO-1, IL-10, and IFN-γ gene levels, with β-actin being the endogenous control. The 2-11CT approach was utilized to determine relative gene expression. Supplementary Table S1 displays primer sequences utilized in this study.

2.11 DNA isolation from intestinal flora and 16S rDNA gene high-throughput sequencing

The DNA Kit (Omega) was utilized for DNA extraction from cecal contents. Universal primers 341F (5'-CCTAYGGGRBGCASCAG-3′) and 806R (5'-GGACTACNNGGGTATCTAAT-3′) were utilized to amplify V3-V4 hypervariable regions of the bacterial 16S rDNA gene. The AxyPrep DNA Gel Recovery Kit (Axygen) was utilized to purify PCR products, whereas QuantiFluor™-ST (Promega) was used for quantification. The TruSeCT60M DNA Sample Prep Kit was employed for constructing the PE library, while the Illumina MiSeq PE300 platform (Illumina) was applied in sequencing in line with specific protocols. UPARSE software was later used in high-quality sequence clustering for obtaining operational taxonomic units (OTUs) according to the 97% similarity level. Alpha- and beta-diversities were examined in line with OTU abundances with the R package. For predominant bacterial species at the phylum and genus levels, their relative abundances were determined. Between-group dominance of microbial communities was analyzed through linear discriminant analysis (LDA) and linear discriminant analysis effect size (LEFSE). Several groups were compared by one-way ANOVA, while two groups were compared by Wilcoxon rank-sum tests.

Note: In the sequencing results of 16S rDNA in this section, in all tables and figures, MLP represents MLP + CTX, while MLE represents MLE + CTX, which means injection of CTX is used to evaluate the improvement effect of MLP and MLE on CTX-induced intestinal dysbiosis. NC group still represents the blank control group, and MC group represents the cyclophosphamide injection group.

2.12 Statistical analysis

Experimental data within tables and figures were represented by mean ± SD, while between-group differences were evaluated through one-way ANOVA and Tukey's multiple comparisons with SPSS. GraphPad Prism 6.0 was applied in graph plotting. Majorbio cloud platform was employed for analyzing 16S rDNA sequencing data. $p < 0.05$ and $p < 0.01$ represent significant and extremely significant differences, separately.

3 Results

3.1 Physicochemical properties of MLP

The MLPs utilized in this study have fundamental features and physicochemical properties of polysaccharides. The Mw values were determined to be 758.773 kDa, 11.968 kDa, 7.643 kDa, and 4.149 kDa, respectively (Figure 1). According to the above findings, there were various polysaccharides within MLP (Figure 2). The absorption band at 3600–3200 cm-1 was ascribed to -OH stretching vibration; typically, absorption peaks within the above region represented the typical peaks of sugars. Later, the peak at 3313 cm-1 stands for an absorption peak related to O-H stretching vibration, and it was the typical peak of sugars. One absorption peak could be detected at 2937 cm-1, probably associated with C-H stretching vibration. The absorption peak detected

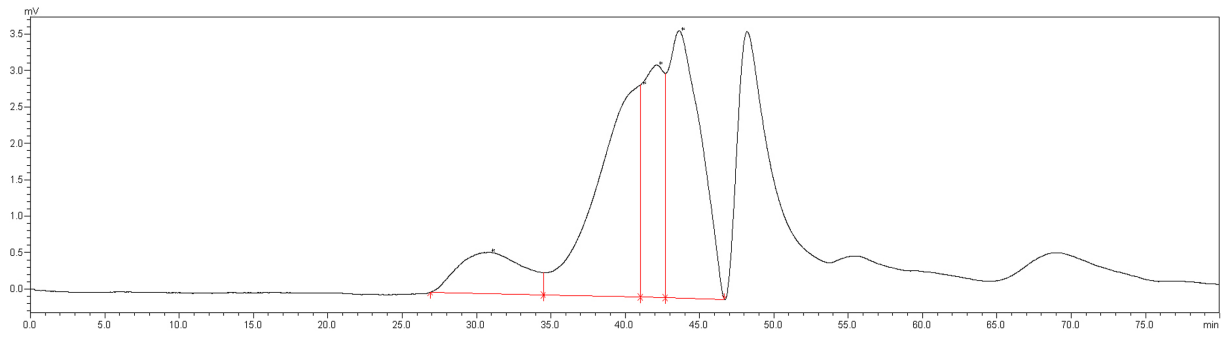

FIGURE 1
Molecular weight detection results of MLP.

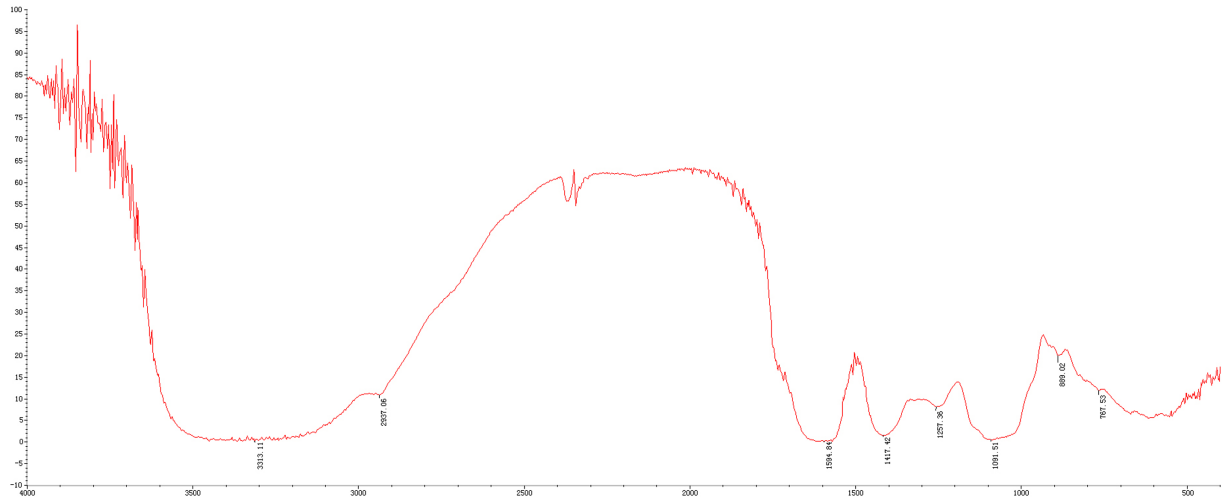

FIGURE 2
FT-IR spectra of MLP.

TABLE 2 Effect of MLP on the growth performance of chicks.

Items	NC	MLP	MLE	*p*-value
D7-D21				
ADG, g/d	3.5 ± 0.19	4.05 ± 0.13*	3.77 ± 0.11	0.062
ADFI, g/d	11.89 ± 0.11	11.79 ± 0.11	11.97 ± 0.07	0.478
FCR	3.44 ± 0.22	2.92 ± 0.08*	3.19 ± 0.09	0081
D21-D28				
ADG, g/d	6.61 ± 0.52	7.66 ± 0.35	6.93 ± 0.29	0.201
ADFI, g/d	19.99 ± 0.82	19.51 ± 0.62	20.27 ± 0.95	0.804
FCR	3.07 ± 0.17	2.56 ± 0.08**	2.94 ± 0.16	0.064
D28-D35				
ADG, g/d	9.55 ± 0.61	12.92 ± 0.41***	9.62 ± 0.47	0.001
ADFI, g/d	30.09 ± 1.21	29.44 ± 1.58	29.36 ± 1.52	0.927
FCR	3.18 ± 0.16	2.28 ± 0.10***	3.08 ± 0.20	0.003

at 889 cm-1 was associated with C-H variable angle vibration of β-terminus differential isomerization of the pyran ring. The absorption peak detected at 767 cm-1 was associated with the symmetric ring stretching vibration of the pyran ring. Based on the above findings, MLP shows typical adsorption of characteristic polysaccharides.

3.2 Effect of MLP on growth performance and the immune organ index in chicks

According to our average daily gain (ADG), average daily feed intake (ADFI), and feed conversion ratio (FCR) results, MLE did not significantly differ in ADG, ADFI, and FCR at all three stages ($p > 0.05$). However, MLP apparently elevated ADG ($p < 0.05$) but significantly declined FCR ($p < 0.05$) of chickens during D7-D21, and MLP highly significantly decreased FCR in chickens during D21-D28 ($p < 0.01$), while during D28-D35, ADG was highly significantly increased ($p < 0.001$), but FCR was extremely markedly reduced ($p < 0.001$) of MLP-treated group relative to NC. In addition, we examined the changes in chick growth performance before and after CTX injection during D28-D35. According to these findings, CTX administration markedly decreased ADG and elevated FCR ($p < 0.001$) in chicks, and the application of MLP significantly restored ADG in chicks ($p < 0.05$) but evidently decreased FCR of the MC group ($p < 0.05$; Tables 2, 3).

In addition, indexes of spleen, thymus, and BF were observed to evaluate the immune function of chicks; as a result, the MC group showed extremely significant lower immune organ indexes relative to the NC group ($p < 0.001$), suggesting the successful establishment of immunosuppression model. On day 35, the spleen index and the thymus index of MLP + CTX and MLE + CTX groups significantly increased relative to the MC group ($p < 0.01$), while the bursa index was not significantly different, but there was an increasing trend. Meanwhile, the spleen index, the thymus index, and the bursa index of the MLP group significantly increased relative to the NC group ($p < 0.05$). The MLE group was not significantly different from the NC group, with the exception of the thymus index that markedly elevated ($p < 0.05$; Figure 3).

TABLE 3 Effect of MLP on the growth performance of immunosuppressed chicks.

D28-D35	NC	MC	MLP + CTX	MLE + CTX	*p*-value
ADG, g/d	9.55 ± 0.61	5.66 ± 0.42***	7.68 ± 1.11$^{\#}$	7.66 ± 0.59$^{\#}$	0.015
ADFI, g/d	30.09 ± 1.21	26.77 ± 1.29	27.72 ± 1.52	29.98 ± 0.56	0.168
FCR	3.18 ± 0.16	4.79 ± 0.32***	3.87 ± 0.45$^{\#}$	3.99 ± 0.27	0.021

Data are expressed as mean ± SD. *$p < 0.05$, **$p < 0.01$, ***$p < 0.001$ compared with the NC group. $^{\#}p < 0.05$, compared with MC.

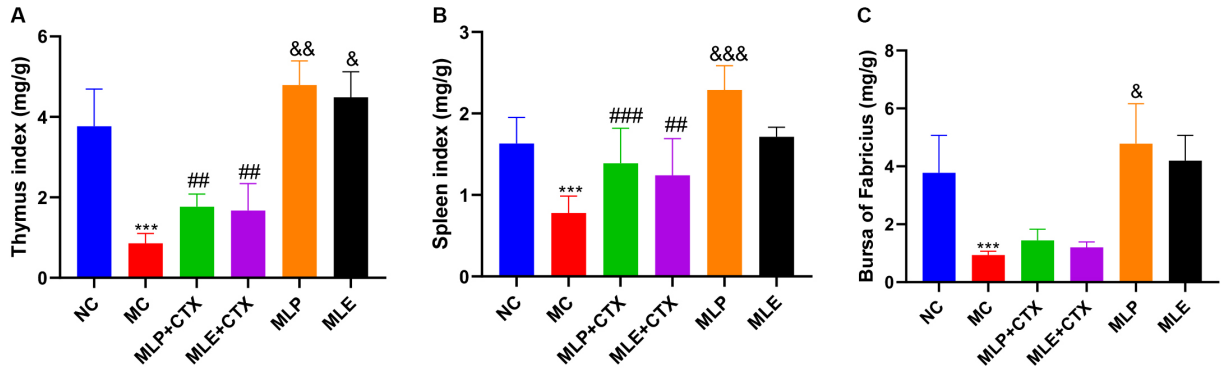

FIGURE 3
Effect of MLP on immune organ indices in chicks. **(A)** Thymus index, **(B)** Spleen index, **(C)** Bursa index. Compared with the NC group, *$p < 0.05$, **$p < 0.01$, ***$p < 0.001$; compared with the MC group, $^{\#}p < 0.05$, $^{\#\#}p < 0.01$, $^{\#\#\#}p < 0.001$; compared with the NC group, $^{\&}p < 0.05$, $^{\&\&}p < 0.01$, $^{\&\&\&}p < 0.001$.

3.3 Function of MLP in serum cytokines and immunoglobulins in chicks

According to our results regarding the function of MLP in cytokines and immunoglobulins of chick serum, serum IL-1β, IL-6, IL-10, IFN-γ, TNF-α, and IgG levels in the MC group showed extremely significant decreased levels relative to the NC group ($p < 0.01$ or $p < 0.001$), and the above results proved that CTX could inhibit the immune activity of chickens. Meanwhile, relative to the MC group, serum cytokines and IgG levels of MLP + CTX group significantly increased ($p < 0.05$ or $p < 0.01$), but the difference was not significant compared with the MLE + CTX group except for levels of IgG ($p < 0.05$). Surprisingly, the MLP group was significantly different from the NC group, with the MLP group had markedly lower IL-1β, IL-6, and TNF-α levels in serum ($p < 0.05$), but evidently higher IL-10, IFN-γ, and IgG levels ($p < 0.05$), while the MLE group, except for the significant elevation of IgG ($p < 0.05$), there was no significant difference in other indicators compared to the NC group (Figure 4).

3.4 Effect of MLP on serum antioxidant enzyme activity in chicks

The results of antioxidant enzyme activities in chick serum showed that the MC group exhibited remarkably decreased SOD, CAT, GPx, and T-AOC serum levels relative to the NC group ($p < 0.01$ or $p < 0.001$), while MDA levels were extremely markedly upregulated relative to the NC group ($p < 0.001$), which proved that CTX could also cause oxidative stress in chicks. Meanwhile, relative to the MC group, antioxidant enzymes highly significantly increased ($p < 0.05$ or $p < 0.01$), while MDA content extremely markedly declined ($p < 0.01$) in the MLP + CTX group, while the MLE + CTX group was not significantly different except for CAT, GPx, and T-AOC contents, which remarkably elevated ($p < 0.05$). The MLP and MLE groups were not significantly different from the NC group. It is thus clear that both MLP and MLE prevent oxidative stress resulting from CTX in the body (Figure 5).

3.5 Effect of MLP on the pathological damage of chick jejunum

Based on the HE staining results, the NC group showed complete and orderly intestinal morphology, complete intestinal villi, complete and fine structure, and shallow crypts. The jejunum morphology in chicks of the MC group was severely impaired, with destructed, short and rough intestinal villi, and deeper recess. After MLP treatment, the intestinal status returned to similar to that of the NC group (Figure 6). By measuring the villus height, crypt depth and intestinal wall thickness of the chicks' jejunum (Figure 7), we can obtain the following conclusions, villi height, villi crypt ratio and intestinal wall thickness of MC group extremely markedly decreased in comparison with NC group ($p < 0.001$) and crypt depth was highly significant higher than NC group ($p < 0.001$), after MLP and MLE administration, villi height, villi crypt ratio and intestinal wall thickness extremely remarkably increased ($p < 0.001$), while crypt depth remarkably decreased ($p < 0.001$) in both MLP and MLE treatment.

3.6 Function of MLP in jejunum-associated genes levels within immunosuppressed chicks

As exhibited by jejunal Occludin, ZO-1, MUC2, TLR4, MyD88, NF-κB, IL-10, and IFN-γ gene levels, the MC group

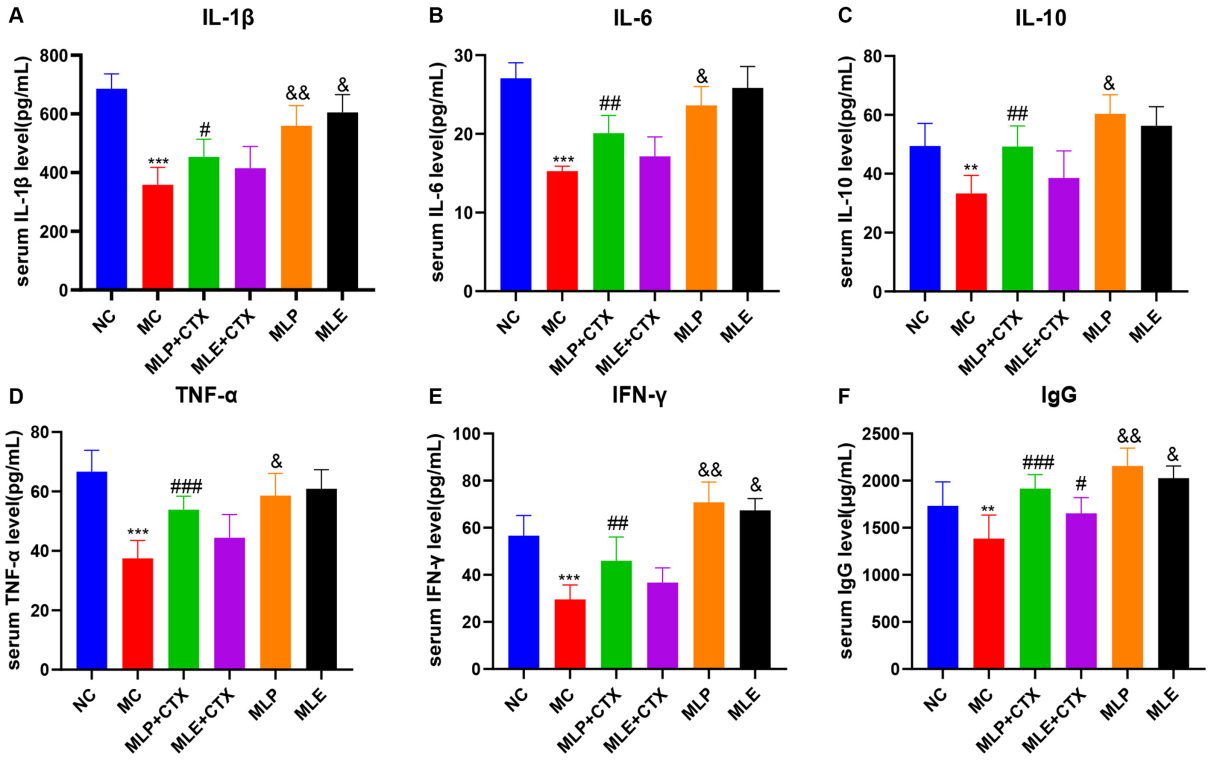

FIGURE 4
Effect of MLP on cytokines and immunoglobulins in the serum of chicks. **(A)** Serum levels of IL-1β, **(B)** serum levels of IL-6, **(C)** serum levels of IL-10, **(D)** serum levels of TNF-α, **(E)** serum levels of IFN-γ, and **(F)** serum levels of IgG. Compared with the NC group, $^{*}p < 0.05$, $^{**}p < 0.01$, $^{***}p < 0.001$; Compared with the MC group, $^{\#}p < 0.05$, $^{\#\#}p < 0.01$, $^{\#\#\#}p < 0.001$; compared with the NC group, $^{\&}p < 0.05$, $^{\&\&}p < 0.01$, $^{\&\&\&}p < 0.001$.

showed significantly decreased expression of Occludin, ZO-1, and MUC2 relative to the NC group ($p < 0.001$, $p < 0.001$, $p < 0.01$), while the expressions in both the MLP + CTX and MLE + CTX groups significantly increased relative to the MC group ($p < 0.001$); meanwhile, the expression of Occludin, ZO-1, and MUC2 of the MLP group significantly increased relative to the NC group ($p < 0.001$), while only ZO-1 and MUC2 levels of the MLE group significantly increased compared with the NC group ($p < 0.001$; Figure 8).

As for mRNA levels, TLR4 and NF-κB levels of the MC group were both extremely remarkably downregulated in comparison with the NC group ($p < 0.01$), MyD88 expression was second ($p > 0.05$), and the difference was not significant, while TLR4, MyD88, and NF-κB of MLP + CTX group were all significantly increased in comparison with the MC group ($p < 0.001$, $p < 0.01$, $p < 0.001$), TLR4 and NF-κB of the MLE + CTX group were significantly upregulated ($p < 0.001$), while MyD88 expression was not significantly different in the MLE + CTX group ($p > 0.05$).

IL-10 and IFN-γ gene expression results in jejunum showed that IL-10 and IFN-γ levels of the MC group were highly significantly lower than NC group ($p < 0.001$), and IL-10 and IFN-γ levels of the MLP + CTX group were significantly higher than MC group ($p < 0.001$) and nearly returned to the level in NC group, meanwhile, the expressions of IL-10 and IFN-γ in MLE+CTX group were significantly higher than those in MC group ($p < 0.01$). This conforms to serum measurements.

3.7 Function of MLP in the intestinal flora within immunosuppressed chicks

Cecal feces in D35 chicks were collected to conduct high-throughput 16S rDNA gene sequencing analysis. First, rarefaction curve analysis revealed the reasonability and reliability of sample number and sequencing depth (Supplementary Figure S1). Alpha-diversities were analyzed to determine microbial community abundance and diversity. The results below were summarized by various indexes for statistical analyses, including the sobs, chao, Shannon, ace, and simpson. Of them, the sobs, chao and ace indexes reflected community richness; as a result, CTX decreased microbial richness within cecal samples in chicks, while MLP and MLE alleviated the decrease in richness caused by CTX ($p > 0.05$), implying that MLP and MLE elevated intestinal microbial number; second, the shannon and simpson indices indicated microbial community diversity, and our results showed that MLP and MLE also elevated microbial community diversity after treatment (Table 4).

Additionally, beta-diversities were analyzed to examine similarities and differences among sample communities. There is a more obvious separation in the NC group compared with the MC group, indicating a large difference between them; also observing the relationship between the MLP and MLE groups and the NC group, it can be found that the MLP group is closer to the NC group relative to the MLE group (Figure 9).

The composition of the intestinal flora of the chicks was analyzed in terms of phylum. As a result, Firmicutes and Bacteroidetes are the

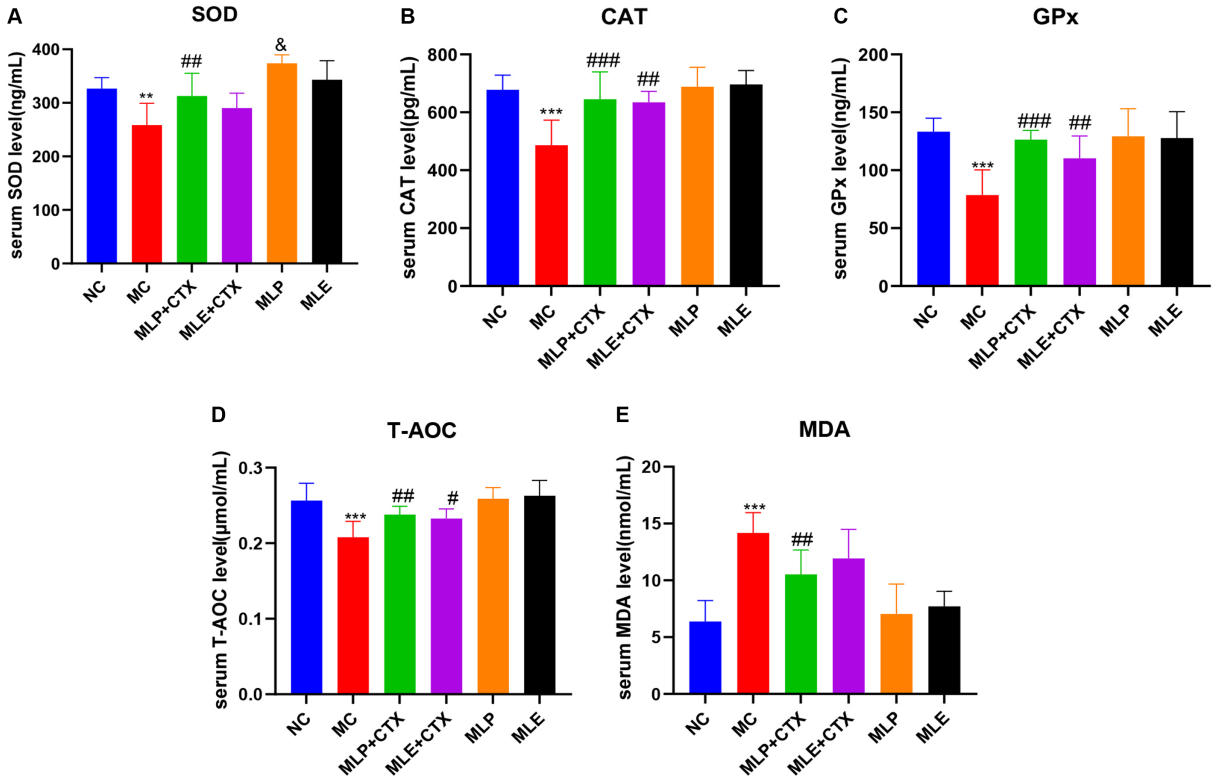

FIGURE 5
Effect of MLP on antioxidant enzymes in the serum of chicks. **(A)** Serum levels of SOD, **(B)** serum levels of CAT, **(C)** serum levels of GPx, **(D)** serum levels of T-AOC, and **(E)** serum levels of MDA. Compared with the NC group, $^{*}p < 0.05$, $^{**}p < 0.01$, $^{***}p < 0.001$; compared with the MC group, $^{\#}p < 0.05$, $^{\#\#}p < 0.01$, $^{\#\#\#}p < 0.001$; compared with the NC group, $^{\delta}p < 0.05$, $^{\delta\delta}p < 0.01$, $^{\delta\delta\delta}p < 0.001$.

two most dominant phyla in microflora. Relative to the MC group, the MLP and MLE groups tended more toward the NC group, with some recovery of several phylum levels. Further analysis revealed that both the MLP and MLE groups increased the proportion of Firmicutes, Verrucomicrobiota, and Actinobacteriota ($p > 0.05$) and reduced that of Bacteroidota and Proteobacteria ($p > 0.05$) in comparison with the MC group (Figure 10E).

Chick intestinal flora were compared at a genus level; as a result, after CTX treatment, chick intestinal flora of Akkermansia, unclassified_f_Peptostreptococcaceae, Anaerofustis, uncultured_f_Peptococcaceae, Family_XIII_UCG-001, norank_f_Erysipelotrichaceae, Eubacterium_nodatum_group, and Lachnospiraceae_FCS020_group, eight bacterial genera, markedly decreased ($p < 0.05$), while Staphylococcus bacterial counts markedly increased ($p < 0.05$). Compared with the MC group: after MLP treatment, the intestinal proportions of *Anaerotruncus*, Ruminococcus_gauvreauii_group and Paludicola significantly elevated in the MLP group ($p < 0.05$); following MLE treatment, Subdoligranulum, DTU089, Paludicola, Lachnospiraceae_FCS020_group, and Lachnospiraceae_UCG-010 were significantly higher ($p < 0.05$), and Limosilactobacillus, Romboutsia, Turicibacter, and Hydrogenoanaerobacterium, Marvinbryantia, and unclassified_c_Bacilli were significantly lower ($p < 0.05$). In conclusion, mulberry leaf polysaccharides and aqueous extracts can improve the intestinal flora disorder caused by CTX to some extent (Figures 10A–D).

As shown in Figure 11, in the NC group c_Verrucomicrobiae, g_Akkermansia, f_Akkermansiaceae, p_Verrucomicrobiota, o_Verrucomicrobiales, and Peptostreptococcales-Tissierellales have increased LDA scores, indicating their higher OUT of the NC group; for the MC group, the high LDA scores are for g_Marvinbryantia, g_Hydrogenoanaerobacterium, and f_norank_o_Oscillospirales These three species indicate that these three species are more susceptible to CTX stimulation; in terms of feeding MLP, g_Anaerotruncus has the highest score; in terms of feeding MLE, c_Clostridia, p_Firmicutes, f_Ruminococcaceae, g_Subdoligranulum, g_Lachnospiraceae_UCG-010, g_DTU089, and g_Paludicola, seven species had higher scores. It indicates that MLP can mitigate CTX-mediated immunosuppression through elevating the intestinal abundance of *Anaerotruncus*.

4 Discussion

Modern industrial poultry farming is very large, so the growth performance of poultry is the fundamental guarantee of the benefits generated by the farming industry. It has been shown that a variety of polysaccharides have the function of enhancing the growth performance of poultry; for example, adding LBP to the diet can enhance growth performance, digestive enzyme activity, and immunity of broilers (Long et al., 2020). In addition, we are examining the effect of both MLP and MLE as a whole for feed additives on chicks and therefore take a common dose of 0.25%. Moreover, the selection of the 0.25% addition amount is determined by the results of the previous preliminary experiment, and the methods and results of the preliminary experiment have been supplemented in the Supplementary material. In this experiment, we first verified whether

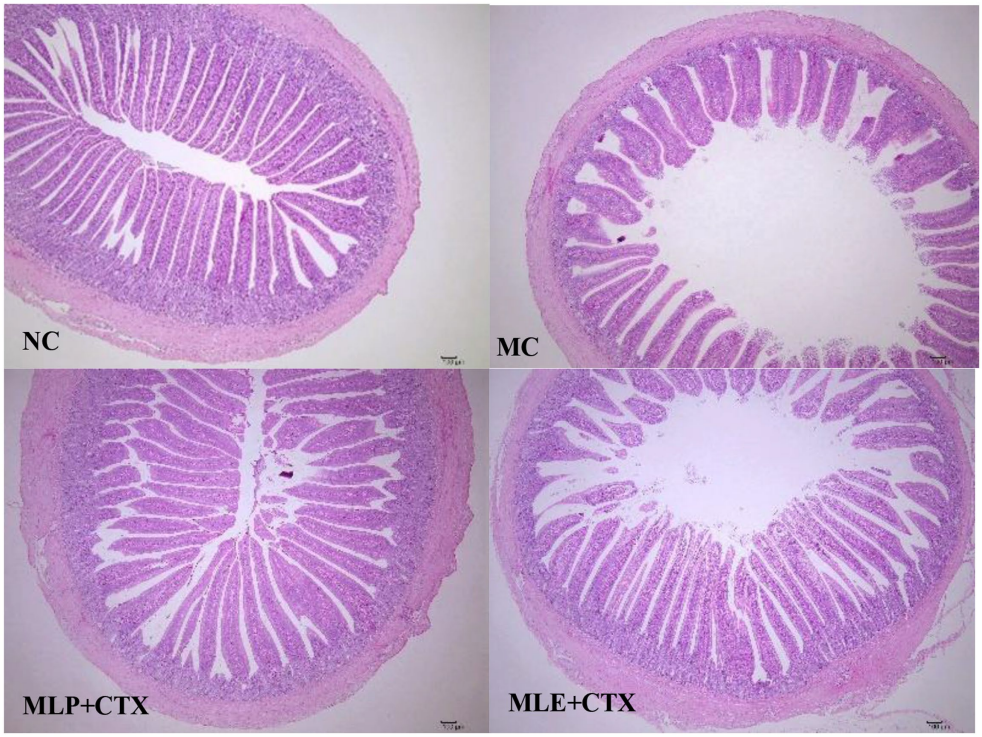

FIGURE 6
Effect of MLP on the histological structure of the jejunum of the chick.

MLP can promote growth performance in chickens. According to the results, adding 0.25% MLP to the diet could significantly improve the ADF of chicks in all periods, but it did not significantly affect AFD in chickens. In terms of feed conversion ratio, MLP could significantly reduce the feed-to-meat ratio of chicks in all periods. CTX injections in chicks resulted in lower average daily weight gain (Cui et al., 2022) and growth performance (Liu et al., 2021). Dietary patterns not only affect weight, but also bone density (Chen et al., 2015). In the present study, growth performance in chicks of the MC group decreased dramatically compared with the NC group, mainly in terms of ADG and ADFI, while the addition of 0.25% MLP in the feed significantly increased the ADG and decreased the FCR of chicks, which shows that MLP promotes growth in chicks in the immunosuppressed state of chicks.

Immune activity is often considered one of the most important defenses against bacterial–viral infections, cancer invasion, or inflammation (Zhu et al., 2016; Li et al., 2019; Qu et al., 2022). The central immune organs include the bursa and thymus, which have a decisive and dominant effect on peripheral lymphoid organ development (Shirani et al., 2015). In some studies, certain natural plant-derived polysaccharide components have the ability to enhance the immune organ index in chickens (Fan et al., 2013; Cui et al., 2022). We found experimentally that CTX extremely markedly reduced the immune organ index in chickens, indicating that the model we established was successful. Meanwhile, the immune organ damage was alleviated by adding MLP and MLE to the feed, but MLE was not as effective as MLP, indicating that MLP promotes immune function in chickens through stimulation of their immune organs.

Cytokines are highly active multi-kinetic protein-peptide molecules produced via immune cells and other related cells, which mainly mediate and regulate the immune response and inflammatory reaction and are involved in tissue repair, among others (Schoenaker et al., 2018). According to the previous articles, some plant-derived polysaccharides mitigate CTX-mediated immunosuppression through immune cell activation, thus promoting cytokine secretion (Zhou et al., 2018; Yang et al., 2021; Zhou et al., 2022). In this study, MLP modulates immunosuppression of chicks through elevating these six cytokine levels, conforming to prior results. Additionally, we examined cytokine secretion in the group without CTX injection, and interestingly, MLP reduced IL-1β, IL-6, and TNF-α secretion compared with the NC group, but those in the MC group significantly increased; it elevated IL-10, IFN-γ, and IgG secretion. The possible reason is that MLP can also regulate the secretion of serum cytokines in chicks to enhance the immunity and anti-inflammatory ability of the organism in the absence of immunosuppression (Zhang et al., 2018). Combining these findings, MLP can enhance cytokine production to alleviate immunosuppression caused by CTX to regulate the systemic immune response.

CTX is capable of causing oxidative stress in the body, after oxidative stress, the antioxidant defense system of the body is disrupted (Has et al., 2019; Zhu et al., 2022). Exogenous dietary additives and ingredients may affect growth performance and antioxidation in animals (Ma et al., 2021; Chen JY et al., 2022; Chen FM et al., 2022). It has been demonstrated that Amaranthus polysaccharides can alleviate CTX-induced oxidative stress in mice (Niu et al., 2020) and enhance the antioxidant enzyme activities of mice in an immunosuppressed state. It has been demonstrated that Mulberry leaf polysaccharides have

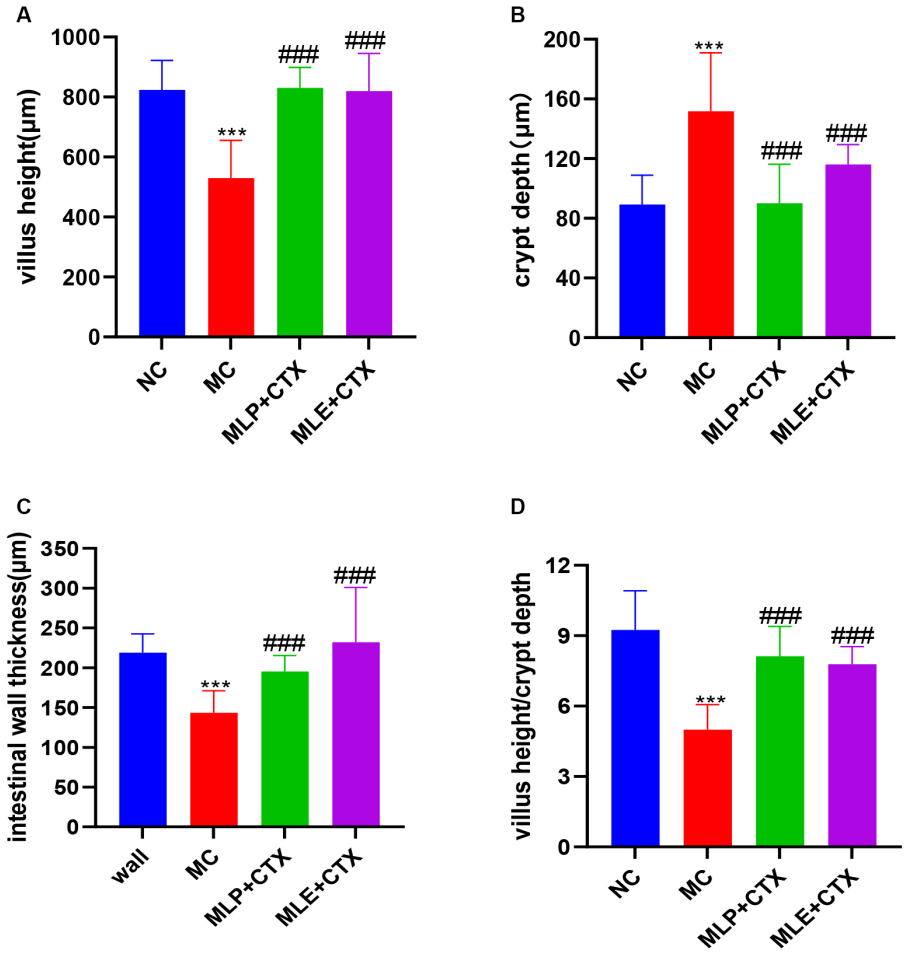

FIGURE 7
Effect of MLP on the intestinal morphology of chicks. **(A)** Villus height, **(B)** crypt depth, **(C)** intestinal wall thickness, and **(D)** villus height/crypt depth. Compared with the NC group, $^{*}p < 0.05$, $^{**}p < 0.01$, $^{***}p < 0.001$; compared with the MC group, $^{\#}p < 0.05$, $^{\#\#}p < 0.01$, $^{\#\#\#}p < 0.001$.

strong *in vitro* antioxidant effects (Yuan et al., 2015; Zhang et al., 2016), so this study analyzed how MLP affected CTX-mediated oxidative stress; as a result, antioxidant enzyme activities in serum were remarkably decreased, while MDA content evidently increased in the MC group, while antioxidant enzyme levels within the serum were higher and MDA level was significantly lower after our MLP treatment, our findings are consistent with previous studies showing that polysaccharides boost antioxidant capacity.

The intestinal mucosal barrier generally refers to the normal intestine having and perfect functional isolation zone that separates the interior of the intestine from the internal environment of the organism, preventing the invasion of pathogenic bacteria, toxic or carcinogenic substances, keeping the internal environment of the organism stable (Bai et al., 2020; Sha et al., 2021) and enabling the maintenance of the collective normal life activities. Dietary nutrients can affect animal small intestine morphology (Chen et al., 2019). An imbalance of gut microbiota–other factor interaction may break the intestinal mucosal homeostasis (Luo et al., 2022). The intestinal epithelial barrier is the first-line defense between the lumen and the host, and if damaged, it may lead to intestinal disorders like inflammation (Wu et al., 2020). According to our results, the intestinal mucosal integrity of chicks was disrupted after CTX injection and the long villi became disorganized and flaccid. After MLP intervention, the morphology of the intestine was changed and the pathological damage was attenuated, indicating that MLP could improve CTX-induced intestinal damage. The intestinal villi and crypt account for critical indexes for describing intestinal function and morphology. This shows that both MLP and MLE significantly affect CTX-mediated intestinal injury, and both can protect intestinal mucosal function by regulating jejunal injury and restoring intestinal absorption and digestive abilities, conforming to previous findings by Cui et al. (2022) and Zhou et al. (2021).

Intestinal tight junction proteins are crucial for keeping intestinal integrity and permeability, with the main function of closing the epithelial cell gap (Schoultz and Keita, 2019). MUC2 represents the intestinal-type mucin produced via cupped cells that forms intestinal mucus while resisting bacterial destruction (Cai et al., 2021). Additionally, defective epithelial MyD88 signaling targeting has been reported to lead to increased mucus-related bacterial number and decreased MUC2 levels (Frantz et al., 2012). Polysaccharides are found to restore CTX into intestinal mucosal injury through regulating intestinal tight junction proteins, for example, Ganoderma lucidum polysaccharides (Ying et al., 2020), *Cordyceps polysaccharides* (Ying et al., 2020), and Oxaliplatin polysaccharides (Chen et al., 2021)

10.3389/fmicb.2024.1382639

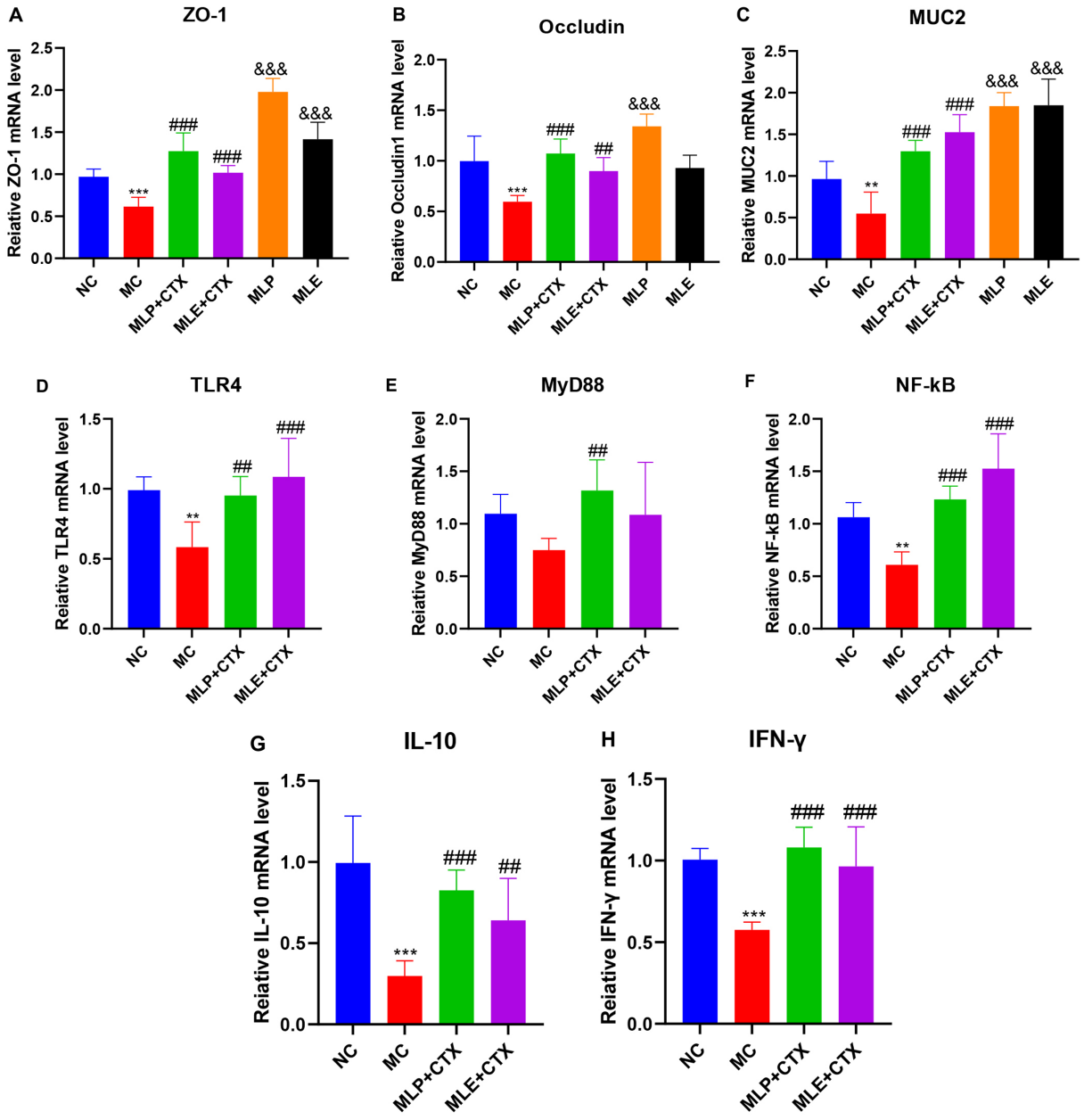

FIGURE 8
Effect of MLP on the expression of jejunum-related genes. **(A)** Expression of ZO-1, **(B)** expression of Occludin, **(C)** expression of MUC2, **(D)** expression of TLR4, **(E)** expression of MyD88, **(F)** expression of NF-κB, **(G)** expression of IL-10, and **(H)** expression of IFN-γ. Compared with the NC group, $^{*}p < 0.05$, $^{**}p < 0.01$, $^{***}p < 0.001$; compared with the MC group, $^{\#}p < 0.05$, $^{\#\#}p < 0.01$, $^{\#\#\#}p < 0.001$.

TABLE 4 α-Diversity indices of gut microbiota in each group.

Groups	NC	MC	MLP + CTX	MLE + CTX	*p*-value
sobs	456.8 ± 57.89	401.7 ± 149.1	413.7 ± 82.42	427.2 ± 54.99	0.8479
chao	513.9 ± 50.31	472.3 ± 172.3	471.8 ± 98.03	492.3 ± 55.58	0.7867
shannon	3.613 ± 0.4203	3.326 ± 0.882	3.691 ± 0.278	3.699 ± 0.2938	0.9204
ace	528.2 ± 53.12	464.5 ± 177.3	472 ± 100.2	498.4 ± 54.88	0.6823
simpson	0.0827 ± 0.037	0.1215 ± 0.1093	0.0652 ± 0.013	0.0644 ± 0.022	0.6106

Data are expressed as mean ± SD. $^{*}p < 0.05$, $^{**}p < 0.01$, $^{***}p < 0.001$ compared with the NC group. $^{\#}p < 0.05$, compared with MC.

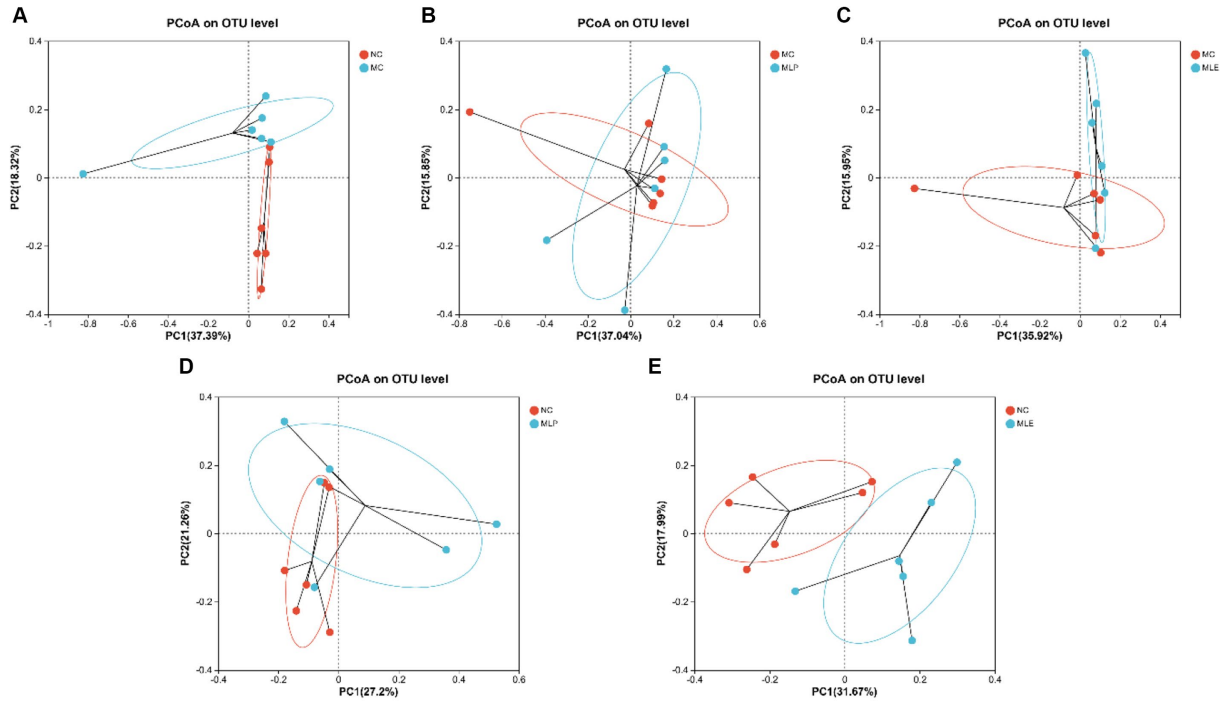

FIGURE 9
PCoA of intestinal microorganisms in chicks **(A)** NCvsMC, **(B)** MCvsMLP, **(C)** MCvsMLE, **(D)** NCvsMLP, and **(E)** NCvsMLE.

reversed intestinal damage by upregulating intestinal tight junction proteins. In the present study, we showed that both MLP and MLE treatment could upregulate MUC2, Occludin, and ZO-1 proteins within the jejunum in chickens after CTX injection, indicating that MLP and MLE can be important for CTX-mediated intestinal mucosal injury. Interestingly, MLP and MLE also remarkably upregulated MUC2, Occludin, and ZO-1 in the group without CTX injection, Occludin, and ZO-1 expression, revealing that MLP and MLE can increase intestinal permeability and digestive absorption through upregulation of MUC2, Occludin and ZO-1 expression, which is related to relationship with growth performance that we previously examined. In addition, we examined IL-10 and IFN-γ levels within chicken jejunum, and our results were consistent with those of our previously examined serum, suggesting that MLP also promotes immune cytokine generation via the intestinal immune system through upregulating IL-10 and IFN-γ expression. Therefore, these cytokines can migrate to the spleen and peripheral lymph nodes, thereby triggering systemic immunity.

The Toll-like receptor (TLR) family has received wide attention as the possible regulatory factors and controllers for immunity by recognizing pathogen-associated molecular patterns (Zuany-Amorim et al., 2002). TLRs are crucial for immune cell regulation, proliferation, and survival, which exert a critical effect on intestinal immunity (Dong et al., 2019). TLRs and glycosyl ligands can bind to and signal MyD88, thereby activating the NF-B pathway while inducing cytokine production, finally stimulating immunity (Zhu et al., 2013; Zhou et al., 2020). It has been demonstrated that the ability of polysaccharides to modulate immunity is linked to TLR4-mediated signaling pathways and that Caulis Spatholobi polysaccharide promotes the increased TLR4, MyD88, and NF-κB levels, key immune signals in the intestine, restoring immune performance (Cui et al., 2022), and it has also been shown that Millettia Speciosa Champ polysaccharide modulate immune performance in mice through TLR4-induced MyD88 pathway activation (Chen et al., 2021). In this study, CTX caused decreased TLR4, MyD88, and NF-κB levels after CTX injection, and we observed that MLP could significantly upregulate TLR4, MyD88, and NF-κB of the MC group. In conclusion: MLP can upregulate intestinal tight junction protein, upregulate TLR4, MyD88, and NF-κB gene expression, and regulate intestinal immunity, thereby protecting the intestinal mucosal barrier while promoting growth.

With the continuous advancement of sequencing technology, we have the opportunity to conduct in-depth research on how dietary alterations affect animal intestinal microbiomes (He et al., 2020; Wang et al., 2022; Chen et al., 2023; Liu et al., 2023). The intestinal microbial milieu has a critical effect on the organism, mainly on inhibiting pathogenic microbial colonization, keeping intestinal epithelial integrity, regulating host organism immunity, and modulating innate immunity. It has been shown that natural plant-derived polysaccharide active ingredients promote immunity through the continuous stimulation of host immunity, thus stimulating changes in the flora to activate the immune response (Zhou et al., 2021); for example, Cordyceps polysaccharides elevate probiotic bacterial abundances in the intestine and decrease pathogenic bacterial production, thus alleviating the side effects associated with CTX (Frantz et al., 2012). First, higher bacterial diversity in the gut usually implies a more stable microbial community in the 'gut of the organism, with a richer microbial community, thus maintaining the health status of the animal organism by suppressing pathogen colonization and maintaining immune homeostasis (Elson and Cong, 2012). In the present study, microbial abundance and

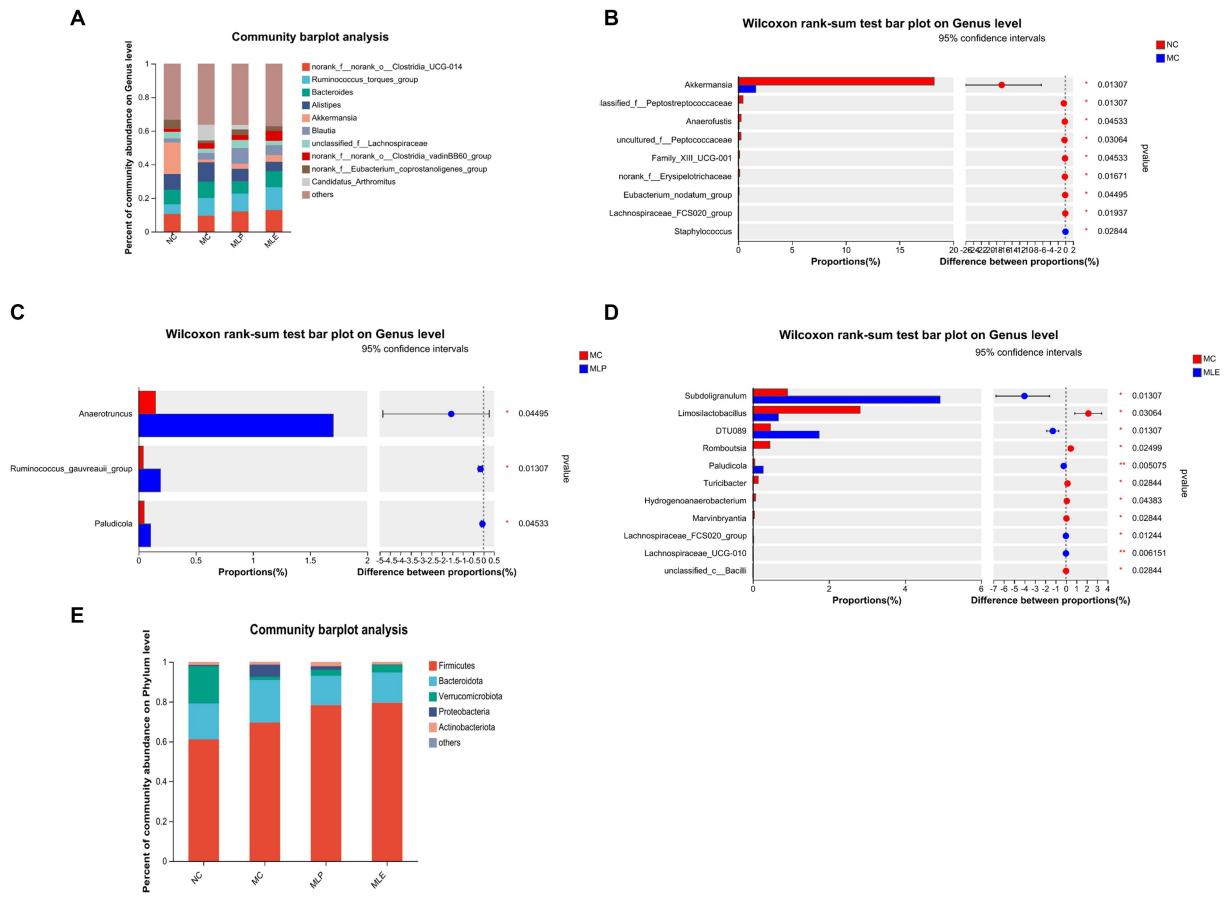

FIGURE 10
Composition of the intestinal flora of chicks at the genus level and their significantly different species at the genus level. **(A)** Composition of gut microbial genus levels in chicks, **(B)** NC versus MC, **(C)** MC versus MLP, and **(D)** MC versus MLE. The right of the bar is the *p*-value; $*p < 0.05$, $**p < 0.01$. **(E)** Composition of each group at the Phylum level.

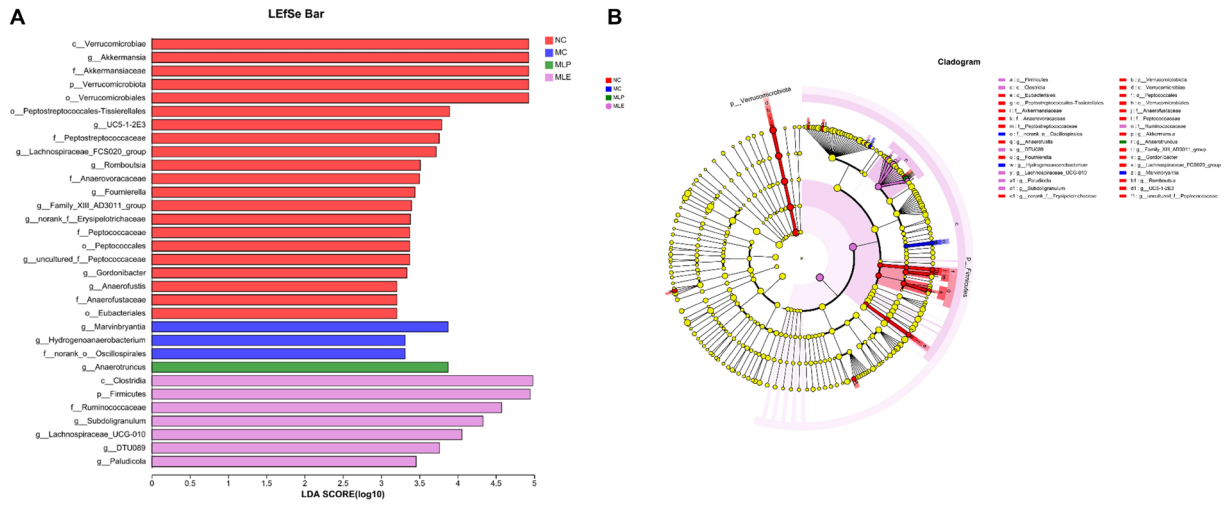

FIGURE 11
Difference in dominant microorganisms among each group via cladogram and distribution histogram based on LDA. **(A)** Histogram of LDA distribution based on LEfSe analysis of classification information and **(B)** evolutionary branching diagram of LEfSe analysis based on classification information.

diversity in the cecum of chicks were reduced after CTX injection, which is consistent with previous studies (Zheng et al., 2022), and were alleviated after MLP and MLE feeding interventions, indicating that dietary MLP and MLE efficiently avoid the reduced bacterial abundance and diversity resulting from CTX. The β-diversity analysis showed that CTX injection significantly altered the microbial community structure, while the dietary MLP resulted in a more convergent microbial community structure toward the NC group, suggesting that MLP can regulate the gut microbial community toward normal levels. To verify this hypothesis, we also examined the alterations of gut microbial composition and specific taxa.

Changing dietary formulas may cause changes in animal gut microbial composition and affect digestion activity (Ji et al., 2019; Wang et al., 2022). We analyzed the MLP and MLE to comparatively analyze intestinal flora at diverse taxonomic levels (phylum and genus levels). At the phylum level, Firmicutes and Bacteroidetes represent phyla with the highest abundances, which use polysaccharides to produce carbohydrate-active enzymes. According to this study, Bacteroidota had an elevated relative abundance of the MC group relative to the NC group, which indicates that Bacteroidetes may use CTX to produce immunosuppression in chicks (Nawaz et al., 2018). In contrast, after feeding MLP and MLE, the Firmicutes, Verrucomicrobiota, and Actinobacteriota percentages increased, whereas Bacteroidota and Proteobacteria percentage decreased in comparison with the MC group, and it has been shown that Firmicutes enhances protein digestion and absorption of animal organism (Janczyk et al., 2009) and can break down the polysaccharide components of plant species, while Verrucomicrobiota can effectively enhance the intestinal immunity in animal organisms (Kong et al., 2020). MLP and MLE enhance the immunity of the intestine of an organism mainly by increasing intestinal Firmicutes and Verrucomicrobiota percentages.

We also analyzed differences in intestinal flora at a genus levela. First, after CTX treatment, altogether eight bacterial genera significantly decreased and one bacterial genus significantly increased, and Staphylococcus apparently elevated of the MC group, suggesting that after CTX administration to the chicks, the immunity of the chicks is reduced, allowing a large invasion of Staphylococcus, which can cause the organism to trigger and promote an inflammatory response. The major bacterial genus Akkermansia was significantly reduced, Akkermansia is a beneficial intestinal bacterium that effectively reduces the level of inflammation in the intestine and gradually decreases with the progression of enteritis (Pope et al., 2012). After MLP feeding, *Anaerotruncus* spp. increased significantly, and it has been shown that *Anaerotruncus* promotes the production of butyric acid (Derrien et al., 2011); butyric acid mainly functions in maintaining intestinal cell stability and protecting them from external pathogens; therefore, the increased abundance of *Anaerotruncus* causes the organism to produce more butyric acid to protect the intestinal cells. This was followed by a significant rise in the genus Ruminococcus_gauvreauii_group. It has been demonstrated that Ruminococcus has highly complex and specific enzymes that have the ability to digest a variety of enzymes, such as cellulase and amylase, and MLP increased the abundance of Ruminococcus, suggesting that MLP enhances digestive enzyme activities through elevating Ruminococcus abundance, which may be associated with capacity of MLP of increasing chick growth performance. First, the MLE group compared with the MC group Subdoligranulum Paludicola was significantly enriched and it has been shown that this species of bacteria produces butyrate, which can help reduce the risk of colon cancer in the organism through promoting intestinal barrier and organism immunity (Zhao et al., 2021). Two genera Lachnospiraceae_FCS020_group, Lachnospiraceae_UCG-010 belong to the genus Trichoderma, represent possible beneficial bacteria related to the metabolism of various carbohydrates, and fermentation can promote acetic acid and butyric acid generation, which provides a major energy source of the host (Suen et al., 2011). Secondly, compared with the MC group, the abundance of six bacteria in the MLE group significantly decreased, while the abundance of the pathogenic bacterium Romboutsia significantly decreased after feeding with MLE, which is consistent with previous research results (Le Roy et al., 2022). In conclusion, MLP and MLE can modulate chick intestinal flora by regulating certain probiotic bacterial enrichment and reducing certain harmful bacterial levels, thus regulating immunity.

5 Conclusion

In conclusion, MLP can restore the growth performance of chicks, protect immune organs, promote production of serum cytokines and immunoglobulins, and modulate humoral immunity of the body. MLP contributes to enhancing the antioxidant capacity of chicks, repairing injured intestinal mucosa, enhancing tight junction protein levels, activating intestinal immune-related pathways, and regulating intestinal immunity. In addition, MLP can increase the diversity of microbial communities while regulating microbial community structure.

Data availability statement

The original contributions presented in the study are included in the article/Supplementary material, further inquiries can be directed to the corresponding authors.

Ethics statement

The animal study was approved by Committee on Ethics of Animal Experiments of Guangxi University. The study was conducted in accordance with the local legislation and institutional requirements.

Author contributions

MC: Formal analysis, Investigation, Methodology, Software, Validation, Visualization, Writing – original draft. YS: Investigation, Validation, Writing – review & editing. YC: Investigation, Writing – review & editing. HH: Software, Supervision, Writing – review & editing. SL: Investigation, Writing – review & editing. YX: Investigation, Writing – review & editing. LH: Investigation, Writing – review & editing. SH: Investigation, Writing – review & editing. YL: Investigation, Writing – review & editing. FC: Investigation, Writing – review & editing. JL: Supervision, Writing – review & editing. HS: Conceptualization, Funding acquisition, Methodology, Project administration, Resources, Writing – review & editing, Formal analysis.

Funding

The author(s) declare that financial support was received for the research, authorship, and/or publication of this article. The present study was supported by Funds of the National Natural Science Foundation of China (U22A20523); Central Guided Local Science and Technological Development Foundation of China (GuiKeJi 202355); the Guangxi University Innovation and Entrepreneurship Training Program Project (S202210593208); the Bama County Talent and Technology Program (20220017); the Science and Technology Plan Project of Guangxi University Fuxile Branch (20210008); and the Science and Technology Plan Project of Guangxi University Fuxile Branch (20210003).

Acknowledgments

We thank the members of the Chinese Veterinarian Laboratory of Guangxi University for their support of the experimental work. We also thank Nanjing Boyan Biotech Co. for testing the experimental data.

Conflict of interest

The authors declare that the research was conducted in the absence of any commercial or financial relationships that could be construed as a potential conflict of interest.

Publisher's note

All claims expressed in this article are solely those of the authors and do not necessarily represent those of their affiliated organizations, or those of the publisher, the editors and the reviewers. Any product that may be evaluated in this article, or claim that may be made by its manufacturer, is not guaranteed or endorsed by the publisher.

Supplementary material

The Supplementary material for this article can be found online at: https://www.frontiersin.org/articles/10.3389/fmicb.2024.1382639/full#supplementary-material

References

Ahlmann, M., and Hempel, G. (2016). The effect of cyclophosphamide on the immune system: implications for clinical cancer therapy. *Cancer Chemother. Pharmacol.* 78, 661–671. doi: 10.1007/s00280-016-3152-1

Has, A. L., Alotaibi, M. F., Bin-Jumah, M., Elgebaly, H., and Mahmoud, A. M. (2019). *Olea europaea* leaf extract up-regulates Nrf2/ARE/HO-1 signaling and attenuates cyclophosphamide-induced oxidative stress, inflammation and apoptosis in rat kidney. *Biomed. Pharmacother.* 111, 676–685. doi: 10.1016/j.biopha.2018.12.112

Bai, Y., Huang, F., Zhang, R., Dong, L., Jia, X., and Liu, L. (2020). Longan pulp polysaccharides relieve intestinal injury in vivo and in vitro by promoting tight junction expression. *Carbohydr. Polym.* 229:et al.:115475. doi: 10.1016/j.carbpol.2019.115475

Cai, G., Wu, Y., Wusiman, A., Gu, P., Mao, N., Xu, S., et al. (2021). Alhagi honey polysaccharides attenuate intestinal injury and immune suppression in cyclophosphamide-induced mice. *Food Funct.* 12, 6863–6877. doi: 10.1039/d1fo01008e

Chen, J. Y., Chen, F. M., Peng, S. M., Ou, Y. J., He, B. S., Li, Y. H., et al. (2022). Effects of Artemisia argyi powder on egg quality, antioxidant capacity, and intestinal development of Roman laying hens. *Front. Physiol.* 13:13. doi: 10.3389/fphys.2022.902568

Chen, F. M., He, J. Y., Wang, X., Lv, T., Liu, C. J., Liao, L. P., et al. (2022). Effect of dietary ramie powder at various levels on the growth performance, meat quality, serum biochemical indices and Antioxidative capacity of Yanling white geese. *Animals* 12:45. doi: 10.3390/ani12162045

Chen, X., Sun, W., Xu, B., Wu, E., Cui, Y., Hao, K., et al. (2021). Polysaccharides from the roots of Millettia speciosa champ modulate gut health and ameliorate cyclophosphamide-induced intestinal injury and immunosuppression. *Front. Immunol.* 12:766296. doi: 10.3389/fimmu.2021.766296

Chen, C., Wang, Z., Li, J., Li, Y., Huang, P., Ding, X., et al. (2019). Dietary vitamin E affects small intestinal histomorphology, digestive enzyme activity, and the expression of nutrient transporters by inhibiting proliferation of intestinal epithelial cells within jejunum in weaned piglets1. *J. Anim. Sci.* 97, 1212–1221. doi: 10.1093/jas/skz023

Chen, F., Wang, Y., Wang, K., Chen, J., Jin, K., Peng, K., et al. (2023). Effects of *Litsea cubeba* essential oil on growth performance, blood antioxidation, immune function, apparent digestibility of nutrients, and fecal microflora of pigs. *Front. Pharmacol.* 14:1166022. doi: 10.3389/fphar.2023.1166022

Chen, Y., Xiang, J., Wang, Z., Xiao, Y., Zhang, D., Chen, X., et al. (2015). Associations of bone mineral density with lean mass, fat mass, and dietary patterns in postmenopausal Chinese women: a 2-year prospective study. *PLoS One* 10:e0137097. doi: 10.1371/journal.pone.0137097

Cui, Y., Sun, W., Li, Q., Wang, K., Wang, Y., Lv, F., et al. (2022). Effects of caulis Spatholobi polysaccharide on immunity, intestinal mucosal barrier function, and intestinal microbiota in cyclophosphamide-induced immunosuppressive chickens. *Front. Vet. Sci.* 9:833842. doi: 10.3389/fvets.2022.833842

Deng, Q., Shao, Y., Wang, Q., Li, J., Li, Y., Ding, X., et al. (2021). Effects and interaction of dietary electrolyte balance and citric acid on growth performance, intestinal histomorphology, digestive enzyme activity and nutrient transporters expression of weaned piglets. *J Anim Physiol Anim Nutr (Berl)* 105, 272–285. doi: 10.1111/jpn.13491

Derrien, M., Van Baarlen, P., Hooiveld, G., Norin, E., Müller, M., and de Vos, W. M. (2011). Modulation of mucosal immune response, tolerance, and proliferation in mice colonized by the mucin-degrader *Akkermansia muciniphila*. *Front. Microbiol.* 2:166. doi: 10.3389/fmicb.2011.00166

Dong, N., Xu, X., Xue, C., Wang, C., Li, X., Shan, A., et al. (2019). Ethyl pyruvate protects against Salmonella intestinal infection in mice through down-regulation of pro-inflammatory factors and inhibition of TLR4/MAPK pathway. *Int. Immunopharmacol.* 71, 155–163. doi: 10.1016/j.intimp.2019.03.019

Duncan, M., and Grant, G. (2003). Oral and intestinal mucositis - causes and possible treatments. *Aliment. Pharmacol. Ther.* 18, 853–874. doi: 10.1046/j.1365-2036.2003.01784.x

Elson, C. O., and Cong, Y. (2012). Host-microbiota interactions in inflammatory bowel disease. *Gut Microbes* 3, 332–344. doi: 10.4161/gmic.20228

Emadi, A., Jones, R. J., and Brodsky, R. A. (2009). Cyclophosphamide and cancer: golden anniversary. *Nat. Rev. Clin. Oncol.* 6, 638–647. doi: 10.1038/nrclinonc.2009.146

Fan, Y., Lu, Y., Wang, D., Liu, J., Song, X., Zhang, W., et al. (2013). Effect of epimedium polysaccharide-propolis flavone immunopotentiator on immunosuppression induced by cyclophosphamide in chickens. *Cell. Immunol.* 281, 37–43. doi: 10.1016/j.cellimm.2013.01.008

Frantz, A. L., Rogier, E. W., Weber, C. R., Shen, L., Cohen, D. A., Fenton, L. A., et al. (2012). Targeted deletion of MyD88 in intestinal epithelial cells results in compromised antibacterial immunity associated with downregulation of polymeric immunoglobulin receptor, mucin-2, and antibacterial peptides. *Mucosal Immunol.* 5, 501–512. doi: 10.1038/mi.2012.23

Fussell, L. W. (1998). Poultry industry strategies for control of immunosuppressive diseases. *Poult. Sci.* 77, 1193–1196. doi: 10.1093/ps/77.8.1193

He, B., Zhu, R., Yang, H., Lu, Q., Wang, W., Song, L., et al. (2020). Assessing the impact of data preprocessing on analyzing next generation sequencing data. *Front. Bioeng. Biotechnol.* 8:817. doi: 10.3389/fbioe.2020.00817

Hoerr, F. J. (2010). Clinical aspects of immunosuppression in poultry. *Avian Dis.* 54, 2–15. doi: 10.1637/8909-043009-Review.1

Jahanian, R., and Rasouli, E. (2015). Dietary chromium methionine supplementation could alleviate immunosuppressive effects of heat stress in broiler chicks. *J. Anim. Sci.* 93, 3355–3363. doi: 10.2527/jas.2014-8807

Janczyk, P., Halle, B., and Souffrant, W. B. (2009). Microbial community composition of the crop and ceca contents of laying hens fed diets supplemented with *Chlorella vulgaris*. *Poult. Sci.* 88, 2324–2332. doi: 10.3382/ps.2009-00250

Jang, Y. J., Kim, W. K., Han, D. H., Lee, K., and Ko, G. (2019). *Lactobacillus fermentum* species ameliorate dextran sulfate sodium-induced colitis by regulating the immune response and altering gut microbiota. *Gut Microbes* 10, 696–711. doi: 10.1080/19490976.2019.1589281

Ji, F. J., Wang, L. X., Yang, H. S., Hu, A., and Yin, Y. L. (2019). Review: the roles and functions of glutamine on intestinal health and performance of weaning pigs. *Animal* 13, 2727–2735. doi: 10.1017/S1751731119001800

Kong, X., Duan, W., Li, D., Tang, X., and Duan, Z. (2020). Effects of polysaccharides from Auricularia auricula on the immuno-stimulatory activity and gut microbiota in immunosuppressed mice induced by cyclophosphamide. *Front. Immunol.* 11:595700. doi: 10.3389/fimmu.2020.595700

Kong, X., Hu, Y., Rui, R., Wang, D., and Li, X. (2004). Effects of Chinese herbal medicinal ingredients on peripheral lymphocyte proliferation and serum antibody titer after vaccination in chicken. *Int. Immunopharmacol.* 4, 975–982. doi: 10.1016/j.intimp.2004.03.008

Le Roy, T., Moens de Hase, E., Van Hul, M., Paquot, A., Pelicaen, R., Régnier, M., et al. (2022). Dysosmobacter welbionis is a newly isolated human commensal bacterium preventing diet-induced obesity and metabolic disorders in mice. *Gut* 71, 534–543. doi: 10.1136/gutjnl-2020-323778

Li, J., Yin, L., Wang, L., Li, J., Huang, P., Yang, H., et al. (2019). Effects of vitamin B6 on growth, diarrhea rate, intestinal morphology, function, and inflammatory factors expression in a high-protein diet fed to weaned piglets1. *J. Anim. Sci.* 97, 4865–4874. doi: 10.1093/jas/skz338

Liu, Y. S., Li, S., Wang, X. F., Xing, T., Li, J. L., Zhu, X. D., et al. (2021). Microbiota populations and short-chain fatty acids production in cecum of immunosuppressed broilers consuming diets containing γ-irradiated Astragalus polysaccharides. *Poult. Sci.* 100, 273–282. doi: 10.1016/j.psj.2020.09.089

Liu, S., Wang, K., Lin, S., Zhang, Z., Cheng, M., Hu, S., et al. (2023). Comparison of the effects between tannins extracted from different natural plants on growth performance, antioxidant capacity, immunity, and intestinal flora of broiler chickens. *Antioxidants (Basel)* 12:441. doi: 10.3390/antiox12020441

Long, L. N., Kang, B. J., Jiang, Q., and Chen, J. S. (2020). Effects of dietary *Lycium barbarum* polysaccharides on growth performance, digestive enzyme activities, antioxidant status, and immunity of broiler chickens. *Poult. Sci.* 99, 744–751. doi: 10.1016/j.psj.2019.10.043

Luo, W. W., Tian, L., Tan, B., Shen, Z. H., Xiao, M. W., Wu, S., et al. (2022). Update: innate lymphoid cells in inflammatory bowel disease. *Dig. Dis. Sci.* 67, 56–66. doi: 10.1007/s10620-021-06831-8

Ma, W. J., Wei, S. S., Peng, W. J., Sun, T. L., Huang, J. H., Yu, R., et al. (2021). Antioxidant effect of Polygonatum sibiricum polysaccharides in D-galactose-induced heart aging mice. *Biomed. Res. Int.* 2021, 1–8. doi: 10.1155/2021/6688855

Nawaz, A., Bakhsh Javaid, A., Irshad, S., Hoseinifar, S. H., and Xiong, H. (2018). The functionality of prebiotics as immunostimulant: evidences from trials on terrestrial and aquatic animals. *Fish Shellfish Immunol.* 76, 272–278. doi: 10.1016/j.fsi.2018.03.004

Niu, Y., Dong, J., Jiang, H., Wang, J., Liu, Z., Ma, C., et al. (2020). Effects of polysaccharide from *Malus halliana* koehne flowers in cyclophosphamide-induced immunosuppression and oxidative stress on mice. *Oxidative Med. Cell. Longev.* 2020:1603735. doi: 10.1155/2020/1603735

Pope, P. B., Mackenzie, A. K., Gregor, I., Smith, W., Sundset, M. A., McHardy, A. C., et al. (2012). Metagenomics of the Svalbard reindeer rumen microbiome reveals abundance of polysaccharide utilization loci. *PLoS One* 7:e38571. doi: 10.1371/journal.pone.0038571

Qu, D., Hu, H., Lian, S., Sun, W., and Si, H. (2022). The protective effects of three polysaccharides from Abrus cantoniensis against cyclophosphamide-induced immunosuppression and oxidative damage. *Front. Vet. Sci.* 9:870042. doi: 10.3389/fvets.2022.870042

Schoenaker, M. H. D., Henriet, S. S., Zonderland, J., van Deuren, M., Pan-Hammarström, Q., Posthumus-van Sluijs, S. J., et al. (2018). Immunodeficiency in bloom's syndrome. *J. Clin. Immunol.* 38, 35–44. doi: 10.1007/s10875-017-0454-y

Schoultz, I., and Keita, Å. V. (2019). Cellular and molecular therapeutic targets in inflammatory bowel disease-focusing on intestinal barrier function. *Cells* 8:193. doi: 10.3390/cells8020193

Sha, Z., Shang, H., Miao, Y., Huang, J., Niu, X., Chen, R., et al. (2021). Polysaccharides from *Pinus massoniana* pollen improve intestinal mucosal immunity in chickens. *Poult. Sci.* 100, 507–516. doi: 10.1016/j.psj.2020.09.015

Shini, S., Huff, G. R., Shini, A., and Kaiser, P. (2010). Understanding stress-induced immunosuppression: exploration of cytokine and chemokine gene profiles in chicken peripheral leukocytes. *Poult. Sci.* 89, 841–851. doi: 10.3382/ps.2009-00483

Shirani, K., Hassani, F. V., Razavi-Azarkhiavi, K., Heidari, S., Zanjani, B. R., and Karimi, G. (2015). Phytotrapy of cyclophosphamide-induced immunosuppression. *Environ. Toxicol. Pharmacol.* 39, 1262–1275. doi: 10.1016/j.etap.2015.04.012

Shu, G., Xu, D., Zhao, J., Yin, L., Lin, J., Fu, H., et al. (2021). Protective effect of Polygonatum sibiricum polysaccharide on cyclophosphamide-induced immunosuppression in chickens. *Res. Vet. Sci.* 135, 96–105. doi: 10.1016/j.rvsc.2020.12.025

Suen, G., Stevenson, D. M., Bruce, D. C., Chertkov, O., Copeland, A., Cheng, J. F., et al. (2011). Complete genome of the cellulolytic ruminal bacterium *Ruminococcus albus* 7. *J. Bacteriol.* 193, 5574–5575. doi: 10.1128/jb.05621-11

Walker, E. M., Thompson, C. A., and Battle, M. A. (2014). GATA4 and GATA6 regulate intestinal epithelial cytodifferentiation during development. *Dev. Biol.* 392, 283–294. doi: 10.1016/j.ydbio.2014.05.017

Wang, H., Hu, C., Cheng, C., Cui, J., Ji, Y., Hao, X., et al. (2019). Unraveling the association of fecal microbiota and oxidative stress with stillbirth rate of sows. *Theriogenology* 136, 131–137. doi: 10.1016/j.theriogenology.2019.06.028

Wang, K., Ma, J., Li, Y., Han, Q., Yin, Z., Zhou, M., et al. (2022). Effects of essential oil extracted from Artemisia argyi leaf on lipid metabolism and gut microbiota in high-fat diet-fed mice. *Front. Nutr.* 9:24722. doi: 10.3389/fnut.2022.1024722

Wang, K., Zhou, M., Gong, X., Zhou, Y., Chen, J., Ma, J., et al. (2022). Starch–protein interaction effects on lipid metabolism and gut microbes in host. *Front. Nutr.* 9:9. doi: 10.3389/fnut.2022.1018026

Wu, F., Guo, X., Zhang, J., Zhang, M., Ou, Z., and Peng, Y. (2017). *Phascolarctobacterium faecium* abundant colonization in human gastrointestinal tract. *Exp. Ther. Med.* 14, 3122–3126. doi: 10.3892/etm.2017.4878

Wu, J., He, C., Bu, J., Luo, Y., Yang, S., Ye, C., et al. (2020). Betaine attenuates LPS-induced downregulation of Occludin and Claudin-1 and restores intestinal barrier function. *BMC Vet. Res.* 16:75. doi: 10.1186/s12917-020-02298-3

Yang, S., Shan, C., Ma, X., Qin, Y., Ju, A., Duan, A., et al. (2021). Immunomodulatory effect of *Acanthopanax senticosus* polysaccharide on immunosuppressed chickens. *Poult. Sci.* 100, 623–630. doi: 10.1016/j.psj.2020.11.059

Yin, L., Li, J., Wang, H., Yi, Z., Wang, L., Zhang, S., et al. (2020). Effects of vitamin B6 on the growth performance, intestinal morphology, and gene expression in weaned piglets that are fed a low-protein diet1. *J. Anim. Sci.* 98:skaa022. doi: 10.1093/jas/skaa022

Ying, M., Yu, Q., Zheng, B., Wang, H., Wang, J., Chen, S., et al. (2020). Cultured Cordyceps sinensis polysaccharides modulate intestinal mucosal immunity and gut microbiota in cyclophosphamide-treated mice. *Carbohydr. Polym.* 235:115957. doi: 10.1016/j.carbpol.2020.115957

Ying, M., Zheng, B., Yu, Q., Hou, K., Wang, H., Zhao, M., et al. (2020). Ganoderma atrum polysaccharide ameliorates intestinal mucosal dysfunction associated with autophagy in immunosuppressed mice. *Food Chem. Toxicol.* 138:111244. doi: 10.1016/j.fct.2020.111244

Yu, Y., Shen, M., Song, Q., and Xie, J. (2018). Biological activities and pharmaceutical applications of polysaccharide from natural resources: a review. *Carbohydr. Polym.* 183, 91–101. doi: 10.1016/j.carbpol.2017.12.009

Yuan, Q., Xie, Y., Wang, W., Yan, Y., Ye, H., Jabbar, S., et al. (2015). Extraction optimization, characterization and antioxidant activity in vitro of polysaccharides from mulberry (*Morus alba* L.) leaves. *Carbohydr. Polym.* 128, 52–62. doi: 10.1016/j.carbpol.2015.04.028

Zhang, C., Li, C. X., Shao, Q., Chen, W. B., Ma, L., Xu, W. H., et al. (2021). Effects of Glycyrrhiza polysaccharide in diet on growth performance, serum antioxidant capacity, and biochemistry of broilers. *Poult. Sci.* 100:100927. doi: 10.1016/j.psj.2020.12.025

Zhang, Y., Ren, C., Lu, G., Mu, Z., Cui, W., Gao, H., et al. (2014). Anti-diabetic effect of mulberry leaf polysaccharide by inhibiting pancreatic islet cell apoptosis and ameliorating insulin secretory capacity in diabetic rats. *Int. Immunopharmacol.* 22, 248–257. doi: 10.1016/j.intimp.2014.06.039

Zhang, D. Y., Wan, Y., Xu, J. Y., Wu, G. H., Li, L., and Yao, X. H. (2016). Ultrasound extraction of polysaccharides from mulberry leaves and their effect on enhancing antioxidant activity. *Carbohydr. Polym.* 137, 473–479. doi: 10.1016/j.carbpol.2015.11.016

Zhang, S., Wang, C., Sun, Y., Wang, G., Chen, H., Li, D., et al. (2018). Xylanase and fermented polysaccharide of Hericium caputmedusae reduce pathogenic infection of broilers by improving antioxidant and anti-inflammatory properties. *Oxidative Med. Cell. Longev.* 2018:4296985. doi: 10.1155/2018/4296985

Zhao, S., Peng, X., Zhou, Q. Y., Huang, Y. Y., Rao, X., Tu, J. L., et al. (2021). Bacillus coagulans 13002 and fructo-oligosaccharides improve the immunity of mice with immunosuppression induced by cyclophosphamide through modulating intestinal-derived and fecal microbiota. *Food Res. Int.* 140:109793. doi: 10.1016/j.foodres.2020.109793

Zhao, X., Yang, R., Bi, Y., Bilal, M., Kuang, Z., Iqbal, H. M. N., et al. (2019). Effects of dietary supplementation with mulberry (*Morus alba* L.) leaf polysaccharides on immune parameters of weanling pigs. *Animals (Basel)* 10:35. doi: 10.3390/ani10010035

Zheng, Y., Li, S., Li, C., Shao, Y., and Chen, A. (2022). Polysaccharides from spores of cordyceps cicadae protect against cyclophosphamide-induced immunosuppression and oxidative stress in mice. *Food Secur.* 11:515. doi: 10.3390/foods11040515

Zheng, Y., Zong, Z. M., Chen, S. L., Chen, A. H., and Wei, X. Y. (2017). Ameliorative effect of Trametes orientalis polysaccharide against immunosuppression and oxidative stress in cyclophosphamide-treated mice. *Int. J. Biol. Macromol.* 95, 1216–1222. doi: 10.1016/j.ijbiomac.2016.11.013

Zhou, Y., Chen, X., Yi, R., Li, G., Sun, P., Qian, Y., et al. (2018). Immunomodulatory effect of tremella polysaccharides against cyclophosphamide-induced immunosuppression in mice. *Molecules* 23:239. doi: 10.3390/molecules23020239

Zhou, R., He, D., Xie, J., Zhou, Q., Zeng, H., Li, H., et al. (2021). The synergistic effects of polysaccharides and ginsenosides from American ginseng (*Panax quinquefolius* L.) ameliorating cyclophosphamide-induced intestinal immune disorders and gut barrier dysfunctions based on microbiome-metabolomics analysis. *Front. Immunol.* 12:665901. doi: 10.3389/fimmu.2021.665901

Zhou, F., Lu, Y., Sun, T., Sun, L., Wang, B., Lu, J., et al. (2022). Antitumor effects of polysaccharides from *Tetrastigma hemsleyanum* Diels et Gilg via regulation of intestinal flora and enhancing immunomodulatory effects in vivo. *Front. Immunol.* 13:1009530. doi: 10.3389/fimmu.2022.1009530

Zhou, Y., Ming, J., Deng, M., Li, Y., Li, B., Li, J., et al. (2020). Berberine-mediated up-regulation of surfactant protein D facilitates cartilage repair by modulating immune

responses via the inhibition of TLR4/NF-κB signaling. *Pharmacol. Res.* 155:104690. doi: 10.1016/j.phrs.2020.104690

Zhou, J. M., Zhang, H. J., Wu, S. G., Qiu, K., Fu, Y., Qi, G. H., et al. (2021). Supplemental xylooligosaccharide modulates intestinal mucosal barrier and cecal microbiota in laying hens fed oxidized fish oil. *Front. Microbiol.* 12:635333. doi: 10.3389/fmicb.2021.635333

Zhu, L., Luo, C., Ma, C., Kong, L., Huang, Y., Yang, W., et al. (2022). Inhibition of the NF-κB pathway and ERK-mediated mitochondrial apoptotic pathway takes part in the mitigative effect of betulinic acid on inflammation and oxidative stress in cyclophosphamide-triggered renal damage of mice. *Ecotoxicol. Environ. Saf.* 246:114150. doi: 10.1016/j.ecoenv.2022.114150

Zhu, N., Lv, X., Wang, Y., Li, J., Liu, Y., Lu, W., et al. (2016). Comparison of immunoregulatory effects of polysaccharides from three natural herbs and cellular uptake in dendritic cells. *Int. J. Biol. Macromol.* 93, 940–951. doi: 10.1016/j.ijbiomac.2016.09.064

Zhu, W., Ma, H., Miao, J., Huang, G., Tong, M., and Zou, S. (2013). β-Glucan modulates the lipopolysaccharide-induced innate immune response in rat mammary epithelial cells. *Int. Immunopharmacol.* 15, 457–465. doi: 10.1016/j.intimp.2012.12.007

Zuany-Amorim, C., Hastewell, J., and Walker, C. (2002). Toll-like receptors as potential therapeutic targets for multiple diseases. *Nat. Rev. Drug Discov.* 1, 797–807. doi: 10.1038/nrd914

frontiers | Frontiers in Microbiology

TYPE Original Research
PUBLISHED 12 June 2024
DOI 10.3389/fmicb.2024.1430276

OPEN ACCESS

EDITED BY
Kang Xu,
Chinese Academy of Sciences (CAS), China

REVIEWED BY
Yu Bai,
Tianjin University of Science and Technology, China
Hui Han,
Chinese Academy of Sciences (CAS), China
Shuting Cao,
Guangdong Academy of Agricultural Sciences (GDAAS), China

*CORRESPONDENCE
Bie Tan
✉ bietan@hunau.edu.cn
Jing Wang
✉ jingwang023@hunau.edu.cn

RECEIVED 09 May 2024
ACCEPTED 03 June 2024
PUBLISHED 12 June 2024

CITATION
Zhang LL, Wu ZC, Kang M, Wang J and Tan BE (2024) Utilization of Ningxiang pig milk oligosaccharides by *Akkermansia muciniphila in vitro* fermentation: enhancing neonatal piglet survival.
Front. Microbiol. 15:1430276.
doi: 10.3389/fmicb.2024.1430276

Utilization of Ningxiang pig milk oligosaccharides by *Akkermansia muciniphila in vitro* fermentation: enhancing neonatal piglet survival

Longlin Zhang[1,2], Zichen Wu[1,2], Meng Kang[1,2], Jing Wang[1,2]* and Bie Tan[1,2]*

[1]Key Laboratory for Quality Regulation of Livestock and Poultry Products of Hunan Province, College of Animal Science and Technology, Hunan Agricultural University, Changsha, China, [2]Yuelushan Laboratory, Changsha, China

Akkermansia muciniphila (*A. muciniphila*), an intestinal symbiont residing in the mucosal layer, shows promise as a probiotic. Our previous study found that the abundance of *A. muciniphila* was significantly higher in Ningxiang suckling piglets compared to other breeds, suggesting that early breast milk may play a crucial role. This study examines *A. muciniphila*'s ability to utilize Ningxiang pig milk oligosaccharides. We discovered that *A. muciniphila* can thrive on both Ningxiang pig colostrum and purified pig milk oligosaccharides. Genetic analysis has shown that *A. muciniphila* harbors essential glycan-degrading enzymes, enabling it to effectively break down a broad spectrum of oligosaccharides. Our findings demonstrate that *A. muciniphila* can degrade pig milk oligosaccharides structures such as 3′-FL, 3′-SL, LNT, and LNnT, producing short-chain fatty acids in the process. The hydrolysis of these host-derived glycan structures enhances *A. muciniphila*'s symbiotic interactions with other beneficial gut bacteria, contributing to a dynamic microbial ecological network. The capability of *A. muciniphila* to utilize pig milk oligosaccharides allows it to establish itself in the intestines of newborn piglets, effectively colonizing the mucosal layer early in life. This early colonization is key in supporting both mucosal and metabolic health, which is critical for enhancing piglet survival during lactation.

KEYWORDS

***Akkermansia muciniphila*, Ningxiang pig, milk oligosaccharides, piglet survival, short-chain fatty acids**

1 Introduction

Ensuring the survival and robust health of newborn piglets is crucial for the economic sustainability of pig farming (Heuß et al., 2019). Notably, approximately 15–20% of piglets succumb within the first 3 days post-birth, primarily due to inadequate immune development and environmental stressors (Bæk et al., 2019; Farmer and Edwards, 2022). Finding certain measures to address these challenges is critical for enhancing piglet survival and overall production efficiency.

Colostrum plays a vital dual role in the early life of piglets. The intake of colostrum within the first 24 h post-birth is essential, not only nourishing the piglets but also fortifying their systemic immune systems, thereby promoting their growth and increasing their resilience against infections

(Ogawa et al., 2016; Kogut and Zhang, 2022). Overall, it serves as an indispensable source of nutrients and crucially shapes the neonatal gut microbiota through its rich content of milk oligosaccharides (MOs) (Zivkovic et al., 2011). MOs are composed of a linear or branched backbone containing galactose, *N*-acetylglucosamine, and glucose, which can be decorated with fucose or sialic acid residues (Li et al., 2022). Although these complex carbohydrates are indigestible by piglets themselves, they are vital for the proliferation of specific beneficial bacteria. This strategic nourishment results in a beneficial microbiota composition that bolsters health and disease resistance, a reflection of evolutionary adaptations aimed at optimizing both infant survival and maternal health.

The Ningxiang breed is known among China's four famous pig breeds for its resilience and notably low rates of diarrhea in neonates (Wang et al., 2014; Ma et al., 2022). In our previous investigations, we observed that *Akkermansia muciniphila* (*A. muciniphila*) was notably more prevalent in Ningxiang suckling piglets compared to other breeds (Unpublished data). This Gram-negative anaerobe from the Verrucomicrobia phylum is renowned for its ability to degrade mucin and colonize the mucus layer of the gastrointestinal tract and convert this polymer into mostly acetate and propionate (Dao et al., 2015; Zhang et al., 2019). The presence of *A. muciniphila* is beneficial for host metabolism and immunity, particularly in mitigating risks associated with chronic conditions such as obesity and diabetes (Zheng et al., 2023). The early colonization by *A. muciniphila*, evident from as early as the first month of life, plays a significant role in the developmental stages of the gut microbiota, facilitated by its ability to utilize MOs (Collado et al., 2007; Derrien et al., 2008).

Based on the above, we hypothesize that the significant presence of *A. muciniphila* in Ningxiang piglets is linked to its ability to metabolize pig milk oligosaccharides (PMOs), which, in turn, would have a beneficial effect on newborn piglets. In this study, an *in vitro* fermentation model to explore the fermentative behavior of *A. muciniphila* on PMOs derived from Ningxiang colostrum, examining growth kinetics and acid production as indicators of PMOs utilization. Through genomic analysis, we have identified the key enzymes responsible for the breakdown of these oligosaccharides, further reinforcing the potential role of *A. muciniphila* in promoting a healthy gut microbiota from the earliest stages of life. By understanding how specific microbial strains such as *A. muciniphila* exploit the unique glycobiome of breast milk, we pave the way for potential interventions aimed at fostering optimal microbial colonization patterns in early life, setting the stage for a healthier adult life.

2 Materials and methods

2.1 Materials

A. muciniphila DSM 22959 was purchased from the German Collection of Microorganisms and Cell Cultures (Braunschweig, Germany). 2′-fucosyllactose [2′-FL] (purity≥95%), 3-fucosyllactose [3′-FL] (purity≥95%), 3′-siallylactose [3′-SL] (purity≥95%), 6′-sialyllactose [6′-SL] (purity≥95%), lacto-*N*-tetraose [LNT] (purity≥95%) and lacto-*N*-neotetraose [LNnT] (purity≥95%) were kindly provided by Zhuo Wang and Siming Jiao, from State Key Laboratory of Biochemical Engineering, Institute of Process Engineering, Chinese Academy of Sciences (Beijing, China). All the reagents used for this study were of analytical grade.

2.2 Bacterial growth curves

A. muciniphila DSM 22959 growth were performed with cells grown in brain heart infusion broth medium (BHI) (1 mL per replicate) broth at 37°C in anaerobic chamber (Whitley A35 anaerobic workstation). Cells were inoculated in BHI broth supplemented with Ningxiang-pig colostrum (10% v/v), Ningxiang-pig purified PMOs (1 mg/mL), neutral trioses (2′-FL and 3′-FL), tetraoses (LNT, LNnT), and acidic trioses (3′-SL, 6′-SL) (10 mM respectively). Medium without any supplementation was included as a control. Cells were incubated anaerobically at 37°C until reaching stationary phase (48 h).

2.3 PMOs extraction

The PMOs were isolated and purified as previously described, with minor modification (Barile et al., 2010). Briefly, frozen milk samples were completely thawed, and a 20 mL aliquot of each sample was mixed with an equal volume of nanopure water and centrifuged at 14,000 × *g* in a microfuge for 30 min at 4°C to remove lipids. The top fat layer was removed, and 4 volumes of chloroform: methanol (2:1, vol/vol) were added, vigorously mixed, and the resulting emulsion was centrifuged at 4,000 × *g* for 30 min at 4°C. The upper methanol layer containing PMOs was transferred to a tube, 2 volumes of cold ethanol were added, and the solution was frozen for 1 h at −30°C, followed by centrifugation for 30 min at 4,000 × *g* and 4°C to precipitate the denatured protein. The supernatant (PMOs-rich fraction) was collected and further purified. Oligosaccharides were purified from the mixture by GCC-SPE. Prior to use, each GCC-SPE cartridge was activated with 3 column volumes of 80% acetonitrile (ACN) and 0.1% trifluoroacetic acid (TFA, vol/vol) and equilibrated with 3 column volumes of nanopure water. The carbohydrate-rich solution was loaded onto the cartridge, and salts and mono- or disaccharides were removed by washing with 10 column volumes of nanopure water. Then, it was eluted with a solution of 40% ACN with 0.1% TFA (vol/vol) in water and the solution was frozen for 1 h at −80°C, with freeze-dried using a lyophilizer overnight to collected purified PMO.

2.4 Carbohydrate-active enzyme (CAZyme) annotation

CAZymes within *A. muciniphila* DSM 22959 (NCBI Reference Sequence: GCF_008000975.1) was annotated using the dbCAN2 metaserver.[1] CAZymes identified by at least two out of three tools were considered for further analysis.

2.5 Quantitative real-time PCR (qPCR)

The abundance of *A. muciniphila* was determined by qPCR as described previously10. Cells (1 mL) were harvested at 21,000 × g for 15 min. DNA extractions were performed using the MasterPure™ Gram Positive DNA Purification Kit (Epicentre, Lucigen, United States). DNA concentrations were measured fuorometrically

1 http://bcb.unl.edu/dbCAN2/

(Qubit dsDNA BR assay, Invitrogen) and adjusted to 1 ng/μL prior to use as the template in qPCR. Primers targeting the 16S rRNA gene of *A. muciniphila* (5′-CAGCACGTGAAGGTGGGGAC-3′ and 5′-CCTTGCGGTTGGCTTCAGAT-3′; 327 bp) were used for quantification. A standard curve was prepared with nine standard concentrations from 100 to 108 gene copies/μL. qPCR was performed in triplicate with iQ SYBR green supermix (Bio-Rad, United States) in a total volume of 10 μL prepared with primers at 500 nM in 384-wells plates with the wells sealed with optical sealing tape. Amplification was performed with an iCycler (Bio-Rad): one cycle of 95°C for 10 min; 40 cycles of 95°C for 15 s, 60°C for 20 s, and 72°C for 30 s each; one cycle of 95°C for 1 min; and a stepwise increase of temperature from 60 to 95°C (at 0.5°C per 5 s) to obtain melt curve data. Data were analyzed using Bio-Rad CFX Manager 3.0. The copy number was corrected for the DNA concentration and for the number of 16S rRNA genes encoded in *A. muciniphila*'s genome.

2.6 SCFAs analysis

The concentrations of SCFAs in *A. muciniphila* fermentation were analyzed using the gas chromatographic (GC) method. Briefly, 1 mL *A. muciniphila* fermentation was first centrifuged at 15,000 × *g* for 10 min at 4°C. The samples were acidified with 25% metaphosphoric acid at a ratio of 1:5 for 30 min on ice. Samples were injected into a GC 8890 series gas chromatograph (Agilent, United States) for detection.

2.7 Statistical analysis

The data were analyzed using SPSS 26.0 statistical software (ver. 26.0 for Windows, SPSS Inc., Chicago, IL, United States). All data were analyzed by Student's *t*-test and expressed as means with their standard errors. And $^{*}p < 0.05$, $^{**}p < 0.01$, and $^{***}p < 0.001$, Colostrum group compared with the CON group. $^{\#}p < 0.05$, $^{\#\#}p < 0.01$, and $^{\#\#\#}p < 0.001$ compared with the same treatment at different time.

3 Results

3.1 *A. muciniphila* DSM 22959 growth in Ningxiang-pig colostrum

Incubation of *A. muciniphila* DSM 22959 on Ningxiang-pig colostrum resulted in growth (Figure 1A). The results showed that presence of Ningxiang-pig colostrum in the basal medium (10% v/v) resulted in a modest increase in *A. muciniphila* growth *in vitro* (Figure 1A). And basal medium supplemented with Ningxiang-pig colostrum (10% v/v) significantly increased the cell number of *A. muciniphila in vitro* at 48 h (Figure 1B). Next, we determined the production of SCFAs by *A. muciniphila* DSM 22959 during fermentation of Ningxiang-pig colostrum at 24 and 48 h. Our results showed that fermentation of Ningxiang-pig colostrum significantly increased production of acetate, propionate and total SCFAs, regardless of whether it was 24 or 48 h (Figures 1C–E). Interestingly,

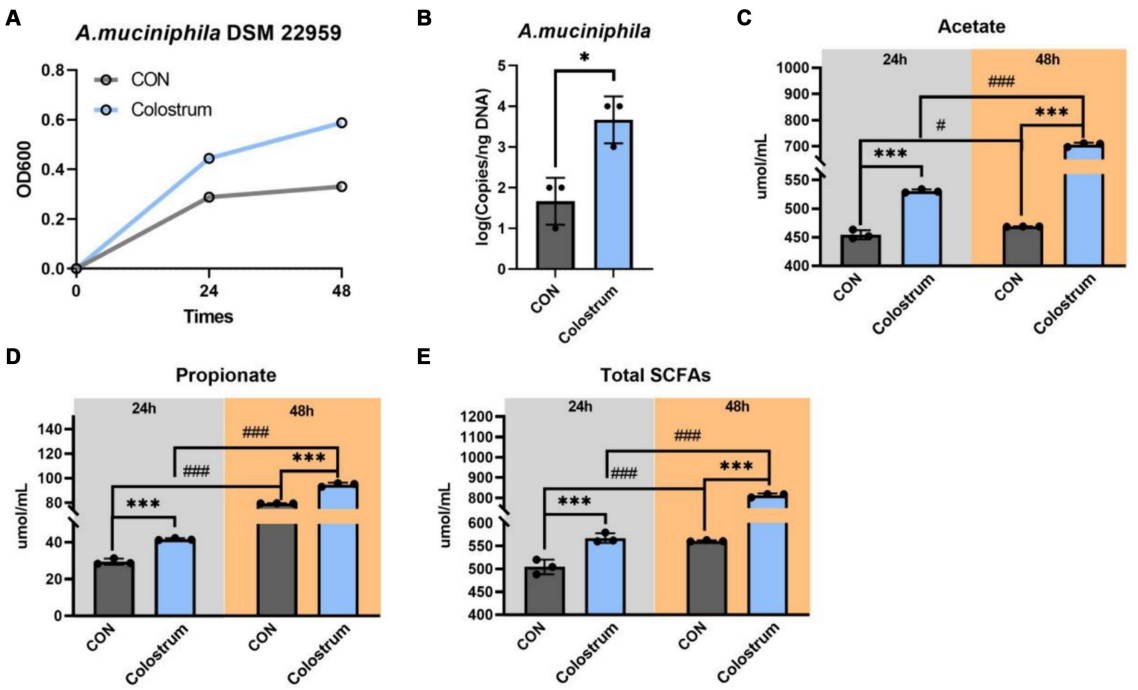

FIGURE 1
Akkermansia muciniphila DSM 22959 growth in Ningxiang-pig colostrum. **(A)** *A. muciniphila* DSM 22959 growth was assessed over a 48 h period by measuring optical density at a wavelength of 600 nm (OD600). Bacteria were grown in brain heart infusion broth medium (BHI), or BHI supplemented with Ningxiang-pig colostrum (10% v/v). **(B)** *A. muciniphila* DSM 22959 was grown *in vitro* in the absence or presence of 10% v/v Ningxiang-pig colostrum until 48 h of growth; *A. muciniphila* was quantified by qPCR. **(C–E)** Changes in SCFA levels in fermentation solutions. Data are expressed as the mean ± standard deviation ($n = 3$). $^{*}p < 0.05$, and $^{***}p < 0.001$, Colostrum group compared with the CON group. $^{\#}p < 0.05$, and $^{\#\#\#}p < 0.001$ compared with the same treatment at different time.

10.3389/fmicb.2024.1430276

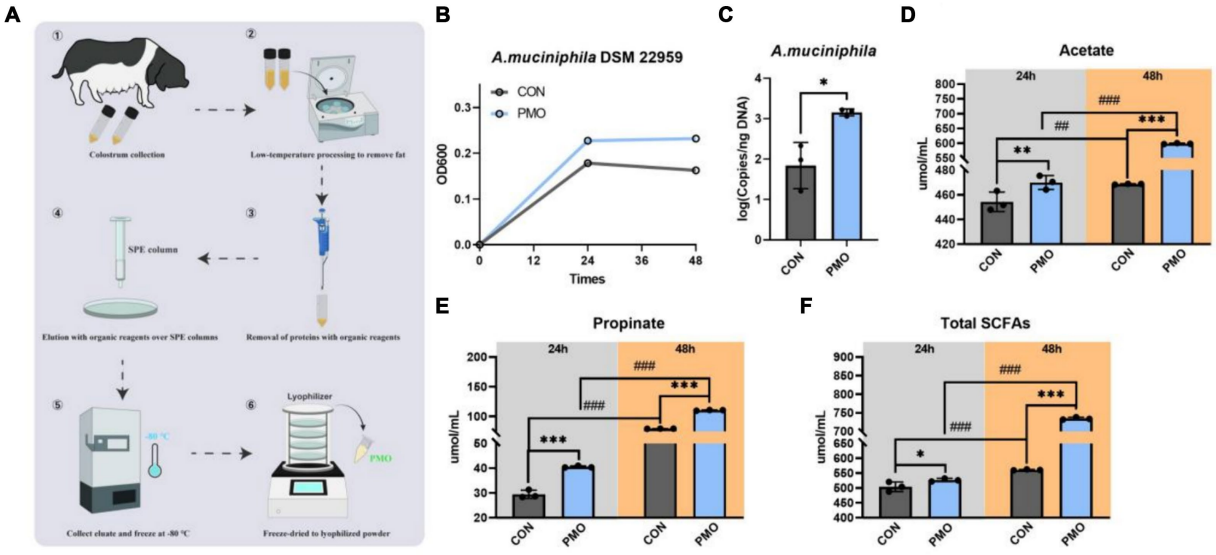

FIGURE 2
Akkermansia muciniphila DSM 22959 growth in Ningxiang-pig purified PMO. **(A)** Schematic illustration of Ningxiang-pig purified PMO preparation. **(B)** *A. muciniphila* DSM 22959 growth was assessed over a 48 h period by measuring optical density at a wavelength of 600 nm (OD600). Bacteria were grown in brain heart infusion broth medium (BHI), or BHI supplemented with Ningxiang-pig purified PMO (1 mg/mL). **(C)** *A. muciniphila* DSM 22959 was grown *in vitro* in the absence or presence of 1 mg/mL Ningxiang-pig purified PMO until 48 h of growth; *A. muciniphila* was quantified by qPCR. **(D–F)** Changes in SCFA levels in fermentation solutions. Data are expressed as the mean ± standard deviation ($n = 3$). $^{*}p < 0.05$, $^{**}p < 0.01$, and $^{***}p < 0.001$, Colostrum group compared with the CON group. $^{\#\#}p < 0.01$, and $^{\#\#\#}p < 0.001$ compared with the same treatment at different time.

the ratio of acetate increase (48 h/24 h) was superior in fermented Ningxiang pig colostrum compared to the increasing trend in the CON group (Figure 1C).

3.2 *A. muciniphila* DSM 22959 growth in Ningxiang-pig purified PMOs

Human milk oligosaccharides (HMOs) play an important role in the early nutrition of nursing infants and can act as substrates to support bacterial growth and thus dominate the gut early in life. In order to determine whether *A. muciniphila* DSM 22959 can utilize breast milk oligosaccharides to promote its own growth, we purified PMOs from the Ningxiang-pig colostrum (Figure 2A). Our results showed that supplemented with PMOs (1 mg/mL) increased the proliferation rate and significantly increased the cell number of *A. muciniphila in vitro* at 48 h (Figures 2B,C). Additionally, PMOs also significantly increased production of acetate, propionate and total SCFAs, regardless of whether it was 24 or 48 h (Figures 2D–F).

3.3 Identification of CAZymes in *A. muciniphila* DSM 22959 genome

To investigate how *A. muciniphila* DSM 22959 can utilize complex PMO, we interrogated the available *A. muciniphila* DSM 22959 genome for the presence of CAZymes using the dbCAN2 metaserver pipeline for automated CAZyme annotation. This pipeline uses a combination of three different annotation tools (Diamond, HMMER and dbCAN_sub) to increase accuracy in predicting and annotating CAZymes within bacterial genomes. This analysis revealed a total of 165 putative ORFs with putative CAZy domains (Figure 3A).

For increased accuracy, we discarded hits that were not identified by at least two out of three tools for further analysis. Among the remaining 118 ORFs multiple types of CAZy domains could be detected, such as glycoside hydrolase (GH), carbohydrate esterase (CE), glycosyl transferase (GT) domains, and carbohydrate-binding modules (CBM), with some genes encoding a combination of multiple domains (Figure 3B). Additionally, most of the putative ORFs belong to the GH and GT classes, and also encode signal peptides, suggests that *A. muciniphila* DSM 22959 was able to utilize multiple MOs.

3.4 The genome of *A. muciniphila* predicts the presence of a wide range of MOs targeting CAZymes

We performed further analysis on the *A. muciniphila* CAZy domains to identify the active enzymes that could contribute to the degradation of PMO (Figure 4A). Closer inspection of the Research Topic of CAZymes identified in the *A. muciniphila* DSM 22959 genome revealed at least 30 glycoside hydrolases that were predicted to utilize MOs, of which the majority contains a signal peptide (Figures 4B,C). Among the 30 glycoside hydrolases are two sialidases (GH33) and four fucosidases (GH29/95), which target the monosaccharides often found at terminal positions of MOs, and six different galactosidases (GH2) and 10 hexosaminidases (GH20/GH40), which are predicted to hydrolyze the underlying glycosidic linkages. The gene structure of the 30 putative enzymes, with the locations of the predicted glycoside hydrolase domains and additional

10.3389/fmicb.2024.1430276

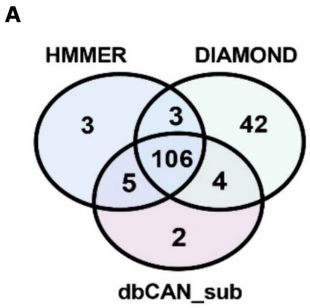

B

Carbohydrate active enzymes of *Akkermansia muciniphila* DSM 22959

CAZY class	a# of identified genes	# of genes with signal peptide
Glycoside hydrolase (GH)	58	40
Carbohydrate esterase (CE)	5	3
Glycosyl transferase (GT)	47	0
Carbohydrate-binding module (CBM)	5	5
Auxiliary activity (AA)	2	1

a# Identified by at least two out of three dbCAN2 tools

FIGURE 3
Identification of carbohydrate active enzymes (CAZymes) in *A. muciniphila* DSM 22959 genome. **(A)** Proportional Venn diagram showing the number of identified CAZyme encoding genes using the Diamond, HMMER and dbCAN_sub tools that are part of the dbCAN2 metaserver analysis. **(B)** The table shows the CAZymes and the presence of signal peptides, separated by CAZyme class, that were identified by at least two out of three dbCAN2 tools.

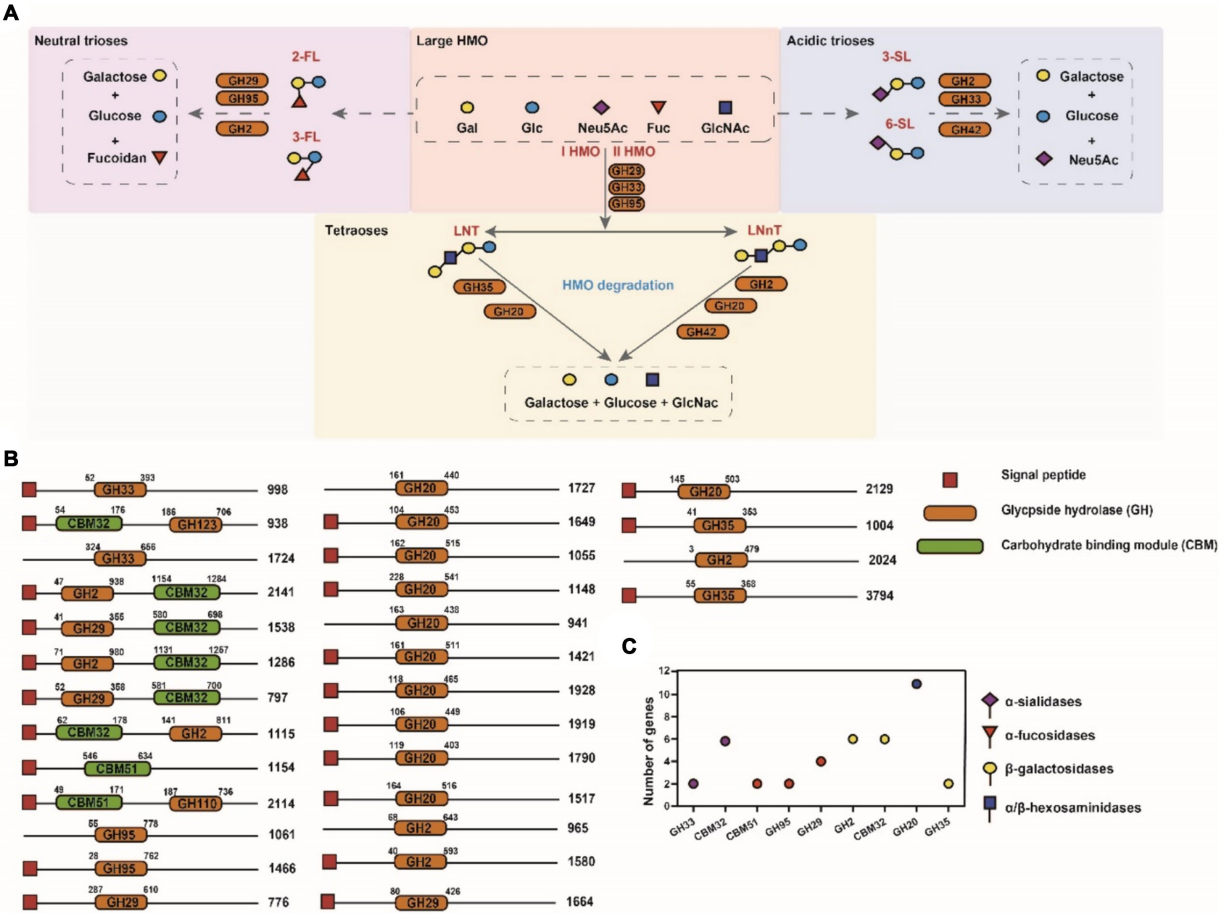

FIGURE 4
Domain architecture of putative MO targeting CAZymes in genome of *A. muciniphila* DSM 22959. **(A)** Simplified schematics of pathways involved in main HMO degradation (acidic trioses, neutral trioses and tetraoses). **(B)** CAZymes are divided in groups based upon their predicted enzyme activity: from top to bottom, α-sialidases, α-fucosidases, β-galactosidases and α/β-hexosaminidases. The displayed domains are those identified by HMMER, in number of amino acids, indicated at the right side of each protein. **(C)** The number of putative MO targeting CAZymes of *A. muciniphila* DSM 22959.

domains clearly demonstrates the great diversity in domains, domain organization and predicted protein sizes – also between genes predicted to encode the same class of enzymes (Figure 4B). Transcription and translation of the entire repertoire of MO-targeting CAZymes would allow degradation of the wide variety of linkages commonly found within MOs. These data demonstrate that *A. muciniphila* DSM 22959 has the enzymatic capacity to utilize a broad range of MOs as well as their constituents.

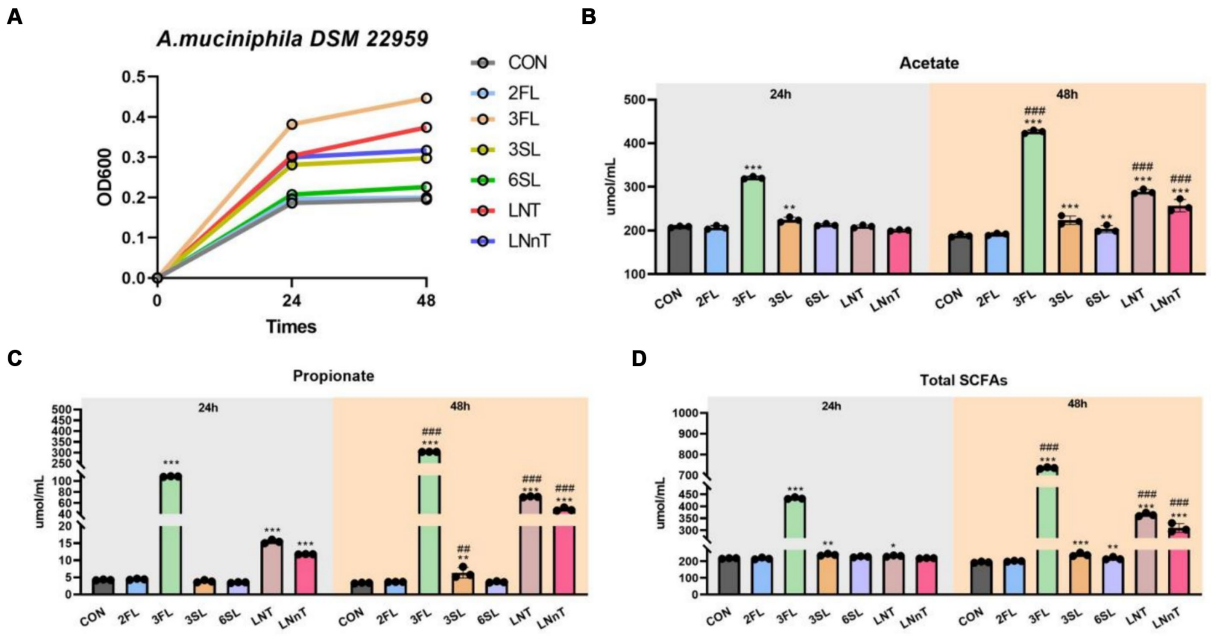

FIGURE 5
A. muciniphila DSM 22959 growth in acidic trioses, neutral trioses and tetraoses. **(A)** *A. muciniphila* DSM 22959 growth was assessed over a 48 h period by measuring optical density at a wavelength of 600 nm (OD600). Bacteria were grown in brain heart infusion broth medium (BHI), or BHI supplemented with neutral trioses (2-fucosyllactose [2-FL] and 3-fucosyllactose [3-FL]), tetraoses (lacto-*N*-tetraose [LNT], lacto-*N*-neotetraose [LNnT]), and acidic trioses (3-siallylactose [3-SL], 6-sialyllactose [6-SL]) (10 mM respectively). **(B–D)** Changes in SCFA levels in fermentation solutions. Data are expressed as the mean ± standard deviation ($n = 3$). $^{*}p < 0.05$, $^{**}p < 0.01$, and $^{***}p < 0.001$, Colostrum group compared with the CON group. $^{\#\#}p < 0.01$, and $^{\#\#\#}p < 0.001$ compared with the same treatment at different time.

3.5 *A. muciniphila* DSM 22959 growth in acidic trioses, neutral trioses and tetraoses

We next sought to investigate which PMOs structures were utilized by *A. muciniphila* during the growth on colostrum. The results showed that *A. muciniphila* DSM 22959 was able to utilize acidic trioses, neutral trioses and tetraoses to grow, especially 3′-FL (Figure 5A). Interestingly, the two type of tetraoses (LNT, LNnT) can all support the growth of *A. muciniphila* DSM 22959, whereas only one type of acidic trioses (3′-FL) and neutral trioses (3′-SL) showed better utilization. Additionally, supplementation with 3′-FL significantly increased production of acetate, propionate and total SCFAs, regardless of whether it was 24 or 48 h (Figures 5B–D).

4 Discussion

The survival rate of newborn piglets significantly impacts the economic viability of the pig industry, with a major focus in animal science being how to enhance piglet vigor through nutrition (Ji et al., 2019; Xu et al., 2019). Based on previous research findings, *A. muciniphila* was able to act as an early characterizing gut microbiota in Ningxiang piglets. *A. muciniphila* consumes mucin and exhibits beneficial effects on the host. Considering the structural similarities between MOs and intestinal mucus, it is plausible that the presence of PMOs in breast milk significantly contributes to the early colonization of *A. muciniphila* in piglets. Studies have identified negative associations between *A. muciniphila* and various diseases such as inflammatory bowel disease, diabetes, and hypertension, and its role in modulating responses to PD-1 blockers in cancer therapy (Derosa et al., 2022). Innovations in bacterial preparation, such as the use of cryopasteurized *A. muciniphila*, have shown metabolic improvements in mice, attributed to the activity of Amuc-1100 protein. This protein interacts with Toll-like receptor 2 to enhance intestinal barrier function and exerts probiotic benefits (Depommier et al., 2019). Furthermore, oral administration of *A. muciniphila* has been demonstrated to boost intestinal stem cell proliferation and promote the differentiation of Paneth and goblet cells, facilitating the regeneration of intestinal epithelia (Kim et al., 2021). Meanwhile, it has been showed that *A. muciniphila* can protect the intestinal health of weaned piglets from damage caused by ETEC infection (Lan et al., 2024).

Colostrum is indispensable for piglet development, serving not only as a vital nutrient source but also significantly shaping the neonatal gut microbiota through its rich content of MOs. Although piglets cannot digest these complex carbohydrates, they are crucial for the proliferation of beneficial bacteria. MOs, primarily undergraded by gastric acid and digestive enzymes, reach the hindgut to undergo microbial fermentation. As a principal carbohydrate source selectively utilized by the gut microbiota, MOs profoundly influence the microbial composition of the host's gut microbiota and are deemed crucial regulators in the development of the neonatal gut microbiota. Extensive studies have shown that MOs provide substrates for the gut microbiota, thereby facilitating the colonization and survival of specific gut microbiota. The complete degradation of MOs, featuring diverse molecular structures, necessitates a variety of glycoside hydrolases or membrane transporters present in the neonatal gut microbiota, essential for the uptake, metabolism, and utilization of MOs by gut microbiota. Recent research has highlighted that certain *Bifidobacteria* spp. can utilize specific MOs

in breast milk for their colonization and growth, thus benefiting the host's immune development, particularly in early life (Lawson et al., 2020; Heiss et al., 2021; Henrick et al., 2021). Furthermore, the mechanisms of MOs degradation and utilization by *Bifidobacteria* spp. are categorized into strategies dependent on bacterial intracellular membrane translocation and those reliant on extracellular glycosidases (Katayama, 2016). Other bacteria like *Bacteroides fragilis* and *Bacteroides vulgatus* also exhibit high MOs metabolizing abilities (Yu et al., 2013), with *Bacteroides fragilis* possessing genes crucial for the metabolism of mucus-sugar conjugates (Marcobal et al., 2011). Our study's detailed genomic analysis has identified specialized CAZymes in *A. muciniphila*, which are specifically adapted for breaking down PMOs from Ningxiang colostrum. These enzymes not only facilitate the ability of gut microbiota to establish and maintain a healthy microbial balance within the neonatal piglet gut but also enable the effective fermentation of a broad range of PMOs. This process highlights *A. muciniphila*'s critical role in shaping the gut microbiota of neonatal piglets, underscoring its evolutionary adaptability and ecological significance, similar to its beneficial functions in human infants.

The MOs have an enormous molecular weight that cannot be directly utilized by cell, but can be catabolized by gut microbiota, then producing SCFAs to respond to various life activities, such as immune regulation and glucose homeostasis (Zhu et al., 2020; Zhang et al., 2021; Chen et al., 2023). SCFAs are the main products of prebiotic fermentation, and the production of these metabolites depends on both dietary fiber types and gut microbiota composition (Bridgman et al., 2017). There is increasing evidence that gut microbial metabolites have wide systemic effects on host through acting as signaling molecules (Gasaly et al., 2021). SCFAs have been implicated in immune system development by modulating the production of immune mediators and regulating the activation and differentiation of immune cells (Yao et al., 2022; Liu et al., 2023). To investigate the metabolic performance of colostrum, purified PMOs and specific MOs fermentation by *A. muciniphila* dominant inocula, the yield of SCFAs were quantified. Our results showed that fermentation of Ningxiang-pig colostrum and purified PMOs significantly increased production of acetate, propionate and total SCFAs, regardless of whether it was 24 or 48 h. The production of SCFAs by *A. muciniphila* during the fermentation of pig colostrum oligosaccharides not only supports its own growth but also mediates significant health benefits for the host. In piglets, these SCFAs can enhance gut integrity, reduce pathogen colonization, and improve nutrient absorption—factors that are crucial for early development and long-term health (Li et al., 2021; Qin et al., 2023). By extending these findings, we can hypothesize that strategic dietary interventions in livestock could replicate these benefits, potentially transforming approaches to neonatal care in pig farming.

In conclusion, this study demonstrated the ability of *A. muciniphila* to grow on Ningxiang PMOs thanks to its expression of a set of PMOs-degrading enzymes using an *in vitro* fermentation model. The fermentation of Ningxiang pig colostrum by *A. muciniphila* degraded acidic trioses, neutral trioses and tetraoses (the mainly PMOs). Our study offers the possibility of controlling colostrum composition or adding prebiotics to piglet diets to promote beneficial bacteria, such as *A. muciniphila*. Such strategies could lead to enhanced survival rates, improved immune functions, and greater resistance to gastrointestinal diseases in neonatal livestock, underscoring the potential of targeted microbial interventions in agricultural settings.

Data availability statement

The original contributions presented in the study are included in the article/supplementary material, further inquiries can be directed to the corresponding authors.

Author contributions

LLZ: Formal analysis, Visualization, Writing – original draft, Writing – review & editing. ZCW: Methodology, Software, Writing – review & editing. MK: Supervision, Validation, Writing – review & editing. JW: Conceptualization, Funding acquisition, Writing – review & editing. BET: Conceptualization, Funding acquisition, Writing – review & editing.

Funding

The author(s) declare that financial support was received for the research, authorship, and/or publication of this article. This study was funded by the National Key R&D Program (2022YFD1300403), Excellent Youth Foundation of Hunan Province (2022JJ20027), Science and Technology Major Project of Yunnan Province (202202AE090032), and Earmarked Fund for China Agriculture Research System (CARS-35).

Acknowledgments

The authors would like to thank HealthSyn Biotechnology (Zhuhai Hengqin) Co., Ltd. for helping our experiments.

Conflict of interest

The authors declare that the research was conducted in the absence of any commercial or financial relationships that could be construed as a potential conflict of interest.

Publisher's note

References

Bæk, O., Sangild, P. T., Thymann, T., and Nguyen, D. N. (2019). Growth restriction and systemic immune development in preterm piglets. *Front. Immunol.* 10, 1–13. doi: 10.3389/fimmu.2019.02402

Barile, D., Marotta, M., Chu, C., Mehra, R., Grimm, R., Lebrilla, C. B., et al. (2010). Neutral and acidic oligosaccharides in Holstein-Friesian colostrum during the first 3 days of lactation measured by high performance liquid chromatography on a microfluidic chip and time-of-flight mass spectrometry. *J. Dairy Sci.* 93, 3940–3949. doi: 10.3168/jds.2010-3156

Bridgman, S. L., Azad, M. B., Field, C. J., Haqq, A. M., Becker, A. B., Mandhane, P. J., et al. (2017). Fecal short-chain fatty acid variations by breastfeeding status in infants at 4 months: differences in relative versus absolute concentrations. *Front. Nutr.* 4:11. doi: 10.3389/fnut.2017.00011

Chen, Y., Wen, Y., Zhu, Y., Chen, Z., Mu, W., and Zhao, C. (2023). Synthesis of bioactive oligosaccharides and their potential health benefits. *Crit. Rev. Food Sci. Nutr.*, 21, 1–13. doi: 10.1080/10408398.2023.2222805

Collado, M. C., Derrien, M., Isolauri, E., de Vos, W. M., and Salminen, S. (2007). Intestinal integrity and *Akkermansia muciniphila*, a mucin-degrading member of the intestinal microbiota present in infants, adults, and the elderly. *Appl. Environ. Microbiol.* 73, 7767–7770. doi: 10.1128/AEM.01477-07

Dao, M. C., Everard, A., Aron-Wisnewsky, J., Sokolovska, N., Prifti, E., Verger, E., et al. (2015). Akkermansia muciniphila and improved metabolic health during a dietary intervention in obesity: rela.Pdf. *Gut* 65, 426–436. doi: 10.1136/gutjnl-2014-308778

Depommier, C., Everard, A., Druart, C., Plovier, H., Van Hul, M., Vieira-Silva, S., et al. (2019). Supplementation with *Akkermansia muciniphila* in overweight and obese human volunteers: a proof-of-concept exploratory study. *Nat. Med.* 25, 1096–1103. doi: 10.1038/s41591-019-0495-2

Derosa, L., Routy, B., Thomas, A. M., Iebba, V., Zalcman, G., Friard, S., et al. (2022). Intestinal *Akkermansia muciniphila* predicts clinical response to PD-1 blockade in patients with advanced non-small-cell lung cancer. *Nat. Med.* 28, 315–324. doi: 10.1038/s41591-021-01655-5

Derrien, M., Collado, M. C., Ben-Amor, K., Salminen, S., and De Vos, W. M. (2008). The mucin degrader *Akkermansia muciniphila* is an abundant resident of the human intestinal tract. *Appl. Environ. Microbiol.* 74, 1646–1648. doi: 10.1128/AEM.01226-07

Farmer, C., and Edwards, S. A. (2022). Review: improving the performance of neonatal piglets. *Animal* 16:100350. doi: 10.1016/j.animal.2021.100350

Gasaly, N., de Vos, P., and Hermoso, M. A. (2021). Impact of bacterial metabolites on gut barrier function and host immunity: a focus on bacterial metabolism and its relevance for intestinal inflammation. *Front. Immunol.* 12, 1–16. doi: 10.3389/fimmu.2021.658354

Heiss, B. E., Ehrlich, A. M., Maldonado-Gomez, M. X., Taft, D. H., Larke, J. A., Goodson, M. L., et al. (2021). Bifidobacterium catabolism of human milk oligosaccharides overrides endogenous competitive exclusion driving colonization and protection. *Gut Microbes* 13:1986666. doi: 10.1080/19490976.2021.1986666

Henrick, B. M., Rodriguez, L., Lakshmikanth, T., Pou, C., Henckel, E., Arzoomand, A., et al. (2021). Bifidobacteria-mediated immune system imprinting early in life. *Cell* 184, 3884–3898.e11. doi: 10.1016/j.cell.2021.05.030

Heuß, E. M., Pröll-Cornelissen, M. J., Neuhoff, C., Tholen, E., and Große-Brinkhaus, C. (2019). Invited review: piglet survival: benefits of the immunocompetence. *Animal* 13, 2114–2124. doi: 10.1017/S1751731119000430

Ji, F. J., Wang, L. X., Yang, H. S., Hu, A., and Yin, Y. L. (2019). Review: the roles and functions of glutamine on intestinal health and performance of weaning pigs. *Animal* 13, 2727–2735. doi: 10.1017/S1751731119001800

Katayama, T. (2016). Host-derived glycans serve as selected nutrients for the gut microbe: human milk oligosaccharides and bifidobacteria. *Biosci. Biotechnol. Biochem.* 80, 621–632. doi: 10.1080/09168451.2015.1132153

Kim, S., Shin, Y. C., Kim, T. Y., Kim, Y., Lee, Y. S., Lee, S. H., et al. (2021). Mucin degrader *Akkermansia muciniphila* accelerates intestinal stem cell-mediated epithelial development. *Gut Microbes* 13, 1–20. doi: 10.1080/19490976.2021.1892441

Kogut, M. H., and Zhang, G. (2022). *Gut microbiota, immunity, and health in production animals*. Springer.

Lan, C., Li, H., Shen, Y., Liu, Y., Wu, A., He, J., et al. (2024). Next-generation probiotic candidates targeting intestinal health in weaned piglets: both live and heat-killed *Akkermansia muciniphila* prevent pathological changes induced by enterotoxigenic *Escherichia coli* in the gut. *Anim. Nutr* 17, 110–122. doi: 10.1016/j.aninu.2024.01.007

Lawson, M. A. E., O'Neill, I. J., Kujawska, M., Gowrinadh Javvadi, S., Wijeyesekera, A., Flegg, Z., et al. (2020). Breast milk-derived human milk oligosaccharides promote Bifidobacterium interactions within a single ecosystem. *ISME J.* 14, 635–648. doi: 10.1038/s41396-019-0553-2

Li, H., Lane, J. A., Chen, J., Lu, Z., Wang, H., Dhital, S., et al. (2022). In vitro fermentation of human milk oligosaccharides by individual *Bifidobacterium longum*-dominant infant fecal inocula. *Carbohydr. Polym.* 287:119322. doi: 10.1016/j.carbpol.2022.119322

Li, Y., Liu, Y., Wu, J., Chen, Q., Zhou, Q., Wu, F., et al. (2021). Comparative effects of enzymatic soybean, fish meal and milk powder in diets on growth performance, immunological parameters, SCFAs production and gut microbiome of weaned piglets. *J. Anim. Sci. Biotechnol.* 12, 106–111. doi: 10.1186/s40104-021-00625-8

Liu, X. F., Shao, J. H., Liao, Y. T., Wang, L. N., Jia, Y., Dong, P. J., et al. (2023). Regulation of short-chain fatty acids in the immune system. *Front. Immunol.* 14, 1–14. doi: 10.3389/fimmu.2023.1186892

Ma, N., Sun, Y., Chen, J., Qi, Z., Liu, C., and Ma, X. (2022). Micro-coevolution of genetics rather than diet with Enterotype in pigs. *Front. Nutr.* 9, 1–11. doi: 10.3389/fnut.2022.846974

Marcobal, A., Barboza, M., Sonnenburg, E. D., Pudlo, N., Martens, E. C., Desai, P., et al. (2011). Bacteroides in the infant gut consume milk oligosaccharides via mucus-utilization pathways. *Cell Host Microbe* 10, 507–514. doi: 10.1016/j.chom.2011.10.007

Ogawa, S., Tsukahara, T., Imaoka, T., Nakanishi, N., Ushida, K., and Inoue, R. (2016). The effect of colostrum ingestion during the first 24 hours of life on early postnatal development of piglet immune systems. *Anim. Sci. J.* 87, 1511–1515. doi: 10.1111/asj.12573

Qin, W., Yu, Z., Li, Z., Liu, H., Li, W., Zhao, J., et al. (2023). Dietary Berberine and Ellagic acid supplementation improve growth performance and intestinal damage by regulating the structural function of gut microbiota and SCFAs in weaned piglets. *Microorganisms* 11, 1–19. doi: 10.3390/microorganisms11051254

Wang, L.-n., Chen, X.-l., Li, X.-G., Shu, G., Yan, H.-c., and Wang, X.-q. (2014). Evaluation of adrenocorticotropin regulated glucocorticoid synthesis pathway in adrenal of different breeds of pigs. *Livest. Sci.* 169, 185–191. doi: 10.1016/j.livsci.2014.08.007

Xu, K., Bai, M., Bin, P., Duan, Y., Wu, X., Liu, H., et al. (2019). Negative effects on newborn piglets caused by excess dietary tryptophan in the morning in sows. *J. Sci. Food Agric.* 99, 3005–3016. doi: 10.1002/jsfa.9514

Yao, Y., Cai, X., Fei, W., Ye, Y., Zhao, M., and Zheng, C. (2022). The role of short-chain fatty acids in immunity, inflammation and metabolism. *Crit. Rev. Food Sci. Nutr.* 62, 1–12. doi: 10.1080/10408398.2020.1854675

Yu, Z. T., Chen, C., and Newburg, D. S. (2013). Utilization of major fucosylated and sialylated human milk oligosaccharides by isolated human gut microbes. *Glycobiology* 23, 1281–1292. doi: 10.1093/glycob/cwt065

Zhang, T., Li, Q., Cheng, L., Buch, H., and Zhang, F. (2019). *Akkermansia muciniphila* is a promising probiotic. *Microb. Biotechnol.* 12, 1109–1125. doi: 10.1111/1751-7915.13410

Zhang, Y., Xie, Q., You, L., Cheung, P. C. K., and Zhao, Z. (2021). Behavior of non-digestible polysaccharides in gastrointestinal tract: a mechanistic review of its anti-obesity effect 2, 59–72. doi: 10.2991/efood.k.210310.001

Zheng, M., Han, R., Yuan, Y., Xing, Y., Zhang, W., Sun, Z., et al. (2023). The role of *Akkermansia muciniphila* in inflammatory bowel disease: current knowledge and perspectives. *Front. Immunol.* 13, 1–19. doi: 10.3389/fimmu.2022.1089600

Zhu, W., Zhou, S., Liu, J., McLean, R. J. C., and Chu, W. (2020). Prebiotic, immuno-stimulating and gut microbiota-modulating effects of *Lycium barbarum* polysaccharide. *Biomed. Pharmacother.* 121:109591. doi: 10.1016/j.biopha.2019.109591

Zivkovic, A. M., German, J. B., Lebrilla, C. B., and Mills, D. A. (2011). Human milk glycobiome and its impact on the infant gastrointestinal microbiota. *Proc. Natl. Acad. Sci. USA* 108, 4653–4658. doi: 10.1073/pnas.1000083107

frontiers | Frontiers in Microbiology

TYPE Original Research
PUBLISHED 17 June 2024
DOI 10.3389/fmicb.2024.1414486

OPEN ACCESS

EDITED BY
Jie Yin,
Hunan Agricultural University, China

REVIEWED BY
Tarique Hussain,
Nuclear Institute for Agriculture and Biology, Pakistan
Yuying Li,
Chinese Academy of Agricultural Sciences, China
Kai Wang,
Chinese Academy of Agricultural Sciences (CAAS), China
Hao Xiao,
Guangdong Academy of Agricultural Sciences, China

*CORRESPONDENCE
Tiejun Li
✉ tjli@isa.ac.cn
Xuping Xiao
✉ 469784129@qq.com
Liuqin He
✉ heliuqin@hunnu.edu.cn

RECEIVED 09 April 2024
ACCEPTED 04 June 2024
PUBLISHED 17 June 2024

CITATION
Zhang H, Xiang X, Wang C, Li T, Xiao X and He L (2024) Different effects of acute and chronic oxidative stress on the intestinal flora and gut-liver axis in weaned piglets. *Front. Microbiol.* 15:1414486. doi: 10.3389/fmicb.2024.1414486

Different effects of acute and chronic oxidative stress on the intestinal flora and gut-liver axis in weaned piglets

Hongyu Zhang[1,2], Xuan Xiang[3], Chenyu Wang[2,3], Tiejun Li[3]*, Xuping Xiao[1]* and Liuqin He[2,3]*

[1]Department of Otorhinolaryngology Head and Neck Surgery, The First Affiliated Hospital of Hunan Normal University (Hunan Provincial People's Hospital), Changsha, China, [2]Hunan Provincial Key Laboratory of Animal Intestinal Function and Regulation, Laboratory of Animal Nutrition and Hunan Health, College of Life Sciences, Hunan Normal University, Changsha, China, [3]Hunan Provincial Key Laboratory of Animal Nutritional Physiology and Metabolic Process, CAS Key Laboratory of Agro-Ecological Processes in Subtropical Region, National Engineering Laboratory for Pollution Control and Waste Utilization in Livestock and Poultry Production, Institute of Subtropical Agriculture, Chinese Academy of Sciences, Changsha, China

Introduction: Oxidative stress plays a pivotal role in modulating the balance of intestinal flora and the gut-liver axis, while also serving as a key determinant of the growth potential of weaned piglets. However, few studies have subdivided and compared acute and chronic oxidative stress.

Methods: In this study, an intestinal model of acute oxidative stress in weaned piglets using paraquat (PQ) and a chronic oxidative stress model using D-galactosa in weaned piglets were conducted. And we further systematically compare their effects.

Results: Both acute and chronic oxidative stress models impaired intestinal barrier function and liver function. Chronic stress caused by D-galactose can result in severe redox dysregulation, while acute stress caused by paraquat can lead to inflammation and liver damage. Additionally, the components involved in the CAR pathway were expressed differently. Chronic or acute oxidative stress can reduce the diversity and composition of intestinal flora. In the PQ group, the richness of Mogibacterium and Denitratisoma improved, but in the D-gal group, the richness of Catenisphaera and Syntrophococcus increased.

Discussion: Not only does this research deepen our understanding of the effects of acute and chronic oxidative stress on intestinal functions, but it also characterizes characteristic changes in the gut flora, potentially identifying novel therapeutic targets and opening new avenues for future research.

KEYWORDS

acute oxidative stress, chronic oxidative stress, gut-liver axis, intestinal flora, weaned piglets

1 Introduction

An oxidative stress condition is defined as the accumulation of reactive oxygen species (ROS) along with a dysfunctional antioxidant system (Forman and Zhang, 2021), which also frequently occurs alongside inflammation and can exacerbate it. Although there is no precise definition, oxidative stress is generally classified as either acute or chronic based on its duration of action. Acute oxidative stress is involved in ischemic stroke, spinal cord injury, acute lung injury, and acute kidney injury, among others, while chronic oxidative stress plays a role in vascular dementia, nonalcoholic liver disease, chronic pancreatitis, and aging (Hajam et al., 2022). Although both result in damage to many intracellular components, particularly mitochondria and DNA (Li X. et al., 2022), there are differences in the mechanisms of acute versus chronic oxidative stress. For instance, in acute lung injury, the production of excess Nitric oxide (NO) induced by ROS causes bronchial arterioles to dilate, increases permeability, and directs blood flow into the lungs through bronchial-pulmonary vascular anastomotic branches, leading to pulmonary edema (Ward, 2010). On the other hand, during cerebral hypoperfusion, increased ROS in the vascular endothelium impairs NO signaling and reduces NO bioavailability (Liu and Zhang, 2012). In addition, excessive ROS in chronic pancreatitis primarily originates from the activation of cytochrome P450 enzymes, and antioxidant therapy has been found to be effective (Petrov, 2010). These studies indicate that acute and chronic oxidative stress have distinct mechanisms of action.

The intestine is a significant source and target of ROS (Feng et al., 2020) and can also induce liver lesions through the gut-liver axis. Through the portal vein system, there is a close anatomical and functional association between liver and intestine. Excessive accumulation of ROS can damage the tight junction proteins between intestinal epithelia, leading to intestinal mucosal epithelial cells becoming abnormally proliferative and differentiated (Liu et al., 2021). It can cause intestinal mucosal barrier dysfunction and alter the intestinal flora (Han et al., 2021). A substantial body of evidence from animal studies indicates that gut microbiota dysbiosis can lead to hepatic injury due to increased gut permeability, which in turn results in increased hepatic exposure to harmful substances (Krawczyk et al., 2018; Rainer et al., 2018). For instance, a significant number of patients with inflammatory bowel disease (IBD) also suffer from Nonalcoholic Fatty Liver Disease (NAFLD) (Younossi et al., 2016). The liver affects the state of intestinal oxidative stress by secreting bile and antibody components into the intestines, providing feedback to the intestines. Individuals with cholangitis have a significantly different intestinal flora than healthy individuals (Tilg et al., 2022). Oxidative stress has a crucial role to liver-gut axis interactions, particularly in intestinal injury. However, previous studies have generally described oxidative stress without distinguishing between acute and chronic forms. Therefore, few comparisons between these two types of oxidative stress have been reported.

Here we constructed two animal models of acute and chronic oxidative stress piglets. Paraquat was used to construct the acute oxidative stress models which is widely used in mammals (Xiang et al., 2022; Xiao et al., 2022). D-galactose, which was previously reported its used in rats and pig models (Sha et al., 2021; Sun et al., 2023), was used in chronic oxidative stress modeling. This study aimed to develop a model of acute and chronic oxidative stress in the porcine intestine and systematically examine its impact on the growth performance, the gut-liver axis and intestinal flora in weaned piglets.

2 Method

2.1 Animal and experimental design

A selection with 21 healthy weaned piglets (Duroc×Landrace×Large) was randomly separated into three groups: control (CON) group, D-galactose (D-gal) group, and paraquat (PQ) group, each with 7 replicates and 1 piglet per pen with comparable body weight (BW = 9.49 ± 0.26 kg). The basal diets were prepared with the NRC (2012) recommended nutrient requirements for piggies weighing 11 ~ 25 kg (Table 1). The experiment was divided into three phases. During the first phase, 5 days of adaptation was followed by feeding all piglets with the basal diet. In the second phase, the CON and PQ groups were fed the basal diet, while the D-gal group was fed the basal diet supplemented with 10 g/kg BW of D-galactose (Hubei Yuying Biotech. Company, Yichang, China) during a chronic stress period. The third phase was the acute stress period. In this phase, the PQ group received intraperitoneal injections of 8 mg/kg BW of PQ (Chengdu HuaXia Chemical Reagent, Chengdu, China) on the days 28, 30, and 32 (Xiang et al., 2022), while the CON group received equal volume of 0.9% sterile saline until they were slaughtered on

TABLE 1 Ingredients and nutrient levels of basal diets (air-dry basis, %).

Ingredients	Content	Nutrient level†	Content
Ripening corn	31.45	NE, kcal/kg	2,450
Ripening rice	25.60	EE	3.76
Flour	12.50	CP	17.32
Extruded soybean	6.40	*CF*	2.18
Fermented soybean meal	5.00	P	0.54
Ripening soybean meal	5.00	Ca	0.63
Fish meal	3.50	Total Lysine	1.39
Sucrose	2.50	Total Valine	1.15
Glucose	2.50	Total Threonine	0.95
Soybean oil	1.25	Total Tryptophan	0.29
50% Choline chloride	0.10	Total Methionine	0.65
$CaHPO_3$	0.80		
Lysine · HCl	0.77		
Limestone	0.50		
NaCl	0.40		
L-Valine	0.38		
Methionine	0.38		
Threonine	0.36		
Premix[1]	0.19		
L-Tryptophan	0.12		
Total	100.00		

NE, net energy; EE, ether extract; CP, crude protein; CF, crude fiber. *Per kilogram of the diet, the premix offered the following: vitamin D, 3000 IU; vitamin A, 10,000 IU; vitamin E, 30 mg; vitamin B2, 10 mg; vitamin B6, 6 mg; vitamin B1 4 mg; vitamin K3, 4 mg; vitamin B12, 0.04 mg; nicotinic acid, 40 mg; pantothenic acid, 20 mg; folic acid, 2 mg; biotin, 0.2 mg; Fe (as ferrous sulfate), 100 mg; Zn (as zinc sulfate), 80 mg; Cu (as copper sulfate pentahydrate), 25 mg; Mn (as manganese sulfate), 25 mg; Co (as cobalt chloride), 0.5 mg; I (as Calcium iodate), 0.8 mg and Se (as sodium selenite), 0.35 mg. †NRC models were used to compute net energy, and values for other nutrients were measured.

day 33. The piglets were housed individually, provided with *ad libitum* feed and water throughout the experiment.

2.2 Sample collection

During the trial, the body weights of the piglets were recorded on days 1, 7, 14, 21, and 28. Daily feed intake and diarrhea were accurately documented. For each week, the average daily feed intake (ADFI), average daily gain (ADG), feed conversion ratio (FCR) and diarrhea rate (DR) were calculated. At the end of the experiment, blood was drawn from the anterior vena cava. After standing for 2 h, the blood was centrifuged for 10 min at 3,000 rpm at 4°C to extract the serum. For histological and pathological examination, 1 cm of liver, jejunum, and ileum tissues were extracted and instantly preserved in 3% glutaraldehyde solutions and 4% paraformaldehyde. For additional analysis, the liver, jejunum, ileum, and colon chyme were obtained, quick frozen in liquid nitrogen and then kept as low as −80°C.

2.3 Serum biochemical and physiological properties

A Cobas c 311 automated biochemical analyzer (Roche, Basel, Switzerland) was used to measure serum total protein (TP), immunoglobulin G (IgG), immunoglobulin M (IgM), alanine aminotransferase (ALT), aspartate aminotransferase (AST), and alkaline phosphatase (ALP). Lactate dehydrogenase (LDH), malondialdehyde (MDA), superoxide dismutase (SOD), total antioxidant capacity (T-AOC) and catalase (CAT) levels are measured with a colorimetric test kit (Beijing BoxBio Science & Tech. Co., Ltd., Beijing, China). and the process was completed in compliance with the instructions of the kit. The levels of glutathione (GSH), glutathione peroxidase (GSH-Px), oxidized glutathione (GSSG), immunoglobulin A (IgA), interleukin 1-β (IL-1β), interleukin-10 (IL-10), interleukin-12 (IL-12), tumor necrosis factor-α (TNF-α), interferon-γ (IFN-γ), intestinal fatty acid binding protein (iFABP), diamine oxidase (DAO), and adenosine triphosphate (ATP) were measured by ELISA (Jiangsu Meimian Industrial, Jiangsu, China), the detailed procedure is based on the kit protocol.

2.4 Tissue histomorphology

Hematoxylin and eosin (H&E) staining was performed on the jejunal and ileal sections after fixing with 4% paraformaldehyde. Villus height and crypt depth were assessed blindly by two separate investigators, same like in the previous study (He et al., 2022). The ileum and liver sections were pre-fixed with 3% glutaraldehyde for lead citrate and uranyl acetate staining. Certain lesions were observed using the JEM-1400 FLASH transmission electron microscope (JEOL, Tokyo, Japan), as reported (Hu et al., 2022).

2.5 Cell apoptosis

A terminal deoxynucleotidyl transferase dUTP nick end labeling (TUNEL) apoptosis assay kit (Beyotime Biotech, Shanghai, China) was used to detect apoptosis. Additionally, sections were examined with DM3000 fluorescence microscopy (Leica, Shanghai, China).

2.6 Immunohistochemical analysis

Immunohistochemical analysis was performed to examine the expression of Occludin, ZO-1 and Claudin 1 in the ileum and jejunum, as previously described (Xiang et al., 2022). Antibodies against the three proteins were used at the following dilution ratios: Claudin 1 (1: 500), Occludin (1: 1000), and ZO-1 (1: 800) (all made by Proteintech, Rosemont, IL, USA).

2.7 Real-time PCR analysis

The quantitative real-time PCR was performed as previously described (He et al., 2017). The primers were designed by Primer Express 5.0 software (Table 2) according to the conserved sequences of pig genes in the NCBI database and the principles of primer design. Total RNA was extracted with TRIzol (Beyotime, Shanghai, China) from the liver and jejunum tissue. The transcript levels of target genes were normalized to either GAPDH or β-actin expression. The relative level of mRNA was normalized to the CON group.

2.8 Gut microbiota profiles

Total microbial DNA was extracted from colon contents samples utilizing the TGuide S96 Magnetic Bead Method Soil/Fecal Genomic DNA Extraction Kit (Tiangen, Beijing, China). Using the primers for the V3-V4 region of the bacterial DNA gene (338F: 5'-ACTCCTACGGGGAGGCGCAGCA-3′ and 806R: 5'-GGACTAC HVGGGTWTCTAAT-3′), 5–50 ng of DNA was extracted and amplified by PCR. The amplified products were homogenized and purified, the libraries were quality-checked by the Qsep-400 method, and the libraries were sequenced using the Illumina Novaseq 6000 platform. High-quality sequences were obtained by first quality filtering the raw sequencing data using Trimmomatic (version 0.33), then identifying and removing primer sequences using Cutadapt (version 1.9.1), splicing bipartite reads using USEARCH (version 10), and lastly removing chimeras using UCHIME (version 8.1). OTUs were classified by clustering/de-noising high-quality sequences, and their species categorization was achieved by analyzing the sequence composition of the OTUs. The BMKCloud[1] platform was used for subsequent bioinformatics research on microbial diversity and differentiation. Raw sequence data reported in this paper have been deposited (CRA015743) in the Genome Sequence Archive in the BIG Data Center, Chinese Academy of Sciences[2] (Members, 2018).

1 http://www.biocloud.net/
2 http://bigd.big.ac.cn/gsa

2.9 Statistical analysis

The data were analyzed using SPSS 20.0 (IBM-SPSS, Chicago, USA) and graphics were processed with GraphPad Prism 8.0 (GraphPad Software, San Diego, USA). Data were analyzed statistically using a *t*-test or one-way ANOVA and Duncan's multiple comparisons test. The data are shown as mean ± standard error, with $p < 0.05$ suggesting a significant difference between groups.

3 Results

3.1 Effect of acute and chronic oxidative stress on intestinal morphology and growth performance in weaned piglets

In comparison to the CON group, the results demonstrated that D-galactose treatment dramatically decreased BW, ADG, and ADFI during the course of the four weeks (Figures 1A–C). Diarrhea rates had no discernible difference in the two groups and both decreased to 0 at 4 weeks as piglets adapted to the environment (Figure 1E). However, at the third week, the D-gal group observed an 8.3% greater rate of diarrhea against the CON group. Furthermore, compared to the CON group, the F/G ratio in the D-gal group exhibited a significant increase in both the second and third weeks (Figure 1D). The ADG was significantly decreased after the paraquat challenge (Figure 1G). However, there were no appreciable variations in rate of diarrhea, BW or ADFI (Figures 1F,H,I).

Oxidative stress induces damage to the intestinal morphology, which is linked to disruptions in the gut epithelial barrier. As shown in our work, PQ and D-galactose treatment resulted in jejunal and ileal morphological damage in weaned piglets (Figure 1J). While the two treatments did not significantly alter the crypt depth (Figure 1L), both PQ and D-galactose challenges, compared to the CON group, caused a drop in the villus height and the villus height to crypt depth ratio (V/C). Additionally, a shorter villi and V/C ratio were observed in the D-gal group (Figures 1K,M). The results suggest that both D-galactose and paraquat have a negative impact on the jejunal and ileal morphology, as well as on the growth performance. However, D-galactose induced chronic oxidative stress caused a more severe impairment of growth potential and morphology.

3.2 Effect of acute and chronic oxidative stress on intestinal permeability in weaned piglets

We evaluated the structure and protein abundances of the tight junction, which are crucial for preserving the integrity and impermeability of the intestinal mucosal barrier. When stimulated by PQ or D-galactose, the intestinal microvilli of piglets were found to be short, thick, loosely organized, and physiologically uneven, as shown in the transmission electron microscope image (Figure 2A). Meanwhile, the group treated with PQ and D-galactose exhibited heterogeneous and fewer mitochondria compared to the control group (CON) (Figure 2C), with reduced and broken cristae. Additionally, the PQ and D-galactose group significantly reduced the number of mitochondria in the ileum and ATP levels (Figure 2D). Weaned piglets treated with PQ or D-galactose showed increased intestinal epithelial cell apoptosis as detected by immunofluorescence (Figures 2B,E).

TABLE 2 Primers for quantitative reverse transcription-PCR.

Accession No.	Gene	Sequence primers (5′ → 3′)
NM_214407.1	GPX4	F: GATTCTGGCCTTCCCTTGC R: TCCCCTTGGGCTGGACTTT
NM_214201.1	GPX1	F: TGGGGAGATCCTGAATTG R: GATAAACTTGGGGTCGGT
NM_001190422.1	CuZnSOD	F: TGAAGGGAGAGAAGACAGTGTTAG R: TCTCCAACGTGCCTCTCTTG
NM_214127.2	MnSOD	F: GGACAAATCTGAGCCCTAACG R: CCTTGTTGAAACCGAGCC
XM_001926378.4	GCLM	F: CACAGCGAGGAGCTTCGAGA R: TGCGTGAGACACAGTACATTCC
XM_021098556.1	GCLC	F: GATCCTCCAGTTCCTGCACA R: GAGAGAGAACCAACCTCGTCG
NM_213948.1	IFN-γ	F: CAGGCCATTCAAAGGAGCAT R: GAGTTCACTGATGGCTTTGCG
NM_214041.1	IL-10	F: CGGCGCTGTCATCAATTTCTG R: CCCCTCTCTTGGAGCTTGCTA
NM_213993.1	IL-12	F: CAGGCCCAGGAATGTTCAAA R: CGTGGCTAGTTCAAGTGGTAAG
NM_214055.1	IL-1β	F: CCAATTCAGGGACCCTACCC R: GTTTTGGGTGCAGCACTTCAT
NM_001037996.1	CAR	F: GTGCCTGAACTGTCTCTGCT R: CCACATGCGCTCCATCTTCT
XM_003131409.5	CCRP	F: TGCCCTAGAATTTGCCCCTG R: GCAAAGACCTCGGACGTACA
XM_001927453.2	RXRα	F: CAAGTGCCTGGAACACCTCT R: ATGGAAGGTAACAGGGTGGC
NM_214366.1	PP2Ac	F: GGTGCCATGACCGGAATGTA R: GTGCTGGGTCAAACTGCAAG
NM_213973.1	HSP90	F: AAGACCGGACCCTCACGATA R: AGGCATACTGCTCGTCATCG
NM_213850.2	GSTA2	F: CTACTACGTGGAAGAGCTGGAC R: GCCCTGCCCACTTTATGAAGAC
NM_214389.2	GSTA1	F: AGGACACCCAGGACCAATCTT R: CTCAGGTACATTCCGGGAGAAG
NM_001159614.1	CYP1A2	F: TTTGTGGAGACCGCCTCATC R: GCTTGAATAGGGCGCTTGTG
NM_214423.1	CYP3A29	F: CCTGAAATTAACCACGCAAGGGCT R: TCTGGGATGCAGCTTTCTTGACCA
NM_214413.1	CYP2B22	F: GGGAACGTTGGAAGACCCTT R: CGGGATCTCTGTAGGCGAAG
NM_001206359.1	GAPDH	F: AAGGAGTAAGAGCCCCTGGA R: TCTGGGATGGAAACTGGAA
XM_003124280.3	β-actin	F: CTGCGGCATCCACGAAACT R: AGGGCCGTGATCTCCTTCTG

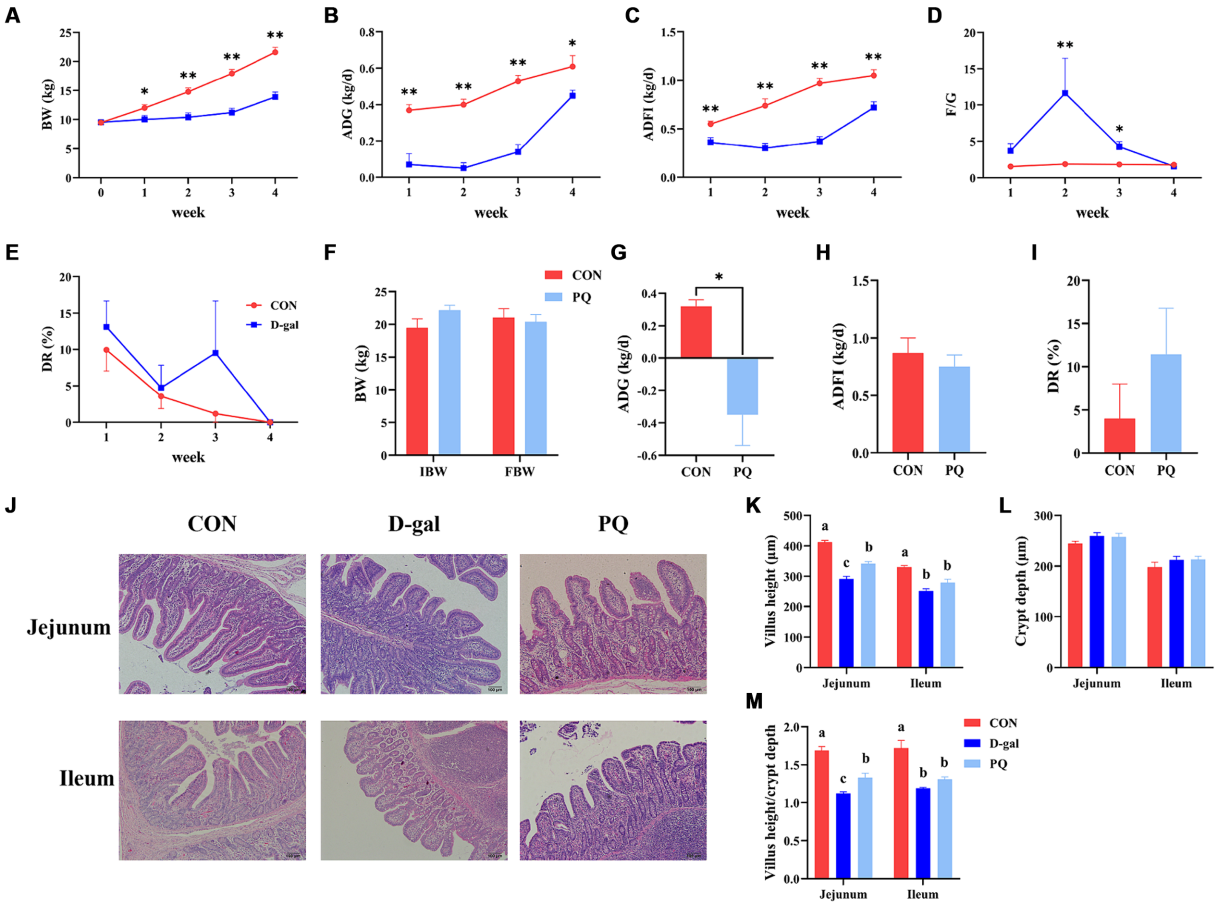

FIGURE 1
Effect of acute and chronic oxidative stress on growth performance and intestinal morphology in weaned piglets. **(A–E)** The BW, ADG, ADFI, F/G, and DR per week for CON group and D-gal group. **(G–I)** The ADG, ADFI, and DR for CON group and PQ group. **(J)** Representative H&E staining of jejunal and ileal tissue for weaned piglets (×100; Scale bars = 100 μm). **(K–M)** The villus height, crypt depth and Villus height to crypt depth ratio of ileum and jejunum in weaned piglets. A significant difference ($p < 0.05$) is indicated by different tiny letter superscripts, whereas no significant difference ($p > 0.05$) is indicated by the same or no letter superscripts. The values are given as Mean ± SE, $n = 7$. CON group, control group; D-gal group, D-galactose induced chronic oxidative stress group; PQ group, paraquat induced acute oxidative stress group; BW, body weight; ADG, average daily gain; ADFI, average daily feed intake; F/G, feed/gain; DR, diarrhea rate.

The effect of PQ and D-galactose on intestinal barrier function was further investigated by examining the localization and expression of intestinal tight junctions, such as Claudin-1, ZO-1, and Occludin protein. The findings (Figures 3A,B,E,F) demonstrated that the expression of Claudin-1, ZO-1, and Occludin protein in the jejunum and ileum of weaned piglets was significantly inhibited by challenging with PQ or D-galactose. Additionally, intestinal permeability was altered (Figures 3C,D), and the DAO content was markedly higher than that of the CON group. As hypothesized, the challenge of PQ and D-galactose could increase the intestinal permeability of weaned piglets.

3.3 Effect of acute and chronic oxidative stress on the gut-liver axis in weaned piglets

TEM confirmed the morphology and quantity of hepatocyte mitochondria (Figure 4A). The PQ group had fewer and more heterogeneous mitochondria than the CON group, with reduced and broken cristae (Figure 4B). Additionally, the hepatic ATP level was significantly decreased (Figure 4C). The PQ group had considerably greater levels of ALT (Figure 4D), AST (Figure 4E), LDH (Figure 4G), and serum TP (Figure 4H) compared with the CON group. However, PQ had little impact on the levels of ALP (Figure 4F), serum IgA (Figure 4I), serum IgG (Figure 4J), and serum IgM (Figure 4K). The D-galactose challenge resulted in similar changes, although not all differences were statistically significant (Figures 4A–K). It is noteworthy that the PQ group had higher levels of AST than the D-gal group. Taken together, our findings indicate that both PQ and D-galactose challenge can damage hepatocytes and their redox system and the PQ group suffered more severe hepatic impairment.

3.4 Effect of acute and chronic oxidative stress on antioxidant capacity and inflammatory cytokines in weaned piglets

To better understand the impact of acute and chronic oxidative stress on the redox system, we examined serological and intestinal

10.3389/fmicb.2024.1414486

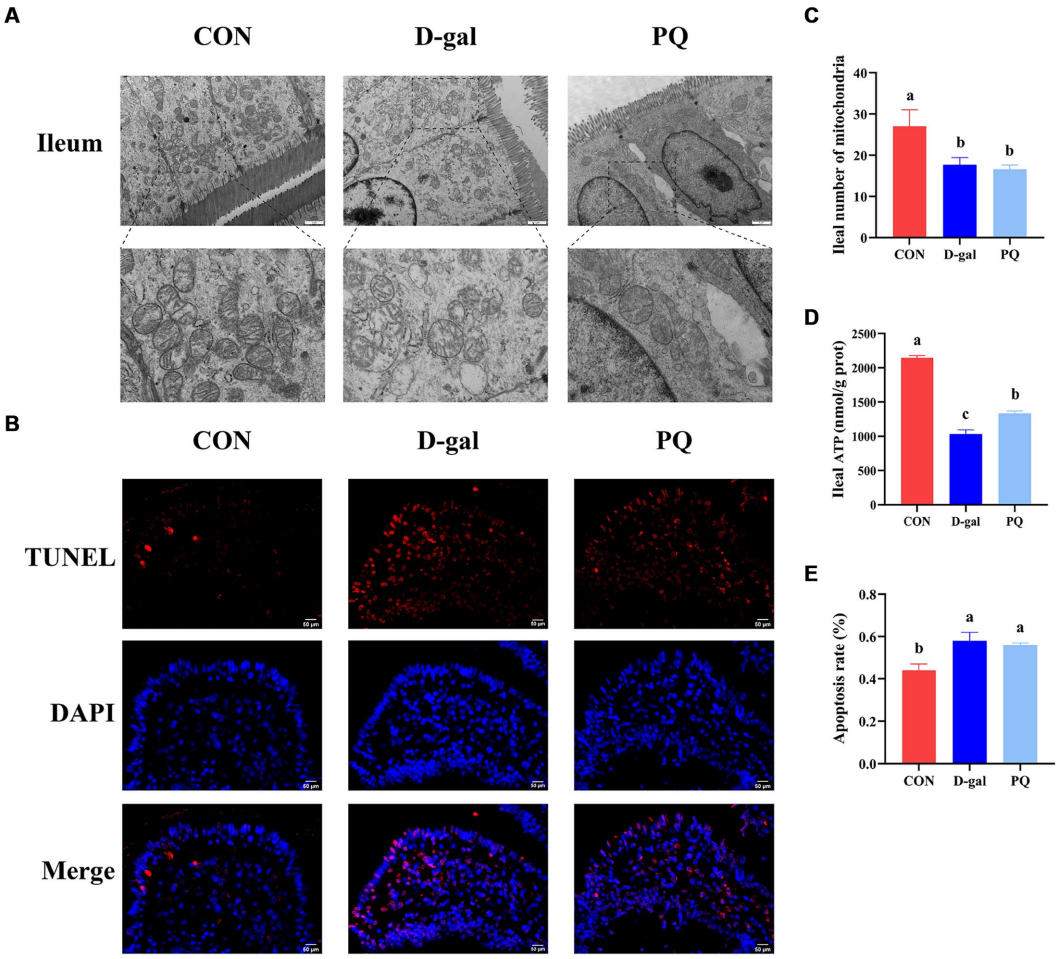

FIGURE 2
Effect of acute and chronic oxidative stress on intestinal epithelial cell in weaned piglets. **(A)** Epithelial cells ultrastructure in the ileum for different group (×15,000; Scale bars=1μm). **(B)** Representative TUNEL staining of ileal tissue (Scale bars=50μm; ×400). **(C)** Number of mitochondria in ileal epithelial cells. **(D)** ATP content in ileal epithelial cells. **(E)** The apoptosis rate quantitation in the ileum. A significant difference ($p<0.05$) is indicated by different tiny letter superscripts, whereas no significant difference ($p>0.05$) is indicated by the same or no letter superscripts. The values are given as Mean±SE, $n=7$. CON group, control group; D-gal group, D-galactose induced chronic oxidative stress group; PQ group, paraquat induced acute oxidative stress group.

antioxidant-related enzymes. The PQ and D-galactose challenge both significantly raised the serum MDA content (Figure 5A) and GSH-PX activity (Figure 5C) compared to the CON group, but a decline in serum T-AOC activity (Figure 5B) and serum SOD (Figure 5D). The ratio of GSH/GSSG in serum, liver, jejunum, and ileum were significantly decreased by PQ and D-galactose challenge (Figures 5E–L). This is due to the fact that the GSH/GSSG ratio is calculated from the previous GSH and GSSH values. Consistent with the results above, our results suggest a decreasing trend in the CuZnSOD and MnSOD mRNA expression while the expressions of GCLC and GCLM tend to increase after PQ or D-galactose challenge. (Figures 5M,N). And this trend was evident in the D-gal group. Our findings demonstrate that PQ and D-galactose challenge disrupt redox balance and impairs antioxidant capacity in weaned piglets.

Since oxidative stress typically triggers an inflammatory response, we further assessed the inflammatory level of weaned piglets. PQ or D-galactose exposure elevated the level of type 1 cytokines in serum, such as IL-1β (Figure 6E) and TNF-α (Figure 6D), which promote type I inflammation. There is no significant difference in IFN-γ and IL-12 (Figures 6B,C). However, PQ and D-galactose decreased the level of IL-10 in serum (Figure 6A), which regulates immunity. Similar results were found in the liver (Figure 6F) and jejunum (Figure 6G) tissues, where PQ or D-galactose increased IL-12 and IFN-γ levels and decreased IL-10 levels. Notably, the PQ group had larger levels of IL-1β, IFN-γ, and IL-12 than the D-gal group did. Overall, the results suggest that PQ and D-galactose induce type 1 proinflammatory cytokines and cause an imbalance in immunity.

3.5 Effect of acute and chronic oxidative stress on CAR pathway in weaned piglets

To fend off oxidative stress brought on by both internal and external stressors, the Constitutive Androstane Receptor (CAR) has the ability to control the production of antioxidant genes like SOD, CAT, and CYP450. In this study, we aimed to determine the potential mechanism underlying the effects of PQ and D-galactose on weaned piglets by examining key targets of the CAR pathway. Compared to the CON group, the PQ group showed an increase in mRNA expression of CAR, HSP90, and CYP2B22 (Figures 7E,F), while also showing a decrease in mRNA expression of PP2Ac and CYP1A2 (Figures 7E,F) in the liver. However, the jejunum of the PQ group

10.3389/fmicb.2024.1414486

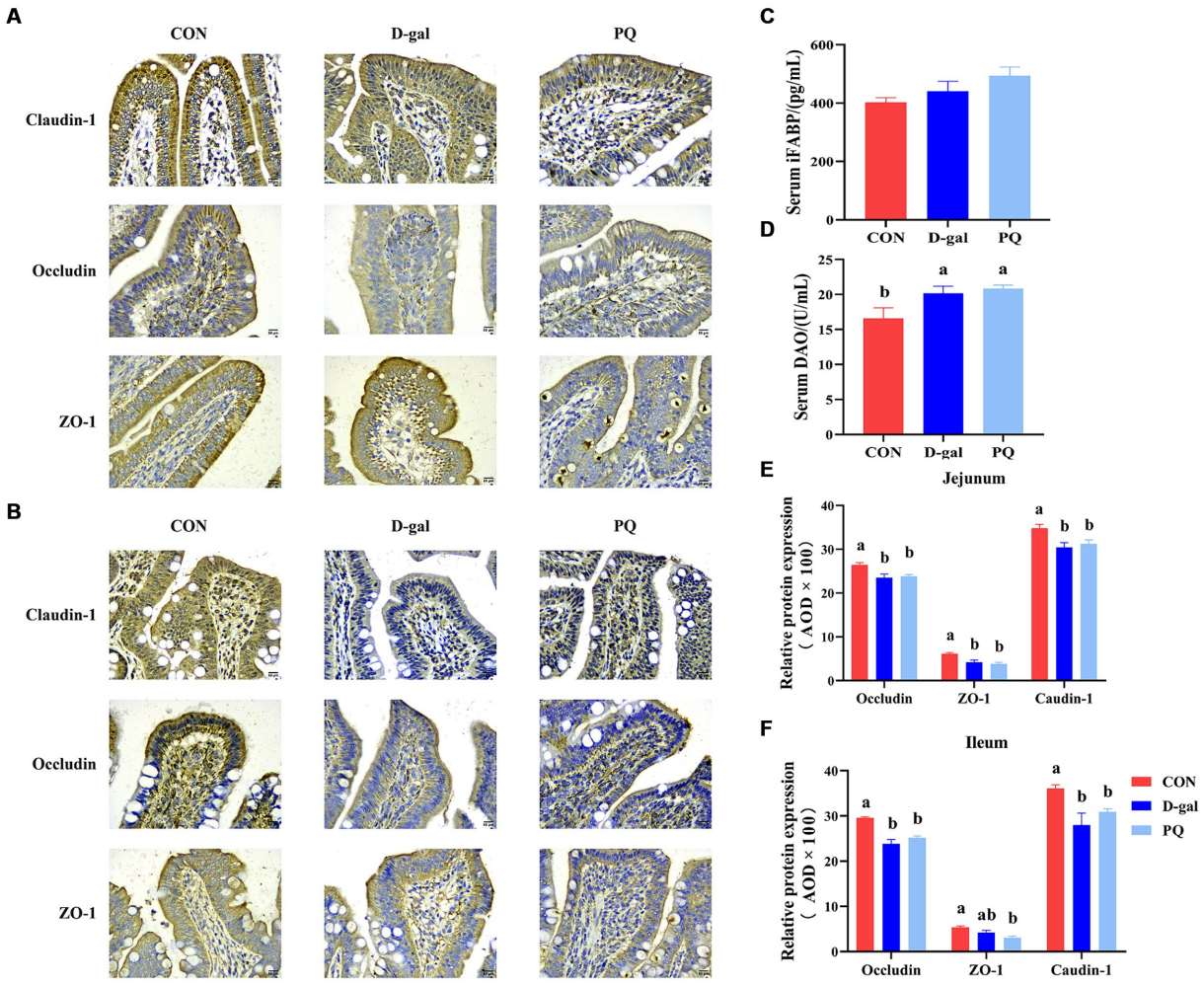

FIGURE 3
Effect of acute and chronic oxidative stress on intestinal barrier function in weaned piglets. Immunohistochemical staining of Claudin-1, Occludin and ZO-1 of jejunum **(A)** and ileum **(B)** (Scale bars = 50 μm; ×400). **(C,D)** Level of serum DAO and iFABP. **(E,F)** The relative expression of Claudin-1, Occludin and ZO-1 in the jejunum and ileum. A significant difference ($p < 0.05$) is indicated by different tiny letter superscripts, whereas no significant difference ($p > 0.05$) is indicated by the same or no letter superscripts. The values are given as Mean ± SE, $n = 7$. CON group, control group; D-gal group, D-galactose induced chronic oxidative stress group; PQ group, paraquat induced acute oxidative stress group; AOD, average optical density.

showed an increase in expression of RXRα, PP2Ac, and CYP1A2 (Figures 7G,H). D-galactose caused the hepatic CCRP and PP2Ac expression to be downregulated, while the expression of PP2Ac and CYP3A29 in the jejunum was upregulated (Figures 7A,C,D). The expression of PP2Ac and CYP3A29 showed no significant difference in liver though (Figure 7B). These findings imply that the CAR signaling pathway may play a different role in liver and gut antioxidant function impairment following stimulation with PQ or D-galactose.

3.6 Effect of acute and chronic oxidative stress on intestinal flora in weaned piglets

The delicate balance of the intestinal flora is essential for preserving intestinal immunity and overall body homeostasis. Many studies have shown a direct relationship between oxidative stress with intestinal flora. The total amount of intestinal flora was estimated to be 2.5 million tons, with 1.5 million bacteria contributing to the antioxidant effect. To identify the bacteria responsible for the antioxidant function, the V3 + V4 regions of 16S rRNA genes were sequenced in order to conduct a microbiota analysis. An average of 76,022 clean reads were clustered after low-quality sequences were eliminated. Based on 97% similarity level, the high-quality sequences were assigned to operational taxonomic units (OTUs). Community richness was assessed using the Chao 1 index, while the Shannon index was chosen as a composite measure of community diversity. Compared to the CON group, both PQ and D-galactose considerably reduced the Chao 1 and Shannon indexes (Figures 8A,B). We assessed β-diversity using Principal Component Analysis (PCA) in order to better understand the variations in microbial composition between the groups. The results indicate that there were variations in the microbial community structure among the three groups (Figure 8C).

The microbial composition of the group differed at the phylum and genus levels. Both PQ and D-galactose decreased the ratio of *Bacteroidota* while improving the relative richness of *Firmicutes* and *Actinobacteriota* at the phylum level (Figure 8D). At the genus level, the

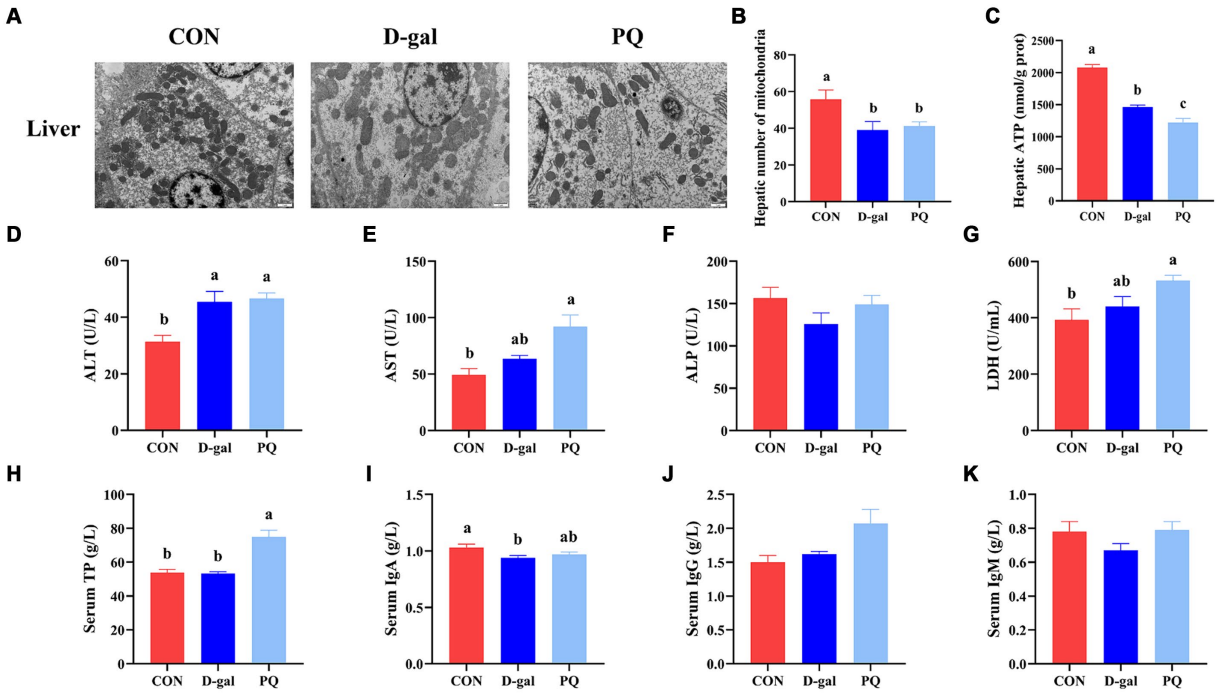

FIGURE 4
Effect of acute and chronic oxidative stress on the gut-liver axis in weaned piglets. **(A)** Liver cells ultrastructure in the liver for different group (×15,000; Scale bars = 1 μm). **(B)** Number of mitochondria in liver cells. **(C)** Level of ATP in liver cells. **(D–K)** The level of ALT, AST, ALP, LDH, TP, IgA, IgG, and IgM in serum. A significant difference ($p < 0.05$) is indicated by different tiny letter superscripts, whereas no significant difference ($p > 0.05$) is indicated by the same or no letter superscripts. The values are given as Mean ± SE, $n = 7$. CON group, control group; D-gal group, D-galactose induced chronic oxidative stress group; PQ group, paraquat induced acute oxidative stress group.

flora composition differed significantly among the three groups (Figure 8E), which is in line with the previous discoveries. We examined the relative richness and found that all 19 genera exhibited significant differences in richness between each pair of the three groups (Figure 8F). *Mogibacterium* and *Denitratisoma* increased in the PQ group, while *Catenisphaera* and *Syntrophococcus* increased in the D-galactose group. *Alloprevotella, Colidextribacter, Ruminococcaceae_Incertae_Sedis, Lachnospira, Lachnospiraceae_ND3007_group, Oscillospira, Prevotella, Prevotella Prevotellaceae_NK3B31_group, Prevotellaceae_UCG_003, Ruminococcus, Schwartzia, [Eubacterium]_xylanophilum_group, unclassified_ Erysipelotrichaceae, unclassified_Lachnospiraceae,* and *unclassified_Prevotellaceae* were decreased in PQ and D-galactose group. We analyzed the association of these groups with the PQ and D-galactose group. In this study, we analyzed the association between these bacteria and oxidative reaction components and inflammatory cytokines (Figure 8G). These findings point to a possible connection between these bacteria and oxidative stress and inflammation. Our findings indicate that a high richness of *Catenisphaera* and *Syntrophococcus,* which increased in the D-galactose group, was associated with lower levels of T-AOC, GSH, ileum GSH/GSSG, SOD and IL-10, and higher level of IL-1β. Additionally, we observed that an increase in the richness of *Mogibacterium* in the PQ group corresponded to lower levels of IgA and serum GSH/GSSG, and higher levels of MDA. On the other hand, *Denitratisoma* tended to increase IL-10 and liver GSH/GSSG. The remaining 15 genera showed opposite effects. These findings suggest that PQ and D-galactose treatment can reduce the diversity and alter the richness of gut flora, leading to imbalances in oxidative and antioxidant processes and inflammatory reactions.

4 Discussion

The gut-liver axis maintains a dynamic balance through the interplay of the intestinal barrier, intestinal flora, and the biological functions of the liver (Ran et al., 2022). The multiple-hit hypothesis proposes that a combination of mechanical, chemical, immunologic, and biologic factors affect the intestinal mucosa. Once the intestinal mucosal barrier is disrupted, intestinal bacteria and their products migrate to the liver, causing a series of immune injuries and inflammatory responses that ultimately lead to liver injury. The intestine is susceptible to damage from ROS due to its exposure to dietary and environmental changes (Hu et al., 2022), as well as its abundance of intrinsically colonized immune cells and intestinal flora, which can produce ROS (Upadhaya and Kim, 2021). Uncontrolled ROS production can directly damage biomolecules and act as a second messenger to activate downstream inflammatory or cell death signaling pathways. Chronic oxidative stress can cause severe redox dysregulation, while acute oxidative stress can easily lead to inflammation and tissue damage. In our study, we used paraquat to generate a model of acute oxidative stress in weaned piglets and utilized D-galactose to create a model of chronic oxidative stress in piglets (Umbayev et al., 2020; Xiao et al., 2022). D-galactose is known to be metabolized to galactitol, which builds up in cells and produces an excess of ROS, causing chronic oxidative stress. The intraperitoneal injection of paraquat is absorbed by the intestinal mesentery and utilizes molecular oxygen within the bloodstream to generate excess ROS, leading to acute oxidative stress. Our data show that piglets given D-galactose displayed lower BW, ADG, and ADFI over a

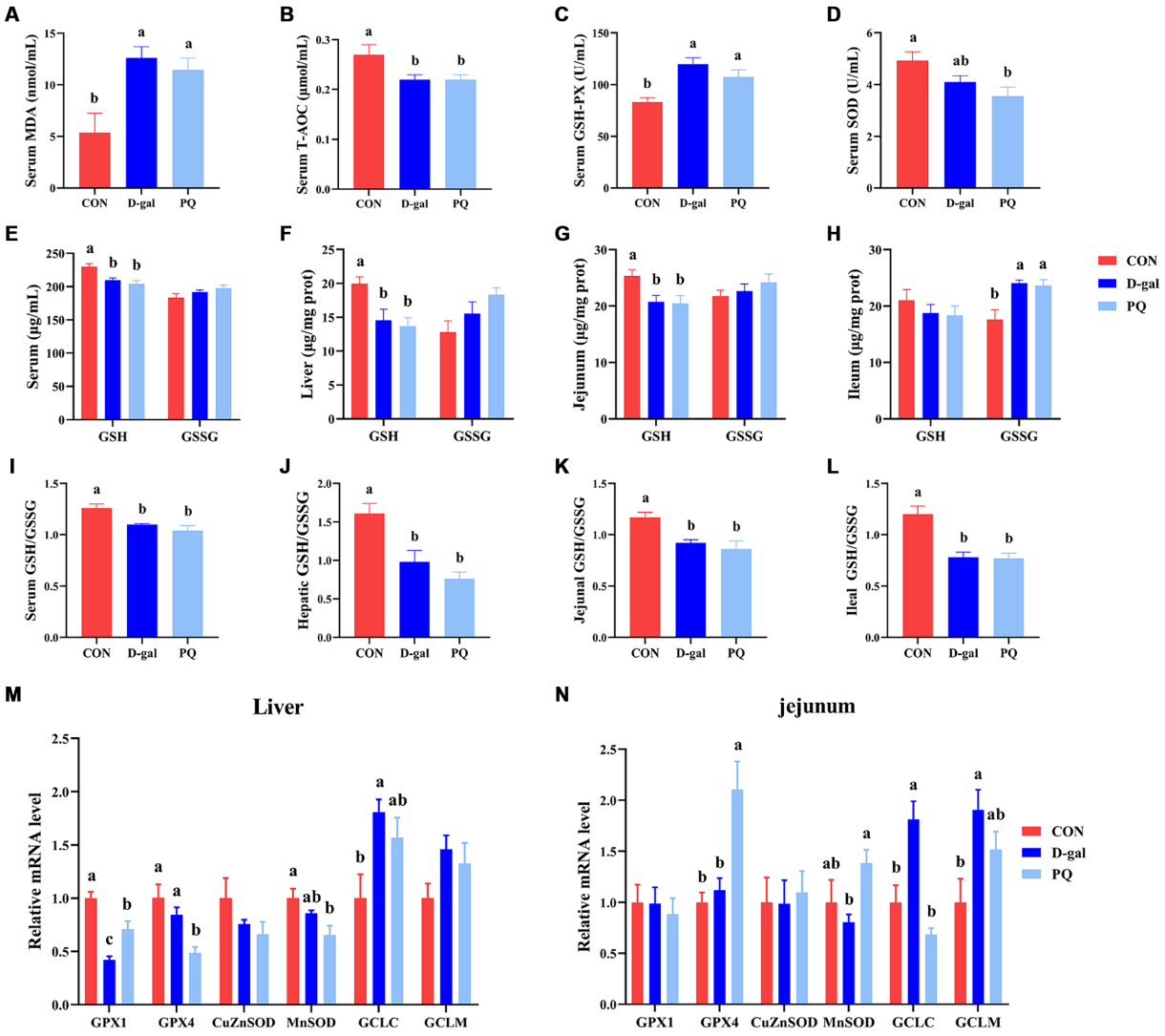

FIGURE 5
Effect of acute and chronic oxidative stress on antioxidant capacity in weaned piglets. **(A–D)** The level of MDA, T-AOC, GSH-PX and SOD in serum. The level of GSH and GSSG in serum **(E)**, liver **(F)**, jejunum **(G)**, and ileum **(H)**. The GSH/GSSG ratio in serum **(I)**, liver **(J)**, jejunum **(K)**, and ileum **(L)**. The relative express of GPX1, GPX4, CuZnSOD, MnSOD, GCLC, and GCLM mRNA in liver **(M)** and jejunum **(N)**. A significant difference ($p < 0.05$) is indicated by different tiny letter superscripts, whereas no significant difference ($p > 0.05$) is indicated by the same or no letter superscripts. The values are given as Mean ± SE, $n = 7$. CON group, control group; D-gal group, D-galactose induced chronic oxidative stress group; PQ group, paraquat induced acute oxidative stress group; MDA, malondialdehyde; T-AOC, total antioxidant capacity; GSH-Px, glutathione peroxidase; SOD, superoxide dismutase; GSH, glutathione; GSSG, oxidized glutathione.

four-week period. Following the paraquat challenge, the ADG was reduced, but no notable variations were observed in BW, ADFI, or diarrhea rate. This suggested that D-galactose induced chronic oxidative stress may cause a more severe impairment of growth potential. These results are consistent with previous reports (Han et al., 2021; Xiang et al., 2022).

The intestine has two primary functions: selective absorption of nutrients and resistance to pathogens and toxins. These functions rely heavily on the intestinal barrier integrity. This study found that acute and chronic oxidative stress decreased the intestinal villus height and V/C ratio in piglets. Higher villi and shallower crypts suggest greater intestinal digestion and absorption, as well as faster cell maturation rates (Ou et al., 2020). This indicates that acute and chronic oxidative stress may impair intestinal absorption function. Oxidative stress damages the tight junctions, microvillus structure, and mitochondrial morphology of ileal epithelial cells. It also increases apoptosis of intestinal epithelial cells and decreases the expression of jejunal tight junction proteins, including Claudin-1, ZO-1, and Occludin. These proteins are critical components of the tight junction structure, which is essential for preserving intestinal permeability (Jiang et al., 2021). In summary, both acute and chronic oxidative stress can cause structural and functional damage to the intestinal tract of weaned piglets. This damage can lead to impaired intestinal barrier function, ultimately affecting piglet growth potential.

Antioxidants help the body defend against the detrimental effects of free radicals, which are continuously produced. Enzymatic and non-enzymatic systems that are comprised of antioxidants are referred to as the antioxidant defense system (Mendonca et al., 2022). GSH-Px,

10.3389/fmicb.2024.1414486

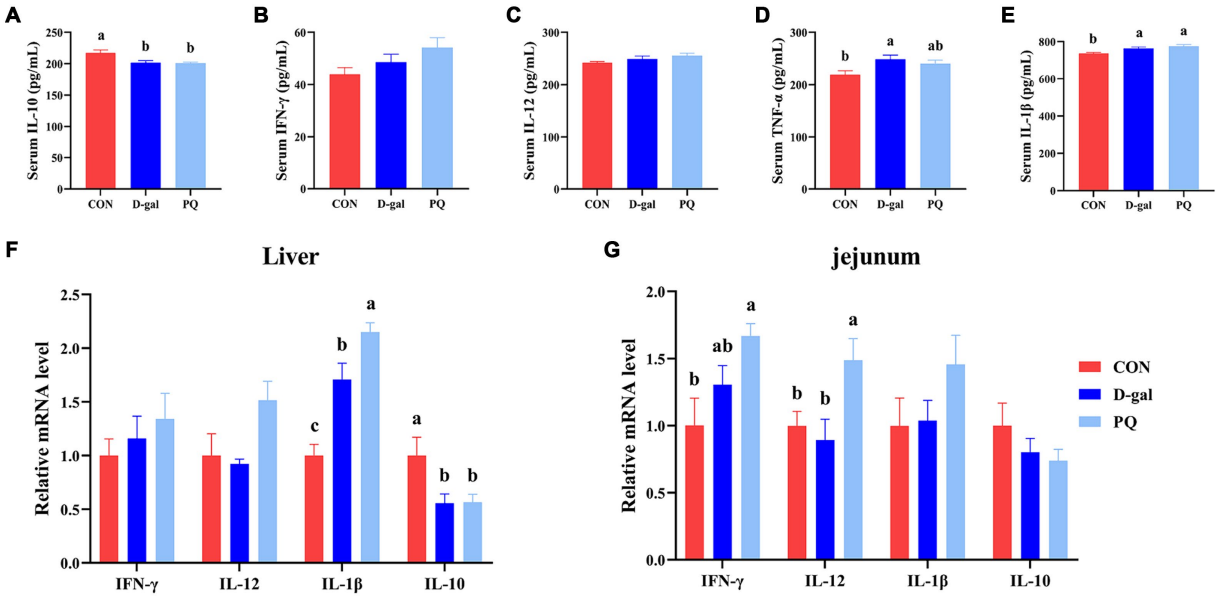

FIGURE 6
Effect of acute and chronic oxidative stress on inflammatory cytokines in weaned piglets. **(A–E)** The level of IL-10, IFN-γ, IL-12, TNF-α, and IL-1β in serum. The relative express of IL-10, IFN-γ, IL-12, TNF-α, and IL-1β mRNA in liver **(F)** and jejunum **(G)**. A significant difference ($p < 0.05$) is indicated by different tiny letter superscripts, whereas no significant difference ($p > 0.05$) is indicated by the same or no letter superscripts. The values are given as Mean ± SE, $n = 7$. CON group, control group; D-gal group, D-galactose induced chronic oxidative stress group; PQ group, paraquat induced acute oxidative stress group.

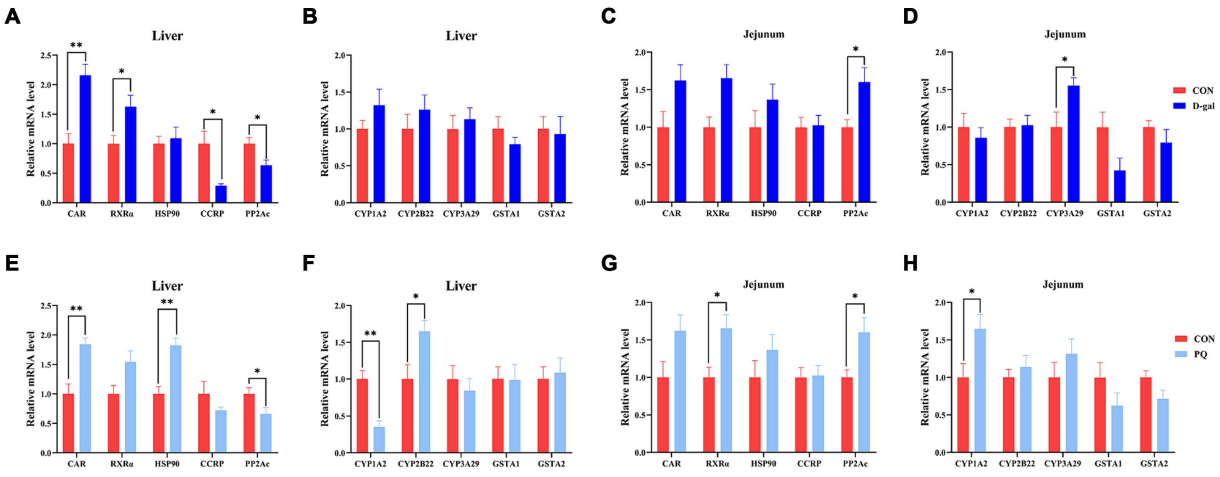

FIGURE 7
Effect of acute and chronic oxidative stress on CAR pathway in weaned piglets. **(A–D)** The relative mRNA expression of CAR, RXRα, HSP0, CCRP, PP2Ac, CYP1A2, CYP2B22, CYP3A29, GSTA1, and GSTA2 in liver and jejunum for CON group and D-gal group. **(E–H)** T The relative mRNA expression of CAR, RXRα, HSP0, CCRP, PP2Ac, CYP1A2, CYP2B22, CYP3A29, GSTA1, and GSTA2 in liver and jejunum for CON group and PQ group. A significant difference ($p < 0.05$) is indicated by different tiny letter superscripts, whereas no significant difference ($p > 0.05$) is indicated by the same or no letter superscripts. The values are given as Mean ± SE, $n = 7$. CON group, control group; D-gal group, D-galactose induced chronic oxidative stress group; PQ group, paraquat induced acute oxidative stress group.

SOD, CAT, and GSH reductase are the main enzymatic antioxidants. Copper, zinc, and selenium are examples of nonenzymatic antioxidant systems that are essential for preventing oxidative stress. Our study found that both acute and chronic oxidative stress can lead to a rise in GSH-Px levels and a reduction in SOD levels in weaned piglets. This, in turn, causes a decrease in the GSH to GSSG ratio and T-AOC of antioxidant indexes and an increase in MDA of oxidized metabolites. The hepatic and jejunal CuZnSOD and MnSOD mRNA expression were reduced after acute and chronic oxidative stress, which coincided with a decrease in serum SOD levels. Glutamate cysteine ligase (GCL) is a rate-limiting enzyme of the cellular antioxidant GSH synthesis. Chronic oxidative stress induced by D-gal upregulated the expression

10.3389/fmicb.2024.1414486

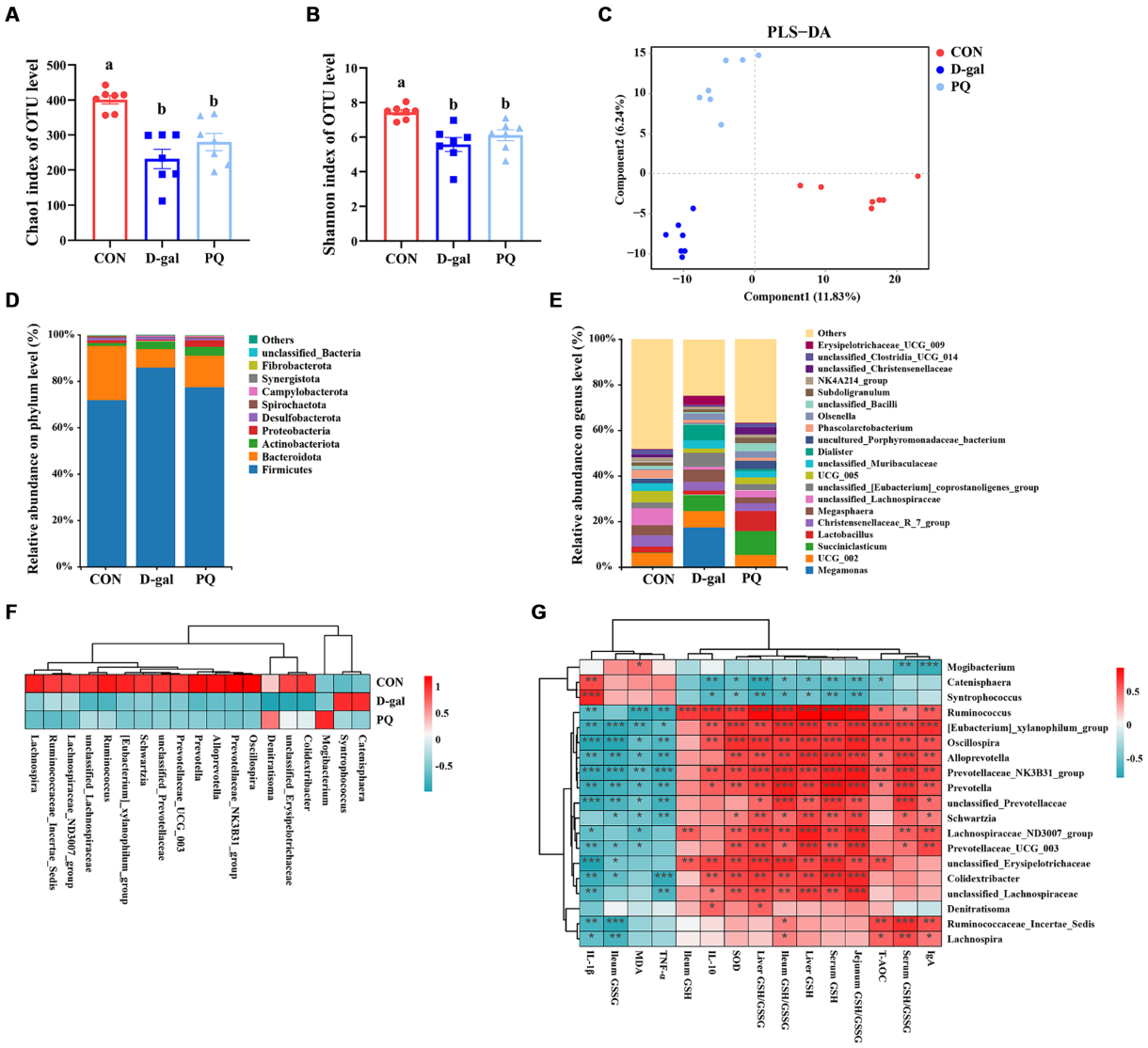

FIGURE 8
Effect of acute and chronic oxidative stress on intestinal flora in weaned piglets. **(A,B)** The Chao 1 index and Shannon index for different group. **(C)** PLS-DA scores plot among the CON group, PQ group, and D-gal group. **(D)** Differences in richness of intestinal flora at the phylum level. **(E)** Differences in richness of intestinal flora at the genus level. **(F)** Heatmap showing the differential richness of intestinal flora among the CON group, PQ group, and D-gal group. **(G)** Correlation analysis of differential flora with indicators of oxidative stress and inflammation. A significant difference ($p < 0.05$) is indicated by different tiny letter superscripts, whereas no significant difference ($p > 0.05$) is indicated by the same or no letter superscripts. The values are given as Mean ± SE, $n = 7$. CON group, control group; D-gal group, D-galactose induced chronic oxidative stress group; PQ group, paraquat induced acute oxidative stress group.

of hepatic and jejunal GCLC and GCLM mRNAs, which are the catalytic and regulatory component of GCL (Lu, 2009). Overall, the antioxidant system is generally decompensated in the D-galactose induced chronic oxidative stress model.

Redox dysregulation in the intestine impairs liver function via the gut-liver axis. Particular markers of liver injury include serum AST, ALP, and ALT. Research has demonstrated that oxidative stress raises AST and ALT levels in the liver and serum in piglets (Zeng et al., 2021). When the liver is injured, the circulatory system receives a rise in AST and ALT concentrations in the serum. The study found that acute and chronic oxidative stress significantly impaired the number and function of mitochondria in hepatocytes. Additionally, serum ALT and AST levels were elevated, while ALP levels showed no statistically significant difference. Liver injury was observed in weaned piglets in both acute and chronic oxidative stress situations. However, statistically significant elevations in LDH and TP levels were observed only in the PQ-induced acute stress model. The heavier diarrhea in the acute model may have caused a short-term decrease in blood volume, which is consistent with the weight loss observed in the acutely stressed piglet group. Additionally, oxidative stress is connected to inflammatory reactions (Tian et al., 2023). Inflammatory processes could be induced by oxidative stress injury, and pro-inflammatory factors increase the production of ROS and RNS (Zong et al., 2023). The

results showed that both acute and chronic oxidative stress can induce inflammation. During acute oxidative stress, the pro-inflammatory factors IL-1β and IFN-γ were upregulated, while the expression of the anti-inflammatory factor IL-10 was inhibited. Chronic oxidative stress additionally led to increased expression of TNF-α. Besides, the PQ group exhibited greater amounts of IL-1β, IL-12, and IFN-γ in contrast to the D-gal group. Both the liver and the jejunum showed a similar trend in inflammatory cytokine levels. The results indicate that acute and chronic oxidative stress cause local destruction of biomolecules and cellular structures, as well as changes in some physiological indicators in the intestine. Furthermore, they cause liver injury and systemic inflammation through the gut-liver axis. Combined with the previous results, it is evident that acute oxidative stress increases the risk of inflammation and liver damage, while chronic oxidative stress causes more severe antioxidant malfunction. This suggests that the molecular mechanisms involved in acute and chronic oxidative stress may differ.

We examined the expression of the CAR signaling pathway to better understand this mechanism. In a physical state, cytoplasmic CAR retention protein (CCRP) binds to HSP70/90 to hold CAR in the cytoplasm, creating the CAR-CCRP-HSP70/90 complex. CAR is translocated to the nucleus after being dephosphorylated by protein phosphatase 2A (PP2A). After that, it forms a heterodimer by binding to RXRα. This heterodimer modifies the activity of downstream target genes to regulate immunological and metabolic functions (Kobayashi et al., 2003). The results show that PQ or D-galactose treatment activated the CAR signaling pathway in both the jejunum and the liver tissues. The mRNA expression of CAR, RXRα, and HSP90 tended to increase, while the expression of PP2Ac increased in the jejunum tissues and decreased in the liver tissues, resulting in differences in the expression of downstream target genes of CAR. This is in line with the results of previous report (Tang et al., 2024), which found that oxidative stress induced by phosphorylates CAR, prevents the CAR-CCRP-HSP90 complex from forming, promotes CAR translocate to nucleus, and binds with RXRa, all of which control downstream target gene expression and hasten CAR activation. In summary, both PQ and D-galactose treatments can activate the CAR signaling pathway, leading to oxidative stress. However, there are differences, and even opposite trends, in the expression of CAR signaling pathway components between acute and chronic oxidative stress, as well as between the intestine and liver. These findings demonstrate differences in the expression of molecules involved in the CAR pathway under acute and chronic oxidative stress. Further studies may be necessary to explore additional mechanistic differences.

The intestinal tract possesses natural properties such as anaerobic, rich nutrition, appropriate temperature and PH, making it an excellent environment for microbial survival and hosting a large number of microorganisms (Zhou et al., 2020). These microorganisms form a complex biological system, also known as intestinal flora, whose diversity exerts a significant influence on the development of the disease (Xing et al., 2024).It is susceptible to attack by oxygen radicals under oxidative stress due to its active energy metabolism (Sebastián Domingo and Sánchez Sánchez, 2018). The relationship between gut flora and the host has drawn more and more attention from researchers in recent years. According to our study, the intestinal flora in weaned piglets significantly declined in the diversity and composition after PQ or D-galactose challenge. This suggests that the balance of intestinal flora can be disrupted by both acute and chronic oxidative stress. We also saw notable alterations in the microbial community structure. The study found that the PQ group experienced an enrichment of *Mogibacterium* and *Denitratisoma*, while the D-galactose intervention group experienced an enrichment of *Catenisphaera* and *Syntrophococcus.* Both intervention groups showed a downgrade of *Alloprevotella, Colidextribacter, Ruminococcaceae_Incertae_Sedis, Lachnospira, Lachnospiraceae_ND3007_group, Oscillospira, Prevotella, Prevotellaceae_NK3B31_group, Prevotellaceae_UCG_003, Ruminococcus, Schwartzia, [Eubacterium]_xylanophilum_group, unclassified_Erysipelotrichaceae, unclassified_Lachnospiraceae,* and *unclassified_Prevotellaceae. Mogibacterium* and *Denitratisoma* have been identified as potential causative agents of gingival disease (Liu et al., 2023; Wu et al., 2023). *Mogibacterium* is also associated with intermaxillary gap infections (Sun et al., 2022). *Denitratisoma* is involved in denitrification and are used in sewage treatment (Wang et al., 2023), but their role in the gut requires further investigation. *Catenisphaera* and *Syntrophococcus* are typically associated with the synthesis of short-chain fatty acids and gut protection (Horvath et al., 2020; Yang et al., 2022). However, they were enriched in the D-galactose group. It is hypothesized that this may be due to a specific competitive advantage in this animal model or the disruption of intestinal homeostasis under certain conditions. *Alloprevotella, Colidextribacter, Lachnospira*, and *Lachnospiraceae_ND3007_group* are associated with anti-inflammation and lipid metabolism (Leibovitzh et al., 2022; Xie et al., 2022; Hou et al., 2023). They are involved in combating oxidative stress and are often considered probiotic. *Oscillospira* is seen as a possible next-generation probiotic, a sign of intestinal health, and a producer of short-chain fatty acids (Yang et al., 2021). The *unclassified Erysipelotrichaceae* family is involved in lipid metabolism and promotes piglet weight gain (Tang et al., 2024). The role of *Prevotella*, *Ruminococcus,* and *Schwartzia*is debated and may be related to different strain. The *Eubacterium xylanophilum* group is typically regarded as a harmful bacterium and has been linked to metabolic diseases and colon cancer (Li et al., 2020; Li H. et al., 2022). The divergent microorganisms upregulated by PQ or D-galactose treatment were strongly correlated with inflammation and oxidative stress, according to subsequent correlational analyses. Conversely, negative correlations were observed for these downregulated microbes. These findings imply that, in weaned pigs under oxidative stress, alterations in the microbe composition can be connected to antioxidant decompensation and inflammatory responses.

Despite the extensive use of the acute and chronic oxidative stress piglet model, there are still some limitations to be considered. The construction of an acute oxidative stress model necessitates the use of paraquat, which is banned in numerous countries and difficult to obtain. Consequently, paraquat administration inevitably causes lung damage and renders the model distinct from the actual pathological state. Furthermore, the construction of a chronic oxidative stress model is more resource-intensive in terms of personnel, material resources, and time. Finally, the intestinal molecular mechanisms involved in acute and chronic oxidative stress modeling remain incompletely understood.

In summary, the two types of oxidative stress can systematically damage the growth performance, antioxidant capacity, inflammation response of weaned piglets, while D-galactose as chronic stress can cause severe redox dysregulation, paraquat as acute stress can easily lead to inflammation and liver damage. Furthermore, chronic or acute oxidative stress can disrupt the dynamic balance of intestinal flora, reducing their diversity and composition. However, the structure of microbes in acute and chronic oxidative stress models differs, indicating that the pathological states or molecular pathways involved in these two models may vary, so further studies are needed to understand the mechanism by gut-liver axis and gut microbiota. These results provide valuable insights and direction for future work exploring the relationship oxidative stress and their associated pathologies.

Data availability statement

The datasets presented in this study can be found in the Genome Sequence Archive (GSA), https://bigd.big.ac.cn/gsa/browse/CRA015743, under accession numbers CRA015743 and CRA015743.

Ethics statement

The animal study was approved by Animal Welfare Committee of the Institute of Subtropical Agriculture, Chinese Academy of Sciences. The study was conducted in accordance with the local legislation and institutional requirements.

Author contributions

HZ: Data curation, Formal analysis, Investigation, Methodology, Visualization, Writing – original draft, Writing – review & editing. XuaX: Formal analysis, Investigation, Methodology, Visualization, Writing – original draft, Data curation. CW: Investigation, Methodology, Writing – original draft. TL: Conceptualization, Project administration, Resources, Supervision, Validation, Writing – review & editing. XupX: Project administration, Resources, Supervision, Validation, Writing – review & editing. LH: Conceptualization, Formal analysis, Funding acquisition, Project administration, Resources, Supervision, Validation, Visualization, Writing – review & editing, Data curation.

Funding

The author(s) declare that financial support was received for the research, authorship, and/or publication of this article. This work was supported by the Postdoctoral Research Funding (20220615-1002), the Natural Science Foundation of China (32172755, 3210099, U23A20233), the science and technology innovation Program of Hunan Province (2023RC1054), Hunan Key Research and Development Plan (2022NK2023).

Conflict of interest

The authors declare that the research was conducted in the absence of any commercial or financial relationships that could be construed as a potential conflict of interest.

Publisher's note

References

Feng, Y., An, Z., Chen, H., He, X., Wang, W., Li, X., et al. (2020). Ulva prolifera extract alleviates intestinal oxidative stress via Nrf2 signaling in weaned piglets challenged with hydrogen peroxide. *Front. Immunol.* 11:599735. doi: 10.3389/fimmu.2020.599735

Forman, H. J., and Zhang, H. (2021). Targeting oxidative stress in disease: promise and limitations of antioxidant therapy. *Nat. Rev. Drug Discov.* 20, 689–709. doi: 10.1038/s41573-021-00233-1

Hajam, Y. A., Rani, R., Ganie, S. Y., Sheikh, T. A., Javaid, D., Qadri, S. S., et al. (2022). Oxidative stress in human pathology and aging: molecular mechanisms and perspectives. *Cells* 11:552. doi: 10.3390/cells11030552

Han, H., Liu, Z., Yin, J., Gao, J., He, L., Wang, C., et al. (2021). D-galactose induces chronic oxidative stress and alters gut microbiota in weaned piglets. *Front. Physiol.* 12:634283. doi: 10.3389/fphys.2021.634283

He, L., Huang, N., Li, H., Tian, J., Zhou, X., Li, T., et al. (2017). AMPK/alpha-ketoglutarate Axis regulates intestinal water and ion homeostasis in young pigs. *J. Agric. Food Chem.* 65, 2287–2298. doi: 10.1021/acs.jafc.7b00324

He, L., Zhou, X., Wu, Z., Feng, Y., Liu, D., Li, T., et al. (2022). Glutamine in suppression of lipopolysaccharide-induced piglet intestinal inflammation: the crosstalk between AMPK activation and mitochondrial function. *Anim. Nutr.* 10, 137–147. doi: 10.1016/j.aninu.2022.03.001

Horvath, A., Durdevic, M., Leber, B., di Vora, K., Rainer, F., Krones, E., et al. (2020). Changes in the intestinal microbiome during a multispecies probiotic intervention in compensated cirrhosis. *Nutrients* 12:1874. doi: 10.3390/nu12061874

Hou, Q., Huang, J., Zhao, L., Pan, X., Liao, C., Jiang, Q., et al. (2023). Dietary genistein increases microbiota-derived short chain fatty acid levels, modulates homeostasis of the aging gut, and extends healthspan and lifespan. *Pharmacol. Res.* 188:106676. doi: 10.1016/j.phrs.2023.106676

Hu, X., He, X., Peng, C., He, Y., Wang, C., Tang, W., et al. (2022). Improvement of ulcerative colitis by aspartate via RIPK pathway modulation and gut microbiota composition in mice. *Nutrients* 14:707. doi: 10.3390/nu14183707

Jiang, Y., Song, J., Xu, Y., Liu, C., Qian, W., Bai, T., et al. (2021). Piezo 1 regulates intestinal epithelial function by affecting the tight junction protein claudin-1 via the ROCK pathway. *Life Sci.* 275:119254. doi: 10.1016/j.lfs.2021.119254

Kobayashi, K., Sueyoshi, T., Inoue, K., Moore, R., and Negishi, M. (2003). Cytoplasmic accumulation of the nuclear receptor CAR by a tetratricopeptide repeat protein in HepG2 cells. *Mol. Pharmacol.* 64, 1069–1075. doi: 10.1124/mol.64.5.1069

Krawczyk, M., Maciejewska, D., Ryterska, K., Czerwinka-Rogowska, M., Jamiol-Milc, D., Skonieczna-Zydecka, K., et al. (2018). Gut permeability might be improved by dietary Fiber in individuals with nonalcoholic fatty liver disease (NAFLD) undergoing weight reduction. *Nutrients* 10:1793. doi: 10.3390/nu10111793

Leibovitzh, H., Lee, S. H., Xue, M., Raygoza Garay, J. A., Hernandez-Rocha, C., Madsen, K. L., et al. (2022). Altered gut microbiome composition and function are associated with gut barrier dysfunction in healthy relatives of patients with Crohn's disease. *Gastroenterology* 163, 1364–1376.e10. doi: 10.1053/j.gastro.2022.07.004

Li, H., Liu, F., Lu, J., Shi, J., Guan, J., Yan, F., et al. (2020). Probiotic mixture of *Lactobacillus plantarum* strains improves lipid metabolism and gut microbiota structure in high fat diet-fed mice. *Front. Microbiol.* 11:512. doi: 10.3389/fmicb.2020.00512

Li, H., Wang, Y., Shao, S., Yu, H., Wang, D., Li, C., et al. (2022). Rabdosia Serra alleviates dextran sulfate sodium salt-induced colitis in mice through anti-inflammation, regulating Th17/Treg balance, maintaining intestinal barrier integrity, and modulating gut microbiota. *J. Pharm. Anal.* 12, 824–838. doi: 10.1016/j.jpha.2022.08.001

Li, X., Zhu, J., Lin, Q., Yu, M., Lu, J., Feng, J., et al. (2022). Effects of curcumin on mitochondrial function, endoplasmic reticulum stress, and mitochondria-associated endoplasmic reticulum membranes in the jejunum of oxidative stress piglets. *J. Agric. Food Chem.* 70, 8974–8985. doi: 10.1021/acs.jafc.2c02824

Liu, L., Liang, L., Yang, C., Zhou, Y., and Chen, Y. (2021). Extracellular vesicles of *Fusobacterium nucleatum* compromise intestinal barrier through targeting RIPK1-mediated cell death pathway. *Gut Microbes* 13, 1–20. doi: 10.1080/19490976.2021.1902718

Liu, S., Xie, G., Chen, M., He, Y., Yu, W., Chen, X., et al. (2023). Oral microbial dysbiosis in patients with periodontitis and chronic obstructive pulmonary disease. *Front. Cell. Infect. Microbiol.* 13:1121399. doi: 10.3389/fcimb.2023.1121399

Liu, H., and Zhang, J. (2012). Cerebral hypoperfusion and cognitive impairment: the pathogenic role of vascular oxidative stress. *Int. J. Neurosci.* 122, 494–499. doi: 10.3109/00207454.2012.686543

Lu, S. C. (2009). Regulation of glutathione synthesis. *Mol. Asp. Med.* 30, 42–59. doi: 10.1016/j.mam.2008.05.005

Members, B. I. G. D. C. (2018). Database resources of the BIG data center in 2018. *Nucleic Acids Res.* 46, D14–D20. doi: 10.1093/nar/gkx897

Mendonca, J. D. S., Guimaraes, R. C. A., Zorgetto-Pinheiro, V. A., Fernandes, C. D. P., Marcelino, G., Bogo, D., et al. (2022). Natural antioxidant evaluation: a review of detection methods. *Molecules* 27:3563. doi: 10.3390/molecules27113563

Ou, J., Courtney, C. M., Steinberger, A. E., Tecos, M. E., and Warner, B. W. (2020). Nutrition in necrotizing enterocolitis and following intestinal resection. *Nutrients* 12:520. doi: 10.3390/nu12020520

Petrov, M. S. (2010). Therapeutic implications of oxidative stress in acute and chronic pancreatitis. *Curr. Opin. Clin. Nutr. Metab. Care* 13, 562–568. doi: 10.1097/MCO.0b013e32833b64b9

Rainer, F., Horvath, A., Sandahl, T. D., Leber, B., Schmerboeck, B., Blesl, A., et al. (2018). Soluble CD163 and soluble mannose receptor predict survival and decompensation in patients with liver cirrhosis, and correlate with gut permeability and bacterial translocation. *Aliment. Pharmacol. Ther.* 47, 657–664. doi: 10.1111/apt.14474

Ran, X., Hu, G., He, F., Li, K., Li, F., Xu, D., et al. (2022). Phytic acid improves hepatic steatosis, inflammation, and oxidative stress in high-fat diet (HFD)-fed mice by modulating the gut-liver Axis. *J. Agric. Food Chem.* 70, 11401–11411. doi: 10.1021/acs.jafc.2c04406

Sebastián Domingo, J. J., and Sánchez Sánchez, C. (2018). From the intestinal flora to the microbiome. *Rev. Esp. Enferm. Dig.* 110, 51–56. doi: 10.17235/reed.2017.4947/2017

Sha, J. Y., Li, J. H., Zhou, Y. D., Yang, J. Y., Liu, W., Jiang, S., et al. (2021). The p53/p21/p16 and PI3K/Akt signaling pathways are involved in the ameliorative effects of maltol on D-galactose-induced liver and kidney aging and injury. *Phytother. Res.* 35, 4411–4424. doi: 10.1002/ptr.7142

Sun, Q., Li, Z., Wang, P., Zhao, J., Chen, S., and Sun, M. (2022). Unveiling the pathogenic Bacteria causing descending necrotizing Mediastinitis. *Front. Cell. Infect. Microbiol.* 12:873161. doi: 10.3389/fcimb.2022.873161

Sun, W., Zhu, J., Qin, G., Huang, Y., Cheng, S., Chen, Z., et al. (2023). *Lonicera japonica* polysaccharides alleviate D-galactose-induced oxidative stress and restore gut microbiota in ICR mice. *Int. J. Biol. Macromol.* 245:125517. doi: 10.1016/j.ijbiomac.2023.125517

Tang, W., Xiang, X., Wang, H., Zhou, W., He, L., Yin, Y., et al. (2024). Zinc lactate alleviates oxidative stress by modulating crosstalk between constitutive androstane receptor signaling pathway and gut microbiota profile in weaned piglets. *Anim. Nutr.* 16, 23–33. doi: 10.1016/j.aninu.2023.10.001

Tian, X., Li, D., Zhao, X., Xiao, Z., Sun, J., Yuan, T., et al. (2023). Dietary grape pomace extract supplementation improved meat quality, antioxidant capacity, and immune performance in finishing pigs. *Front. Microbiol.* 14:1116022. doi: 10.3389/fmicb.2023.1116022

Tilg, H., Adolph, T. E., and Trauner, M. (2022). Gut-liver axis: pathophysiological concepts and clinical implications. *Cell Metab.* 34, 1700–1718. doi: 10.1016/j.cmet.2022.09.017

Umbayev, B., Askarova, S., Almabayeva, A., Saliev, T., Masoud, A. R., and Bulanin, D. (2020). Galactose-induced skin aging: the role of oxidative stress. *Oxidative Med. Cell. Longev.* 2020, 7145656–7145615. doi: 10.1155/2020/7145656

Upadhaya, S. D., and Kim, I. H. (2021). The impact of weaning stress on gut health and the mechanistic aspects of several feed additives contributing to improved gut health function in weanling piglets-a review. *Animals (Basel)* 11:2418. doi: 10.3390/ani11082418

Wang, Q., Lin, Y., Peng, L., Wang, Y., Ma, S., Ren, H., et al. (2023). Weak magnetic field enhances waste molasses-driven denitrification during wastewater treatment. *Bioresour. Technol.* 387:129697. doi: 10.1016/j.biortech.2023.129697

Ward, P. A. (2010). Oxidative stress: acute and progressive lung injury. *Ann. N. Y. Acad. Sci.* 1203, 53–59. doi: 10.1111/j.1749-6632.2010.05552.x

Wu, L., Ma, B., Yu, F., Ma, Z., Meng, Q., Li, Z., et al. (2023). Salivary microbiome diversity in Chinese children with various caries states. *Clin. Oral Investig.* 27, 773–785. doi: 10.1007/s00784-022-04825-y

Xiang, X., Wang, H., Zhou, W., Wang, C., Guan, P., Xu, G., et al. (2022). Glutathione protects against Paraquat-induced oxidative stress by regulating intestinal barrier, antioxidant capacity, and CAR signaling pathway in weaned piglets. *Nutrients* 15:198. doi: 10.3390/nu15010198

Xiao, Y., Huang, R., Wang, N., Deng, Y., Tan, B., Yin, Y., et al. (2022). Ellagic acid alleviates oxidative stress by mediating Nrf2 signaling pathways and protects against Paraquat-induced intestinal injury in piglets. *Antioxidants (Basel)* 11:252. doi: 10.3390/antiox11020252

Xie, Q., Li, H., Ma, R., Ren, M., Li, Y., Li, J., et al. (2022). Effect of Coptis chinensis franch and Magnolia officinalis on intestinal flora and intestinal barrier in a TNBS-induced ulcerative colitis rats model. *Phytomedicine* 97:153927. doi: 10.1016/j.phymed.2022.153927

Xing, J. H., Niu, T. M., Zou, B. S., Yang, G. L., Shi, C. W., Yan, Q. S., et al. (2024). Gut microbiota-derived LCA mediates the protective effect of PEDV infection in piglets. *Microbiome* 12:20. doi: 10.1186/s40168-023-01734-4

Yang, Y., Jiang, X., Cai, X., Zhang, L., Li, W., Che, L., et al. (2022). Deprivation of dietary Fiber enhances susceptibility of piglets to lung immune stress. *Front. Nutr.* 9:827509. doi: 10.3389/fnut.2022.827509

Yang, J., Li, Y., Wen, Z., Liu, W., Meng, L., and Huang, H. (2021). Oscillospira – a candidate for the next-generation probiotics. *Gut Microbes* 13:1987783. doi: 10.1080/19490976.2021.1987783

Younossi, Z. M., Blissett, D., Blissett, R., Henry, L., Stepanova, M., Younossi, Y., et al. (2016). The economic and clinical burden of nonalcoholic fatty liver disease in the United States and Europe. *Hepatology* 64, 1577–1586. doi: 10.1002/hep.28785

Zeng, X., Liu, R., Li, Y., Li, J., Zhao, Q., Li, X., et al. (2021). Excessive ammonia inhalation causes liver damage and dysfunction by altering gene networks associated with oxidative stress and immune function. *Ecotoxicol. Environ. Saf.* 217:112203. doi: 10.1016/j.ecoenv.2021.112203

Zhou, B., Yuan, Y., Zhang, S., Guo, C., Li, X., Li, G., et al. (2020). Intestinal Flora and Disease mutually shape the regional immune system in the intestinal tract. *Front. Immunol.* 11:575. doi: 10.3389/fimmu.2020.00575

Zong, Q., Li, K., Qu, H., Hu, P., Xu, C., Wang, H., et al. (2023). Sodium butyrate ameliorates Deoxynivalenol-induced oxidative stress and inflammation in the porcine liver via NR4A2-mediated histone acetylation. *J. Agric. Food Chem.* 71, 10427–10437. doi: 10.1021/acs.jafc.3c02499

Glossary

ROS	Reactive oxygen species
BW	Body weight
ADFI	Average daily feed intake
ADG	Average daily gain
FCR	Feed conversion ratio
DR	Diarrhea rate
TP	Total protein
IgG	Immunoglobulin G
IgM	Immunoglobulin M
ALT	Alanine aminotransferase
AST	Aspartate aminotransferase
ALP	Alkaline phosphatase
LDH	Lactate dehydrogenase
MDA	Malondialdehyde
SOD	Superoxide dismutase
T-AOC	Total antioxidant capacity
CAT	Catalase
GSH	Glutathione
GSH-Px	Glutathione peroxidase
GSSG	Oxidized glutathione
IgA	Immunoglobulin A
L-1β	Interleukin 1-β
IL-10	Interleukin-10
IL-12	Interleukin-12
TNF-α	Tumor necrosis factor-α
IFN-γ	Interferon-γ
iFABP	Intestinal fatty acid binding protein
DAO	Diamine oxidase
ATP	Adenosine triphosphate
V/C	Villus height to crypt depth ratio
CAR	Constitutive androstane receptor
OTUs	Operational taxonomic units
GCL	Glutamate cysteine ligase
CCRP	Cytoplasmic CAR retention protein
PP2A	Protein phosphatase 2A

frontiers | Frontiers in Microbiology

TYPE Original Research
PUBLISHED 19 June 2024
DOI 10.3389/fmicb.2024.1422172

OPEN ACCESS

EDITED BY
Gabriele Brecchia,
University of Milan, Italy

REVIEWED BY
Yuying Li,
Chinese Academy of Agricultural Sciences (CAAS), China
Yu Bai,
Tianjin University of Science and Technology, China

*CORRESPONDENCE
Qinghua He
✉ qinghua.he@szu.edu.cn
Xiangfeng Kong
✉ nnkxf@isa.ac.cn

RECEIVED 23 April 2024
ACCEPTED 27 May 2024
PUBLISHED 19 June 2024

CITATION
Li Z, Qin B, Chen T, Kong X, Zhu Q, Azad MAK, Cui Y, Lan W and He Q (2024) Fermented *Aronia melanocarpa* pomace improves the nutritive value of eggs, enhances ovarian function, and reshapes microbiota abundance in aged laying hens.
Front. Microbiol. 15:1422172.
doi: 10.3389/fmicb.2024.1422172

Fermented *Aronia melanocarpa* pomace improves the nutritive value of eggs, enhances ovarian function, and reshapes microbiota abundance in aged laying hens

Zhihua Li[1,2], Binghua Qin[2], Ting Chen[2], Xiangfeng Kong[2]*, Qian Zhu[2], Md. Abul Kalam Azad[2], Yadong Cui[3], Wei Lan[3] and Qinghua He[1]*

[1]Department of Food Science and Engineering, College of Chemistry and Environmental Engineering, Shenzhen University, Shenzhen, China, [2]Hunan Provincial Key Laboratory of Animal Nutritional Physiology and Metabolic Process, National Engineering Laboratory for Pollution Control and Waste Utilization in Livestock and Poultry Production, Institute of Subtropical Agriculture, Chinese Academy of Sciences, Changsha, China, [3]School of Biology and Food Engineering, Fuyang Normal University, Fuyang, China

Introduction: There is a decline in the quality and nutritive value of eggs in aged laying hens. Fruit pomaces with high nutritional and functional values have gained interest in poultry production to improve the performance.

Methods: The performance, egg nutritive value, lipid metabolism, ovarian health, and cecal microbiota abundance were evaluated in aged laying hens (320 laying hens, 345-day-old) fed on a basal diet (control), and a basal diet inclusion of 0.25%, 0.5%, or 1.0% fermented *Aronia melanocarpa* pomace (FAMP) for eight weeks.

Results: The results show that 0.5% FAMP reduced the saturated fatty acids (such as C16:0) and improved the healthy lipid indices in egg yolks by decreasing the atherogenicity index, thrombogenic index, and hypocholesterolemia/hypercholesterolemia ratio and increasing health promotion index and desirable fatty acids ($P < 0.05$). Additionally, FAMP supplementation (0.25%–1.0%) increased ($P < 0.05$) the ovarian follicle-stimulating hormone, luteinizing hormone, and estrogen 2 levels, while 1.0% FAMP upregulated the *HSD3B1* expression. The expression of *VTG II* and *ApoVLDL II* in the 0.25% and 0.5% FAMP groups, *APOB* in the 0.5% FAMP group, and *ESR2* in the 1% FAMP group were upregulated ($P < 0.05$) in the liver. The ovarian total antioxidant capacity was increased ($P < 0.05$) by supplementation with 0.25%–1.0% FAMP. Dietary 0.5% and 1.0% FAMP downregulated ($P < 0.05$) the *Keap1* expression, while 1.0% FAMP upregulated ($P < 0.05$) the *Nrf2* expression in the ovary. Furthermore, 1.0% FAMP increased cecal acetate, butyrate, and valerate concentrations and Firmicutes while decreasing Proteobacteria ($P < 0.05$).

Conclusion: Overall, FAMP improved the nutritive value of eggs in aged laying hens by improving the liver–blood–ovary function and cecal microbial and metabolite composition, which might help to enhance economic benefits.

KEYWORDS

aged laying hens, nutritive value, fermented *Aronia melanocarpa* pomace, ovarian function, microbiota

1 Introduction

Eggs are excellent sources of nutrients, such as proteins, lipids, and micronutrients, which are highly beneficial to the physical health of humans (Kovacs-Nolan et al., 2005). However, laying hens are afflicted by a series of physiological health complications, resulting in a decline in their egg-laying performance and egg quality with age. Lipid precursor substances in egg yolk are mainly derived from the liver. The yolk formation and deposition of laying hens are largely determined by the multifunction of the liver–blood–ovary (LBO) axis, including lipid metabolism and hormone regulations of various forms (Wu et al., 2023). The recession activities of the liver and ovary in aged laying hens arise from endocrine disorders and decrease in antioxidant capacity and follicle formation (Gu et al., 2021; Wu et al., 2023). Ovarian dysfunction in laying hens results in the decline of egg-laying performance and quality of eggs, for which decrease in antioxidant capacity is one of the main reasons (Bao et al., 2022). Moreover, modulation of gut microbiota is a prospective approach to alleviating the common problems of aged laying hens, such as the decline in the quality and nutritive value of eggs (Feng et al., 2021; Dai et al., 2022). Hence, strengthening the LBO and gut functions in aged laying hens can contribute to improving their egg-laying performance and quality.

Recently, numerous natural plants or their extracts have been employed as feed additives to promote the production of eggs in aged laying hens. *Aronia melanocarpa*, known as black chokeberry, originated from North America and spread to European and other regions, especially in Poland, with a yearly yield of 14,000–15,000 tons of fresh fruits (Jurikova et al., 2017) and 600–700 tons in China (Ren et al., 2022). It is mainly industrially processed as different food products, such as juice, jams, and dietary supplements for humans (Sidor and Gramza-Michalowska, 2019). After production and processing, it produces large amounts of pomace. *Aronia melanocarpa* pomace (AMP) contains phenolic phytochemicals, dietary fiber, free glucose, fructose, and other bioactive substances (Schmid et al., 2020). It has been reported that AMP can serve as a feed additive to increase production in animals (Lipinska et al., 2017; Ren et al., 2022). AMP contains a relatively high content of fiber. Meanwhile, avians lack enzymes that degrade non-starch polysaccharides, which may affect the adequate absorption of AMP (Erinle and Adewole, 2022). Microbial fermentation helps to enhance the nutritional quality of agricultural by-products as alternative feed ingredients (Cui et al., 2023) and increases the content and bioavailability of dietary polyphenols (Du and Myracle, 2018; Esatbeyoglu et al., 2023). Fermentation of AMP may improve its nutritive value by decreasing fruit wastes generated in the food industry and feed costs in animal husbandry, which is environmentally friendly and economical. However, studies regarding the influence of the fermented AMP (FAMP) on the production performance, quality and nutritive value of eggs in aged laying hens, and the potential mechanisms of FAMP's action remain unclear. Hence, this study explored the effects of the addition of FAMP to aged laying hens' diet on the production performance, quality and nutritive value of eggs, ovarian function, and cecal microbiota and metabolite composition, which might lay the theoretical foundation for improving the nutritive value of eggs due to the FAMP additive.

2 Materials and methods

2.1 Fermentation of *Aronia melanocarpa* pomace

Dried and cleaned AMP was obtained from Fuyang Fruit Wine Engineering Technology Center (Fuyang, China). FAMP was prepared according to the following procedure. A compound starter culture was prepared to ferment the raw material (AMP). The compound starter culture was composed of a microbial agent mixture, enzyme, medium 1, medium 2, and sucrose at a mass ratio of 1:1:1:1:1. Among them, the microbial agent mixture (Guangdong Microbial Culture Collection Center, Guangzhou, China) contained *Bacillus subtilis* GDMCC 1.372, *Bacillus licheniensis* GDMCC 1.182, *Lactobacillus plantarum* GDMCC 1.648, and *Rhodotorula benthica* GDMCC 2.215 at a mass ratio of 1:1:1:1. The active enzyme was a mixture of cellulase and papain at a mass ratio of 1:1. Medium 1 consisted of cultivated ginseng leaves, which were dried and crushed to a 40-mesh powder. Medium 2 was soybean flour. The above compound starter culture and AMP were blended at a mass ratio of 1:100. The fermentation conditions were as follows: fermentation temperature, 75°C; dissolved oxygen, 3–10%; moisture content, 30–80%; and fermentation method, solid fermentation. The measured nutrient levels (%; dry matter basis) of FAMP were as follows: ash, 5.20; crude protein, 10.63; ether extract, 4.80; crude fiber, 15.90; calcium, 0.55; total phosphorus, 0.28; and gross energy, 18.65 MJ/kg. Amino acid and fatty acid profiles of FAMP are presented in Supplementary Tables S1 and S2, respectively.

2.2 Animals, diets, and treatments

A total of 320 Yukou Jingfen No. 8 laying hens that were 345 days old with similar health conditions were selected and randomly allocated into one of the four treatment groups with eight replicates per treatment (ten birds/replicate). The four treatment groups were fed on a basal diet with the addition of 0 (control, CON), 0.25%, 0.5%, and 1.0% FAMP, respectively. The basal diet for laying hens was formulated based on the standard nutriment requirements (Supplementary Table S3). The trial continued for eight weeks and there was a 1-week pre-feeding trial. All laying hens were raised in a controlled environment at 18–24 °C, humidity of 45–60%, and 16 h/day of illumination. The other feeding management followed routine commercial feeding management protocols during the trial.

2.3 Determination of laying performance

The weight and number of eggs and feed intake in each replicate were recorded during the whole trial. Then, average laying rate (ALR), average egg weight (AEW), average daily feed intake (ADFI), and feed-to-egg ratio (FER) were analyzed from weeks 1 to 2, 3 to 4, 5 to 6, 7 to 8, and 1 to 8 of the trial.

2.4 Egg quality analysis

Three eggs per replicate were randomly collected for egg quality measurement every two weeks during the trial. The egg shape index was determined by a Vernier caliper and calculated using previous formulas described by Feng et al. (2021). The eggshell strength, egg weight, albumen height, Haugh unit, and yolk color (Roche colorimetric unit) were measured with an Egg Force Reader and an EggAnalyzer (ORKA Food Technology Ltd., Ramat HaSharon, Israel), respectively. Then, the eggshell, yolk, and albumen were separated, weighed, and their percentages calculated. The eggshell thickness was measured by a hand-held micrometer (Deli Group, Ningbo, China).

2.5 Sample collection and plasma preparation

Three eggs from each replicate were collected to obtain the egg yolk and egg albumen for further nutritive value analyses after the 8-week animal trial. The plasma samples were obtained through wing vein-blood collection and centrifugation and kept at −80°C for plasma hormone, biochemical parameter, and antioxidant indicator analyses. Then, hens from each replicate were euthanized by jugular vein bleeding. The liver and ovary were dissected and kept at −80°C for mRNA extraction, and the ovary samples were also collected for hormone and antioxidant indicator analyses. The cecal contents were collected to determine the microbiota abundance and short-chain fatty acids (SCFA).

2.6 Count of ovarian follicles

In hens' ovaries, numbers of large white (2–5 mm), small yellow (6–8 mm), and hierarchical (>9 mm) follicles were recorded based on previously described methods (Li et al., 2020; Huang et al., 2021).

2.7 Determination of ether extract concentration and fatty acid profiles in yolks

The ether extract level of egg yolks was determined by a Soxhlet extraction with petroleum. The fatty acid composition was determined by employing the area normalization method (Hu et al., 2017). Briefly, total lipids were taken from egg yolks following the chloroform–methanol process. The fatty acid methyl ester was obtained with KOH/methanol and determined by a gas chromatograph (GC2030, Shimadzu Corporation, Kyoto, Japan).

According to the percentage of particular fatty acids of egg yolks, saturated fatty acids (SFA), polyunsaturated fatty acids (PUFA), monounsaturated fatty acids (MUFA), n-3 PUFA, and n-6 PUFA percentages were counted as follows: SFA = C14:0 + C16:0 + C17:0 + C18:0, MUFA = C16:1n-7 + C18:1n-9 + C20:1n-9, n-3 PUFA = C18:3n-3 + C22:6n-3, n-6 PUFA = C18:2n-6 + C18:3n-6 +C20:2n-6 + C20:3n-6 + C20:4n-6, and PUFA= n-3 PUFA + n-6 PUFA. Meanwhile, the health lipid indices related to fatty acids, such as atherogenicity index (AI), thrombogenic index (TI), hypocholesterolemic/hypercholesterolaemic ratio (H/H), health promotion index (HPI), and desirable fatty acids (DFA), were calculated as reported in our previous study (Li et al., 2024): AI = (C12:0 + 4 × C14:0 + C16:0)/UFA, TI = (C14:0 + C16:0 + C18:0)/(0.5 × MUFA + 0.5 × n-6 PUFA + 3 × n-3 PUFA + n-3/ n-6 PUFA), H/H ratio = (C18:1n-9 + C18:2n-6 + C20:4n-6 + C18:3n-3 + C20:5n-3 + C22:5n-3+C22:6n-3)/(C14:0 + C16:0), HPI = (MUFA + PUFA)/(C12:0 + 4 × C14:0 +C16:0), and DFA = C18:0 + MUFA + PUFA.

2.8 Measurement of crude protein and amino acid content in egg albumen

The crude protein content in egg albumen was evaluated by the Kjeldahl method. The content of amino acids in egg albumen was determined using a previously described method (Hu et al., 2017). Briefly, freeze-dried egg albumen samples were prepared using 6 mol/L hydrochloric acid at 110°C for 24 h. Then, the suspensions were filtered and detected by an ion-exchange AA analyzer (LA8080, Hitachi, Tokyo, Japan).

2.9 Analysis of plasma and ovary homogenate hormones

Ovary samples were placed in normal saline, vortexed, and then centrifuged at 4°C for supernatant collection. The protein content in ovary homogenate was measured with a bicinchoninic acid assay kit (Nanjing Jiancheng Bioengineering Institute, Nanjing, China).

The content of estrogen 2 (E_2), follicle-stimulating hormone (FSH), and luteinizing hormone (LH) in plasma and ovary homogenate was determined using the enzyme-linked immunosorbent assay (ELISA) kits (Hunan Richamp Biotechnology Co., Ltd., Changsha, China). The optical density (OD) values were obtained on a spectrophotometer (Tecan, Infinite M200 Pro, Basel, Switzerland).

2.10 Determination of plasma and ovary redox status and plasma biochemical parameters

The content of superoxide dismutase (SOD), glutathione peroxidase (GPX), total antioxidant capacity (T-AOC), glutathione (GSH), and malondialdehyde (MDA) in plasma and ovary homogenate was determined by colorimetry (Nanjing Jiancheng Bioengineering Institute, Nanjing, China) on a spectrophotometer (Tecan, Infinite M200 Pro, Basel, Switzerland). The protein content of each ovary homogenate sample was used to normalize the indexes mentioned above. The content of total cholesterol (TC) and triglyceride (TG), alanine aminotransferase (ALT), and aspartate aminotransferase (AST) in plasma was also determined by colorimetry (Nanjing Jiancheng Bioengineering Institute, Nanjing, China) on a spectrophotometer (Tecan, Infinite M200 Pro, Basel, Switzerland).

TABLE 1 Effects of FAMP on productive performance of aged laying hens.

Items	CON	Dietary FAMP level			SEM	*P*-value
		0.25%	0.5%	1.0%		
1 to 2 weeks						
ALR (%)	71.79	65.63	69.46	70.98	1.555	0.529
AEW (g)	51.10	51.60	51.75	51.19	0.231	0.726
ADFI (g)	95.31	96.09	95.34	95.47	0.454	0.742
FER	2.60	2.89	2.73	2.66	0.064	0.452
3 to 4 weeks						
ALR (%)	69.91	70.45	71.43	69.20	1.195	0.934
AEW (g)	52.67	51.31	50.84	51.43	0.287	0.131
ADFI (g)	91.74	90.48	89.33	89.51	0.305	0.023
FER	2.51	2.52	2.50	2.53	0.042	0.997
5 to 6 weeks						
ALR (%)	73.21	72.86	70.27	72.50	1.213	0.840
AEW (g)	51.54	51.45	51.47	51.45	0.224	0.999
ADFI (g)	100.75	101.76	101.74	101.68	0.121	0.056
FER	2.69	2.74	2.84	2.75	0.044	0.716
7 to 8 weeks						
ALR (%)	71.43	76.03	70.18	75.80	1.306	0.275
AEW (g)	51.01	52.06	52.00	51.76	0.244	0.413
ADFI (g)	97.37^{c}	99.46^{a}	98.90^{ab}	97.93^{bc}	0.230	0.003
FER	2.71	2.53	2.72	2.52	0.046	0.243
1 to 8 weeks						
ALR (%)	71.58	71.20	70.33	72.12	1.035	0.947
AEW (g)	51.57	51.61	51.50	51.47	0.198	0.995
ADFI (g)	96.29	96.94	96.33	96.15	0.138	0.082
FER	2.62	2.65	2.69	2.60	0.036	0.858

Data are represented as means with SEM; $n = 8$. Values with different lowercase letters within the same row differ significantly ($P < 0.05$). FAMP, fermented *Aronia melanocarpa* pomace; ALR, average laying rate; ADFI, average daily feed intake; AEW, average egg weight; FER, feed-to-egg ratio.

2.11 RNA extraction and mRNA quantification

The total RNA in both liver and ovary samples was measured using the TransZol agent (TransGen Biotech, Beijing, China). The concentration and purity of extracted RNA samples were evaluated by a Nanophotometer N60 (Implen, GmbH, Germany). The total RNA was reverse transcribed into cDNA following instructions provided in the RT Kit (Accurate Biology, Changsha, China). Quantitative PCR amplification was carried out on the LightCycler R 480II Real-Time PCR System (Roche, Basel, Switzerland) using the qPCR Kit (Accurate Biology, Changsha, China) following the manufacturer's instructions. Characteristic primer sequences devised through the Primer 3 web (https://primer3.ut.ee/) are available in Supplementary Table S4. The relative gene expression was computed with the $2^{-\Delta\Delta Ct}$ method (Livak and Schmittgen, 2001).

2.12 Cecal microbial analysis

The cecal microbiota composition analysis was performed by the Shanghai Personal Biotechnology Co., Ltd., Shanghai, China (Zhu et al., 2022). Briefly, the total microbial DNA of cecal contents was extracted and amplified with specific primers (forward primer: 5′-ACTCCTACGGGAGGCAGCA-3′ and reverse primer: 5′-GGACTACHVGGGTWTCTAAT-3′) to obtain bacterial V3-V4 sequences. After purification and amplification, the PCR products were paired-end sequenced on an Illumina NovaSeq platform (Illumina, San Diego, CA, USA). After quality control and chimera removal, amplified sequence variants (ASVs) were taxonomically aligned with species annotation using the Greengenes database. The α and β diversity indices were analyzed to detect the diversity, richness, and dissimilarity of the microbiota. Kruskal–Wallis test was performed to determine the differential phyla and genera. The linear discriminant analysis (LDA) effect size (LEfSe; LDA ≥ 2, $P < 0.05$) and random forest analysis were applied to identify and distinguish the microbiota in the four groups. The Kyoto Encyclopedia of Genes and Genomes (KEGG) pathway analysis of the microbiota was conducted with the Phylogenetic Investigation of Communities by Reconstruction of Unobserved States (PICRUSt2) method. The correlation between cecal microbiota abundance (top 50 genera) and phenotypes was performed using Spearman correlation by the R package ($|R| > 0.50$, $P < 0.05$).

2.13 Measurement of cecal short-chain fatty acid profile

The concentrations of cecal SCFA were measured according to our previous study (Li et al., 2021) using Agilent 7890A gas chromatograph (Agilent Inc., Palo Alto, CA, USA).

2.14 Statistical analysis

All data analyses were performed using the SPSS 22.0 software (SPSS Inc., Chicago, IL, USA) package. The normality and homogeneity of variances of the data were assessed using the Shapiro–Wilk test and Levene's test, respectively. When applicable, the one-way analysis of variance (ANOVA) following Tukey's *post-hoc* test was performed to assess significant differences. Otherwise, Welch's ANOVA and Games-Howell tests were performed for the significant difference analyses. The results are expressed as means with standard error of the mean (SEM). $P < 0.05$ was considered statistically significant, whereas $0.05 \leq P < 0.1$ suggested a trend.

3 Results

3.1 Laying performance and egg quality

Table 1 showed no notable differences ($P > 0.05$) in the ALR, AEW, and FER among the four groups during 1 to 2, 3 to 4,

10.3389/fmicb.2024.1422172

TABLE 2 Effects of FAMP on egg quality of aged laying hens.

Items	CON	Dietary FAMP level			SEM	*P*-value
		0.25%	0.5%	1.0%		
Week 2						
Eggshell strength (N)	38.72	42.25	40.35	40.59	0.794	0.499
Shape index	1.33^{a}	1.29^{b}	1.35^{a}	1.33^{ab}	0.007	0.007
Albumen height (mm)	3.38	3.70	4.44	3.77	0.157	0.104
Yolk color	13.67	14.04	13.88	13.79	0.122	0.763
Haugh unit	55.04	57.72	64.04	56.82	1.600	0.215
Eggshell thickness (mm)	0.34	0.33	0.34	0.34	0.003	0.548
Eggshell percent (%)	13.34	12.88	12.66	12.91	0.105	0.133
Yolk percent (%)	32.72	32.60	31.91	31.59	0.331	0.588
Albumen percent (%)	53.88	54.56	55.43	55.59	0.377	0.357
Week 4						
Eggshell strength (N)	40.74	40.32	40.24	39.84	0.746	0.982
Shape index	1.32	1.34	1.33	1.33	0.005	0.627
Albumen height (mm)	5.17	4.05	4.37	4.31	0.173	0.113
Yolk color	13.96	13.50	13.21	13.31	0.132	0.191
Haugh unit	68.70	61.70	64.59	63.25	1.632	0.488
Eggshell thickness (mm)	0.34	0.33	0.33	0.32	0.002	0.120
Eggshell percent (%)	13.24	13.07	13.06	12.98	0.113	0.890
Yolk percent (%)	30.48	30.97	30.78	30.82	0.304	0.955
Albumen percent (%)	56.29	55.96	56.16	56.21	0.318	0.987
Week 6						
Eggshell strength (N)	39.81	43.09	40.65	40.20	0.738	0.408
Shape index	1.36	1.34	1.34	1.33	0.006	0.568
Albumen height (mm)	4.21	5.51	4.94	5.51	0.251	0.217
Yolk color	13.75	14.38	14.17	14.38	0.104	0.104
Haugh unit	63.86	71.31	69.12	71.31	1.731	0.393
Eggshell thickness (mm)	0.344^{ab}	0.354^{a}	0.345^{ab}	0.334^{b}	0.002	0.012
Eggshell percent (%)	13.12	13.41	12.96	13.38	0.104	0.368
Yolk percent (%)	31.34	30.94	30.48	30.33	0.237	0.436
Albumen percent (%)	55.54	55.64	56.56	56.30	0.292	0.561
Week 8						
Eggshell strength (N)	40.14	39.18	39.80	41.24	0.912	0.891
Shape index	1.32	1.34	1.34	1.34	0.005	0.665
Albumen height (mm)	5.18	5.01	4.89	4.81	0.100	0.618
Yolk color	14.04	14.17	14.10	14.08	0.091	0.973
Haugh unit	71.25	70.11	68.97	68.60	0.959	0.776
Eggshell thickness (mm)	0.33	0.33	0.34	0.34	0.003	0.683
Eggshell percent (%)	13.05	13.24	12.69	13.05	0.101	0.294
Yolk percent (%)	31.25	30.62	31.26	30.37	0.250	0.506
Albumen percent (%)	55.70	56.15	56.04	56.58	0.268	0.732

Data are represented as means with SEM; $n = 8$. Values with different lowercase letters within the same row differ significantly ($P < 0.05$). FAMP, fermented *Aronia melanocarpa* pomace.

10.3389/fmicb.2024.1422172

TABLE 3 Effects of FAMP on ether extract concentration, fatty acid profile, and health lipid indices of egg yolk.

Items	CON	Dietary FAMP level			SEM	*P*-value
		0.25%	0.5%	1.0%		
Ether extract (g/100g tissue)	33.89	34.55	34.36	34.94	0.309	0.712
C14:0	0.40	0.41	0.38	0.39	0.006	0.419
C16:0	25.78^{a}	25.23^{ab}	24.55^{b}	24.93^{ab}	0.146	0.013
C16:1n-7c	3.12	2.88	2.69	2.74	0.076	0.192
C17:0	0.14	0.15	0.17	0.15	0.005	0.282
C18:0	8.26	8.17	8.05	8.11	0.112	0.940
C18:1n-9c	42.90	42.95	44.47	42.60	0.435	0.446
C18:2n-6c	16.26	17.22	16.60	17.90	0.448	0.610
C18:3n-6	0.12	0.13	0.11	0.12	0.004	0.636
C18:3n-3	0.65	0.68	0.70	0.74	0.022	0.594
C20:1n-9c	0.22	0.21	0.21	0.21	0.003	0.538
C20:2n-6	0.13	0.14	0.13	0.14	0.004	0.797
C20:3n-6	0.14	0.12	0.12	0.12	0.003	0.059
C20:4n-6	1.29^{a}	1.18^{b}	1.22^{ab}	1.26^{ab}	0.016	0.037
C22:6n-3	0.60	0.54	0.60	0.58	0.010	0.157
Health lipid indices						
SFA(%)	34.58^{a}	33.96^{ab}	33.15^{b}	33.59^{ab}	0.168	0.010
MUFA(%)	46.23	46.04	47.37	45.55	0.441	0.542
PUFA(%)	19.19	20.00	19.48	20.86	0.482	0.662
PUFA/SFA	0.56	0.59	0.59	0.62	0.016	0.552
n-3 PUFA(%)	1.25	1.22	1.30	1.32	0.028	0.575
n-6 PUFA(%)	17.94	18.78	18.18	19.54	0.461	0.646
n-6/n-3 PUFA	14.32	15.50	13.89	14.80	0.255	0.135
AI	0.42^{a}	0.41^{ab}	0.39^{b}	0.40^{ab}	0.003	0.006
TI	0.96^{a}	0.94^{ab}	0.90^{b}	0.91^{ab}	0.008	0.022
H/H	2.36^{b}	2.44^{ab}	2.55^{a}	2.50^{ab}	0.022	0.007
HPI	2.39^{b}	2.46^{ab}	2.57^{a}	2.51^{ab}	0.021	0.008
DFA(%)	73.68^{b}	74.21^{ab}	74.91^{a}	74.52^{ab}	0.147	0.015

Data are represented as means with SEM; $n = 6$. Values with different lowercase letters within the same row differ significantly ($P < 0.05$). FAMP, fermented *Aronia melanocarpa* pomace; SFA, saturated fatty acids; PUFA, polyunsaturated fatty acids; MUFA, monounsaturated fatty acids; AI, atherogenicity index; TI, thrombogenic index; H/H, hypocholesterolaemic-to-hypercholesterolaemic ratio; HPI, health promotion index; DFA, desirable fatty acids.

5 to 6, 7 to 8, and 1 to 8 weeks of the trial. The ADFI was elevated ($P < 0.05$) in the 0.25% and 0.5% FAMP groups relative to that in the CON group during 7–8 weeks. The ADFI in the 0.25% FAMP group was higher ($P < 0.05$) than that of the 1% FAMP group during 7 to 8 weeks, and showed an increasing trend ($P = 0.082$) during 1 to 8 weeks. As presented in Table 2, the addition of 0.25% FAMP decreased ($P < 0.05$) the egg shape index relative to that in the CON and 0.5% AMP groups at week 2. The eggshell thickness was higher ($P < 0.05$) in the 0.25% FAMP group than in the 1% FAMP group at week 6. No notable differences ($P > 0.05$) were found in the eggshell strength, Haugh unit, albumen height, yolk color, and percentages of eggshell, yolk, and albumen among the four groups throughout the trial.

3.2 The ether extract and fatty acid profiles in the egg yolk

As seen in Table 3, the C16:0 percentage was lower ($P < 0.05$) in the 0.5% FAMP group than that of the CON group. The C20:4n-6 percentage showed a decrease ($P < 0.05$) in the 0.25% FAMP group compared to the CON group. Moreover, FAMP supplementation exhibited a declining trend ($P = 0.059$) in the C20:3n-6 percentage compared to the CON group. Additionally, the SFA percentage and AI and TI indexes were reduced ($P < 0.05$), whereas H/H, HPI, and DFA indexes were elevated ($P < 0.05$) in the 0.5% FAMP group by comparison with the CON group. PUFA, PUFA/SFA, n-3 PUFA, and n-6 PUFA in the four groups showed no obvious distinctions ($P > 0.05$).

10.3389/fmicb.2024.1422172

3.3 Crude protein and amino acid content in egg albumen

The valine content in egg albumen was reduced ($P < 0.05$) in the 0.25% FAMP group than in the CON group. The 0.25% and 0.5% FAMP groups exhibited a decreasing trend with regard to the content of histidine ($P = 0.093$), proline ($P = 0.060$), and branched-chain amino acid (BCAA, $P = 0.089$) of egg albumen relative to the CON group (Table 4).

TABLE 4 Effects of FAMP on crude protein and amino acid content of egg albumen.

Items, %	CON	Dietary FAMP level			SEM	*P*-value
		0.25%	0.5%	1.0%		
Crude protein	9.93	9.27	9.60	9.50	0.154	0.535
EAA	5.11	4.60	4.75	4.92	0.091	0.227
Arginine	0.57	0.51	0.52	0.55	0.010	0.249
Histidine	0.23	0.21	0.21	0.22	0.004	0.093
Isoleucine	0.53	0.47	0.48	0.50	0.010	0.118
Leucine	0.86	0.77	0.80	0.83	0.015	0.160
Lysine	0.65	0.60	0.60	0.66	0.012	0.173
Methionine	0.49	0.46	0.52	0.46	0.015	0.496
Phenylalanine	0.62	0.56	0.58	0.61	0.011	0.162
Threonine	0.46	0.42	0.43	0.45	0.008	0.187
Valine	0.69^{a}	0.60^{b}	0.61^{ab}	0.65^{ab}	0.012	0.025
NEAA	4.83	4.34	4.43	4.64	0.082	0.153
Alanine	0.61	0.55	0.56	0.59	0.011	0.131
Aspartic acid	1.06	0.95	0.96	1.01	0.018	0.104
Glutamic acid	1.37	1.23	1.25	1.31	0.023	0.129
Glycine	0.36	0.32	0.33	0.35	0.006	0.139
Proline	0.34	0.30	0.30	0.33	0.006	0.060
Serine	0.70	0.64	0.65	0.68	0.012	0.272
Tyrosine	0.39	0.35	0.38	0.38	0.007	0.387
TAA	9.94	8.94	9.18	9.56	0.173	0.189
FAA	3.97	3.56	3.62	3.79	0.068	0.135
BCAA	2.08	1.84	1.89	1.98	0.037	0.089

Data are represented as means with SEM; $n = 6$. Values with different lowercase letters within the same row differ significantly ($P < 0.05$). FAMP, fermented *Aronia melanocarpa* pomace; EAA, essential amino acid, containing arginine, histidine, isoleucine, leucine, lysine, methionine, phenylalanine, threonine, tryptophan, and valine; NEAA, non-essential amino acid, containing alanine, aspartic acid, cystine, glutamic acid, glycine, proline, serine, and tyrosine; TAA, total amino acid; FAA, flavor amino acid, containing aspartic acid, glutamic acid, glycine, alanine, and arginine; BCAA, branched-chain amino acid, containing isoleucine, leucine, and valine.

3.4 The number of ovarian follicles, hormone levels of plasma and ovary, and hormone synthesis and receptor genes in the ovary

The results of ovarian follicles are shown in Figure 1A. The number of large white follicles in the FAMP groups exhibited an increasing trend ($P = 0.092$) relative to the CON group. There were no significant changes ($P > 0.05$) in plasma FSH, LH, and E_2 contents among the four groups (Figure 1B). However, ovary FSH, LH, and E_2 levels were higher ($P < 0.05$) in the 0.25%, 0.5%, and 1.0% FAMP groups relative to the CON group (Figure 1C). The ovary *HSD17B1* expression was upregulated ($P < 0.05$) in the 1.0% FAMP group relative to the CON group. The mRNA expression involved in hormonogenesis (including *CYP11A1*, *HSD3B1*, *CYP17A1*, and *CYP19A1*) and hormone receptors (including *ESR1*, *ESR2*, *FSHR*, and *LHCGR*) in ovarian tissues did not differ among the four groups (Figures 1D, E).

3.5 Plasma biochemical indicators and expression of genes involved in egg yolk precursor synthesis and transport

As shown in Figure 2A, plasma TC, TG, ALT, and AST levels of the four groups showed no significant differences ($P > 0.05$). The gene expression involved in the synthesis of yolk precursor (including *ACC*, *FAS*, and *SCD1*) and *ESR2* in the liver was upregulated ($P < 0.05$) in the 1.0% FAMP group compared with the CON group (Figures 2B, E). The gene expressions of the liver-respecting egg yolk precursor transportation (including *VTG II*, *ApoVLDL II*, and *APOB*) were upregulated ($P < 0.05$) in the 0.5% FAMP group relative to the CON group (Figure 2C). As for the *VLDR* gene expression of the ovary, no difference ($P > 0.05$) was observed among the four groups (Figure 2D).

3.6 Plasma and ovary redox status and the *Keap1/Nrf2* pathway of the ovary

The levels of plasma redox status-related parameters, including T-AOC, GSH, GSH-PX, SOD, and MDA, were not changed ($P > 0.05$) by dietary FAMP supplementation (Figure 3A). In the ovary, T-AOC ($P < 0.05$) and SOD ($P = 0.064$) levels were increased in the 0.5% FAMP group in comparison to the CON group (Figure 3B). Furthermore, the *Keapl* expression of the 0.5% and 1.0% FAMP groups was decreased ($P < 0.05$) relative to the CON group. Moreover, the *Nrf2* expression of the 0.5% FAMP group was higher ($P < 0.05$) than in the 1.0% FAMP group.

3.7 Microbiota structure and community in cecal contents

The results of the α-diversity are presented in Figure 4A. The Observed_species, Chao1, and Faith-pd indexes were higher, whereas the Goods coverage index was lower in the 0.25% FAMP group relative to the CON group ($P < 0.05$). The Pielou_e index of the 1.0% FAMP group was higher ($P < 0.05$) relative to the 0.5% FAMP group. The β-diversity analysis (non-metric

10.3389/fmicb.2024.1422172

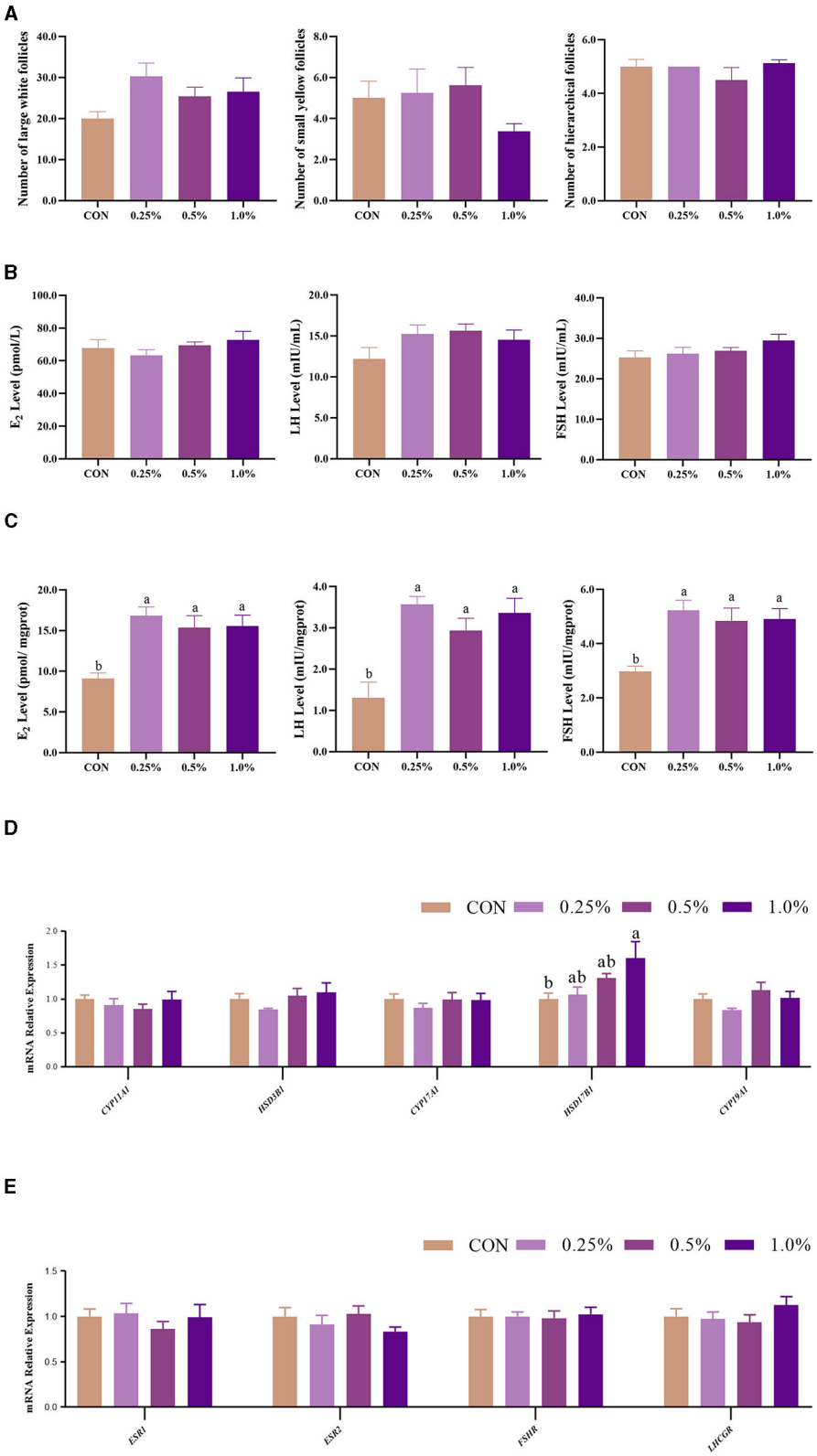

FIGURE 1
FAMP affected the number of follicles, hormone levels, and gene expression related to hormone synthesis/receptors. The number of follicles **(A)**, hormone levels in plasma **(B)** and ovary **(C)**, and gene expression related to hormone synthesis **(D)** and receptor **(E)** of the ovary. The hens in the CON, 0.25%, 0.5%, and 1.0% groups were fed the basal diet supplemented with 0, 0.25%, 0.5%, and 1.0% fermented *Aronia melanocarpa* pomace (FAMP), respectively. Data are represented as means with SEM; $n = 8$. Values with different lowercase letters in the histogram differ significantly ($P < 0.05$). *CYP11A1*, cytochrome P450 family 11 subfamily A member 1; *HSD3B1*, 3 beta- and steroid delta-isomerase 1; *CYP17A1*, cytochrome P450 family 17 subfamily A member 1; *HSD17B1*, hydroxysteroid 17-beta dehydrogenase 1; *CYP19A1*, cytochrome P450 family 19 subfamily A member 1; *ESR1*, estrogen receptor 1; *ESR2*, estrogen receptor 2; *FSHR*, follicle stimulating hormone receptor; *LHCGR*, luteinizing hormone/choriogonadotropin receptor.

10.3389/fmicb.2024.1422172

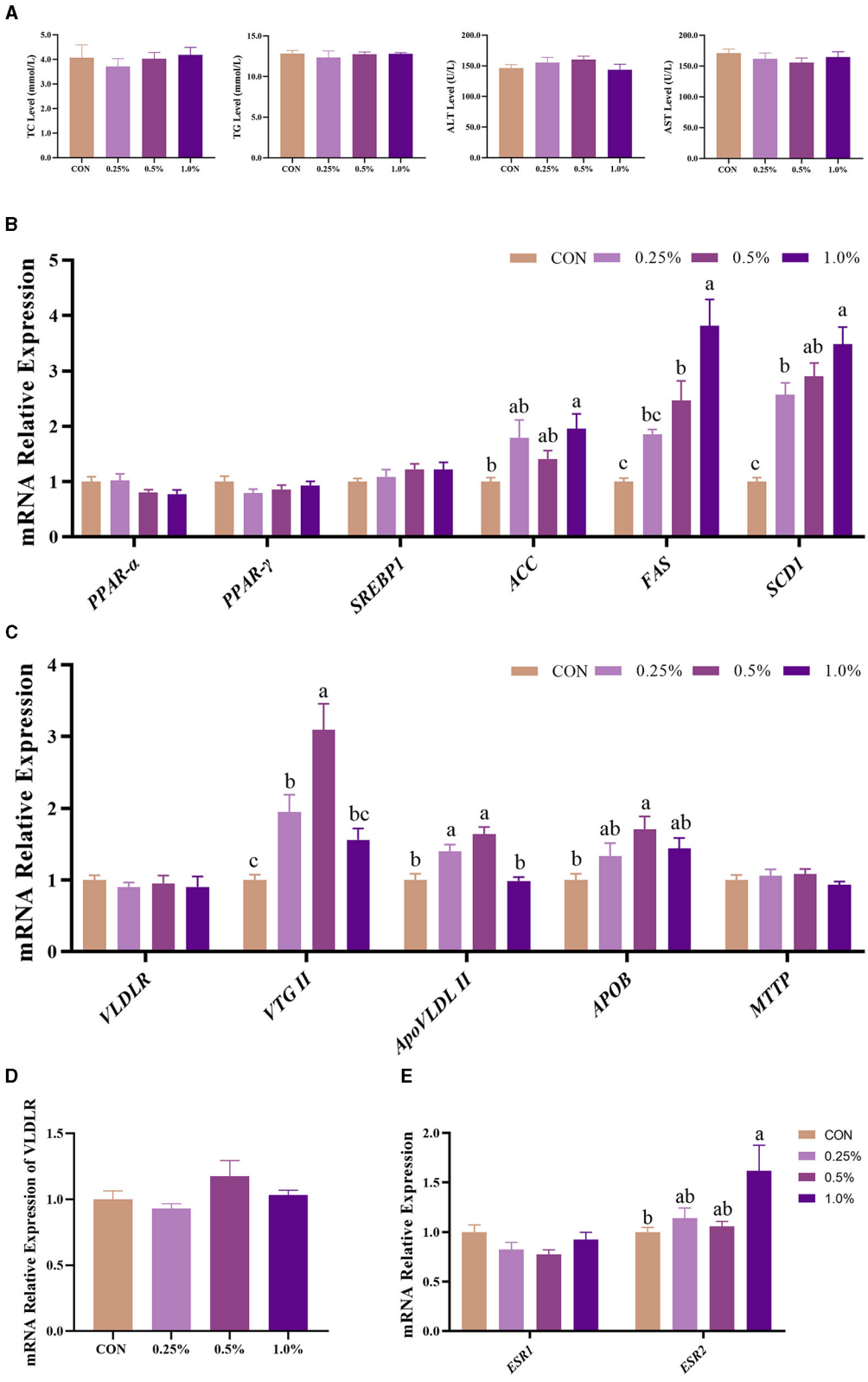

FIGURE 2
FAMP affected plasma biochemical indicators and egg yolk precursors synthesis and transport of the liver. The plasma biochemical indicators **(A)** and expression of genes related to egg yolk precursor synthesis **(B)** and transport **(C)** of the liver. The mRNA expression of *VLDLR* of the ovary **(D)** and *ESR1* and *ESR2* of the liver **(E).** The hens in the CON, 0.25%, 0.5%, and 1.0% groups were fed the basal diet supplemented with 0, 0.25%, 0.5%, and 1.0% fermented *Aronia melanocarpa* pomace (FAMP), respectively. Data are represented as means with SEM; $n = 8$. Values with different lowercase letters in the histogram differ significantly ($P < 0.05$). *ACC*, acetyl-CoA carboxylase; *APOB*, apolipoprotein B; *ApoVLDL II*, apo very low-density lipoprotein II; *ESR1*, estrogen receptor 1; *ESR2*, estrogen receptor 2; *FAS*, fatty acid synthase; *MTTP*, microsomal triglyceride transfer protein; *PPARα*, peroxisome proliferator-activated receptor alpha; *PPAR-γ*, peroxisome proliferator-activated receptor gamma; *SCD1*, stearoyl-CoA desaturase 1; *SREBP1*, sterol regulatory element binding protein 1; TC, total cholesterol; TG, triglyceride; *VLDLR*, very low-density lipoprotein receptor; *VTG* II, vitellogenin 2.

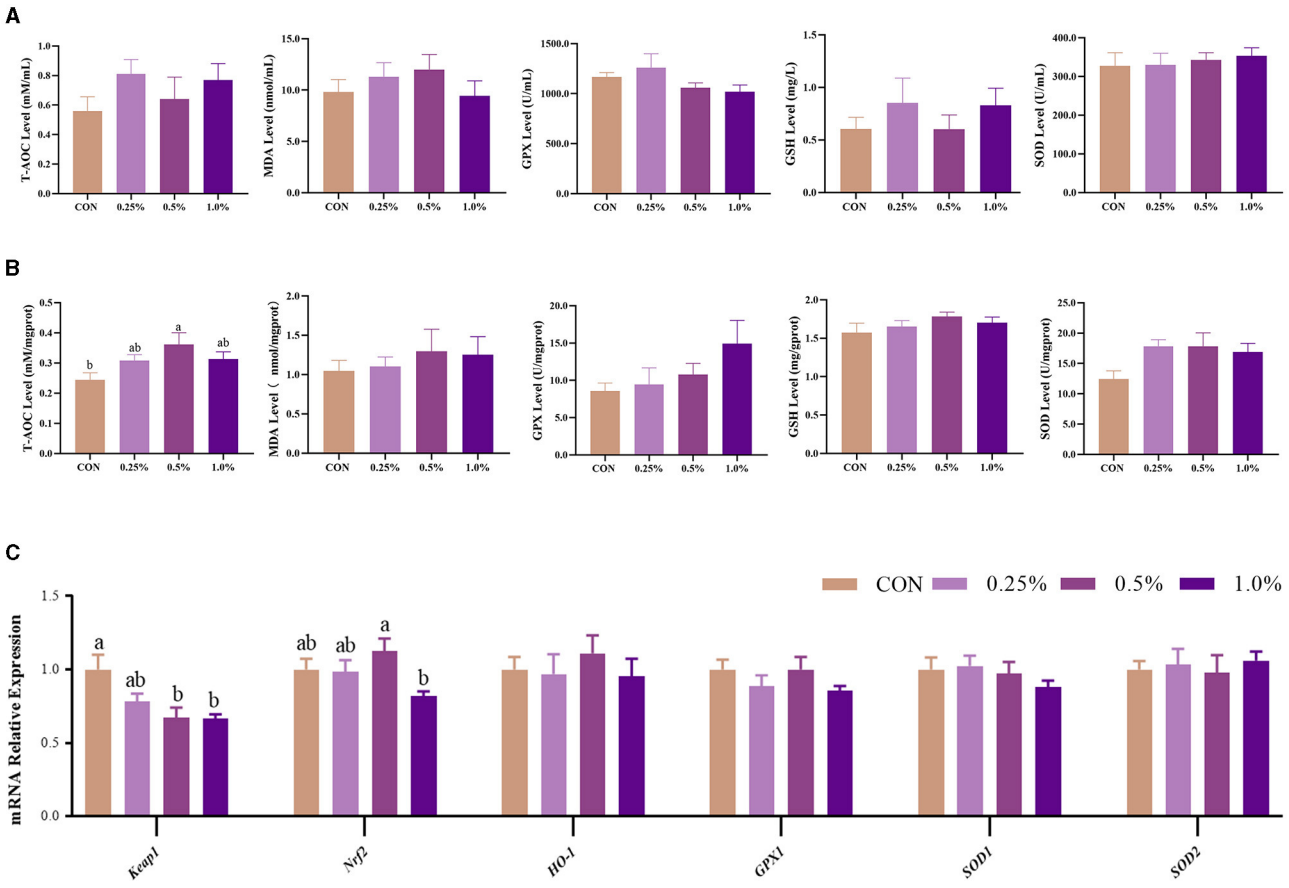

FIGURE 3
FAMP-affected the antioxidant capacity of the plasma and ovary. The plasma **(A)** and ovary **(B)** redox level and gene expression in the Keap1/Nrf2 signaling pathway of the ovary **(C)**. The hens in CON, 0.25%, 0.5%, and 1.0% groups were fed the basal diet supplemented with 0, 0.25%, 0.5%, and 1.0% fermented *Aronia melanocarpa* pomace (FAMP), respectively. Data are represented as means with SEM; $n = 8$. Values with different lowercase letters in the histogram differ significantly ($P < 0.05$). T-AOC, total antioxidant capacity; SOD, superoxide dismutase; GSH, glutathione; GPX, glutathione peroxidase; MDA, malondialdehyde; *Keap1*, Kelch-like ECH-associated protein 1; *Nrf2*, NF-E2-related factor 2; *HO-1*, heme oxygenase 1; *GPX1*: glutathione peroxidase 1; *SOD1*, superoxide dismutase 1; *SOD2*, superoxide dismutase 2.

multidimensional scaling ordination plot) indicated that cecal microbial communities were differentiated between the CON and the three FAMP groups (Figure 4B). Bacteroidetes, Firmicutes, and Proteobacteria predominated in the cecal phyla (Figure 4C). An increase ($P < 0.05$) in the relative abundance of Bacteroidetes was found in the 0.25% and 0.5% FAMP groups relative to the 1.0% FAMP group. The relative abundance of Firmicutes was increased ($P < 0.05$) in the 1.0% FAMP group relative to the other three groups. Especially, we found a decrease ($P < 0.05$) in the relative abundance of Proteobacteria in the FAMP groups in comparison to the CON group (Figure 4E). Furthermore, the top ten genera were *Bacteroides*, *Lactobacillus*, *Megamonas*, *Faecalibacterium*, *Phascolarctobacterium*, *Prevotella*, *Oscillospira*, *[Ruminococcus]*, *Desulfovibrio*, and *Subdoligranulum* (Figure 4D). Notably, the relative abundance of *Lactobacillus* of the 1.0% FAMP group was the highest ($P < 0.05$) among all groups. The 0.5% and 1% FAMP groups exhibited a decrease in the relative abundances of *Oscillospira* and *[Ruminococcus]* ($P < 0.05$) relative to the 0.25% FAMP group. The relative abundance of *[Ruminococcus]* of the 0.5% FAMP group was decreased ($P < 0.05$) relative to the CON group (Figure 4F).

3.8 Cecal microbiota biomarkers and function prediction

As presented in Figure 5A, the LEfSe analysis of taxa with LDA score ≥ 2 showed that Proteobacteria in the CON group; Armatimonadetes, Chloroflexi, GNO4, OD1, Planctomycetes, and WS3 in the 0.25% FAMP group, Bacteroidetes in the 0.5% FAMP, and Firmicutes in the 1.0% FAMP group were enriched. At the genus level, *Streptomyces*, *Symbiobacterium*, *Methylobacterium*, *Massilia*, *Shigella*, *Acinetobacter*, and *Pseudomonas* in the CON group, *Alistipes*, *Candidatus_Brocadia*, *Nitrosomonas*, and *Psychrobacter* in the 0.25% FAMP group, *Weissella* and *Streptococcus* in the 0.5% FAMP group, and *Lactobacillus*, *Acetobacter*, and *Ralstonia* in the 1.0% FAMP group were enriched. The random forest model was performed to further identify the biomarkers. As shown in Figure 5B, the top five marker genera among the four groups were *Methylobacterium*, *Ralstonia*, *Alistipes*, *Olsenella*, and *Weissella* at the genus level. Meanwhile, the 0.25% FAMP group had increased *Alistipes*, *Olsenella*, *Oscillospira*, and others. Furthermore, the pathways at level 3 were further identified (Figure 5C). The results showed

10.3389/fmicb.2024.1422172

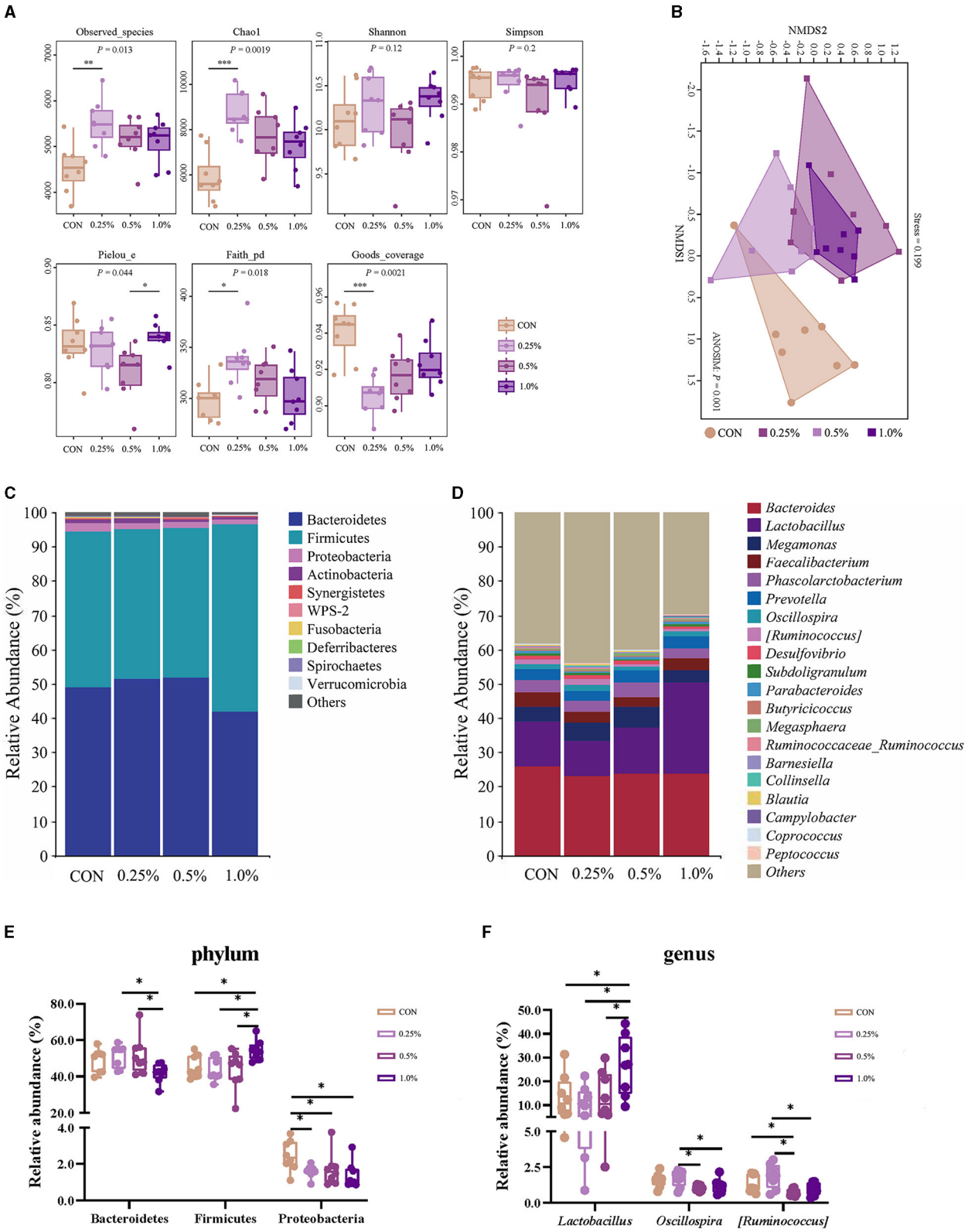

FIGURE 4
FAMP affected the cecal microbiota composition. The α- **(A)** and β-diversity **(B)** indices and community composition of cecal microbiota of aged laying hens at the phylum **(C, E)** and genus **(D, F)** levels. The hens in the CON, 0.25%, 0.5%, and 1.0% groups were fed the basal diet supplemented with 0, 0.25%, 0.5%, and 1.0% fermented *Aronia melanocarpa* pomace (FAMP), respectively. Data are represented as means with SEM; $n = 8$. *$P < 0.05$.

10.3389/fmicb.2024.1422172

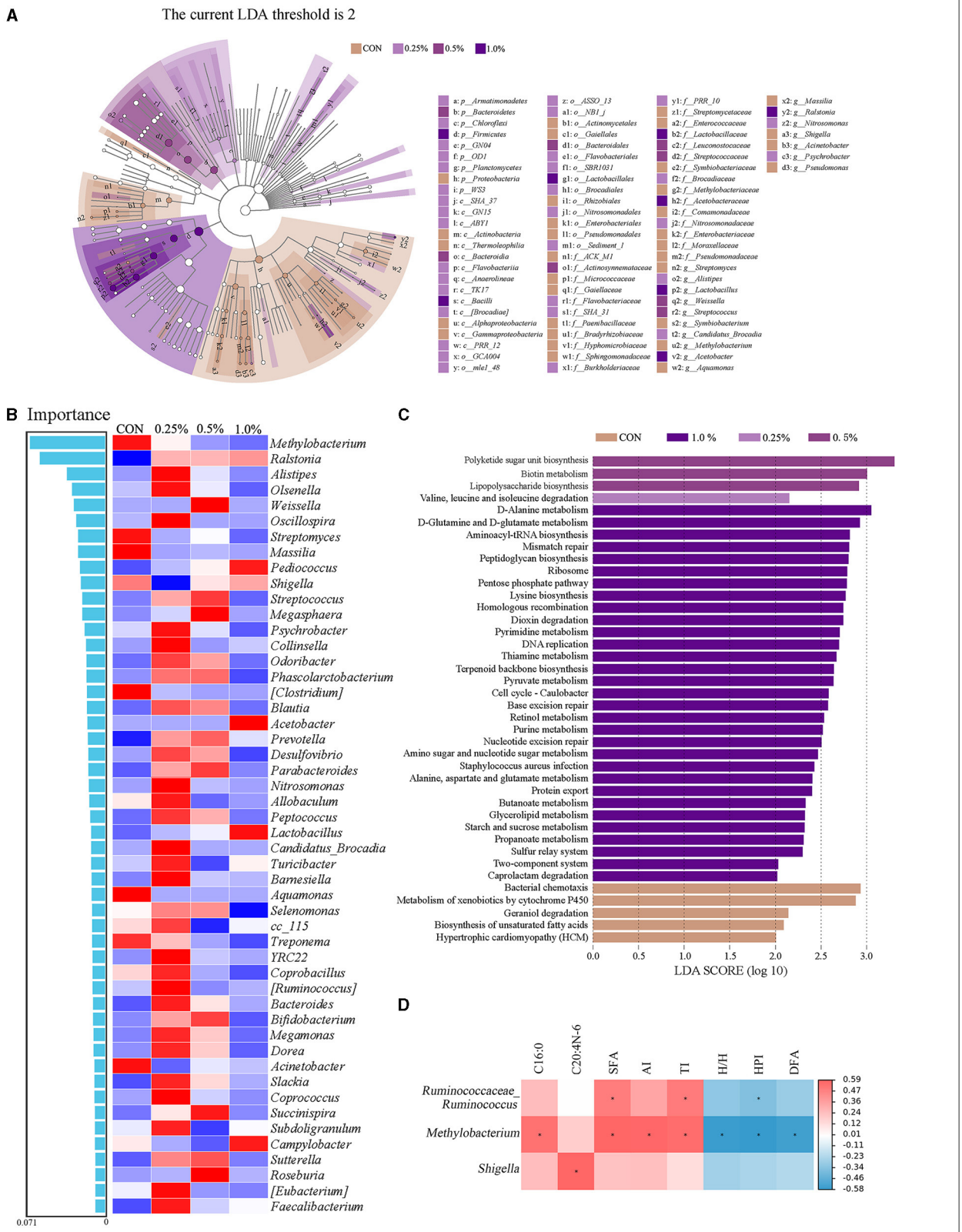

FIGURE 5
FAMP affected the predicted microbiota functions in cecal contents. Linear discriminant analysis effect size (LEfSe analysis, LDA score ≥ 2) for taxonomic abundance analysis **(A)**, random forest for identifying microbial markers **(B)**, different enrichment pathways for predicted function **(C)**, and correlation analysis ($|R| > 0.50$, $P < 0.05$) between microbiota (top 50 genera) and differential fatty acid indices **(D)** of cecal microbiota of aged laying hens. The hens in the CON, 0.25%, 0.5%, and 1.0% groups were fed the basal diet supplemented with 0, 0.25%, 0.5%, and 1.0% fermented *Aronia melanocarpa* pomace (FAMP), respectively.

10.3389/fmicb.2024.1422172

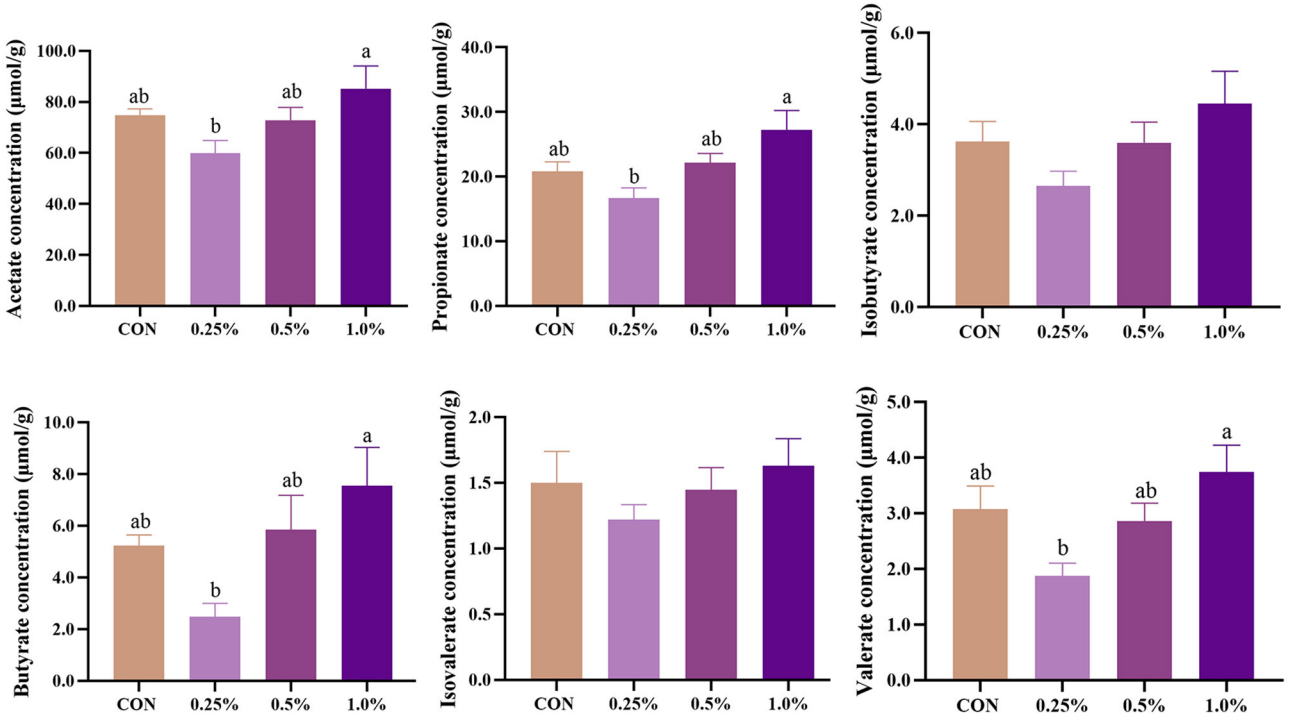

FIGURE 6
FAMP affected the concentrations of short-chain fatty acids in cecal content. The hens in CON, 0.25%, 0.5%, and 1.0% groups were fed the basal diet supplemented with 0, 0.25%, 0.5%, and 1.0% fermented *Aronia melanocarpa* pomace (FAMP), respectively. Data are represented as means with SEM; $n = 8$. Values with different lowercase letters in the histogram differ significantly ($P < 0.05$).

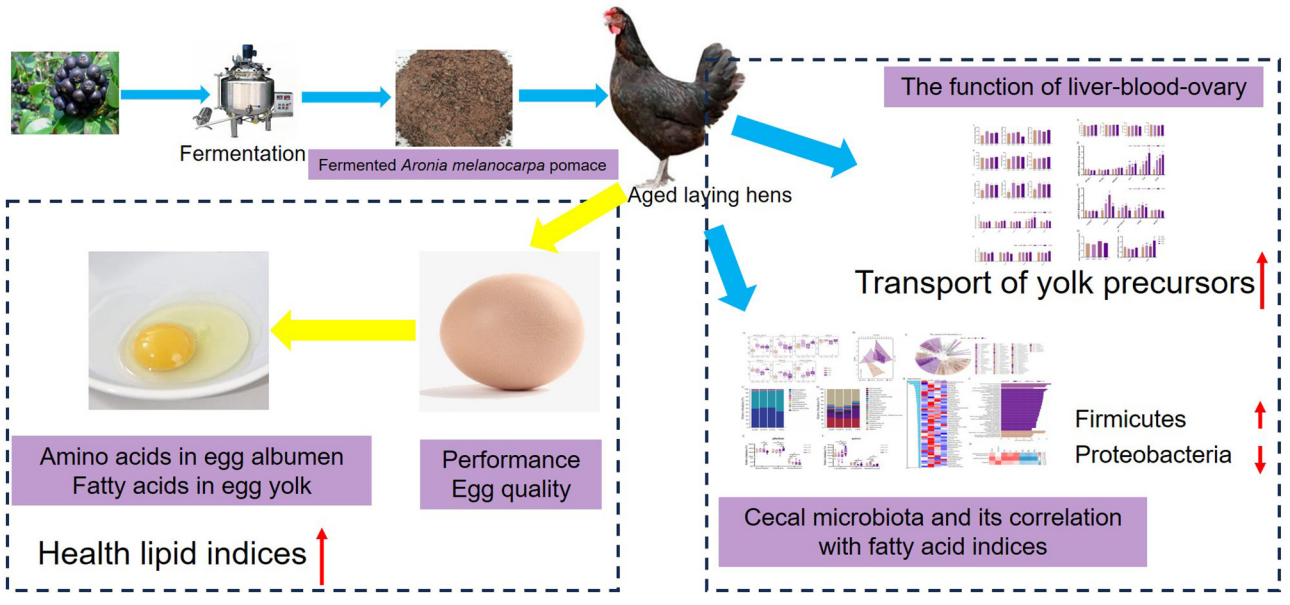

FIGURE 7
Effects and potential mechanisms of fermented *Aronia melanocarpa* pomace on performance, quality, and nutritive value of eggs, ovarian function, and cecal microbiota composition of aged laying hens.

that the CON, 0.25%, 0.5%, and 1.0% FAMP groups significantly enriched 5, 1, 3, and 31 pathways, respectively. There were five significantly enriched pathways in the CON group, namely, bacterial chemotaxis, metabolism of xenobiotics by cytochrome P450, geraniol degradation, biosynthesis of unsaturated fatty acids, and hypertrophic cardiomyopathy. The pathway enriched

in the 0.25% FAMP group was valine, leucine, and isoleucine degradation. There were three significantly enriched pathways in the 0.5% FAMP group, namely polyketide sugar unit biosynthesis, biotin metabolism, and lipopolysaccharide biosynthesis. The 1.0% FAMP group enriched 31 pathways, and the top 10 pathways included D-alanine metabolism, D-glutamine and D-glutamate metabolism, aminoacy1-tRNA biosynthesis, mismatch repair, peptidoglycan biosynthesis, ribosome, pentose phosphate pathway, lysine biosynthesis, homologous recombination, and dioxin degradation.

3.9 Correlations between microbiota and differential fatty acid indices of egg yolk

As shown in Figure 5D, the positive correlations were obtained between *Ruminococcaceae_Ruminococcus* with SFA and TI, *Methylobacterium* with C16:0, SFA, AI, and TI, and *Shigella* with C20:4n-6 ($|R| > 0.50$, $P < 0.05$). The negative correlations ($|R| > 0.50$, $P < 0.05$) were obtained between *Ruminococcaceae_Ruminococcus* with HPI, and *Methylobacterium* with H/H, HPI, and DFA.

3.10 Cecal short-chain fatty acid composition

The levels of cecal SCFA of aged laying hens are presented in Figure 6. The levels of acetate, propionate, butyrate, and valerate were increased ($P < 0.05$) in the 1.0% FAMP group relative to the 0.25% FAMP group. Dietary 0.25%−1.0% FAMP did not ($P > 0.05$) affect the level of isobutyrate.

4 Discussion

Increasing evidence suggests that a reduction in performance and egg quality influences the nutritive and economic value of eggs in aged hens after high-intensity metabolism at the peak laying period (He et al., 2023), which refers to the stage after 48 weeks of age, accounting for about half of the entire laying period. Therefore, modulating the aging of the ovary is essential to enhance the egg quality of aged laying hens. In this trial, we observed the addition of FAMP improved the health lipid indices of yolk and nutritive value of eggs, enhanced lipid metabolism in the LBO axis, regulated the reproductive hormone metabolism, increased ovarian antioxidant function and cecal SCFA, and reshaped cecal microbiota composition in Yukou Jingfen No. 8 laying hens at 50 and 58 weeks of age. Thus, the findings support the reuse of fermented AMP, a byproduct of the food industry, in the feed of laying hens to enhance the nutritive value of eggs.

Laying performance and egg quality are important indicators in the poultry industry, and these parameters are dependent on the diverse organs participating in reproduction. Aging can alter the body's genome, proteome, and metabolome, leading to diverse damages and metabolic dysfunctions, hindering the normal function of multiple organs, such as the ovary, liver, and intestine (Li G. et al., 2023). Our results showed that FAMP (0.25%−1.0%) supplementation did not significantly improve the laying performance (including ALR, AEW, and FER) and egg quality (e.g., yolk color, Haugh unit, albumen height, and other indicators). Similarly, supplementation of 3% dried AMP (Sosnówka-Czajka and Skomorucha, 2021), 2.5% AMP (Loetscher et al., 2014), and 4% grape pomace (Kara et al., 2016) in laying hens' diets also had no obvious effects on laying performance and egg quality. However, the inclusion of 3% dried AMP (Sosnówka-Czajka and Skomorucha, 2021) in the diet tended to increase AEW, which may be related to its beneficial effects on body metabolism due to the higher proportion of AMP in the diet (corresponding to higher anthocyanins).

The nutritive value of eggs depends upon the composition of lipids, proteins, and other active substances. Lipid is the main component (30%) of egg yolk, which has a large content of fatty acids (Nielsen, 1998). C18:1n9-c and C16:0 are the most abundant fatty acids in egg yolks. In this trial, the addition of 0.5% FAMP reduced the percentage of C16:0 in egg yolks. The excess content of C16:0 may be harmful to the human body by increasing the production of harmful lipids, impairing cellular function, and inducing inflammation (Palomer et al., 2018). Meanwhile, FAMP supplementation decreased the SFA, especially 0.5% FAMP, which is partially in line with Selim et al. (2023), who found that supplementing grape pomace in laying hens' diets reduced the SFA. The CON group had a higher content of arachidonic acid in egg yolk, which may partly result from its increased biosynthesis of the unsaturated fatty acids pathway of cecal microbiota. Moreover, we found that the addition of FAMP (0.25%−0.1%) had beneficial impacts on the health lipid indices of egg yolk, which decreased the AI and TI while increasing the H/H, HPI, and DFA values. A relatively lower AI or TI value is beneficial to coronary artery health due to lower platelet aggregation (Woloszyn et al., 2020). The H/H index is defined as the Σhypercholesterolemic fatty acids/Σhypercholesterolemic fatty acids ratio and is also strongly associated with cholesterol metabolism. With respect to nutriology, the relatively higher H/H value is considered to have a greater potential to maintain physical health (Fernandes et al., 2014). The higher H/H and HPI (the reciprocal of AI) ratios provide protection against cardiovascular diseases (Hanus et al., 2018). The DFA index involves fatty acids, which are considered to have either neutral or cholesterol-lowering effects (Banskalieva et al., 2000). Thus, dietary FAMP supplementation positively affected the nutritive value of egg yolk. The optimal dosage was 0.5% FAMP, suggesting that FAMP had quadratic effects on fatty acid indices in egg yolk.

Egg albumen is rich in proteins, peptides, and amino acids (Sun et al., 2019), which possess antimicrobial, antioxidant, and anti-inflammatory functions (Lee and Paik, 2019). In the present study, the addition of 0.25% FAMP decreased the valine concentration, which may be related to its increased valine, leucine, and isoleucine degradation pathway of cecal microbiota. The addition of FAMP had no significant impact on most of the amino acid composition of egg albumen (Table 4). In contrast, a diet supplemented with 120–360 mg/kg anthocyanin-rich purple corn extract could improve most EAA and NEAA concentrations in eggs (Li J. et al., 2023). This disagreement is possibly influenced by the differences in feed composition, breeds, and ages of laying hens. For example,

L-glutamine supplementation increased the levels of asparagine, phenylalanine, tryptophan, and tyrosine of albumen (Tomaszewska et al., 2021).

The growth and the role of ovarian follicles affect the laying performance of layers (Song et al., 2023), which is closely related to hormone regulation (Brady et al., 2020). The aged laying hens exhibit abnormal secretion of steroid hormones (Wu et al., 2023). In our study, the inclusion of 0.25%−1.0% FAMP increased the white follicles and the ovarian FSH, LH, and E_2 levels. The small white follicles are involved in the estradiol secretion (Huang et al., 2021). FSH stimulates 3b-hydroxysteroid dehydrogenase (HSD3B1) production in granulosa cells by combining it with its receptor (FSHR) (Huang et al., 2021). Our findings suggested that the addition of 1% FAMP increased ovarian *HSD17B1* expression. HSD17B1 catalyzes the transformation process of estrone into estradiol (the most active type of estrogen), which is responsible for testosterone generation (Ruan et al., 2023). These findings indicate that FAMP supplementation could enhance ovary function by regulating follicle development and hormone synthesis.

Yolk precursors formed in the liver are transported into the ovary of laying hens through blood circulation (Li et al., 2015). Estrogen stimulates the synthesis of apo very low-density lipoprotein II (ApoVLDL II) and apolipoprotein B (APOB) and the induction of hepatic very low-density lipoprotein (VLDL) assembly procedures for VLDL Y (VLDLy) formation (Walzem et al., 1999). ApoVLDL-II prevents the lipolytic action of lipoprotein lipase on VLDLy for lipid deposition in the oocyte (Schneider et al., 1990). Aged laying hens tend to have abnormalities in their LBO axis function (Amevor et al., 2021). Our findings showed that genes related to yolk precursors synthesis (e.g., *ACC*, *FAS*, and *SCD*) and transport (e.g., *VTG II*, *ApoVLDL II*, and *APOB*) of the liver were upregulated in aged laying hens after FAMP supplementation, which could coordinately generate yolk lipids (Amevor et al., 2021). Li et al. observed that the *ESR2* expression in the liver was significantly upregulated in hens with higher laying performance (Li et al., 2015). We found that 1.0% FAMP increased *ESR2* expression in the liver. Similarly, the addition of 1.0% and 4.0% *Aronia melanocarpa* increased the levels of estrogen and proteins as manifested by yolk precursors in the liver of laying hens (Jing et al., 2022). Collectively, the addition of FAMP may contribute to the yolk lipid deposition in the ovary by regulating the function of the LBO axis.

Oxidative stress is a critical cause of ovarian recession, accompanied by decreased laying performance and egg quality of aged hens (Bao et al., 2022). In this study, 0.5% FAMP supplementation increased the ovarian T-AOC and SOD levels, which belong to the enzymatic defense system of the body (Wu et al., 2023). AMP contains total polyphenols, which have antioxidant potential (Sidor and Gramza-Michalowska, 2019). Dietary 2.5% AMP increased tocopherol content and exhibited better antioxidant properties in egg yolk (Loetscher et al., 2014). Polyphenol-rich additives like AMP, *Aronia melanocarpa* (Jing et al., 2022), grape pomace (Reis et al., 2019), and purple corn extract fed to laying hens (Li J. et al., 2023) improved ovary or plasma antioxidant capacity via regulating the Keap1/Nrf2 signaling pathway, which is responsible for xenobiotic and oxidant elimination (Bhattacharyya et al., 2014). Nrf2 regulates defensive gene expression concerning antioxidant proteins, such as HO-1, GPX1, SOD1, and SOD2, which exert antioxidant effects (Tonelli et al., 2018). Keap1, a negative regulator of Nrf2, contributes to its retention in the cytosol. The present study showed that supplementation of 0.5% FAMP in layer diets upregulated the *Nrf2* and downregulated the *Keap1* expressions in the ovary. Our results suggest the addition of FAMP could enhance the antioxidant function of aged laying hens.

Intestinal microbiota communities and their metabolites are essential for the host physiology metabolism. The cecum has been regarded as the main site for containing relatively higher dominant microbial communities in laying hens (Ricke et al., 2022). The present study revealed that the addition of 0.25% FAMP increased the α-diversity of cecal microbiota, including richness indexes (Observed_species and Chao1) and the evolutionary diversity index (Faith-pd), but decreased the coverage index (Goods coverage), indicating that laying hens fed with 0.25% FAMP has the higher species abundance in the cecum. FAMP supplementation resulted in a difference in the β-diversity index, suggesting the addition of FAMP could alter the cecal microbiota composition. In line with previous studies, Bacteroidetes and Firmicutes were the predominant phyla of aged laying hens (Dai et al., 2022). The decline in the value of Firmicutes/Bacteroidetes may be associated with intestinal inflammation (Stojanov et al., 2020). The addition of 1% FAMP had higher Firmicutes and lower Bacteroidetes abundance, suggesting the addition of 1% FAMP was beneficial for the gut health of the laying hens. Dietary 1% FAMP supplementation also increased probiotic species such as *Pediococcus*, *Lactobacillus*, and *Acetobacter*, which can produce lactic acid and SCFA and modulate the elements of the gut–liver axis (Yu et al., 2021; Wen et al., 2023). Meanwhile, *Lactobacillus* was more abundant in laying hens with high laying performance (Wang et al., 2020). In addition, Proteobacteria is considered a potential diagnostic criterion for dysbiosis and other diseases (Shin et al., 2015). In the present study, the addition of FAMP (0.25%−1.0%) significantly decreased the Proteobacteria abundance, including *Methylobacterium* (Kovaleva et al., 2014), *Ralstonia* (Ryan and Adley, 2013), *Shigella* (Feng et al., 2021), and *Acinetobacter* (Maslova et al., 2022), which can be opportunistic pathogens. Additionally, there is an interplay between the cecal microbiota and phenotypic indicators (e.g., metabolites) of egg yolk (Tian et al., 2024). In this study, *Methylobacterium* and *Shigella* showed positive correlations with SFA, AI, and TI, and those also presented negative correlations with H/H, HPI, and DFA. Thus, FAMP could improve egg yolk health indexes, which may be related to reducing harmful bacteria.

The SCFA are the main metabolites of dietary fiber fermented by gut microbiota, which participate in energy and lipid metabolism and maintain gut homeostasis (He et al., 2020). Our findings show that the addition of 1% FAMP increased cecal acetate, propionate, butyrate, and valerate concentrations, which may be closely associated with the changes in microbial community structure. For instance, butyrate and Firmicutes (a butyrate-producing bacteria) were uniformly enhanced in the 1% FAMP group. Meanwhile, the pathway of butanoate metabolism and propanoate was also enriched in the 1% FAMP group by the PICRUSt2 analysis of microbiota. It is consistent with the fact that the 4% AMP supplementation increased the cecal acetate and butyrate concentrations in growing pigs (Ren et al., 2022).

Therefore, the above findings suggest that the addition of FAMP contributes to increasing the cecal SCFA content, which may also have positive effects on gut health.

5 Conclusion

The inclusion of FAMP in aged laying hen diet improved the health lipid indices in the egg yolk by decreasing the total SFA, AI, and TI indices, as well as increasing the H/H, HPI, and DFA indices. The addition of FAMP improved ovarian function by regulating the yolk precursor formation in the LBO axis and enhancing the antioxidant function of aged laying hens. Meanwhile, FAMP addition could regulate the cecal microbiota composition and increase SCFA concentrations of aged laying hens to promote gut health (Figure 7). Our findings provide fundamental evidence for the utilization of FAMP in aged laying hens due to its positive effects on the nutritive value of egg yolks by improving the LBO function and microbiota composition.

Data availability statement

The original contributions presented in the study are publicly available. This data can be found here: Science Data Bank, https://doi.org/10.57760/sciencedb.09193.

Ethics statement

The animal study was approved by the Animal Care and Use Committee of the Institute of Subtropical Agriculture, Chinese Academy of Sciences. The study was conducted in accordance with the local legislation and institutional requirements.

Author contributions

ZL: Conceptualization, Data curation, Formal analysis, Investigation, Methodology, Visualization, Writing – original draft. BQ: Investigation, Writing – review & editing. TC: Investigation, Writing – review & editing. XK: Conceptualization, Funding acquisition, Project administration, Writing – review & editing, Writing – original draft. QZ: Validation, Writing – review & editing. MA: Validation, Writing – review & editing. YC: Supervision, Writing – review & editing. WL: Supervision, Writing – review & editing. QH: Conceptualization, Funding acquisition, Writing – review & editing.

Funding

The author(s) declare financial support was received for the research, authorship, and/or publication of this article. This study was supported by the City-School Cooperation Project of the Fuyang Science and Technology Special Fund undertaken by Fuyang Normal University (SXHZ2020007), the National Key Research and Development Project (2022YFC3400700), the Shenzhen Science and Technology Program (ZDSYS20210623100800001), and the Special Commissioner for Rural Science and Technology of Guangdong Province (KTP20210345).

Conflict of interest

The authors declare that the research was conducted in the absence of any commercial or financial relationships that could be construed as a potential conflict of interest.

The author(s) declared that they were an editorial board member of Frontiers, at the time of submission. This had no impact on the peer review process and the final decision.

Publisher's note

Supplementary material

The Supplementary Material for this article can be found online at: https://www.frontiersin.org/articles/10.3389/fmicb.2024.1422172/full#supplementary-material

SUPPLEMENTARY TABLE S1
Amino acid composition of the fermented *Aronia melanocarpa pomace*.

SUPPLEMENTARY TABLE S2
Fatty acid composition of the fermented *Aronia melanocarpa* pomace.

SUPPLEMENTARY TABLE S3
Composition and nutrient levels of basal diet.

SUPPLEMENTARY TABLE S4
Specific primers for PCR analysis.

References

Amevor, F. K., Cui, Z., Du, X., Ning, Z., Shu, G., Jin, N., et al. (2021). Combination of quercetin and vitamin E supplementation promotes yolk precursor synthesis and follicle development in aging breeder hens via liver-blood-ovary signal axis. *Animals* 11:1915. doi: 10.3390/ani11071915

Banskalieva, V. V., Sahlu, T., and Goetsch, A. L. (2000). Fatty acid composition of goat muscles and fat depots: A review. *Small Rumin. Res.* 37, 255–268. doi: 10.1016/S0921-4488(00)00128-0

Bao, T., Yao, J., Zhou, S., Ma, Y., Dong, J., Zhang, C., et al. (2022). Naringin prevents follicular atresia by inhibiting oxidative stress in the aging chicken. *Poult. Sci.* 101:101891. doi: 10.1016/j.psj.2022.101891

Bhattacharyya, A., Chattopadhyay, R., Mitra, S., and Crowe, S. E. (2014). Oxidative stress: An essential factor in the pathogenesis of gastrointestinal mucosal diseases. *Physiol. Rev.* 94, 329–354. doi: 10.1152/physrev.00040.2012

Brady, K., Porter, T. E., Liu, H.-C., and Long, J. A. (2020). Characterization of the hypothalamo–pituitary–gonadal axis in low and high egg producing turkey hens. *Poult. Sci.* 99, 1163–1173. doi: 10.1016/j.psj.2019.12.028

Cui, Y., Peng, S., Deng, D., Yu, M., Tian, Z., Song, M., et al. (2023). Solid-state fermentation improves the quality of chrysanthemum waste as an alternative feed ingredient. *J. Environ. Manage.* 330:117060. doi: 10.1016/j.jenvman.2022.117060

Dai, D., Qi, G. H., Wang, J., Zhang, H. J., Qiu, K., and Wu, S. G. (2022). Intestinal microbiota of layer hens and its association with egg quality and safety. *Poult. Sci.* 101:102008. doi: 10.1016/j.psj.2022.102008

Du, X., and Myracle, A. D. (2018). Fermentation alters the bioaccessible phenolic compounds and increases the alpha-glucosidase inhibitory effects of aronia juice in a dairy matrix following *in vitro* digestion. *Food Funct.* 9, 2998–3007. doi: 10.1039/C8FO00250A

Erinle, T. J., and Adewole, D. I. (2022). Fruit pomaces–their nutrient and bioactive components, effects on growth and health of poultry species, and possible optimization techniques. *Anim. Nutr.* 9, 357–377. doi: 10.1016/j.aninu.2021.11.011

Esatbeyoglu, T., Fischer, A., Legler, A. D. S., Oner, M. E., Wolken, H. F., Köpsel, M., et al. (2023). Physical, chemical, and sensory properties of water kefir produced from *Aronia melanocarpa* juice and pomace. *Food Chem. X* 18, 100683. doi: 10.1016/j.fochx.2023.100683

Feng, J., Lu, M., Wang, J., Zhang, H., Qiu, K., Qi, G., et al. (2021). Dietary oregano essential oil supplementation improves intestinal functions and alters gut microbiota in late-phase laying hens. *J. Anim. Sci. Biotechnol.* 12:72. doi: 10.1186/s40104-021-00600-3

Fernandes, C. E., Vasconcelos, M. A., de Almeida Ribeiro, M., Sarubbo, L. A., Andrade, S. A. C., and Filho, A.B. (2014). Nutritional and lipid profiles in marine fish species from Brazil. *Food Chem.* 160, 67–71. doi: 10.1016/j.foodchem.2014.03.055

Gu, Y., Chen, Y., Jin, R., Wang, C., Wen, C., and Zhou, Y. (2021). Age-related changes in liver metabolism and antioxidant capacity of laying hens. *Poult. Sci.* 100:101478. doi: 10.1016/j.psj.2021.101478

Hanus, O., Samkova, E., Krizova, L., Hasonova, L., and Kala, R. (2018). Role of fatty acids in milk fat and the influence of selected factors on their variability-A review. *Molecules* 23, 1636. doi: 10.3390/molecules23071636

He, J., Zhang, P., Shen, L., Niu, L., Tan, Y., Chen, L., et al. (2020). Short-chain fatty acids and their association with signalling pathways in inflammation, glucose and lipid metabolism. *Int. J. Mol. Sci.* 21: 6356. doi: 10.3390/ijms21176356

He, W., Wang, H., Tang, C., Zhao, Q., and Zhang, J. (2023). Dietary supplementation with astaxanthin alleviates ovarian aging in aged laying hens by enhancing antioxidant capacity and increasing reproductive hormones. *Poult. Sci.* 102:102258. doi: 10.1016/j.psj.2022.102258

Hu, C. J., Jiang, Q. Y., Zhang, T., Yin, Y. L., Li, F. N., Deng, J. P., et al. (2017). Dietary supplementation with arginine and glutamic acid modifies growth performance, carcass traits, and meat quality in growing-finishing pigs. *J. Anim. Sci.* 95, 2680–2689. doi: 10.2527/jas2017.1388

Huang, S. J., Purevsuren, L., Jin, F., Zhang, Y. P., Liang, C. Y., Zhu, M. Q., et al. (2021). Effect of anti-müllerian hormone on the development and selection of ovarian follicle in hens. *Poult. Sci.* 100:100959. doi: 10.1016/j.psj.2020.12.056

Jing, B., Xiao, H., Yin, H., Wei, Y., Wu, H., Zhang, D., et al. (2022). Feed supplemented with *Aronia Melanocarpa* (AM) relieves the oxidative stress caused by ovulation in peak laying hens and increases the content of yolk precursors. *Animals* 12:3574. doi: 10.3390/ani12243574

Jurikova, T., Mlcek, J., Skrovankova, S., Sumczynski, D., Sochor, J., Hlavacova, I., et al. (2017). Fruits of black chokeberry *Aronia melanocarpa* in the prevention of chronic diseases. *Molecules* 22:944. doi: 10.3390/molecules22060944

Kara, K., Gülü, B. K., Baytok, E., and Research, M. (2016). Effects of grape pomace supplementation to laying hen diet on performance, egg quality, egg lipid peroxidation and some biochemical parameters. *J. Appl. Anim. Res.* 44, 303–310. doi: 10.1080/09712119.2015.1031785

Kovacs-Nolan, J., Phillips, M., and Mine, Y. (2005). Advances in the value of eggs and egg components for human health. *J. Agric. Food Chem.* 53, 8421–8431. doi: 10.1021/jf050964f

Kovaleva, J., Degener, J. E., van der Mei, H. C., and Doern, G. V. (2014). *Methylobacterium* and its role in health care-associated infection. *J. Clin. Microbiol.* 52, 1317–1321. doi: 10.1128/JCM.03561-13

Lee, J. H., and Paik, H. D. (2019). Anticancer and immunomodulatory activity of egg proteins and peptides: A review. *Poult. Sci.* 98, 6505–6516. doi: 10.3382/ps/pez381

Li, G., Feng, Y., Cui, J., Hou, Q., Li, T., Jia, M., et al. (2023). The ionome and proteome landscape of aging in laying hens and relation to egg white quality. *Sci. China Life Sci.* 66, 2020–2040. doi: 10.1007/s11427-023-2413-4

Li, G. M., Liu, L. P., Yin, B., Liu, Y. Y., Dong, W. W., Gong, S., et al. (2020). Heat stress decreases egg production of laying hens by inducing apoptosis of follicular cells via activating the FasL/Fas and TNF-α systems. *Poult. Sci.* 99, 6084–6093. doi: 10.1016/j.psj.2020.07.024

Li, H., Wang, T., Xu, C., Wang, D., Ren, J., Li, Y., et al. (2015). Transcriptome profile of liver at different physiological stages reveals potential mode for lipid metabolism in laying hens. *BMC Genomics* 16:763. doi: 10.1186/s12864-015-1943-0

Li, J., Zhou, D., Li, H., Luo, Q., Wang, X., Qin, J., et al. (2023). Effect of purple corn extract on performance, antioxidant activity, egg quality, egg amino acid, and fatty acid profiles of laying hen. *Front. Vet. Sci.* 9:1083842. doi: 10.3389/fvets.2022.1083842

Li, Z., Meng, C., Azad, M. A. K., Lin, W., Gui, J., Cui, Y., et al. (2024). Dietary Chinese herbal formula supplementation improves yolk fatty acid profile in aged laying hens. *Vet. Quart.* 44, 1–11. doi: 10.1080/01652176.2024.2319828

Li, Z., Zhu, Q., Azad, M. A. K., Li, H., Huang, P., and Kong, X. (2021). The impacts of dietary fermented mao-tai lees on growth performance, plasma metabolites, and intestinal microbiota and metabolites of weaned piglets. *Front. Microbiol.* 12:778555. doi: 10.3389/fmicb.2021.778555

Lipinska, P., Atanasov, A. G., Palka, M., and Jozwik, A. (2017). Chokeberry pomace as a determinant of antioxidant parameters assayed in blood and liver tissue of Polish merino and Wrzosowka lambs. *Molecules* 22:1461. doi: 10.3390/molecules22111461

Livak, K. J., and Schmittgen, T. D. (2001). Analysis of relative gene expression data using real-time quantitative PCR and the $2^{-\Delta\Delta CT}$ method. *Methods* 25, 402–408. doi: 10.1006/meth.2001.1262

Loetscher, Y., Kreuzer, M., and Messikommer, R. E. (2014). Late laying hens deposit dietary antioxidants preferentially in the egg and not in the body. *J. Appl. Poult. Res.* 23, 647–660. doi: 10.3382/japr.2014-00973

Maslova, O., Mindlin, S., Beletsky, A., Mardanov, A., and Petrova, M. (2022). Plasmids as key players in *Acinetobacter* adaptation. *Int. J. Mol. Sci.* 23, 10893. doi: 10.3390/ijms231810893

Nielsen, H. (1998). Hen age and fatty acid composition of egg yolk lipid. *Br. Poult. Sci.* 39, 53–56. doi: 10.1080/00071669889394

Palomer, X., Pizarro-Delgado, J., Barroso, E., and Vázquez-Carrera, M. (2018). Palmitic and oleic acid: The Yin and Yang of fatty acids in type 2 diabetes mellitus. *Trends Endocrinol. Metab.* 29, 178–190. doi: 10.1016/j.tem.2017.11.009

Reis, J. H., Gebert, R. R., Barreta, M., Boiago, M. M., Souza, C. F., Baldissera, M. D., et al. (2019). Addition of grape pomace flour in the diet on laying hens in heat stress: Impacts on health and performance as well as the fatty acid profile and total antioxidant capacity in the egg. *J. Therm. Biol.* 80, 141–149. doi: 10.1016/j.jtherbio.2019.01.003

Ren, Z., Fang, H., Zhang, J., Wang, R., Xiao, W., Zheng, K., et al. (2022). Dietary *Aronia melanocarpa* pomace supplementation enhances the expression of ZO-1 and Occludin and promotes intestinal development in pigs. *Front. Vet. Sci.* 9:904667. doi: 10.3389/fvets.2022.904667

Ricke, S. C., Dittoe, D. K., and Olson, E. G. (2022). Microbiome applications for laying hen performance and egg production. *Poult. Sci.* 101, 101784. doi: 10.1016/j.psj.2022.101784

Ruan, G., Ye, L., Lin, J., Lin, H., Yu, L., Wang, C., et al. (2023). An integrated approach of netstudy pharmacology, molecular docking, and experimental verification uncovers kaempferol as the effective modulator of HSD17B1 for treatment of endometrial cancer. *J. Transl. Med.* 21:204. doi: 10.1186/s12967-023-04048-z

Ryan, M. P., and Adley, C. C. (2013). *Ralstonia* spp.: Emerging global opportunistic pathogens. *Eur. J. Clin. Microbiol. Infect. Dis.* 33, 291–304. doi: 10.1007/s10096-013-1975-9

Schmid, V., Steck, J., Mayer-Miebach, E., Behsnilian, D., Briviba, K., Bunzel, M., et al. (2020). Impact of defined thermomechanical treatment on the structure and content of dietary fiber and the stability and bioaccessibility of polyphenols of chokeberry (*Aronia melanocarpa*) pomace. *Food Res. Int.* 134:109232. doi: 10.1016/j.foodres.2020.109232

Schneider, W. J., Carroll, R., Severson, D. L., and Nimpf, J. (1990). Apolipoprotein VLDL-II inhibits lipolysis of triglyceride-rich lipoproteins in the laying hen. *J. Lipid Res.* 31, 507–513. doi: 10.1016/S0022-2275(20)43172-4

Selim, S., Abdel-Megeid, N. S., Alhotan, R. A., Ebrahim, A., and Hussein, E. (2023). Grape pomace: agrifood by-product with potential to enhance performance, yolk quality, antioxidant capacity, and eggshell ultrastructure in laying hens. *Vet. Sci.* 10:61. doi: 10.3390/vetsci10070461

Shin, N. R., Whon, T. W., and Bae, J. W. (2015). *Proteobacteria*: *Microbial* signature of dysbiosis in gut microbiota. *Trends Biotechnol.* 33, 496–503. doi: 10.1016/j.tibtech.2015.06.011

Sidor, A., and Gramza-Michalowska, A. (2019). Black chokeberry *Aronia melanocarpa* L.-A qualitative composition, phenolic profile and antioxidant potential. *Molecules* 24:3710. doi: 10.3390/molecules24203710

Song, X., Wang, D., Zhou, Y., Sun, Y., Ao, X., Hao, R., et al. (2023). Yolk precursor synthesis and deposition in hierarchical follicles and effect on egg production performance of hens. *Poult. Sci.*102:102756. doi: 10.1016/j.psj.2023.102756

Sosnówka-Czajka, E., and Skomorucha, I. (2021). Effect of supplementation with dried fruit pomace on the performance, egg quality, white blood cells, and lymphatic organs in laying hens. *Poult. Sci.*100:101278. doi: 10.1016/j.psj.2021.101278

Stojanov, S., Berlec, A., and Štrukelj, B. (2020). The influence of probiotics on the Firmicutes/Bacteroidetes ratio in the treatment of obesity and inflammatory bowel disease. *Microorganisms* 8:1715. doi: 10.3390/microorganisms8111715

Sun, C., Liu, J., Yang, N., and Xu, G. (2019). Egg quality and egg albumen property of domestic chicken, duck, goose, turkey, quail, and pigeon. *Poult. Sci.* 98, 4516–4521. doi: 10.3382/ps/pez259

Tian, Y., Zhang, R., Li, G., Zeng, T., Chen, L., Xu, W., et al. (2024). Microbial fermented feed affects flavor amino acids and yolk trimethylamine of duck eggs via cecal microbiota–yolk metabolites crosstalk. *Food Chem.* 430:137008. doi: 10.1016/j.foodchem.2023.137008

Tomaszewska, E., Arczewska-Wlosek, A., Burmanczuk, A., Pyz-Lukasik, R., Donaldson, J., Muszynski, S., et al. (2021). The effect of L-glutamine on basal albumen and yolk indices, and albumen amino acids composition. *Animals* 11:556. doi: 10.3390/ani11123556

Tonelli, C., Chio, I. I. C., and Tuveson, D. A. (2018). Transcriptional regulation by Nrf2. *Antioxid Redox Signal.* 29, 1727–1745. doi: 10.1089/ars.2017.7342

Walzem, R. L., Hansen, R. J., Williams, D. L., and Hamilton, R. L. (1999). Estrogen induction of VLDLy assembly in egg-laying hens. *J. Nutr.* 129, 467s−472s. doi: 10.1093/jn/129.2.467S

Wang, Y., Xu, L., Sun, X., Wan, X., Sun, G., Jiang, R., et al. (2020). Characteristics of the fecal microbiota of high- and low-yield hens and effects of fecal microbiota transplantation on egg production performance. *Res. Vet. Sci.* 129, 164–173. doi: 10.1016/j.rvsc.2020.01.020

Wen, X., Wang, Z., Liu, Q., Lessing, D. J., and Chu, W. (2023). *Acetobacter pasteurianus* BP2201 alleviates alcohol-induced hepatic and neuro-toxicity and modulate gut microbiota in mice. *Microb. Biotechnol.* 16, 1834–1857. doi: 10.1111/1751-7915.14303

Woloszyn, J., Haraf, G., Okruszek, A., Werenska, M., Goluch, Z., and Teleszko, M. (2020). Fatty acid profiles and health lipid indices in the breast muscles of local Polish goose varieties. *Poult. Sci.* 99, 1216–1224. doi: 10.1016/j.psj.2019.10.026

Wu, H., Yuan, J., Yin, H., Jing, B., Sun, C., Nguepi Tsopmejio, I. S., et al. (2023). *Flammulina velutipes* stem regulates oxidative damage and synthesis of yolk precursors in aging laying hens by regulating the liver-blood-ovary axis. *Poult. Sci.* 102:102261. doi: 10.1016/j.psj.2022.102261

Yu, J. S., Youn, G. S., Choi, J., Kim, C. H., Kim, B. Y., Yang, S. J., et al. (2021). *Lactobacillus lactis* and *Pediococcus pentosaceus*-driven reprogramming of gut microbiome and metabolome ameliorates the progression of non–alcoholic fatty liver disease. *Clin. Transl. Med.* 11:e634. doi: 10.1002/ctm2.634

Zhu, Q., Cheng, Y., Song, M., Liu, Y., Azad, M. A. K., Liu, Y., et al. (2022). Probiotics or synbiotics addition to sows' diets alters colonic microbiome composition and metabolome profiles of offspring pigs. *Front. Microbiol.* 13:934890. doi: 10.3389/fmicb.2022.934890

frontiers | Frontiers in Microbiology

TYPE Original Research
PUBLISHED 03 July 2024
DOI 10.3389/fmicb.2024.1435503

OPEN ACCESS

EDITED BY
Jie Yin,
Hunan Agricultural University, China

REVIEWED BY
Shimeng Huang,
China Agricultural University, China
Long Pan,
Nanjing Agricultural University, China

*CORRESPONDENCE
Xueli Cao
✉ caoxl@th.btbu.edu.cn

RECEIVED 20 May 2024
ACCEPTED 05 June 2024
PUBLISHED 03 July 2024

CITATION
Wang L, Liu P, Wu Y, Pei H and Cao X (2024) Inhibitory effect of *Lonicera japonica flos* on *Streptococcus mutans* biofilm and mechanism exploration through metabolomic and transcriptomic analyses. *Front. Microbiol.* 15:1435503. doi: 10.3389/fmicb.2024.1435503

Inhibitory effect of *Lonicera japonica flos* on *Streptococcus mutans* biofilm and mechanism exploration through metabolomic and transcriptomic analyses

Lin Wang, Ping Liu, Yulun Wu, Hairun Pei and Xueli Cao*

Beijing Technology and Business University, Beijing Advanced Innovation Centre for Food Nutrition and Human Health, Beijing, China

Introduction: *Streptococcus mutans* was the primary pathogenic organism responsible for dental caries. *Lonicera japonica flos* (LJF) is a traditional herb in Asia and Europe and consumed as a tea beverage for thousands of years.

Methods: The inhibitory effect and mechanism of LJF on biofilm formation by *S. mutans* was investigated. The active extracts of LJF were validated for their inhibitory activity by examining changes in surface properties such as adherence, hydrophobicity, auto-aggregation abilities, and exopolysaccharides (EPS) production, including water-soluble glucan and water-insoluble glucan.

Results and discussion: LJF primarily inhibited biofilm formation through the reduction of EPS production, resulting in alterations in cell surface characteristics and growth retardation in biofilm formation cycles. Integrated transcriptomic and untargeted metabolomics analyses revealed that EPS production was modulated through two-component systems (TCS), quorum sensing (QS), and phosphotransferase system (PTS) pathways under LJF stress conditions. The sensing histidine kinase VicK was identified as an important target protein, as LJF caused its dysregulated expression and blocked the sensing of autoinducer II (AI-2). This led to the inhibition of response regulator transcriptional factors, down-regulated glycosyltransferase (Gtf) activity, and decreased production of water-insoluble glucans (WIG) and water-soluble glucans (WSG). This is the first exploration of the inhibitory effect and mechanism of LJF on *S. mutans*, providing a theoretical basis for the application of LJF in functional food, oral health care, and related areas.

KEYWORDS

***Lonicera japonica flos*, *S. mutans*, quorum sensing, metabolomic and transcriptomic, biofilm**

1 Introduction

With the acceleration of contemporary lifestyles and the proliferation of highly processed foods, individuals increasingly sought sugar to enhance their gustatory experience. Dental caries, a biofilm-mediated oral disease, were closely associated with suboptimal dietary habits and the consumption of high-sugar foods (Chen et al., 2021; Park et al., 2023). As a result, dental caries remained a common oral health issue over time. *Streptococcus mutans* (*S. mutans*)

was the primary pathogenic organism responsible for dental caries, as biofilm formation was the main virulence factor (Barran-Berdon et al., 2020; Bhatt et al., 2020). Therefore, identifying and understanding the main virulence factors of *S. mutans* that form biofilm becomes crucial for preventing dental caries.

Biofilm represents a structured bacterial community enveloped by an extracellular polymeric matrix (Matsumoto-Nakano, 2018). The accepted theory of plaque formation was roughly divided into three stages. Firstly, glycoproteins in saliva adhered to the tooth surface to form an acquired membrane. Next, *S. mutans* cells adhered to this membrane. Once firmly attached, further adhesion between bacteria led to aggregation and the formation of a biofilm, commonly known as dental plaque (Chen et al., 2019; Li J. et al., 2020). Once formed, the biofilm could resist environmental stress. Exopolysaccharides (EPS) were the main components of the biofilm, and along with extracellular proteins and water, they formed extracellular polymers. The extracellular matrix within the biofilm provided protection from harmful factors. *S. mutans* was the leading producer of EPS and could encode multiple exoenzymes, such as glycosyltransferases (Gtf) and glucan-binding proteins. Gtfs were produced inside the cells and secreted outside, meaning they were present in the extracellular medium. Sucrose was the substrate of Gtfs and was used to synthesize glucans (Sutherland, 2001; Hoshino and Fujiwara, 2022). Glucans were the main EPS in biofilm and provided additional microbial binding sites (Schilling and Bowen, 1992; Steinberg et al., 1993; Venkitaraman et al., 1995). Despite the emergence of new strategies such as secondary messenger signaling pathway, quorum sensing pathway, and eDNA, controlling EPS production is still the main way to inhibit biofilm formation.

For treatment of cariogenic biofilms, CH was considered the gold standard in dentistry and was recommended to prevent dental caries (Persson et al., 2007). However, conventional medications, including CH, cipyridine, triclosan, etc., exhibited limited efficacy over a short duration. Long-term use of these therapies could decrease oral microbial diversity (Scully and Greenman, 2012; Pragman et al., 2021). Thus, they are not suitable for daily prevention. There is an urgent need for treatments of oral diseases with low side effects. The utilization of phytochemicals presented a promising approach, as evidence indicated the impact of plant extracts on the virulence of *S. mutans*. For instance, *Kaffir Lime leaf* exhibited an anti-biofilm effect by regulating genes associated with biofilm formation (Rather et al., 2021), *Emblica officinalis* extract reduced surface properties and glucan synthesis, and *Achyranthes aspera* extract inhibited Gtf activity (Murugan et al., 2013). Overall, phytomedicine are considered a valuable source of inhibitory substances involved in biofilm formation.

Lonicerae japonica flos (LJF, known as Jinyinhua in Chinese), the dried flowers or flower buds of *Lonicera japonica Thunberg*, is a medicinal-edible herb antibacterial, antiviral, and anti-inflammatory properties that have been well-studied and widely used for thousands of years (Li et al., 2014; Cai et al., 2020; Zheng et al., 2022). It is also consumed as a tea beverage in Asia and Europe because of its unique aroma and flavor (Li et al., 2014; Yang et al., 2017). Moreover, chlorogenic acid, the main component of LJF, has been shown in previous studies to inhibit the biofilm formation of *Pseudomonas*, *Staphylococcus aureus*, and *Salmonella enteritidis* (Sun et al., 2021, 2022; Wang L. et al., 2023). This suggests that LJF may have inhibitory effects on the biofilm formation of *S. mutans*. However, the current assessment of anti-biofilm effect is insufficient and the inhibition mechanism lacks comprehensiveness.

In the last years, integrated transcriptomic and metabolomic analyses provide a molecular-scale perspective on the response of crops to pesticides (Liu and Zhu, 2020), the effects on the interaction of tea plant and *Colletotrichum camelliae* (Lu et al., 2020). Integrated multi omics analyses aroused a high interest because of their potential for the identification of molecular features and target discovery. In the present study, the inhibitory effect of LJF samples from different origins on *S. mutans* was examined. The active extracts were evaluated for the inhibitory activity in terms of changes in surface properties, EPS production, and quorum-sensing (QS) signaling molecule AI-2. Integrated metabolomics and transcriptomic analyses were applied to investigate the differentiation of metabolites and gene expression in biofilms, elucidating inhibitory mechanisms of LJF on biofilm formation.

2 Materials and methods

2.1 Materials and reagents

Dried LJF samples were collected from four different origins in 2021. Sample information is provided in Supplementary Table S1, and plant morphology is shown in Figure 1A. *S. mutans* strain UA159 (ATCC700610) was purchased from the China General Microbiological Culture Collection Center and sub-cultured under anaerobic conditions for experiments. The anaerobic environment was maintained in a 2.5 L anaerobic incubator (D-110, Mitsubishi, Japan) using a disposable AnaeroPack (MGC AnaeroPack Series D-04, Mitsubishi, Japan). For biofilm formation, 1% sucrose was added to Brain Heart Infusion medium (BHIS).

2.2 Preparation of LJF extract

LJF extracts were prepared as previously elucidated (Wang S. et al., 2023). Each sample (10.0 g) was extracted with 100 mL of 60% aqueous methanol under ultrasonication, yielding approximately 1 g of extract from 10 g of dry sample.

2.3 Minimum inhibitory concentration assay of LJF and biofilm formation of *Streptococcus mutans*

The minimum inhibitory concentration (MIC) of the LJF extract against *S. mutans* was tested as described with some modification (Li et al., 2018). Firstly, 1.5 g of LJF extract was dissolved in 45 mL sterile BHIS, and the bacteria-free solution was obtained by filtering through a 0.22-μm membrane. Then, 190 μL BHIS containing diluted LJF extract (30.00, 27.00, 24.00, 21.00, 18.00, 15.00, 12.00, 9.00, 6.00, 3.00, and 0.00 mg/mL) was added to a 96-well plate. Each well was supplemented with 10 μL *S. mutans* culture (OD_{600nm} 0.17). Five replicates were performed at each concentration. Positive control groups contained BHIS culture, while background control groups were supplemented with 10 μL saline instead of *S. mutans* culture. After 16 h of incubation, data was read at 600 nm using a microplate

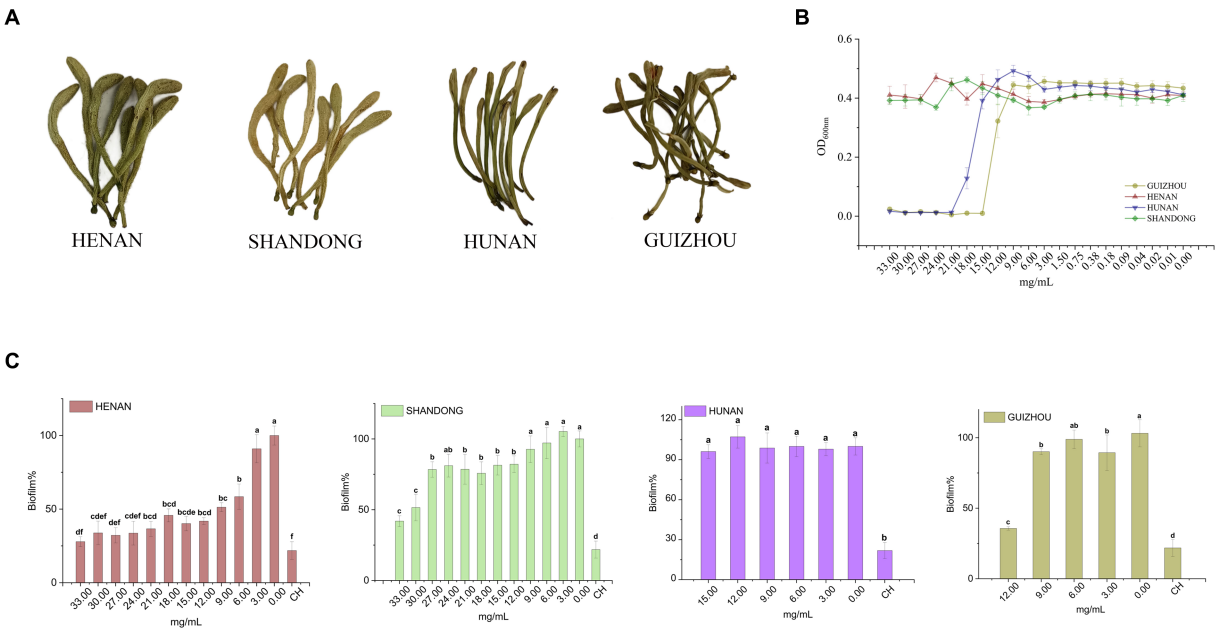

FIGURE 1
Inhibitory effect of different cultivars of LJF on planktonic *S. mutans* and biofilm production. **(A)** Four cultivars of LJF. **(B)** Inhibitory effect of different LJF cultivars on *S. mutans*. **(C)** Inhibitory effect of different LJF cultivars on *S. mutans* biofilm production. For the letters a–f, mean values ($n = 5$) with different letters within the same column are significantly different ($p < 0.05$).

reader (Infinite M200PRO, TESCAN, Mannedorf, Switzerland). MIC was determined as the lowest concentration with no inhibitory effect. Biofilm formation was assessed as described (De Jesus and Dedeles, 2020), with data read at 590 nm using the microplate reader, and the percentage of biofilm formation calculated.

2.4 Morphology of *Streptococcus mutans* biofilm

First, 1.9 mL of 21.00 mg/mL LJF was added to each well containing a slice (φ15 mm, NEST, Wuxi, China) in a 24-well plate. Then, 100 μL of a bacterial suspension of *S. mutans* (OD_{600nm} 0.17) was added to each well. The plate was incubated at 37°C for 16 h. After incubation, the biofilm was fixed as described (Jiang et al., 2022). Images were obtained using SEM (SU8020, Hitachi, Japan). For Fourier Transform Infrared Spectroscopy (FTIR) (Nicolet IS10, Thermo Fisher, USA), 1 mg of biofilm from each slice was mixed with 100 mg of KBr and ground (Chang et al., 2021; Howard et al., 2023).

2.5 Analysis of the main components of *Streptococcus mutans* biofilm

2.5.1 Viability of biofilm-entrapped cells

After incubation in the 96-well plate, the supernatants were removed, and the biofilm formed on the plates was rinsed twice with PBS. Then, 200 μL of 0.5 mg/mL 3,-3′-bis (4-methoxy-6-nitro) benzene sulfonic acid (XTT) was added to each well and incubated in an opaque black plastic bag at 37°C for 4 h. The absorbance at 490 nm was recorded as viability, as described (Kim et al., 2022).

2.5.2 Contents of EPS

The water-soluble glucan (WSG) and water-insoluble glucan (WIG) of the *S. mutans* biofilms were extracted as previously described with some modifications (Zhang H. et al., 2022; Rudin et al., 2023). The detailed steps are shown in Supplementary Figure S1. The absorbance of WSG and WIG was measured using the anthrone method.

2.6 Surface properties of *Streptococcus mutans* in biofilm

The adherence of cells in each group was measured using the method of Islam et al. (2008). The hydrophobicity of biofilm cells in each group was determined according to the method of Ullah et al. (2023). The aggregation capacity (AC) was evaluated as described by Kolenbrander (Bosch et al., 2012). Detailed steps for these determinations are shown in Supplementary Figure S1. Data was read at 600 nm using a microplate reader.

2.7 Autoinducer-2 bioassay

Autoinducer-2 (AI-2) was determined using methods previously described, with some modifications. To begin the assay, 9.0 mL of a *V. harveyi* BB170 cell culture diluted 1:100 was placed into a set of sterile plastic rocker tubes. Then, 1.0 mL of tested samples, negative control, positive control, and chemically synthesized pure AI-2 (10 μM) were added separately to each tube (Supplementary Figure S2). The luminescence value (RL) (SpectraMax®i3, Molecular Devices, Shanghai, China) was measured in photons/s mode every 60–120 min for a total of 8 h. AI-2 content was determined as described (Vilchez et al., 2007; Cuadra et al., 2016; Muras et al., 2018; Zhang Y. et al.,

2022). The relative luminescence intensity (RLI) and the content of AI-2 was determined as follows:

$$RLI = \frac{RL_{sample} - RL_{medium\ control}}{RL_{BB170} - RL_{AB\ medium}}$$

$$AI-2 = \frac{RLI_{sample} \times 10_{10\,\mu M\ AI-2}}{RLI_{10\,\mu M\ AI-2}}$$

2.8 Metabolomics analysis of *Streptococcus mutans* biofilm

First, 10 mL of 21.00 mg/mL LJF was added into a tissue culture-treated dish (NEST, Cat.No:704001, Jiangsu, China). Then, 1,000 μL bacterial suspension was added into each dish. After 16 h incubation, dishes were rinsed with sterile water twice. Biofilms cultured in the same volume of non-LJF BHIS were set as control group. An amount of 50 mg of each biofilm sample was weighed accurately and added into 2 mL centrifuge tubes. Metabolites extraction and MS data collection were according to the previous method (Li et al., 2024). Metabolomics data have been deposited to the EMBL-EBI MetaboLights database: with the identifier MTBLS9711. The complete dataset could be accessed at "https://www.ebi.ac.uk/metabolights/MTBLS9711".

2.9 Transcriptomic analysis of *Streptococcus mutans* biofilm

A total of 100 mg biofilm cells were collected using 1 mL of PBS from dishes. Total RNA was isolated as described (Li et al., 2019). Whole mRNAseq libraries were generated by Guangdong Magigene Biotechnology Co., Ltd. Result of the quality control can be seen from Supplementary Table S3. Differentially expressed genes (DEG) were selected according to the criterion: genes with FDR ≤ 0.05 and |log2(fold change)| ≥ 1. Enrichment analysis of differentially expressed genes were performed by Heml, referred to the website of KEGG. Pathways with FDR ≤ 0.05 were considered significantly enriched. The RNA-seq datasets are available at the NCBI Sequence Read Archive (SRA) database under accession number PRJNA1119033. The complete dataset could be accessed at "https://www.ncbi.nlm.nih.gov/sra/PRJNA1119033".

2.10 Quantitative reverse transcriptional polymerase chain reaction (qRT-PCR)

Primers for target genes were designed for biofilm formation-related DEGs in *S. mutans*. Primers were synthesized by Ruiboxingke Biotechnology Co. Ltd. (Beijing, China) and were shown in Supplementary Table S2. The PCR reactions were conducted according to the previous described method (Park et al., 2023).

2.11 Statistical analysis

A one-way analysis of variance (ANOVA) was conducted using SPSS to determine significant differences in biofilm formation properties, with a significance level set at $p < 0.05$. Data were visualized using Origin 9. Chemometrics for metabolomics and transcriptomics were performed in R (4.3.1) and Biodeep.[1] Finally, a mechanism diagram was created using Adobe Illustrator.

3 Results

3.1 Effects of different cultivars on *Streptococcus mutans* biofilm formation

The inhibitory effect of LJF extracts from different cultivars was initially evaluated through a series of concentration tests to determine their impact on the planktonic growth of *S. mutans*. As shown in Figure 1B, LJF samples from Hunan and Guizhou exhibited no inhibitory effect at concentrations below 15.00 mg/mL and 12.00 mg/mL, respectively, indicating MIC values higher than these concentrations. Similarly, LJF samples from Henan and Shandong showed no inhibitory effect at concentrations lower than 33.00 mg/mL, suggesting an MIC higher than 33.00 mg/mL. The antibacterial efficacy of Guizhou and Hunan extracts were significantly superior to that of the other two extracts.

However, as depicted in Figure 1C, the crystal violet staining assay revealed that Henan cultivar exhibited a robust dose-dependent inhibition of biofilm formation at concentrations below MIC, demonstrating an impressive inhibition rate of 72% (compared to control group) at 33.00 mg/mL. This rate was slightly below the positive control effect achieved by CH at 12.5 μM (79%). The Shandong cultivar displayed an inhibition rate of approximately 50% within the range of 30.00–33.00 mg/mL. In contrast, the Guizhou cultivar showed a modest inhibitory effect, while the Hunan cultivar exhibited no discernible inhibitory effect on biofilm formation at concentrations below the MIC, despite its demonstrated inhibitory effect on planktonic *S. mutans* growth. Consequently, the Henan cultivar was selected for subsequent investigations due to its superior performance in biofilm inhibition compared to other tested varieties.

3.2 Effect on the biofilm characteristics of *Streptococcus mutans*

3.2.1 Morphology analysis

In control group, clusters of *S. mutans* exhibited a uniformly distributed multilayer and reticular biofilm (Figure 2A). But when cultured in the concentration of LJF and CH (24.00 mg/mL and 12.5 μM, respectively), the density of biofilm decreased, and the network structure was damaged to varying degrees. Biofilms in treated group displayed wider channels compared to biofilm in control group, such as fewer bacteria and channels, primarily attributed to the underdeveloped biofilm structure. Additionally, bacteria were arranged in a three-dimensional stacking pattern in both control group and treated group. It means that cell membrane permeability remained unaltered in LJF group at this concentration.

FTIR spectra of biofilm in control group and LJF group was measured to determine changes biofilm structure, chemical groups

1 https://www.biodeep.cn/

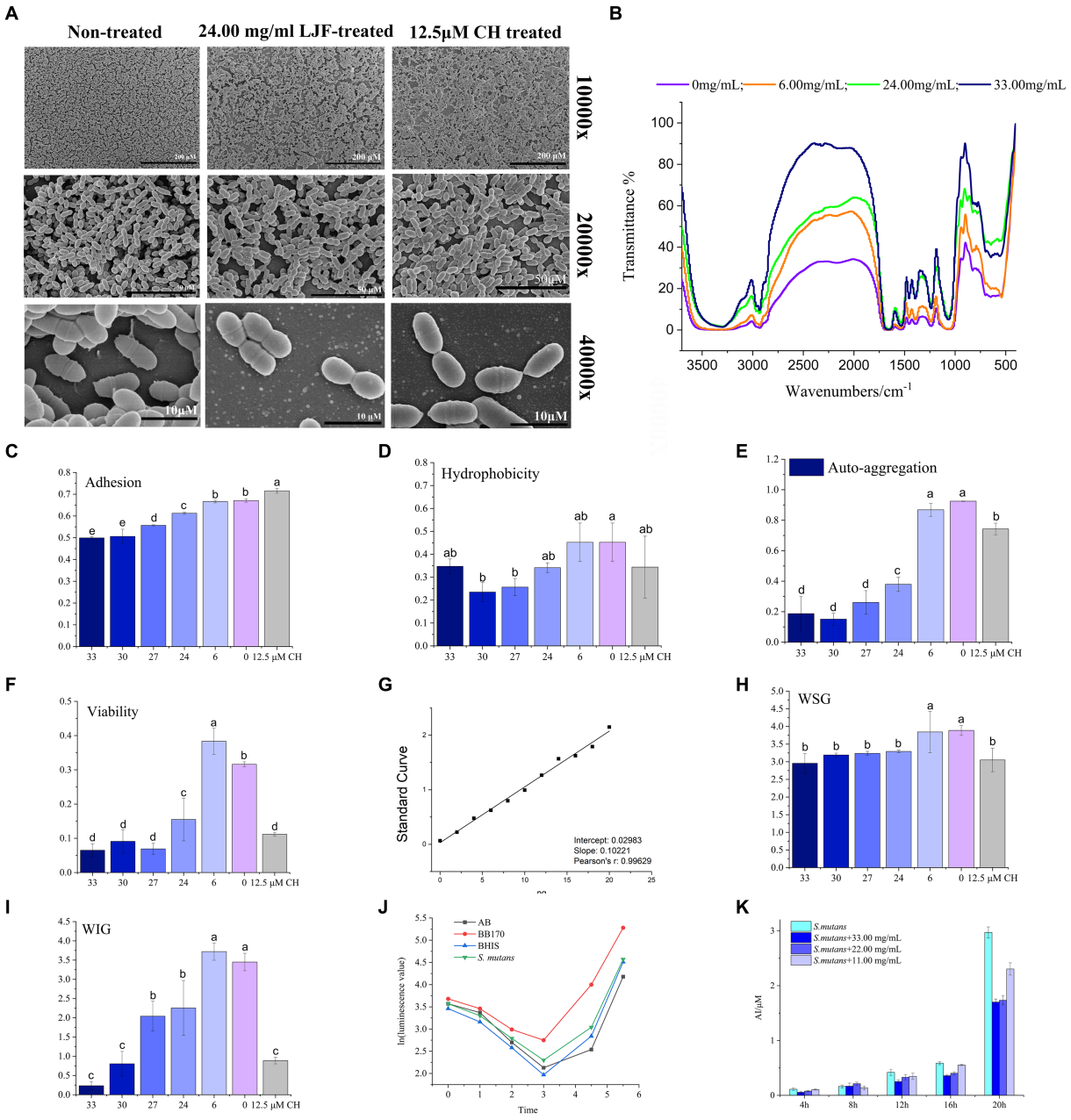

FIGURE 2
Effect of LJF on *S. mutans* biofilm. **(A)** Microstructure of *S. mutans* biofilm. **(B)** FTIR of *S. mutans* biofilm (Blank line: non-LJF treated sample; Yellow line: 6.00 mg/mL LJF inhibition sample; Light blue line: 21 mg/mL LJF inhibition sample; Pink line: 33.00 mg/mL LJF inhibition sample). **(C)** Effect of the LJF on the adhesion of *S. mutans* ($p<0.05$). **(D)** Effect of the LJF on the hydrophobicity of *S. mutans* ($p < 0.05$). **(E)** Effect of the LJF on the self-aggregation of *S. mutans* ($p < 0.05$). **(F)** Viability of bacteria in *S. mutans* biofilm ($p < 0.05$). **(G)** Standard curve of glucan. **(H)** Water soluble glucans (WSG) production of *S. mutans* biofilm ($p < 0.05$). **(I)** Water insoluble glucans (WIG) production of *S. mutans* biofilm. **(J)** AI-2 production of *S. mutans*. **(K)** Inhibitory effect of LJF on AI-2 production of *S. mutans*. Colors of column indicated the different concentration of LJF. For the letters a–e, mean values ($n = 4$) with different letters within the same column are significantly different ($p < 0.05$).

and compounds of unknown substances of biofilms, as presented in Figure 2B. Compared to the black line, the other three lines were narrow at 3,600–3,000 cm^{-1}, 3,000–2,800 cm^{-1}, 1,600–1,500 cm^{-1}, and 1,200–1,000 cm^{-1}. There is a broad peak at 3,600–3,000 cm^{-1}. Maybe it caused by the hydration of EPS in biofilm and surface polysaccharide of biofilm cells. Additionally, a peak at 3,000–2,800 cm^{-1} corresponded to the C-H of EPS. A peak at 1,600–1,500 cm^{-1} was assigned to the C=O of polysaccharides. Peaks at 1,200–1,000 cm^{-1} were maybe caused by two kinds of C-O stretching vibration. The morphological analysis using SEM and FTIR indicated structural alterations in the biofilm structure of LJF-treated groups compared to the control group.

3.2.2 Surface properties of biofilm cells

The main surface properties of biofilm include adherence, hydrophobicity, and auto-aggregation ability. LJF effectively inhibited the adherence of *S. mutans* biofilm in a dose-dependent manner

(Figure 2C). Adherence of cells is likely attributed to the hydrophobic interaction between cells and the contact surface. Both LJF-treated and CH-treated groups exhibited lower hydrophobicity compared to the control group (Figure 2D) ($p < 0.05$). Auto-aggregation refers to the phenomenon of cellular aggregation in a bacterial culture, indicating the interaction of the mass and the rapid propagation of bacteria during the culture process. There was less auto-aggregation in the LJF-treated and CH-treated groups than in the control group (Figure 2E) ($p < 0.05$). Inhibition at 24.00–33.00 mg/mL occurred in a dose-dependent manner. Cell clumping properties were mainly regulated by surface EPS.

3.3 Effect on the main components of *Streptococcus mutans* biofilm

3.3.1 Viability of biofilm-entrapped cells

The migratory capacity of the biofilm is contingent upon the bacterial activity within it. The XTT method represents a widely employed approach for assessing bacterial metabolic function. The viability of biofilm-entrapped cells significantly decreased in the presence of LJF, comparable to that of CH treatment (Figure 2F). This suggested that the metabolic capability of *S. mutans* biofilm decreased under LJF treatment.

3.3.2 Extracellular polysaccharides of biofilms

As the survival of living bacteria in biofilm primarily relies on the polysaccharide matrix and dead bacteria for protective measures, glucan polymers play a crucial role in maintaining the three-dimensional structure of biofilms. EPS was the main component of polysaccharide matrix and primarily consist of two types of glucans, WSG and WIG. Figure 2G illustrated the standard curve used for quantitative detection of polysaccharides. As depicted in Figures 2H,I, both WSG and WIG production exhibited significant inhibition compared to the control group ($p < 0.05$). The application of LJF resulted in a significant reduction of 50–90% in WIG production, which is particularly noteworthy.

3.4 Effect on the AI-2 production

The LuxS/AI-2 quorum sensing (QS) system has been widely reported to play a role in biofilm formation in *S. mutans*. It can been seen from Figure 2J, there was low expression of AI-2 within the first 4 h, followed by a gradual increase. Compared to the control group (BHIS without *S. mutans*), the secretion of AI-2 by *S. mutans* was significantly higher in the group of inoculated BHIS. The observed trend exhibited a similar pattern to that of the positive control, indicating successful production of the AI-2 signal molecule by *S. mutans*. To investigate the impact of LJF on the LuxS/AI-2 QS system, we assessed changes in AI-2 secretion by *S. mutans* at different concentrations of LJF. Notably, presence of LJF resulted in decreased production of AI-2 by *S. mutans* (Figure 2K), confirming its inhibitory effect on biofilm through LuxS/AI-2.

In all, LJF-induced changes in surface features and EPS formation of *S. mutans* biofilm were confirmed. LuxS/AI-2 was identified as one of the inhibitory pathways associated with this phenomenon. In fact, the unique composition and characteristics of biofilms make combating biofilm infections extremely difficult due to their multi-microbial nature, which results in synergistic tolerance of multiple resistance mechanisms. Single-target treatments are usually ineffective against biofilm formation (Seneviratne et al., 2020). Therefore, we hypothesized that the inhibition of biofilm formation by LJF exhibited a multi-target mechanism.

3.5 Metabolomics analysis

Untargeted metabolomics analysis was performed to achieve profiling changes of all metabolites with the exclusion of antibacterial function. The variation of critical metabolites revealed the regulated metabolic pathway. The UPLC-Qtof MS system was employed to harvest a total of 6,803 and 11,695 metabolites in the positive and negative modes, respectively. Principal component analysis (PCA) of the positive mode metabolome data (Figure 3A) revealed that PC-1 accounted for 41.2% of the variance, while PC-2 explained 12.1%, primarily contributing to the observed differences along PC-1 axis. In the negative mode (Figure 3B), PC-1 accounted for 53.7% of the variance, with PC-2 explaining 13.3%. The volcano plot depicted variations among all metabolites, where differential expressed metabolites (DEMs) were selected based on $p < 0.05$ and VIP ≥ 1.0 criteria: up-regulated metabolites were represented by red dots, down-regulated ones by blue dots, and grey dots indicated those not meeting screening criteria. In positive mode, a total of 1981 compounds were upregulated while 979 compounds were down-regulated; in negative mode, there were 4,783 up-regulated compounds and 1,643 down-regulated compounds identified separately as DEMs.

Therefore, we further identified key metabolites by integrating data from open-source databases and local databases, and explored the metabolic pathways associated with biofilm formation capacity. In total, 394 differentially expressed metabolites (DEMs) were identified using secondary mass spectrometry, and their clustering analysis is shown in the heatmap (Figure 3C1). The information of these identified metabolites can be found in Supplementary Table S4. Figure 3C2 illustrates the up-regulated and down-regulated DEMs, which include fatty acyls, carboxylic acids and derivatives, steroids and steroid derivatives, benzene and substituted derivatives, prenol lipids, organooxygen compounds, as well as pyrimidine nucleotides. The subclasses of these compounds are presented in Figures 3D1–D5. Most of DEMs were the metabolites regulated in alanine, aspartate and glutamate metabolism, biosynthesis of various secondary metabolites, lysine degradation, glyoxylate and dicarboxylate metabolism, two-component system (TCS), pyrimidine metabolism, purine metabolism, and ABC transporters. At the metabolic level, all but ABC transporters were the pathways that inhibited biofilm formation and significantly regulated by DEMs.

3.6 Transcriptomic analysis

The LJF-treated and control groups exhibited a conspicuous disparity, characterized by a substantial variance in PC-1 and a considerable dissimilarity over long distances (Figures 4A,B). DEGs with |Fold change| (|FC|) ≥ 2, p-value < 0.05, FDR ≤ 0.05 were selected. The LJF group exhibited a total of 389 up-regulated genes, while the remaining 368 genes were down-regulated (Figure 4C). The

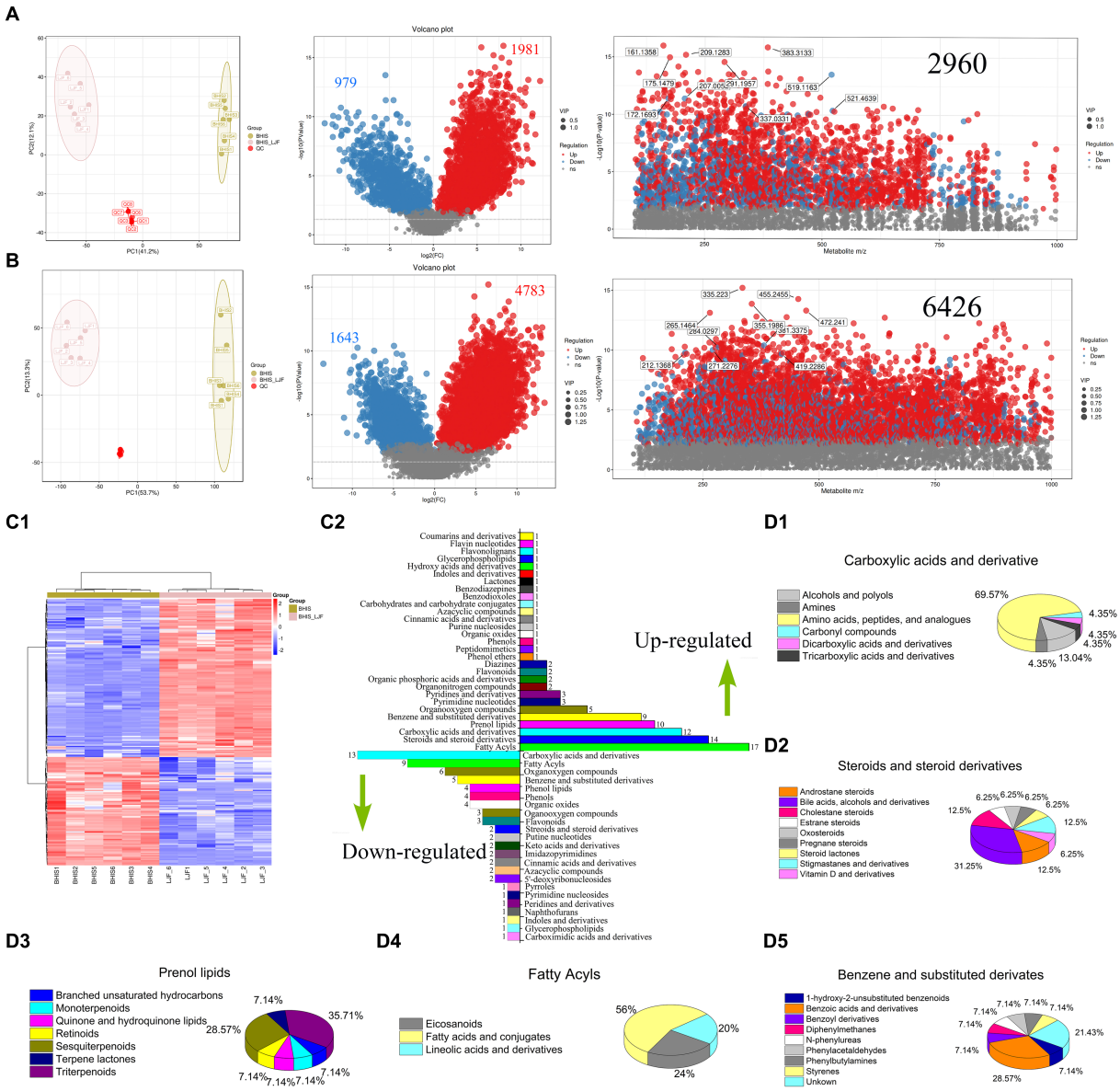

FIGURE 3
Differential analysis and metabolite identification. **(A)** Differential analysis in ESI positive mode. **(B)** Differential analysis in ESI negative mode. In the volcano plots, each compound is represented in red (up-regulated) or blue (down-regulated). In the scatter plot, the horizontal coordinate indicates the m/z of the compound. The ordinate represents the logarithm of the *p*-value. Each dot represents a compound. The red dot represents up-regulate and the blue dot represents down-regulate. The grey dot represents the metabolite that is below the screening criteria. The dot size represents the VIP value. **(C)** Cluster analysis by the metabolites identified in MS/MS mode. Upregulated metabolites were the right column. Down-regulated metabolites were left columns. **(D)** Composition of the main metabolite classes.

prominently up-regulated genes were associated with ABC transporters, TCS, and phosphotransferase system (PTS). Conversely, the down-regulated genes primarily participated in ribosome function, QS, and TCS (Figure 4D). We further validated the altered expression of these genes induced by LJF using quantitative real-time PCR assay. This finding is consistent with the mRNA-seq analysis results for gene expression levels (Supplementary Table S5). These screened genes for RT-PCR validation involved in biofilm formation. The expression levels of the aforementioned genes were consistent with the results obtained from mRNA-seq analysis (Supplementary Figure S3), thereby establishing confidence in the enrichment analysis. Most of DEGs were enriched in the pathways of TCS, purine metabolism, PTS, histidine metabolism, glycine, serine and threonine metabolism, galactose metabolism, fructose and mannose metabolism. At the level of transcription, PTS, histidine metabolism, galactose metabolism, glycine, serine and threonine metabolism were the most regulated pathways by LJF.

Mechanism analysis based on transcriptomics and metabolomics obtained several pathways that regulated biofilm formation, but the information obtained by the two kinds of omics analysis could not be completely consistent, and the target information could not be judged. Therefore, it is necessary to integrate transcriptomics and metabolomics analyses to focus on the target of LJF inhibiting biofilm formation.

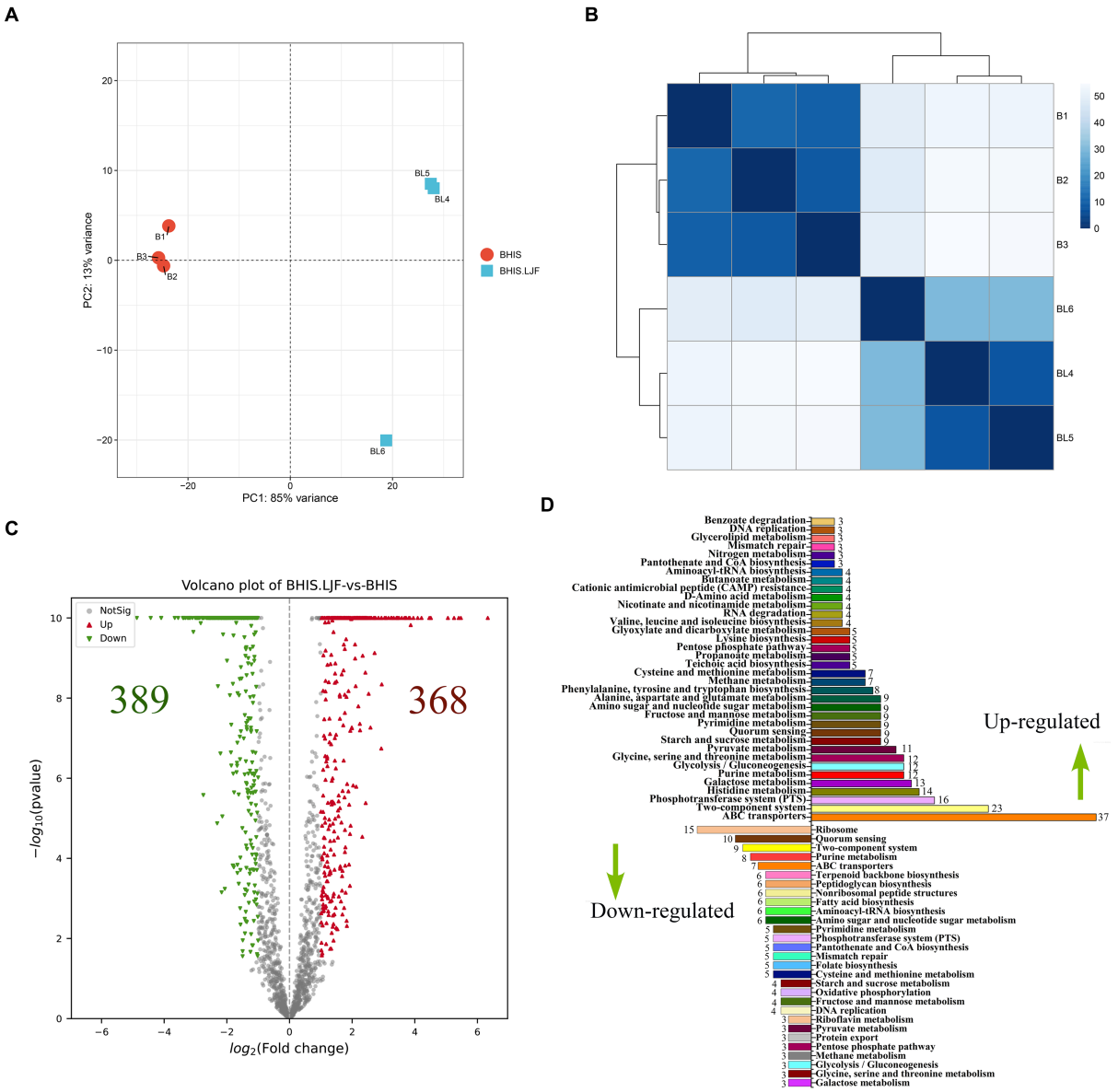

FIGURE 4
Transcriptomic analysis. **(A)** PCA score plot. **(B)** Distance heatmap. **(C)** Volcano plots of DEG on RNA-seq analysis of untreated and LJF-treated *S. mutans*. Each gene is represented in red (upregulated) and green (downregulated) and they are DEGs with >2 fold change and $p < 0.05$. **(D)** Numbers of DEGs and RT-PCR validation. Up-regulated DEGs were the right columns and down-regulate DEMs were the left columns.

3.7 Conjoint analysis of transcriptomic and metabolomics data

A four-image map of DEGs and DEMs, visually represented the correlation between gene expression and metabolite changes (Figure 5A). Purple points in parts two, four, five, six, and eight indicated non-correlated DEMs and DEGs, while green points represented significant co-differentials with a screening criterion of $|FC| \geq 2$. There were more points in the parts that indicated correlated DEMs and DEGs. These findings established a foundation for further exploration of the anti-biofilm mechanism of LJF. KEGG pathway enrichment analysis identified 55 pathways in both transcriptomic and metabolomic analyses (Figure 5B). The transcriptomic results supported the metabolomic analysis. Pathway enrichments of DEMs and DEGs are presented in Figure 5C based on *p*-value, impact (metabolomic), and rich factor (transcriptomic). In the enrichment scatter plot, TCS and PTS exhibited the most significant changes across both two omics datasets. Additionally, top pathways such as ABC transporter, purine metabolism, QS, starch and sucrose metabolism, alanine/aspartate/glutamate metabolism, and glyoxylate/dicarboxylate metabolism remained highly enriched. In these pathways, TCS, QS, and PTS were known to be involved in biofilm formation. Therefore, the DEMs and DEGs regulated in the three pathways were further screened.

In the regulatory network diagram of the screened DEGs and DEMs, blue lines represent QS, orange lines indicate TCS, and purple lines depict the PTS pathway (Figure 5D). These pathways play a crucial role in regulating metabolism. Norepinephrine was

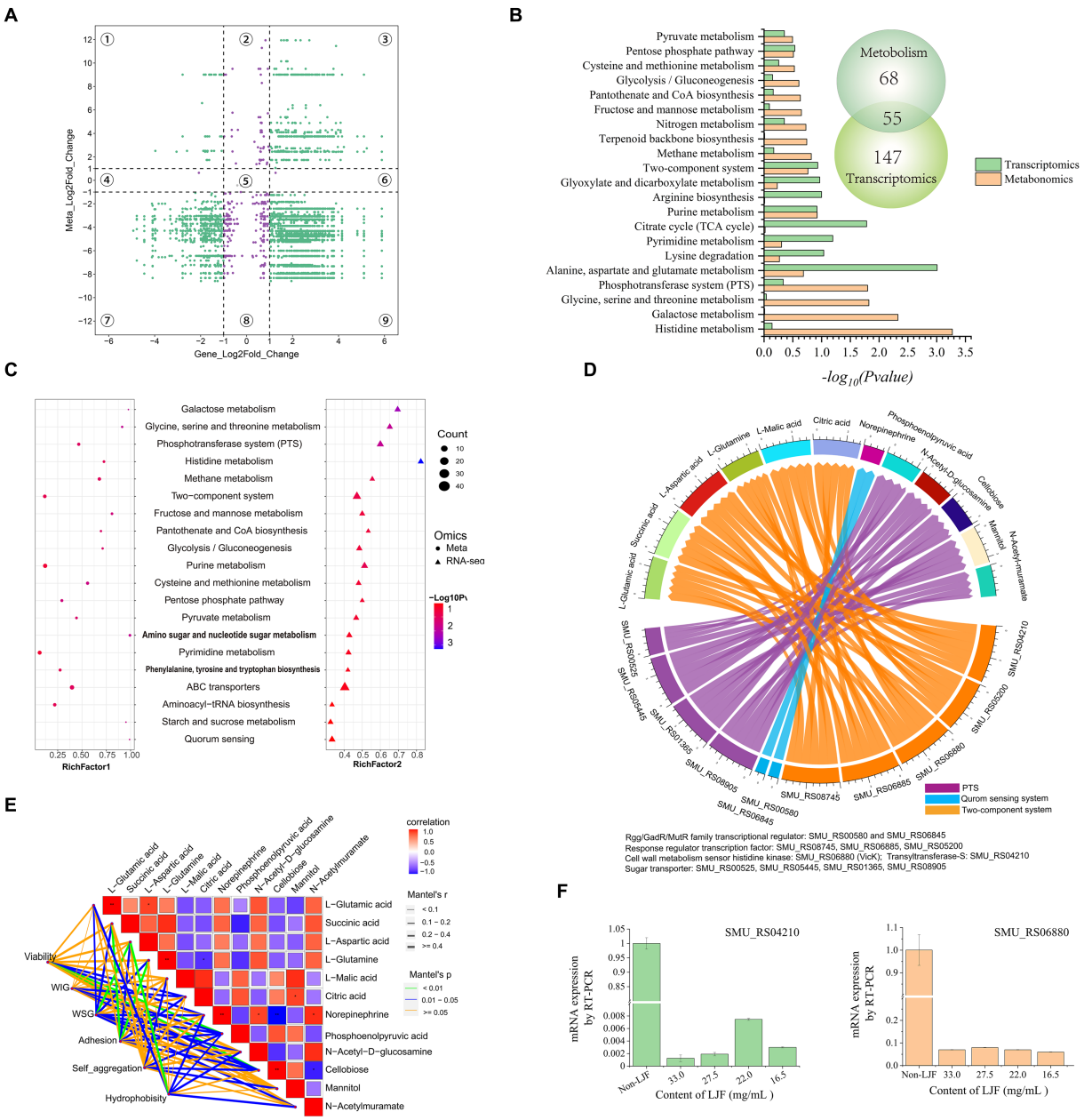

FIGURE 5
The conjoint analysis of metabolomics and transcriptomics. **(A)** A four-image map to analyze the relationship between DEMs and DEGs. **(B)** KEGG pathway analysis of DEGs and DEMs. **(C)** KEGG enrichment scatter plot. **(D)** Chord diagram of metabolites and genes. **(E)** Association analysis of biofilm character and biofilm character. **(F)** Gene expression level of SMU_RS04210 (*gtfS*) and SMU_RS06880 (*vicK*).

down-regulated by the *Rgg/GadR/MutR* family transcriptional regulators *rgg3* and *rgg2*. The response regulator transcription factors *arlR*, *vicR*, *ciaR*, *vicK*, and *gtfS* down-regulated L-glutamic acid, L-glutamine, and L-aspartic acid expression levels while up-regulating succinic acid, L-malic acid, and citric acid expression levels. Additionally, four subunits of sugar transporters were down-regulated along with N-acetyl-D-glucosamine. Conversely, PTS mediated the up-regulation of phosphoenolpyruvic acid and cellobiose.

Pearson correlation analysis was used to explore the relationship between metabolites and biofilm characteristics (Figure 5E). The green line represents the most significant characteristic, blue lines depict other noteworthy features, and yellow lines indicate insignificance. All investigated characteristics demonstrated a substantial association with metabolites. For instance, phosphoenolpyruvic acid and cellobiose were highly related to viability. L-aspartic acid significantly related to WSG and hydrophobicity. L-glutamine was related to adhesion.

While phosphoenolpyruvic acid and cellobiose were down-regulated by the sugar transporter protein in the PTS pathway, viability was down-regulated by phosphoenolpyruvic acid and cellobiose (Figures 5D,E). After L-aspartic acid was regulated by the response regulator transcription factor, cell wall metabolism sensor histidine, and glycosyltransferase in TCS, WSG and hydrophobicity were then down-regulated. Moreover, adhesion was down-regulated

by L-glutamine through its regulation via TCS. WIG was down-regulated by PTS-mediated regulation of phosphoenolpyruvic acid. *Rgg/GadR/MutR* family transcriptional regulators were associated with norepinephrine through the QS signaling pathway, which had a relationship with viability, WSG, and hydrophobicity. Rgg/GadR/MutR family transcriptional regulators was an important part of TCS. In all, TCS was the central pathway regulated by LJF.

Interestingly, genes of *gtfS* and *vicK* were crucial within TCS, validating their role in this mechanism. Both genes exhibited down-regulation upon exposure to LJF (Figure 5F). The observed changes in *gtfS* expression suggested that LJF influenced *Gtf* activity while decreasing WIG and WSG production. Alterations in *vicK* expression provided evidence for TCS-mediated biofilm inhibition under LJF-induced stress conditions (see Figure 6).

4 Discussion

Until the 2005 Edition of Chinese patent medicines, LJF (Henan and Shandong in Figure 1) and *Lonicerae flos* (LF, Hunan and Guizhou in Figure 1) were long considered the same herb. Relevant pharmacological distinctions between them have been scarcely investigated. From previous study, LJF and LF have similar antibacterial spectrums (Li Y. et al., 2020). But in this study, LJF exhibited stronger antibacterial activity than LF. The origin of LJF and LF used in our study differs from previous studies, leading to different results. Studies showed that the antibacterial activity was highly correlated with the phenolic acid content and phenolic acid content can be reflected by lower chromatic value (Shan et al., 2007; Gao et al., 2021). As indicated in Supplementary Table S1, the chromatic value of LJF was lower than that of LF. It means the content of phenolic acid in LJF was higher than that in LF. From Figure 1B, LJF has the more anti-biofilm activity than LF. Therefore, the content of phenolic acid in LJF may also related to the inhibitory effect of biofilm formation. In recent years, there are few studies focus on plant extracts' inhibitory effect of biofilm formation. *Cymbopogon citratus* displayed the highest efficacy in reducing *S. mutans* biofilm formation and adhesion activity, achieving 90% inhibition at an MIC value of 12 μg/mL (Preeti Pallavi, 2024). However, the LJF has inhibitory effect at more than 6.00 mg/mL in our study. Maybe it caused by the different methods of extracts preparation. Different methods of extracts preparation leaded to difference phytochemicals and functionality in extracts.

The mechanisms of antibacterial activity and anti-biofilm formation are distinct. Antibacterial activity involves cell wall synthesis suppression, membrane permeability alteration, protein synthesis inhibition, nucleic acid metabolism perturbation, and folate metabolism modulation (Silva et al., 2016). The anti-biofilm mechanisms are less understood, focusing on quorum sensing inhibition, adhesion protein disruption, and second messenger pathways (Koo et al., 2017). Biofilms are complex, including bacteria, metabolites, polysaccharide matrix, fibrin, and lipids, and are susceptible to environmental influences (Yadav et al., 2020; Rather et al., 2021). Polysaccharide matrix was the main component of biofilm. EPS was the polysaccharide matrix outside bacteria cells. The components of EPS varied among different bacteria. For *S. mutans*, the main constituent of EPS is predominantly glucan. WIG and WSG are crucial for biofilm formation and resistance to environmental factors, with their reduction consistent with observed inhibitory effect of biofilm formation. In biofilm formation, *S. mutans* adheres to *in situ* glucans formed by Gtfs and glucan-binding proteins (Gbps). Gtfs hydrolyze sucrose, with *S. mutans* possessing multiple Gbps (GbpA, GbpB, GbpC, and GbpD) facilitating adhesion (Bhatt et al., 2020). WIG, rich in α-1,3-glucosidic linkages, is synthesized by GtfB and GtfC and plays a crucial role in biofilm accumulation and adhesion, while GtfD synthesizes WSG rich in α-1,6-glucosidic linkages

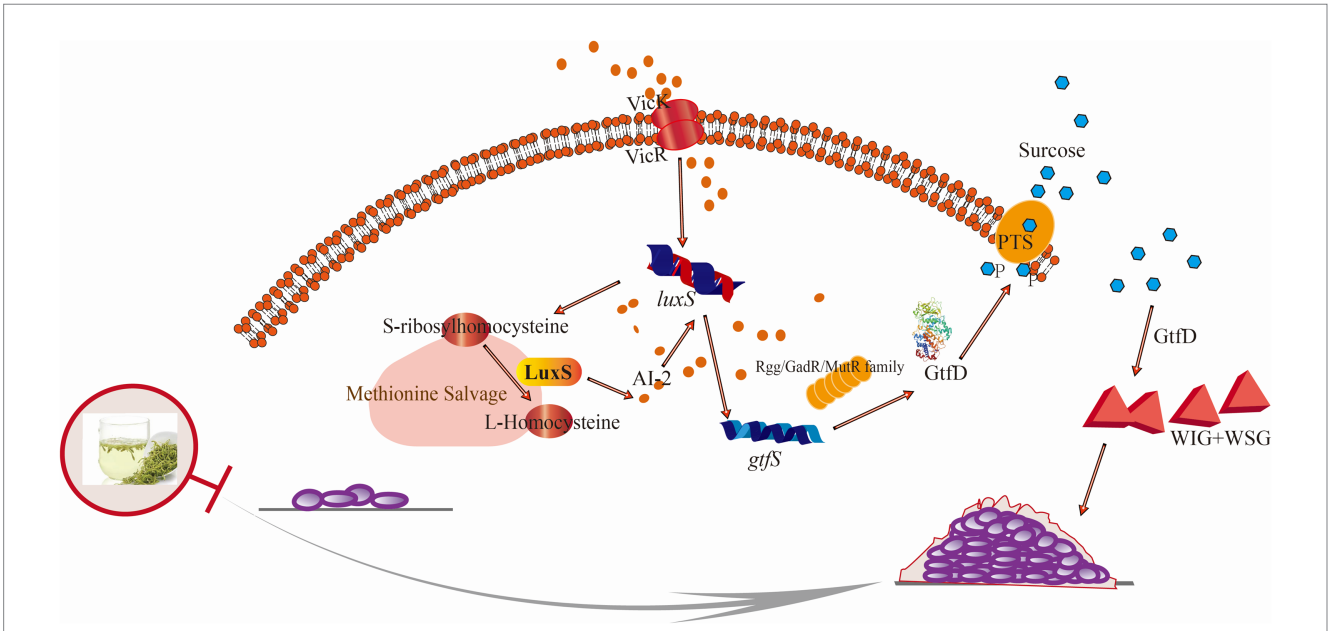

FIGURE 6
Schematic illustration of the anti-biofilm mechanism of LJF against *S. mutans*. Briefly, the sensing histidine VicK was expressed disorderly and AI-2 sensing was blocked by LJF. The corresponding response regulator transcriptional factor was inhibited, leading to the down-regulated glycosyltransferase by gtf family and decreased in WIG and WSG.

(Matsumoto-Nakano, 2018; Zhang H. et al., 2022). Reduced Cellular aggregation reflects inter-bacterial interaction, with stronger aggregation indicating higher invasiveness, driven by extracellular glucan (Vickerman and Jones, 1995; Yi Wang, 2014). Cell surface hydrophobicity, influenced by dextran-bound hydrophobic moieties, affects biofilm formation, with reduced hydrophobicity indicating modified dextran properties (Schormann et al., 2023; Zheng et al., 2023). In LJF, not only the WSG and WIG were down-regulated (Figures 2H,I), but also the expression level of *gtfS* was inhibited. It proposed that the down-regulated in WIG and WSG production indicated the decreased Gtf activity. LJF disrupted the EPS-mediated adherence pathway, impacting biofilm surface properties.

AI-2, a ubiquitous signaling molecule, plays a crucial role in various metabolic pathways and the LuxS/AI-2 QS system in *S. mutans*, which governs drug resistance, biofilm formation, motility, adherence, and virulence (Zhang et al., 2019). AI-2, produced through the LuxS-catalyzed S-ribosyl homocysteine (SRH) pathway, decreased in the presence of LJF, confirming its inhibitory effect on biofilm formation. The AI-2 inhibition mechanism involves obstructing the histidine kinase VicK or using LJF components as AI-2 analogs (Li et al., 2021; Yuan et al., 2021; Zhang Y. et al., 2022). Despite many studies identifying anti-biofilm inhibitors, understanding the biofilm inhibition mechanism is limited. The crystal violet assay, transcriptome analysis, PCR, and microstructure analyses reveal phytochemicals' potential in combating biofilm formation, but their mechanisms remain elusive.

Untargeted metabolomics analyses using LC–MS can identify new biomarkers and diagnostics, with bacterial metabolites identified as lipids, amino sugars, nucleotides, amines, organic acids, peptides, amino acids, and terpenes (Depke et al., 2020; Zhao et al., 2023; Bernardo-Bermejo et al., 2024). Although there are many bacterial metabolites identified, reports on biofilm bacteria metabolites are scarce. Maytham Hussein pioneered the application of a non-targeted metabolomics approach to elucidate the mechanism of action of Texobatine against methicillin-resistant *S. aureus* (Hussein et al., 2020). A total of 6,209 differential metabolites can be screened to explore the mechanism of lipoic acid against *Y. enterocolitica* (Yang et al., 2022). It is valuable to for understanding these mechanisms. In fact, to the best of our knowledge, few studies have been conducted on *S. mutan*'s metabolomics based on LC–MS. The current research on the anti-biofilm mechanism is still limited. As many regulators and effectors of virulence are small-molecule secondary metabolites that can be generally amenable to LC–MS (Letieri et al., 2022), the development of an untargeted metabolomics approach based on LC–MS for comprehensive analysis of the known metabolome at a large scale would be highly valuable in elucidating the molecular mechanisms underlying anti-biofilm activity. In this study, under LJF stress, fatty acyls, carboxylic acids, amino acids, steroids, prenol lipids, and benzene derivatives were the main DEMs (Figure 3). Amino acids, serving as energy precursors, indicated high metabolic activity and biofilm maturity under LJF stress (Sadiq et al., 2020). Biofilm development is energy-intensive, with histidine and alanine metabolism crucial for *E. coli* and *S. mutans* biofilm formation, respectively. Methionine metabolism also plays a role in biofilm structure phenotype by regulating the LuxS QS system in *S. mutans* (Hu et al., 2018).

In response to LJF, all the DEGs attributed in peptidoglycan biosynthesis and terpenoid backbone biosynthesis were down-regulated. Peptidoglycan is a crucial component of the cell wall, consisting of peptide and glycan molecules (Sara Marti, 2017). Peptidoglycan enhances bacterial resistance to stressful environments, while down-regulating its synthesis pathway can reduce bacteria's adaptability to their surroundings (Christopher Ealand and Germar Beukes, 2024). It means that the inhibitory effect of LJF on decreasing bacterial resistance prevented drug resistance. Terpenoid backbone biosynthesis in bacteria is a complex biochemical process that involves the synthesis of terpene precursors and their subsequent modification to form various terpenoid compounds. But the biosynthesis of terpenoids remains unclear (Duan et al., 2023). LJF down-regulated DEGs involved in peptidoglycan and terpenoid backbone biosynthesis, reducing bacterial resistance and adaptability. Dextransucrase, down-regulated by LJF, inhibited dextran synthesis, the main WIG in EPS (Fujiwara et al., 1998). From the decreased WIG production, it can be inferred that the activity of dextransucrase may also inhibited by LJF. Levanbiose, the main WSG, was produced through the enzymatic conversion of sucrose by levansucrase, followed by levanase-catalyzed formation (Pereira et al., 2001). LJF impeded the activity of glycosyltransferase, reducing glucan production. *S. mutans* has two sucrose metabolic pathways: extracellular Gtf metabolism and intracellular PTS transporter, with extracellular Gtf activity being the primary biofilm formation mechanism. LJF inhibited Gtf expression (Figure 5F), suppressing Gtf activity through the Rgg/GadR/MutR family transcriptional regulator and the QS system (Supplementary Figure S3). Conjoint analysis revealed that WSG is influenced by the QS system (Figures 5D,E). Decreased expression of *rgg3* and *rgg2*, were validated by RT-PCR (Supplementary Figure S3). It indicated that the impact of LJF on Gtf activity was through TCS. The expression of the histidine kinase VicK (Supplementary Table S5) was disrupted and AI-2 sensing was blocked (Figure 2K), hindering response regulator transcription factors (Supplementary Figure S3), resulting in decreased Gtf activity and reduced WIG and WSG production (Figures 2H,I). L-aspartic acid and norepinephrine, regulated by TCS and QS, influenced WSG. Phosphoenolpyruvic acid, inhibited via PTS and regulated WIG (Figures 5D,E). In summary, LJF primarily inhibited biofilm formation by suppressing glucan production through the QS system, TCS, and PTS. This inhibition was triggered by LJF disrupting the expression of histidine kinase VicK and blocking AI-2 sensing, leading to the down-regulation of Gtf activity and a decrease in both WIG and WSG. For LJF, the primary targets of inhibitory effects on biofilm formation were VicK and Gtf.

5 Conclusion

Lonicera japonica flos (LJF) significantly reduced EPS production within the biofilm, accounting for its inhibitory activity. Mechanistically, WIG and WSG were down-regulated by Gtf, associated with TCS, QS, and PTS pathways, leading to the reduced EPS production. WSG synthesis was regulated by L-aspartic acid and norepinephrine via TCS and QS pathways, respectively, while WIG synthesis was regulated by phosphoenolpyruvic acid via the PTS pathway. The regulation trigger was that LJF disrupted VicK and blocked AI-2 sensing, inhibiting response regulator transcriptional factors. This pioneering study on LJF's inhibitory mechanism against *S. mutans* provides a solid foundation for developing LJF-based functional food and oral health care products.

Data availability statement

In the part of 2.9, the RNA-seq datasets are available at the NCBI Sequence Read Archive (SRA) database under accession number PRJNA1119033. The complete dataset could be accessed at https://www.ncbi.nlm.nih.gov/sra/PRJNA1119033. In the part of 2.8, Metabolomics data have been deposited to the EMBL-EBI Metabolites database: with the identifier MTBLS9711. The complete dataset could be accessed at https://www.ebi.ac.uk/metabolights/MTBLS9711.

Author contributions

LW: Conceptualization, Investigation, Methodology, Writing – original draft, Writing – review & editing. PL: Data curation, Investigation, Writing – review & editing. YW: Data curation, Writing – review & editing. HP: Investigation, Writing – review & editing. XC: Methodology, Funding acquisition, Resources, Writing – review & editing, Supervision, Project administration.

Funding

The author(s) declare financial support was received for the research, authorship, and/or publication of this article. This work was supported by the Beijing Natural Science Foundation and Beijing Municipal Education Committee (KZ202010011017).

Conflict of interest

The authors declare that the research was conducted in the absence of any commercial or financial relationships that could be construed as a potential conflict of interest.

Publisher's note

Supplementary material

The Supplementary material for this article can be found online at: https://www.frontiersin.org/articles/10.3389/fmicb.2024.1435503/full#supplementary-material

References

Barran-Berdon, A. L., Ocampo, S., Haider, M., Morales-Aparicio, J., Ottenberg, G., Kendall, A., et al. (2020). Enhanced purification coupled with biophysical analyses shows cross-β structure as a core building block for *Streptococcus mutans* functional amyloids. *Sci. Rep.* 10:5138. doi: 10.1038/s41598-020-62115-7

Bernardo-Bermejo, S., Castro-Puyana, M., Sánchez-López, E., Fernández-Martínez, A. B., Javier Lucio-Cazaña, F., and Luisa Marina, M. (2024). UHPLC-MS-based untargeted metabolomic strategy to reveal the metabolic differences between cisplatin first and second generation apoptotic bodies from hk-2 cells. *Microchem. J.* 200:110406. doi: 10.1016/j.microc.2024.110406

Bhatt, L., Chen, L., Guo, J., Klie, R. F., Shi, J., and Pesavento, R. P. (2020). Hydrolyzed ce(iv) salts limit sucrose-dependent biofilm formation by *Streptococcus mutans*. *J. Inorg. Biochem.* 206:110997. doi: 10.1016/j.jinorgbio.2020.110997

Bosch, M., Nart, J., Audivert, S., Bonachera, M. A., Alemany, A. S., Fuentes, M. C., et al. (2012). Isolation and characterization of probiotic strains for improving oral health. *Arch. Oral Biol.* 57, 539–549. doi: 10.1016/j.archoralbio.2011.10.006

Cai, Z., Liao, H., Wang, C., Chen, J., Tan, M., Mei, Y., et al. (2020). A comprehensive study of the aerial parts of *Lonicera japonica thunb.* based on metabolite profiling coupled with PLS-DA. *Phytochem. Anal.* 31, 786–800. doi: 10.1002/pca.2943

Chang, A., He, Q., Li, L., Yu, X., Sun, S., and Zhu, H. (2021). Exploring the quorum sensing inhibition of isolated chrysin from *Penicillium Chrysogenum* DXY-1. *Bioorg. Chem.* 111:104894. doi: 10.1016/j.bioorg.2021.104894

Chen, X., Daliri, E. B., Tyagi, A., and Oh, D. (2021). Cariogenic biofilm: pathology-related phenotypes and targeted therapy. *Microorganisms* 9:1311. doi: 10.3390/microorganisms9061311

Chen, X., Liu, C., Peng, X., He, Y., Liu, H., Song, Y., et al. (2019). Sortase A-mediated modification of the *Streptococcus mutans* transcriptome and virulence traits. *Mol. Oral Microbiol.* 34, 219–233. doi: 10.1111/omi.12266

Christopher Ealand, B. R. J. C., and Germar Beukes, E. M. S. J. (2024). Resuscitation-promoting factors are required for *Mycobacterium smegmatis* biofilm formation. *Appl. Environ. Microbiol.* 84, e618–e687. doi: 10.1128/AEM.00687-18

Cuadra, G. A., Frantellizzi, A. J., Gaesser, K. M., Tammariello, S. P., and Ahmed, A. (2016). Autoinducer-2 detection among commensal oral *streptococci* is dependent on ph and boric acid. *J. Microbiol.* 54, 492–502. doi: 10.1007/s12275-016-5507-z

De Jesus, R., and Dedeles, G. (2020). Data on quantitation of *Bacillus cereus sensu lato* biofilms by microtiter plate biofilm formation assay. *Data Brief* 28:104951. doi: 10.1016/j.dib.2019.104951

Depke, T., Thöming, J. G., Kordes, A., Häussler, S., and Brönstrup, M. (2020). Untargeted LC-MS metabolomics differentiates between virulent and avirulent clinical strains of *Pseudomonas aeruginosa*. *Biomol. Ther.* 10:1041. doi: 10.3390/biom10071041

Duan, Y., Koutsaviti, A., Harizani, M., Ignea, C., Roussis, V., Zhao, Y., et al. (2023). Widespread biosynthesis of 16-carbon terpenoids in bacteria. *Nat. Chem. Biol.* 19, 1532–1539. doi: 10.1038/s41589-023-01445-9

Fujiwara, T., Terao, Y., Hoshino, T., Kawabata, S., Ooshima, T., Sobue, S., et al. (1998). Molecular analyses of glucosyltransferase genes among strains of *Streptococcus mutans*. *FEMS Microbiol. Lett.* 161, 331–336. doi: 10.1111/j.1574-6968.1998.tb12965.x

Gao, Y., Wang, F., Liu, Q., Qi, Y., Wang, Q., and Liu, H. (2021). Comparison of anti-inflammatory effects of *Lonicerae japonicae flos* and *Lonicerae flos* based on network pharmacology. *Chin. Herb. Med.* 13, 332–341. doi: 10.1016/j.chmed.2021.06.005

Hoshino, T., and Fujiwara, T. (2022). The findings of glucosyltransferase enzymes derived from oral *streptococci*. *Jpn. Dent. Sci. Rev.* 58, 328–335. doi: 10.1016/j.jdsr.2022.10.003

Howard, S. A., Carr, C. M., Sbahtu, H. I., Onwukwe, U., López, M. J., Dobson, A. D. W., et al. (2023). Enrichment of native plastic-associated biofilm communities to enhance polyester degrading activity. *Environ. Microbiol.* 25, 2698–2718. doi: 10.1111/1462-2920.16466

Hu, X., Wang, Y., Gao, L., Jiang, W., Lin, W., Niu, C., et al. (2018). The impairment of methyl metabolism from *luxS* mutation of *Streptococcus mutans*. *Front. Microbiol.* 9:404. doi: 10.3389/fmicb.2018.00404

Hussein, M., Karas, J. A., Schneider-Futschik, E. K., Chen, F., Swarbrick, J., Paulin, O., et al. (2020). The killing mechanism of teixobactin against methicillin-resistant *Staphylococcus aureus*: an untargeted metabolomics study. *Msystems* 5:e00077–20. doi: 10.1128/mSystems.00077-20

Islam, B., Khan, S. N., Haque, I., Alam, M., Mushfiq, M., and Khan, A. U. (2008). Novel anti-adherence activity of mulberry leaves: inhibition of *Streptococcus mutans* biofilm by 1-Deoxynojirimycin isolated from *Morus alba*. *J. Antimicrob. Chemother.* 62, 751–757. doi: 10.1093/jac/dkn253

Jiang, X., Lin, A., Li, S., Shi, Y., Zhou, F., Felix, G. G., et al. (2022). Effects of artificial honey and epigallocatechin-3-gallate on *Streptococcus pyogenes*. *BMC Microbiol.* 22:207. doi: 10.1186/s12866-022-02611-0

Kim, N., Kim, B. S., Lee, H. B., An, S., Kim, D., and Kang, S. (2022). Effect of bacteriocin-like inhibitory substance (BLIS) from *Enterococcus faecium* DB1 on cariogenic *Streptococcus mutans* biofilm formation. *Food Sci. Anim. Resour.* 42, 1020–1030. doi: 10.5851/kosfa.2022.e49

Koo, H., Allan, R. N., Howlin, R. P., Stoodley, P., and Hall-Stoodley, L. (2017). Targeting microbial biofilms: current and prospective therapeutic strategies. *Nat. Rev. Microbiol.* 15, 740–755. doi: 10.1038/nrmicro.2017.99

Letieri, A. S., Freitas-Fernandes, L. B., Souza, I. P. R., Valente, A. P., and Fidalgo, T. K. S. (2022). Metabolomic signatures of in vitro biofilm maturation of *Streptococcus mutans*. *Curr. Microbiol.* 79:86. doi: 10.1007/s00284-022-02778-9

Li, J., Fan, Q., Jin, M., Mao, C., Zhang, H., Zhang, X., et al. (2021). Paeoniflorin reduce *luxS/AI-2* system-controlled biofilm formation and virulence in *Streptococcus suis*. *Virulence* 12, 3062–3073. doi: 10.1080/21505594.2021.2010398

Li, J., Jin, S., Zu, Y., Luo, M., Wang, W., Zhao, C., et al. (2014). Rapid preparative extraction and determination of major organic acids in honeysuckle (*Lonicera japonica thunb.*) tea. *J. Food Compos. Anal.* 33, 139–145. doi: 10.1016/j.jfca.2013.12.007

Li, Y., Li, W., Fu, C., Song, Y., and Fu, Q. (2020). *Lonicerae japonicae flos* and *Lonicerae flos*: a systematic review of ethnopharmacology, phytochemistry and pharmacology. *Phytochem. Rev.* 19, 1–61. doi: 10.1007/s11101-019-09655-7

Li, B., Li, X., Lin, H., and Zhou, Y. (2018). Curcumin as a promising antibacterial agent: effects on metabolism and biofilm formation in *S. mutans*. *Biomed. Res. Int.* 2018, 1–11. doi: 10.1155/2018/4508709

Li, Q., Lin, B., and Tang, J. (2024). Studying on genetic diversity and metabolic differences of *saccharomyces cerevisiae* in baijiu. *Eur. Food Res. Technol.* 250, 1619–1640. doi: 10.1007/s00217-024-04489-w

Li, W., Ma, Y., Xie, X., Shi, Q., Wen, X., Sun, T., et al. (2019). Diallyl disulfide from garlic oil inhibits *Pseudomonas aeruginosa* quorum sensing systems and corresponding virulence factors. *Front. Microbiol.* 9:3222. doi: 10.3389/fmicb.2018.03222

Li, J., Wu, T., Peng, W., and Zhu, Y. (2020). Effects of resveratrol on cariogenic virulence properties of *Streptococcus mutans*. *BMC Microbiol.* 20:99. doi: 10.1186/s12866-020-01761-3

Liu, N., and Zhu, L. (2020). Metabolomic and transcriptomic investigation of metabolic perturbations in *Oryza sativa* L. triggered by three pesticides. *Environ. Sci. Technol.* 54, 6115–6124. doi: 10.1021/acs.est.0c00425

Lu, Q., Wang, Y., Xiong, F., Hao, X., Zhang, X., Li, N., et al. (2020). Integrated transcriptomic and metabolomic analyses reveal the effects of callose deposition and multihormone signal transduction pathways on the tea plant-colletotrichum camelliae interaction. *Sci. Rep.* 10:12858. doi: 10.1038/s41598-020-69729-x

Matsumoto-Nakano, M. (2018). Role of *Streptococcus mutans* surface proteins for biofilm formation. *Jpn. Dent. Sci. Rev.* 54, 22–29. doi: 10.1016/j.jdsr.2017.08.002

Muras, A., Mayer, C., Romero, M., Camino, T., Ferrer, M. D., Mira, A., et al. (2018). Inhibition of *Steptococcus mutans* biofilm formation by extracts of *Tenacibaculum* sp. 20J, a bacterium with wide-spectrum quorum quenching activity. *J. Oral Microbiol.* 10:1429788. doi: 10.1080/20002297.2018.1429788

Murugan, K., Sekar, K., Sangeetha, S., Ranjitha, S., and Sohaibani, S. A. (2013). Antibiofilm and quorum sensing inhibitory activity of *Achyranthes aspera* on cariogenic *Streptococcus mutans*: an *in vitro* and in silico study. *Pharm. Biol.* 51, 728–736. doi: 10.3109/13880209.2013.764330

Park, S., Raka, R. N., Hui, X., Song, Y., Sun, J., Xiang, J., et al. (2023). Six Spain thymus essential oils composition analysis and their *in vitro* and in silico study against *Streptococcus mutans*. *BMC Complement. Altern. Med.* 23:106. doi: 10.1186/s12906-023-03928-7

Pereira, Y., Petit-Glatron, M. F., and Chambert, R. (2001). *Yveb*, encoding endolevanase LevB, is part of the sacB-yveB-yveA levansucrase tricistronic operon in *Bacillus subtilis*. *Microbiology* 147, 3413–3419. doi: 10.1099/00221287-147-12-3413

Persson, G. R., Yeates, J., Persson, R. E., Hirschi-Imfeld, R., Weibel, M., and Kiyak, H. A. (2007). The impact of a low-frequency chlorhexidine rinsing schedule on the subgingival microbiota (the teeth clinical trial). *J. Periodontol.* 78, 1751–1758. doi: 10.1902/jop.2007.070138

Pragman, A. A., Fieberg, A. M., Reilly, C. S., and Wendt, C. (2021). Chlorhexidine oral rinses for symptomatic COPD: a randomised, blind, placebo-controlled preliminary study. *BMJ Open* 11:e50271:e050271. doi: 10.1136/bmjopen-2021-050271

Preeti Pallavi, P. P. S. S. (2024). Comparative evaluation of anti-biofilm and anti-adherence potential of plant extracts against *Streptococcus mutans*: a therapeutic approach for oral health. *Microb. Pathog.* 188:106514. doi: 10.1016/j.micpath.2023.106514

Rather, M. A., Gupta, K., and Mandal, M. (2021). Microbial biofilm: formation, architecture, antibiotic resistance, and control strategies. *Braz. J. Microbiol.* 52, 1701–1718. doi: 10.1007/s42770-021-00624-x

Rudin, L., Bornstein, M. M., and Shyp, V. (2023). Inhibition of biofilm formation and virulence factors of cariogenic oral pathogen *Streptococcus mutans* by natural flavonoid phloretin. *J. Oral Microbiol.* 15:2230711. doi: 10.1080/20002297.2023.2230711

Sadiq, F. A., Yan, B., Zhao, J., Zhang, H., and Chen, W. (2020). Untargeted metabolomics reveals metabolic state of *Bifidobacterium bifidum* in the biofilm and planktonic states. *Lwt* 118:108772. doi: 10.1016/j.lwt.2019.108772

Sara Marti, C. P. A. M. (2017). Bacterial lysis through interference with peptidoglycan synthesis increases biofilm formation by nontypeable *Haemophilus influenzae*. *Msphere* 2, 316–329. doi: 10.1128/mSphere.00329-16

Schilling, K. M., and Bowen, W. H. (1992). Glucans synthesized in situ in experimental salivary pellicle function as specific binding sites for *Streptococcus mutans*. *Infect. Immun.* 60, 284–295. doi: 10.1128/iai.60.1.284-295.1992

Schormann, N., Patel, M., Thannickal, L., Purushotham, S., Wu, R., Mieher, J. L., et al. (2023). The catalytic domains of *Streptococcus mutans* glucosyltransferases: a structural analysis. *Acta Crystallogr. F-Struct. Biol. Commun.* 79, 119–127. doi: 10.1107/S2053230X23003199

Scully, C., and Greenman, J. (2012). Halitology (breath odour: aetiopathogenesis and management). *Oral Dis.* 18, 333–345. doi: 10.1111/j.1601-0825.2011.01890.x

Seneviratne, C. J., Suriyanarayanan, T., Widyarman, A. S., Lee, L. S., Lau, M., Ching, J., et al. (2020). Multi-omics tools for studying microbial biofilms: current perspectives and future directions. *Crit. Rev. Microbiol.* 46, 759–778. doi: 10.1080/1040841X.2020.1828817

Shan, B., Cai, Y., Brooks, J. D., and Corke, H. (2007). The *in vitro* antibacterial activity of dietary spice and medicinal herb extracts. *Int. J. Food Microbiol.* 117, 112–119. doi: 10.1016/j.ijfoodmicro.2007.03.003

Silva, L. N., Zimmer, K. R., Macedo, A. J., and Trentin, D. S. (2016). Plant natural products targeting bacterial virulence factors. *Chem. Rev.* 116, 9162–9236. doi: 10.1021/acs.chemrev.6b00184

Steinberg, D., Kopec, L. K., and Bowen, W. H. (1993). Adhesion of actinomyces isolates to experimental pellicles. *J. Dent. Res.* 72, 1015–1020. doi: 10.1177/00220345930720060401

Sun, J., Sun, Z., Wang, D., Liu, F., and Wang, D. (2022). Contribution of ultrasound in combination with chlorogenic acid against *Salmonella enteritidis* under biofilm and planktonic condition. *Microb. Pathog.* 165:105489. doi: 10.1016/j.micpath.2022.105489

Sun, J., Wang, D., Sun, Z., Liu, F., Du, L., and Wang, D. (2021). The combination of ultrasound and chlorogenic acid to inactivate *Staphylococcus aureus* under planktonic, biofilm, and food systems. *Ultrason. Sonochem.* 80:105801. doi: 10.1016/j.ultsonch.2021.105801

Sutherland, I. (2001). Biofilm exopolysaccharides: a strong and sticky framework. *Microbiology* 147, 3–9. doi: 10.1099/00221287-147-1-3

Ullah, A., Mirani, Z. A., Binbin, S., Wang, F., Chan, M. W. H., Aslam, S., et al. (2023). An elucidative study of the anti-biofilm effect of selenium nanoparticles (SeNPs) on selected biofilm producing pathogenic bacteria: a disintegrating effect of SeNPs on bacteria. *Process Biochem.* 126, 98–107. doi: 10.1016/j.procbio.2022.12.031

Venkitaraman, A. R., Vacca-Smith, A. M., Kopec, L. K., and Bowen, W. H. (1995). Characterization of GlucosyltransferaseB, GtfC, and GtfD in solution and on the surface of hydroxyapatite. *J. Dent. Res.* 74, 1695–1701. doi: 10.1177/00220345950740101101

Vickerman, M. M., and Jones, G. W. (1995). Sucrose-dependent accumulation of oral *streptococci* and their adhesion-defective mutants on saliva-coated hydroxyapatite. *Oral Microbiol. Immunol.* 10, 175–182. doi: 10.1111/j.1399-302X.1995.tb00139.x

Vilchez, R., Lemme, A., Thiel, V., Schulz, S., Sztajer, H., and Wagner-Döbler, I. (2007). Analysing traces of autoinducer-2 requires standardization of the *Vibrio harveyi* bioassay. *Anal. Bioanal. Chem.* 387, 489–496. doi: 10.1007/s00216-006-0824-4

Wang, L., Cao, X., Pei, H., Liu, P., Song, Y., and Wu, Y. (2023). Anti-biofilm activity of chlorogenic acid against *Pseudomonas* using quorum sensing system. *Food Secur.* 12:3601. doi: 10.3390/foods12193601

Wang, S., Yang, L., Hou, A., Liu, S., Yang, L., Kuang, H., et al. (2023). Screening hepatoprotective effective components of *Lonicerae japonica flos* based on the spectrum-effect relationship and its mechanism exploring. *Food Sci. Human Wellness* 12, 283–294. doi: 10.1016/j.fshw.2022.07.018

Yadav, P., Verma, S., Bauer, R., Kumari, M., Dua, M., Johri, A. K., et al. (2020). Deciphering streptococcal biofilms. *Microorganisms* 8:1835. doi: 10.3390/microorganisms8111835

Yang, X., Liu, Y., Hou, A., Yang, Y., Tian, X., and He, L. (2017). Systematic review for geo-authentic *Lonicerae japonicae flos*. *Front. Med.* 11, 203–213. doi: 10.1007/s11684-017-0504-0

Yang, S., Tian, L., Wang, X., Wu, M., Liao, S., Fu, J., et al. (2022). Metabolomics analysis and membrane damage measurement reveal the antibacterial mechanism of lipoic acid against *Yersinia enterocolitica*. *Food Funct.* 13, 11476–11488. doi: 10.1039/d2fo01306a

Yi Wang, S. M. L. G. (2014). Growth in the presence of sucrose may decrease attachment of some oral bacteria to abiotic surfaces. *Ann. Microbiol.* 65, 1159–1163. doi: 10.1007/s13213-014-0883-2

Yuan, K., Hou, L., Jin, Q., Niu, C., Mao, M., Wang, R., et al. (2021). Comparative transcriptomics analysis of *Streptococcus mutans* with disruption of Luxs/AI-2 quorum sensing and recovery of methyl cycle. *Arch. Oral Biol.* 127:105137. doi: 10.1016/j.archoralbio.2021.105137

Zhang, Y., Gu, Y., Wu, R., Zheng, Y., Wang, Y., Nie, L., et al. (2022). Exploring the relationship between the signal molecule AI-2 and the biofilm formation of *Lactobacillus sanfranciscensis*. *Lwt.* 154:112704. doi: 10.1016/j.lwt.2021.112704

Zhang, B., Ku, X., Zhang, X., Zhang, Y., Chen, G., Chen, F., et al. (2019). The AI-2/LuxS quorum sensing system affects the growth characteristics, biofilm formation, and virulence of *Haemophilus parasuis*. *Front. Cell. Infect. Microbiol.* 9:62. doi: 10.3389/fcimb.2019.00062

Zhang, H., Xia, M., Zhang, B., Zhang, Y., Chen, H., Deng, Y., et al. (2022). Sucrose selectively regulates *Streptococcus mutans* polysaccharide bygcrr. *Environ. Microbiol.* 24, 1395–1410. doi: 10.1111/1462-2920.15887

Zhao, Z., Wu, J., Sun, Z., Fan, J., Liu, F., Zhao, W., et al. (2023). Postbiotics derived from *L. paracasei* ET-22 inhibit the formation of *S. mutans* biofilms and bioactive substances: an analysis. *Molecules* 28:1236. doi: 10.3390/molecules28031236

Zheng, T., Jing, M., Gong, T., Yan, J., Wang, X., Xu, M., et al. (2023). Regulatory mechanisms of exopolysaccharide synthesis and biofilm formation in *Streptococcus mutans*. *J. Oral Microbiol.* 15:2225257. doi: 10.1080/20002297.2023.2225257

Zheng, S., Liu, S., Hou, A., Wang, S., Na, Y., Hu, J., et al. (2022). Systematic review of *Lonicerae japonicae flos*: a significant food and traditional Chinese medicine. *Front. Pharmacol.* 13:1013992. doi: 10.3389/fphar.2022.1013992

10.3389/fmicb.2024.1435503

Glossary

LJF	*Lonicera japonica* flos
S. mutans	*Streptococcus mutans*
RT-PCR	Real-time fluorescent quantitative Polymerase Chain Reaction
EPS	Exopolysaccharides
CH	Chlorhexidine
BHI	Brain-heart infusion
BHIS	Brain-heart infusion containing 1% sucrose
MIC	minimum inhibitory concentration
CV	crystal violet
SEM	scanning electron microscopy
FTIR	Fourier transform infrared spectroscopy
WIG	Water insoluble glucan
WSG	Water soluble glucan
AC	Aggregation capacity
RLI	Relative luminescence intensity
UPLC	Ultrahigh-performance liquid chromatography
MS	Mass spectrometry
VIP	Variable Important in projection
FDR	False discovery rate
TCS	two-component system
QS	quorum sensing system
PTS	phosphotransferase system

frontiers | Frontiers in Microbiology

TYPE Original Research
PUBLISHED 30 August 2024
DOI 10.3389/fmicb.2024.1425764

OPEN ACCESS

EDITED BY
Kang Xu,
Chinese Academy of Sciences (CAS), China

REVIEWED BY
Rui Wang,
Shanghai Jiao Tong University, China
Shiqi He,
Northeast Agricultural University, China

*CORRESPONDENCE
Shuangshuang Wang
✉ wangss1023@126.com

RECEIVED 30 April 2024
ACCEPTED 19 August 2024
PUBLISHED 30 August 2024

CITATION
Zhu J, Liu X, Liu N, Zhao R and Wang S (2024) *Lactobacillus plantarum* alleviates high-fat diet-induced obesity by altering the structure of mice intestinal microbial communities and serum metabolic profiles. *Front. Microbiol.* 15:1425764. doi: 10.3389/fmicb.2024.1425764

Lactobacillus plantarum alleviates high-fat diet-induced obesity by altering the structure of mice intestinal microbial communities and serum metabolic profiles

Junwen Zhu[1,2], Xueying Liu[2], Naiyuan Liu[2], Ruochi Zhao[3] and Shuangshuang Wang[1,3]*

[1]Department of Cardiology, The First People's Hospital of Wenling, Wenling Hospital of Wenzhou Medical University, Wenling, China, [2]Hunan Provincial Engineering Research Center of Applied Microbial Resources Development for Livestock and Poultry, College of Bioscience and Biotechnology, Hunan Agricultural University, Changsha, China, [3]Key Laboratory of Precision Medicine for Atherosclerotic Diseases of Zhejiang Province, Affiliated First Hospital of Ningbo University, Ningbo, China

Obesity, which is always accompanied by disorders of lipid metabolism and dysbiosis of the gut microbiota, has become a global epidemic recognised by the World Health Organisation, necessitating innovative strategies and a globally accepted agreement on treating obesity and its related complications. Probiotics, as major active ingredients in many foods, offer potential as biological treatments for obesity prevention and management. *Lactobacillus plantarum* (*L. plantarum*) possesses a wide range of biological activities and is widely used to alleviate and ameliorate various diseases. This research demonstrated that *Lactobacillus plantarum* reduces the weight increase and fat build-up caused by a high-fat diet (HFD) in mice, while also improving glucose tolerance and insulin sensitivity in obese mice. Results indicated that *L. plantarum* effectively controlled the intestinal microbial community's structure, counteracted disruptions in gut flora caused by HFD, normalized the Firmicutes to Bacteroidota ratio (F/B), and decreased the prevalence of detrimental bacteria *Desulfovibrio* and Clostridia. Serum metabolomics findings indicate notable alterations in serum metabolites across various groups, notably the increased levels of Isoprothiolane and Inosine, key regulators of lipid metabolism disorders and enhancers of fat burning. These differential metabolites were mainly enriched in unsaturated fatty acid biosynthesis, sulfur metabolism, fatty acid biosynthesis, and purine metabolism. Consequently, we propose that *L. plantarum* has the potential to alter the gut microbial community's composition, positioning it as a promising option for obesity therapy.

KEYWORDS

obesity, probiotics, *Lactobacillus plantarum*, intestinal microbes, fat metabolism, differential metabolites

1 Introduction

Obesity is defined as excess adiposity and adipose tissue expansion, which occurs through adipocyte hypertrophy and hyperplasia (Cai et al., 2022; Hotamisligil, 2017). Numerous research works suggest that obesity may lead to the emergence of several illnesses (Hoyt et al., 2014), such as metabolic syndrome, Type 2 diabetes mellitus (DMTII) (Youn et al., 2021),

heart-related diseases, and fatty liver disease (Hotamisligil, 2017). Statistical data indicates that obesity is responsible for 44% of Type 2 diabetes, 23% of ischaemic heart disease, and as much as 41% of specific cancer types (Boccellino and D'Angelo, 2020). The intestinal microbiota is involved in lipid synthesis and metabolism and is an important component of host energy intake and metabolism (Backhed et al., 2004). It has been demonstrated that the ratio (F/B) of the colonic contents of HFD-induced obese mice (Torres-Fuentes et al., 2017), represented by the Firmicutes and Bacteroidota (Shen et al., 2018), showed a significant increase, which led to metabolic dysregulation and fat accumulation.

With the deeper understanding of a large number of studies, it has been found that probiotics can be used as an effective strategy for obesity prevention (Abenavoli et al., 2019). Probiotics play an irreplaceable role in improving the structure of gut microbial community (Backhed et al., 2004). Studies have proposed that the antagonistic effect that probiotics can have on the growth of pathogenic microorganisms, as well as their ability to modulate the gastrointestinal immune system, results in the modulation of the composition of the gut microbiota and host lipid metabolism (Lee et al., 2018). As a probiotic, *Lactobacillus plantarum* serves as a key component in numerous food items, exhibiting diverse functional characteristics including reducing cholesterol, acting as an antioxidant, and modulating immune responses (Han et al., 2020). It is also able to interact directly with host immune cells and improve intestinal barrier function, which has led to its use in the alleviation and treatment of many diseases, including obesity. A multitude of research indicate s that *L. plantarum* can preserve mitochondrial health and integrity by activating PPAR-α (Cai et al., 2020), simultaneously inhibiting genes related to fatty acid production and the repair of the intestinal barrier. Moreover, *in vitro* and *in vivo* studies have found that *Lactobacillus plantarum* is highly resistant to artificial gastric and intestinal fluids, ensuring that it can survive in large quantities after digestion in the stomach and intestines (Zhang et al., 2022; Rahayu et al., 2021).

This research aimed to explore the capabilities of *L. plantarum*, known for its various bioactivities affecting gut microbiota, in mitigating and treating obesity (Zhou et al., 2021). *L. plantarum* was administered by gavage to HFD-induced obese mice, and the therapeutic effect of *L. plantarum* was determined by recording changes in body weight and detecting subcutaneous and perirenal fat content (Long et al., 2020). Furthermore, alterations in gut flora and metabolic patterns in living organisms were examined through extensive sequencing of colon contents and serum metabolomic studies. This serves as a theoretical foundation for considering *L. plantarum* as a potential treatment option for obesity.

2 Materials and methods

2.1 Animals

The animal study adhered to Hunan Agricultural University's established protocols for laboratory animal care and usage in animal research. All animal experiments were approved by the Animal Ethics Committee of Hunan Agricultural University (approval number: 2023-251). We acquired 30 female ICR mice, each approximately 8 weeks old, from Hunan Sileike Jingda Co (Changsha, China). All animals passed safety quarantine. The mice were kept at a temperature of 25 ± 1°C and on a light or dark cycle for 12 h. The acclimatisation period was 1 week, during which all mice drank water and consumed feed normally. At the end of the acclimatisation period, 30 mice were randomly divided into three groups according to body weight: normal control group (CON): fed normal chow (10% kcal from fat, XTCON50J, Xietong Pharmaceutical Bio-engineering Co., Jiangsu, China), high fat control group (HFD): fed high fat chow (60% kcal from fat, XTHF60, Xietong Pharmaceutical Bio-engineering Co., Jiangsu, China), and high fat-*L. plantarum* treatment group (HFD-ZW), with 10 mice in a group and every two in a cage ($n = 5$) (Table 1). The experimental period was 15 weeks, of which the obesity modelling lasted for 10 weeks with weekly weighing, but in week 11, mice in the HFD-ZW group received 150 μL of *Lactobacillus plantarum* HMRS-6 for 14 straight days, whereas those in the CON and HFD groups were administered an identical saline dose, and the mice were resumed the original food and water intake after 14 days until the last day of the experiments when the mice were put to death and the samples were collected for the subsequent analyses (Figure 1).

2.2 Strain activation and oral gavage

Lactobacillus plantarum HMRS-6 was isolated from pickles in Hunan, China, and stored in 30% glycerol test tubes at −80°C in the Microbiology Laboratory, Hunan Agricultural University (Changsha, China). The bacteria were inoculated into the MRS activation medium (Solarbio Science & Technology Co., Ltd., Beijing, China) and placed in a shaker for 24 h at an incubation temperature of 25°C and a rotational speed of 180 rpm. 1 mL of activated bacterial solution was aspirated and diluted to obtain a gradient dilution of 10^{-1} to 10^{-9} bacterial solution, 100 mL of MRS solid medium was configured and distributed into multiple dry sterilised Petri dishes, and after solidification, 100 μL was aspirated after solidification, 100 μL of the gradient-diluted bacterial solution was added to the solid petri dishes and coated evenly, and the plates were counted after being inverted and incubated at 25°C for 24 h. The amount of bacterial solution for each mouse was 1×10^9 CFU, divided by the number of colonies per milliliter counted on the plate, namely, the amount of bacterial solution for each mouse in the HFD-ZW group was 150 μL/d. The amount of bacterial solution required for each mouse per day was aspirated, and then placed into a centrifuge and centrifuged at 10,000 rpm for 15 min. After centrifugation, the supernatant was skimmed, and the bacterial solution was resuspended by adding an

TABLE 1 Formula table of mice diet.

Ingredients	CON (kcal)	HFD (kcal)
Corn Starch	0.0	2024.8
Casein	800.0	800.0
Sucrose	291.2	291.2
Soybean oil	225.0	225.0
Lard	2205.0	180.0
L-cystine	12.0	12.0
Maltodextrin	500.0	500.0

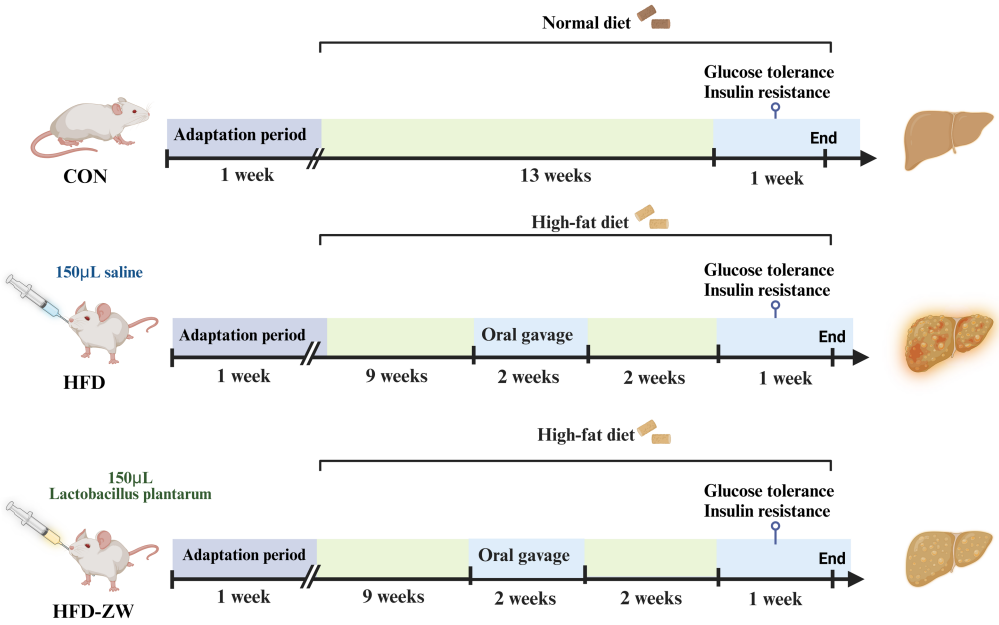

FIGURE 1
Experimental group assignment and workflow. The 30 mice were divided into three different groups (CON group, HFD group and HFD-ZW group) for 15 weeks.

appropriate amount of sterile water to get the amount of bacterial solution for the daily gastric gavage.

2.3 Glucose and insulin tolerance tests

Mice underwent the Intraperitoneal Glucose Tolerance Test (IPGTT) following 10–14 h of fasting. Every mice received a gavage of 2.5 g/kg of glucose, followed by measuring their tail vein blood glucose levels using a glucometer for the subsequent 0, 15, 30, 60, and 120 min. Every mice received an intraperitoneal injection of 0.75 U/Kg insulin, followed by measuring their tail vein blood glucose levels using a glucometer at intervals of 0, 15, 30, 60, and 120 min. Mice underwent the Insulin Tolerance Test (ITT) following a fasting period of 10–14 h. Every mice received an intraperitoneal insulin injection, and their blood sugar levels in the tail vein were monitored using a glucometer at intervals of 0, 15, 30, 60, and 120 min.

2.4 Sampling and sample preservation

After completing the insulin resistance test and glucose tolerance test, blood was collected from mice into centrifuge tubes using the eyeball blood collection method. Following the gathering of blood, the mice underwent cervical dislocation, with rapid dissection, followed by the collection and weighing of subcutaneous and visceral fat. Subsequently, the mice colon samples were placed in centrifuge tubes and promptly immersed in liquid nitrogen for a brief period of rapid freezing. Post-sampling, the gathered blood underwent swift centrifugation at 3,500 rpm for a duration of 10 min in a freezing centrifuge. Subsequently, the clear liquid above the sediment was moved to a fresh centrifuge tube and chilled at 4°C, whereas the accumulated colon samples were kept in a refrigerator at −80°C.

2.5 Serum metabolome prep

The procedure involved naturally defrosting pre-stored mice serum, extracting 100 μL of this serum into a 1 mL centrifuge tube, then mixing it fourfold (400 μL) with a 1:1 methanol/acetonitrile solvent mixture. This mixture was agitated in a vortex shaker for 30 s, thoroughly mixed, ultrasonicated in an ice bath at 4°C for 10 min, refrigerated at −80°C for 8 h post-ultrasonication, and finally centrifuged for 15 min at 4°C and 12,000 rpm. Following a 15-min centrifugation, the clear liquid above the sediment was drawn into a fresh centrifuge tube and dehydrated to a dry state using a vacuum dryer. Introduce 100 μL of a solvent (methanol/acetonitrile), proceed to sonicate the mixture at 4°C for a duration of 10 min, followed by centrifugation at 4°C and 12,000 rpm for 15 min. Subsequently, transfer the supernatant into a fresh tube, and ultimately store the sample in an ultra-low temperature fridge at −80°C to freeze.

2.6 Ultrahigh-performance liquid chromatography-quadrupole time-of-flight mass spectrometry (UHPLC/Q-TOF-MS) analysis

Fifteen mice serum specimens were gathered in total, from which 10 μL was extracted, blended, and segmented into five parts, designated as a Quality control (QC) group to stabilize the device and adjust the data for pre-treatment. UHPLC: An Agilent 1290HPLC system; Column: Eclipse Plus C18, RRHD 1.8um, 2.1 × 100 mm, temperature set to 30°C; utilizing mobile phases: a mixture of 0.1% formic acid in water (Mobile

10.3389/fmicb.2024.1425764

TABLE 2 Elution procedure.

Time (min)	Mobile phase A (%)	Mobile phase B (%)	Flow velocity (mL/min)	Critical pressure (bar)
0	95	5	0.3	1,300
2	95	5	0.3	
20	0	100	0.3	
25	0	100	0.3	

phase A) and 0.1% formic acid acetonitrile (Mobile phase B). The flow rate was regulated to 0.3 mL/min, with a controlled injection volume of 2 μL, and the elution method is detailed in Table 2. The rate of ionization flow was established at 1.2 L/min, the interval for mass scanning ranged from 20 to 100 meters per second, and the temperature of the drying gas was fixed at 200°C. The data output from the mass spectrometer (Agilent 6,545 Q-TOF LC/MS) were processed and interpreted using the appropriate mass spectrometry software to determine the mass peak areas or peak heights of the target compounds and analyzed quantitatively by HPLC-MS/MS in combination with known standards.

2.7 Microbiota profiling by 16S rRNA amplicon sequencing

Total mice intestinal microbial DNA was extracted from mouse colonic content species by referring to the QIAamp Power Fecal DNA kit instructions, and the V3V4 variable region of the mouse intestinal bacterial 16S rRNA gene was specifically amplified using the polymerase chain reaction (PCR), with the primers 27F 5′-AGRG TTTGATYNTGGCTCAG-3′ and 1492R 5′-TASGGHTACCTTGTT ASGACTT-3′, in which each sample was repeated three times, the PCR products were purified by the kit, and then gel recovery was carried out by agarose gel electrophoresis at a concentration of 1.8%, and the results of the electrophoresis and PCR were imaged using a nucleic acid gel imager and characterised using ImageJ software. The recovered PCR products were subjected to bipartite sequencing and library construction using Illumina NovaSeq second-generation sequencing platform. Initial identification and quality control of the raw data was performed using QIIME2 (2023.6) software to remove low-quality, repetitive and short sequences (<100 bp) from the library. Sequencing splices during sequencing and library construction were removed using the Cutadapt program, sequence chimeras in the library were removed and sequencing fragments were spliced using the Usearch program, a filter condition of 97% similarity with a threshold of 0.005% was set, and OTU clustering and downscaling was performed on the filtered data, resulting in a total of 698 OTUs being identified for the complete study using the available faecal samples. QIIME2 was used to analyse the α-diversity and β-diversity of microorganisms in the samples, as well as the distribution of microorganisms in each treatment group at each taxonomic level and the dominant flora in each group.

2.8 Differential metabolite screening and pathway analysis

The raw data obtained were uploaded to Human Metabolome Database (HMDB) and MetaboAnalyst databases after noise reduction and data normalization using Metaboscape software, and the basic information of metabolites was obtained by preliminary retrieval. The screening conditions were VIP > 1, p-value<0.05, FC > 2. Finally, differential metabolite pathways were analyzed using the pathway analysis panel in the MetaboAnalyst website.[1]

2.9 Data and statistical analyses

The experiment's data is presented as the mean plus or minus the standard error of the mean (SEM). The variance among group averages was examined through one-way ANOVA and evaluated via Duncan's multiple comparison method. IBM SPSS Statistics 22 for Windows was utilized to conduct these studies. The correlation between colonic microorganisms and serum metabolites was assessed using Spearman's correlation coefficient. Statistical significance was attributed to $P < 0.05$.

3 Results

3.1 *Lactobacillus plantarum* inhibits HFD-induced obesity in mice

From week 3, the body weights of mice in the high-fat-fed HFD and HFD-ZW groups were significantly higher than those in the regular-fed CON group ($p < 0.05$), and the most pronounced difference was observed at week 8 (Figure 2A), with the body weights of mice in the HFD group and the HFD-ZW group being approximately 1.21 and 1.07 times that of those in the CON group, respectively ($p < 0.01$). Prior to week 11, the average body weight of mice in the CON group was 30.55 g, whereas that of mice in the HFD and HFD-ZW groups was 38.97 g. The overweight rate of the HFD group was 27.56% compared with that of the standard CON group ($p < 0.001$). Starting from the 11th week, mice in the HFD-ZW group were intragastrically gavaged with 150 μL of *L. plantarum*, and both mice in the CON group and the HFD-ZW group showed different degrees of body weight loss in the first week of gavage, with a significant 5.72% decrease in body weight of the mice in the HFD-ZW group in the 11th week (Figure 2B). Meanwhile, significant differences in body weight were also observed between the HFD-ZW-treated group and the HFD modeling group ($p < 0.05$), and the gavage test showed that the body weights of each group decreased by 6.23 and 2.87%, respectively (Figures 2B–E), which indicated the therapeutic efficacy of *L. plantarum* administered by gavage on obesity and significantly reduced the body weights of the mice in the modeling group ($p < 0.05$).

3.2 *Lactobacillus plantarum* enhances glucose tolerance and insulin resistance in obese mice

During the intraperitoneal glucose tolerance examination, it was observed that every mice exhibited a notable rise in blood sugar

1 https://genap.metaboanalyst.ca/MetaboAnalyst/home.xhtml

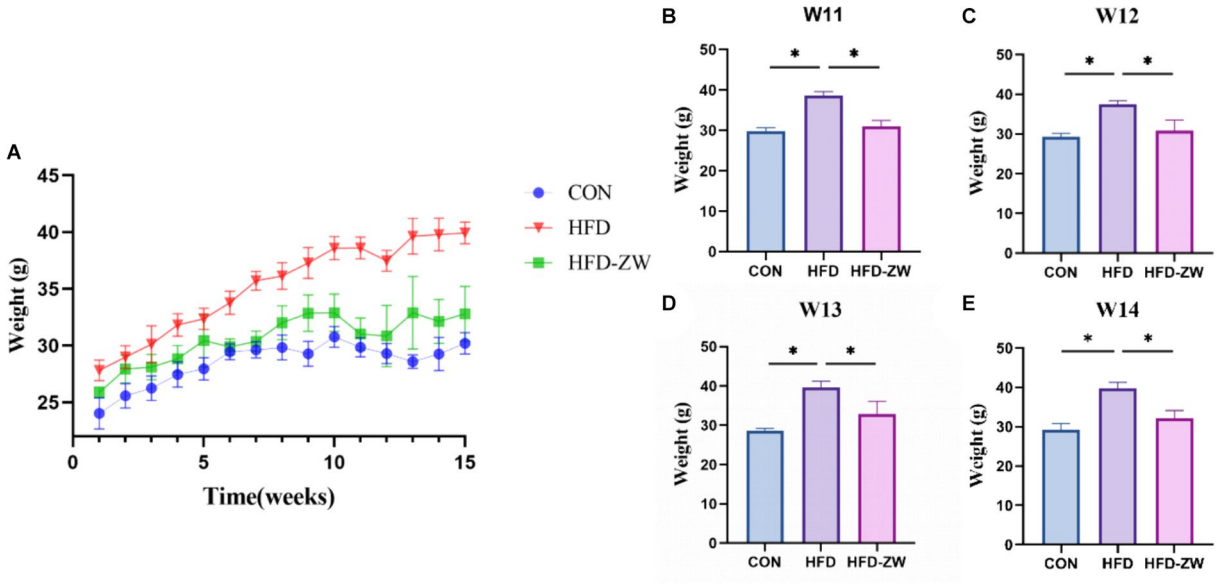

FIGURE 2
L. plantarum on body weight in obese mice. **(A)** Change in body weight of mice. **(B–E)** Weight changes in each treatment group during gavage. Data are means ± standard deviation and were analysed by one-way ANOVA. *$p < 0.05$ ($n = 5$).

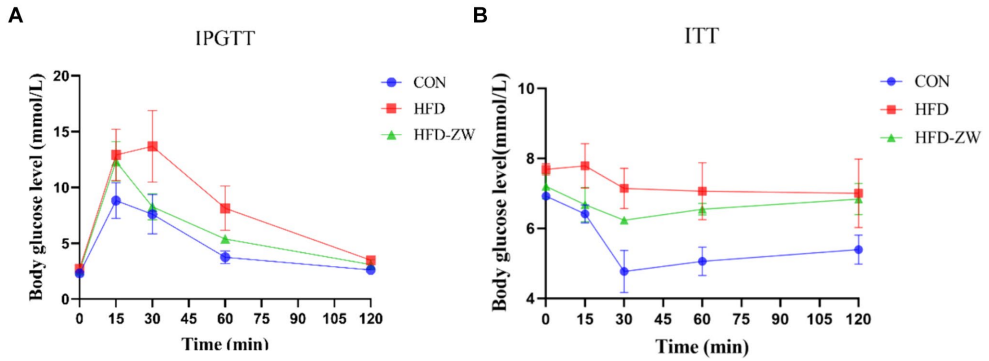

FIGURE 3
Effect of *L. plantarum* on glucose tolerance and insulin resistance in obese mice. **(A)** Plasma glucose levels in the mice glucose tolerance test; **(B)** plasma glucose levels in the mice insulin resistance test.

levels 15 min subsequent to receiving an intraperitoneal glucose injection (Figure 3A), yet in a span of 15–30 min, there was a notable reduction in the blood sugar levels of mice in the HFD-ZW group relative to those in the CON and HFD groups. Variations in blood sugar levels among mice during the glucose tolerance test consistently exhibited a pattern of rising and then falling, with the glucose area under the curve (AUC) in the HFD group mice notably exceeding that in the CON and HFD-ZW groups. The insulin resistance test revealed (Figure 3B). It was observed that the HFD group consistently exhibited the highest blood glucose levels, in contrast to the CON group, which had the lowest during the 0–120 min. The HFD group did not demonstrate a notable reduction in blood glucose levels in the 0–15 min period, in contrast to the other two groups, indicating a remarkable imbalance in insulin sensitivity.

3.3 *Lactobacillus plantarum* reduces HFD-induced adiposity gain and decreases adipocyte size

The HFD group exhibited notably greater subcutaneous and visceral fat weights with regard to the CON group ($p < 0.05$). Additionally, the proportions of subcutaneous and visceral fat to body weight (%) were notably greater in the HFD group than in the CON and HFD-ZW groups (Figures 4A,B). Additionally, we conducted HE staining on both subcutaneous and visceral fat in mice, discovering a notable reduction in adipocyte size in the CON and HFD-ZW compared to the HFD group ($p < 0.05$). Consistently, accumulated lipid droplets and balloon-like structures, which are markers of hepatic steatosis, were observed in the hepatocytes of the HFD group (Figure 4C). After plant lactic rod treatment, lipid droplet size was

significantly reduced and hepatic steatosis was significantly improved in the HFD-ZW in comparison to HFD-fed mice.

3.4 Analysis of microbial diversity in the mice colon

The distribution of OTUs in each group was as follows: 380 in the CON group, 365 in the HFD group, and 360 in the HFD-ZW group, of which the number of featured articles was 155, 135, and 145, respectively (Figure 5A). From this, it can be preliminarily hypothesised that obesity had reduced the species richness of the microorganisms of the mice colon to a greater extent, and that *L. plantarum* gastric gavage had restored the species richness of the microorganisms of the mice intestine to a certain degree.

According to the analysis of α-diversity indices of each treatment group, ACE and Chao1 indices could be used to measure the number of species (Figures 5B,C), and Shannon and Simpson indices were used to assess the diversity of species (Figures 5D,E). The ACE, Shannon and Chao1 indices of the HFD group had the lowest values among all treatment groups, and the three indices were significantly higher in the HFD-ZW and CON groups ($p < 0.05$), and the ACE, Shannon and Chao1 indices tended to increase in the HFD-ZW with regard to the CON group, which indicated that *L. plantarum* gavage increased the species richness of mice colon microorganisms to a greater extent, which was consistent with the results of the OTU distribution; the α-diversity indices of the HFD group were lower than those of the other treatment groups, which may indicate that the obesity environment reduced the microbial diversity of the mice colon to a greater extent. In addition to measure the degree of similarity between microbial communities, β-diversity was further assessed using Binary-jaccard PCoA. In this study, PCoA was used to analyse the microbial community structure of colon contents from different groups of mice. The results showed that the probiotic group had the greatest variability after the intervention *L. plantarum* after the intervention (Figure 5F). However, the UPGMA results showed that the HFD-ZW group was closer to the CON group than the HFD group at the phylum level (Figure 5G).

3.5 Analysis of colonic microflora composition in mice

3.5.1 *Lactobacillus plantarum* affects the abundance of microorganisms at phylum level under high fat diet induced obesity

Within the phylum, the leading five microbial phyla were Bacteroidota, Firmicutes, Proteobacteria, Actinobacteriota, and Desulfobacterota, representing over 90% of the overall count (Figure 6A). In each group, the relative abundance of Bacteroidetes was 49.32, 38.31, and 52.90% (Figure 6B), and the high-fat environment significantly decreased the abundance of Bacteroidetes, on the contrary, the gavage of *L. plantarum* significantly increased the relative abundance of Bacteroidetes in the colons of the mice ($p < 0.05$), and even marginally exceeded the CON group's by 3.58%. Meanwhile, as the relative abundance of the Firmicutes in the HFD group increased, its relative abundance in the CON and HFD-ZW groups was 35.40 and 29.19%, respectively (Figure 6C), 8.29 and 14.6%, respectively, lower than in the HFD group. Consequently, there was a notable rise in the proportion of F/B within the HFD group (Figure 6D). Furthermore, the comparative prevalence of the Proteobacteria in each experimental group stood at 5.47, 3.95, and

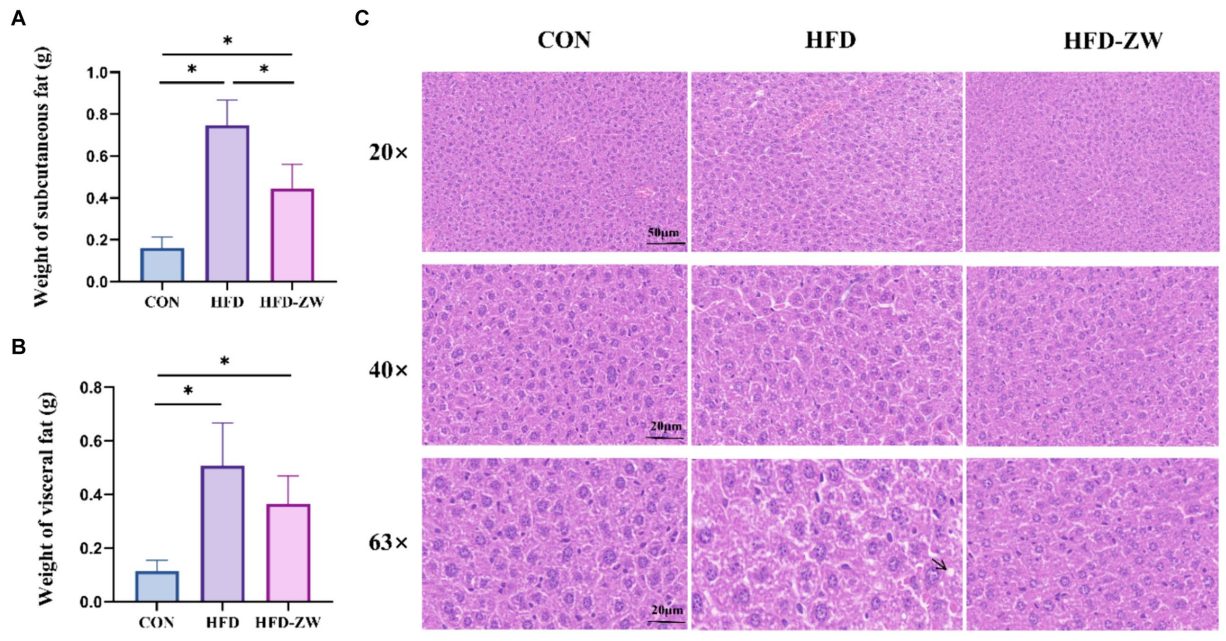

FIGURE 4
Effects of *L. plantarum* on adipocyte and liver histological changes in obese mice. **(A)** Changes in subcutaneous fat weight; **(B)** changes in visceral fat weight; **(C)** histological changes in liver sections measured by H&E staining with 20×, 40× and 63× magnification, respectively. Data are mean ± standard deviation and were analysed by one-way ANOVA. *$p < 0.05$ ($n = 5$).

10.3389/fmicb.2024.1425764

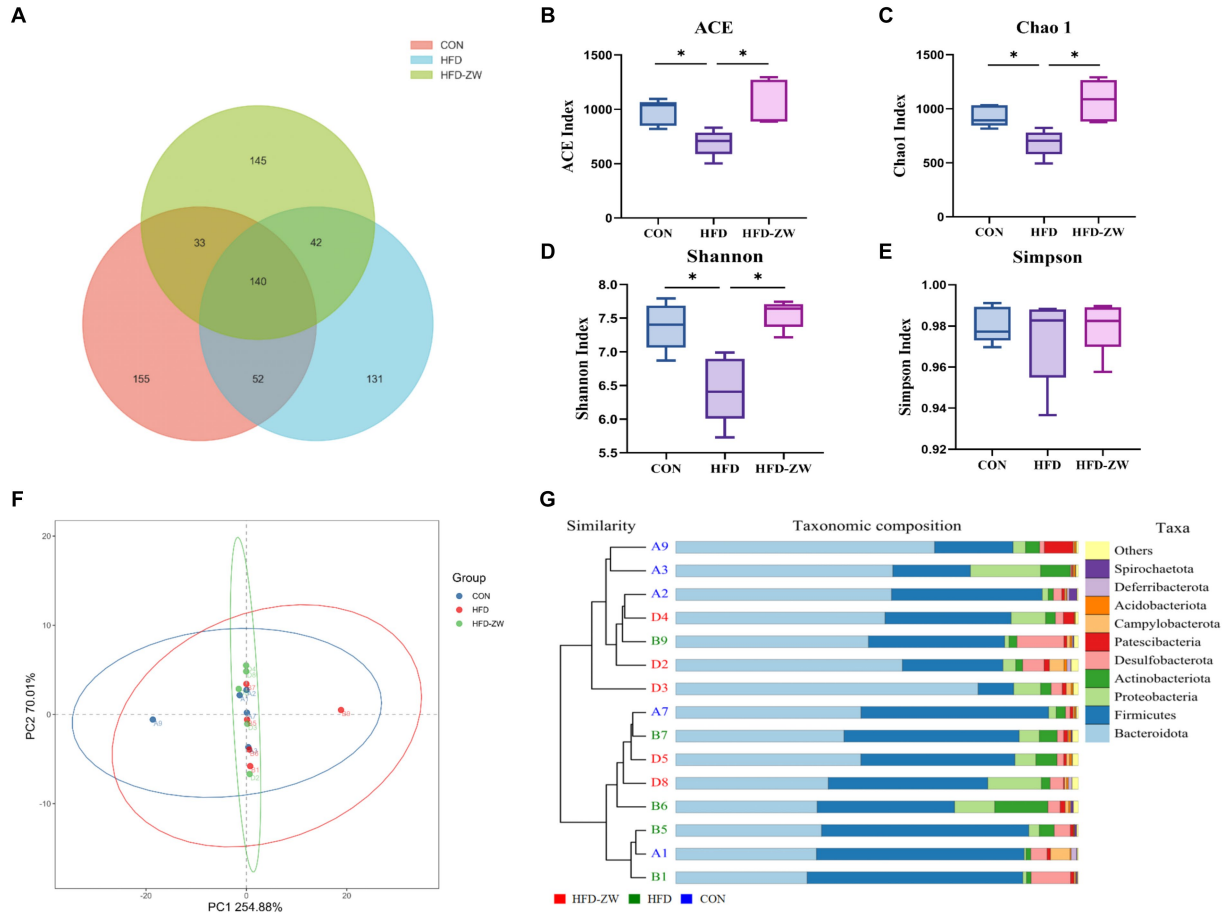

FIGURE 5
Effect of *L. plantarum* treatment on microbial species richness, α and β diversity indices in mice colon. **(A)** Venn diagram of OTU distribution. **(B)** ACE index. **(C)** Chao 1 index. **(D)** Shannon's index. **(E)** Simpson's index. **(F)** Principal co-ordinate analysis (PCoA) showing microbial community distances between baseline of the CON group (blue circles), the HFD group (red circles), and the baseline of the group after *L. plantarum* intervention (green circles). **(G)** Unweighted pair group method with arithmetic mean (UPGMA) analysis. Data are means ± standard deviation and were analyzed using one-way ANOVA. *$p < 0.05$ ($n = 5$).

7.06% correspondingly (Figure 6E), indicating a downward trend in the HFD group, yet the difference was not statistically meaningful. Both Actinobacteria phylum and Desulfobacterota significantly reversed the increasing trend in high-fat environment after gavage by *L. plantarum* (Figures 6F,G) ($p < 0.05$).

3.5.2 *Lactobacillus plantarum* affects the abundance of microorganisms at class level under high fat diet induced obesity

The microbial composition in the mice colon was examined, revealing the top 15 microorganisms at the Class level, as illustrated in Figure 7A. Notably, the predominant microorganisms, including Bacteroidia, Clostridia, Bacilli, Actinobacteria, and Deferribacteres, collectively accounted for more than 80% of the total microbial population. Specifically, under high-fat conditions, a reduction of 11.01% in the relative abundance of Bacteroidia was observed (Figure 7B), mirroring the trends seen in the Bacteroidota phylum. However, administration of *L. plantarum* through gavage resulted in a significant increase in the relative abundance of Bacteroidia ($p < 0.05$). In the CON, HFD, and HFD-ZW groups, the relative abundance of Clostridia was found to be 27.35, 30.90, and 20.90%, respectively (Figure 7C). Similarly, the relative abundance of Bacilli was observed to be 7.98, 12.82, and 8.20%, respectively (Figure 7D). Notably, both the CON group and the HFD-ZW group exhibited a significant increasing trend in Bacilli abundance. Additionally, the relative abundance of Actinobacteria was found to be 1.81, 5.94, and 3.03% (Figure 7E), while the relative abundance of Deferribacteres in each treatment group was 5.29, 3.69, and 4.68%, with no statistically significant difference observed ($p > 0.05$) (Figure 7F). Comparative analysis revealed a significant increase in the abundance of Clostridia and Bacilli ($p < 0.05$) in the HFD group compared to CON. Importantly, administration of *L. plantarum* effectively restored the altered microbial abundance induced by the high-fat conditions.

3.5.3 *Lactobacillus plantarum* affects microbial abundance at the genus level under high-fat diet-induced obesity

By analysing the composition of microorganisms in the mice colon, the five dominant genera at the level of the 15 most abundant genera were *Dubosiella*, *Parasutterella*, *Desulfobibrio*, *Bacteroides* and

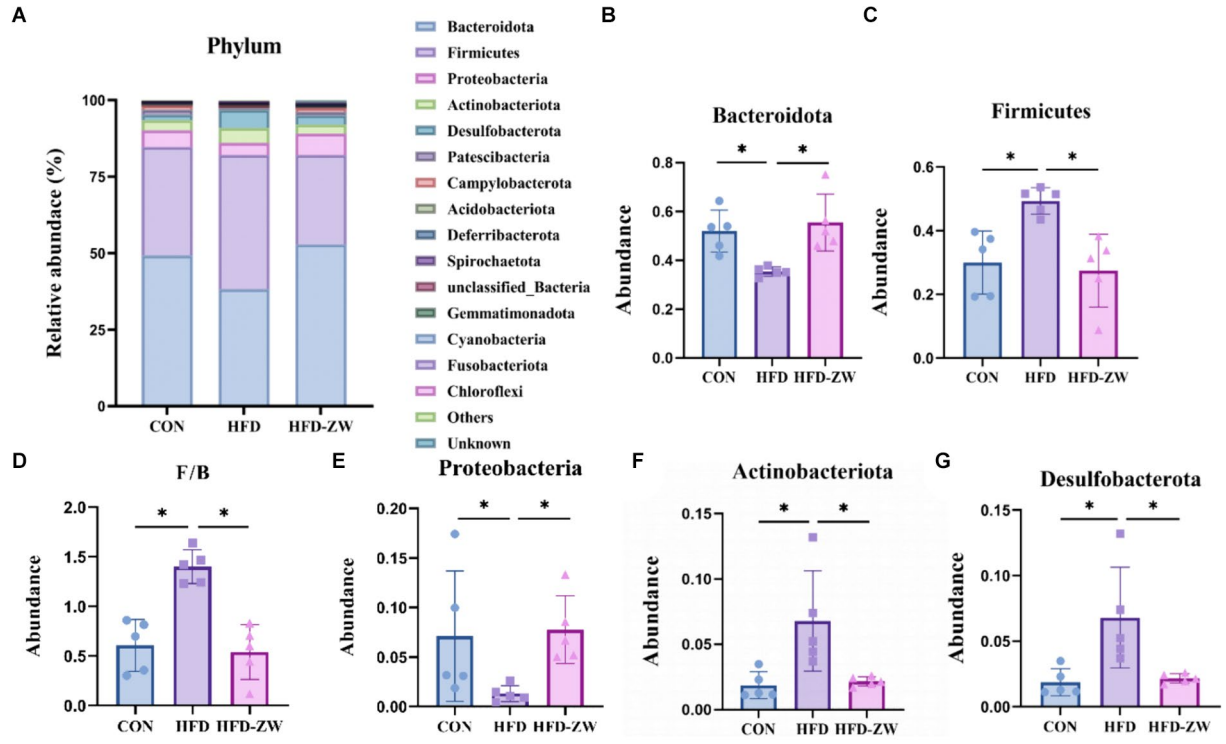

FIGURE 6
Analysis of microbial components at the phylum level. **(A)** Relative abundance of microbial phyla in the mice colon. Components of the relative abundance of the Bacteoidota **(B)**, Firmicutes **(C)**, F/B ratio **(D)**, Proteobacteria **(E)**, Actinobacteria **(F)**, and Desulfobacterota **(G)** in the colons of mice in the CON, HFD, and HFD-ZW groups. *$p < 0.05$ ($n = 5$).

Odoribacter (Figure 8A). *Parasutterella*, *Bacteroides*, and *Odoribacter* decreased by 1.66, 0.37, and 0.97%, respectively, under high-fat conditions compared to the CON group (Figures 8C,E,F). In addition, the relative abundance of *Dubosiella* was 1.54, 9.37, and 4.01% (Figure 8B), and that of *Desulfobibrio* was 0.83, 4.99, and 2.27% (Figure 8D), respectively, which were significantly increased ($p < 0.05$) in the HFD group. Whereas, using *L. plantarum* gavage treatment, *Parasutterella*, *Bacteroides* and *Odoribacter* all had a tendency to recover the same abundance as that of the CON group (Figures 8C,E,F), but there was no statistical difference. Meanwhile, *Dubosiella* and *Desulfobibrio* in the HFD-ZW group reversed the abundance changes induced by the high-fat environment (Figures 8B,D) and showed a significant recovery in abundance ($p < 0.05$).

3.6 LEfSe analysis of microbiota in colon contents

The results of LEfSe analysis of colonic microorganisms in the CON, HFD, and HFD-ZW groups are shown in Figure 9A ($p < 0.05$). We found that the order of significant enrichment in the CON group was Bacteroidales, Oscillospirales, and Lacteobacillales; the families Prevotellaceae and Lactobacillaceae; and the genus *Alloprevotella*. The HFD group was remarkably enriched in the genera Lachnospirales, Erysipelotrichales, Desulfovibrionales, order Coriobacteriales; families Lachnospiraceae, Erysipelotrichaceae, Desulfovibrionaceae; *Dubosiella*, *unclassified_Lachnospireaceae*, *Desulfovibrio* and *Lachnospiraceae_NK4A136_groups* were significantly enriched. The HFD-ZW group was in the orders Burkholderiales, Richettsiales; Families Muribaculaceae, Sutterellaceae, Rickettsiaceae, Atopobiaceae; *unclassified_ Muribaculaceae*, *Ligilactobacillus*, *Parasutterella*, *unclassified_ Rickettsiaceae* genera were significantly enriched. By identifying Linear Discriminant Analysis (LDA) scores above 2 (Figure 9B), it was possible to determine that species abundance differed in each group. In the HFD-ZW group, the order Cyanobacteriia; the orders Richettsiales, Cyanobacteriia, Cyannobacteriales, Sphingomonadales; the families Rickettsiaceae, Sphingomonadaceae; The species abundance of the genera *Spingomonas*, *unclassified_Sphingomonas*, and *Plesiomonas* had the most notably effect on the abundance of differential bacteria. Further revealed significant differences in biological branching composition between the control, HFD and HFD-ZW groups, which is consistent with the above results.

3.7 Influence of *Lactobacillus plantarum* treatment on serum levels of total metabolites in mice

The serum differential metabolites of mice from the CON, HFD, and HFD-ZW groups were comprehensively analyzed through pairwise comparisons, as depicted in Figure 10. Notably, metabolites with *p*-values <0.05 and FC-values >1 were considered significant. The differential metabolite volcano plot revealed a total of 554 distinctive metabolites between the CON and HFD groups (Figure 10A). Among these, Rosmic acid, Edulisin III,

10.3389/fmicb.2024.1425764

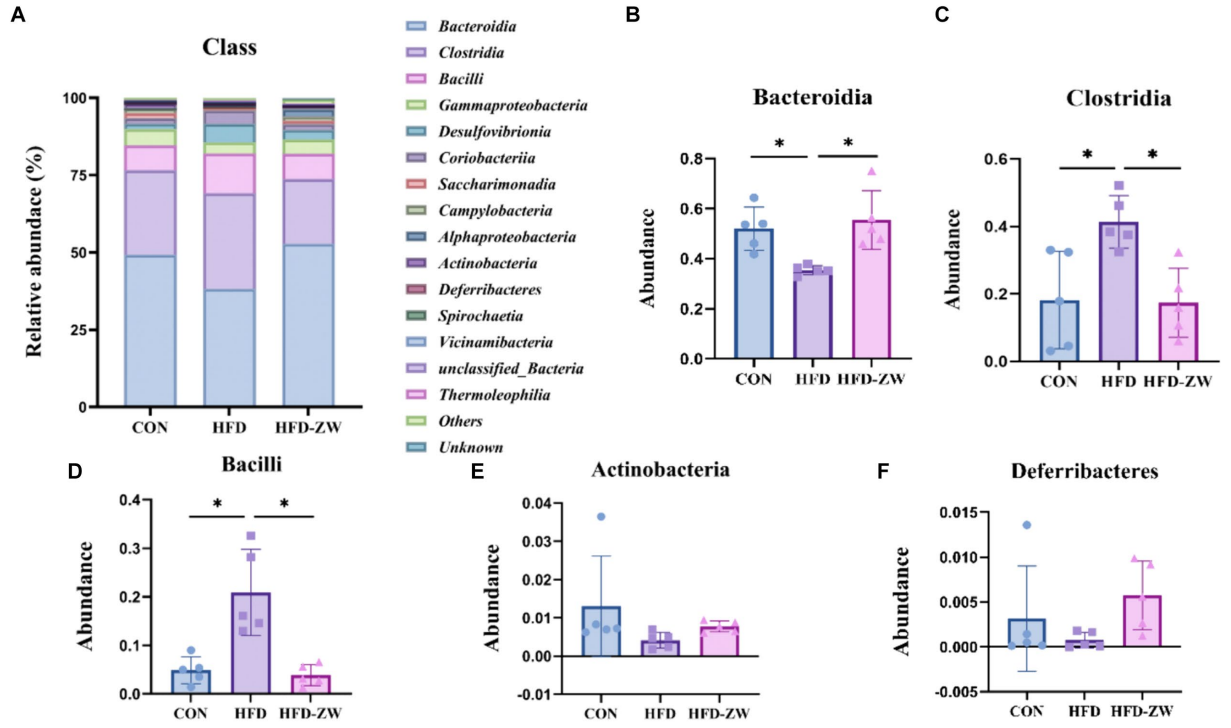

FIGURE 7
Analysis of microbial components at the class level. **(A)** Relative abundance of microbial class in the mice colon. Components of the relative abundance of Bacteroidia **(B)**, Clostridia **(C)**, Bacilli **(D)**, Actinobacteria **(E)**, and Deferribacteres **(F)** in the colons of mice in the CON, HFD, and HFD-ZW groups. *$p < 0.05$ ($n = 5$).

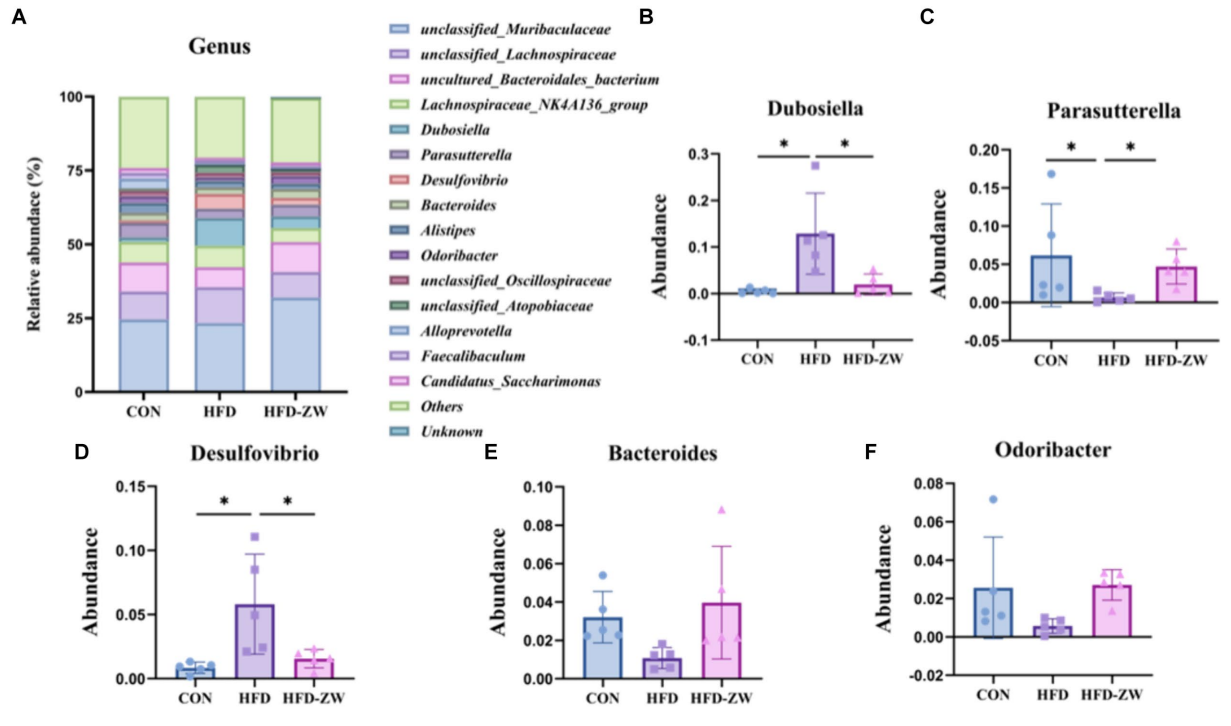

FIGURE 8
Analysis of microbial components at the genus level. **(A)** Relative abundance of microbial genus in the mice colon. Components of the relative abundance of *Dubosiella* **(B)**, *Parasutterella* **(C)**, *Desulfovibrio* **(D)**, *Bacteroides* **(E)**, and *Odoribacter* **(F)** in the colons of mice in the CON, HFD, and HFD-ZW groups. *$p < 0.05$ ($n = 5$).

10.3389/fmicb.2024.1425764

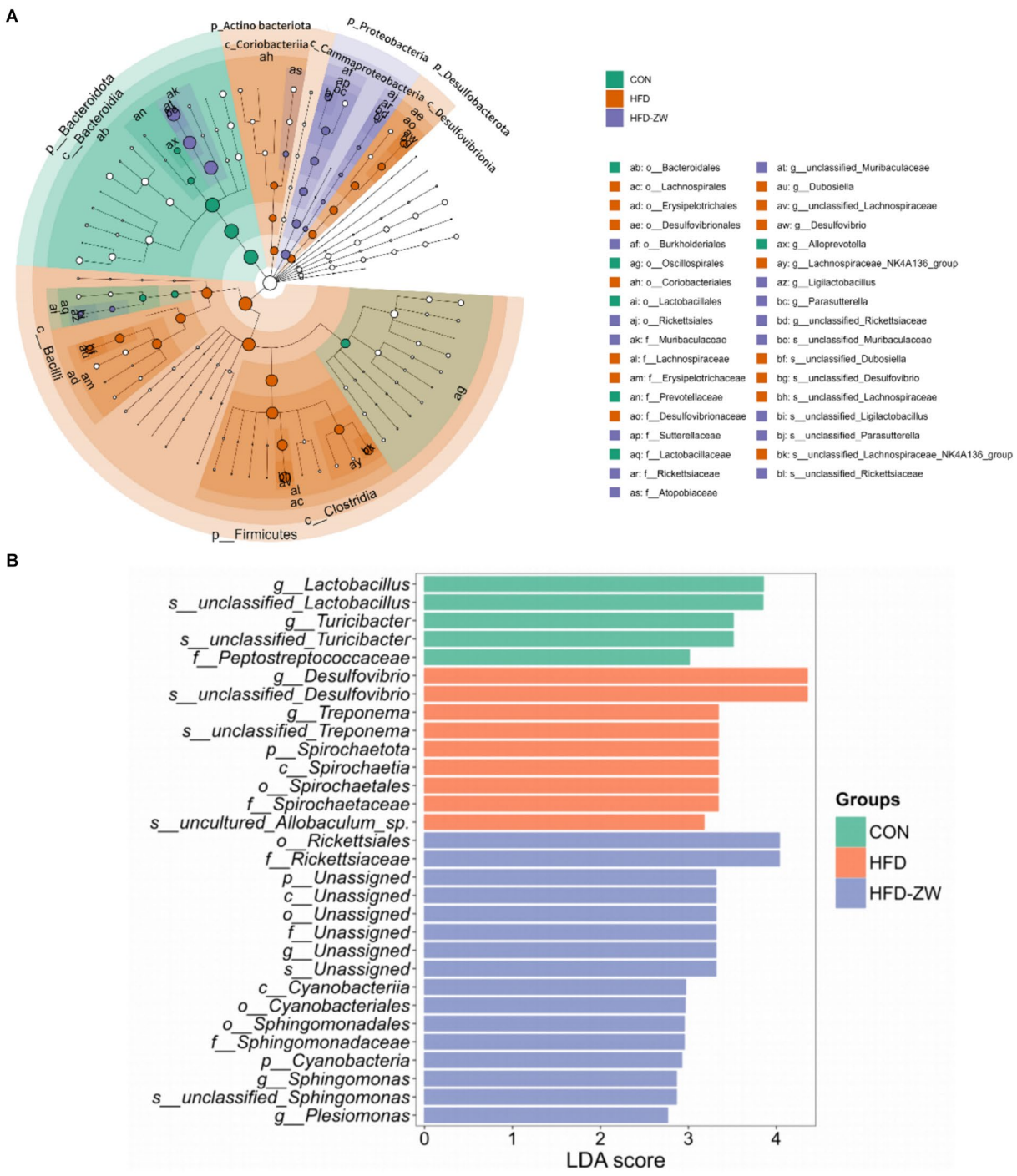

FIGURE 9
Characterisation of mice colonic microorganisms identified by *L. plantarum* treatment. **(A)** LEfSe taxonomic branching diagram, different colours indicate enrichment of certain taxonomic units in the CON group (green), the HFD group (orange) and the HFD-ZW group (purple); **(B)** LDA scores, LDA scores higher than 2 were considered to be significant contributors to the model.

1-Hexadecen-3-one, Armillaricin, PS (18:0/13:0), PE (20:0/0:0), and 10,20-Dihydroxyeicosanoic acid were found to be significantly up-regulated in the CON group. On the other hand, there were 84 differential metabolites identified between the HFD and HFD-ZW groups (Figure 10C). Following the administration of *Lactobacillus plantarum* gavage treatment, metabolites including PE (22:6(4Z,7Z,10Z,13Z,16Z,19Z)/0:0), 1-Methyl-3-(2-thiazolyl)-1H-indole, Lupinate, Pemetrexed, Isoprothiolane, Inosine, and Cerberin showed significant up-regulation, whereas Sophoranol, 4-Heptyloxyphenol, and Capsianoside VI displayed decreased expression. Notably, similar trends were observed in the CON group for metabolites such as PE-Cer(d16:1(4E)/19:0), Cycloartanyl ferulate, Cer(d18:1/24:1), and Tetrahydroaldosterone-3-glucuronide following *L. plantarum* treatment.

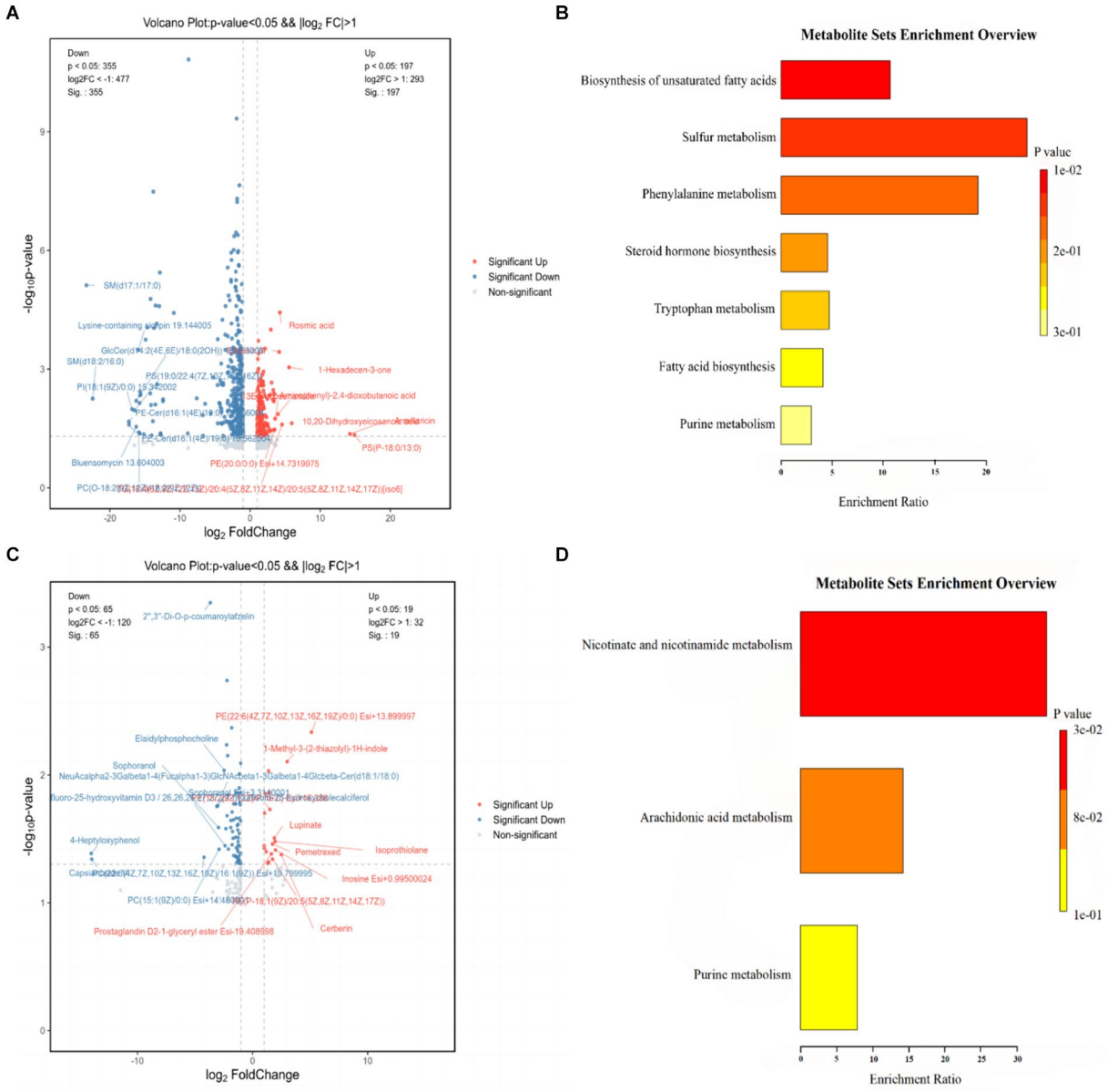

FIGURE 10
Differential metabolite and KEGG pathway enrichment analysis results. **(A)** Analysis of differential metabolites between CON and HFD; **(B)** results of enrichment analysis of KEGG pathways between CON and HFD; **(C)** analysis of differential metabolites between HFD and HFD-ZW; **(D)** results of enrichment analysis of KEGG pathways between HFD and HFD-ZW.

The results of the Kyoto Encyclopedia of Genes and Genomes (KEGG) database enrichment analysis of the major differentiated metabolites indicated distinct pathways associated with unsaturated fatty acid biosynthesis, sulfur metabolism, phenylalanine metabolism, steroid hormone biosynthesis, tryptophan metabolism, fatty acid biosynthesis, and purine metabolism between the CON and the HFD group (Figure 10B). In contrast, differential metabolites in the HFD and HFD-ZW groups were largely enriched in domains of nicotinic acid and nicotinamide metabolism, arachidonic acid metabolism, and purine metabolism (Figure 10D). These findings provide valuable insights into the metabolic alterations associated with high-fat diet-induced conditions, as well as the potential modulatory effects of *L. plantarum* intervention.

3.8 Correlation between intestinal microbes and serum metabolites

The genus-level network Spearman correlation analysis of the intestinal flora of each group of mice (Figure 11A) revealed that unclassified_UCG_010, unclassified_Ruminococcaceae, Colidextribacter, and Lachnospiraceae_UCG_006 showed high correlation with other microorganisms showed high positive correlation,

while unclassified_Oscillospiraceae, Parasutterella, unclassified_Ruminococcaceae and Incertae_Sedis presented high negative correlation. And the relative abundance of Oscillibacter, unclassified_Ruminococcaceae, Incertae_Sedis and Lachnospiraceae_NK4A136_group was found to be at a high level according to node size. By analysing the heatmap of mice colon microbial correlation with serum differential metabolites it was found (Figure 11B) that LysoPC (18:1 (11Z)) showed a significant positive correlation with Paraclostridium, unclassified_Lactobacillaceae, uncultured_Barnesiella_sp. and Serratia were significantly positively correlated with each other. While unclassified_Cyanobacteriales and Sulfurimonas were significantly negatively correlated with LysoPC (18:2 (9Z, 12Z)), LysoPC (0:0/18:0).

4 Conclusion

This research delved into the healing capabilities of *L. plantarum*, a probiotic known for its diverse bioactivities (Li et al., 2020), by inducing obesity in mice on a high-fat diet and tube-feeding them with a probiotic with a wide range of bioactivities. The study showed

FIGURE 11
Spearman correlation analysis of gut flora with serum metabolites. **(A)** Network plot of gut flora correlation in mice; **(B)** heat map of gut differential microbiota versus raw serum differential metabolites. *$p < 0.05$ and **$p < 0.01$.

that *L. plantarum* significantly alleviated and reduced body weight in obese mice. Besides, it can inhibit the accumulation of lipids in the liver. *L. plantarum* treatment promoted the restoration of glucose tolerance and insulin sensitivity in obese mice according to IPGTT and ITT results. Analysis of mice colon samples revealed that treatment with *L. plantarum* enhanced the alpha variety in intestinal microbes. There was a rise in the number of advantageous bacteria, a fall in the quantity of detrimental bacteria, and a reduction in the balance between Firmicutes and Bacteroidota. Serum metabolomics analysis revealed notable alterations in serum metabolites across all three mice groups. During obesity modelling and *L. plantarum* treatment, *L. plantarum* significantly increased Isoprothiolane, Inosine and Cerberin levels, inhibited lipid accumulation in adipocytes as well as facilitated fat burning, leading to obesity alleviation. Meanwhile the differential metabolites were significantly enriched in purine metabolism. These findings suggest that *L. plantarum* is expected to be able to be a new strategy for the effective treatment of obesity, providing a more optimised alternative to achieve therapeutic goals. In addition, more future studies are needed to explore in depth and comprehensively the specific mechanisms involved in alleviating obesity and to clarify the dosage of *L. plantarum* treatment. This will help to maximise therapeutic benefits when managing obesity.

5 Discussion

Obesity and its associated chronic diseases have become an important risk factor threatening global health (O'Neill and O'Driscoll, 2015). Several studies have proposed the potential efficacy of probiotics in the effective alleviation and treatment of obesity due to their modulation of gut microbial composition and maintenance of the functional integrity of the intestinal barrier (In Kim et al., 2019; Quigley, 2019). Thus, *L. plantarum*, which has a variety of bioactive functions, was selected for our study to investigate its efficacy in ameliorating obesity (Zhu et al., 2019; Park and Oh, 2007). It was found that treatment of high-fat diet-induced obesity by *L. plantarum* reduced body weight, subcutaneous and visceral fat weight as well as reduced lipid droplet size in the liver and improved liver function in obese mice (Leung et al., 2016; Wei et al., 2023). The data suggest that *L. plantarum* improves glucose tolerance, insulin resistance and regulates serum metabolites (Han et al., 2020). It is consistent with the findings of Ho et al. on the anti-obesity potential of *Lactobacillus rhamnosus* SG069 (LR069) and *Lactobacillus brevis* SG031 (LB031) as well as their ability in preventing diet-induced insulin resistance (Ho et al., 2024).

There exists a tight association between blood glucose and lipid metabolism (Kojta et al., 2020). Studies have shown that when the blood glucose level in the host body exceeds a certain threshold, the acetyl CoA, citric acid and ultimately ATP generated during the oxidative decomposition of glucose, the three can be allosterically activated acetyl CoA carboxylase, which ultimately leads to the conversion of glucose into fat stored in the adipose tissue (Saltiel and Kahn, 2001). However, we found that obese mice treated with *L. plantarum* by gavage had the ability to regulate blood glucose levels compared with the model group, as shown by the significant reduction of blood glucose levels in the treated group of obese mice 30 min after receiving intraperitoneal glucose injection. This indicates that *L. plantarum* is able to ameliorate the abnormal elevation of blood glucose values and reduce the conversion of glycogen into energy storage in the form of fat (Youn et al., 2021). Meanwhile, insulin plays a major role in reducing plasma glucose levels by controlling hepatic glucose metabolism. It was found by insulin resistance experiments that mice fed under high-fat conditions consistently had the highest blood glucose levels and within 15 min for showed the ability to lower blood glucose. However, both the HFD-ZW group and the CON group showed a tendency to lower blood glucose at 15 min, it is consistent with the findings of Zhao et al. (2022) and further indicates that *Lactobacillus plantarum* tube-feeding-treated mice were able to inhibit the level of insulin resistance in high-fat mice to a certain extent (Paranjape et al., 2010; Chao et al., 2019).

Notable alterations ($p < 0.05$) in the gut microbe makeup of mice were noted during the development of the obesity model and the ensuing application of *L. plantarum* (Moorthy et al., 2021). A notable reduction in Bacteroidota was noted in obese mice nurtured in a high-fat setting, contrasted by a marked rise in the HFD-ZW group (Furet et al., 2010). At the same time, the abundance of Firmicutes increased in the HFD group (Rastmanesh, 2011), which led to an increasing trend in the ratio of Firmicutes to Bacteroidota in high-fat conditions. It is well known that the elevated F/B ratio is widely recognized as a key factor in the emergence and advancement of obesity (Chang et al., 2015). It was found that Firmicutes can produce more harvestable energy than Bacteroidota, so that in the presence of an increase in the relative abundance of Firmicutes and a decrease in the relative abundance of Bacteroidota, calorie uptake is increased, which then promotes obesity (Ma et al., 2022; Li et al., 2020). Subsequently, HFD-fed obese mice significantly restored the F/B ratio to normal levels after treatment with *L. plantarum* gavage (Stojanov et al., 2020). This conclusion was also confirmed by a study on *Lactobacillus gasseri* (de Moura et al., 2023). In addition, we found that *L. plantarum* dietary intervention also reduced *Desulfovibrio* expression in the HFD group (Wang et al., 2020). It has been proposed that increased *Desulfovibrio* abundance is a key feature of obesity (Katamoto et al., 1991). At the same time with the increase of *Desulfovibrio* there is an antagonistic effect on Clostridia. High abundance of *Desulfovibrio* and low abundance of Clostridia ultimately lead to a decrease in the expression of CD36 (Buttet et al., 2014), a key regulator of lipid absorption in the intestinal tract, and its deficiency leads to lipid metabolism disorders and excessive accumulation of adipocytes in the body (Buttet et al., 2016), which in turn increases the chances of obesity and metabolic syndrome caused by HFD feeding (Ma et al., 2022). More notably, we found that tube-feeding treatment with *L. plantarum* also reduced the expression of *Clostridium difficile* in the HFD group. A previous study by Ma Yong et al. also found that high abundance of Clostridium can metabolise and produce excess faecal deoxycholic acid (DCA). This ecological disturbance further reduced bile acid uncoupling, and DCA stimulated S1PR2 expression ultimately inducing activation of NLRP3 inflammatory vesicles (Ma et al., 2022). Furthermore, *Dubosiella* abundance was significantly reduced following *L. plantarum* gavage treatment, showing a positive association with weight increase and a reduction in the proliferation of short-chain fatty acid (SCFA) producing bacteria (Qiu et al., 2021; Martin-Gallausiaux et al., 2021). Mariana et al. study similarly found that disturbances in the intestinal flora were negatively correlated with total SCFA production and were able to reverse this adverse effect after probiotic intervention (de Moura et al., 2023). These bacteria are synthesized by intestinal Bacteroides through the fermentation of polysaccharides and carbohydrates, which pose challenges for the host to assimilate and digest (Blaak et al., 2020). Also, *L. plantarum* was able to enhance the expression of Bacteroides, and

these results suggest that it has a role in alleviating obesity (Backhed et al., 2004; Parnell and Reimer, 2012).

By analysing serum metabolomics, it was shown that metabolites PS-18:0/13:0 and PE (20:0/0:0) were significantly up-regulated in HFD-fed obese mice, PS-18:0/13:0 and PE (20:0/0:0) are important phospholipids in cell membranes and one of the important components of lipid metabolism (Xie et al., 2023), so it can be hypothesized that obese environments significantly reduce the metabolism of mice role in lipid metabolism in mice (Martinic et al., 2018). Serum metabolomics research was employed to evaluate the effectiveness of treating obese mice with *L. plantarum* and to understand its fundamental mechanisms. In obese mice treated with *L. plantarum*, the varied metabolites observed were PE (22:6(4Z,7Z,10Z,13Z,16Z,19Z)/0:0), 1-Methyl-3-(2-thiazolyl)-1H-indole, Pemetrexed, Isoprothiolane, Inosine, Cerberin, Cer(d18:1/24:1), 4-Heptyloxyphenol and Capsianoside VI. There was a notable rise in Isoprothiolane concentrations in the HFD-ZW relative to the HFD group. The study demonstrated that Isoprothiolane increased the levels of non-esterified fatty acids (NEFA) and was able to block lipid deposition into adipocytes (Katamoto et al., 1991), while having a common effect by accelerating the desaturation of fatty acids in tissue lipids. It is well known that obesity occurs as a result of excessive energy intake accumulating in the body in the form of fat, and increased Inosine expression promotes fat burning (Crunkhorn, 2022). Cer(d18:1/24:1) resumed the same decreasing trend as the CON group after *L. plantarum* gavage treatment (Yu et al., 2023). This is consistent with the findings of Yu Baowen et al. It was proposed that Cer(d18:1/24:1) levels are increased in the metabolic profile of obese subjects, which leads to reduced insulin sensitivity and is associated with metabolic disturbances in obesity and may also contribute to obesity comorbidities (Yu et al., 2023). The study suggests that increased levels of Cer(d18:1/24:1) may be a potential biomarker for obesity (Yu et al., 2023). Analysis of differential metabolites for potential signalling pathways involved in obesity showed that the CON vs. HFD group and the HFD vs. HFD-ZW group of varied microorganisms showed a notable increase in purine metabolism.

Data availability statement

The datasets presented in this study can be found in online repositories. The names of the repository/repositories and accession number(s) can be found at: https://www.ncbi.nlm.nih.gov/genbank/, PRJNA1104806.

Ethics statement

The animal study was approved by Animal Care Committee of Hunan Agricultural University (2023-51). The study was conducted in accordance with the local legislation and institutional requirements.

Author contributions

JZ: Data curation, Writing – original draft, Writing – review & editing. XL: Data curation, Writing – review & editing. NL: Data curation, Writing – review & editing. RZ: Data curation, Writing – review & editing. SW: Funding acquisition, Writing – review & editing.

Funding

The author(s) declare financial support was received for the research, authorship, and/or publication of this article. The research was supported by the grants from: Zhejiang Provincial Program for Medicine and Health (2023KY411), Key Laboratory of Precision Medicine for Atherosclerotic Diseases of Zhejiang Province (Grant No. 2022E10026), Social Development Science and Technology Foundation of Taizhou (21ywb115), Social Development Science and Technology Foundation of Wenling (2021S00197) and Hunan Provincial Science and Technology Department (2019TP2004).

Conflict of interest

The authors declare that the research was conducted in the absence of any commercial or financial relationships that could be construed as a potential conflict of interest.

Publisher's note

All claims expressed in this article are solely those of the authors and do not necessarily represent those of their affiliated organizations, or those of the publisher, the editors and the reviewers. Any product that may be evaluated in this article, or claim that may be made by its manufacturer, is not guaranteed or endorsed by the publisher.

References

Abenavoli, L., Scarpellini, E., Colica, C., Boccuto, L., Salehi, B., Sharifi-Rad, J., et al. (2019). Gut microbiota and obesity: a role for probiotics. *Nutrients* 11, 17–21. doi: 10.3390/nu11112690

Backhed, F., Ding, H., Wang, T., Hooper, L. V., Koh, G. Y., Nagy, A., et al. (2004). The gut microbiota as an environmental factor that regulates fat storage. *Proc. Natl. Acad. Sci. USA* 101, 15718–15723. doi: 10.1073/pnas.0407076101

Blaak, E. E., Canfora, E. E., Theis, S., Frost, G., Groen, A. K., Mithieux, G., et al. (2020). Short chain fatty acids in human gut and metabolic health. *Benef. Microbes* 11, 411–455. doi: 10.3920/BM2020.0057

Boccellino, M., and D'Angelo, S. (2020). Anti-obesity effects of polyphenol intake: current status and future possibilities. *Int. J. Mol. Sci.* 21, 1–2. doi: 10.3390/ijms21165642

Buttet, M., Poirier, H., Traynard, V., Gaire, K., Tran, T. T., Sundaresan, S., et al. (2016). Deregulated lipid sensing by intestinal CD36 in diet-induced hyperinsulinemic obese mouse model. *PLoS One* 11:e0145626. doi: 10.1371/journal.pone.0145626

Buttet, M., Traynard, V., Tran, T. T., Besnard, P., Poirier, H., and Niot, I. (2014). From fatty-acid sensing to chylomicron synthesis: role of intestinal lipid-binding proteins. *Biochimie* 96, 37–47. doi: 10.1016/j.biochi.2013.08.011

Cai, H., Wen, Z., Li, X., Meng, K., and Yang, P. (2020). *Lactobacillus plantarum* FRT10 alleviated high-fat diet-induced obesity in mice through regulating the PPARalpha signal pathway and gut microbiota. *Appl. Microbiol. Biotechnol.* 104, 5959–5972. doi: 10.1007/s00253-020-10620-0

Cai, H., Wen, Z., Zhao, L., Yu, D., Meng, K., and Yang, P. (2022). *Lactobacillus plantarum* FRT4 alleviated obesity by modulating gut microbiota and liver metabolome in high-fat diet-induced obese mice. *Food Nutr. Res.* 66, 1–2. doi: 10.29219/fnr.v66.7974

Chang, C. J., Lin, C. S., Lu, C. C., Martel, J., Ko, Y. F., Ojcius, D. M., et al. (2015). Ganoderma lucidum reduces obesity in mice by modulating the composition of the gut microbiota. *Nat. Commun.* 6:7489. doi: 10.1038/ncomms8489

Chao, H. W., Chao, S. W., Lin, H., Ku, H. C., and Cheng, C. F. (2019). Homeostasis of glucose and lipid in non-alcoholic fatty liver disease. *Int. J. Mol. Sci.* 20, 2–4. doi: 10.3390/ijms20020298

Crunkhorn, S. (2022). Inosine boosts fat burning. *Nat. Rev. Drug Discov.* 21:633. doi: 10.1038/d41573-022-00126-x

de Moura, E. D. M., da Silva Duarte, V., Mota, L. F. M., De Cassia Avila Alpino, G., Dos Reis Louzano, S. A., Da Conceicao, L. L., et al. (2023). *Lactobacillus gasseri* LG-G12 restores gut microbiota and intestinal health in obesity mice on ceftriaxone therapy. *Food Secur.* 12, 6–7. doi: 10.3390/foods12051092

Furet, J. P., Kong, L. C., Tap, J., Poitou, C., Basdevant, A., Bouillot, J. L., et al. (2010). Differential adaptation of human gut microbiota to bariatric surgery-induced weight loss: links with metabolic and low-grade inflammation markers. *Diabetes* 59, 3049–3057. doi: 10.2337/db10-0253

Han, K. J., Lee, J. E., Lee, N. K., and Paik, H. D. (2020). Antioxidant and anti-inflammatory effect of probiotic *Lactobacillus plantarum* KU15149 derived from Korean homemade diced-radish kimchi. *J. Microbiol. Biotechnol.* 30, 591–598. doi: 10.4014/jmb.2002.02052

Ho, P. Y., Chou, Y. C., Koh, Y. C., Lin, W. S., Chen, W. J., Tseng, A. L., et al. (2024). *Lactobacillus rhamnosus* 069 and *Lactobacillus brevis* 031: unraveling strain-specific pathways for modulating lipid metabolism and attenuating high-fat-diet-induced obesity in mice. *ACS Omega* 9, 28520–28533. doi: 10.1021/acsomega.4c02514

Hotamisligil, G. S. (2017). Inflammation, metaflammation and immunometabolic disorders. *Nature* 542, 177–185. doi: 10.1038/nature21363

Hoyt, C. L., Burnette, J. L., and Auster-Gussman, L. (2014). "Obesity is a disease": examining the self-regulatory impact of this public-health message. *Psychol. Sci.* 25, 997–1002. doi: 10.1177/0956797613516981

In Kim, H., Kim, J. K., Kim, J. Y., Jang, S. E., Han, M. J., and Kim, D. H. (2019). *Lactobacillus plantarum* LC27 and *Bifidobacterium longum* LC67 simultaneously alleviate high-fat diet-induced colitis, endotoxemia, liver steatosis, and obesity in mice. *Nutr. Res.* 67, 78–89. doi: 10.1016/j.nutres.2019.03.008

Katamoto, H., Yoneda, N., and Shimada, Y. (1991). Effects of isoprothiolane and phytosterol on adipocyte metabolism and fatty acid composition of serum and tissue lipids in rats. *J. Vet. Med. Sci.* 53, 905–910. doi: 10.1292/jvms.53.905

Kojta, I., Chacinska, M., and Blachnio-Zabielska, A. (2020). Obesity, bioactive lipids, and adipose tissue inflammation in insulin resistance. *Nutrients* 12, 1–3. doi: 10.3390/nu12051305

Lee, E., Jung, S. R., Lee, S. Y., Lee, N. K., Paik, H. D., and Lim, S. I. (2018). *Lactobacillus plantarum* strain Ln4 attenuates diet-induced obesity, insulin resistance, and changes in hepatic mRNA levels associated with glucose and lipid metabolism. *Nutrients* 10, 11–13. doi: 10.3390/nu10050643

Leung, C., Rivera, L., Furness, J. B., and Angus, P. W. (2016). The role of the gut microbiota in NAFLD. *Nat. Rev. Gastroenterol. Hepatol.* 13, 412–425. doi: 10.1038/nrgastro.2016.85

Li, H., Liu, F., Lu, J., Shi, J., Guan, J., Yan, F., et al. (2020). Probiotic mixture of *Lactobacillus plantarum* strains improves lipid metabolism and gut microbiota structure in high fat diet-fed mice. *Front. Microbiol.* 11:512. doi: 10.3389/fmicb.2020.00512

Li, X., Xiao, Y., Song, L., Huang, Y., Chu, Q., Zhu, S., et al. (2020). Effect of *Lactobacillus plantarum* HT121 on serum lipid profile, gut microbiota, and liver transcriptome and metabolomics in a high-cholesterol diet-induced hypercholesterolemia rat model. *Nutrition* 79-80:110966. doi: 10.1016/j.nut.2020.110966

Long, X., Zeng, X., Tan, F., Yi, R., Pan, Y., Zhou, X., et al. (2020). *Lactobacillus plantarum* KFY04 prevents obesity in mice through the PPAR pathway and alleviates oxidative damage and inflammation. *Food Funct.* 11, 5460–5472. doi: 10.1039/d0fo00519c

Ma, Y., Fei, Y., Han, X., Liu, G., and Fang, J. (2022). *Lactobacillus plantarum* alleviates obesity by altering the composition of the gut microbiota in high-fat diet-fed mice. *Front. Nutr.* 9:947367. doi: 10.3389/fnut.2022.947367

Martin-Gallausiaux, C., Marinelli, L., Blottiere, H. M., Larraufie, P., and Lapaque, N. (2021). SCFA: mechanisms and functional importance in the gut. *Proc. Nutr. Soc.* 80, 37–49. doi: 10.1017/S0029665120006916

Martinic, A., Barouei, J., Bendiks, Z., Mishchuk, D., Heeney, D. D., Martin, R., et al. (2018). Supplementation of *Lactobacillus plantarum* improves markers of metabolic dysfunction induced by a high fat diet. *J. Proteome Res.* 17, 2790–2802. doi: 10.1021/acs.jproteome.8b00282

Moorthy, M., Sundralingam, U., and Palanisamy, U. D. (2021). Polyphenols as prebiotics in the management of high-fat diet-induced obesity: a systematic review of animal studies. *Food Secur.* 10, 23–24. doi: 10.3390/foods10020299

O'Neill, S., and O'Driscoll, L. (2015). Metabolic syndrome: a closer look at the growing epidemic and its associated pathologies. *Obes. Rev.* 16, 1–12. doi: 10.1111/obr.12229

Paranjape, S. A., Chan, O., Zhu, W., Horblitt, A. M., McNay, E. C., Cresswell, J. A., et al. (2010). Influence of insulin in the ventromedial hypothalamus on pancreatic glucagon secretion in vivo. *Diabetes* 59, 1521–1527. doi: 10.2337/db10-0014

Park, K. B., and Oh, S. H. (2007). Cloning, sequencing and expression of a novel glutamate decarboxylase gene from a newly isolated lactic acid bacterium, *Lactobacillus brevis* OPK-3. *Bioresour. Technol.* 98, 312–319. doi: 10.1016/j.biortech.2006.01.004

Parnell, J. A., and Reimer, R. A. (2012). Prebiotic fiber modulation of the gut microbiota improves risk factors for obesity and the metabolic syndrome. *Gut Microbes* 3, 29–34. doi: 10.4161/gmic.19246

Qiu, X., Macchietto, M. G., Liu, X., Lu, Y., Ma, Y., Guo, H., et al. (2021). Identification of gut microbiota and microbial metabolites regulated by an antimicrobial peptide lipocalin 2 in high fat diet-induced obesity. *Int. J. Obes.* 45, 143–154. doi: 10.1038/s41366-020-00712-2

Quigley, E. M. M. (2019). Prebiotics and probiotics in digestive health. *Clin. Gastroenterol. Hepatol.* 17, 333–344. doi: 10.1016/j.cgh.2018.09.028

Rahayu, E. S., Mariyatun, M., Putri Manurung, N. E., Hasan, P. N., Therdtatha, P., Mishima, R., et al. (2021). Effect of probiotic *Lactobacillus plantarum* Dad-13 powder consumption on the gut microbiota and intestinal health of overweight adults. *World J. Gastroenterol.* 27, 107–128. doi: 10.3748/wjg.v27.i1.107

Rastmanesh, R. (2011). High polyphenol, low probiotic diet for weight loss because of intestinal microbiota interaction. *Chem. Biol. Interact.* 189, 1–8. doi: 10.1016/j.cbi.2010.10.002

Saltiel, A. R., and Kahn, C. R. (2001). Insulin signalling and the regulation of glucose and lipid metabolism. *Nature* 414, 799–806. doi: 10.1038/414799a

Shen, Z. H., Zhu, C. X., Quan, Y. S., Yang, Z. Y., Wu, S., Luo, W. W., et al. (2018). Relationship between intestinal microbiota and ulcerative colitis: mechanisms and clinical application of probiotics and fecal microbiota transplantation. *World J. Gastroenterol.* 24, 5–14. doi: 10.3748/wjg.v24.i1.5

Stojanov, S., Berlec, A., and Strukelj, B. (2020). The influence of probiotics on the Firmicutes/Bacteroidetes ratio in the treatment of obesity and inflammatory bowel disease. *Microorganisms* 8, 1–6. doi: 10.3390/microorganisms8111715

Torres-Fuentes, C., Schellekens, H., Dinan, T. G., and Cryan, J. F. (2017). The microbiota-gut-brain axis in obesity. *Lancet Gastroenterol. Hepatol.* 2, 747–756. doi: 10.1016/S2468-1253(17)30147-4

Wang, L., Gong, Z., Zhang, X., Zhu, F., Liu, Y., Jin, C., et al. (2020). Gut microbial bile acid metabolite skews macrophage polarization and contributes to high-fat diet-induced colonic inflammation. *Gut Microbes* 12, 1819155–1819120. doi: 10.1080/19490976.2020.1819155

Wei, B., Peng, Z., Xiao, M., Huang, T., Yang, S., Liu, K., et al. (2023). Modulation of the microbiome-fat-liver Axis by lactic acid Bacteria: a potential alleviated role in high-fat-diet-induced obese mice. *J. Agric. Food Chem.* 71, 10361–10374. doi: 10.1021/acs.jafc.3c03149

Xie, P., Xie, J. B., Xiao, M. Y., Guo, M., Qi, Y. S., Li, F. F., et al. (2023). Liver lipidomics analysis reveals the anti-obesity and lipid-lowering effects of gypnosides from heat-processed Gynostemma pentaphyllum in high-fat diet fed mice. *Phytomedicine* 115:154834. doi: 10.1016/j.phymed.2023.154834

Youn, H. S., Kim, J. H., Lee, J. S., Yoon, Y. Y., Choi, S. J., Lee, J. Y., et al. (2021). *Lactobacillus plantarum* reduces low-grade inflammation and glucose levels in a mouse model of chronic stress and diabetes. *Infect. Immun.* 89:e0061520. doi: 10.1128/IAI.00615-20

Yu, B., Hu, M., Jiang, W., Ma, Y., Ye, J., Wu, Q., et al. (2023). Ceramide d18:1/24:1 as a potential biomarker to differentiate obesity subtypes with unfavorable health outcomes. *Lipids Health Dis.* 22:166. doi: 10.1186/s12944-023-01921-0

Zhang, L., Meng, Y., Li, J., Yu, J., Mu, G., and Tuo, Y. (2022). Lactiplantibacillus plantarum Y42 in biofilm and planktonic states improves intestinal barrier integrity and modulates gut microbiota of Balb/c mice. *Food Secur.* 11, 5–6. doi: 10.3390/foods11101451

Zhao, L., Shen, Y., Wang, Y., Wang, L., Zhang, L., Zhao, Z., et al. (2022). *Lactobacillus plantarum* S9 alleviates lipid profile, insulin resistance, and inflammation in high-fat diet-induced metabolic syndrome rats. *Sci. Rep.* 12:15490. doi: 10.1038/s41598-022-19839-5

Zhou, M., Zheng, X., Zhu, H., Li, L., Zhang, L., Liu, M., et al. (2021). Effect of *Lactobacillus plantarum* enriched with organic/inorganic selenium on the quality and microbial communities of fermented pickles. *Food Chem.* 365:130495. doi: 10.1016/j.foodchem.2021.130495

Zhu, Y., Wang, X., Pan, W., Shen, X., He, Y., Yin, H., et al. (2019). Exopolysaccharides produced by yogurt-texture improving *Lactobacillus plantarum* RS20D and the immunoregulatory activity. *Int. J. Biol. Macromol.* 121, 342–349. doi: 10.1016/j.ijbiomac.2018.09.201

frontiers | Frontiers in Marine Science

TYPE Original Research
PUBLISHED 03 September 2024
DOI 10.3389/fmars.2024.1441921

OPEN ACCESS

EDITED BY
Jie Yin,
Hunan Agricultural University, China

REVIEWED BY
Cunxin Sun,
Chinese Academy of Fishery Sciences (CAFS), China
Zhigang Zhou,
Chinese Academy of Agricultural Sciences, China

*CORRESPONDENCE
Lingrui Ge
gelingrui@hunau.edu.cn

RECEIVED 31 May 2024
ACCEPTED 16 August 2024
PUBLISHED 03 September 2024

CITATION
Wen X, Ge L, Liu K, Tan S and Hu Y (2024) Effects of *Atractylodes macrocephala* polysaccharide on growth performance, serum biochemical indexes, and intestinal microflora of largemouth bass (*Micropterus salmoides*). *Front. Mar. Sci.* 11:1441921. doi: 10.3389/fmars.2024.1441921

Effects of *Atractylodes macrocephala* polysaccharide on growth performance, serum biochemical indexes, and intestinal microflora of largemouth bass (*Micropterus salmoides*)

Xingxing Wen, Lingrui Ge*, Kejun Liu, Shengguo Tan and Yi Hu

College of Animal Science and Technology, Hunan Biological and Electromechanical Polytechnic, Changsha, China

Introduction: As the aquaculture industry intensifies to enhance production efficiency and capacity, the risk of disease outbreaks in high-density systems, such as those for largemouth bass, has escalated. This necessitates the exploration of novel strategies for disease prevention and control. Studies have shown that Atractylodes macrocephala polysaccharide (AMP) possesses the functions of promoting growth and enhancing immune capacity, making it a potential feed additive in animal production.

Methods: This study aimed to assess the impact of AMP on the growth performance, serum biochemical indices, and intestinal flora structure of largemouth bass. A total of 360 healthy largemouth bass (mean weight: 15.25 ± 1.29 g) were randomly assigned to four groups, each with three replicates. The groups were fed diets supplemented with 0% (Group D, control group), 0.4% (Group A), 0.8% (Group B), or 1.2% (Group C) AMP for 42 days.

Results: The results showed that the addition of an appropriate amount of AMP in the feed significantly improved the weight gain rate (WGR) and specific growth rate (SGR) of largemouth bass, reduced the feed conversion ratio (FCR), and enhanced growth performance. AMP reduced the levels of AST and ALT, indicating a hepatoprotective effect on largemouth bass, with significant differences from the control group ($P < 0.05$). AMP also improved the intestinal microbiota composition of largemouth bass, positively affecting intestinal health. The analysis of intestinal microbiota revealed 1,288 amplicon sequence variants (ASVs) in the intestine of largemouth bass in Group B, dominated by Firmicutes and Bacteroidota. In contrast, Group C (1.2%) had 920 ASVs, with Fusobacteriota and Firmicutes as the major components, while the relative abundance of Firmicutes was lower, showing significant differences from the control Group D. The functional analysis of intestinal microbiota based on KEGG showed significant differences ($P < 0.05$) among the four groups in Carbon metabolism, Biosynthesis of amino acids, and Metabolic pathways.

Discussion: The study concludes that the inclusion of AMP at 0.8% – 1.2% in the feed can enhance the growth performance and intestinal health of largemouth bass, offering a promising strategy for disease prevention and control in intensive aquaculture settings.

KEYWORDS

Atractylodes macrocephala polysaccharide, *Micropterus salmoides*, growth performance, serum biochemical indexes, intestinal microflora

1 Introduction

The largemouth bass, a carnivorous fish native to North America, was introduced to China in 1983 (He et al., 2020). It is popular among aquaculturists due to its strong adaptability, rapid growth, ease of catching, and short breeding cycle. In addition, its delicious and nutritious meat, absence of intramuscular bones, and elegant appearance render it suitable for consumption, which leads to promising market prospects, making it one of the main freshwater fish breeding species in China (Zhang and He, 1994; Bai et al., 2008). According to the statistical data from "China Fishery Statistical Yearbook 2023," the annual output of largemouth bass in China in 2022 was 802,500 tons, with a production value exceeding 20 billion yuan. In pursuit of higher production efficiency and increased capacity, the aquaculture industry is gravitating towards intensification, making largemouth bass vulnerable to diseases under artificial high-density breeding conditions. This necessitates enhanced disease prevention strategies. Research has shown that polysaccharides can reduce the incidence of diseases by enhancing the immunity of animals, serving as potential immune enhancers (Huang et al., 2015; Kong et al., 2020; Li et al., 2019; Wang et al., 2023). *Atractylodes macrocephala* Polysaccharide (AMP), an extract of the traditional Chinese medicine *Atractylodes macrocephala*, is the core active ingredient of the herb. It possesses pharmacological effects such as immune regulation, gastrointestinal mucosa protection, liver protection, antibacterial, and antioxidant properties, making it an efficient, low-toxicity, and well-defined polysaccharide from traditional Chinese medicine (National Pharmacopoeia Commission, 2020; Bailly, 2021). As a feed additive, AMP is widely used in animal production. AMP has significant effects on promoting growth, enhancing macrophage phagocytosis, and enhancing cellular and humoral immunity in livestock and poultry within a certain dose range (Yang et al., 2018; Wang et al., 2023). In the aquaculture industry, studies have also found that extracts of *Atractylodes macrocephala* can improve the growth performance and disease resistance of *Macrobrachium* nipponense, *Oncorhynchus* mykiss, and *Pseudobagrus* fulvidraco (Bai et al., 2023; Lu et al., 2024; Zhuo et al., 2022). Currently, there are few reports on the application of AMP as a feed additive in largemouth bass, and its mechanism of action remains unclear. Therefore, this study takes largemouth bass as the research subject, analyzing the effects of different addition levels of AMP on the growth performance, serum biochemical indicators, and intestinal flora of largemouth bass. This marks the first comprehensive exploration of the optimal additive concentration range of AMP in largemouth bass, aiming to provide a theoretical basis for the application of AMP in the basic feed for largemouth bass aquaculture.

2 Materials and methods

2.1 Experimental feed design

Three experimental diets with a control were prepared. The nutritional composition and levels of the experimental feeds are shown in Table 1. The protein sources for the test feeds were imported fishmeal, soybean meal, and other raw materials, while the fat sources were fish oil, peanut oil, and other raw materials. The experimental diet contained three concentrations of 0.4%, 0.8%, or 1.2% AMP. The control did not add AMP. AMP was purchased from Shanxi Senyuan Biotechnology Co., Ltd., Xi'an, China. The initial materials were crushed using an 80-mesh screen to remove large particles and then precisely weighed according to the specific feed formula's proportions. The mixed feed was put into a batch mixer, where a measured amount of distilled water was added to ensure thorough blending. Subsequently, a ring die granulator was employed to shape the mixed feed into pellets with a standardized diameter of 1.5 mm. These pellets were then dried in an oven at 60 °C. Finally, the feed was air-dried and collected in sealed bags, which were subsequently placed in a freezer at a temperature of -25°C for preservation.

2.2 Husbandry methods

The largemouth bass were obtained from Hunan Aoyu Aquaculture Co., Ltd. (Yueyang, China) and were temporarily reared in a laboratory recirculating aquaculture system for 2 weeks to adapt to the environment, during which they were fed a

10.3389/fmars.2024.1441921

TABLE 1 Nutrient composition and nutrient level of experimental feed.

Nutritional composition	Content(%)			
	Control group (D, 0%)	Experimental group (A, 0.4%)	Experimental group (B, 0.8%)	Experimental group (C, 1.2%)
Imported Fishmeal	40.00	40.00	40.00	40.00
Soybean Meal	6.00	6.00	6.00	6.00
Corn Gluten Meal	16.50	16.50	16.50	16.50
Corn Starch	15.00	15.00	15.00	15.00
Wheat Bran	10.00	9.60	9.20	8.80
Fish Oil	5.00	5.00	5.00	5.00
Peanut Oil	2.00	2.00	2.00	2.00
AMP	0.00	0.40	0.80	1.20
Vitamin Premix ①	1.00	1.00	1.00	1.00
Mineral Premix ②	2.00	2.00	2.00	2.00
Dicalcium Phosphate	1.50	1.50	1.50	1.50
Microcrystalline Cellulose	1.00	1.00	1.00	1.00
Total	100.00	100.00	100.00	100.00
Nutrient levels ③	Content(%)			
Crude Protein (CP)	50.12	50.06	50.13	50.08
Crude Fat (EE)	8.15	8.17	8.18	8.13
Crude Ash	14.35	14.34	14.38	14.42
Total Calcium	0.68	0.67	0.66	0.67
Total Phosphorus	1.14	1.14	1.13	1.13

① Add premix according to the requirements of feed per kilogram. Vitamin content in premix: Vit A 6000 IU, Vit B1 6 mg, Vit B2 15 mg, Vit B6 8 mg, Vit C 8 mg, Vit D 2000 IU, Vit E 100 IU, folic acid 7 mg;
② Add premix according to the requirements of feed per kilogram. Mineral content: Se 0.5 mg, I 1 mg, Cu 5 mg, Mn 20 mg, Zn 65 mg, Fe 70 mg.
③Nutrient levels were measured by instruments in our laboratory.

basic diet ad libitum every day. All animals studies were performed according to protocols approved by the Animal Care Advisory Committee of Animal Science and Technology, Hunan Biological And Electromechanical Polytechnic. A total of 360 healthy largemouth bass (mean weight: 15.25 ± 1.29 g) were randomly divided into four groups with three parallel sets in each group. Each group was fed a diet supplemented with 0% (Group D, control group), 0.4% (Group A), 0.8% (Group B), and 1.2% (Group C) AMP for 42 days. The largemouth bass were raised in an indoor culture barrels (200 L) with water exchanged once every two weeks to ensure optimal growth conditions. During the experiment, the water temperature in the tanks was maintained at 23-25 °C. The feeding amount for the largemouth bass was determined based on their body weight, and feeding was conducted at 7:00 am, 12:00 pm, and 6:00 pm every day and adjusted promptly according to feeding intensity or other factors. The remaining feed was collected one hour after each feeding to avoid its influence on water quality. Regular inspections were conducted, and the water quality in the barrels was monitored daily, including dissolved oxygen, ammonia nitrogen, pH, and water temperature, to ensure favorable breeding conditions. At 42 d, The growth performance of each group was tested and 8 largemouth bass were randomly selected from each group, and serum immune indexes and intestinal microbial population data were collected. The control group (Group D) consisted of largemouth bass labeled D1-D8, while the experimental groups (Groups A, B and C) consisted of largemouth bass labeled A1-A8, B1-B8 and C1-C8 respectively.

2.3 Measurement and calculation of growth performance

Each group of largemouth bass individuals was weighed on day 42 of the experiment, and the body weight gain, body length and number of deaths of largemouth bass were recorded. The daily food intake of largemouth bass was calculated, and the liver mass of largemouth bass was weighed. The following formulae were used to calculate growth performance of largemouth bass:

$$\text{Weight gain rates (WGR, \%)} = (W_2 - W_1)/W_1 \times 100 \quad (1)$$

$$\text{Specific growth rates (SGR, \%)} = (\ln W_2 - \ln W_1)/t \times 100 \quad (2)$$

$$\text{Feed conversion ratio (FCR)} = W_{TF}/W_{TG} \quad (3)$$

$$\text{Hepatopancreas somatic indices (HSI, \%)} = W_h/W_2 \times 100 \quad (4)$$

$$\text{Survival rate (SR, \%)} = N_2/N_1 \times 100 \quad (5)$$

The variables used in the calculations were as follows: W_2 represents the body mass of largemouth bass at 42 d; W_1 represents for the initial mass of largemouth bass; t represents the number of days of testing largemouth bass; W_{TF} represents for the total feed intake during the trial phase of largemouth bass per replicate; W_{TG} represents total weight gain per replicate; W_h represents for the liver mass of largemouth bass; N_2 represents for the final quantity; N_1 represents the initial number of largemouth bass.

2.4 Determination of serum indexes

After the feeding, 8 largemouth bass were randomly selected from each group for blood collection. Blood was collected from the tail vein of the fish using a 2 mL sterile syringe. The blood samples were refrigerated at 4 °C for 4 h, and then centrifuged at 4 °C and 5000 RPM for 10 minutes. Subsequently, the serum was separated and analyzed for various indicators. The kits from Nanjing Jiancheng Bioengineering Institute were utilized to detect biochemical parameters like cholesterol (CHOL), triglyceride (TG), alkaline phosphatase (ALP), total protein (TP), serum albumin (ALB), aspartate aminotransferase (AST), and alanine aminotransferase (ALT). Additionally, serum immune indices including superoxide dismutase (SOD), malondialdehyde (MDA), complement C3, and C4 were also measured.

2.5 Intestinal microflora changes and bioinformatics analysis

2.5.1 Intestinal sample collection

In order to study the microbial population in the intestinal tract of largemouth bass, the intestinal tracts of largemouth bass in the experimental group and the control group were sampled respectively. Before sampling, we anesthetized the largemouth bass by placing them in water to which 100 μg MS-222 had been added per liter of water for 2 min. After removal, wipe 75% ethanol on the body surface of the largemouth bass quickly disassembled and removed the intestine, and squeezed the intestinal contents into a 5 ml centrifuge tube. The samples were then frozen with liquid nitrogen and stored at -80 °C for analysis of intestinal flora changes of largemouth bass.

2.5.2 Analysis of microflora changes in intestinal samples

The intestinal genome DNA of largemouth bass was extracted and sequenced using the combined multiomics technology of Shanghai OE Biotech Co., Ltd. Genomic DNA extraction was performed using a dedicated DNA extraction kit, and its concentration was accurately determined through agarose gel electrophoresis and NanoDrop spectrophotometric analysis. This purified genomic DNA served as the template for defining the sequencing region, with specific primers added to ensure thorough mixing. The resulting mixture was then processed in a Takara PCR instrument, ensuring the validity and precision of the detection values.

The FASTQ-formatted raw data underwent primer sequence trimming using cutadapt software. Subsequently, DADA2 processed the raw sequences in accordance with Qiime2's established protocols, yielding high-quality sequences and ASV abundance tables. The diversity of the obtained data was analyzed, and the intestinal microflora information of largemouth bass was obtained through various algorithms. This information was used to analyze the changes of intestinal microflora of largemouth bass by AMP.

2.6 Statistical analysis

Statistical analysis was performed according to Excel to sort out the recorded data. The recorded data results were expressed as (Mean ± SD). The normality of the data was tested by SPSSAU, and then Duncan was used to conduct one-way ANOVA on the obtained data to find significant differences between the data ($P < 0.05$).

3 Results

3.1 Changes in growth performance

According to Table 2, it can be seen that the WGR and SGR of largemouth bass with AMP added to the feed exhibited an upward trend within a certain concentration range. The WGR and SGR of each experimental group were significantly improved compared to the control group ($P < 0.05$), with Group B (0.8% AMP) demonstrating the best effect. The feed coefficient of each experimental group decreased significantly compared to the control group ($P < 0.05$). However, there was no significant difference between Group B (0.8% AMP) and Group C (1.2% AMP) ($P > 0.05$). The hepatosomatic index (HSI) of each experimental group was significantly lower than that of the control group ($P < 0.05$), and the HSI increased with the increase in concentration among the experimental groups. However, there was no significant difference between the experimental groups. ($P > 0.05$).

3.2 Changes in serum biochemical indicators

3.2.1 Effect of AMP on serum liver function indicators

The serum liver function index data are shown in Table 3. There were no significant differences in the levels of TP and ALB in the

TABLE 2 Growth performance of largemouth bass.

Items	Control group (D, 0%)	Experimental group (A, 0.4%)	Experimental group (B, 0.8%)	Experimental group (C, 1.2%)
IBW (g)	15.24 ± 1.46	15.26 ± 1.07	15.23 ± 1.58	15.29 ± 1.25
FBW (g)	30.25 ± 7.13^{d}	37.12 ± 4.58^{c}	63.28 ± 6.69^{a}	52.51 ± 7.77^{b}
WGR (%)	98.37 ± 38.50^{c}	145.88 ± 46.44^{c}	321.80 ± 81.43^{a}	246.78 ± 64.96^{b}
SGR (%/d)	1.59 ± 0.44^{d}	2.11 ± 0.44^{c}	3.39 ± 0.42^{a}	2.92 ± 0.46^{b}
SR (%)	91.11 ± 1.92^{b}	95.56 ± 1.92^{ab}	96.67 ± 3.33^{a}	96.67 ± 3.33^{a}
FCR	1.30 ± 0.01^{a}	1.18 ± 0.02^{b}	1.06 ± 0.03^{c}	1.11 ± 0.03^{c}
HSI (%)	1.57 ± 0.19^{a}	1.41 ± 0.07^{b}	1.46 ± 0.21^{b}	1.53 ± 0.20^{b}

In the data, letters are used to indicate significant differences in the data of the group ($P < 0.05$), and the same or no letters are used to indicate no significant differences in the data of the group ($P > 0.05$). IBW, Initial body weight; FBW, final body weight; WGR, weight gain rate; SGR, specific growth rate; SR, survival rate; FCR, feed conversion ratio; HIS, hepatosomatic index.

serum of largemouth bass among the experimental groups, except for Group C (1.2% AMP) where the TP level decreased slightly and was significantly different from the control group and other experimental groups. The levels of AST and ALT showed a downward trend with increasing amounts of AMP added within a certain range and were significantly different from the control group ($P < 0.05$). The ALP level showed an upward trend with increasing amounts of AMP added within a certain range. Compared to the control group, Groups A and B did not have significant differences, while Group C (1.2% AMP) had a significant increase compared to the control group.

3.2.2 Effect of AMP on lipid metabolism indicators

As shown in Table 4, with the increasing dosage of AMP, the levels of TG and CHOL in the serum of the experimental groups exhibited a trend of initially increasing and then decreasing. Specifically, the TG level in the high-dosage group (Group C, 1.2% AMP) was significantly lower than that of the other groups ($P < 0.05$), while the TG levels in the low-dosage group (Group A, 0.4% AMP) and the medium-dosage group (Group B, 0.8% AMP) were significantly higher than that of the control group ($P < 0.05$). In terms of CHOL levels, Group A and Group C were significantly lower than the control group, while there was no significant difference between Group B and the control group.

3.2.3 Effect of AMP on serum antioxidant and non-specific immune indicators

As shown in Table 5, with the increase in the dosage of AMP, the SOD content in each experimental group exhibited a trend of first increasing and then decreasing. Group B (0.8% AMP) was significantly higher than the other groups ($P < 0.05$). Additionally, the MDA content in each experimental group was significantly lower than that in the control group, with Group B (0.8% AMP) being significantly lower than the other groups ($P < 0.05$). Furthermore, the C3 content of each experimental group was higher than that of the control group, and Group B (0.8% AMP) showed a significantly higher content than the other groups ($P < 0.05$). However, there was no significant difference in C4 content among the remaining groups.

3.3 Structural characteristics of intestinal flora

3.3.1 Analysis of differences in intestinal flora groups

The changes in intestinal flora may be the primary reason for the enhancement of largemouth bass growth and metabolic levels by AMP. The structure of intestinal flora was studied using 16S rDNA amplicon sequencing technology. First, principal co-ordinates analysis (PCoA) was performed based on Weighted Unifrac distance to reflect the beta diversity of different groups.

TABLE 3 Serum liver function indicators of largemouth bass.

Items	Control group (D, 0%)	Experimental group (A, 0.4%)	Experimental group (B, 0.8%)	Experimental group (C, 1.2%)
TP(g/L)	34.75 ± 3.74^{a}	34.99 ± 4.62^{a}	35.16 ± 3.18^{a}	29.81 ± 2.07^{b}
ALB(g/L)	7.95 ± 1.07	8.16 ± 1.26	8.74 ± 0.74	7.65± 1.11
ALT(U/L)	54.30 ± 14.25^{a}	20.08 ± 8.58^{b}	2.85 ± 1.52^{c}	3.29 ± 1.62^{c}
AST(U/L)	229.88 ± 29.55^{a}	170.50 ± 12.04^{b}	68.88 ± 7.00^{c}	77.13± 9.55^{c}
ALP(U/L)	64.00 ± 15.70^{b}	59.25 ± 8.97^{b}	72.88 ± 9.46^{ab}	81.63 ± 18.78^{a}

In the data, letters are used to indicate significant differences in the data of the group ($P < 0.05$), and the same or no letters are used to indicate no significant differences in the data of the group ($P > 0.05$).

TABLE 4 Serum lipid metabolism indicators of largemouth bass.

Items	Control group (D, 0%)	Experimental group (A, 0.4%)	Experimental group (B, 0.8%)	Experimental group (C, 1.2%)
TG(mmol/L)	8.65 ± 1.87^{b}	10.94 ± 2.02^{a}	11.53 ± 2.00^{a}	5.44 ± 1.89^{c}
CHOL(mmol/L)	9.81 ± 1.19^{a}	9.02 ± 1.52^{b}	11.06 ± 1.43^{ab}	8.54 ± 0.76^{b}

In the data, letters are used to indicate significant differences in the data of the group ($P < 0.05$), and the same or no letters are used to indicate no significant differences in the data of the group ($P > 0.05$).

The PCoA plot (Figure 1) showed that the intestinal flora of Group C was significantly different from that of groups A, B, and D [permutation multivariate analysis of variance (PerMANOVA), P=0.001], indicating that Group C formed a unique flora.

3.3.2 Characteristics and changes of intestinal flora

Analysis of the composition and structure of the intestinal flora revealed that Group B (0.8% AMP) possessed the highest number of ASVs (amplicon sequence variants) in largemouth bass intestinal flora, reaching 1288 species, followed by groups D (0% AMP) and C (1.2% AMP) with 943 and 920 species respectively, and group A (0.4% AMP) had the least (714 species). There were few shared ASVs among the four groups, indicating significant individual differences among the samples within each group. Specifically, each sample shared only 2 ASVs (Figures 2A, B).

Differences were observed in the intestinal flora structure of largemouth bass among the groups (Figure 2C). In Group A (0.4% AMP), the relative abundance of *Firmicutes*, *Actinobacteriota*, *Bacteroidota*, and *Proteobacteria* accounted for over 99%, with *Firmicutes* comprising 80.9%. In Group B (0.8% AMP), the relative abundance of *Firmicutes*, *Bacteroidota*, and *Actinobacteriota* totaled more than 84%, with *Firmicutes* accounting for 62.7%. Group D (0% AMP) exhibited a relative abundance of *Firmicutes*, *Bacteroidota*, *Actinobacteriota*, *Fusobacteriota*, and *Proteobacteria* that exceeded 98%, with *Firmicutes* comprising 66.5%. Notably, Group C (1.2% AMP) differed significantly from groups A, B, and D, with *Fusobacteriota*, *Firmicutes*, and *Proteobacteria* accounting for 85.5%, of which *Fusobacteriota* comprised 56.6%.

Cluster analysis was performed on the top 15 bacterial genera with relative abundance, and a heat map was drawn (Figure 2D). It was evident that the relative abundance of the four groups differed significantly at the genus level. When comparing the variations in bacterial abundance among individual samples, we found that in Group A (0.4% AMP), the relative abundance of *Mycoplasma* and others was high. In Group B (0.8% AMP), the relative abundance of *Bifidobacterium*, *Bacteroides*, and others was relatively high. In Group C (1.2% AMP), the relative abundance of *Cetobacterium* and *Aeromonas* was relatively high. In Group D (0% AMP), the relative abundance of *Prevotella*, *Bacteroides*, *Muribaculaceae*, and others was relatively high, and there were significant abundance differences among the different groups. Additionally, the abundance of *Cetobacterium* and *Aeromonas* in Group C (1.2% AMP) was lower compared to other groups.

The alpha diversity index of the intestinal flora can intuitively reflect the species diversity within each group. As shown in Figure 2E, there are differences in the Chao1 index, ACE index, Shannon index, Simpson index, and PD_whole_tree index among the four groups. Specifically, the median values of Chao1 index, ACE index, and PD_whole_tree index were Group C > Group D > Group A > Group B. The median values of Shannon index and Simpson index were Group C > Group B > Group D > Group A.

3.3.3 Analysis of differential bacterial groups

In order to further analyze the differences in the composition of intestinal flora in each group, LEfSe analysis was performed to find biomarkers in each group. From the bar chart showing the distribution of linear discriminant analysis (LDA) scores in Figure 3A, we can see that 9 biomarkers were discovered in the intestinal microbiota of Group A (0.4% AMP), with 8 having LDA scores greater than 4, including *Firmicutes*, *Bacilli*, *Mycoplasma*, *Mycoplasmatales*, *Mycoplasmataceae*, *Clostridiales*, *Clostridiaceae*, and *Clostridia*. In Group B (0.8% AMP), 4 biomarkers were identified, with only 1 having an LDA score greater than 4, belonging to the class *Acidimicrobiia*. Group C (1.2% AMP) exhibited 18 biomarkers, with 10 having LDA scores greater than 4, including Fusobacteriia, *Fusobacteriota*, *Fusobacteriales*, *Fusobacteriaceae*, *Cetobacterium*, *Aeromonadales*, *Aeromonadaceae*, *Aeromonas*, *Ruminobacter*, and *Alloscardovia*. 7 biomarkers were found in the intestinal microbiota of Group D (0% AMP), with only 1 having an LDA score greater than 4, belonging to the genus *Gardnerella*.

TABLE 5 Serum antioxidant and non-specific immune indicators of largemouth bass.

Items	Control group (D, 0%)	Experimental group (A, 0.4%)	Experimental group (B, 0.8%)	Experimental group (C, 1.2%)
SOD/(U/L)	96.81 ± 1.73^{b}	97.34 ± 2.64^{b}	131.46 ± 6.19^{a}	103.43 ± 1.04^{b}
MDA(nmol/L)	8.48 ± 0.16^{a}	6.44 ± 0.11^{b}	5.51 ± 0.28^{c}	6.46 ± 0.11^{b}
C3/(mg/L)	0.24 ± 0.09^{a}	0.32 ± 0.08^{a}	0.43 ± 0.08^{b}	0.31 ± 0.11^{a}
C4/(mg/L)	0.05 ± 0.02	0.09 ± 0.03	0.11 ± 0.04	0.06 ± 0.03

In the data, letters are used to indicate significant differences in the data of the group ($P < 0.05$), and the same or no letters are used to indicate no significant differences in the data of the group ($P > 0.05$).

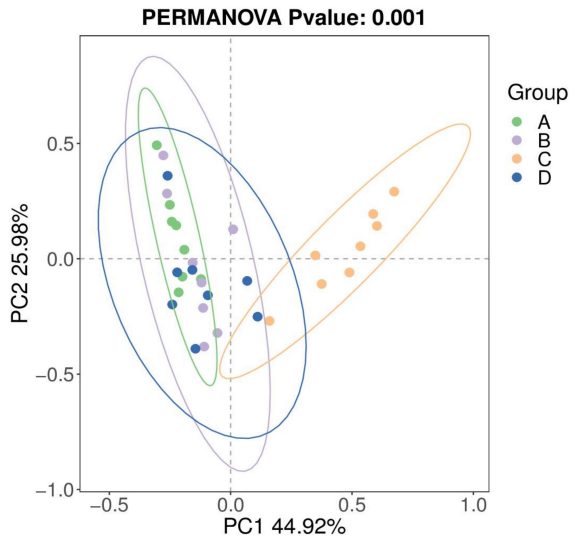

FIGURE 1
PCOA based on Weighted Unifrac distance. Each point in the figure represents a sample, samples in the same group are represented by the same color, and the color area represents the confidence interval. A1-8 are the 8 samples from Group A; B1~8 are the 8 samples from Group B; C1~8 are the 8 samples from Group C; D1~8 are the 8 samples from Group D. FIGURE 2, FIGURE 4 and FIGURE 5 are the same.

As shown in the cladogram (Figure 3B), the biomarkers in Group C (1.2% AMP) are not only numerous but also distributed across multiple distant genetic evolutionary branches.

The relative abundance box plot of the top 10 differential bacterial genera (biomarkers) between groups (Figure 4A) and the relative abundance heat map of the top 15 differential bacterial genera (biomarkers) between samples (Figure 4B) shows that *Bacteroidales*_RF16_group, *Mycoplasma*, and Others have higher abundance in Group A (0.4% AMP), *Mycoplasma* has higher abundance in Group B (0.8% AMP), *Alloscardovia*, *Cetobacterium*, *Ruminobacter*, and *Citrobacter* are commonly found in relatively higher abundance in each sample in Group C (1.2% AMP). In Group D (0% AMP), The abundance of *Acinetobacter* and *Streptococcus* was higher.

3.3.4 Functional differences of intestinal flora

Use PICRUSt2 (2.3.0b0) to predict the functional composition of known microbial genes based on 16S sequences, thereby counting the functional differences between different samples and groups. Functional prediction at level 3 based on KEGG shows that Group A, Group B, Group C, and Group D have important roles in ABC transporters, Carbon metabolism, Biosynthesis of amino acids, Microbial metabolism in diverse environments, Biosynthesis of secondary metabolites, Metabolic There are significant differences in pathways ($P < 0.05$, Figure 5A), and there are individual differences in the samples in each group (Figure 5B). After comparison, it was found that compared with Groups A, B, and D, Group C had better metabolism in Starch and sucrose metabolism, Purine metabolism, Pyruvate metabolism, Carbon metabolism, Metabolic pathways, Amino sugar and nucleotide sugar metabolism, Pyrimidine metabolism, and Microbial metabolism in diverse environments. Biosynthesis of amino acids, Biosynthesis of secondary metabolites, Arinoacyl-tRNA biosynthesis, ABC transporters, Quorum sensing, Ribosome, Glycolysis/Gluconeogenesis were significantly enhanced, and the order of strength was Group C > Group D > Group B > Group A.

4 Discussion

AMP is widely used as a feed additive in livestock and poultry production. Research indicates that AMP can promote the growth of weaned piglets and increase WGR by enhancing immunity, improving intestinal health, and reducing diarrhea rates (Li et al., 2009, 2011; Zhao and Wang, 2015; Chai et al., 2020). AMP also enhances production performance and disease resistance of ruminants by improving the immune function and anti-stress ability of poultry (Cao et al., 2022; Jing et al., 2019; Xu et al., 2015)In recent years, its application in aquatic animals has also been reported. A study by Zhuo et al. found that replacing 25% of fish meal with protein sources like soybean meal adversely affects the growth and physiological metabolism of *Pseudobagrus fulvidraco* (Zhuo et al., 2022). Adding AMP to the feed significantly improved these effects, indicating that AMP has a protective effect on the health of *Pseudobagrus fulvidraco*. Bai Ruxue et al. discovered that Atractylodes macrocephala extract can improve the growth performance, antioxidant capacity, and disease resistance of *Macrobrachium* japonicum (Bai et al., 2023). Lu's research demonstrates that AMP, as a feed additive, can enhance the growth performance, immunity, antioxidant capacity, and resistance of rainbow trout against *Aeromonas salmonicida* (Lu et al., 2024). In our study, adding 0.4%, 0.8%, and 1.2% AMP to the feed all exhibited significant growth-promoting effects, and the FCR showed a downward trend. The WGR and SGR were highest when the concentration was 0.8%, indicating the best growth-promoting effect.

Serum biochemistry is a fundamental blood test that can quickly reflect organ inflammation, damage, and metabolic abnormalities in the body. Among these parameters, AST and ALT are commonly used clinical indicators to assess liver damage. Research indicates that the application of AMP can reduce AST and ALT levels in rats and goslings, thus playing a protective role in preventing and treating non-alcoholic steatohepatitis and improving liver immune function (Che et al., 2017; Li et al., 2022). Furthermore, studies show that with an increase in the amount of AMP added, the contents of AST and ALT exhibit a downward trend within a certain range, suggesting that AMP plays a hepatoprotective role in largemouth bass. Additionally, blood lipid levels are closely linked to the body's lipid metabolism capabilities (Zhang et al., 2018). Serum TG and CHOL are closely related to lipid metabolism. When there is excess fat in the liver or fat metabolism disorders, their levels tend to increase (Zhang et al., 2018; Wei et al., 2019). In this study, the TG and CHOL levels in the serum of the experimental groups exhibited a trend of first increasing and then decreasing. Notably, the TG of the high-dose group (Group C) was significantly lower than that of

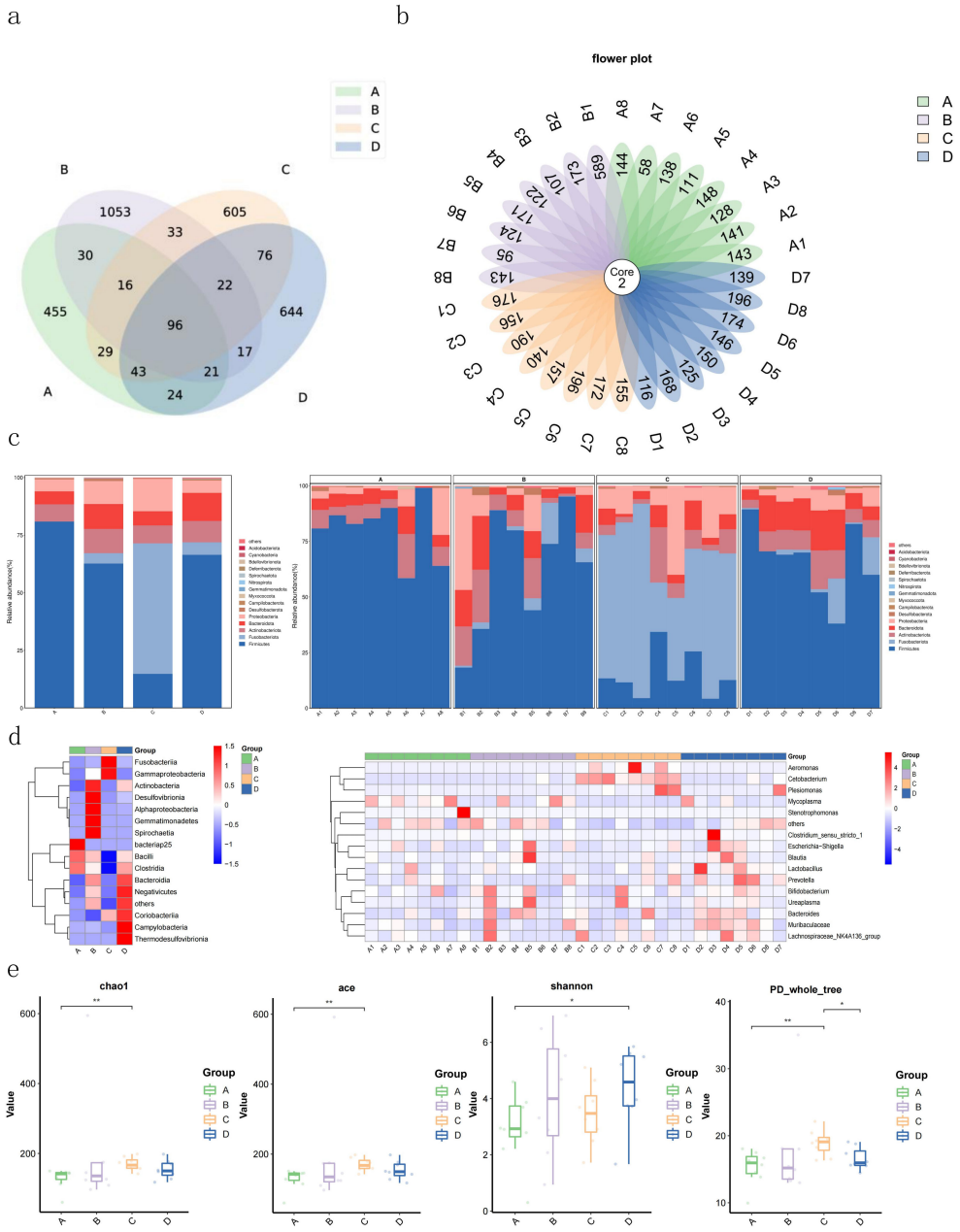

FIGURE 2
Effects of AMP on Intestinal Microflora of Largemouth Bass. **(A, B)** Venn diagram based ASVs; **(C)** relative abundance analysis of dominant bacterial phyla in intestinal microflora; **(D)** heatmap of species abundance at genus level of intestinal microflora for each sample and each group; **(E)** diversity analysis. In the figure, * mean $P < 0.05$, ** mean $P < 0.01$, and *** mean $P < 0.001$.

the other groups, and the CHOL content was also significantly lower than the control group. This suggests that AMP can regulate lipid metabolism in largemouth bass, promoting lipid metabolism. These results are similar to Zhuo et al.'s study on the effects of AMP on the growth and health maintenance of *Pseudobagrus fulvidraco* (Zhuo et al., 2022). Moreover, peroxide ions, hydroxyl free radicals, and other reactive species generated during metabolic processes can cause cellular damage. The stronger the antioxidant capacity of an animal's body, the more effectively it can avoid the adverse effects of oxidative reactions on the body (Chen et al., 2023).

AMP, as an immune polysaccharide, has been demonstrated by numerous studies to enhance the body's antioxidant and non-specific immune functions (Chen et al., 2023; Miao et al., 2021). In this experiment, the SOD content and C3 levels in each test group were significantly higher than those in the control group. Conversely, the MDA content of each test group was significantly lower than that of the control group. This finding aligns with Yang's study on the impact of AMP on growth performance, serum biochemical indicators, and intestinal morphology in broiler chickens (Yang, 2023), indicating that AMP also enhances the

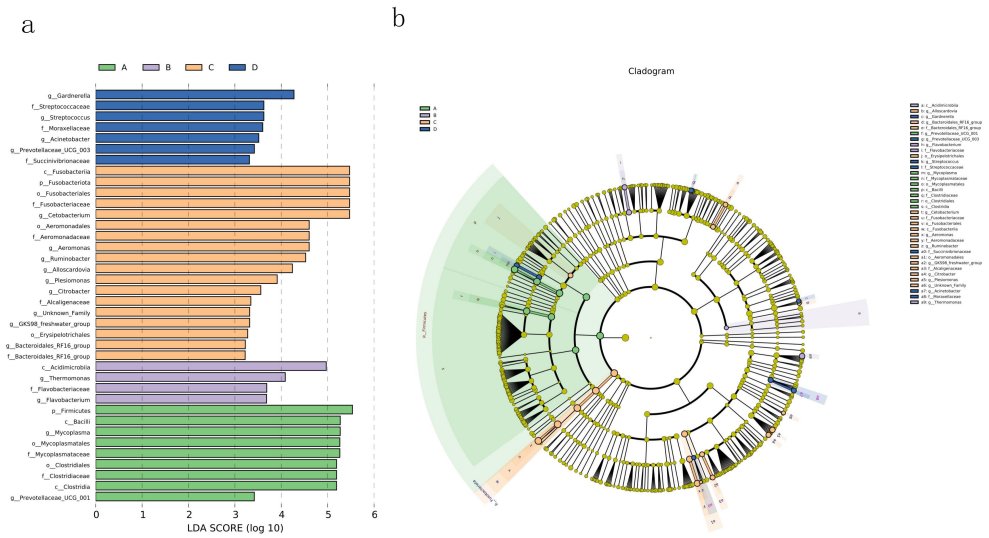

FIGURE 3
LEfSe analysis identified the biomarkers in different groups. **(A)** The LDA score distribution histogram mainly displays the species with LDA scores greater than the preset values (less strict sets as 2; more strict sets as 4), indicates that the biomarker has statistical difference; the color of the bar represents their respective groups, while the length represents the LDA score. **(B)** In the cladogram, the circle radiating from inside to outside in the diagram represents the classification level from kingdom (single circle) to genus (or species); each small circle at different classification levels represents a classification at that level, and the diameter of the small circle is proportional to the relative abundance. Different colors represent the microbial groups that play an important role in each group.

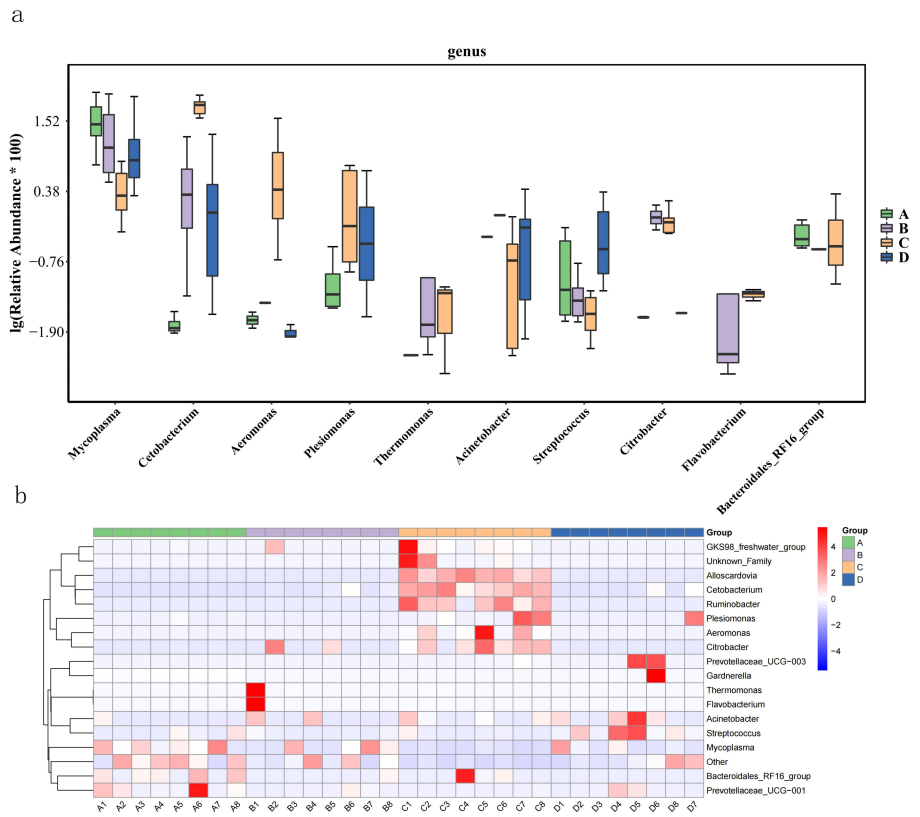

FIGURE 4
Effects of AMP on relative abundances of differential bacteria genus (biomarkers) in intestinal microflora of largemouth bass. **(A)** box diagram of relative abundance of the top 10 differential bacterial genus (biomarkers) among groups; **(B)** heatmap of relative abundance of the top 15 differential bacterial genus (biomarkers) among samples.

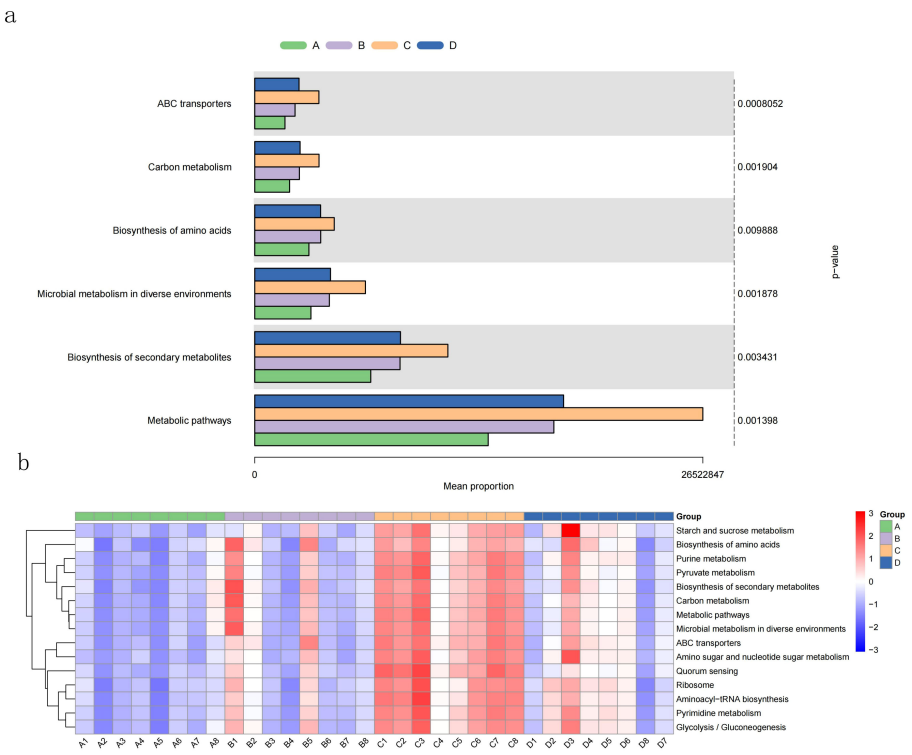

FIGURE 5
KEGG function prediction based on 16S of largemouth bass intestinal flora. **(A)** KEGG prediction results with significant differences among groups using Kruskal-Wallis method; **(B)** the heatmap of top15 mean proportion of predicted KEGG results with significant differences among difference samples.

resistance, antioxidant capacity, and immune response of aquatic animals.

Intestinal tissue and intestinal contents, together, constitute the intestinal environment, which serves as a habitat for a large number of microorganisms. These microorganisms participate in the digestion and absorption of nutrients and the regulation of the body's immunity during the growth and development of animals, thereby having a significant impact on animal health. They play an extremely important role in growth, development, and overall well-being (Zhang, 2020; Xu and Knight, 2015). Studies have shown that the diversity and structure of fish intestinal flora are influenced by various factors, including their own genetics, the environment, individual size, and food composition. Among these factors, food composition and environmental status are the most influential (Bolnick et al., 2014; Sullam et al., 2012).

Shang et al (Shang et al., 2016). found that some bacteria in the intestine may be related to the polysaccharide content in food. Ingesting fucoidan can increase the number of lactobacilli in the intestine and reduce the number of harmful bacteria such as *Escherichia coli*. Huang et al (Huang et al., 2022). found in a study on mice that the addition of fucoidan changed the composition of the main intestinal flora of mice, significantly increased the abundance of beneficial bacteria at the genus *Lactobacillus*, and also made some beneficial bacteria The abundance of functional genes is increased. In this study, adding 1.2% AMP to the feed increased the abundance of intestinal flora of largemouth bass, but the diversity of each group decreased.

At the phylum level, the relatively abundant bacterial groups in the intestinal tract of largemouth bass in each group were *Firmicutes*, *Actinobacteriota*, *Bacteroidota*, *Fusobacteriota*, and *Proteobacteria*. Studies have found that among bacteria, many pathogenic bacteria are members of the *Proteobacteria* phylum, which increase the risk of disease in the body (Shin et al., 2015). *Fusobacteria* can trigger inflammation in certain parts of the host under certain conditions (Han et al., 2005). Some bacteria in the *Firmicutes* phylum can play important roles in cellulose decomposition and polysaccharide fermentation (Ji et al., 2016). *Actinobacteria* are opportunistic pathogens that may infect animals when their immunity is low, causing them to develop some chronic or subacute diseases (Mai et al., 2020). *Bacteroidetes* can participate in the conversion of proteins, lipids, etc., and can also participate in the metabolism of sugars and bile acids (Michaud et al., 2009). In this study, as the concentration of AMP added to the feed gradually increased, the abundance of *Firmicutes* in the intestinal tract of largemouth bass significantly decreased, and the abundance of *Fusobacteriota* and *Proteobacteria* increased significantly, indicating that the addition of *Atractylodes* macrocephala to the feed Excessive concentration of AMP is not conducive to the conversion and absorption of nutrients in the intestinal tract of largemouth bass, and protects intestinal health, thereby reducing the immunity of largemouth bass and increasing the probability of disease occurrence.

At the bacterial genus level, in this study, the dominant species of the intestinal flora of the 4 groups of largemouth bass were

different. Group A (0.4% AMP)was mainly *Mycoplasma*, Group B (0.8% AMP) was mainly *Bifidobacterium* and *Bacteroides*, Group C (1.2% AMP) was mainly *Cetobacterium* and *Aeromonas*, and Group D was mainly intestinal flora. There are abundant probiotics such as *Prevotella* (Galvez et al., 2020) and *Muribaculaceae* (Lagkouvardos et al., 2019) in the intestinal flora, but the relative abundance of these bacteria in the AMP-added group was low, and compared with the control group, most samples in Group C had Cetobacterium, the relative abundance of *Aeromonas* is high, which shows that compared with the individual diversity of the intestinal flora of the fish group in the control group, Group C adjusted the intestinal flora structure of the fish group to make the intestinal flora structure of the entire fish group tend to be consistent. In this study, the addition of AMP had a significant regulatory effect on the intestinal flora structure of largemouth bass. The relationship between the intestinal flora structure and its relationship needs further study.

At the same time, KEGG function prediction based on 16S rRNA sequencing revealed that the intestinal flora regulated by Group C strengthened amino acid metabolism, fat metabolism, sugar metabolism, and various biosynthesis pathways compared to Group D. The effects observed in groups A and B were opposite. These findings (Li et al., 2023) are consistent with previous research results. It is speculated that the diverse functions of the intestinal flora in largemouth bass in this experiment also play a crucial role in metabolism and contribute to maintaining the stability of the microbiota structure. The experiment found that as the concentration increased, the metabolic function, body system, and genetic information processing expression in the intestinal tract of largemouth bass in groups A, B, and C gradually improved. At low concentrations, AMP had an inhibitory effect on these pathways. However, when the concentration reached 1.2%, it effectively promoted the expression of bodily functions, which benefits the utilization of fish body nutrients and the development of cell functions. This increase in nutrient utilization further promotes the survival and growth of the fish (Zhang et al., 2023).

5 Conclusion

Adding an appropriate amount of AMP to the feed can increase the WGR and SGR of largemouth bass, reduce the FCR, and improve the growth performance of largemouth bass. It can also lower the AST and ALT levels, protecting the liver function of largemouth bass. Additionally, it enhances the activity of serum SOD, C3, and C4 in largemouth bass, reduces MDA content, and improves the antioxidant and disease resistance of largemouth bass. It improves the composition of intestinal flora in largemouth bass, which has a positive effect on intestinal health. Based on comprehensive analysis, the recommended range of AMP in the feed is 0.8% – 1.2%.

Data availability statement

The data presented in the study are deposited in the Sequence Read Archive (https://www.ncbi.nlm.nih.gov/sra), under accession number PRJNA1118736 (https://www.ncbi.nlm.nih.gov/bioproject/PRJNA1118736/).

Ethics statement

The animal study was approved by Hunan Biological And Electromechanical Polytechnic. The study was conducted in accordance with the local legislation and institutional requirements.

Author contributions

XW: Conceptualization, Data curation, Formal analysis, Writing – original draft. LG: Supervision, Validation, Writing – review & editing. KL: Methodology, Writing – original draft. ST: Project administration, Software, Writing – review & editing. YH: Methodology, Resources, Writing – original draft.

Funding

The author(s) declare financial support was received for the research, authorship, and/or publication of this article. This work was supported by the Hunan Provincial Education Department Funding Project (23C0777); the Natural Science Foundation of Hunan Province (2024JJ8038).

Conflict of interest

The authors declare that the research was conducted in the absence of any commercial or financial relationships that could be construed as a potential conflict of interest.

Publisher's note

References

Bai, J. J., Lutz-Carillo, D. J., Ouan, Y. C., and Liang, S. (2008). Taxonomic status and genetic diversity of cultured largemouth bass Micropterus salmoides in China. *Aquaculture* 278, 27–30. doi: 10.1016/j.aquaculture.2008.03.016

Bai, R. X., Hua, L. H., Liu, H. K., Zhang, Y. X., Zhu, X. M., Yang, Y. X., et al. (2023). Effects of adding Atractylodes macrocephala extract to feed on the growth, health and disease resistance of Macrobrachium japonicum. *Acta Hydrobiologica Sin.* 06, 30. doi: 10.7541/2023.2023.0097

Bailly, C. (2021). Atractylenolides, essential components of atractylodes-based traditional hebal medicines: Antioxidant, anti-inflammatory and anticancer properties. *Eur. J. Pharmacol.* 891, 173735. doi: 10.1016/j.ejphar.2020.173735

Bolnick, D. I., Snowberg, L. K., Hirsch, P. E., Lauber, C. L., Knight, R., Caporaso, J. G., et al. (2014). Individuals' diet diversity influences gut microbial diversity in two freshwater fish (threespine stickleback and Eurasian perch). *Ecol. Lett.* 17, 979–987. doi: 10.1111/ele.12301

Cao, N., Yang, S. Z., Hu, C. Y., Lu, Z. E., Liu, J. N., Qian, L., et al. (2022). Effects of Atractylodes polysaccharide on growth performance, slaughter performance, and immune organ development of Lingnan yellow chickens. *J. Anim. Nutr.* 34, 205–214. doi: 10.3969/j.issn.1006-267x.2022.01.020

Chai, Y., Li, Q. H., Jia, J. J., Zhang, W. J., Lu, Q. F., Chen, T., et al. (2020). Effects of Atractylodes polysaccharide on production performance and intestinal tissue morphology of weaned piglets. *China Feed* 15, 49–54. doi: 10.15906/j.cnki.cn11-2975/s.20201513

Che, C. Y., Li, H. S., Ying, H., and Zhou, F. (2017). Study on the preventive and therapeutic effects of Atractylodes polysaccharide on non-alcoholic steatohepatitis. *Chin. J. Traditional Chin. Med.* 35, 1801–1803. doi: 10.13193/j.issn.1673-7717.2017.07.045

Chen, H. X., Yang, S. Z., Lu, Z., Qian, L., Li, B. X., Li, W. Y., et al. (2023). Atractylodes polysaccharide alleviates cyclophosphamide-induced oxidative stress and liver cell apoptosis in Lingnan yellow chickens. *J. Anim. Nutr.* 35, 1976–1984. doi: 10.12418/CJAN2023.185

Galvez, E. J. C., Iljazovic, A., Amend, L., Lesker, T. R., Renault, T., Thiemann, S., et al. (2020). Distinct polysaccharide utilization determines interspecies competition between intestinal Prevotella spp. *Cell Host Microbe* 28, 838–852.e6. doi: 10.1016/j.chom.2020.09.012

Han, Y. W., Ikegami, A., Rajanna, C., Kawsar, H. I., Zhou, Y., Li, M., et al. (2005). Identification and characterization of a novel adhesin unique to oral Fusobacteria. *J. Bacteriology* 187, 5330–5340. doi: 10.1128/JB.187.15.5330-5340.2005

He, M., Li, X., Poolsawat, L., Guo, Z., Yao, W., Zhang, C., et al. (2020). Effects of fish meal replaced by fermented soybean meal on growth performance, intestinal histology and microbiota of largemouth bass (Micropterus salmoides). *Aquaculture Nutr.* 26, 1058–1071. doi: 10.1111/anu.13064

Huang, J., Huang, H. L., Sun, J. Y., Li, Y., and Li, H. J. (2023). Regulatory effect of golden algae polysaccharide on immune function and intestinal flora in immunocompromised mouse model. *Chin. J. Food Sci.* 32, 92–102. doi: 10.16429/j.1009-7848.2022.05.011

Huang, X. W., Yang, S. S., Liu, Y., Fan, T., Ming, W., Lin, R. N., et al. (2015). Effect of dietary chitosan on growth performance, lipid metabolism, non-specific immune function and intestinal health of juvenile Jian carp (Cyprinus carpiovar. jian). *Chin. J. Anim. Nutr.* 27, 2106–2114. doi: 10.3969/j.issn.1006-267x.2015.07.016

Ji, Y. J., Zhu, Q., Geng, M. M., Chen, W., Yin, Y. L., and Kong, X. F. (2016). Effects of high and low nutritional level diets on the structure and metabolites of colonic flora of Huanjiang Xiang pigs. *Bull. Microbiol.* 43, 1650–1659. doi: 10.13344/j.microbiol.china.150594

Jing, J. L., Zhao, G. X., Gong, J. G., Hao, Y. S., and Feng, Z. H. (2019). Effects of Atractylodes polysaccharide on growth performance and serum immune indicators of laying hens during the breeding period. *Feed Res.* 42, 35–37. doi: 10.13557/j.cnki.issn1002-2813.2019.02.011

Kong, X., Duan, W., Li, D., Tang, X., and Duan, Z. (2020). Effects of polysaccharides from Auricularia auricula on the immuno-stimulatory activity and gut microbiota in immunosuppressed mice induced by cyclophosphamide. *Front. Immunol.* 11. doi: 10.3389/fimmu.2020.595700

Lagkouvardos, I., Lesker, T. R., Hitch, T. C. A., Gálvez, E. J., Smit, N., Neuhaus, K., et al. (2019). Sequence and cultivation study of Muribaculaceae reveals novel species, host preference, and functional potential of this yet undescribed family. *Microbiome* 7, 28. doi: 10.1186/s40168-019-0637-2

Li, L., Yin, F., Zhang, B., Peng, H. Z., Li, F. N., Zhu, N. S., et al. (2011). Dietary supplementation with Atractylodes macrophala Koidz polysaccharides ameliorates metabolic status and improves immune function in early-weaned pigs. *Livestock Sci.* 142, 33–41. doi: 10.1016/j.livsci.2011.06.013

Li, L. L., Zhang, B., Zhu, N. S., Yin, Y. L., Peng, H. Z., Yin, X. M., et al. (2009). Effects of polysaccharides on lymphocyte proliferation and cytokines in early weaned piglets. *Agric. Modernization Res.* 30, 495–497.

Li, C. J., Zhang, J., Zhu, Y. C., and Kong, X. H. (2019). Application of Astragalus polysaccharide in aquatic animal disease control. *Fisheries Sci.* 38, 881–886. doi: 10.16378/j.cnki.1003-1111.2019.06.021

Li, Q. J., Zhu, H. J., Qiang, J., Nie, Z. J., Gao, J. C., Sun, Y., et al. (2023). Effects of adding Acanthopanax to feed on lipid deposition, antioxidant capacity, intestinal digestive enzymes and microorganisms of Tilapia jifu. *Acta Hydrobiologica Sin.* 47, 1396–1407. doi: 10.7541/2023.2022.0281

Li, W. Y., Wang, Y. F., Li, B. X., Xu, S. P., Zheng, M., Cao, N., et al. (2022). Study on the protective effect of Atractylodes polysaccharide on the liver immune function of goslings. *Guangdong Anim. Husbandry Veterinary Sci. Technol.* 47, 6–13. doi: 10.19978/j.cnki.xmsy.2022.02.02

Lu, S., Bian, X., Wang, C. A., Wang, D., Shi, H., Wang, S., et al. (2024). Protective effects of polysaccharide from Atractylodes macrocephala Koidze (AMP) as a feed additive on growth performance, immunity, antioxidant capacity, and disease resistance against Aeromonas salmonicida in rainbow trout (Oncorhynchus mykiss). *Aquaculture Int.*, 1–16. doi: 10.1007/s10499-024-01521-4

Mai, H. B., Guo, X. W., Wang, J. G., Chi, S. Y., Dong, X. H., Yang, Q. H., et al. (2020). Effects of eating different dietary proteins on the intestinal tissue morphology and bacterial composition of juvenile pearl gentian grouper. *J. Dalian Ocean Univ.* 35, 63–70. doi: 10.16535/j.cnki.dlhyxb.2019-123

Miao, Y. F., Gao, X. N., Xu, D. N., Li, M. C., Gao, Z. S., Tang, Z. H., et al. (2020). Protective effect of the newly prepared Atractylodes macrocephala Koidz polysaccharide on fatty liver hemorrhagic syndrome in laying hens. *Poultry Sci.* 100, 938–948. doi: 10.1016/j.psj.2020.11.036

Michaud, L., Lo Giudice, A., Troussellier, M., Smedile, F., Bruni, V., and Blancheton, J. P. (2009). Phylogenetic characterization of the heterotrophic bacterial communities inhabiting a marine recirculating aquaculture system. *J. Appl. Microbiol.* 107, 1935–1946. doi: 10.1111/jam.2009.107.issue-6

National Pharmacopoeia Commission (2020). *Pharmacopoeia of the People's Republic of China* (Beijing: China Medical Science and Technology Press).

Shang, Q. S., Shan, X. D., Cai, C., Hao, J. J., Li, G. Y., and Yu, G. L. (2016). Dietary fucoidan modulates the gut microbiota in mice by increasing the abundance of Lactobacillus and Ruminococcaceae. *Food Funct.* 7, 3224–3232. doi: 10.1039/C6FO00309E

Shin, N. R., Whon, T. W., and Bae, J. E. (2015). Proteobacteria: microbial signature of dysbiosis in gut microbiota. *Trends Biotechnol.* 33, 496–503. doi: 10.1016/j.tibtech.2015.06.011

Sullam, K. E., Essinger, S. D., Lozupone, C. A., O'Connor, M. P., Rosen, G. L., Knight, R., et al. (2012). Environmental and ecological factors that shape the gut bacterial communities of fish: a meta-analysis. *Mol. Ecol.* 21, 3363–3378. doi: 10.1111/j.1365-294X.2012.05552.x

Wang, L., Wang, B., and Wang, R. C. (2023). Research progress on the biological functions of Atractylodes extracts and their application in animal production. *Feed Res.* 46, 160–163. doi: 10.13557/j.cnki.issn1002-2813.2023.01.034

Wang, Y. Z., Xin, Y. X., Li, X. Y., Guo, X. Z., Liu, W. S., Liu, W. Z., et al. (2023). Research progress on the application of lentinan in aquaculture. *Feed Industry*. 45, 37–42. doi: 10.13302/j.cnki.fi.2024.02.007

Wei, F. F., Wang, W. J., He, Q. H., and Zhang, B. (2019). Protective mechanism of Lycium Barbarum Polysaccharide on alcohol-induced liver injury in mice. *Drug Eval. Res.* 42, 852–857. doi: 10.7501/j.issn.1674-6376.2019.05.008

Xu, W., Guan, R., Shi, F. S., Du, A., and Hu, S. (2015). Structural analysis and immunomodulatory effect of polysaccharide from Atractylodes macrocephalae Koidz. on bovine lymphocytes. *Carbohydr. Polymers* 174, 1213–1223.

Xu, Z., and Knight, R. (2015). Dietary effects on human gut microbiome diversity. *Br. J. Nutr.* 113, S1–S5. doi: 10.1017/S0007114514004127

Yang, Z. Z. (2023). Effects of Atractylodes polysaccharide on growth performance, serum biochemical indicators, and intestinal morphology of broiler chickens. *Feed Res.* 46, 46–50. doi: 10.13557/j.cnki.issn1002-2813.2023.12.010

Yang, J. T., Cheng, X., Chen, H. W., Wu, J. W., and Zeng, Y.-M. (2018). Research progress on the immunomodulatory mechanism of Atractylodes polysaccharide. *Chin. J. Veterinary Drugs* 52, 80–85. doi: 10.11751/ISSN.1002-1280.2018.06.13

Zhang, H. X. (2020). *Effects of large daphnia powder on the growth, digestion, some biochemical indicators, and intestinal health of yellow catfish* (Tianjin Agricultural University).

Zhang, Y. T., and He, Y. F. (1994). Research on largemouth bass culture. *J. Zhanjiang Fisheries Univ.* 1994, 23–28.

Zhang, J. Y., Wang, S. X., Liu, D. J., Du, X. K., Mu, J. H., and Shen, X. H. (2023). Research on the intestinal flora of wheat ear fish in aquaponics system. *J. Fisheries* 36, 104–111. doi: 1005- 3832(2023)03- 0104- 08

Zhang, D. D., Yan, Y. A., Tian, H. Y., Jiang, G., Li, X., and Liu, W. (2018). Resveratrol supplementation improves lipid and glucose metabolism in high-fat diet-fed blunt snout bream. *Fish Physiol. Biochem.* 44, 163–173. doi: 10.1007/s10695-017-0421-9

Zhao, Y. F., and Wang, Y. Z. (2015). Effects of Atractylodes macrocephala, micron Atractylodes macrocephala and Atractylodes macrocephala polysaccharide on growth performance, intestinal morphology and microecological flora of weaned piglets. *Chin. J. Anim. Husbandry* 51, 65–69.

Zhuo, W. W., Ren, S. G., Wang, X., Gu, X. L., Li, D. G., and Xie, R. C. (2022). Research on the effects of Atractylodes polysaccharide on the growth and health maintenance of yellow catfish. *Aquaculture* 43, 32–38. doi: 10.13302/j.cnki.fi.2022.24.006

frontiers | Frontiers in Microbiology

TYPE Original Research
PUBLISHED 09 September 2024
DOI 10.3389/fmicb.2024.1445223

OPEN ACCESS

EDITED BY
Jie Yin,
Hunan Agricultural University, China

REVIEWED BY
Limei Lin,
Nanjing Agricultural University, China
Lifeng Dong,
Chinese Academy of Agricultural Sciences, China

*CORRESPONDENCE
Zhongquan Zhao
✉ zhongquanzhao@126.com
Juncai Chen
✉ juncai.chen@hotmail.com

†These authors have contributed equally to this work

RECEIVED 07 June 2024
ACCEPTED 30 August 2024
PUBLISHED 09 September 2024

CITATION
Chen J, Zhang X, Chang X, Wei B, Fang Y, Song S, Gong D, Huang D, Sun Y, Dong X, Zhao Y and Zhao Z (2024) Multi-omics analysis reveals the effects of host-rumen microbiota interactions on growth performance in a goat model. *Front. Microbiol.* 15:1445223. doi: 10.3389/fmicb.2024.1445223

Multi-omics analysis reveals the effects of host-rumen microbiota interactions on growth performance in a goat model

Juncai Chen[1*†], Xiaoli Zhang[1†], Xuan Chang[1], Bingni Wei[1], Yan Fang[1], Shanshan Song[1], Daxiang Gong[2], Deli Huang[2], Yawang Sun[1], Xianwen Dong[3], Yongju Zhao[1] and Zhongquan Zhao[1*]

[1]College of Animal Science and Technology, Chongqing Key Laboratory of Herbivore Science, Southwest University, Chongqing, China, [2]Tengda Animal Husbandry Co., Ltd., Chongqing, China, [3]Chongqing Academy of Animal Science, Chongqing, China

The growth rate of young ruminants has been associated with production performance in later life, with recent studies highlighting the importance of rumen microbes in supporting the health and growth of ruminants. However, the specific role of rumen epithelium bacteria and microbiota-host interactions in influencing the early life growth rate of ruminants remains poorly understood. In this study, we investigated the rumen fermentation pattern, microbiota characteristics, and global gene expression profiles of the rumen epithelium in 6-month-old goats with varying growth rates. Our results showed that goats with high average daily gain (HADG) exhibited higher rumen propionate concentrations. Goats with low average daily gain (LADG) had the higher relative abundances of rumen epithelium bacteria genera U29-B03 and *Quinella*, while exhibiting a lower relative abundance of *Lachnospiraceae* UCG-009. In the rumen fluid, the relative abundances of bacteria genus *Alloprevotella* were lower and *Desulfovibrio* were higher in LADG goats compared to HADG goats. Additionally, the relative abundance of fungal genus *Symmetrospora* was lower in LADG goats compared to HADG goats. Transcriptome analysis showed that 415 genes were differentially expressed between LADG and HADG goats, which were enriched in functions related to cell junction and cell adhesion, etc. Correlation analysis revealed that rumen epithelium bacteria genera *UCG-005* and Candidatus *Saccharimonas* were negatively associated, while *Lachnospiraceae* NK3A20 group and *Oscillospiraceae* NK4A214 group were positively associated with average daily gain (ADG) and genes related to barrier function. The rumen fluid bacteria genus *Alloprevotella* was positively correlated, while *Desulfovibrio* was negatively correlated with rumen propionate and ammoniacal nitrogen (NH_3-N) concentrations, as well as genes related to barrier function and short chain fatty acids (SCFAs) transport. In summary, our study reveals that the higher ruminal fermentation efficiency, improved rumen epithelial barrier functions, and enhanced SCFAs transport in HADG goats could be attributed to the rumen microbiota, particularly the rumen epithelium bacteria, such as *Lachnospiraceae* and *Oscillospiraceae* NK4A214 group.

KEYWORDS

microbes, rumen epithelium, transcriptome, growth rate, goat

Introduction

The rumen constitutes a complex natural ecosystem that harbors diverse microbes responsible for biomass degradation, which provide nutrients for the host's physiological needs. In return, the rumen provides a unique environment characterized by anaerobic conditions, stable temperature, and high osmotic pressure for the rumen microbes (Kamra, 2005). Emerging evidence suggests that the stable mutualistic relationship between rumen and its microbial inhabitants is pivotal for the growth, development (Malmuthuge et al., 2019; Jize et al., 2022), feed efficiency (Fonseca et al., 2023), and mitigation of acidosis (Li et al., 2019) in ruminants. However, these studies predominantly focused on rumen fluid-associated bacteria, which are more sensitive to the changes in environmental conditions (Liu et al., 2016) and differ from rumen epithelium bacteria (Pei et al., 2010). Rumen epithelium bacteria, directly adhering to the epithelium, likely engage in more interactions with the host. Moreover, fungi are immensely important for degrading ligno-carbohydrate complex in rumen (Bhagat et al., 2023). Yin et al. (2023) identified several fungal biomarkers in both rumen and rectum that were associated with growth rate in lambs. However, our understanding of the functional roles of rumen fungi remains limited and further investigations are required.

Early-life growth rate significantly influences later-life production performance. The pre-weaning and pre-pubertal average daily gain (ADG) has been reported to be correlated with milk production (Soberon and Van Amburgh, 2013; Gelsinger et al., 2016) and fertility (Schubach et al., 2019; Costa et al., 2021) in ruminants. There is a growing interest in exploring key microbes that affect the health and growth performance of ruminant animals. Yin et al. (2023) identified several microbes in both the rumen and the rectum associated with post-weaning ADG in lambs. The ADG-related rumen fluid microbiota, including the *Prevotellaceae* family, *Streptococcus*, and Candidatus *Saccharimonans*, is believed to contribute to nutrient metabolism functions and short chain fatty acids (SCFAs) production in dairy goats (Wang et al., 2023). Nevertheless, the role of rumen epithelium bacteria and microbiota-host interactions in influencing the early-life growth performance of goats remains unclear.

The objective of the present study was to investigate the relationships between ruminal microbiota and early-life growth performance in ruminants, and to further explore the underlying mechanisms involved in the microbiota-host interactions at transcriptome level. Here, 6-month-old goats with different ADG, raised under identical conditions, were selected as model animals to assess their rumen fermentation patterns, rumen microbiota characteristics, and global gene expression profiles of the rumen epithelium. The findings of this study may contribute to the development of novel strategies aimed at improving the growth rate of young ruminants, thereby potentially enhancing production performance in later life.

Materials and methods

Ethics statement

All animal experimental and protocols were approved by the Institutional Animal Care and Use Committee of Southwest University, Beibei, China (approval IACUC-20220630-04).

Animal experiment design

A total of 49 female Dazu black kids from Tengda Animal Husbandry Co., Ltd. (Chongqing, China) were used for the experiment. Birth weights of all goat kids were recorded immediately after birth and they were weaned at 2 months of age. The goats were fed with a total mixed ration (TMR) *ad libitum* twice daily at 0700 and 1,600, consisting of corn grain (475 g/kg), soybean meal (40 g/kg), alfalfa hay (450 g/kg), NaCl (5 g/kg), dicalcium phosphate (10 g/kg), sodium bicarbonate (10 g/kg), and a trace minerals and vitamins supplement (10 g/kg). The diet was antibiotic-free, meeting the recommendations of the Feeding Standard of Meat-producing Sheep and Goats of China, NY/T 816–2004 (Ministry of Agriculture, MOA, PRC, 2004).

At approximately 6 months of age (183.4 ± 6.2 days), the goats were weighed before morning feeding and then slaughtered after anesthesia. The ADG was calculated as the weight gain from birth to 6 months of age divided by the number of days. The average ADG for all 49 goats was 86.8 ± 10.9 g/day (Supplementary Table S1), after which goats were ranked based on individual ADG. The top 10% of goats were designated as the high ADG group (HADG, 99.8 ± 12.8 g/day), while the bottom 10% were designated as the low ADG group (LADG, 63.6 ± 3.94 g/day).

Dry matter intake was continuously measured for 2 days before slaughtering (844 ± 28 g/day for LADG goats and 857 ± 37 g/day for HADG goats, $p = 0.55$). The rumen fluid was filtered using a four-layer cheesecloth, and pH values were measured with a portable pH meter (PHB-4, Rex Instrument, Shanghai, China). Rumen epithelium samples were collected from the ventral sac of each goat immediately after slaughter and rinsed with 0.01 M phosphate-buffered saline (PBS) buffer. All samples were promptly immersed in liquid nitrogen and then stored at −80°C for subsequent analysis.

The SCFAs and NH_3-N analysis

The rumen fluid was centrifuged for 10 min at 10,000 × g, and the supernatants were filtered with a membrane (0.22 μm). Acetate, propionate, and butyrate concentrations were determined using high-performance liquid chromatography (KC-811 column, Shodex; mobile phase, 3 mM perchloric acid; flow rate, 1.0 mL/min; temperature: 50°C). Ammonia-N (NH_3-N) concentration was determined using the phenol-hypochlorite colorimetric method.

Rumen microbiota analysis

Total microbial DNA was extracted from rumen fluid and epithelial samples using the E.Z.N.A.® stool DNA Kit (Omega Bio-tek, Norcross, GA, U.S.) according to the manufacturer's protocol. The quality of the DNA was determined by 1% agarose gel electrophoresis. Bacterial 16S rRNA gene fragments (V3-V4) were amplified with primers 338F (5'-ACTCCTACGGGAGGCAGCAG-3′) and 806R (5'-GGACTACHVGGGTWTCTAAT-3′), and fungi ITS rRNA gene was amplified with primers ITS1F (5'-CTTGGTCATTTAGAGGAAGTAA-3′) and ITS2R (5'-GCTGCGTTCTTCATCGATGC-3′) using an ABI GeneAmp® 9,700 PCR thermocycler (ABI, CA, United States). The amplicons were paired-end sequenced using the Illumina PE250

platform (Illumina, San Diego, USA). The raw sequencing reads were deposited in the NCBI Sequence Read Archive (SRA) database (Accession Number: PRJNA1099693). The resulting sequences were filtered using FASTP (version 0.19.6) and merged using FLASH (version 1.2.11). The amplicon sequence variant (ASV), obtained using DADA2 in QIIME2 (version 2020.2), were assigned to taxonomies using SILVA database (version 138) and UNITE database (version 8.0) for bacteria and fungi, respectively. The alpha diversity indices, including Chao1, ACE, Sobs, Shannon, and Simpson, were analyzed using Mothur (version 1.30.2). Principal coordinate analysis (PCoA) was performed based on weighted UniFrac distances and significance was determined using ANOSIM with 999 permutations.

Transcriptome analysis

Total RNA was extracted from rumen epithelium using Trizol reagent (Tiangen Biotech, Beijing, China) according to the manufacturer's protocol. RNA quality was determined by a 5,300 (Bioanalyser Agilent, Palo Alto, CA, United States) and high-quality RNA samples were sent to Majorbio Biotech (Shanghai, China) for commercial library preparation and sequencing on the Illumina Novaseq 6,000. The DEGs (differential expression genes) between groups were analyzed using DESeq2. Genes with $|\log_2 FC| \geq 1$ and FDR < 0.05 were considered as differentially expressed. The gene ontology (GO) functional-enrichment analyses were performed by Goatools to identify significantly enriched GO terms at a Bonferroni-corrected *p*-value ≤0.05. RNA sequencing data were deposited in the NCBI's Gene Expression Omnibus under the accession number PRJNA1101717.

Tissue RNA extraction and real-time quantitative PCR

Total RNA was extracted from rumen epithelium using Trizol reagent (Tiangen Biotech, Beijing, China) according to the manufacturer's protocol. RNA degradation and contamination were monitored through 1% agarose gels electrophoresis. RNA concentration and purity were examined using a NanoDrop spectrophotometer (NanoDrop Technologies, Wilmington, DE, United States). The gene expression was detected by quantitative real-time PCR (RT-qPCR) using the $2^{-\Delta\Delta CT}$ method. The primer sequences are listed in Supplementary Table S2. β-actin and GAPDH were used as the endogenous reference genes. All reactions were run in triplicate for each sample.

Statistical analysis

Statistical significance was assessed using an unpaired Student's two-tailed t-test for average daily gain, ruminal pH, NH_3-N, and SCFAs, or the one-way ANOVA with Tukey's *post hoc* tests for alpha diversity of the bacterial community, using GraphPad Prism (version 9.2.0, GraphPad Software, San Diego, CA, United States). Results are expressed as means with the standard error of the means (SEM). A *p*-value of less than 0.05 was considered statistically significant. Correlations between rumen microbiota and growth performance, ruminal SCFAs and NH_3-N, or gene expression were estimated by Spearman correlation analysis using the 'Hmisc' and 'Corrplot' packages in R (version 4.3.2).

Results

Ruminal pH, NH_3-N, and short-chain fatty acids concentrations

HADG goats had higher rumen propionate concentrations ($p < 0.05$) and tended to have higher rumen NH_3-N concentration ($p = 0.07$, Figure 1). However, no significant differences were found in rumen fluid pH, and ruminal acetate and butyrate concentrations between HADG and LADG goats.

Microbiota composition of rumen fluid and epithelium

In the current study, 16 s and ITS gene sequencing techniques were used to determine the differences in rumen microbiota, especially for rumen epithelium bacteria, between HADG and LADG goats, aiming to explore the potential microbial targets for the development of novel intervention strategies to improve the growth performance of young ruminants.

The alpha diversity of the bacterial community in rumen fluid and epithelium is shown in Table 1. Bacterial community richness indices (Chao1, Ace, and Sobs) were greater in rumen epithelium of both HADG and LADG goats compared with rumen fluid of the same groups ($p < 0.01$). Nonetheless, no significant difference was observed in bacterial community composition between HADG and LADG goats in either rumen fluid or epithelium. In rumen fluid, the bacterial diversity of HADG was higher than that of LADG ($p < 0.01$), as indicated by Shannon indices.

As shown in Figure 2A, bacterial communities of rumen epithelium were well separated from those in the rumen fluid, with 52.25 and 15.57% of the variations explained by principal component 1 (PC1) and PC2, respectively. The rumen fluid bacterial composition of LADG goats was separated from the HADG goats (Figure 2C). However, the rumen epithelium bacterial composition was similar between LADG and HADG goats (Figure 2B).

We found that the *Butyrivibrio* (12.6% in HADG goats and 12.9% in LADG goats), *Prevotellaceae* UCG-001 (8.5% in HADG goats and 6.5% in LADG goats), *Blvii28* wastewater-sludge group (6.3% in HADG goats and 7.3% in LADG goats), *Rikenellaceae* RC9 gut group (5.9% in HADG goats and 7.6% in LADG goats), *Treponema* (5.9% in HADG goats and 7.1% in LADG goats), and norank_f_F082 (5.0% in HADG goats and 5.4% in LADG goats) were predominant genera in the rumen epithelium (Figure 2D). In contrast, the *Prevotella* (12.6% in HADG goats and 12.9% in LADG goats), norank_f_F082 (12.3% in HADG goats and 16.2% in LADG goats), *Rikenellaceae* RC9 gut group (8.6% in HADG goats and 11.8% in LADG goats), *Quinella* (2.1% in HADG goats and 17.9% in LADG goats), norank_f_*Muribaculaceae* (7.8% in HADG goats and 4.8% in LADG goats), *Succiniclasticum* (5.1% in HADG goats and 2.2% in LADG goats) were predominant genus in the rumen fluid.

In rumen epithelium, the relative abundances of genera U29-B03 and *Quinella* were higher, while *Lachnospiraceae*_UCG-009, norank_f_norank_o_WCHB1-41, and *Lachnospiraceae*_FCS020_group were lower in LADG goats compared with HADG goats ($p < 0.05$, Figure 3A). Additionally, the relative abundance of unclassified_c_*Clostridia* tended to be lower ($p = 0.06$), and *Desulfovibrio* tended to be higher ($p = 0.09$)

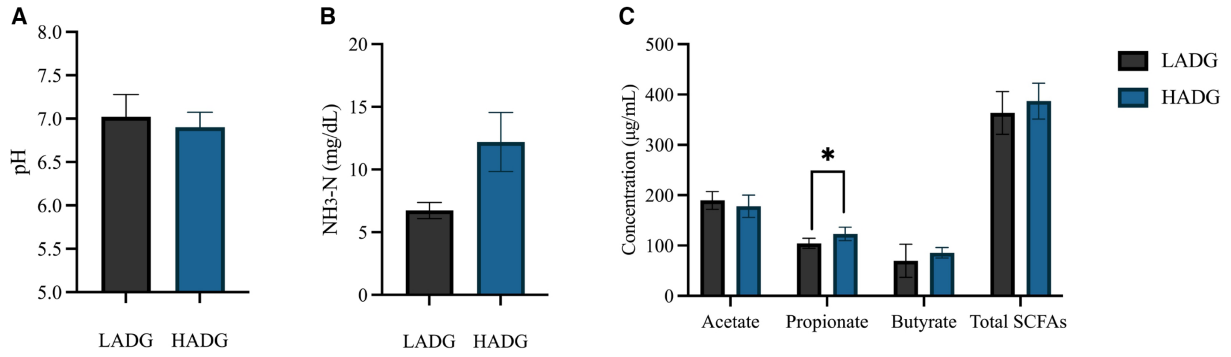

FIGURE 1
The ruminal pH **(A)**, NH3-N **(B)**, and short-chain fatty acids (SCFAs) concentrations **(C)** of low average daily gain (LADG) or high average daily gain (HADG) goats. * $p < 0.05$.

TABLE 1 The alpha diversity of rumen fluid or rumen epithelium microbiota in goats.

Items	RE-LADG	RE-HADG	RF-LADG	RF-HADG	*p* values
ACE index	953.6 ± 347.0 [a]	931.8 ± 265.3 [a]	225.4 ± 31.3 [b]	224.7 ± 42.4 [b]	< 0.01
Chao1 index	898.7 ± 353.5 [a]	866.4 ± 196.1 [a]	225.4 ± 31.3 [b]	225.0 ± 42.7 [b]	< 0.01
Sobs index	624.6 ± 184.6 [a]	635.6 ± 104.4[a]	224.0 ± 30.5 [b]	223.2 ± 42.1 [b]	< 0.01
Shannon index	4.88 ± 0.33 [a]	5.05 ± 0.28 [a]	4.07 ± 0.58 [b]	4.60 ± 0.34 [a]	< 0.01
Simpson index	0.022 ± 0.003 [b]	0.018 ± 0.006 [b]	0.085 ± 0.085 [a]	0.027 ± 0.024 [ab]	0.04

Significant differences were tested by one-way ANOVA with Tukey's post hoc tests ($n = 5$ per group). The variant letter indicates a significant difference when $P < 0.05$. RE-LADG, rumen epithelium of low average daily gain goat; RE-HADG, rumen epithelium of high average daily gain goat; RF-LADG, rumen fluid of low average daily gain goat; RF-HADG, rumen fluid of high average daily gain goat.

in rumen epithelium of LADG goats compared with HADG goats. In rumen fluid, the relative abundances of genera *Alloprevotella* and unclassified_o_*Bacteroidales* were lower, and *Desulfovibrio* and U23-B03 were higher in LADG goats compared with HADG goats ($p < 0.05$, Figure 3B). Moreover, the relative abundance of norank_f_*Bacteroidales*_BS11_gut_group tended to be lower ($p = 0.06$), and *Quinella* ($p = 0.09$) tended to be higher in LADG goats compared with HADG goats.

To explore whether rumen fungi were related to the growth performance, we analyzed the fungal compositions of rumen fluid in LADG and HADG goats (Figure 4). The *Saccharomyces* (42.6% in HADG goats and 34.8% in LADG goats), *Cladosporium* (25.7% in HADG goats and 8.1% in LADG goats), *Wallemia* (3.0% in HADG goats and 10.3% in LADG goats), and *Monascus* (4.4% in HADG goats and 6.0% in LADG goats) were predominant genera in the rumen fluid. Alpha diversity analysis showed that the rumen fluid fungal composition of LADG goats was not clearly separated from the HADG goats. However, the relative abundance of genus *Symmetrospora* was lower in LADG goats compared with HADG goats ($p < 0.05$). Additionally, the relative abundance of genus unclassified_f_*Cladosp oriaceae* tended to be lower ($p = 0.06$), and *Aspergillus* ($p = 0.06$) tended to be higher in LADG goats compared with HADG goats.

RNA-Seq analysis of the rumen epithelium

Principal components analysis (PCA) did not reveal strong clustering, with 34.41 and 14.76% variations explained by PC1 and PC2, respectively (Figure 5A). Further analysis of differentially expressed genes (DEGs) showed that 168 DEGs were upregulated, while 147 DEGs were downregulated in HADG goats compared with LADG goats (Figure 5B). 65 GO terms, including cell adhesion, cell junction, positive regulation of vascular endothelial growth factor production, regulation of developmental process, positive regulation of immune system process, etc., were identified (Figure 5C). Specifically, three DEGS, *SPON2*, *SCARF2*, *VNN1*, were upregulated and *POSTN* was downregulated, which were involved in regulation of cell adhesion, in HADG goats compared with LADG goats. Three upregulated genes (*CDH24*, *ITGB2, APOE*) and one downregulated gene (*ACTN2*) were enriched in the GO terms of cell junction in HADG goats. The *ARNT* and *CCBE1* involved in regulation of vascular endothelial growth factor production were upregulated in HADG goats. Five upregulated genes (*GPR4*, *CTSK*, *MDK*, *SNAI1*, *TMEM119*, *CYP126B1*) and 1 downregulated gene (*FRZB*) were enriched in the GO terms of regulation of developmental process in HADG goats. Additionally, three genes (*ITGAM*, *STXBP1*, and *PLVAP*) involved in regulation of immune system process were upregulated in HADG goats.

Relative gene expression of the rumen epithelium

The relative mRNA expression levels associated with tight junction, SCFAs transport, and inflammation are shown in Figure 6. The results demostrated that the relative expressions of *ZO-1* ($p = 0.01$), *Occludin* ($p = 0.02$), *NHE-2* ($p = 0.03$), and *NHE-3* ($p = 0.03$) were higher in the rumen epithelium of HADG goats compared with LADG

10.3389/fmicb.2024.1445223

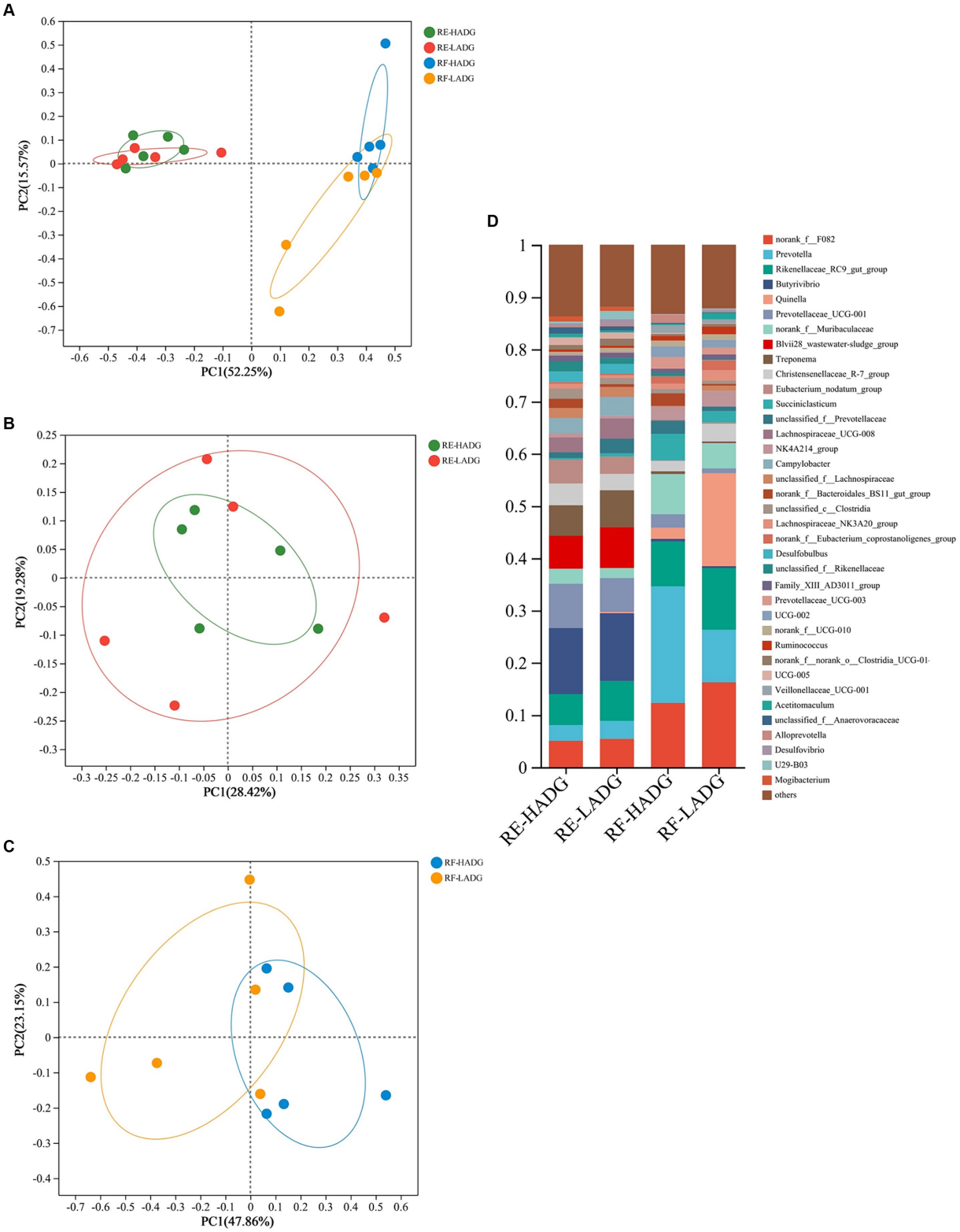

FIGURE 2
Principal coordinate analysis (PCoA) of bacterial compositional profiles of all samples **(A)**, rumen epithelium samples **(B)**, and rumen fluid samples **(C)** between LADG and HADG goats, based on weighted UniFrac distances. Abundant genera **(D)** in the rumen bacteria of LADG or HADG goats. Data are shown as means. RE-LADG, rumen epithelium of low average daily gain goat; RE-HADG, rumen epithelium of high average daily gain goat; RF-LADG, rumen fluid of low average daily gain goat; RF-HADG, rumen fluid of high average daily gain goat.

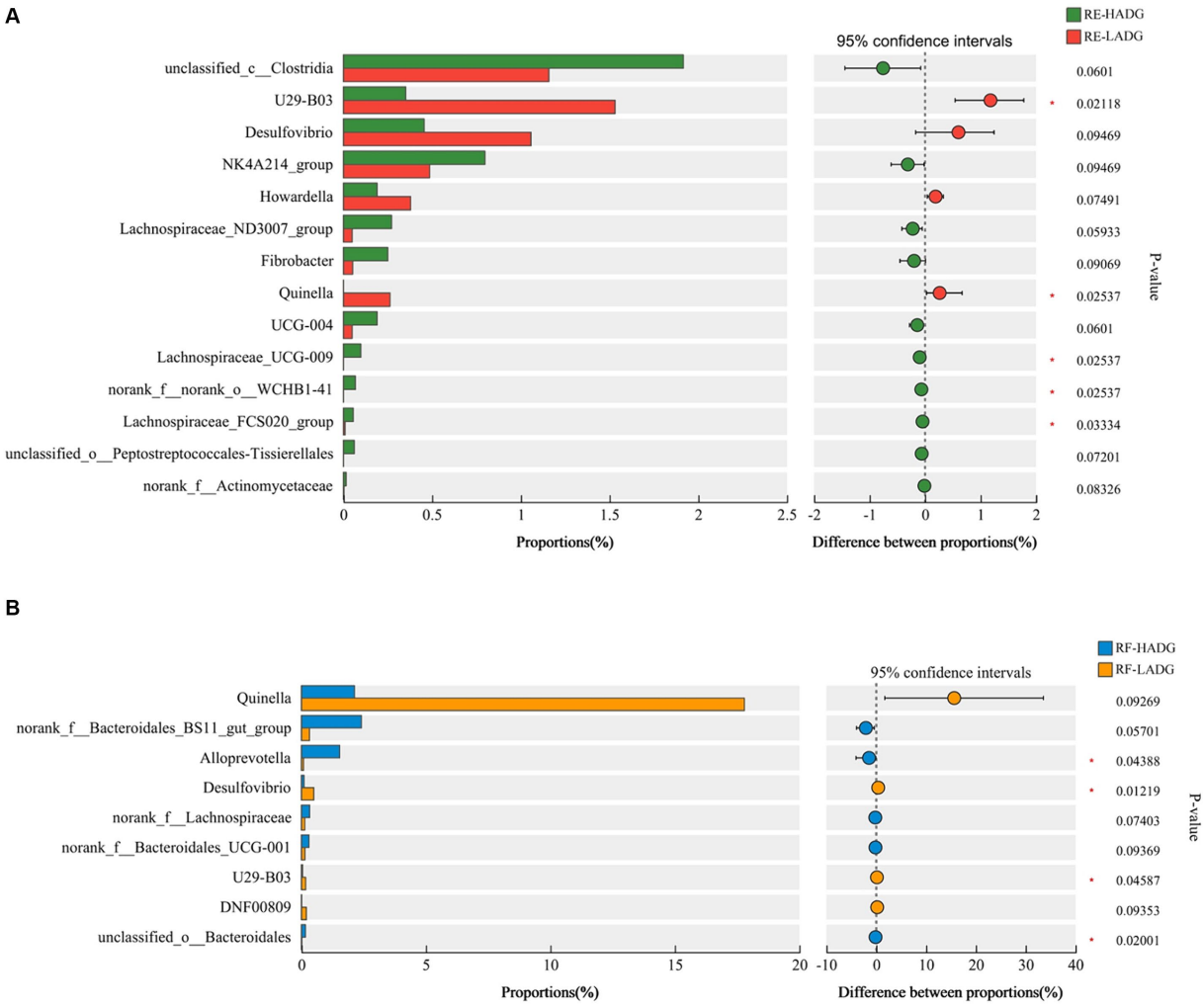

FIGURE 3
Differential enrichment of bacterial genera in rumen epithelium samples **(A)** and rumen fluid samples **(B)** between LADG and HADG goats, based on Wilcoxon rank-sum test. Data are shown as means. RE-LADG, rumen epithelium of low average daily gain goat; RE-HADG, rumen epithelium of high average daily gain goat; RF-LADG, rumen fluid of low average daily gain goat; RF-HADG, rumen fluid of high average daily gain goat.

goats. Furthermore, the relative expressions of *Claudin-1* ($p = 0.10$), *Claudin-4* ($p = 0.09$), and *MCT-4* ($p = 0.08$) tended to increase in the rumen epithelium of HADG goats compared with LADG goats. However, the relative mRNA expressions related to inflammation did not show significant differences between the two groups.

Correlation analyses of the rumen microbiota, growth performance, rumen SCFAs and NH3-N concentrations, or gene expression levels

The Spearman correlation analysis revealed that the relative abundances of genera *UCG-005* and Candidatus *Saccharimonas* in rumen epithelium were negatively associated with ADG, and relative expressions of *ZO-1* and *Occludin* ($p < 0.05$, Figure 7). The relative abundances of genera *Lachnospiraceae* NK3A20 group and *Oscillospiraceae* NK4A214 group in the rumen epithelium were positively correlated with ADG and the relative expressions of *ZO-1* and *Occludin* ($p < 0.05$). Additionally, the relative abundances of genera norank_f_norank_o_*Clostridia*_UCG-014 and *Desulfovibrio* in rumen epithelium were negatively associated with the relative expressions of *ZO-1* and *Occludin* ($p < 0.05$), while the relative abundance of genus *Oscillospiraceae* NK4A214 group in the rumen epithelium was positively associated with the relative expressions of *MCT-4*, *NHE-2*, *NHE-3*, and *AE2* ($p < 0.05$).

In rumen fluid, the relative abundance of *Quinella* had a negative correlation with the relative expressions of *claudin-4* and *NHE-3* ($p < 0.05$). Notably, the relative abundances of *Alloprevotella* in rumen fluid had a positive correlation with rumen propionate ($p < 0.01$) and NH_3-N ($p < 0.05$) concentrations, and the relative expressions of *Claudin-1* ($p < 0.01$). Conversely, the relative abundance of *Desulfovibrio* in rumen fluid had a negative correlation with weaning weight ($p < 0.01$), rumen propionate ($p < 0.01$) and NH_3-N ($p < 0.05$) concentrations, and the relative expressions of *ZO-1* ($p < 0.01$) and *NHE-3* ($p < 0.05$).

Furthermore, the relative abundances of fungal genera *Cladosporium* ($p < 0.01$), unclassified_f_*Cladosporiaceae* ($p < 0.01$),

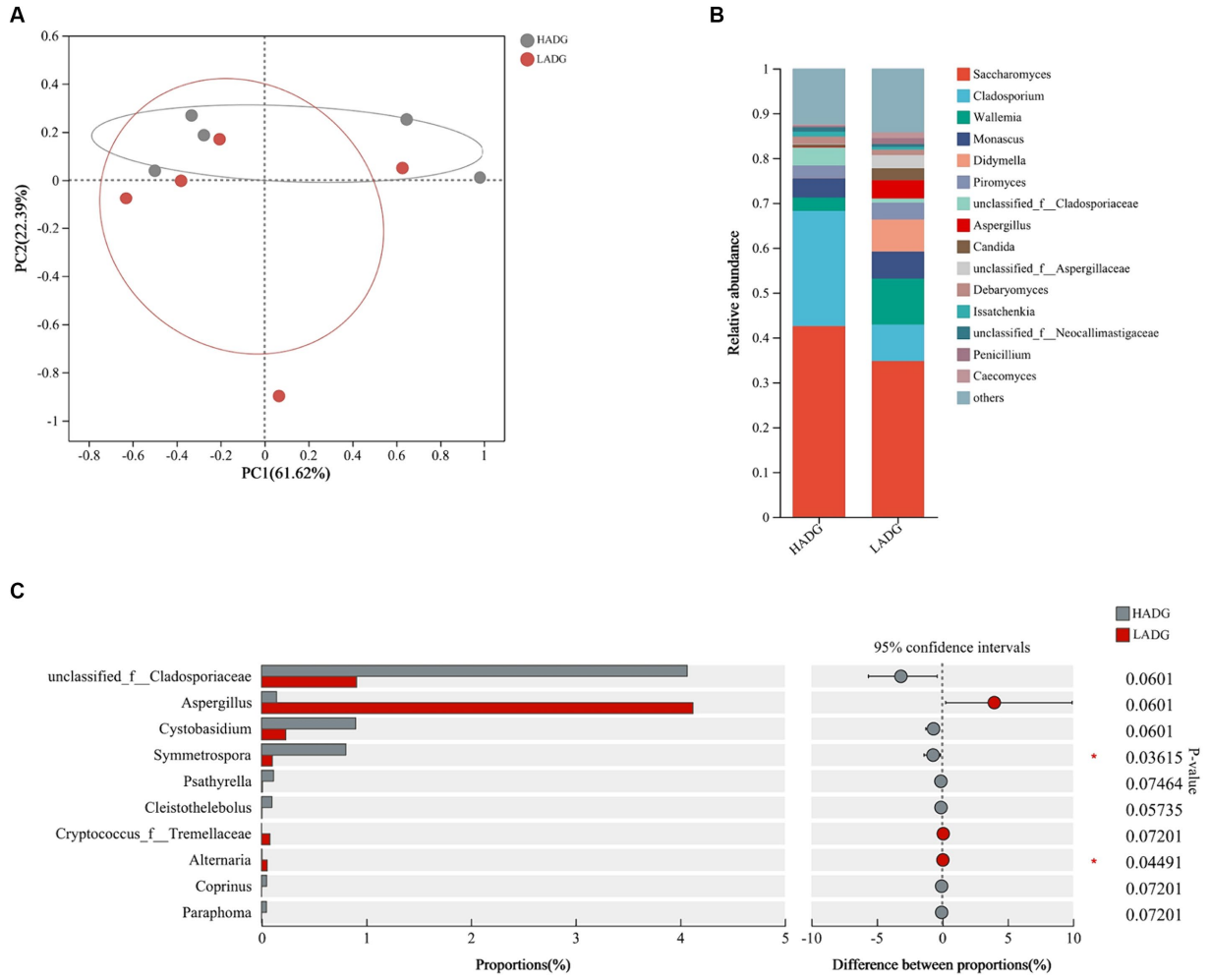

FIGURE 4
Principal coordinate analysis (PCoA) of fungal compositional profiles of rumen fluid samples between LADG and HADG goats, based on weighted UniFrac distances **(A)**. Abundant genera in the rumen fungi of LADG or HADG goats **(B)**. Differential enrichment of fungus genera of rumen epithelium samples **(C)** between LADG and HADG goats, based on Wilcoxon rank-sum test. Data are shown as means. $n = 5$ per group. LADG, low average daily gain goats; HADG, high average daily gain goats.

and *Cystobasidium* ($p < 0.05$) showed positive correlations with the relative expressions of *Claudin-1*. The relative of fungal genus *Issatchenkia* were positively ($p < 0.01$), and *Pseudopithomyces* were negatively ($p < 0.01$) associated with rumen acetate concentration.

Discussion

We observed distinct rumen fermentation patterns between LADG and HADG goats, as reflected by lower rumen propionate and NH_3-N concentrations in LADG goats. Propionate, a crucial precursor for gluconeogenesis in ruminants, is known to consume hydrogen and contribute to higher energy utilization efficiency and reduced methane formation in the rumen (Moss et al., 2000; Goopy et al., 2011). Shabat et al. (2016) further demonstrated that efficient ruminants exhibit higher ruminal propionate concentrations. Moreover, the tendency of higher rumen NH_3-N concentration observed in HADG goats may favor microbial protein production. These findings suggest that the rumen microbiota of HADG goats likely had higher fermentation efficiency, supporting the higher ADG of these goats compared with LADG goats.

While most studies have focused on the rumen fluid associated bacteria, it is crucial to acknowledge the distinct microbiota residing in the rumen epithelium (Pei et al., 2010). Malmuthuge et al. (2019) emphasized the inadequacy of studies only based only on rumen contents in capturing the complete rumen microbiome. In our current study, alpha diversity analysis revealed higher bacterial diversity and richness in rumen epithelium compared to rumen fluid. Notably, *Butyrivibrio* and *Prevotellaceae* UCG-001 were predominant in rumen epithelium, contrasting with *Prevotella* and norank_f_F082, which dominated the rumen fluid. However, it is worth noting that diversity indices were reported to be higher in rumen digesta than in mucosal tissue in pre-weaning calves (Malmuthuge et al., 2014), likely due to the differences in growth stage and diet between weaned and pre-weaned ruminants.

The higher bacterial diversity and richness imply a more intricate microbial population and complex host-bacteria interactions within

10.3389/fmicb.2024.1445223

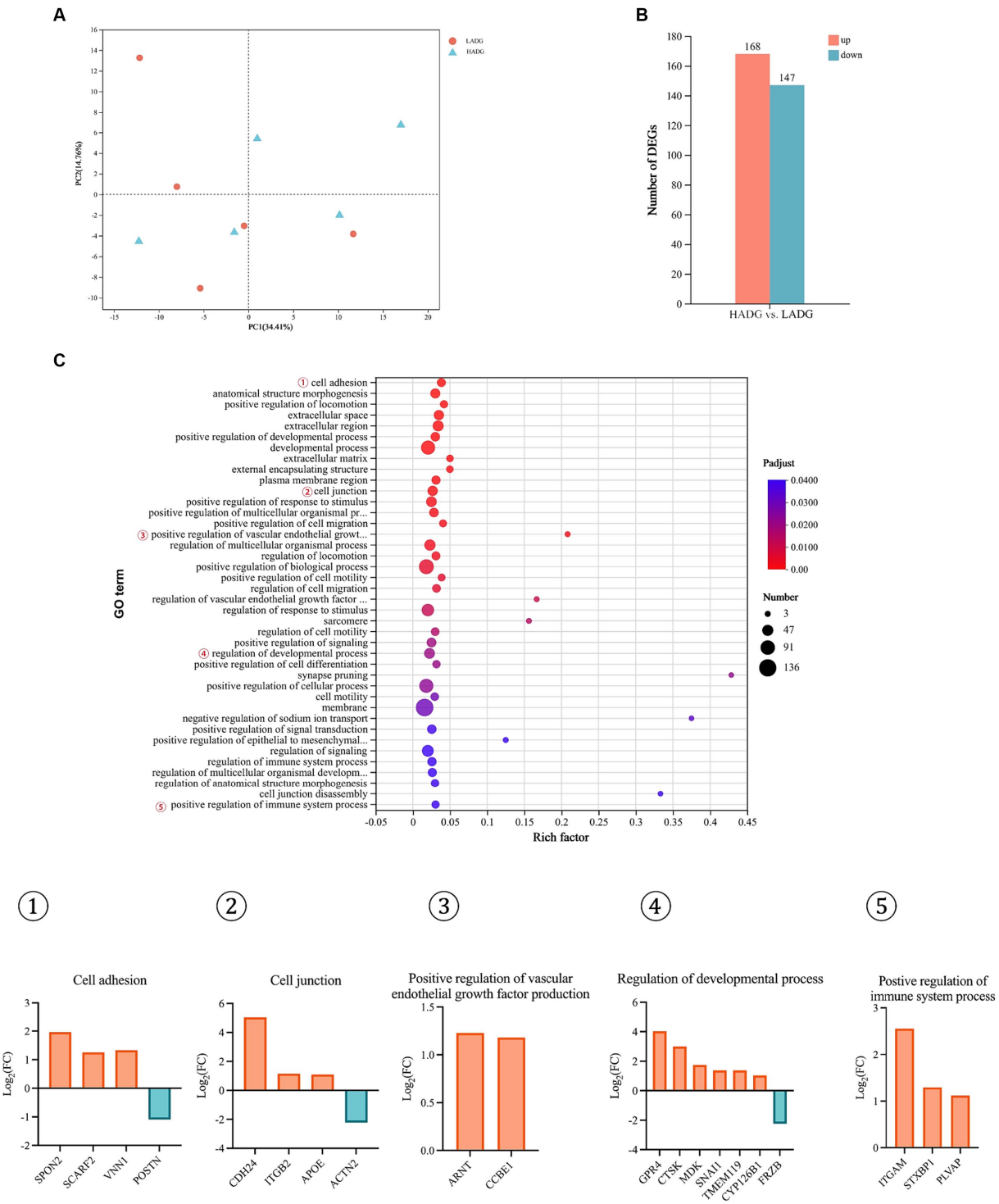

FIGURE 5
RNA-seq analysis of the rumen epithelium of HADG and LADG goats. Principal component analysis (PCA) of gene expressions in rumen epithelium between LADG and HADG goats **(A)**. The number of differentially expressed genes (DEGs) between HADG and LADG goats **(B)**. The GO pathways significantly enriched in the DEGs in rumen epithelium between LADG and HADG goats **(C)**. *n* = 5 per group. LADG, low average daily gain goats; HADG, high average daily gain goats.

the rumen epithelium. Previous studies have highlighted the involvement of ruminal epithelium bacteria in various crucial processes such as oxygen scavenging, tissue recycling, urea digestion, and anatomic and functional development of rumen (Cheng et al., 1979; Jiao et al., 2015). In our study, we observed that LADG goats had higher abundances of the genera U29-B03 and *Quinella* in the rumen epithelium compared to HADG goats. While U29-B03, a member of the *Rikenellaceae* family, has been reported to positively influence SCFAs production (Du et al., 2021), it is worth noting that Wang et al. (2023) found an unclassified *Rikenellaceae* to be positively correlated

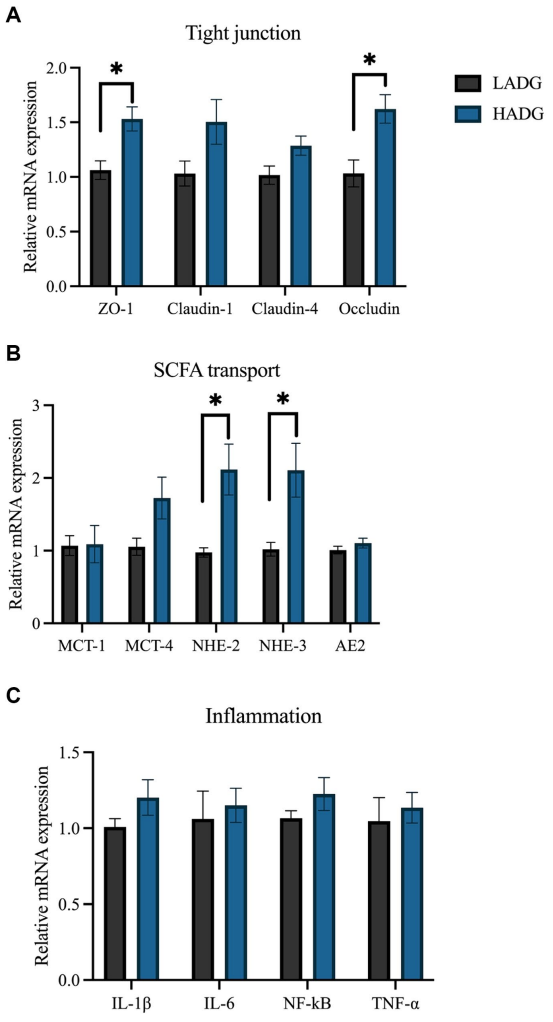

FIGURE 6
RT-PCR analyses of the relative mRNA expression of genes associated with tight junction **(A)**, short-chain fatty acids (SCFAs) transport **(B)**, and inflammation **(C)**. The values represent the mean ± SD ($n = 5$ per group). *$p < 0.05$.

with the acetate levels but negatively correlated with growth performance traits in dairy goats. Additionally, Yi et al. (2022) reported a negative correlation between *Quinella* abundance and propionate concentration. When enriched, *Quinella* cells, were found to predominantly ferment glucose into lactate, with minimal production of acetate, propionate, and CO_2 (Brough et al., 1970). Furthermore, genera U29-B03 and *Quinella* abundances were higher in the rumen fluid of LADG goats compared with HADG goats in the current study. Thus, these findings suggest that the genera U29-B03 and *Quinella* may be the key bacteria influencing the fermentation pattern, which could partly explain the lower propionate concentration observed in LADG goats.

The genus *Desulfovibrio* comprises the predominant sulfate-reducing bacteria in the rumen (Drewnoski et al., 2014; Zhao et al., 2020). Hydrogen sulfide gas (H_2S) is the principal terminal metabolite produced by *Desulfovibrio* via the dissimilatory sulfate reduction pathway (Rey et al., 2013). In our study, the abundance of *Desulfovibrio* was found to be higher in both the rumen epithelium and fluid in LADG goats compared with HADG goats. Although the relationship between ruminal *Desulfovibrio* and the production performance of ruminants remains unclear, overgrowth of *Desulfovibrio* is known to correlate with several human intestinal and extra-intestinal diseases (Singh et al., 2023). Wu et al. (2021) found that a high sulfur diet increases the ruminal abundance of *Desulfovibrio* and compromises the integrity and barrier function of the rumen epithelium. According to the Spearman correlation analysis, the abundance of *Desulfovibrio* was negatively correlated with ruminal propionate and NH_3-N concentrations, as well as with the expressions of epithelial tight junction-related genes. Based on these findings, we speculated that *Desulfovibrio* may play a critical role in influencing the growth performance of LADG goats, but further investigations are warranted to clarify the ecological functions of *Desulfovibrio* in the rumen.

In our study, we observed lower abundances of the genus *Alloprevotella* in the rumen fluid and several members of family *Lachnospiraceae* (e.g., *Lachnospiraceae*_ND3007_group and *Lachnospiraceae*_UCG-009) in the rumen epithelium of LADG goats compared with HADG goats. *Alloprevotella,* belonging to the family *Prevotellaceae,* has the capacity to produce moderate amounts of acetate and significant amounts of succinic acid (Downes et al., 2013). Our findings revealed a positive correlation between propionate concentration in the rumen and *Alloprevotella*, consistent with previous research by Fan et al. (2020). Furthermore, Xie et al. (2022) proposed that species within the *Lachnospiraceae* family may play a key role in carbohydrate metabolism and influence feed efficiency in dairy cows. In our study, genera within *Lachnospiraceae* showed positive correlation with ADG, ruminal butyrate concentration, and the expression of genes related to epithelial tight junction. These results suggest that *Alloprevotella* and *Lachnospiraceae* could potentially serve as probiotics, enhancing fermentation efficiency and promoting host health.

We further explored the differences in fungal composition to gain a comprehensive understanding of the rumen microbiota between LADG and HADG goats. We observed a lower abundance of genus *Symmetrospora* and a tendency towards higher abundances of the genera unclassified_f_*Cladosporiaceae* and *Aspergillus* in LADG goats. *Symmetrospora foliicola* has previously been associated with body weight in lambs at 90 days of age (Yin et al., 2023). Moreover, several mycotoxins, such as aflatoxins and ochratoxin A, can be produced by *Aspergillus* fungi and may disrupt ruminal functions (Loh et al., 2020). We also observed a negative correlation between the abundance of *Aspergillus*and and the mRNA expression of *Claudin-4*, suggesting that *Aspergillus* may impair the integrity of the ruminal barrier.

The rumen epithelium serves as a critical site for host-bacteria interactions, acting as the first line of defense against pathogens and facilitating nutrient uptake to support the development and growth of host (Petri et al., 2018). Transcriptome analysis in our study revealed differential expression of 415 genes between LADG and HADG goats, with enrichment in cell junction (*CDH24*, *ITGB2*, *APOE*, and *ACTN2*), cell adhesion (*SPON2*, *SCARF2*, *VNN1*, and *POSTN*), and others. The tight junction barrier of rumen epithelium plays a pivotal role in preventing microbial invasion and the entry of harmful substances, which is crucial for the growth and health of ruminants (Aschenbach et al., 2019). Our findings indicated lower expression levels of *CDH24, ZO-1,* and *Occludin* in the rumen epithelium of LADG goats. Additionally, *PLVAP* was demonstrated to play a critical role in endothelial barrier function and intestinal homeostasis (Stan et al., 2012). Consistent with our results, studies on monogastric animals have shown lower expression of tight junction proteins in

10.3389/fmicb.2024.1445223

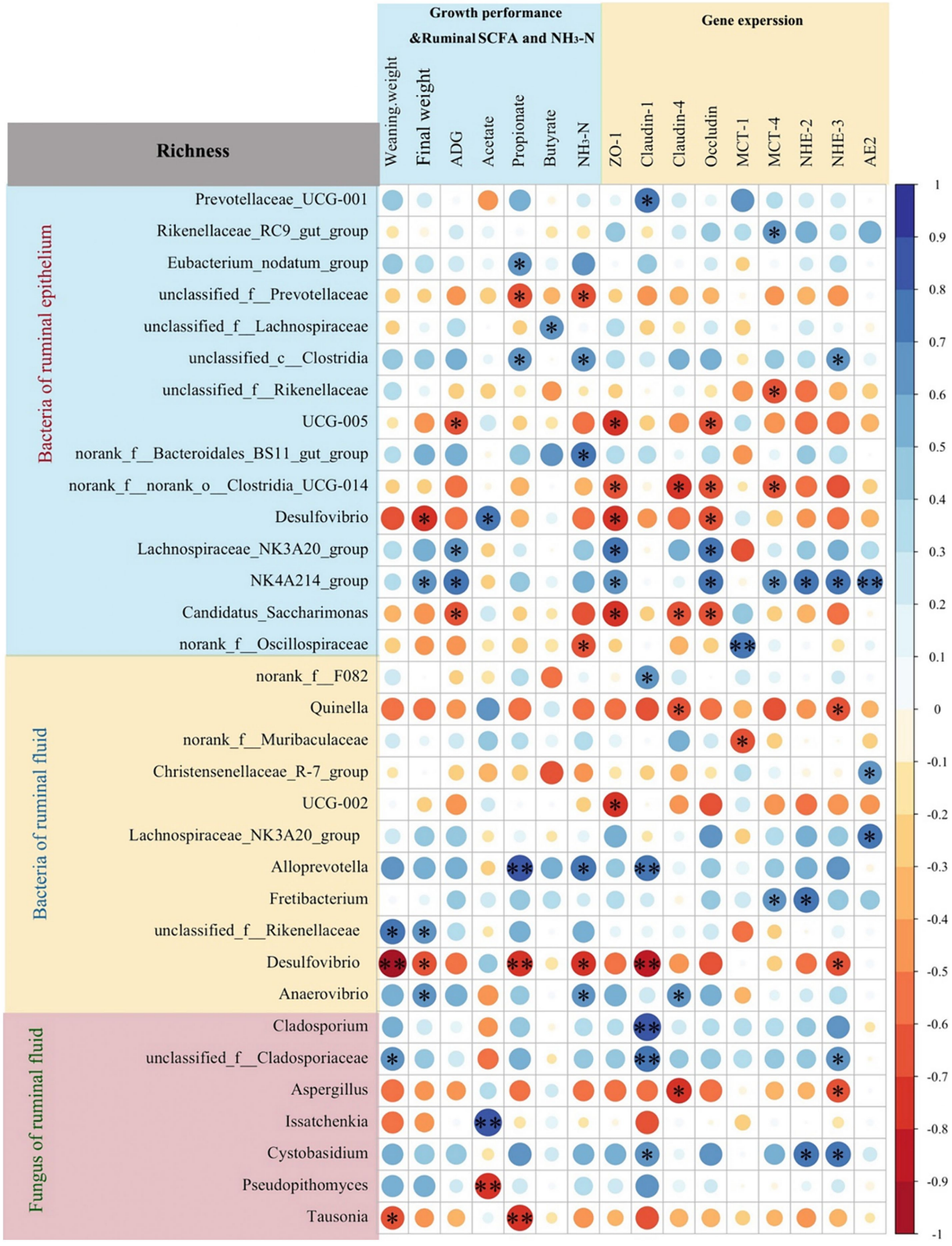

FIGURE 7
Spearman correlation analysis between rumen microbiota richness (fungi and bacteria of rumen fluid, and bacteria of rumen epithelium) and growth performance, ruminal short-chain fatty acids (SCFAs) and NH3-N concentrations, or gene expression levels. *$p<0.05$, **$p<0.01$.

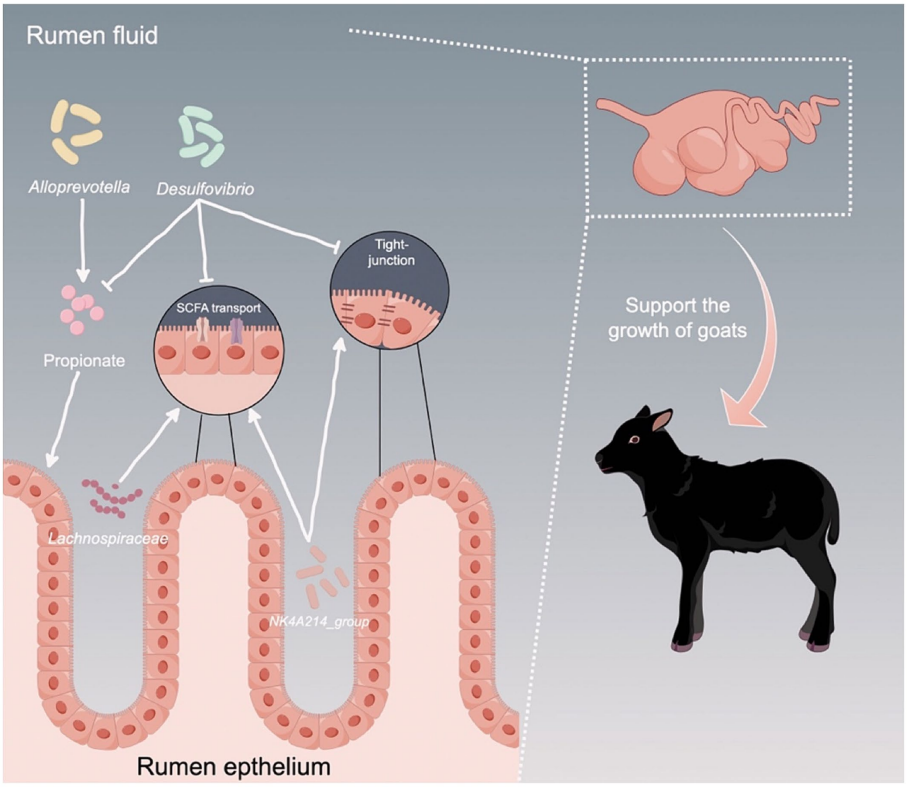

FIGURE 8
Proposed model of the interactions between ruminal microbiota and the host to support the growth of young ruminants. Arrows indicates upregulation, while T bars indicate downregulation.

low-birth-weight piglets (Huang et al., 2021; Wang et al., 2023). Furthermore, several bacteria inhabiting the rumen epithelium were significantly associated with the mRNA expression of *ZO-1* and *Occludin* in our study, suggesting that these bacteria may influence the growth performance by regulating the rumen epithelial barrier.

In the current study, the transcriptome analysis showed that cell adhesion related genes, such as *SPON2*, *VNN1*, and *CTSK*, were upregulated in HADG goats. The *SPON2* encodes mind in, which binds to bacteria and their components, acting as an opsonin (He et al., 2004). *VNN1*, which encodes pantetheinase, is involved in coenzyme A metabolism, lipid metabolism, and energy production (Bartucci et al., 2019). Salzano et al. (2023) suggested that the increased *VNN1* expression in rumen epithelium of buffaloes fed a green feed diet was associated with the anti-inflammatory activities. Moreover, the gene *CTSK*, involved in the regulation of developmental processes, has been shown to maintain the normal composition of intestinal microbiota (Sina et al., 2013). However, the functions of these DEGs in ruminants are not well understood, and further research is needed to confirm these findings.

In our study, the mRNA expressions of *NHE-2* and *NHE-3* were found to be higher in HADG goats. The Na^+/H^+ exchanger (NHE) proteins regulate the intracellular pH of rumen epithelium by transporting H^+ to the lumen or extracellular space and taking up Na^+ into epithelial cells (Schlau et al., 2012). Increased NHE activities are known to lower the local pH near epithelial cells, thereby enhancing the uptake of the undissociated form of SCFAs via simple diffusion (Graham et al., 2007). In addition, the presence of the genus *Oscillospiraceae* NK4A214 group in the rumen epithelium was positively associated with the relative expressions of *MCT-4*, *NHE-2*, *NHE-3*, and *AE2*. Previously classified in the family *Ruminococcaceae*, *Oscillospiraceae* NK4A214 group has been linked to improving growth and lactation performance in ruminants (Tong et al., 2018; Huang et al., 2021; Wang et al., 2023). Consequently, *Oscillospiraceae* NK4A214 group could serve as a potential probiotic to enhance growth or production by mediating SCFAs transport-related genes in the rumen epithelium. However, *Oscillospiraceae* NK4A214 group remains uncultured, and its exact mechanism of action in rumen remains unclear, warranting further investigation.

Conclusion

In summary, our study reveals that HADG goats exhibit higher ruminal fermentation efficiency, improved rumen epithelial barrier functions, and enhanced SCFAs transport, all of which support the development and growth of goats. These differences can be attributed to the rumen microbiota, particularly to the rumen epithelium bacteria (Figure 8). Thus, our findings offer a deeper understanding of the association between rumen microbiota and growth performance, and identify several potential microbial targets for the development of novel intervention strategies to improve the growth performance of young ruminants.

Data availability statement

The raw sequencing reads of the rumen microbiota, along with the RNA sequencing data, were deposited into the NCBI Sequence Read

Archive (SRA) database and NCBI's Gene Expression Omnibus under the accession numbers PRJNA1099693 and PRJNA1101717, respectively.

Ethics statement

The animal study was approved by Institutional Animal Care and Use Committee of Southwest University. The study was conducted in accordance with the local legislation and institutional requirements.

Author contributions

JC: Conceptualization, Funding acquisition, Writing – original draft, Writing – review & editing. XZ: Methodology, Writing – original draft, Writing – review & editing. XC: Methodology, Writing – original draft. BW: Methodology, Writing – original draft. YF: Funding acquisition, Investigation, Resources, Writing – original draft. SS: Investigation, Resources, Writing – original draft. DG: Investigation, Resources, Writing – original draft. DH: Investigation, Resources, Writing – review & editing. YS: Investigation, Resources, Writing – original draft. XD: Investigation, Methodology, Writing – original draft. YZ: Conceptualization, Funding acquisition, Writing – review & editing. ZZ: Conceptualization, Funding acquisition, Writing – review & editing.

Funding

The author(s) declare that financial support was received for the research, authorship, and/or publication of this article. This study was supported by the National Natural Science Foundation of China (32202686), Key project of Chong Qing Natural Science Foundation (grant number. cstc2020jcyj-zdxmX0005), The Strategic Collaboration Project jointly funded by Chongqing Municipal People's Government and Chinese Academy of Agricultural Sciences, and Chongqing Municipal Training Program of Innovation and Entrepreneurship for Undergraduates (grant number X202310635055).

Acknowledgments

The authors appreciated the Figdraw (www.figdraw.com) for their assistance in drawing figure.

Conflict of interest

DG and DH were employed by the Tengda Animal Husbandry Co., Ltd.

The remaining authors declare that the research was conducted in the absence of any commercial or financial relationships that could be construed as a potential conflict of interest.

Publisher's note

Supplementary material

The Supplementary material for this article can be found online at: https://www.frontiersin.org/articles/10.3389/fmicb.2024.1445223/full#supplementary-material

References

Aschenbach, J. R., Zebeli, Q., Patra, A. K., Greco, G., Amasheh, S., and Penner, G. B. (2019). Symposium review: the importance of the ruminal epithelial barrier for a healthy and productive cow. *J. Dairy Sci.* 102, 1866–1882. doi: 10.3168/jds.2018-15243

Bartucci, R., Salvati, A., Olinga, P., and Boersma, Y. L. (2019). Vanin 1: its physiological function and role in diseases. *Int. J. Mol. Sci.* 20:3891. doi: 10.3390/ijms20163891

Bhagat, N. R., Kumar, S., Kumari, R., and Bharti, V. K. (2023). A review on rumen anaerobic fungi: current understanding on carbohydrate fermentation and roughages digestion in ruminants. *Appl. Biochem. Microbiol.* 59, 231–249. doi: 10.1134/S0003683823030043

Brough, B. E., Reid, T., and Howard, B. (1970). The biochemistry of the rumen bacterium" Quin's oval" —part 1. *N. Z. J. Sci.* 13, 570–575.

Cheng, K., McCowan, R., and Costerton, J. (1979). Adherent epithelial bacteria in ruminants and their roles in digestive tract function. *Am. J. Clin. Nutr.* 32, 139–148. doi: 10.1093/ajcn/32.1.139

Costa, A., Boselli, C., and De Marchi, M. (2021). Effect of body weight and growth in early life on the reproductive performances of Holstein heifers. *Agriculture* 11:159. doi: 10.3390/agriculture11020159

Downes, J., Dewhirst, F. E., Tanner, A. C., and Wade, W. G. (2013). Description of Alloprevotella rava gen. Nov., sp. nov., isolated from the human oral cavity, and reclassification of *Prevotella tannerae* Moore et al. 1994 as Alloprevotella tannerae gen. Nov., comb. nov. *Int. J. Syst. Evol. Microbiol.* 63, 1214–1218. doi: 10.1099/ijs.0.041376-0

Drewnoski, M., Pogge, D., and Hansen, S. (2014). High-sulfur in beef cattle diets: a review. *J. Anim. Sci.* 92, 3763–3780. doi: 10.2527/jas.2013-7242

Du, M., Yang, C., Liang, Z., Zhang, J., Yang, Y., Ahmad, A. A., et al. (2021). Dietary energy levels affect carbohydrate metabolism-related bacteria and improve meat quality in the longissimus thoracis muscle of yak (*Bos grunniens*). *Front. Vet. Sci.* 8:718036. doi: 10.3389/fvets.2021.718036

Fan, Q., Wanapat, M., Yan, T., and Hou, F. (2020). Altitude influences microbial diversity and herbage fermentation in the rumen of yaks. *BMC Microbiol.* 20, 1–13. doi: 10.1186/s12866-020-02054-5

Fonseca, P., Lam, S., Chen, Y., Waters, S., Guan, L., and Cánovas, A. (2023). Multi-breed host rumen epithelium transcriptome and microbiome associations and their relationship with beef cattle feed efficiency. *Sci. Rep.* 13:16209. doi: 10.1038/s41598-023-43097-8

Gelsinger, S., Heinrichs, A., and Jones, C. (2016). A meta-analysis of the effects of preweaned calf nutrition and growth on first-lactation performance. *J. Dairy Sci.* 99, 6206–6214. doi: 10.3168/jds.2015-10744

Goopy, J. P., Woodgate, R., Donaldson, A., Robinson, D. L., and Hegarty, R. (2011). Validation of a short-term methane measurement using portable static chambers to estimate daily methane production in sheep. *Anim. Feed. Sci. Tech.* 166, 219–226. doi: 10.1016/j.anifeedsci.2011.04.012

Graham, C., Gatherar, I., Haslam, I., Glanville, M., and Simmons, N. L. (2007). Expression and localization of monocarboxylate transporters and sodium/proton exchangers in bovine rumen epithelium. *Am. J. Physiol. Regul. Integr. Comp. Physiol.* 292, R997–R1007. doi: 10.1152/ajpregu.00343.2006

He, Y. W., Li, H., Zhang, J., Hsu, C. L., Lin, E., Zhang, N., et al. (2004). The extracellular matrix protein mindin is a pattern-recognition molecule for microbial pathogens. *Nat. Immunol.* 5, 88–97. doi: 10.1038/ni1021

Huang, C., Ge, F., Yao, X., Guo, X., Bao, P., Ma, X., et al. (2021). Microbiome and metabolomics reveal the effects of different feeding systems on the growth and ruminal development of yaks. *Front. Microbiol.* 12:682989. doi: 10.3389/fmicb.2021.682989

Jiao, J., Huang, J., Zhou, C., and Tan, Z. (2015). Taxonomic identification of ruminal epithelial bacterial diversity during rumen development in goats. *Appl. Environ. Microb.* 81, 3502–3509. doi: 10.1128/AEM.00203-15

Jize, Z., Zhuoga, D., Xiaoqing, Z., Na, T., Jiacuo, G., Cuicheng, L., et al. (2022). Different feeding strategies can affect growth performance and rumen functions in Gangba sheep as revealed by integrated transcriptome and microbiome analyses. *Front. Microbiol.* 13:908326. doi: 10.3389/fmicb.2022.908326

Kamra, D. N. (2005). Rumen microbial ecosystem. *Curr. Sci. India* 10, 124–135.

Li, W., Gelsinger, S., Edwards, A., Riehle, C., and Koch, D. (2019). Transcriptome analysis of rumen epithelium and meta-transcriptome analysis of rumen epimural microbial community in young calves with feed induced acidosis. *Sci. Rep.* 9:4744. doi: 10.1038/s41598-019-40375-2

Liu, J. H., Zhang, M. L., Zhang, R. Y., Zhu, W. Y., and Mao, S. Y. (2016). Comparative studies of the composition of bacterial microbiota associated with the ruminal content, ruminal epithelium and in the faeces of lactating dairy cows. *Microb. Biotechnol.* 9, 257–268. doi: 10.1111/1751-7915.12345

Loh, Z. H., Ouwerkerk, D., Klieve, A. V., Hungerford, N. L., and Fletcher, M. T. (2020). Toxin degradation by rumen microorganisms: a review. *Toxins* 12:664. doi: 10.3390/toxins12100664

Malmuthuge, N., Griebel, P. J., and Guan, L. L. (2014). Taxonomic identification of commensal bacteria associated with the mucosa and digesta throughout the gastrointestinal tracts of preweaned calves. *Appl. Environ. Microb.* 80, 2021–2028. doi: 10.1128/AEM.03864-13

Malmuthuge, N., Liang, G., and Guan, L. L. (2019). Regulation of rumen development in neonatal ruminants through microbial metagenomes and host transcriptomes. *Genome Biol.* 20, 1–16. doi: 10.1186/s13059-019-1786-0

Moss, A. R., Jouany, J. P., and Newbold, J. (2000). Methane production by ruminants: its contribution to global warming. *Ann. Zootech.* 49, 231–253. doi: 10.2527/1995.7382483x

Pei, C. X., Mao, S. Y., Cheng, Y. F., and Zhu, W. Y. (2010). Diversity, abundance and novel 16S rRNA gene sequences of methanogens in rumen liquid, solid and epithelium fractions of Jinnan cattle. *Animal* 4, 20–29. doi: 10.1017/S1751731109990681

Petri, R., Kleefisch, M., Metzler-Zebeli, B., Zebeli, Q., and Klevenhusen, F. (2018). Changes in the rumen epithelial microbiota of cattle and host gene expression in response to alterations in dietary carbohydrate composition. *Appl. Environ. Microb.* 84, e00384–e00318. doi: 10.1128/AEM.00384-18

Rey, F. E., Gonzalez, M. D., Cheng, J., Wu, M., Ahern, P. P., and Gordon, J. I. (2013). Metabolic niche of a prominent sulfate-reducing human gut bacterium. *Proc. Natl. Acad. Sci.* 110, 13582–13587. doi: 10.1073/pnas.1312524110

Salzano, A., Fioriniello, S., D'Onofrio, N., Balestrieri, M. L., Aiese Cigliano, R., Neglia, G., et al. (2023). Transcriptomic profiles of the ruminal wall in Italian Mediterranean dairy buffaloes fed green forage. *BMC Genomics* 24:133. doi: 10.1186/s12864-023-09215-6

Schlau, N., Guan, L., and Oba, M. (2012). The relationship between rumen acidosis resistance and expression of genes involved in regulation of intracellular pH and butyrate metabolism of ruminal epithelial cells in steers. *J. Dairy Sci.* 95, 5866–5875. doi: 10.3168/jds.2011-5167

Schubach, K. M., Cooke, R. F., Brandão, A. P., Schumaher, T. F., Pohler, K. G., Bohnert, D. W., et al. (2019). Impacts of postweaning growth rate of replacement beef heifers on their reproductive development and productivity as primiparous cows. *J. Anim. Sci.* 97, 4171–4181. doi: 10.1093/jas/skz262

Shabat, S. K. B., Sasson, G., Doron-Faigenboim, A., Durman, T., Yaacoby, S., Berg Miller, M. E., et al. (2016). Specific microbiome-dependent mechanisms underlie the energy harvest efficiency of ruminants. *ISME J.* 10, 2958–2972. doi: 10.1038/ismej.2016.62

Sina, C., Lipinski, S., Gavrilova, O., Aden, K., Rehman, A., Till, A., et al. (2013). Extracellular cathepsin K exerts antimicrobial activity and is protective against chronic intestinal inflammation in mice. *Gut* 62, 520–530. doi: 10.1136/gutjnl-2011-300076

Singh, S. B., Carroll-Portillo, A., and Lin, H. C. (2023). Desulfovibrio in the gut: the enemy within? *Microorganisms* 11:1772. doi: 10.3390/microorganisms11071772

Soberon, F., and Van Amburgh, M. (2013). Lactation biology symposium: the effect of nutrient intake from milk or milk replacer of preweaned dairy calves on lactation milk yield as adults: a meta-analysis of current data. *J. Anim. Sci.* 91, 706–712. doi: 10.2527/jas.2012-5834

Stan, R. V., Tse, D., Deharvengt, S. J., Smits, N. C., Xu, Y., Luciano, M. R., et al. (2012). The diaphragms of fenestrated endothelia: gatekeepers of vascular permeability and blood composition. *Dev. Cell* 23, 1203–1218. doi: 10.1016/j.devcel.2012.11.003

Tong, J., Zhang, H., Yang, D., Zhang, Y., Xiong, B., and Jiang, L. (2018). Illumina sequencing analysis of the ruminal microbiota in high-yield and low-yield lactating dairy cows. *PLoS One* 13:e0198225. doi: 10.1371/journal.pone.0198225

Wang, D., Chen, L., Tang, G., Yu, J., Chen, J., Li, Z., et al. (2023). Multi-omics revealed the long-term effect of ruminal keystone bacteria and the microbial metabolome on lactation performance in adult dairy goats. *Microbiome* 11:215. doi: 10.1186/s40168-023-01652-5

Wu, H., Li, Y., Meng, Q., and Zhou, Z. (2021). Effect of high sulfur diet on rumen fermentation, microflora, and epithelial barrier function in steers. *Animals* 11:2545. doi: 10.3390/ani11092545

Xie, Y., Sun, H., Xue, M., and Liu, J. (2022). Metagenomics reveals differences in microbial composition and metabolic functions in the rumen of dairy cows with different residual feed intake. *Anim. Microbiome* 4:19. doi: 10.1186/s42523-022-00170-3

Yi, S., Dai, D., Wu, H., Chai, S., Liu, S., Meng, Q., et al. (2022). Dietary concentrate-to-forage ratio affects rumen bacterial community composition and metabolome of yaks. *Front. Nutr.* 9:927206. doi: 10.3389/fnut.2022.927206

Yin, X., Duan, C., Ji, S., Tian, P., Ju, S., Yan, H., et al. (2023). Average daily gain in lambs weaned at 60 days of age is correlated with rumen and rectum microbiota. *Microorganisms* 11:348. doi: 10.3390/microorganisms11020348

Zhao, Y., Xie, B., Gao, J., and Zhao, G. (2020). Dietary supplementation with sodium sulfate improves rumen fermentation, fiber digestibility, and the plasma metabolome through modulation of rumen bacterial communities in steers. *Appl. Environ. Microb.* 86, e01412–e01420. doi: 10.1128/AEM.01412-20

frontiers | Frontiers in Microbiology

TYPE Original Research
PUBLISHED 17 September 2024
DOI 10.3389/fmicb.2024.1442077

OPEN ACCESS

EDITED BY
Gabriele Brecchia,
University of Milan, Italy

REVIEWED BY
Francesca Romana Massacci,
Experimental Institute of Zooprophylaxis of Umbria and Marche (IZSUM), Italy
Yu Pi,
Chinese Academy of Agricultural Sciences, China

*CORRESPONDENCE
Rui Li
✉ lirui181000@163.com

RECEIVED 01 June 2024
ACCEPTED 16 August 2024
PUBLISHED 17 September 2024

CITATION
Feng G, Deng M, Li R, Hou G, Ouyang Q, Jiang X, Liu X, Tang H, Chen F, Pu S, Wan D and Yin Y (2024) Gastrointestinal microbiota and metabolites responses to dietary cereal grains in an adult pig model. *Front. Microbiol.* 15:1442077. doi: 10.3389/fmicb.2024.1442077

Gastrointestinal microbiota and metabolites responses to dietary cereal grains in an adult pig model

Ganyi Feng[1], Menglong Deng[2], Rui Li[1]*, Gaifeng Hou[1], Qing Ouyang[2], Xianji Jiang[1,2], Xiaojie Liu[1,2], Hui Tang[1,2], Fengming Chen[3], Shihua Pu[4,5], Dan Wan[1] and Yulong Yin[1]

[1]Key Laboratory of Agro-Ecological Processes in Subtropical Region, Hunan Provincial Key Laboratory of Animal Nutritional Physiology and Metabolic Process, Hunan Research Center of Livestock and Poultry Sciences, South Central Experimental Station of Animal Nutrition and Feed Science in the Ministry of Agriculture, National Engineering Laboratory for Poultry Breeding Pollution Control and Resource Technology, Institute of Subtropical Agriculture, Chinese Academy of Sciences, Changsha, China, [2]College of Animal Science and Technology, Hunan Co-Innovation Center of Animal Production Safety, Hunan Agricultural University, Changsha, China, [3]Hunan Provincial Key Laboratory of the TCM Agricultural Biogenomics, Changsha Medical University, Changsha, China, [4]Chongqing Academy of Animal Science, Rongchang, Chongqing, China, [5]National Center of Technology Innovation for Pigs, Chongqing, China

Corn (C), wheat (W), and paddy rice (PR) are important energy sources and are commonly used in feed production for swine. This study mainly focuses on the variation and regularities of microbiota and metabolites in the gastrointestinal tract (GIT) of pigs in response to C, W, and PR. A total of 18 pigs were allotted into three dietary groups with six replicated pigs and received diets containing C, W, or PR as the sole energy source, respectively. The results showed that digestive parts significantly affected the diversity of microbial communities. Cereal grain sources significantly influenced the β-diversity of microbial communities in the colon and rectum. Campylobacterota and Proteobacteria are mainly distributed in the duodenum, *Lactobacillus* in the jejunum, and Bacteroidota in the colon and rectum. The W diet increased the Bacteroidota, Spirochaetota, and *Prevotellaceae_NK3B31_group* abundances and showed the highest concentrations of all short-chain fatty acids (SCFAs) in the hindgut. Fibrobacterota, Bacteroidota, Spirochaetota, *Prevotellaceae_NK3B31_group*, *Prevotella*, and *Treponema* in the colon or rectum were positively correlated with acetate, propionate, butyrate, and total SCFAs. These findings suggested that aerobic bacteria and facultative anaerobes in the foregut will gradually be replaced by anaerobes in the hindgut. The W diet had the best fermentability and was beneficial to the colonization of microbial communities that mainly used carbohydrates. The hindgut flora of the PR diet group may be more balanced with fewer potential pathogenic bacteria. Many microbial communities have been identified to contribute positively to the SCFA production of the hindgut. Collectively, our study revealed the spatial variation regularities of GIT microbial communities in an adult pig model and provided new insights into GIT microbiota and responses of metabolites to cereal grain diets.

KEYWORDS

corn, wheat, paddy rice, GIT, microbial community, SCFAs

1 Introduction

Cereal grains are the most important energy component in the diet of monogastric animals and are widely used in the feed industry. Cereal grains contain easily digestible starch and high-quality plant-based protein (Singh et al., 2010; Gidley, 2023). Although resistant starch (RS) and dietary fibers (DFs) in cereal grains cannot be digested and absorbed by the stomach and small intestine, they will be fermented by microorganisms in the large intestine to produce SCFAs (Jaworski and Stein, 2015; Rodehutscord et al., 2016; Holscher, 2017; Walsh et al., 2022; Gidley, 2023). The physicochemical properties and chemical composition of different cereal grains vary considerably, especially the composition of DF (Cervantes-Pahm et al., 2014; Tan et al., 2021). Fermentable DF from different cereal grains may regulate the microbial community composition in the host GIT and affect the metabolism of SCFAs in the hindgut (O'Connell et al., 2005; Wong et al., 2006; Van der Meulen and Jansman, 2010; Liu et al., 2012; Ma et al., 2018; Zhao et al., 2019). A previous study found that a barley-based diet increased the ratio of *Lactobacillus* spp. to *Enterobacteriaceae* in ileal digesta and fecal samples of pigs, while a W-based diet promoted the proliferation of *Roseburia* spp. in the ileum and *Bifidobacterium* spp. in the fecal samples (Weiss et al., 2016). Zhao et al. (2019) reported that different DF influenced the abundances of *Filifactor* and *Intestinibacter* in ileal digesta, as well as *Ruminococcus_1* and *Lachnoclostridium* in the feces of pigs. In addition, the production of SCFAs in ileal digesta and feces was associated with microbial compositions.

The GIT microbiota is a huge, dynamic, and complex ecosystem and plays an important role in nutrient digestion, absorption, and metabolism, as well as in the maintenance of intestinal health (Lallès, 2016; Holman et al., 2017; Tan et al., 2018). Fully understanding the dynamic distribution of the gut microbiota in pigs is essential (Luo et al., 2022). At present, although there are many studies on the composition and distribution of intestinal microbiota in pigs, most of them selected colonic or fecal samples with more abundant microorganisms (O'Hara and Shanahan, 2006; Gao et al., 2019a; Gao et al., 2019b; Li et al., 2019a; Li et al., 2019b; Li et al., 2023). Few studies have focused on the whole-gut microbiota of pigs, which limits a comprehensive understanding of the spatial variation and regularities of the GIT microbiota in swine.

Zhao et al. (2015) highlighted that although the composition and structure of the microbial community become stable when the host is mature, and there are significant similarities between feces and the large intestine microbiome, using fecal samples alone cannot fully represent the microbial profile of the GIT. Therefore, observing the dynamic variation of microorganisms along the GIT is a necessary consideration when studying the interaction between hosts and microorganisms. In recent years, some researchers have explored and summarized the characteristics and dynamic distribution of gut microbiota across different ages and GIT segments of pigs (Zhao et al., 2015; Liu et al., 2019; Luo et al., 2022; Fabà et al., 2024). However, it is worth noting that these studies have selected young pigs (newborn piglets and nursery pigs) as models. There have been no relevant reports on the dynamic distribution of the GIT microbiota in adult pigs (especially for finishing pigs with heavier weight) models, which is not conducive to enriching the scientific community's understanding of the gut microbiome dynamics for swine.

C, W, and PR were the three important food crops in terms of total production around the world (FAOSTAT, 2023). They are also widely used in pig's diets. However, few studies have investigated the effect of these cereal grains on the GIT microbiota and metabolites. Therefore, this study aimed to characterize the microbial composition of adult pigs from the stomach to the rectum and to investigate the effects of C, W, and PR on the composition and SCFA production of the GIT microbiota.

2 Materials and methods

2.1 Animals, diets, and experimental design

In total, 18 pigs (Duroc × Yorkshire × Landrace, initial body weight of 73.58 ± 6.44 kg) fitted with a simple T-cannula in their distal ileum were allotted to three dietary treatments with six replicated pigs (Figure 1). During the 14-day experimental period, pigs were fed diets with C, W, and PR as the sole energy source, respectively (Table 1). Vitamins and minerals were supplemented to meet or exceed the nutrient requirements recommended by the NRC (2012). Pigs were placed in individual metabolism crates (1.4 m × 0.7 m × 0.5 m) and kept in an environmentally controlled room (23 ± 1°C). From days 1 to 14, the daily feeding schedule was divided into two equal meals provided at 0830 and 1730 h, respectively. The daily feeding amount of each pig was fixed at 4% of the average initial weight of pigs (Adeola, 2000). Each pig had free access to water via a nipple drinker.

2.2 Sample collection

From 0800 h on 15th d, all pigs were slaughtered, the GIT was removed immediately, and the stomach (S), duodenum (D), jejunum (J), ileum (I), colon (C), and rectum (R) were carefully identified, separated, and ligated with a thin thread. While ensuring that digesta did not move as much as possible, a scissor was used to cut open each digestive part, and digesta from six digestive parts was collected as much as possible using numbered 50 ml centrifuge tubes or beakers with larger volumes. After stirring evenly with a glass rod, four representative samples of the stomach, duodenal, jejunal, ileal, colonic, and rectal digesta from each pig were collected using a 1.5 ml centrifuge tube. These samples were divided into 18 groups ($n = 6$) according to the corresponding digestive part and dietary treatment. Each group was named according to the form "cereal grain abbreviation_digestive part abbreviation" (e.g., C_S group). These samples were first snap-frozen in liquid nitrogen and stored in a −80°C refrigerator at the end of sampling. One digesta sample per pig from 18 groups was selected for 16S rRNA gene sequence analysis ($n = 108$). One additional digesta sample from each of the ileum, colon, and rectum was selected for SCFA analysis ($n = 54$).

2.3 Chemical composition analysis of experiment diets

The C diet, W diet, and PR diet were finely ground to pass through a 1-mm screen. The dry matter (DM, 930.15), ether extract (EE, 920.39), and ash (942.05) contents of diets were analyzed using the Association

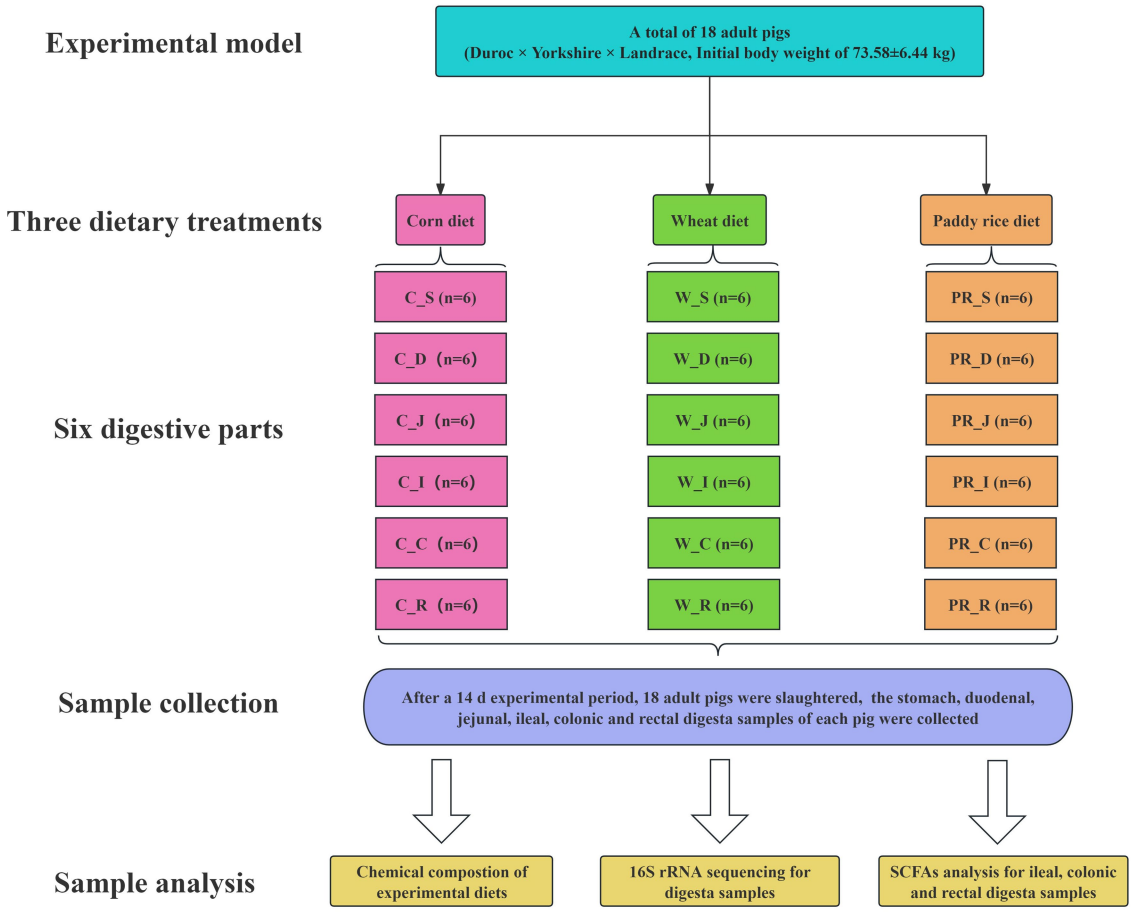

FIGURE 1
Flow diagram of the experimental design. C, corn; W, wheat; PR, paddy rice; S, stomach; D, duodenum; J, jejunum; I, ileum; C, colon; R, rectum.

Official Analytical Chemists (AOAC, 2012). The crude protein (CP) content of diets was determined by the various MAX cube Carbon/Nitrogen/Sulfur Elemental Analyzer (Elementar Analysensysteme GmbH, Frankfurt, Hessian, Germany). The content of gross energy (GE) in diets was determined by an HXR-6000 Oxygen Bomb Automatic Calorimeter (Hunan Huaxing Energy Sources Instrument Co. Ltd., Changsha, China). The contents of crude fiber (*CF*), neutral detergent fiber (NDF), and acid detergent fiber (ADF) were determined using fiber bags and the FT12 automatic fiber analyzer (Gerhardt Analytical Instrument Co., Ltd., Konigswinter, North Rhine-Westphalia, Germany) by the basic procedures of Van Soest et al. (1991). The contents of soluble dietary fiber (SDF) and insoluble dietary fiber (IDF) were analyzed according to the procedure described in a commercial reagent kit (K-TDFR-200A, Megazyme Inc., Wicklow, Ireland). Total starch (TS) was measured according to the AOAC Method 996.11 with the K-TSTA TS assay kit (Megazyme Inc., Wicklow, Ireland).

2.4 SCFA analysis

The SCFA concentrations in the ileal, colonic, and rectal digesta samples were analyzed according to the method described by Wang et al. (2017). Briefly, approximately 150 mg samples were weighed into a 1.5 ml centrifuge tube, then diluted with 450 µl of deionized water, including 1.68 mM heptanoic acid/L as an internal standard (Sigma Chemical Co., St. Louis, MO, USA). The samples were centrifuged at 10,000 rpm for 10 min at 4°C after thoroughly mixing with the OSE-Y50 high-speed grinder (Tiangen Biochemical Technology Co., Ltd., Beijing, China), and the supernatant was all absorbed and filtered with a 0.22 µm membrane. The acetate, propionate, isobutyrate, butyrate, isovalerate, valerate, and total SCFAs were measured and quantified using the 7820A gas chromatography (GC) system (Agilent Technologies, Palo Alto, CA, USA).

2.5 DNA extraction, GIT microbes, and 16S rRNA sequencing

Total microbial genomic DNA in digesta (the stomach, duodenum, jejunum, ileum, colon, and rectum) was extracted using the E.Z.N.A.® Soil DNA Kit (Omega Bio-Tek Inc., Norcross, GA, USA). The quality and concentration of DNA were detected by 1.0% agarose gel electrophoresis and the NanoDrop® ND-2000 spectrophotometer, respectively (Thermo Scientific Inc., Boston, MA, USA). The hypervariable V3–V4 region of the bacterial 16S rRNA gene was amplified with primer pairs 338F (5′-ACTCCTACG

TABLE 1 Ingredient and analyzed chemical compositions of diets (as-fed basis, %).

Items	Corn diet	Wheat diet	Paddy rice diet
Corn	97.00	-	-
Wheat	-	97.00	-
Paddy rice	-	-	97.00
Dicalcium phosphate	1.00	1.00	1.00
Limestone	0.90	0.90	0.90
Sodium chloride	0.30	0.30	0.30
Titanium dioxide	0.30	0.30	0.30
Vitamin and mineral premix[1]	0.50	0.50	0.50
Total	100.00	100.00	100.00
Analyzed composition			
DM	88.53	90.23	88.98
CP	8.44	11.12	7.57
GE, MJ/kg	14.51	13.21	14.51
EE	0.86	1.80	1.89
Ash	3.08	4.42	6.29
NDF	25.21	17.75	22.89
ADF	2.41	3.02	13.93
CF	1.26	1.59	8.24
IDF	8.92	10.21	17.44
SDF	1.16	1.37	0.83
TDF	10.08	11.58	18.27
TS	56.22	46.21	56.88

DM, dry matter; CP, crude protein; GE, gross energy; EE, ether extract; NDF, neutral detergent fiber; ADF, acid detergent fiber; CF, crude fiber; IDF; insoluble dietary fiber; SDF; soluble dietary fiber; TDF, total dietary fiber; TS, total starch.[1]The premix provided the following per kg of diets: Vitamin A 4,200 IU, VD_3 400 IU, VE 36 IU, VK_3 1.2 mg, VB_{12} 23 μg, VB_2 5.63 mg, VB_5 20.5 mg, VB_3 28 mg, Choline chloride 1.00 g, Folic acid 0.8 mg, VB_1 3.4 mg, VB_6 2.7 mg, VB_7 0.18 mg, Mn (as manganese sulfate) 40.0 mg, Fe (as ferrous sulfate) 70.0 mg, Zn (as zinc sulfate) 70.0 mg, Cu (as copper sulfate) 70 mg, I (as potassium iodide) 0.3 mg, and Se (as sodium selenite) 0.3 mg.

GGAGGCAGCAG-3′) and 806R (5′-GGACTACHVGGTWTCTAAT-3′) using the ABI GeneAmp® 9700 PCR thermocycler (Applied Biosystems Inc., Los Angeles, CA, USA; Liu et al., 2016). PCR was carried out in triplicate using 20 μl reactions containing 10 ng of template DNA, 4 μl of 5 × Fast Pfu buffer, 2 μl of dNTPs, 0.8 μl of each primer, 0.4 μl of Fast Pfu polymerase, 0.2 μl of BSA, and 12.6 μl of ddH_2O. The PCR product was extracted from 2% agarose gel, purified using the AxyPrep DNA Gel Extraction Kit (Axygen Biosciences, Union City, CA, USA), and quantified using the Quantus™ fluorometer (Promega Inc., Madison, WI, USA). Purified amplicons were pooled in equimolar amounts and paired-end sequenced on an Illumina MiSeq PE300 platform/NovaSeq PE250 platform (Illumina Inc., San Diego, CA, USA).

2.6 Bioinformatics analysis

Raw sequence data were quality-filtered and merged using Fastp (version 0.19.6) and Flash (version 1.2.11) software, respectively (Magoč and Salzberg, 2011; Chen et al., 2018). The optimized sequences were clustered into operational taxonomic units (OTUs) using Uparse software with a 97% sequence similarity level (Stackebrandt and Goebel, 1994; Edgar, 2013). The number of 16S rRNA gene sequences from each sample was rarefied to 66,859, and the average coverage index of samples was 99.66% after rarefying. OTUs representing <0.005% of the population were removed, and taxonomy was assigned using the RDP classifier (Wang et al., 2007; Li et al., 2023). R Programming Language (version 3.3.1) was used to generate Venn diagrams to visualize the occurrence of shared and unique OTUs among groups and to make pie and bar plots to represent the relative abundance of taxonomic groups on the phylum and genus levels.

The Mothur software (version 1.30.2) was used for calculating the Shannon, Ace, Simpson, and Chao1 indices on the OTU level (Schloss et al., 2009; Edgar, 2013). The principal coordinate analysis (PCoA) based on the Bray–Curtis dissimilarity was performed to determine the similarity among the microbial communities in different groups (Li et al., 2021). Analysis of similarities (ANOSIM) was performed to compare the difference in microbial communities at six digestive parts and three dietary treatments. The significantly abundant bacterial taxa from the phylum to genus level among the different groups (LDA score > 2, $p < 0.05$) were identified using the linear discriminant analysis (LDA) effect size (LEfSe) software (Wang et al., 2007; Segata et al., 2011). The pheatmap package of R programming language (version 3.3.1) was used to calculate Spearman's coefficient and draw the correlation heatmap.

2.7 Statistical analysis

GraphPad Prism (version 10.1.2, La Jolla, CA, USA) and IBM SPSS Statistics (version 22.0, IBM, Chicago, IL, USA) software were used for plotting graphs and statistical analysis. For Shannon, Simpson, Ace, and Chao1 index data, significant differences between treatments were assessed by two-way ANOVA using Turkey's multiple comparisons test with each pig as an experimental unit, and digestive parts and treatment diet were two fixed effects, considering their interaction. For SCFA concentration data from the ileum to the rectum, significant differences between treatments were assessed by one-way ANOVA using Duncan's multiple comparisons test with each pig as an experimental unit, and treatment diet was the only fixed effect. For data on the relative abundances of microbial communities, the Kruskal–Wallis and Tukey–Kramer tests were used to evaluate the statistical significance among the multiple groups. Statistical significance was declared at a p-value of <0.05.

3 Results

3.1 Tag- and OTU-based analysis

A total of 25,880,835 sequences passed the quality control, with an average of 239,637 high-quality sequences per sample and an average sequence length of 416 bp. As shown in Supplementary Figure 1, the Venn analysis identified 1,497, 1,302, 1,091, 1,120, 3,076, and 2,972 unique OTUs in the stomach, duodenum, jejunum, ileum, colon, and rectum groups, respectively.

3.2 The diversity of bacterial communities in samples

As shown in Table 2, non-dietary grain sources but digestive parts significantly affect the α-diversity indices of microbial communities ($p < 0.01$). The interaction effect of diets and digestive parts had a significant effect on Simpson and Ace indices ($p < 0.05$). The microbial community in the colon and rectum groups mostly showed higher Shannon, Ace, Chao1, and lower Simpson indices than other groups ($p < 0.01$ or $p < 0.05$, Table 2 and Supplementary Figures 2, 3). The results of PCoA based on Bray–Curtis distance and evaluated by the ANOSIM test indicated significant differences in microbial communities in the colon and rectum compared to other digestive parts (Figure 2A, $p < 0.01$) There are no significant differences in the stomach, duodenal, jejunal and ileal microbiota among three dietary treatments (Figures 2B–E). There are significant differences in the colonic and rectal microbiota among three dietary treatments (Figures 2F,G, $p < 0.01$).

3.3 Composition and differential analysis of microbial communities among six digestive parts

As shown in Figure 3, Firmicutes was the most dominant phylum among six digestive parts, its relative abundance was 84.76% (the stomach), 74.09% (the duodenum), 91.91% (the jejunum), 98.58% (the ileum), 78.15% (the colon), and 74.31% (the rectum), respectively. Bacteroidota is another dominant phylum in the colon and rectum, with relative abundance of 14.51% (colon) and 16.38% (rectum), respectively. *Turicibacter*, *Lactobacillus*, and *Clostridium_sensu_stricto_1* were the

TABLE 2 Effects of grain diets on intestinal microbial α-diversity indexes of adult pigs.

Treatment	Digestive parts	Shannon index	Simpson index	Ace index	Chao1 index
Corn diet	Stomach	1.22 ± 0.57^{b}	0.44 ± 0.15^{a}	292.04 ± 86.88^{b}	279.52 ± 103.21^{b}
	Duodenum	1.71 ± 1.01^{b}	0.28 ± 0.14^{ab}	367.14 ± 215.32^{b}	368.68 ± 222.13^{b}
	Jejunum	1.56 ± 0.96^{b}	0.39 ± 0.23^{a}	370.31 ± 130.37^{b}	373.00 ± 132.86^{b}
	Ileum	1.83 ± 0.32^{b}	0.25 ± 0.07^{abc}	212.79 ± 132.26^{b}	170.47 ± 64.65^{b}
	Colon	4.30 ± 0.67^{a}	0.08 ± 0.09^{bc}	2361.40 ± 332.38^{a}	1994.75 ± 219.05^{a}
	Rectum	4.79 ± 0.17^{a}	0.02 ± 0.00^{c}	2156.24 ± 325.48^{a}	1967.71 ± 172.00^{a}
Wheat diet	Stomach	2.26 ± 0.86^{b}	0.25 ± 0.15^{ab}	567.11 ± 459.52^{b}	557.87 ± 442.03^{bc}
	Duodenum	2.39 ± 1.23^{b}	0.28 ± 0.22^{ab}	676.40 ± 466.45^{b}	660.97 ± 470.59^{b}
	Jejunum	1.95 ± 1.11^{b}	0.38 ± 0.25^{a}	359.67 ± 112.32^{b}	342.02 ± 114.82^{bc}
	Ileum	1.72 ± 0.32^{b}	0.28 ± 0.12^{ab}	222.82 ± 110.35^{b}	163.41 ± 63.38^{c}
	Colon	4.24 ± 0.57^{a}	0.09 ± 0.08^{b}	2051.29 ± 354.80^{a}	1992.74 ± 339.20^{a}
	Rectum	4.57 ± 0.19^{a}	0.04 ± 0.01^{b}	2165.32 ± 257.56^{a}	2091.11 ± 197.56^{a}
Paddy rice diet	Stomach	2.07 ± 1.22^{c}	0.21 ± 0.11	564.66 ± 337.37^{b}	576.81 ± 345.22^{b}
	Duodenum	1.93 ± 1.09^{c}	0.22 ± 0.14	535.92 ± 150.98^{b}	481.70 ± 131.46^{b}
	Jejunum	2.25 ± 1.14^{bc}	0.21 ± 0.10	587.70 ± 228.86^{b}	560.71 ± 227.45^{b}
	Ileum	1.76 ± 0.75^{c}	0.32 ± 0.10	471.79 ± 449.22^{b}	420.24 ± 449.22^{b}
	Colon	3.60 ± 1.28^{ab}	0.21 ± 0.24	1864.45 ± 363.87^{a}	1197.63 ± 359.39^{a}
	Rectum	3.90 ± 0.67^{a}	0.12 ± 0.13	1961.49 ± 163.62^{a}	1911.61 ± 145.90^{a}
Corn diet					
Wheat diet					
Paddy rice diet					
	Stomach	1.85 ± 0.99^{b}	0.30 ± 0.16^{a}	474.60 ± 339.78^{b}	471.40 ± 339.42^{b}
	Duodenum	2.01 ± 1.08^{b}	0.26 ± 0.16^{ab}	526.48 ± 318.21^{b}	503.78 ± 316.33^{b}
	Jejunum	1.92 ± 1.04^{b}	0.33 ± 0.21^{a}	439.22 ± 189.22^{b}	425.24 ± 184.85^{b}
	Ileum	1.77 ± 0.48^{b}	0.28 ± 0.10^{a}	302.46 ± 288.58^{b}	251.37 ± 277.25^{b}
	Colon	4.04 ± 0.90^{a}	0.13 ± 0.16^{bc}	2092.38 ± 391.07^{a}	1928.37 ± 308.20^{a}
	Rectum	4.42 ± 0.55^{a}	0.06 ± 0.08^{c}	2094.34 ± 260.58^{a}	1990.14 ± 179.98^{a}
p-value	Diets	0.287	0.636	0.765	0.167
	Digestive parts	<0.01	<0.01	<0.01	<0.01
	Diets × Digestive parts	0.290	0.047	0.019	0.187

All data were analyzed by the Kruskal-Wallis and Tukey-Kramer test. The results were presented as mean values ± standard deviation ($n = 6$ per treatment). Means in each column with different letters differs significantly ($p < 0.05$).

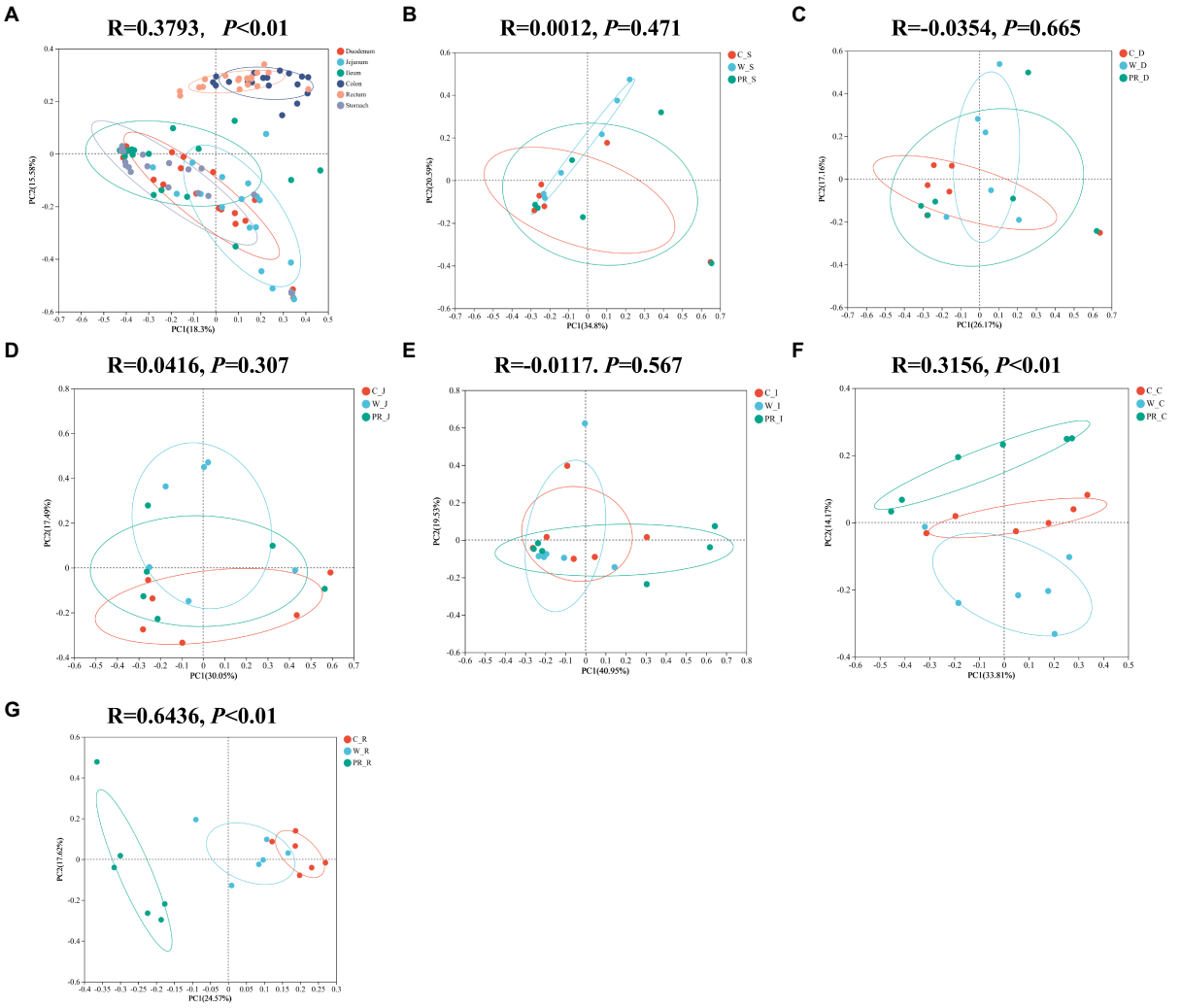

FIGURE 2
Principal coordinates analysis (PcoA) of microbial composition in six digestive parts **(A)**. PcoA of microbial composition in the stomach **(B)**, duodenal **(C)**, jejunal **(D)**, ileal **(E)**, colonic **(F)**, and rectal **(G)** digesta of adult pigs fed with different cereal diets. C, corn; W, wheat; PR, paddy rice; S, stomach; D, duodenum; J, jejunum; I, ileum; C, colon; R, rectum.

dominant genera in the stomach, duodenum, jejunum and ileum. *Streptococcus* (23.13%) was the most dominant genus in the colon, whereas *Turicibacter* (10.33%) was dominant in the rectum (Figure 4). The jejunum and ileum groups had a high abundance of Firmicutes ($p < 0.05$, Figure 5A). The colon and rectum groups showed greater Bacteroidota abundance than other groups ($p < 0.05$, Figure 5B). The populations of Campylobacterota, Proteobacteria, and *Sarcina* were largest in the duodenum group ($p < 0.05$, Figures 5C,D,I). *Lactobacillus* in the jejunum and *Streptococcus* in the colon had the highest relative abundance, respectively ($p < 0.05$, Figures 5F,H). The ileum group showed higher relative abundances of *Turicibacter* and *Clostridium_sensu_stricto_1* than the jejunum and colon groups ($p < 0.05$, Figures 5E,G).

3.4 Composition and differential analysis of microbial communities among dietary treatments

As shown in Figure 6, Firmicutes was the most dominant phylum among dietary treatments. Campylobacterota was the second dominant phylum in the C_S and C_D groups (4.11 and 23.73%, respectively), while Proteobacteria was the second dominant phylum in the W_D group (10.06%). The W_S, PR_S, and PR_S groups have abundant Campylobacterota (6.90, 8.94, and 15.45%, respectively) and Proteobacteria (7.02, 6.87, and 12.81%, respectively). Actinobacteriota was the second dominant phylum in the W_J group (8.75%). Bacteroidota was the second dominant phylum in the C_C, W_C, PR_C, and PR_R groups (16.22, 21.56, 5.74, and 6.19%, respectively). Bacteroidota and Spirochaetota were the second (22.44 and 20.14%, respectively) and third (6.19 and 5.26%, respectively) dominant phyla in C_R and W_R, respectively. The top five genera in the relative abundances of all groups were *Turicibacter*, *Lactobacillus*, *Clostridium_sensu_stricto_1*, *Streptococcus*, and *Sarcina* (Figure 7). W_C and W_R groups had greater Bacteroidota, Spirochaetota, and *Prevotellaceae_NK3B31_group* abundances, but showed lower Firmicutes abundance than the PR_C and PR_R groups, respectively ($p < 0.05$, Figures 8A–H). The population of *Sarcina* in the W_S and W_D groups was the largest ($p < 0.05$, Figures 8I,J).

10.3389/fmicb.2024.1442077

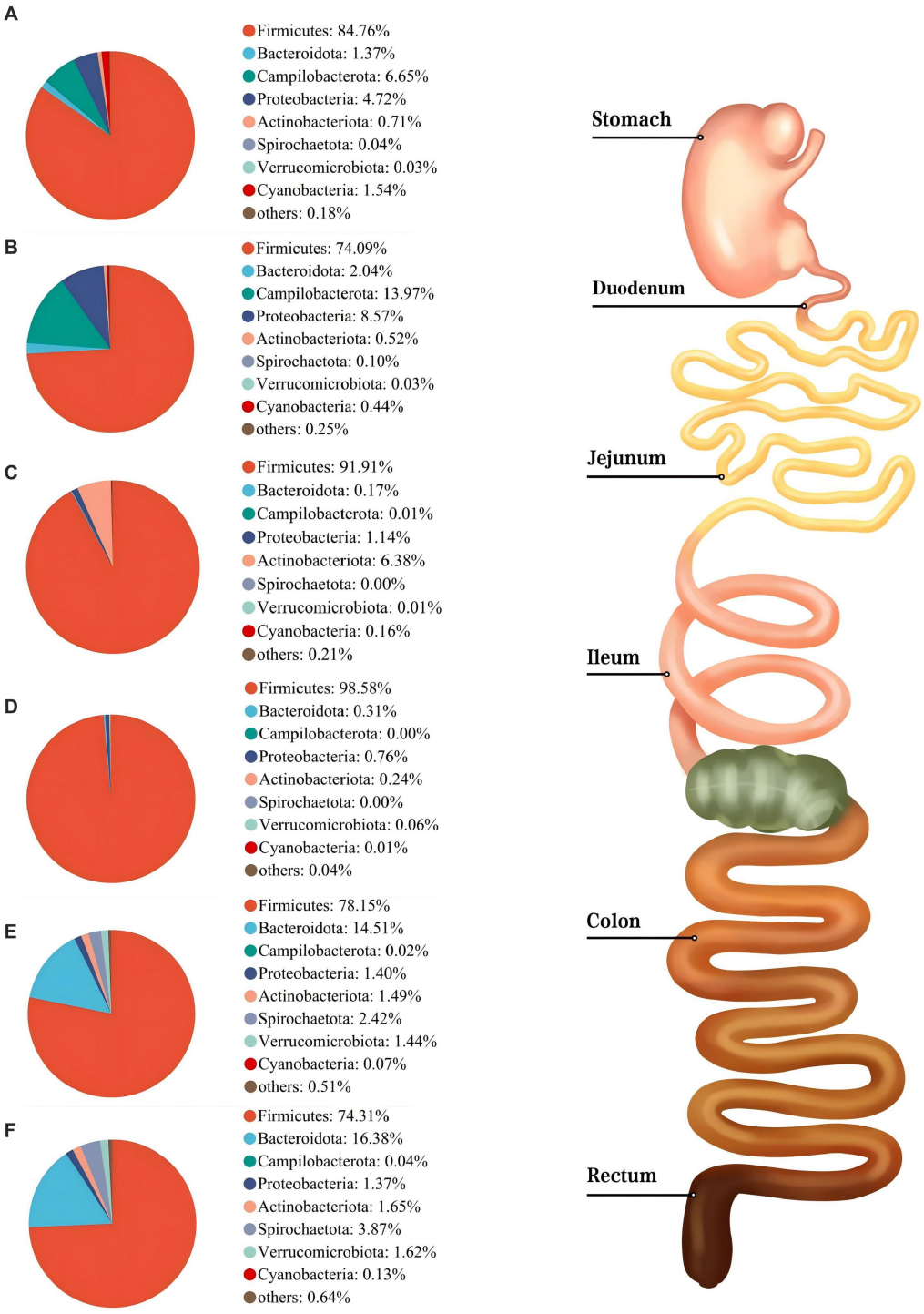

FIGURE 3
Composition of microbiota in the stomach **(A)**, duodenum **(B)**, jejunum **(C)**, ileum **(D)**, colon **(E)**, and rectum **(F)** based on the phylum level.

3.5 Cladogram of LEfSe from the phylum to the genus level

From the phylum to the genus level, 8 taxa including *Sarcina* and 22 taxa, including Fibrobacterota, were significantly enriched in the W_S and PR_S groups, respectively (Figure 9A). Seven taxa, including *Propionibacteriales,* and nine taxa, including *paenibacillales*, were significantly enriched in the W_D and PR_D groups, respectively (Figure 9B). In the C_J, W_J, and PR_J groups, four specific enriched taxa, including *Acidobacteria*, two specific enriched taxa, including *NK4A214*, and 25 specific enriched taxa, including Kiritimatiellae, were detected, respectively (Figure 9C). Two (e.g., *Clostridium_sensu_strico_6*), four (e.g., *Clostridia*), and eight (e.g., *Bacilli*) taxa in the C_I, W_I, and PR_I groups were significantly enriched, respectively

10.3389/fmicb.2024.1442077

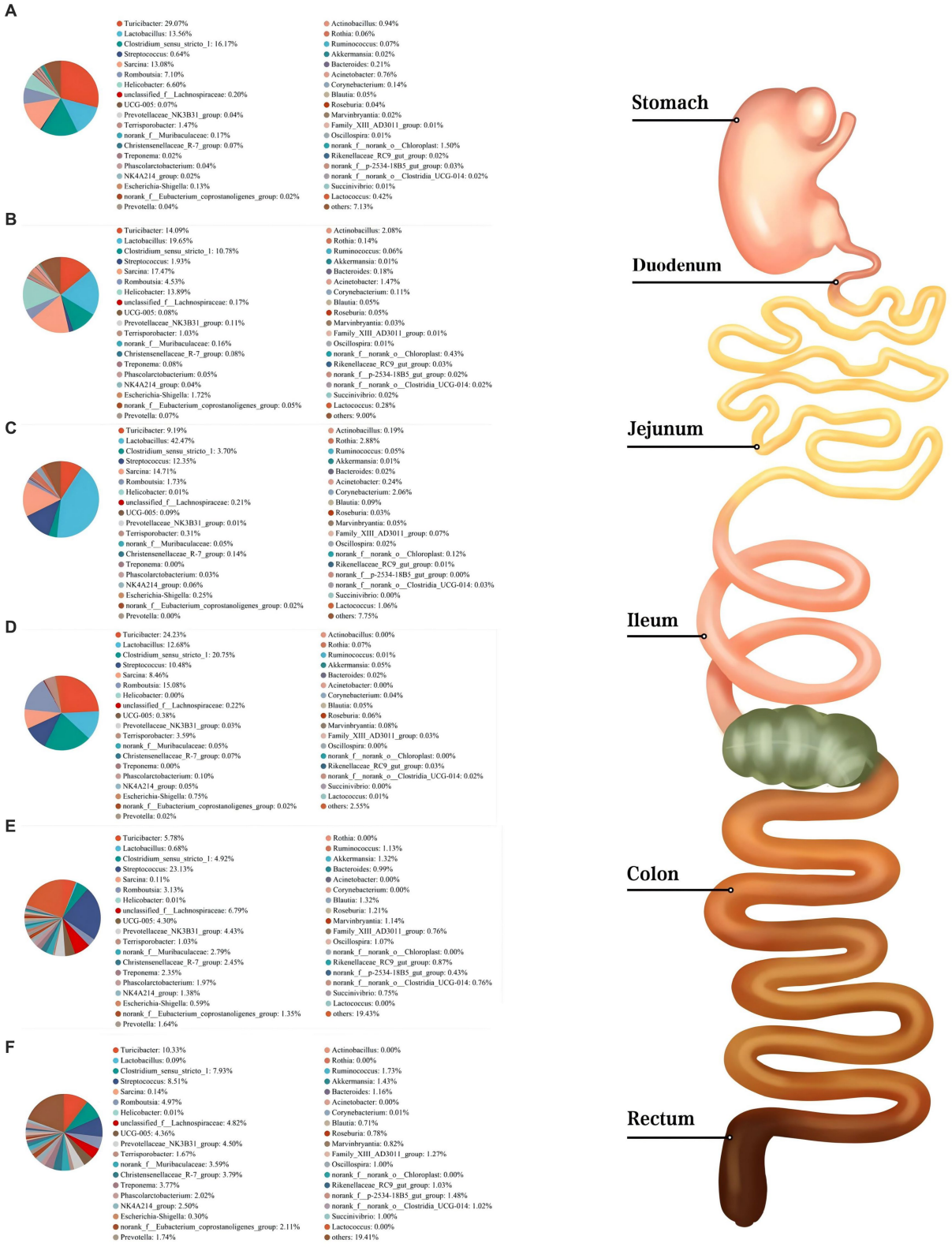

FIGURE 4
Composition of microbiota in the stomach **(A)**, duodenum **(B)**, jejunum **(C)**, ileum **(D)**, colon **(E)**, and rectum **(F)** based on the genus level.

(Figure 9D). In total, 32 taxa, including Actinobacteriota, were significantly enriched in the C_C group, while 47 taxa, including Spirochaetota, Proteobacteria, Fibrobacterota, and Bacteroidota were significantly enriched in the W_C group, and 28 taxa, including Firmicutes, were significantly enriched in the PR_C group, respectively (Figure 9E). A total of 47 taxa represented by Spirochaetota and

10.3389/fmicb.2024.1442077

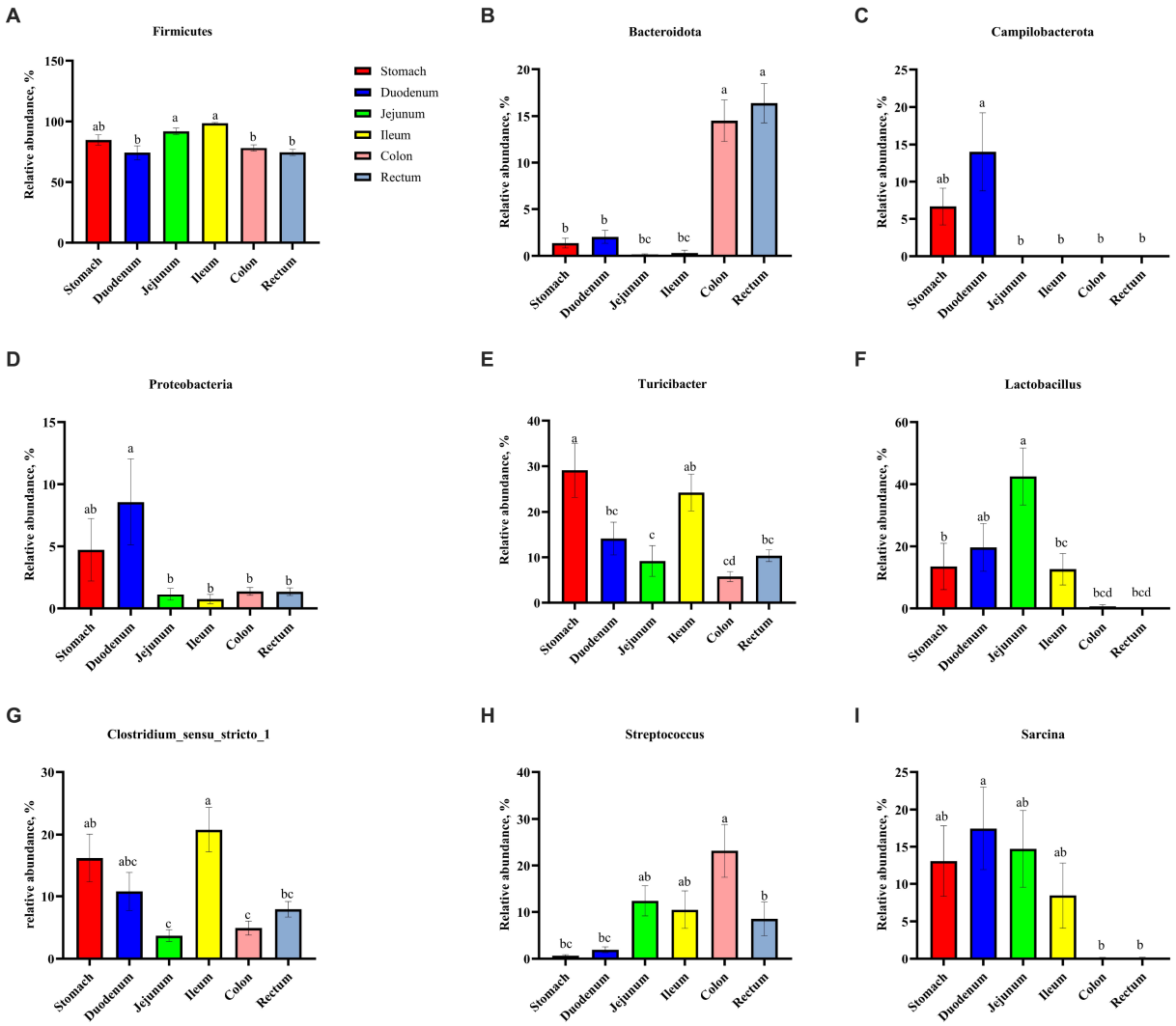

FIGURE 5
Comparative analysis of microbiota among six digestive parts based on the phylum **(A–D)** and the genus **(E–I)** levels. All data were analyzed by the Kruskal–Wallis and Tukey–Kramer test and presented as the mean percentage of different bacteria (group = 6, $n = 18$ per treatment). The different letters mean $p < 0.05$.

Bacteroidota were significantly enriched in the C_R group, while 39 taxa, including *Prevotellaceae_NK3B31_group,* were enriched in the W_R group, and 46 taxa, including Firmicutes and Actinobacteriota, were enriched in the PR_R group, respectively (Figure 9F).

3.6 SCFAs production

Acetate was the main SCFAs in the ileal digesta, while acetate, propionate, and butyrate were the dominant acids in the colonic and rectal digesta (Table 3). In ileal digesta, the contents of acetate and isovalerate in the W diet group were higher than in the C diet group ($p < 0.01$). The concentrations of propionate and total SCFAs in the W groups were higher than in other dietary groups ($p < 0.01$ and $p < 0.05$, respectively). The concentration of isobutyrate in the PR diet group was the lowest ($p < 0.01$). In the colonic digesta, the W diet group had greater acetate, propionate, butyrate, isobutyrate, isovalerate, and total SCFA contents compared with other dietary groups ($p < 0.01$ or $p < 0.05$). In the rectal digesta, the C and W diet groups showed higher acetate, propionate, and total SCFA contents than the PR group ($p < 0.01$). The W diet group had the highest concentration of butyrate ($p < 0.05$) and showed greater isobutyrate and isovalerate contents than other dietary groups ($p < 0.01$).

3.7 Correlation analysis between the relative abundance of microbial community and SCFAs production

In the ileal digesta, Planctomycetota and *Sarcina* were positively correlated with propionate ($p < 0.05$, Figures 10A, 11A). In the colonic digesta, Fibrobacterota, Spirochaetota, *Prevotellaceae_NK3B31_group*, *Treponema,* and *Prevotella* showed positive correlations with acetate, propionate, butyrate, and total SCFAs ($p < 0.05$ or $p < 0.01$ or $p < 0.001$, Figures. 10B, 11B). Bacteroidota

10.3389/fmicb.2024.1442077

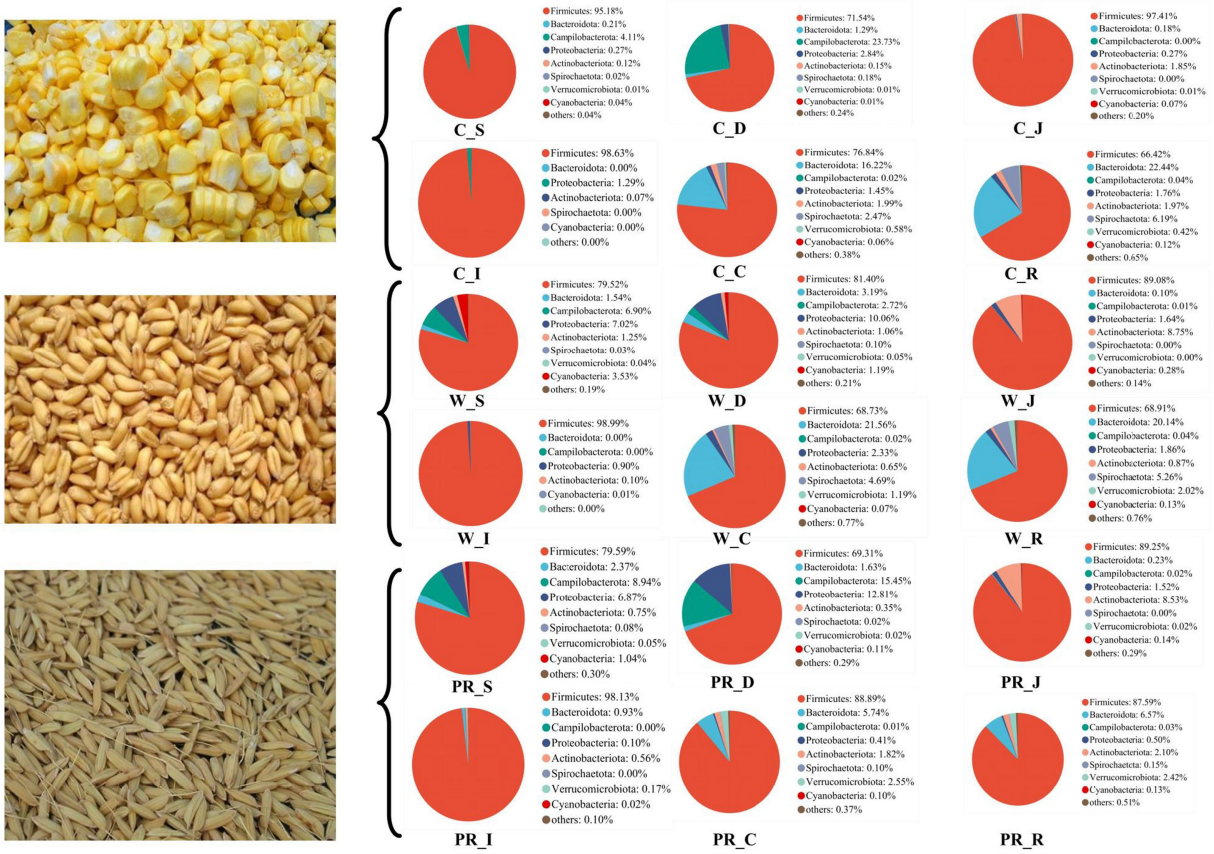

FIGURE 6
Composition of microbiota in the digesta of pigs fed with corn, wheat, and paddy rice diets based on the phylum level. C, corn; W, wheat; PR, paddy rice; S, stomach; D, duodenum; J, jejunum; I, ileum; C, colon; R, rectum.

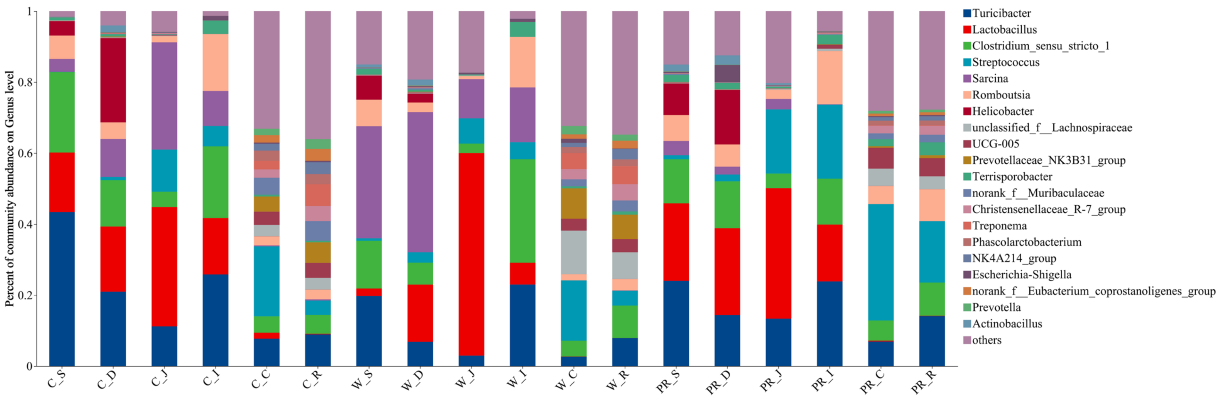

FIGURE 7
Composition of microbiota in the digesta of pigs fed with corn, wheat, and paddy rice diets based on the genus level. C, corn; W, wheat; PR, paddy rice; S, stomach; D, duodenum; J, jejunum; I, ileum; C, colon; R, rectum.

was positively correlated with propionate, butyrate, and total SCFAs, while Firmicutes was on the contrary ($p < 0.05$ or $p < 0.01$, Figure 10B). In the rectal digesta, Bacteroidota and *Prevotellaceae_NK3B31_group* showed strong positive correlations with acetate, propionate, butyrate, and total SCFAs, while Firmicutes was on the contrary ($p < 0.01$ or $p < 0.001$, Figures 10C, 11C). Spirochaetota and *Treponema* were positively correlated with acetate, propionate, and total SCFAs ($p < 0.05$ or $p < 0.01$, Figures 10C, 11C). Actinobacteriota in the colonic and rectal digesta were negatively correlated with acetate, propionate, butyrate, isobutyrate, isovalerate, and total SCFAs ($p < 0.05$ or $p < 0.01$ or $p < 0.001$, Figures 10B,C).

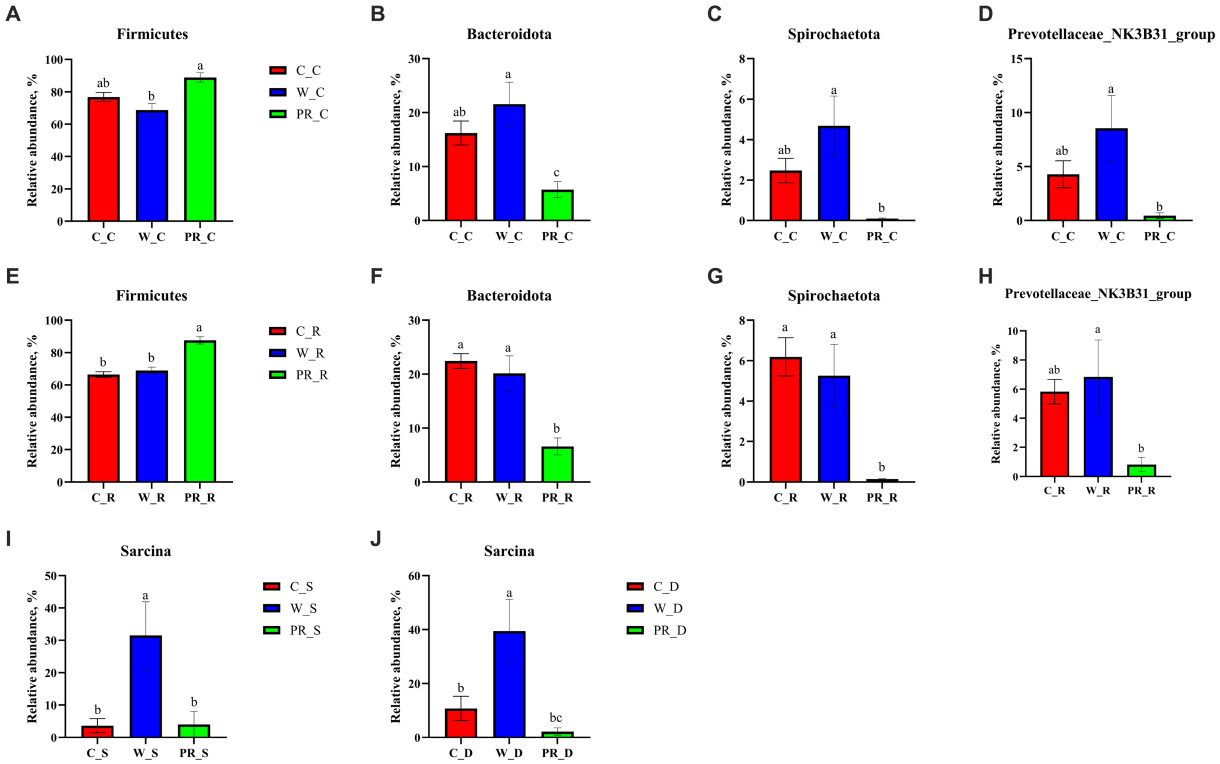

FIGURE 8
Comparative analysis of microbiota in the stomach **(I)**, duodenal **(J)**, colonic **(A–D)**, and rectal **(E–H)** digesta of adult pigs fed with corn, wheat, and paddy rice diets based on the phylum and the genus levels. All data were analyzed by the Kruskal–Wallis and Tukey-Kramer test and presented as the mean percentage of different bacteria (group = 3, $n = 6$ per treatment). The different letters mean $p < 0.05$. C, corn; W, wheat; PR, paddy rice; S, stomach; D, duodenum; C, colon; R, rectum.

4 Discussion

4.1 α- and β-diversity of the samples

In this study, a greater number of unique OTUs (Supplementary Figure 1) and higher Shannon, Ace, and Chao1 indices were often observed in the colon and rectum compared with other digestive parts (Table 2, Supplementary Figures 2, 3). These indicate that the microbial communities in the colonic and rectal digesta samples had greater species richness and compositional diversity (Shannon, 1948; Simpson, 1949; Chao, 1984). Interestingly, we found that it was the digestive parts rather than dietary treatment that had a highly significant effect on the α-diversity indices of the samples (Table 2), which is similar to the previous study (Li et al., 2023). The PcoA results showed that the composition of microbial communities from the stomach to the ileum was approximate, but differed significantly from that of the colon and rectum (Figure 2A). These results were expected and consistent with the previous studies (Liu et al., 2019; Zhao et al., 2015). Anatomically, the duodenum, jejunum, and ileum belong to the small intestine, while the colon and rectum belong to the large intestine. The small intestine primarily relies on enzymes to digest most of the starch, protein, and fat in feed. However, the large intestine is the main site for the fermentation of DF, a small amount of protein and peptides produced by microorganisms. Therefore, different digestive patterns determine that the distribution of microorganisms will inevitably be segmented at the boundary between the small and large intestines (DiBaise et al., 2008; Liu et al., 2019; Zhao et al., 2015). In addition, compared with the large intestine, the pH value in the stomach is lower, the oxygen content in the stomach and small intestine (e.g., duodenum and jejunum) is higher, with more antimicrobials, faster peristalsis speed, and shorter transit time of digesta (Kelly et al., 2017). These factors are not conducive to the colonization of a large number of microorganisms. Therefore, there are only 10^3–10^4 bacteria/ml in the stomach and small intestine contents, mainly acid-tolerant lactobacilli and streptococci (Hao and Lee, 2004). As the oxygen concentration from the small intestine to the large intestine gradually decreases, the intestine peristalsis speed slows down, the pH value gradually increases, making it easier for microorganisms to colonize, and the number of microbial communities becomes more abundant and diverse (Hao and Lee, 2004). The colon also becomes the main site for microbial colonization, and a large number of specialized anaerobic bacteria adapted to this environmental condition, such as *Prevotellaceae*, which is intolerant to oxygen, gradually occupy a dominant position (Kelly et al., 2017). In summary, based on the different digestion patterns and physiological characteristics between the small intestine and the large intestine, it is reasonable to observe significant differences in the quantity and diversity of microbial communities between the anterior and posterior intestinal segments.

The composition of microbial communities in the colonic and rectal digesta also differed among three dietary treatment groups (Figures 2F,G), which is similar to the previous findings (Nielsen et al.,

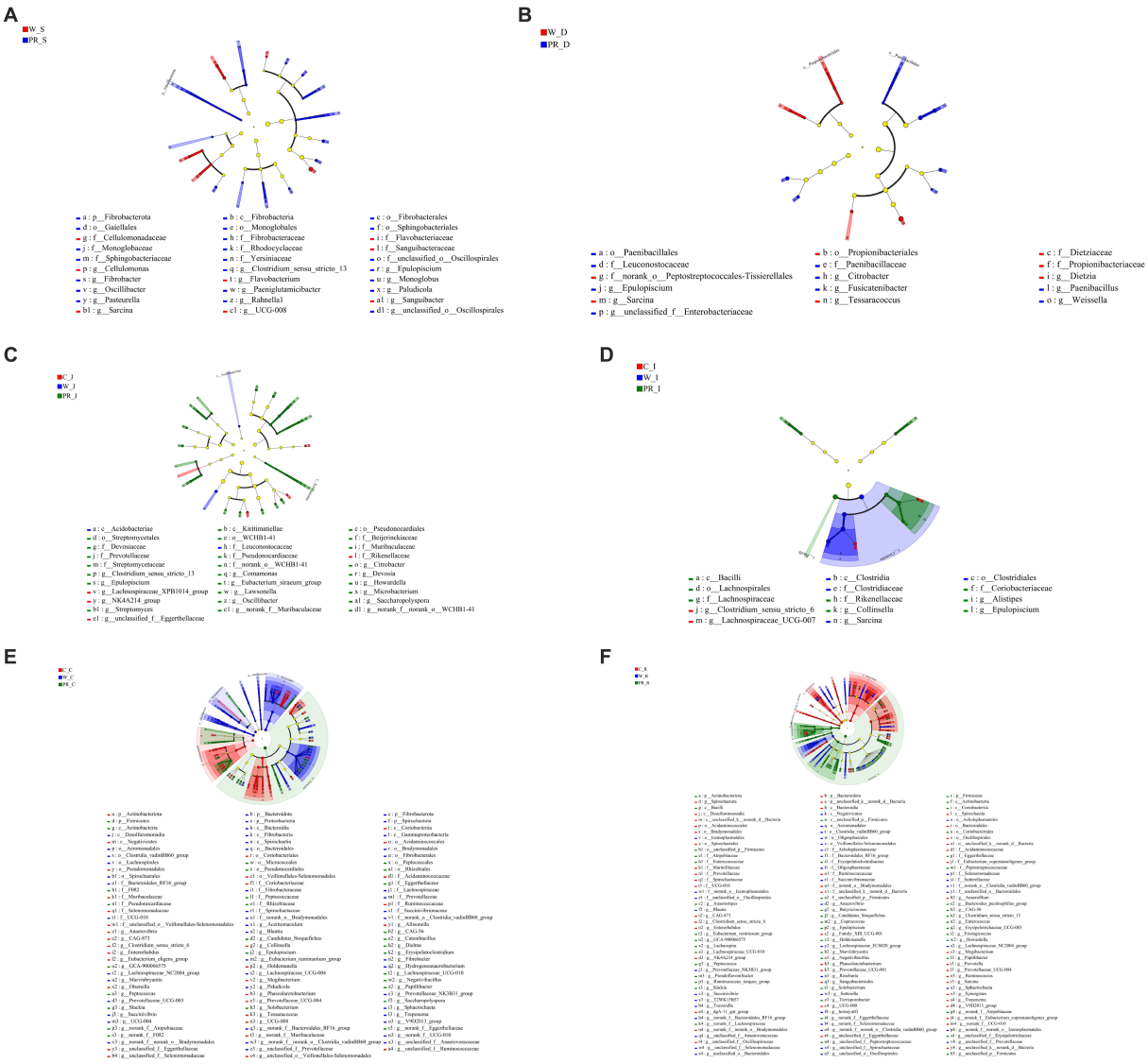

FIGURE 9
Cladogram of LEfSe demonstrates taxonomic profiling for the distinct bacteria in the stomach **(A)**, duodenal **(B)**, jejunal **(C)**, ileal **(D)**, colonic **(E)**, and rectal **(F)** digesta among three dietary treatments. C, corn; W, wheat; PR, paddy rice; S, stomach; D, duodenum; J, jejunum; I, ileum; C, colon; R, rectum.

2014; Burbach et al., 2017; Li et al., 2023). This may be attributed to the difference in fermentation substrates in the large intestine. The responses of the microbiota to dietary intervention can be rapid and are also sensitive to structural changes in fermentation substrates (Turnbaugh et al., 2009; David et al., 2014; Hamaker and Tuncil, 2014; Fouhse et al., 2017). For each whole grain used in this experiment, due to its unique composition matrix, it affects the fluidity and availability of fermentation substrates entering the large intestine, thereby manipulating the microbial composition (Hamaker and Tuncil, 2014; Fouhse et al., 2017). Several previous studies have confirmed these viewpoints. It has been reported that a barley-based diet has a higher concentration of non-starch polysaccharides (NSP) and better water solubility than a W-based diet. Therefore, it increased the number of Firmicutes and decreased the number of Proteobacteria in the feces of pigs. Burbach et al. (2017) and Ellner et al. (2022) suggested that due to the higher cellulose and lower CP contents in rye than in triticale, cellulolytic species of *Clostridium_sensu_stricto* dominated in the ileum and feces of pigs fed with a rye-based diet, while the *Clostridium XI* level in the rye-based diet group was lower than that in the triticale-based diet group. Fouhse et al. (2017) reported that a large number of *Phascolarctobacterium* and *Oscillospira* were observed in the feces of pigs fed with a low-fermentability barley diet and hard red spring W diet, and speculated that this may be related to the high ADF content in these two diets. Snart et al. (2006) found that pigs consuming an oat-based diet showed significantly greater increases in Bifidobacteria compared with pigs consuming a barley-based diet, which may be related to the different structures and molecular weights of β-glucans and other polysaccharides, as well as differences in non-DF components. Similarly, the composition and structure of fermentation substrates entering the hindgut (e.g., cellulose, hemicellulose, lignin, and RS), vary greatly among C, W, and PR. This will inevitably change the composition of microbial communities and fermentation patterns

TABLE 3 Effects of different cereal grains on the concentrations of short-chain fatty acids in the intestine of pigs (μmol/g).

Items	Corn diet	Wheat diet	Paddy rice diet	SEM	*p*-value
Ileal digesta					
Acetate	4.96 ± 1.03^{b}	20.54 ± 12.20^{a}	12.06 ± 1.71^{ab}	2.210	$p < 0.01$
Propionate	0.59 ± 0.21^{b}	1.16 ± 0.30^{a}	0.52 ± 0.40^{b}	0.098	$p < 0.01$
Butyrate	0.83 ± 0.65	0.85 ± 0.48	0.85 ± 0.64	0.132	0.999
Isobutyrate	0.50 ± 0.01^{a}	0.30 ± 0.00^{b}	0.19 ± 0.04^{c}	0.031	$p < 0.01$
Valerate	0.65 ± 0.09^{a}	0.49 ± 0.00^{b}	0.68 ± 0.10^{a}	0.026	$p < 0.01$
Isovalerate	0.26 ± 0.08^{b}	0.43 ± 0.06^{a}	0.30 ± 0.18^{ab}	0.032	$p < 0.01$
Total SCFAs	8.18 ± 1.88^{b}	24.06 ± 12.37^{a}	13.62 ± 3.94^{b}	2.316	0.011
Colonic digesta					
Acetate	43.27 ± 15.78^{b}	70.27 ± 11.34^{a}	28.99 ± 4.95^{c}	4.879	$p < 0.01$
Propionate	15.59 ± 5.31^{b}	27.75 ± 5.25^{a}	10.25 ± 2.82^{b}	2.049	$p < 0.01$
Butyrate	11.43 ± 4.01^{b}	28.32 ± 2.47^{a}	6.79 ± 2.83^{c}	2.351	$p < 0.01$
Isobutyrate	0.47 ± 0.01^{c}	0.73 ± 0.13^{a}	0.60 ± 0.04^{b}	0.031	$p < 0.01$
Valerate	2.63 ± 2.05	2.03 ± 0.40	1.16 ± 0.36	0.308	0.147
Isovalerate	1.18 ± 0.20^{b}	1.82 ± 0.45^{a}	1.41 ± 0.08^{b}	0.090	0.028
Total SCFAs	71.79 ± 22.60^{b}	134.62 ± 23.79^{a}	49.20 ± 10.07^{b}	9.802	$p < 0.01$
Rectal digesta					
Acetate	35.38 ± 2.30^{a}	38.62 ± 4.72^{a}	22.43 ± 3.31^{b}	1.873	$p < 0.01$
Propionate	13.36 ± 3.11^{a}	14.31 ± 4.48^{a}	6.09 ± 0.98^{b}	1.138	$p < 0.01$
Butyrate	7.88 ± 4.19^{ab}	13.68 ± 8.24^{a}	3.49 ± 1.36^{b}	1.565	0.023
Isobutyrate	0.49 ± 0.10^{b}	0.91 ± 0.08^{a}	0.48 ± 0.07^{b}	0.052	$p < 0.01$
Valerate	1.16 ± 0.20	1.53 ± 0.40	1.16 ± 0.34	0.084	0.103
Isovalerate	1.42 ± 0.32^{b}	2.36 ± 0.14^{a}	1.26 ± 0.22^{b}	0.129	$p < 0.01$
Total SCFAs	57.47 ± 5.10^{b}	70.59 ± 16.85^{a}	35.08 ± 5.31^{c}	4.262	$p < 0.01$

The results were presented as mean values ± standard deviation ($n = 6$ per treatment). Means in each line with different letters differs significantly ($p < 0.05$).

in the hindgut (Bach-Knudsen, 2014; NRC, 2012; Cervantes-Pahm et al., 2014; Menkovska et al., 2017; Li et al., 2020; Kaur et al., 2021).

4.2 Differences in the microbial community among six digestive parts

The relative abundance of Firmicutes was dominant in six digestive parts (Figure 3), which is in agreement with previous findings (Gao et al., 2019a; Gao et al., 2019b; Zhao et al., 2019; Li et al., 2023). Firmicutes are believed to be involved in fat metabolism and energy absorption processes in the host (Zhao et al., 2015; Gao et al., 2019a). Some previous studies found that the Firmicutes level in the large intestine was greater than that in the small intestine and inferred that the large intestine might undertake more tasks of fat deposition compared to the small intestine (Mao et al., 2015; Zhao et al., 2015; Liu et al., 2018). However, our results do not concord with this inference (Figure 5A). In fact, Gao et al. (2019b) also suggested that the above inference might not be correct because they observed that there was no difference in the relative abundance of Firmicutes between the cecum and the small intestine of pigs. In this study, we observed that the Bacteroidota was mainly distributed in the colonic and rectal digesta (Figure 5B). Bacteroidota is rich in carbohydrate-active enzyme (CAZyme) genes, which can degrade plant cell walls and produce acetate and propionate in the large intestine (Morrison and Preston, 2016; Liu et al., 2021). Therefore, our result was as expected and close to the previous studies (Looft et al., 2014; Crespo-Piazuelo et al., 2018; Gao et al., 2019b). Campylobacterota is considered to be one of the important pathogens causing diarrhea in piglets after weaning (Adhikari et al., 2019). The increase of Proteobacteria abundance can be considered as one of the potential features of gut dysbiosis (Shin et al., 2015). Fortunately, compared to other groups, only the stomach and duodenum groups showed greater Campylobacterota and Proteobacteria abundances (Figures 5C,D).

On the genus level, we found that *Lactobacillus* was mainly distributed in the jejunum (Figure 5F), which is similar to the previous findings (Crespo-Piazuelo et al., 2018; Gao et al., 2019b). *Lactobacillus* is the most common probiotic, which contributes greatly to preventing potential infections and maintaining host intestinal health (Che et al., 2014; Ahn et al., 2018). Previous studies have shown that *Lactobacillus* was the major amylolytic genus (Pandey et al., 2023). Therefore, it was not surprising that abundant *Lactobacillus* appeared in the jejunum. Interestingly, we found that *Turicibacter* and *Clostridium_sensu_stricto_1* showed similar spatial regularities in the GIT, especially their high abundances in the ileum (Figures 5E,G), which is similar to some previous studies (Crespo-Piazuelo et al., 2018; Liu et al., 2019; Zhao et al., 2019). Some previous studies indicated that *Turicibacter* had good adaptability to an ileal environment with 5% oxygen content (Hillman et al., 1993; Cuiv

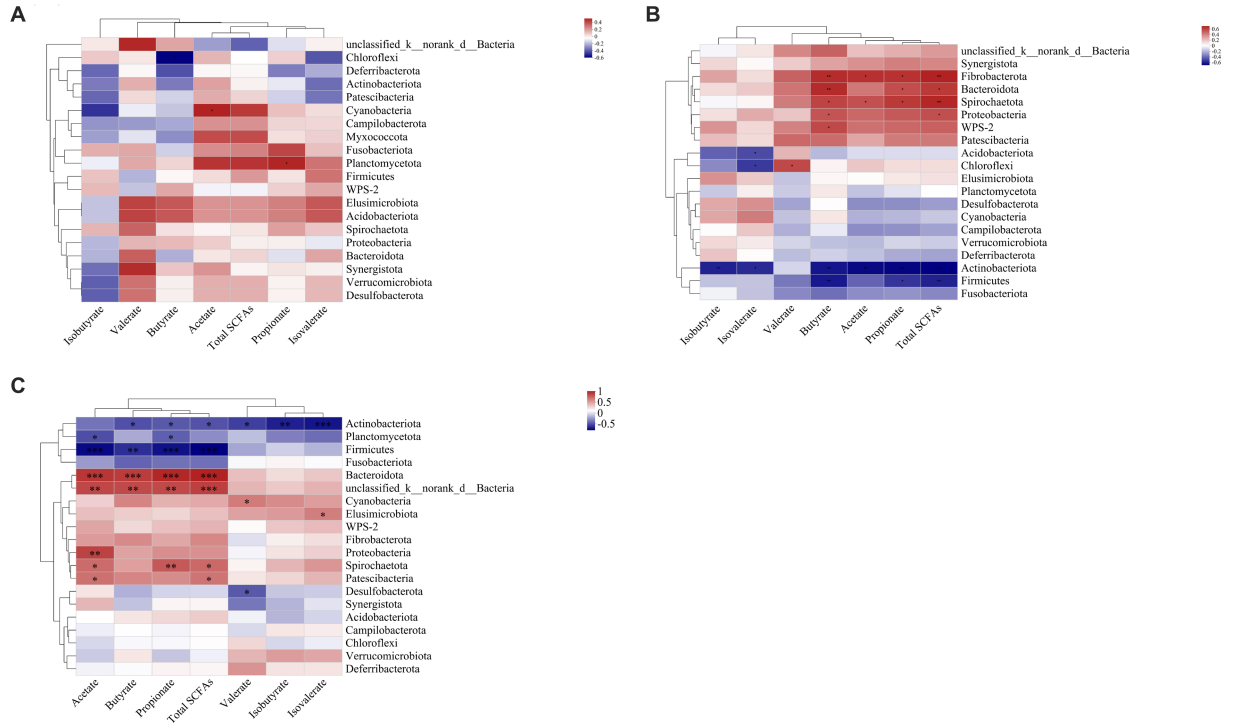

FIGURE 10
Correlation heatmaps between the short-chain fatty acid (SCFA) concentrations and the relative abundances of the top 20 phyla in the ileal **(A)**, colonic **(B)**, and rectal **(C)** digesta. Correlation is indicated by a color gradient from blue to red based on Spearman's correlation coefficients. The asterisk indicates a significant correlation between two variables, $*p < 0.05$, $**p < 0.01$, $***p < 0.001$.

et al., 2011; Looft et al., 2014). Meanwhile, a previous study has confirmed that the ileal effluent from ileostomy patients showed a high relative abundance of *Clostridium cluster I* (Zoetendal et al., 2012). Therefore, our results may be explained by the special environment of the ileum and the installation of the T-cannula. Currently, a higher relative abundance of *Streptococcus* in the colon was found Some members of Streptococcus are known for their high virulence (Spellerberg and Brandt, 2015) (Figure 5H), which may be due to its involvement in the fermentation of cereal grains through the Wood–Ljungdahl pathway (Koh et al., 2016). *Sarcina* has been demonstrated as a causative organism in the abomasa bloat and death of livestock (DeBey et al., 1996; Sopha et al., 2015). Crespo-Piazuelo et al. (2018) found that *Sarcina* was the relatively abundant genus in the duodenum, jejunum, and ileum of pigs, which is consistent with our results (Figure 5I).

In summary, the relative abundance of microbial communities from the stomach to the rectum was dynamically changing. Among them, some results can be explained by the decrease in oxygen concentration from the small intestine to the large intestine (Bergey et al., 2001; Albenberg et al., 2014; Donaldson et al., 2016). For example, we observed that aerobic bacteria or facultative anaerobes, such as Campylobacterota, Proteobacteria, and *Lactobacillus* in the foregut, were gradually replaced by anaerobic Bacteroidota and partially anaerobic *Streptococcus* in the hindgut (Figures 5B–D,F,H), which is strong evidence.

4.3 Differences in the microbial community among dietary treatment

Various grains contain different contents of macronutrients, organic, and inorganic micronutrients. This directly determines different fermentation substrates for intestinal microbiota and profoundly influences the relative abundances of specific dominant bacterial groups (Scott et al., 2008; Walker et al., 2011; Power et al., 2014; Gidley, 2023). In the current study, PR_C and PR_R groups had greater Firmicutes abundance than W_C and W_R groups, respectively (Figures 8A,E), suggesting that fat metabolism may be more vigorous in the hindgut of adult pigs fed with the PR diet (Li et al., 2023). However, the lower Bacteroidota abundance in the PR_C and PR_R groups may be associated with the high levels of ADF, *CF*, and IDF in the PR diet. These components are difficult to ferment due to their poor water solubility, which may inhibit the colonization of Bacteroidota (Urriola et al., 2010; Navarro et al., 2019a). The PR_C and PR_R groups showed lower Spirochaetota abundance than W_C and W_R, respectively (Figures 8C,G), indicating that the hindgut flora of pigs fed with PR may be more balanced (Litvak et al., 2017). This result may be explained by the different structure of arabinoxylan (AX) between W and PR. AX is one of the main components of NSP in cereal grains (Bach-Knudsen et al., 2017). AX in PR is located in the pericarp or testa with abundant branched chains, and the ratio of arabinose to xylose (A:X) is higher than that of W (0.8 versus 0.5–0.7; Zhang et al., 2015). Therefore, it is difficult to depolymerize. On the one hand, this ensures that the carbohydrates in PR are still slowly fermented in the distal part of the colon (Zhang et al., 2015; Bach-Knudsen et al., 2017). On the other hand, this will help reduce protein fermentation and the release of toxic substances and inhibit the proliferation of pathogenic microbes (Williams et al., 2005; Jha and Berrocoso, 2016). On the contrary, for W, AX is located in its aleurone layer with few branches and good water solubility (Zhang et al., 2015; Bach-Knudsen et al., 2017; Tiwari et al., 2019). These characteristics allow it to be rapidly fermented in the cecum and proximal colon

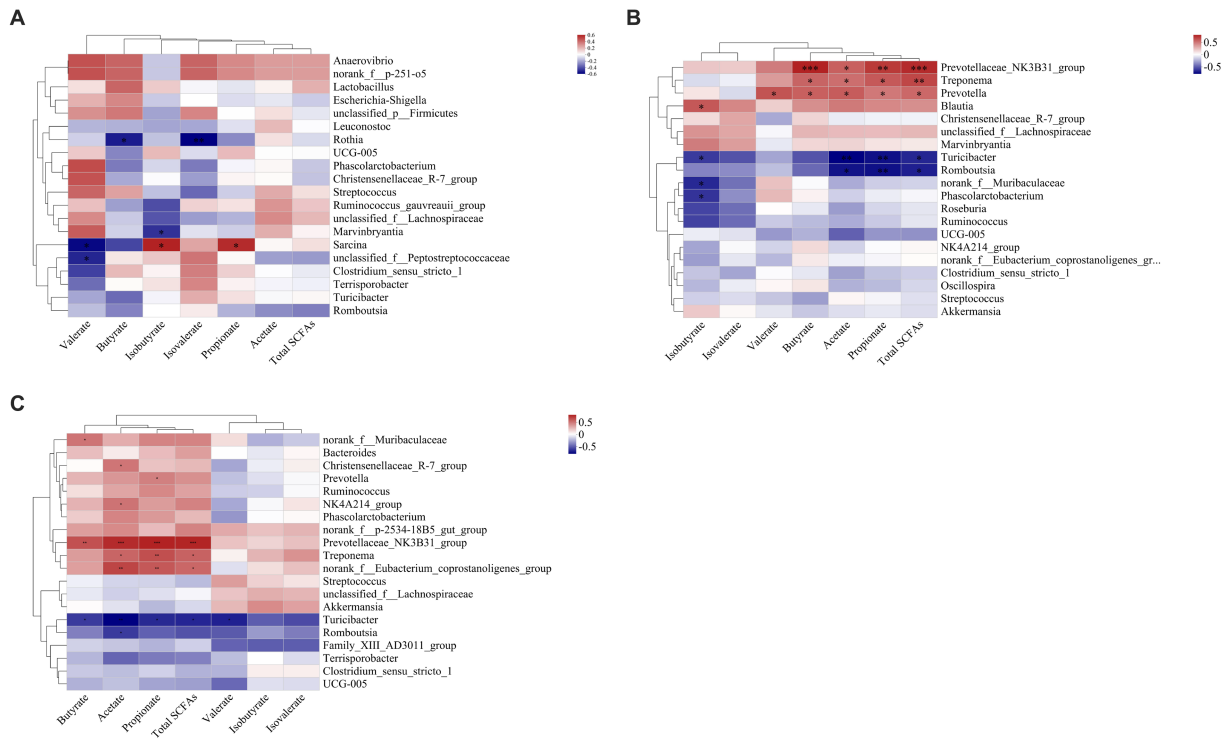

FIGURE 11
Correlation heatmaps between the short-chain fatty acid (SCFA) concentrations and the relative abundances of the top 20 genera in the ileal **(A)**, colonic **(B)**, and rectal **(C)** digesta. Correlation is indicated by a color gradient from blue to red based on Spearman's correlation coefficients. The asterisk indicates a significant correlation between two variables, $*p < 0.05$, $**p < 0.01$, $***p < 0.001$.

(Bach-Knudsen et al., 2017). In addition, the protein level in the W diet is higher than that in the PR diet (11.12 versus 7.57%), thus there may be more undigested protein entering the hindgut. When the carbon source is gradually depleted in the hindgut, protein fermentation will occur in the distal of the colon, producing toxic metabolites such as ammonia, biogenic amines, hydrogen sulfide, indenol, and phenolic compounds (Rist et al., 2013; Molist et al., 2014; Giuberti et al., 2015; Pieper et al., 2016; Jha et al., 2019). This may provide a favorable growth environment for the colonization of potential pathogenic bacteria such as Spirochaetota (Shin et al., 2015).

Prevotella mainly uses carbohydrates as substrates and has the ability to hydrolyze protein, hemicellulose, and pectin (Varel and Yen, 1997; Burbach et al., 2017; Zhu et al., 2017; Han et al., 2023; Pandey et al., 2023). In this study, the cell wall of W contains abundant and highly soluble AX (Nortey et al., 2008; Bach-Knudsen, 2015; Jaworski et al., 2015), which may provide substrates for the colonization of *Prevotellaceae_NK3B31_group* in W_C and W_R groups (Figures 8D,H).

4.4 Effect of diet and digestive parts on SCFAs production

The DF, protein, and peptide in the cereal grain diet will be fermented by the microbiota in the cecum and colon (Macfarlane and Macfarlane, 2012). The main products are acetate, propionate, butyrate, H_2, CH_4, and CO_2 (Cummings et al., 1987; Macfarlane and Macfarlane, 1993; Williams et al., 2001). The proportion of acetate can reach approximately two-thirds of the produced SCFAs (Williams et al., 2001; Lunn and Buttriss, 2007), which is consistent with our results (Table 3). Due to the large number of microbial communities that are highly active in the cecum and proximal colon, the concentrations of almost all kinds of SCFAs were increased in the colonic and rectal digesta (Louis et al., 2007). However, with the gradual consumption of fermentation substrates in the colon, a portion of SCFAs is utilized by colonocytes or absorbed into portal vein blood (Nielsen et al., 2014; Koh et al., 2016). These resulted in a decrease in the majority of SCFA contents in the rectum.

Our results showed that the W diet group had the highest concentrations of acetate, propionate, butyrate, and total SCFAs in the colonic and rectal digesta (Table 3). This means that microorganisms have a stronger fermentation effect on the W diet. Similarly, a previous study reported that whole-W diets exhibited higher SCFA concentrations in the cecum and colon of rats compared to the rice diet (Han et al., 2018). AX is the main type of NSP in W, with a high content (5.85–6.74%), less branched chains, and good water solubility, which makes it easy to be rapidly fermented (Zhang et al., 2015; Weiss et al., 2016; Bach-Knudsen et al., 2017; Navarro et al., 2019b). On the contrary, PR is difficult to ferment because of high IDF content, heavily branched AX, and the poor water solubility of β-glucan and lignin (Bach-Knudsen, 2014; Zhang et al., 2015; Tiwari et al., 2019). Isobutyrate and isovalerate are mainly formed by the metabolism of branched-chain amino acids such as valine, leucine, and isoleucine (Macfarlane et al., 1992). For the W diet group, we found that isobutyrate and isovalerate contents were the highest in the colonic and rectal digesta (Table 3). These results reveal that stronger protein fermentation appears in the hindgut of adult pigs fed a W diet.

4.5 Effect of microbial communities on SCFAs production

SCFAs are mainly the result of carbohydrate fermentation by specific microbial communities through different metabolic pathways (Gong et al., 2018). *Bacteroides* spp. and *Prevotella* spp. may convert pyruvate to acetate through the acetyl-CoA or the Wood–Ljungdahl pathway (Ragsdale and Pierce, 2008; Koh et al., 2016). Thus, in this study, we observed the significant positive relationships between Bacteroidota, *Prevotellaceae_NK3B31_group,* and acetate in the colon and rectum (Figures 10B,C, 11B,C). Propionate can be formed by some members of Bacteroidota via the succinate pathway (Scott et al., 2006; Reichardt et al., 2014). Therefore, we found that propionate was significantly positively correlated with Bacteroidota in the colon and rectum (Figures 10B,C), which is in line with our expectations. Butyrate is the preferred metabolic substrate and the main energy source of colon cells (Gardiner et al., 2020; Han et al., 2023). Butyrate is formed mainly through the phosphotransbutyrylase and butyrate kinase pathways, the butyryl-CoA: acetyl-CoA transferase pathway, and the lysine pathway (Duncan et al., 2002; Louis et al., 2004; Vital et al., 2014). Previous studies have shown that butyrate-producing bacteria are mainly *Clostridium clusters* IV and XIVa (Louis and Flint, 2009). However, no similar results were obtained in this study. Interestingly, some flora in the colon and rectum that were positively correlated with butyrate tend to be positively associated with acetate (Figures 10B,C, 11B,C). It has been shown that the presence of acetate results in the production of butyrate (Diez-Gonzalez et al., 1999). Based on this, we speculate that Fibrobacterota, Bacteroidota, Spirochaetota, *Prevotella_NK3B31_group,* and *Treponema* may have the ability to convert acetate to butyrate. Fibrobacterota in the colon was positively correlated with acetate, propionate, butyrate, and total SCFAs (Figure 10B), which is expected because Fibrobacterota can degrade cellulose and convert it to various SCFAs (Miron and Ben-Ghedalia, 1993).

A previous review summarized that Firmicutes and Actinobacteriota are important SCFA-producing bacteria (Gong et al., 2018). However, we found that Firmicutes and Actinobacteriota in the colon and rectum were negatively correlated with multiple SCFAs, while Spirochaetota, Proteobacteria, and *Treponema* were in contrast (Figures 10B,C, 11B,C). In general, higher concentrations of SCFAs will lead to a more acidic environment in the hindgut, which may inhibit the survival of potential pathogens such as Spirochaetota and Proteobacteria. Indeed, our results contradict it, which requires further experiments to explore the mechanism of this phenomenon in an adult pig model.

5 Conclusion

The diversity of microbial communities in the colon and rectum was similar but markedly different from that in the stomach, duodenum, jejunum, and ileum. From the stomach to the rectum, the evolution from aerobic bacteria and facultative anaerobes to anaerobes was observed. The W diet was more conducive to the colonization of Bacteroidota and *Prevotellaceae_NK3B31_group* that mainly used carbohydrates in the hindgut, however, a greater abundance of potential pathogenic bacteria was found. Meanwhile, the W diet showed higher concentrations of all SCFAs in the hindgut compared to the PR diet. These findings reveal the spatial variation regularities of GIT microbiota in the adult pig model, suggesting that W has better fermentability than C and PR, and provide new insights for GIT microbiota and metabolites responses to cereal grains diets.

Data availability statement

The data presented in the study are deposited into the Sequence Read Archive (SRA) database (https://www.ncbi.nlm.nih.gov/sra), under accession number PRJNA1091723 (https://www.ncbi.nlm.nih.gov/bioproject/PRJNA1091723).

Ethics statement

The animal experiments were carried out in the metabolism laboratory of the Institute of Subtropical Agriculture, Chinese Academy of Sciences (Changsha, China). The experimental protocols, including animal care and use, were reviewed and approved by the Animal Care and Use committee at the Institute of Subtropical Agriculture, Chinese Academy of Sciences (IACUC#201302). The studies were conducted in accordance with the local legislation and institutional requirements. Written informed consent was obtained from the owners for the participation of their animals in this study.

Author contributions

GF: Conceptualization, Data curation, Formal analysis, Investigation, Methodology, Project administration, Resources, Software, Supervision, Visualization, Writing – original draft, Writing – review & editing. MD: Data curation, Formal analysis, Methodology, Writing – review & editing. RL: Conceptualization, Formal analysis, Funding acquisition, Investigation, Methodology, Project administration, Resources, Supervision, Writing – review & editing. GH: Data curation, Formal analysis, Methodology, Writing – review & editing. QO: Writing – review & editing. XJ: Data curation, Formal analysis, Methodology, Writing – review & editing. XL: Formal analysis, Methodology, Writing – review & editing. HT: Formal analysis, Methodology, Writing – review & editing. FC: Formal analysis, Methodology, Writing – review & editing. SP: Formal analysis, Methodology, Writing – review & editing. DW: Formal analysis, Methodology, Writing – review & editing. YY: Conceptualization, Funding acquisition, Investigation, Project administration, Writing – review & editing.

Funding

The author(s) declare that financial support was received for the research, authorship, and/or publication of this article. This study is supported by grants from the National Natural Science Foundation of China (32472957), National Key Research and Development Program (2021YFD1300201 and 2021YFD1301004), National Center of Technology Innovation for Pigs (NCTIP- XDB18), the Ministry of Agriculture and Rural Affairs (16190298, 16200142, and 20210406), the Key Project of Science and Technology of Yunnan Province

(202202AE090032), the Science and Technology Innovation Program of Hunan Province (2020RC2063), the Natural Science Foundation of Hunan Province (2022JJ40532), and the Open Fund of Key Laboratory of Agro-ecological Processes in Subtropical Region, Chinese Academy of Sciences (ISA2021103 and ISA2023201).

Conflict of interest

The authors declare that the research was conducted in the absence of any commercial or financial relationships that could be construed as a potential conflict of interest.

The handling editor GB declared a past co-authorship with the author YY.

Publisher's note

Supplementary material

The Supplementary material for this article can be found online at: https://www.frontiersin.org/articles/10.3389/fmicb.2024.1442077/full#supplementary-material

References

Adeola, O. (2000). "Digestion and balance techniques in pigs" in Swine nutrition. eds. J. Austin, L. Lewis and S. Lee (Boca Raton, FL: CRC Press), 923–936.

Adhikari, B., Kim, S. W., and Kwon, Y. M. (2019). Characterization of microbiota associated with digesta and mucosa in different regions of gastrointestinal tract of nursery pigs. *Int. J. Mol. Med. Adv. Sci.* 20:1630. doi: 10.3390/ijms20071630

Ahn, K. B., Baik, J. E., Park, O. J., Yun, C. H., and Han, S. H. (2018). *Lactobacillus plantarum* lipoteichoic acid inhibits biofilm formation of *Streptococcus mutans*. *PLoS One* 13:e0192694. doi: 10.1371/journal.pone.0192694

Albenberg, L., Esipova, T. V., Judge, C. P., Bittinger, K., Chen, J., Laughlin, A., et al. (2014). Correlation between intraluminal oxygen gradient and radial partitioning of intestinal microbiota. *Gastroenterology* 147, 1055–1063.e8. doi: 10.1053/j.gastro.2014.07.020

AOAC (2012). Official methods of analysis. *19th* Edn. Arlington, Va: Off. Assoc. Anal. Chem.

Bach-Knudsen, K. E. (2014). Fiber and nonstarch polysaccharide content and variation in common crops used in broiler diets. *Poult. Sci.* 93, 2380–2393. doi: 10.3382/ps.2014-03902

Bach-Knudsen, K. E. (2015). Microbial degradation of whole-grain complex carbohydrates and impact on short-chain fatty acids and health. *Adv. Nutr.* 6, 206–213. doi: 10.3945/an.114.007450

Bach-Knudsen, K. E., Nørskov, N. P., Bolvig, A. K., Hedemann, M. S., and Lærke, H. N. (2017). Dietary fibers and associated phytochemicals in cereals. *Mol. Nutr. Food Res.* 61:1600518. doi: 10.1002/mnfr.201600518

Bergey, D. H., Harrison, F. C., Breed, R. S., Hammer, B. W., and Huntoon, F. M. (2001) in Bergey's manual of systematic bacteriology. eds. G. M. Garrity, D. R. Boone and R. W. Castenholz, vol. *2-4. 2nd.* ed (New York, NY: Springer Press).

Burbach, K., Strang, E. J. P., Mosenthin, R., Camarinha-Silva, A., and Seifert, J. (2017). Porcine intestinal microbiota is shaped by diet composition based on rye or triticale. *J. Appl. Microbiol.* 123, 1571–1583. doi: 10.1111/jam.13595

Cervantes-Pahm, S. K., Liu, Y. H., and Stein, H. H. (2014). Comparative digestibility of energy and nutrients and fermentability of dietary fiber in eight cereal grains fed to pigs. *J. Sci. Food Agric.* 94, 841–849. doi: 10.1002/jsfa.6316

Chao, A. (1984). Non-parametric estimation of the number of classes in a population. *Scand. J. Stat.* 11, 265–270. doi: 10.2307/4615964

Che, L. Q., Chen, H., Yu, B., He, J., Zheng, P., Mao, X. B., et al. (2014). Long-term intake of pea fiber affects colonic barrier function, bacterial and transcriptional profile in pig model. *Nutr. Cancer* 66, 388–399. doi: 10.1080/01635581.2014.884229

Chen, S. F., Zhou, Y. Q., Chen, Y. R., and Gu, J. (2018). Fastp: an ultra-fast all-in-one FASTQ preprocessor. *Bioinformatics* 34, i884–i890. doi: 10.1093/bioinformatics/bty560

Crespo-Piazuelo, D., Estellé, J., Revilla, M., Criado-Mesas, L., Ramayo-Caldas, Y., Óvilo, C., et al. (2018). Characterization of bacterial microbiota compositions along the intestinal tract in pigs and their interactions and functions. *Sci. Rep.* 8:12727. doi: 10.1038/s41598-018-30932-6

Cuiv, P. O., Klaassens, E. S., Durkin, A. S., Harkins, D. M., Foster, L., McCorrison, J., et al. (2011). Draft genome sequence of *Turicibacter sanguinis* PC909, isolated from human feces. *J. Bacteriol.* 193, 1288–1289. doi: 10.1128/jb.01328-10

Cummings, J. H., Pomare, E. W., Branch, W. J., Naylor, C. P., and MacFarlane, G. (1987). Short chain fatty acids in human large intestine, portal, hepatic and venous blood. *Gut* 28, 1221–1227. doi: 10.1136/gut.28.10.1221

David, L. A., Maurice, C. F., Carmody, R. N., Gootenberg, D. B., Button, J. E., Wolfe, B. E., et al. (2014). Diet rapidly and reproducibly alters the human gut microbiome. *Nature* 505, 559–563. doi: 10.1038/nature12820

DeBey, B. M., Blanchard, P. C., and Durfee, P. T. (1996). Abomasal bloat associated with Sarcina-like bacteria in goat kids. *J. Am. Vet. Med. Assoc.* 209, 1468–1469.

DiBaise, J. K., Zhang, H., Crowell, M. D., Krajmalnik-Brown, R., Decker, G. A., and Rittmann, B. E. (2008). Gut microbiota and its possible relationship with obesity. *Mayo Clin. Proc.* 83, 460–469. doi: 10.4065/83.4.460

Diez-Gonzalez, F., Bond, D. R., Jennings, E., and Russell, J. B. (1999). Alternative schemes of butyrate production in Butyrivibrio fibrisolvens and their relationship to acetate utilization, lactate production, and phylogeny. *Arch. Microbiol.* 171, 324–330. doi: 10.1007/s002030050717

Donaldson, G. P., Lee, S. M., and Mazmanian, S. K. (2016). Gut biogeography of the bacterial microbiota. *Nat. Rev. Microbiol.* 14, 20–32. doi: 10.1038/nrmicro3552

Duncan, S. H., Barcenilla, A., Stewart, C. S., Pryde, S. E., and Flint, H. J. (2002). Acetate utilization and butyryl coenzyme A (CoA): acetate-CoA transferase in butyrate-producing bacteria from the human large intestine. *Appl. Environ. Microbiol.* 68, 5186–5190. doi: 10.1128/aem.68.10.5186-5190.2002

Edgar, R. C. (2013). UPARSE: highly accurate OTU sequences from microbial amplicon reads. *Nat. Methods* 10, 996–998. doi: 10.1038/nmeth.2604

Ellner, C., Wessels, A. G., and Zentek, J. (2022). Effects of dietary cereal and protein source on fiber digestibility, composition, and metabolic activity of the intestinal microbiota in weaner piglets. *Animals* 12:109. doi: 10.3390/ani12010109

Fabà, L., Hulshof, T. G., Venrooij, K. C., and Van Hees, H. M. (2024). Variability in feed intake the first days following weaning impacts gastrointestinal tract development, feeding patterns, and growth performance in nursery pigs. *J. Anim. Sci.* 102, 1–12. doi: 10.1093/jas/skad419

FAOSTAT (2023). Gateway to crops and livestock products. Available at: https://www.fao.org/faostat/en/#data/QCL (Accessed March 24, 2023).

Fouhse, J. M., Gänzle, M. G., Beattie, A. D., Vasanthan, T., and Zijlstra, R. T. (2017). Whole-grain starch and fiber composition modifies ileal flow of nutrients and nutrient availability in the hindgut, shifting fecal microbial profiles in pigs. *J. Nutr.* 147, 2031–2040. doi: 10.3945/jn.117.255851

Gao, P. F., Guo, Y. L., Zhang, N. F., Zhang, W. F., Wang, H. J., Guo, X. H., et al. (2019b). Characterization and comparisons of microbiota in different intestinal segments between adult Chinese Shanxi black pigs and large white pigs. *Ann. Microbiol.* 69, 447–456. doi: 10.1007/s13213-018-1430-3

Gao, P. F., Liu, Y. D., Le, B. Y., Qin, B. Y., Liu, M., Zhao, Y. Y., et al. (2019a). A comparison of dynamic distributions of intestinal microbiota between large white and Chinese Shanxi black pigs. *Arch. Microbiol.* 201, 357–367. doi: 10.1007/s00203-019-01620-4

Gardiner, G. E., Metzler-Zebeli, B. U., and Lawlor, P. G. (2020). Impact of intestinal microbiota on growth and feed efficiency in pigs: a review. *Microorganisms* 8:1886. doi: 10.3390/microorganisms8121886

Gidley, M. J. (2023). Grain factors in food and feed that influence digestion and gut fermentation outcomes. *Cereal Chem.* 101, 288–298. doi: 10.1002/cche.10718

Giuberti, G., Gallo, A., Moschini, M., and Masoero, F. (2015). New insight into the role of resistant starch in pig nutrition. *Anim. Feed Sci. Technol.* 201, 1–13. doi: 10.1016/j.anifeedsci.2015.01.004

Gong, L. X., Cao, W. Y., Chi, H. L., Wang, J., Zhang, H. J., Liu, J., et al. (2018). Whole cereal grains and potential health effects: involvement of the gut microbiota. *Food Res. Int.* 103, 84–102. doi: 10.1016/j.foodres.2017.10.025

Hamaker, B. R., and Tuncil, Y. E. (2014). A perspective on the complexity of dietary fiber structures and their potential effect on the gut microbiota. *J. Mol. Biol.* 426, 3838–3850. doi: 10.1016/j.jmb.2014.07.028

Han, X. B., Ma, Y., Ding, S. J., Fang, J., and Liu, G. (2023). Regulation of dietary fiber on intestinal microorganisms and its effects on animal health. *Anim. Nutr.* 14, 356–369. doi: 10.1016/j.aninu.2023.06.004

Han, F., Wang, Y., Han, Y., Zhao, J., Han, F., Song, G., et al. (2018). Effects of whole-grain rice and wheat on composition of gut microbiota and short-chain fatty acids in rats. *J. Agric. Food Chem.* 66, 6326–6335. doi: 10.1021/acs.jafc.8b01891

Hao, W. L., and Lee, Y. K. (2004). Microflora of the gastrointestinal tract: a review. *Methods Mol. Biol.* 268, 491–502. doi: 10.1385/1-59259-766-1:491

Hillman, K., Whyte, A. L., and Stewart, C. S. (1993). Dissolved oxygen in the porcine gastrointestinal tract. *Lett. Appl. Microbiol.* 16, 299–302. doi: 10.1111/j.1472-765X.1993.tb00362.x

Holman, D. B., Brunelle, B. W., Trachsel, J., and Allen, H. K. (2017). Meta-analysis to define a core microbiota in the swine gut. *MSystems* 2, 10–1128. doi: 10.1128/msystems.00004-17

Holscher, H. D. (2017). Dietary fiber and prebiotics and the gastrointestinal microbiota. *Gut Microbes* 8, 172–184. doi: 10.1080/19490976.2017.1290756

Jaworski, N. W., Lærke, H. N., Bach Knudsen, K. E., and Stein, H. H. (2015). Carbohydrate composition and in vitro digestibility of dry matter and nonstarch polysaccharides in corn, sorghum, and wheat and coproducts from these grains. *J. Anim. Sci.* 93, 1103–1113. doi: 10.2527/jas.2014-8147

Jaworski, N. W., and Stein, H. H. (2015). Disappearance of nutrients and energy in the stomach and small intestine, cecum, and colon of pigs fed corn-soybean meal diets containing distillers dried grains with solubles, wheat middlings, or soybean hulls. *J. Anim. Sci.* 93, 1103–1113. doi: 10.2527/jas2016.0752

Jha, R., and Berrocoso, J. F. (2016). Dietary fiber and protein fermentation in the intestine of swine and their interactive effects on gut health and on the environment: a review. *Anim. Feed Sci. Technol.* 212, 18–26. doi: 10.1016/j.anifeedsci.2015.12.002

Jha, R., Fouhse, J. M., Tiwari, U. P., Li, L., and Willing, B. P. (2019). Dietary fiber and intestinal health of monogastric animals. *Front. Vet. Sci.* 6:48. doi: 10.3389/fvets.2019.00048

Kaur, H., Singh, B., and Singh, A. (2021). Comparison of dietary fibers obtained from seven Indian cereal grains. *J. Cereal Sci.* 102:103331. doi: 10.1016/j.jcs.2021.103331

Kelly, J., Daly, K., Moran, A. W., Ryan, S., Bravo, D., and Shirazi-Beechey, S. P. (2017). Composition and diversity of mucosa-associated microbiota along the entire length of the pig gastrointestinal tract; dietary influences. *Environ. Microbiol.* 19, 1425–1438. doi: 10.1111/1462-2920.13619

Koh, A., De Vadder, F., Kovatcheva-Datchary, P., and Bäckhed, F. (2016). From dietary fiber to host physiology: short-chain fatty acids as key bacterial metabolites. *Cell* 165, 1332–1345. doi: 10.1016/j.cell.2016.05.041

Lallès, J. P. (2016). Microbiota-host interplay at the gut epithelial level, health and nutrition. *J. Anim. Sci. Biotechnol.* 7, 66–68. doi: 10.1186/s40104-016-0123-7

Li, R., Chang, L., Hou, G. F., Song, Z. H., Fan, Z. Y., He, X., et al. (2019a). Colonic microbiota and metabolites response to different dietary protein sources in a piglet model. *Front. Nutr.* 6:151. doi: 10.3389/fnut.2019.00151

Li, R., Hou, G. F., Jiang, X. D., Song, Z. H., Fan, Z. Y., Hou, D. X., et al. (2019b). Different dietary protein sources in low protein diets regulate colonic microbiota and barrier function in a piglet model. *Food Funct.* 10, 6417–6428. doi: 10.1039/c9fo01154d

Li, D. F., Qiao, S. Y., Chen, D. W., Wu, D., Jiang, Z. Y., Liu, Z. H., et al. (2020). Nutrient requirements of swine in China. Beijing: China Agric. Sci. Tech. Press.

Li, Z. Q., Tang, L. Z., Liu, N., Zhang, F., Liu, X., Jiang, Q., et al. (2021). Comparative effects of compound enzyme and antibiotics on growth performance, nutrient digestibility, blood biochemical index, and intestinal health in weaned pigs. *Front. Microbiol.* 12:768767. doi: 10.3389/fmicb.2021.768767

Li, Z. Q., Zhang, F., Zhao, Y. R., Liu, X., Xie, J. Y., and Ma, X. K. (2023). Effects of different starch diets on growth performance, intestinal health and faecal microbiota of growing pigs. *J. Anim. Physiol. Anim. Nutr.* 107, 1043–1053. doi: 10.1111/jpn.13810

Litvak, Y., Byndloss, M. X., Tsolis, R. M., and Bäumler, A. J. (2017). Dysbiotic Proteobacteria expansion: a microbial signature of epithelial dysfunction. *Curr. Opin. Microbiol.* 39, 1–6. doi: 10.1016/j.mib.2017.07.003

Liu, H. Y., Ivarsson, E., Dicksved, J., Lundh, T., and Lindberg, J. E. (2012). Inclusion of chicory (*Cichorium intybus* L.) in pigs' diets affects the intestinal microenvironment and the gut microbiota. *Appl. Environ. Microbiol.* 78, 4102–4109. doi: 10.1128/AEM.07702-11

Liu, G. S., Li, P. H., Hou, L. M., Niu, Q., Pu, G., Wang, B. B., et al. (2021). Metagenomic analysis reveals new microbiota related to fiber digestion in pigs. *Front. Microbiol.* 12:746717. doi: 10.3389/fmicb.2021.746717

Liu, H., Wang, J., He, T., Becker, S., Zhang, G. L., Li, D. F., et al. (2018). Butyrate: a double-edged sword for health? *Adv. Nutr.* 9, 21–29. doi: 10.1093/advances/nmx009

Liu, C. S., Zhao, D. F., Ma, W. J., Guo, Y. D., Wang, A. J., Wang, Q. L., et al. (2016). Denitrifying sulfide removal process on high-salinity wastewaters in the presence of *Halomonas* sp. *Appl. Microbiol. Biotechnol.* 100, 1421–1426. doi: 10.1007/s00253-015-7039-6

Liu, Y., Zheng, Z. J., Yu, L. H., Wu, S. L., Sun, L., Wu, S. L., et al. (2019). Examination of the temporal and spatial dynamics of the gut microbiome in newborn piglets reveals distinct microbial communities in six intestinal segments. *Sci. Rep.* 9:3453. doi: 10.1038/s41598-019-40235-z

Looft, T., Allen, H. K., Cantarel, B. L., Levine, U. Y., Bayles, D. O., Alt, D. P., et al. (2014). Bacteria, phages and pigs: the effects of in-feed antibiotics on the microbiome at different gut locations. *ISME J.* 8, 1566–1576. doi: 10.1038/ismej.2014.12

Louis, P., Duncan, S. H., McCrae, S. I., Millar, J., Jackson, M. S., and Flint, H. J. (2004). Restricted distribution of the butyrate kinase pathway among butyrate-producing bacteria from the human colon. *J. Bacteriol.* 186, 2099–2106. doi: 10.1128/jb.186.7.2099-2106.2004

Louis, P., and Flint, H. J. (2009). Diversity, metabolism and microbial ecology of butyrate-producing bacteria from the human large intestine. *FEMS Microbiol. Lett.* 294, 1–8. doi: 10.1111/j.1574-6968.2009.01514.x

Louis, P., Scott, K. P., Duncan, S. H., and Flint, H. J. (2007). Understanding the effects of diet on bacterial metabolism in the large intestine. *J. Appl. Microbiol.* 102, 1197–1208. doi: 10.1111/j.1365-2672.2007.03322.x

Lunn, J., and Buttriss, J. L. (2007). Carbohydrates and dietary fibre. *Nutr. Bull.* 32, 21–64. doi: 10.1111/j.1467-3010.2007.00616.x

Luo, Y. H., Ren, W., Smidt, H., Wright, A. D. G., Yu, B., Schyns, G., et al. (2022). Dynamic distribution of gut microbiota in pigs at different growth stages: composition and contribution. *Microbiol. Spectrum.* 10, e00688–e00621. doi: 10.1128/spectrum.00688-21

Ma, N., Guo, P. T., Zhang, J., He, T., Kim, S. W., Zhang, G. L., et al. (2018). Nutrients mediate intestinal bacteria–mucosal immune crosstalk. *Front. Immunol.* 9:317319. doi: 10.3389/fimmu.2018.00005

Macfarlane, G. T., Gibson, G. R., Beatty, E., and Cummings, J. H. (1992). Estimation of short-chain fatty acid production from protein by human intestinal bacteria based on branched-chain fatty acid measurements. *FEMS Microbiol. Ecol.* 10, 81–88. doi: 10.1111/j.1574-6941.1992.tb00002.x

Macfarlane, G. T., and Macfarlane, S. (1993). Factors affecting fermentation reactions in the large bowel. *Proc. Nutr. Soc.* 52, 367–373. doi: 10.1079/PNS19930072

Macfarlane, G. T., and Macfarlane, S. (2012). Bacteria, colonic fermentation, and gastrointestinal health. *J. AOAC Int.* 95, 50–60. doi: 10.5740/jaoacint.SGE_Macfarlane

Magoč, T., and Salzberg, S. L. (2011). FLASH: fast length adjustment of short reads to improve genome assemblies. *Bioinformatics* 27, 2957–2963. doi: 10.1093/bioinformatics/btr507

Mao, S. Y., Zhang, M. L., Liu, J. H., and Zhu, W. J. (2015). Characterising the bacterial microbiota across the gastrointestinal tracts of dairy cattle: membership and potential function. *Sci. Rep.* 5:16116. doi: 10.1038/srep16116

Menkovska, M., Levkov, V., Damjanovski, D., Gjorgovska, N., Knezevic, D., Nikolova, N., et al. (2017). Content of TDF, SDF and IDF in cereals grown by organic and conventional farming-a short report. *Polish J. Food Nut. Sci.* 67, 241–244. doi: 10.1515/pjfns-2016-0030

Miron, J., and Ben-Ghedalia, D. (1993). Digestion of cell-wall monosaccharides of ryegrass and alfalfa hays by the ruminal bacteria Fibrobacter succinogenes and *Butyrivibrio fibrisolvens*. *Can. J. Microbiol.* 39, 780–786. doi: 10.1139/m93-115

Molist, F., Van Oostrum, M., Pérez, J. F., Mateos, G. G., Nyachoti, C. M., and Van Der Aar, P. J. (2014). Relevance of functional properties of dietary fibre in diets for weanling pigs. *Anim. Feed Sci. Technol.* 189, 1–10. doi: 10.1016/j.anifeedsci.2013.12.013

Morrison, D. J., and Preston, T. (2016). Formation of short chain fatty acids by the gut microbiota and their impact on human metabolism. *Gut Microbes* 7, 189–200. doi: 10.1080/19490976.2015.1134082

Navarro, D. M. D. L., Abelilla, J. J., and Stein, H. H. (2019b). Structures and characteristics of carbohydrates in diets fed to pigs: a review. *J. Anim. Sci. Biotechnol.* 10, 39–17. doi: 10.1186/s40104-019-0345-6

Navarro, D. M. D. L., Bruininx, E. M. A. M., De Jong, L., and Stein, H. H. (2019a). Effects of inclusion rate of high fiber dietary ingredients on apparent ileal, hindgut, and total tract digestibility of dry matter and nutrients in ingredients fed to growing pigs. *Anim. Feed Sci. Technol.* 248, 1–9. doi: 10.1016/j.anifeedsci.2018.12.001

Nielsen, T. S., Lærke, H. N., Theil, P. K., Sørensen, J. F., Saarinen, M., Forssten, S., et al. (2014). Diets high in resistant starch and arabinoxylan modulate digestion processes and SCFA pool size in the large intestine and faecal microbial composition in pigs. *Br. J. Nutr.* 112, 1837–1849. doi: 10.1017/S000711451400302X

Nortey, T. N., Patience, J. F., Sands, J. S., Trottier, N. L., and Zijlstra, R. T. (2008). Effects of xylanase supplementation on the apparent digestibility and digestible content of energy, amino acids, phosphorus, and calcium in wheat and wheat by-products from dry milling fed to grower pigs. *J. Anim. Sci.* 86, 3450–3464. doi: 10.2527/jas.2007-0472

NRC (2012). Nutrient requirements of swine. *11th rev.* Edn. Washington, DC: Natl. Acad. Press.

O'Connell, J. M., Sweeney, T., Callan, J. J., and O'Doherty, J. V. (2005). The effect of cereal type and exogenous enzyme supplementation in pig diets on nutrient digestibility, intestinal microflora, volatile fatty acid concentration and manure ammonia emissions from finisher pigs. *Anim. Sci.* 81, 357–364. doi: 10.1079/ASC42040357

O'Hara, A. M., and Shanahan, F. (2006). The gut flora as a forgotten organ. *EMBO Rep.* 7, 688–693. doi: 10.1038/sj.embor.7400731

Pandey, S., Kim, E. S., Cho, J. H., Song, M., Doo, H., Kim, S., et al. (2023). Swine gut microbiome associated with non-digestible carbohydrate utilization. *Front. Vet. Sci.* 10:1231072. doi: 10.3389/fvets.2023.1231072

Pieper, R., Tudela, C. V., Taciak, M., Bindelle, J., Pérez, J. F., and Zentek, J. (2016). Health relevance of intestinal protein fermentation in young pigs. *Anim. Health Res. Rev.* 17, 137–147. doi: 10.1017/s1466252316000141

Power, S. E., O'Toole, P. W., Stanton, C., Ross, R. P., and Fitzgerald, G. F. (2014). Intestinal microbiota, diet and health. *Br. J. Nutr.* 111, 387–402. doi: 10.1017/S0007114513002560

Ragsdale, S. W., and Pierce, E. (2008). Acetogenesis and the wood-Ljungdahl pathway of CO_2 fixation. *Biochim. Biophys. Acta* 1784, 1873–1898. doi: 10.1016/j.bbapap.2008.08.012

Reichardt, N., Duncan, S. H., Young, P., Belenguer, A., McWilliam Leitch, C., Scott, K. P., et al. (2014). Phylogenetic distribution of three pathways for propionate production within the human gut microbiota. *ISME J.* 8, 1323–1335. doi: 10.1038/ismej.2014.14

Rist, V. T. S., Weiss, E., Eklund, M., and Mosenthin, R. (2013). Impact of dietary protein on microbiota composition and activity in the gastrointestinal tract of piglets in relation to gut health: a review. *Animal* 7, 1067–1078. doi: 10.1017/S1751731113000062

Rodehutscord, M., Rückert, C., Maurer, H. P., Schenkel, H., Schipprack, W., Bach Knudsen, K., et al. (2016). Variation in chemical composition and physical characteristics of cereal grains from different genotypes. *Arch. Anim. Nutr.* 70, 87–107. doi: 10.1080/1745039X.2015.1133111

Schloss, P. D., Westcott, S. L., Ryabin, T., Hall, J. R., Hartmann, M., Hollister, E. B., et al. (2009). Introducing mothur: open-source, platform-independent, community-supported software for describing and comparing microbial communities. *Appl. Environ. Microbiol.* 75, 7537–7541. doi: 10.1128/AEM.01541-09

Scott, K. P., Duncan, S. H., and Flint, H. J. (2008). Dietary fibre and the gut microbiota. *Nutr. Bull.* 33, 201–211. doi: 10.1111/j.1467-3010.2008.00706.x

Scott, K. P., Martin, J. C., Campbell, G., Mayer, C. D., and Flint, H. J. (2006). Whole-genome transcription profiling reveals genes up-regulated by growth on fucose in the human gut bacterium "*Roseburia inulinivorans*". *J. Bacteriol.* 188, 4340–4349. doi: 10.1128/jb.00137-06

Segata, N., Izard, J., Waldron, L., Gevers, D., Miropolsky, L., Garrett, W. S., et al. (2011). Metagenomic biomarker discovery and explanation. *Genome Biol.* 12, R60–R18. doi: 10.1186/gb-2011-12-6-r60

Shannon, C. E. (1948). A mathematical theory of communication. *Bell Syst. Tech. J.* 27, 379–423. doi: 10.1002/j.1538-7305.1948.tb01338.x

Shin, N. R., Whon, T. W., and Bae, J. W. (2015). Proteobacteria: microbial signature of dysbiosis in gut microbiota. *Trends Biotechnol.* 33, 496–503. doi: 10.1016/j.tibtech.2015.06.011

Simpson, E. H. (1949). Measurement of species diversity. *Nature* 163:688.

Singh, J., Dartois, A., and Kaur, L. (2010). Starch digestibility in food matrix: a review. *Trends Food Sci. Technol.* 21, 168–180. doi: 10.1016/j.tifs.2009.12.001

Snart, J., Bibiloni, R., Grayson, T., Lay, C., Zhang, H., Allison, G. E., et al. (2006). Supplementation of the diet with high-viscosity beta-glucan results in enrichment for lactobacilli in the rat cecum. *Appl. Environ. Microbiol.* 72, 1925–1931. doi: 10.1128/AEM.72.3.1925-1931.2006

Sopha, S. C., Manejwala, A., and Boutros, C. N. (2015). Sarcina, a new threat in the bariatric era. *Hum. Pathol.* 46, 1405–1407. doi: 10.1016/j.humpath.2015.05.021

Spellerberg, B., and Brandt, C. (2015). "Streptococcus," in *Manual of Clinical Microbiology*, eds. J. H. Jorgensen, M. A. Pfaller, K. C. Carroll, G. Funke, M. L. Landry, S. S. Richter, and D. W. Warnock (Washington DC: ASM press), 11th ed, 1, 383–402. doi: 10.1128/9781555817381.ch22

Stackebrandt, E., and Goebel, B. M. (1994). Taxonomic note: a place for DNA-DNA reassociation and 16S rRNA sequence analysis in the present species definition in bacteriology. *Int. J. Syst. Evol. Microbiol.* 44, 846–849. doi: 10.1099/00207713-44-4-846

Tan, F. P., Wang, L. F., Gao, J., Beltranena, E., Vasanthan, T., and Zijlstra, R. T. (2021). Hindgut fermentation of starch is greater for pulse grains than cereal grains in growing pigs. *J. Anim. Sci.* 99, 1–13. doi: 10.1093/jas/skab306

Tan, Z., Wang, Y., Yang, T., Ao, H., Chen, S. K., Xing, K., et al. (2018). Differences in gut microbiota composition in finishing landrace pigs with low and high feed conversion ratios. *Antonie Van Leeuwenhoek* 111, 1673–1685. doi: 10.1007/s10482-018-1057-1

Tiwari, U. P., Singh, A. K., and Jha, R. (2019). Fermentation characteristics of resistant starch, arabinoxylan, and β-glucan and their effects on the gut microbial ecology of pigs: a review. *Anim. Nutr.* 5, 217–226. doi: 10.1016/j.aninu.2019.04.003

Turnbaugh, P. J., Ridaura, V. K., Faith, J. J., Rey, F. E., Knight, R., and Gordon, J. I. (2009). The effect of diet on the human gut microbiome: a metagenomic analysis in humanized gnotobiotic mice. *Sci. Transl. Med.* 1:6ra14. doi: 10.1126/scitranslmed.3000322

Urriola, P. E., Shurson, G. C., and Stein, H. H. (2010). Digestibility of dietary fiber in distillers coproducts fed to growing pigs. *J. Anim. Sci.* 88, 2373–2381. doi: 10.2527/jas.2009-2227

Van der Meulen, J., and Jansman, A. J. M. (2010). Effect of pea and faba bean fractions on net fluid absorption in ETEC-infected small intestinal segments of weaned piglets. *Livest. Sci.* 133, 207–209. doi: 10.1016/j.livsci.2010.06.065

Van Soest, P. J., Robertson, J. B., and Lewis, B. A. (1991). Methods for dietary Fiber, neutral detergent Fiber, and nonstarch polysaccharides in relation to animal nutrition. *J. Dairy Sci.* 74, 3583–3597. doi: 10.3168/jds.S0022-0302(91)78551-2

Varel, V. H., and Yen, J. T. (1997). Microbial perspective on fiber utilization by swine. *J. Anim. Sci.* 75, 2715–2722. doi: 10.2527/1997.75102715x

Vital, M., Howe, A. C., and Tiedje, J. M. (2014). Revealing the bacterial butyrate synthesis pathways by analyzing (meta) genomic data. *MBio* 5:e00889-14. doi: 10.1128/mbio.00889-14

Walker, A. W., Ince, J., Duncan, S. H., Webster, L. M., Holtrop, G., Ze, X., et al. (2011). Dominant and diet-responsive groups of bacteria within the human colonic microbiota. *ISME J.* 5, 220–230. doi: 10.1038/ismej.2010.118

Walsh, S. K., Lucey, A., Walter, J., Zannini, E., and Arendt, E. K. (2022). Resistant starch-an accessible fiber ingredient acceptable to the Western palate. *Compr. Rev. Food Sci. Food Saf.* 21, 2930–2955. doi: 10.1111/1541-4337.12955

Wang, Q., Garrity, G. M., Tiedje, J. M., and Cole, J. R. (2007). Naive Bayesian classifier for rapid assignment of rRNA sequences into the new bacterial taxonomy. *Appl. Environ. Microbiol.* 73, 5261–5267. doi: 10.1128/AEM.00062-07

Wang, K., Jin, X. L., You, M. M., Tian, W. L., Le Leu, R. K., Topping, D. L., et al. (2017). Dietary propolis ameliorates dextran sulfate sodium-induced colitis and modulates the gut microbiota in rats fed a western diet. *Nutrients* 9:875. doi: 10.3390/nu9080875

Weiss, E., Aumiller, T., Spindler, H. K., Rosenfelder, P., Eklund, M., Witzig, M., et al. (2016). Wheat and barley differently affect porcine intestinal microbiota. *J. Sci. Food Agric.* 96, 2230–2239. doi: 10.1002/jsfa.7340

Williams, B. A., Bosch, M. W., Boer, H., Verstegen, M. W. A., and Tamminga, S. (2005). An in vitro batch culture method to assess potential fermentability of feed ingredients for monogastric diets. *Anim. Feed Sci. Technol.* 123-124, 445–462. doi: 10.1016/j.anifeedsci.2005.04.031

Williams, B. A., Verstegen, M. W., and Tamminga, S. (2001). Fermentation in the large intestine of single-stomached animals and its relationship to animal health. *Nutr. Res. Rev.* 14, 207–228. doi: 10.1079/NRR200127

Wong, J. M., De Souza, R., Kendall, C. W., Emam, A., and Jenkins, D. J. (2006). Colonic health: fermentation and short chain fatty acids. *J. Clin. Gastroenterol.* 40, 235–243.doi: 10.1097/00004836-200603000-00015

Zhang, S., Li, W. C. J. S., Smith, C. J., and Musa, H. (2015). Cereal-derived arabinoxylans as biological response modifiers: extraction, molecular features, and immune-stimulating properties. *Crit. Rev. Food Sci. Nutr.* 55, 1035–1052. doi: 10.1080/10408398.2012.705188

Zhao, J. B., Bai, Y., Tao, S. Y., Zhang, G., Wang, J. J., Liu, L., et al. (2019). Fiber-rich foods affected gut bacterial community and short-chain fatty acids production in pig model. *J. Funct. Foods* 57, 266–274. doi: 10.1016/j.jff.2019.04.009

Zhao, W. J., Wang, Y. P., Liu, S. Y., Huang, J. J., Zhai, Z. X., He, C., et al. (2015). The dynamic distribution of porcine microbiota across different ages and gastrointestinal tract segments. *PLoS One* 10:e0117441. doi: 10.1371/journal.pone.0117441

Zhu, Y., Shi, X., Ye, K., Xu, X., Li, C., and Zhou, G. (2017). Beef, chicken, and soy proteins in diets induce different gut microbiota and metabolites in rats. *Front. Microbiol.* 8:1395. doi: 10.3389/fmicb.2017.01395

Zoetendal, E. G., Raes, J., Van Den Bogert, B., Arumugam, M., Booijink, C. C., Troost, F. J., et al. (2012). The human small intestinal microbiota is driven by rapid uptake and conversion of simple carbohydrates. *ISME J.* 6, 1415–1426. doi: 10.1038/ismej.2011.212

frontiers | Frontiers in Microbiology

TYPE Original Research
PUBLISHED 20 November 2024
DOI 10.3389/fmicb.2024.1501211

OPEN ACCESS

EDITED BY
Kang Xu,
Chinese Academy of Sciences (CAS), China

REVIEWED BY
Yu Bai,
Tianjin University of Science and Technology, China
Yu Pi,
Chinese Academy of Agricultural Sciences, China

*CORRESPONDENCE
Jun He
✉ hejun8067@163.com

†These authors have contributed equally to this work and share first authorship

RECEIVED 24 September 2024
ACCEPTED 29 October 2024
PUBLISHED 20 November 2024

CITATION
Zheng Y, Li Y, Yu B, Huang Z, Luo Y, Zheng P, Mao X, Yu J, Tan H, Luo J, Yan H and He J (2024) Grape seed proanthocyanidins improves growth performance, antioxidative capacity, and intestinal microbiota in growing pigs.
Front. Microbiol. 15:1501211.
doi: 10.3389/fmicb.2024.1501211

Grape seed proanthocyanidins improves growth performance, antioxidative capacity, and intestinal microbiota in growing pigs

Yuyang Zheng[1,2†], Yan Li[1,2†], Bing Yu[1,2], Zhiqing Huang[1,2], Yuheng Luo[1,2], Ping Zheng[1,2], Xiangbing Mao[1,2], Jie Yu[1,2], Huize Tan[3], Junqiu Luo[1,2], Hui Yan[1,2] and Jun He[1,2]*

[1]Institute of Animal Nutrition, Sichuan Agricultural University, Chengdu, Sichuan, China, [2]Key Laboratory of Animal Disease-Resistant Nutrition, Chengdu, Sichuan, China, [3]Wens Foodstuff Group Co., Ltd., Yunfu, China

Grape seed proanthocyanidin (GSP) is a kind of plant polyphenols with a wide variety of biological activities. In this study, we explored the effect of dietary GSP supplementation on growth performance, nutrient digestibility, and intestinal microbiota in growing pigs. A total of 180 growing pigs (30.37 ± 0.31 kg) were randomly assigned to five treatment groups, each consisting of six replicate pens with six pigs per pen. The pigs received either a basal diet (control) or a basal diet supplemented with GSP at 15, 30, 60, or 120 mg/kg. The trial lasted for 33 days, and blood and fecal samples were collected for biochemical measurements. GSP supplementation at a dose from 30 to 120 mg/kg decreased the ratio of feed intake to gain (*F*:*G*) ($p < 0.05$). GSP also increased the digestibility of dry matter, crude protein, ether extract, and gross energy ($p < 0.05$). GSP supplementation at 30 mg/kg increased the serum concentrations of immunoglobulin (Ig) A ($p < 0.05$). Interestingly, GSP supplementation at 60 mg/kg decreased the serum concentrations of urea and malondialdehyde ($p < 0.05$). However, the serum concentrations of glutathione peroxidase and total superoxide dismutase were significantly increased upon GSP supplementation ($p < 0.05$). Importantly, GSP supplementation at 120 mg/kg significantly increased the abundance of the phylum Firmicutes, but decreased the abundance of phylum Bacteroidetes and Epsilonbacteraeota in the feces ($p < 0.05$). Moreover, GSP supplementation significantly elevated the abundance of genus Lactobacillus, but decreased the abundance of genus Prevotellaceae NK3B31 ($p < 0.05$). Dietary GSP supplementation improves the growth performance and nutrient digestibility in growing pigs, which may be associated with enhancement of the antioxidative capacity, as well as improvement in gut microbiota. This study may promote the use of GSP in animal nutrition and the feed industry.

KEYWORDS

GSP, growth performance, nutrient digestibility, antioxidant capacity, intestinal microbiota, growing pigs

1 Introduction

Oxidative stress is characterized by excessive production of reactive oxygen species (ROS) within the cell, which leads to disruption of the redox balance in the body (Bhor et al., 2004). Various factors contribute to oxidative stress in pigs, including weaning stress, mycotoxin contamination, social interactions, and the feeding environment (Novais et al.,

2021; Zhao et al., 2013; Yang et al., 2020). Accumulating evidence showed that the modulation of the diet of pigs can also significantly reduce oxidative stress. For instance, dietary supplementation of probiotics during the weaning period was found to attenuate oxidative stress and improve the growth performance of piglets by improving the gut microbiota and inhibiting intestinal inflammation (Xiang et al., 2020). Moreover, dietary supplementation of an antioxidant compound can enhance feed conversion and increase oxidative defense in finishing pigs (Zhu et al., 2022).

Proanthocyanidin is a natural pigment that is abundant in numerous plant species and belongs to a kind of flavonoid compound. Grape seed proanthocyanidin (GSP), is extracted from grape seeds, which is a polymeric compound formed by the condensation of phenolic compounds with trihydroxyflavones. Their chemical structure comprises the core anthocyanin structure, wherein a benzene ring is attached to a tricyclic flavonoid scaffold, featuring hydroxyl and methoxy functional groups (Rodríguez et al., 2019). Prior research has demonstrated that GSP possesses a range of bioactive properties. For instance, GSP exhibits strong antioxidant properties, capable of scavenging free radicals and mitigating oxidative stress, thereby aiding in cellular protection against oxidative damage (Chedea et al., 2010). It also has anti-bacterial (Guo et al., 2020), anti-inflammatory (Tyagi et al., 2013), anti-viral (Ignea et al., 2013), immunomodulatory (Tong et al., 2011), etc. Recently, GSP has been utilized by a wide variety of animal species. For instance, GSP can improve the health status of tilapia and enhance its growth rate (Zhai et al., 2016). GSP has also been reported to enhance rumen fermentation function in cattle, thereby increasing nutrient digestibility (Ma et al., 2023). Moreover, GSP can protect the integrity of the goose intestinal barrier, increase the abundance and diversity of cecal microflora, and promote the growth of beneficial bacteria (Deng et al., 2023).

Although a number of studies revealed a prominent health-promoting effect of GSP, clear evidence establishing direct links among GSP dosage, product origin, developmental stage, and animal species is lacking. Furthermore, the biological events influenced by GSP are still not fully understood in terms of their underlying mechanisms. This study investigated the impact of dietary GSP supplementation on growth performance and intestinal microbiota in growing pigs. We found that GSP significantly improved growth performance in growing pigs, which may be associated with improvement in nutrient digestibility, antioxidative capacity, and intestinal microbiota. This study not only sheds light on the mechanisms underlying GSP's effects on growth in pigs, but may also facilitate its application in animal nutrition and the feed industry.

2 Materials and methods

2.1 Ethics statement

The research underwent submission and approval by the Committee on Animal Care Advisory of Sichuan Agricultural University, with the authorization number SICAU-2021-007. The experiment procedures were conducted in accordance with the Guidelines for the Care and Use of Laboratory Animals.

2.2 Experimental design and diet

A total of 180 pigs (Duroc × Landrace × Yorkshire) with an initial BW of 30.37 ± 0.66 kg (90 barrows and 90 gilts) were allocated to five treatments based on Randomized Complete Block Design. Each treatment group comprised six replicate pens (6 pigs per pen). For each treatment, three replicate pens were utilized to house the barrows and another three pens were utilized to house the gilts (pigs of the same gender were housed in a pen). The treatments were a control diet formulated to meet the requirements from NRC (2012) nutrient requirements (Table 1) with no addition of GSP, and the control diet with four increasing levels of GSP (15, 30, 60, and 120 mg/kg). The GSP was supplied by Fengpeng Biotechnology Co., Ltd. (Guilin, China) and contains 86.81% proanthocyanidin oligomers, 1.52% catechin, 2.41% epicatechin, and 0.98% proanthocyanidin B_2, with a total proanthocyanidin purity of 96.58%. The feeders were refilled three times a day, and drinking water *ad libitum* throughout the experimental period (33 days). The feed intake was recorded every day. The final body weight, average daily feed intake (ADFI), average daily gain (ADG), and the ratio of feed intake to gain (*F*:*G*) were measured at the end of the experiment.

TABLE 1 Composition and nutrient levels of the experimental diets (air-dry basis, %).

Ingredient	%	Nutrient composition[3]	Contents
Corn	72.58	Analyzed nutrient levels	
Soybean meal	17.93	Gross energy, MJ/kg	18.95
Bran	2.50	Crude protein, %	18.48
Fish meal	2.50	Ether extract, %	3.12
Soybean oil	2.00	Calcium, %	0.71
Limestone	0.69	Total phosphorus, %	0.47
Dicalcium phosphate	0.58	Calculated nutrient levels	
Salt	0.30	Digestible energy, MJ/kg	14.23
L-Lysine HCl	0.31	Crude protein, %	15.88
DL-Methionine	0.03	Ether extract, %	5.08
L-Threonine	0.07	Calcium, %	0.66
L-Tryptophan	0.01	Total phosphorus, %	0.51
Choline chloride	0.15	Available phosphorus, %	0.31
Vitaminic premix[1]	0.05	SID[4] Lysine, %	0.98
Mineral premix[2]	0.30	SID Methionine + Cystine, %	0.50
		SID Threonine, %	0.59
		SID Tryptophan, %	0.17

[1]Provided the following (per kilogram of complete diet): 15,000 IU of vitamin A; 5,000 IU of vitamin D_3; 40 IU of vitamin E; 5 mg of vitamin K; 5 mg of vitamin B_1; 12.5 mg of vitamin B_2; 6 mg of vitamin B_6; 0.06 mg of vitamin B_{12}; 50 mg of nicotinic acid; 25 mg of pantothenic acid; 2.5 mg of folic acid; 0.25 mg of biotin.

[2]Provided the following (per kilogram of complete diet): 60.0 mg of Fe (as ferrous sulfate); 4 mg of Cu (as copper sulfate); 60.0 mg of Zn (as zinc sulfate); 2.0 mg of Mn (as manganese sulfate); 0.14 mg of I (as KI); 0.2 mg of Se (as Na_2SeO_3).

[3]The calculated nutrient levels of the diet were obtained from the China Feed Database (2020).

[4]SID = standardized ileal digestibility.

2.3 Sample collection

At the outset of the experiment, feed samples were gathered and preserved for subsequent analysis. During days 25–28 of the experiment, fecal samples were collected daily for four consecutive days from each replicate to assess nutrient digestibility. Hydrochloric acid at a concentration of 10% was added to the fecal samples for nitrogen fixation, and then the samples were dried in an oven at 60°C. The dried samples were then pulverized in a high-speed pulverizer and passed through 0.45 pm filters for chemical assay. Additionally, a portion of fecal samples was collected and stored at −80°C for 16S rDNA sequencing. Approximately 15 mL of blood was drawn from the anterior vena cava of one randomly selected pig from each of the six pens per group on day 33 of the experiment. The blood samples were then centrifuged at 3,000 × *g* for 20 min at 4°C to isolate the serum.

2.4 Apparent total tract nutrient digestibility analysis

Dried and ground feed and fecal samples were utilized for nutrient digestibility analysis, employing acid-insoluble ash (AIA) as an endogenous indicator. The AIA in diet and fecal samples was measured as described by National National Standard (2009). The diet and fecal samples were evaluated for dry matter (DM), crude protein (CP) (Method 976.05; AOAC, 2007), and ether extract (EE) (Method 922.06; AOAC, 2007). An automated oxygen bomb calorimeter (Model 6,400, Parr, United States) was used to evaluate the gross energy (GE). The apparent total tract nutrient digestibility for all parameters was calculated using the following formula:

$$\left[\left(1-\mathrm{A1F2}/\mathrm{A2F1}\right)\times 100\right],$$

in which A1: is the AIA content of the diet, A2: is the AIA content of fecal, F1: is the nutrient content of the diet, F2: is the nutrient content of fecal. The diet was analyzed for calcium and total phosphorus content by inductively coupled plasma spectroscopy (method 985.01 A, B, and C; AOAC, 2007). The calculated nutrient levels of the diet were obtained from the China Feed Database (2020).

2.5 Serum biochemical, immunoglobulin, and antioxidant parameters

Serum biochemical parameters were measured using an Olympus automatic analyzer (Shanghai, China). Utilizing ELISA kits (MEIMIAN, Yancheng, Jiangsu, China), the concentrations of immunoglobulins (Ig) A (MM-090502), G (MM-040302), and M (MM-040202) were measured. Commercial kits from Nanjing Jiancheng Bioengineering Institute (Nanjing, Jiangsu, China) were utilized to measure the concentrations of total antioxidative capacity (T-AOC) (Cat. No. A015-1-2), glutathione peroxidase (GSH-Px) (Cat. No. A005-1-2), catalase (CAT) (Cat. No. A007-1-1), total superoxide dismutase (T-SOD) (Cat. No. A001-1-1), and malondialdehyde (MDA) (Cat. No. A003-1-2).

2.6 Diversity and composition of the bacterial community

From 0.5 g of fecal samples, nucleic acids were extracted with the Stool DNA kit (TIANGEN, China) in accordance with the manufacturer's guidelines. The analysis of bacterial community diversity and composition was conducted using the Quantitative Insights Into Microbial Ecology (QIIME) software package. The PCR amplification focused on the V4 region of the 16S rRNA gene, employing primers 515F (5'-GTGYCAGCMGCCGCGGTAA-3′) and 806R (5'-GGACTACHVGGGTWTCTAAT-3′). The PCR conditions were as follows: initial denaturation at 94°C for 1 min, followed by 1 cycle; denaturation at 94°C for 20 s, annealing at 54°C for 30 s, and extension at 72°C for 30 s for 25–30 cycles; final extension at 72°C for 5 min; held at 4°C. Amplification was carried out using a Verity Thermocycler (Applied Biosystems). PCR products were purified through electrophoresis on a 2% agarose gel. Desired bands were excised from qualified samples and purified using the Zymoclean Gel Recovery Kit (D4008), quantified with a Qubit 2.0 Fluorometer (Thermo Scientific), and mixed in equimolar amounts. Sequencing was conducted using the PE250 method with the Illumina NovaSeq 6,000 SP Reagent Kit V1.5.

Paired-end reads were merged using FLASH. Sequences were demultiplexed based on barcodes with SABRE, followed by barcode trimming, and quality control was performed using QIIME2. Within QIIME2, sequences were denoised and chimeras were removed using the Deblur algorithm, generating an ASV feature table and feature sequences. A 97% similarity threshold was used to define operational taxonomic units (OTUs). The analysis of community composition was performed in R, employing various data transformations and utilizing the ggplot2 package for visualization. The alpha diversity was analyzed in R, with PD index calculations performed using the Picante package, while other indices were calculated using the Vegan package. Bray–Curtis distance was computed using the vegdits function in Vegan, and PCoA analysis was conducted with the ape package.

2.7 Sample size calculation and statistical analysis

Data were analyzed by IBM SPSS 27.0 software (Statistical Product and Service Solutions, Inc., United States). In the context of growth performance and nutrient digestibility, each pen is regarded as the experimental unit; however, for other experimental data, individual pigs are treated as the experimental unit. The growth performance data were analyzed utilizing Linear Mixed Model (LMM), considering dietary treatment and sex as fixed effects with an interaction term for dietary treatment × sex, while considering pen as a random effect. Other data were analyzed using a general linear model (GLM), with dietary treatment and sex as fixed effects with an interaction term for dietary treatment × sex. The effects of dietary treatment were evaluated using one-way ANOVA, followed by Duncan's multiple comparison test to assess mean differences. Results are expressed as mean ± standard error of the mean (SEM), with statistical significance set at $p < 0.05$ and trends defined as $0.05 < p < 0.10$.

3 Results

3.1 Growth performance and nutrient digestibility

As shown in Table 2, dietary GSP supplementation at a dose from 30 to 120 mg/kg significantly increased the ADG and decreased the *F*:*G* ratio of the pigs ($p < 0.05$). Moreover, with dietary GSP supplementation, the digestibility of dry matter, crude protein, ether extract, and gross energy increased quadratically (quadratic, $p < 0.05$).

3.2 Serum biochemical parameters

As shown in Table 3, dietary GSP supplementation did not affect serum biochemical parameters such as the ALT, AST, CK, and TP ($p > 0.05$). Nevertheless, the serum concentration of urea decreased quadratically by GSP supplementation (quadratic, $p < 0.05$).

3.3 Serum immunoglobulins and antioxidative capacity

As shown in Table 4, GSP supplementation at 30 mg/kg significantly elevated serum IgA levels ($p < 0.05$). Additionally, serum MDA levels decreased quadratically with GSP supplementation (quadratic, $p < 0.05$), while serum levels of GSH-Px and T-SOD exhibited a quadratic increase (quadratic, $p < 0.05$).

3.4 Intestinal microbiota

Following OTU assignment and chimera checking, a total of 1,002,573 effective tags representing the 16S rRNA gene V4 region

TABLE 2 Effect of GSP on growth performance and nutrient digestibility in growing pigs.

Items	GSP (mg/kg)					SEM	*p*-value		
	0	15	30	60	120		LMM	Linear	Quadratic
Initial weight, kg	30.39	30.29	30.42	30.33	30.42	0.66	0.75	0.98	1.00
Final weight, kg	57.99	58.88	59.99	59.00	59.53	0.41	0.11	0.28	0.41
ADFI, kg/d	1.95	1.95	1.93	1.89	1.96	0.02	0.30	0.73	0.58
ADG, kg/d	0.84^{c}	0.87^{b}	0.90^{a}	0.87^{ab}	0.88^{ab}	0.01	<0.01	0.23	0.30
F:*G*	2.35^{a}	2.26^{ab}	2.16^{b}	2.19^{b}	2.24^{b}	0.03	<0.01	0.23	0.18
DM, %	85.66^{b}	86.64^{ab}	87.52^{a}	87.84^{a}	86.93^{a}	0.26	0.01	0.04	0.01
CP, %	82.63^{c}	83.07^{bc}	84.59^{ab}	85.11^{a}	84.45^{ab}	0.33	0.02	0.01	0.02
EE, %	66.77^{b}	66.84^{b}	69.39^{a}	70.03^{a}	69.73^{a}	0.40	<0.01	<0.01	<0.01
GE, %	88.34^{c}	89.03^{bc}	89.48^{b}	90.68^{a}	89.35^{bc}	0.24	<0.01	0.03	0.02

Data are shown as mean ± SEM ($n = 6$ replicates per treatment).
[a,b,c]Means lacking a common uppercase superscript differ ($p < 0.05$) using Duncan test.
GSP, Grape Seed Proanthocyanidin; SEM, standard error of the mean; LMM, Linear Mixed Model; ADFI, average daily feed intake; ADG, average daily gain; *F*:*G*, feed to gain ratio; DM, dry matter; CP, crude protein; EE, ether extract; GE, gross energy.

TABLE 3 Effects of dietary GSP on serum biochemical parameters in growing pigs.

Items	GSP (mg/kg)					SEM	*P*-value		
	0	15	30	60	120		GLM	Linear	Quadratic
ALT, U/L	52.29	48.02	45.42	44.54	45.29	1.99	0.77	0.22	0.37
AST, U/L	64.83	39.63	34.00	33.43	37.95	4.59	0.24	0.06	0.04
ALP, U/L	103.83	105.00	104.17	112.00	104.83	5.60	0.99	0.83	0.96
ALB, g/L	27.08	24.69	23.78	25.10	28.87	0.79	0.34	0.48	0.06
TP, g/L	52.70	48.96	50.66	54.25	59.02	1.50	0.36	0.09	0.07
GLU, mmol/L	4.59	4.18	4.28	4.22	4.91	0.11	0.23	0.38	0.05
TG, mmol/L	0.59	0.58	0.57	0.54	0.70	0.05	0.88	0.59	0.63
TC, mmol/L	2.13	1.92	1.96	2.06	2.15	0.05	0.53	0.62	0.29
CK, U/L	64.83	39.63	34.00	33.43	37.95	4.56	0.24	0.06	0.04
CREA, μmol/L	85.51	72.49	83.64	80.12	84.39	2.75	0.64	0.79	0.68
UREA, mmol/L	3.15^{a}	2.46^{bc}	2.14^{c}	2.95^{ab}	3.20^{a}	0.11	<0.01	0.48	< 0.01
LDH, U/L	832.30	492.27	413.02	360.13	457.98	58.36	0.12	0.03	0.01

Data are shown as mean ± SEM ($n = 6$ replicates per treatment).
[a,b,c]Means lacking a common uppercase superscript differ ($P < 0.05$) using Duncan test.
GSP, Grape Seed Proanthocyanidin; SEM, standard error of the mean; GLM, General Linear Model; ALT, alanine aminotransferase; AST, aspartate aminotransferase; ALP, alkaline phosphatase; ALB, albumin; TP, total Protein; GLU, glucose; TG, triglyceride; TC, total cholesterol; CK, creatine kinase; CREA, creatinine; UREA, urea; LDH, lactate Dehydrogenase.

TABLE 4 Effects of GSP on serum immunoglobulin and antioxidant parameters in growing pigs.

Items	GSP (mg/kg)					SEM	*P*-value		
	0	15	30	60	120		GLM	Linear	Quadratic
IgA, μg/mL	36.39^{b}	35.31^{b}	42.17^{a}	39.07^{ab}	37.28^{ab}	0.76	0.05	0.31	0.12
IgG, μg/mL	525.91	507.05	608.03	574.92	569.47	22.42	0.67	0.34	0.54
IgM, μg/mL	7.69	7.97	8.69	10.04	8.19	0.47	0.47	0.36	0.44
MDA, nmol/mL	4.13^{a}	3.60^{ab}	3.42^{ab}	3.07^{b}	3.15^{b}	0.13	0.10	<0.01	0.01
T-AOC, U/mL	3.81	3.81	3.94	4.55	4.64	0.18	0.49	0.07	0.17
CAT, U/mL	2.04	2.05	2.53	2.69	2.42	0.11	0.16	0.06	0.11
GSH-Px, U/mL	526.57^{c}	560.36^{bc}	605.64^{ab}	642.64^{a}	598.11^{ab}	11.48	< 0.01	<0.01	<0.01
T-SOD, U/mL	141.12^{b}	147.14^{ab}	149.34^{ab}	157.24^{a}	161.58^{a}	2.34	0.04	<0.01	<0.01

Data are shown as mean ± SEM ($n = 6$ replicates per treatment).
^{a,b,c}Means lacking a common uppercase superscript differ ($P < 0.05$) using Duncan test.
GSP, Grape Seed Proanthocyanidin; SEM, standard error of the mean; GLM, General Linear Model; IgA, immunoglobulin A; IgG, immunoglobulin G; IgM, immunoglobulin M; MDA, malondialdehyde; T-AOC, total antioxidant capacity; CAT, catalase; GSH-Px, glutathione peroxidase; T-SOD, total supemxide dismutase.

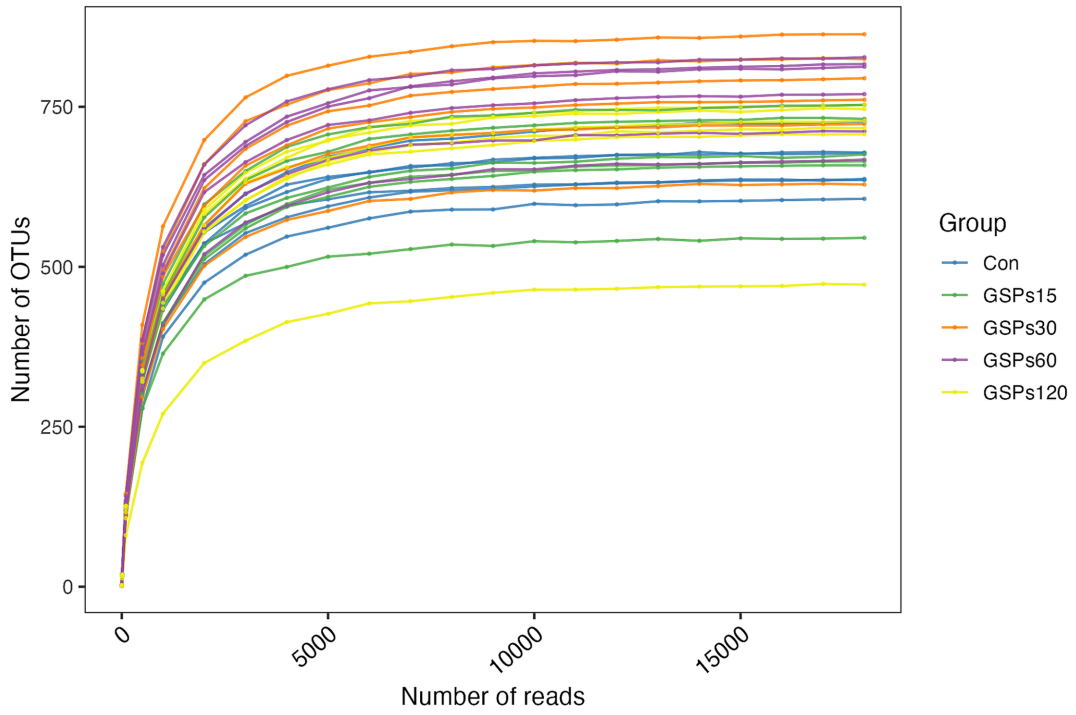

FIGURE 1
Rarefaction curves. Con, control group; GSPs15, 15 mg/kg GSP group; GSPs30, 30 mg/kg GSP group; GSPs60, 60 mg/kg GSP group; GSPs120, 120 mg/kg GSP group ($n = 6$).

were selected from 1,027,009 tags, yielding an average of 33,419 sequences per fecal sample. The percentage of combined sequences for each sample ranged from 97.17 to 98.04% (Supplementary Table S1). The rarefaction curves indicated that the depth of sampling was adequate to assess the bacterial communities (Figure 1).

The alpha diversity index is shown in Figure 2 and Supplementary Table S2. Dietary GSP supplementation has no significant differences in the alpha diversity index. Principal coordinate analysis (PCoA) based on Bray–Curtis distance metrics (Figure 3) indicated a distinct separation in microbiota composition between the 120 mg/kg GSP group and other treatment groups ($p < 0.05$).

At the phylum level, all of the qualified sequences were assigned to 21 known phyla (Figure 4A and Supplementary Table S3). Among these predominant phyla, GSP supplementation at 120 mg/kg enhanced the abundance of Firmicutes compared to the CON group ($p < 0.05$), but decreased the abundance of the phylum Bacteroidetes in fecal samples ($p < 0.05$). At the genus level, the sequences derived from fecal samples were to 21 known genera (Figure 4B and Supplementary Table S4). GSP supplementation at 120 mg/kg increased the abundance of the *Lactobacillus* ($p < 0.05$). Moreover, GSP supplementation at 120 mg/kg decreased the *Prevotellaceae NK3B31 group* and *Alloprevotella* abundance at the genus level ($p < 0.05$). The heatmap displays the abundance of selected phyla and genera across

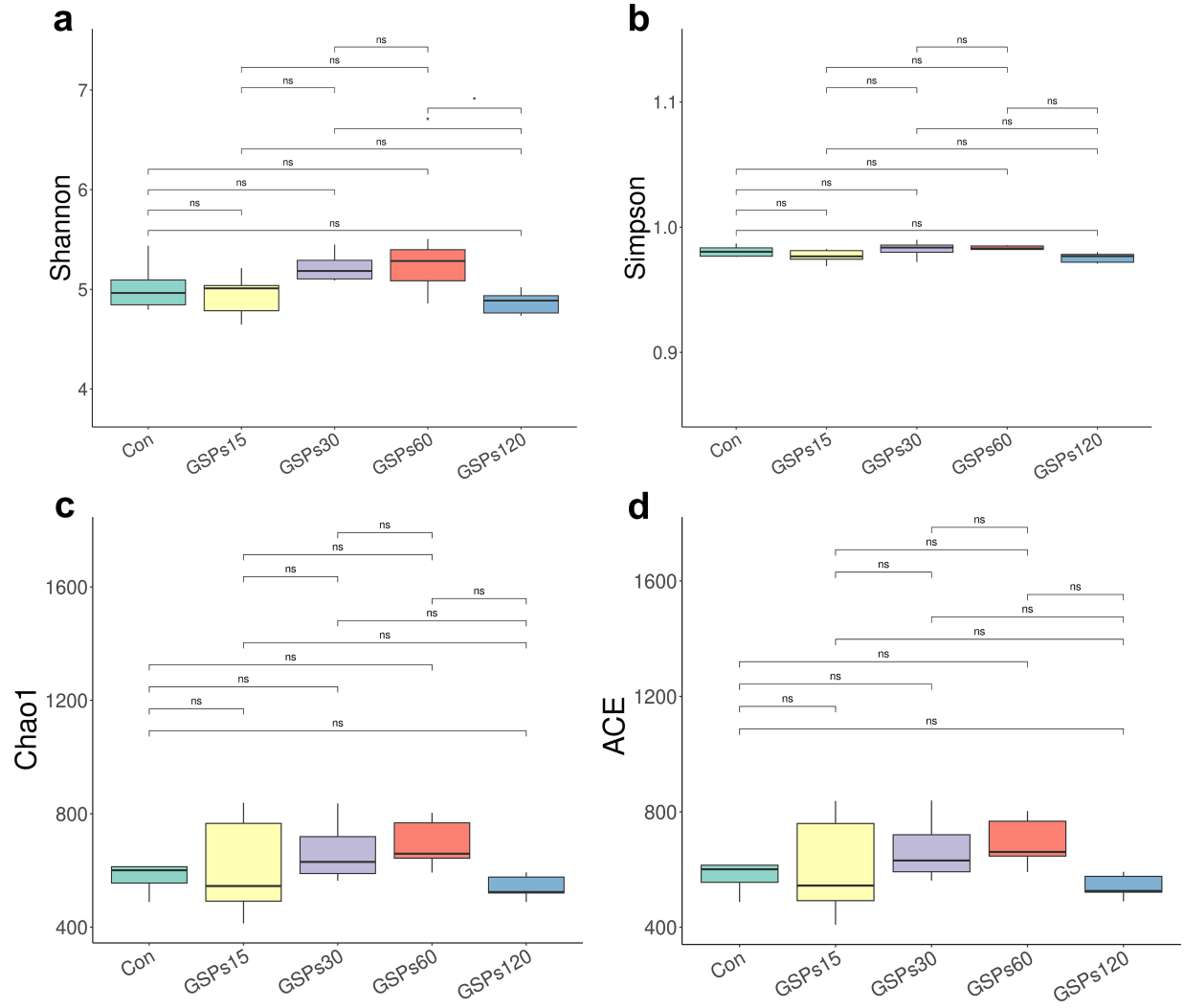

FIGURE 2
The boxplot of differences on bacterial community diversity and richness. (a) Shannon index. (b) Simpson index. (c) Chao1 index. (d) ACE index. Con, control group; GSPs15, 15 mg/kg GSP group; GSPs30, 30 mg/kg GSP group; GSPs60, 60 mg/kg GSP group; GSPs120, 120 mg/kg GSP group ($n = 6$). *Means significant difference ($p < 0.05$) between groups.

samples, clearly highlighting significant differences in distribution between the treatment groups (Figure 5).

Analysis using Spearman correlation (Figure 6) demonstrated significant links between the top 30 genera of intestinal microbiota and essential metrics such as growth performance, nutrient digestibility, and antioxidant capacity in growing pigs. A notable negative correlation was observed between average ADG and the relative abundance of *Alloprevotella* ($p < 0.05$). Additionally, dry matter digestibility showed an inverse relationship with the relative abundances of *Clostridium sensu stricto 1*, the *Prevotellaceae NK3B31 group*, and *Ruminococcus 1* ($p < 0.05$). Moreover, the digestibility of GE was negatively associated with the relative abundance of *Clostridium sensu stricto 1* ($p < 0.05$). A negative correlation was found between the digestibility of CP and the relative abundances of *Clostridium sensu stricto 1*, *Prevotella 1*, and *Ruminococcus 1* ($p < 0.05$). Negative associations were observed between the digestibility of EE and the relative abundances of *Clostridium sensu stricto 1* and *Campylobacter* ($p < 0.05$). Furthermore, serum MDA levels were negatively correlated with the *Ruminococcaceae NK4A214 group* ($p < 0.05$). A positive correlation was identified between serum GSH-Px levels and the relative abundances of *Streptococcus*, *Ruminococcaceae UCG-014*, *Oscillospira*, *Eubacterium coprostanoligenes group*, and *Prevotellaceae UCG-003* ($p < 0.05$). Moreover, the serum T-SOD concentration was negatively correlated with the relative abundance of *Alloprevotella*, but was positively correlated with the relative abundances of *Selenomonas* and *Ruminococcaceae NK4A214 group* ($p < 0.05$).

4 Discussion

In the present study, we explored the effect of dietary GSP supplementation on growth performance and nutrient digestibility in growing pigs. We found that GSP supplementation significantly increased the feed efficiency, as indicated by the decrease in the ratio of *F:G* and the increase in the digestibility of DM, CP, EE, and

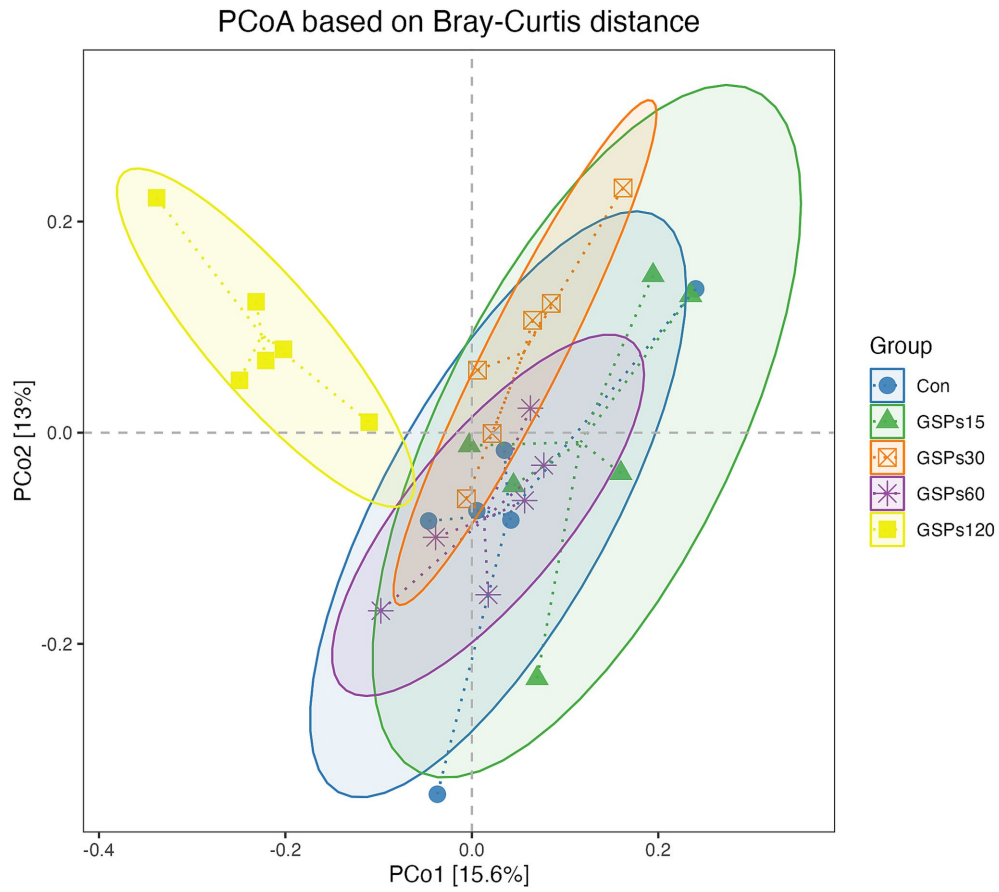

FIGURE 3
The PCoA analysis based on Bray–Curtis distance. Con, control group; GSPs15, 15 mg/kg GSP group; GSPs30, 30 mg/kg GSP group; GSPs60, 60 mg/kg GSP group; GSPs120, 120 mg/kg GSP group ($n = 6$).

GE. This finding aligns with earlier research conducted on piglets and growing pigs (Fiesel et al., 2014; Park et al., 2014). Improved feed efficiency may be linked to enhanced immunity and antioxidative capacity resulting from GSP supplementation (Chedea et al., 2010; Hao et al., 2021; Tong et al., 2011). In this study, serum concentrations of IgA were significantly elevated by dietary supplementation of GSP at 30 mg/kg, which predominantly exists on mucosal surfaces, such as those of the respiratory and digestive tracts, where it serves as a crucial first line of defense by preventing pathogen adhesion and penetration of the mucosa (Pabst, 2012). Previous study also indicated that polyphenolic compounds, such as magnolol, can enhance amino acid absorption and protein synthesis in growing pigs, thereby maintaining immune homeostasis (Liu et al., 2023).

Oxidative stress can induce acute inflammatory response in the intestine, leading to structural and functional disruptions in the intestinal epithelium and increasing intestinal permeability (Assimakopoulos et al., 2004; John et al., 2011). Moreover, oxidative stress can also lead to oxidative modifications of digestive enzymes, resulting in decreased enzyme activity, which impairs the digestion and absorption of nutrients (Bhor et al., 2004). In recent years, various antioxidants have been utilized to enhance the antioxidant capacity of pigs. For instance, certain plant extracts such as resveratrol, β-glucans, daidzein, etc., have been reported to scavenge excessive free radicals in the body, effectively alleviate intestinal oxidative damage, promote villus growth and increase intestinal wall thickness, thereby enhancing feed efficiency (Goh et al., 2023; Li et al., 2021; Meng et al., 2018). The GSP has potent antioxidant properties, as the multiple hydroxyl groups in its polyphenolic structure can effectively neutralize free radicals and reduce their activity through resonance stabilization (Spranger et al., 2008). By activating the Nrf2 signaling pathway and enhancing the expression of downstream antioxidant enzymes, GSP can also mitigate oxidative stress (Xu et al., 2019). In this study, the antioxidative capacity of the pigs was significantly enhanced by GSP supplementation, as indicated by the decrease in serum concentration of MDA. The MDA is one of the end products of lipid peroxidation and can indirectly reflect the extent of oxidative damage in the body (Marnett, 1999). Moreover, GSP supplementation also enhanced the concentrations of T-SOD and GSH-Px. GSH-Px is a selenium-containing enzyme that catalyzes the reduction of hydrogen peroxide and organic peroxides to water and the corresponding alcohol using reduced glutathione as a substrate, and the T-SOD is a type of metal-containing enzyme that is the first line of defense in the detoxification of oxidative stress products (Ceballos-Picot et al., 1996; Fattman et al., 2003). These

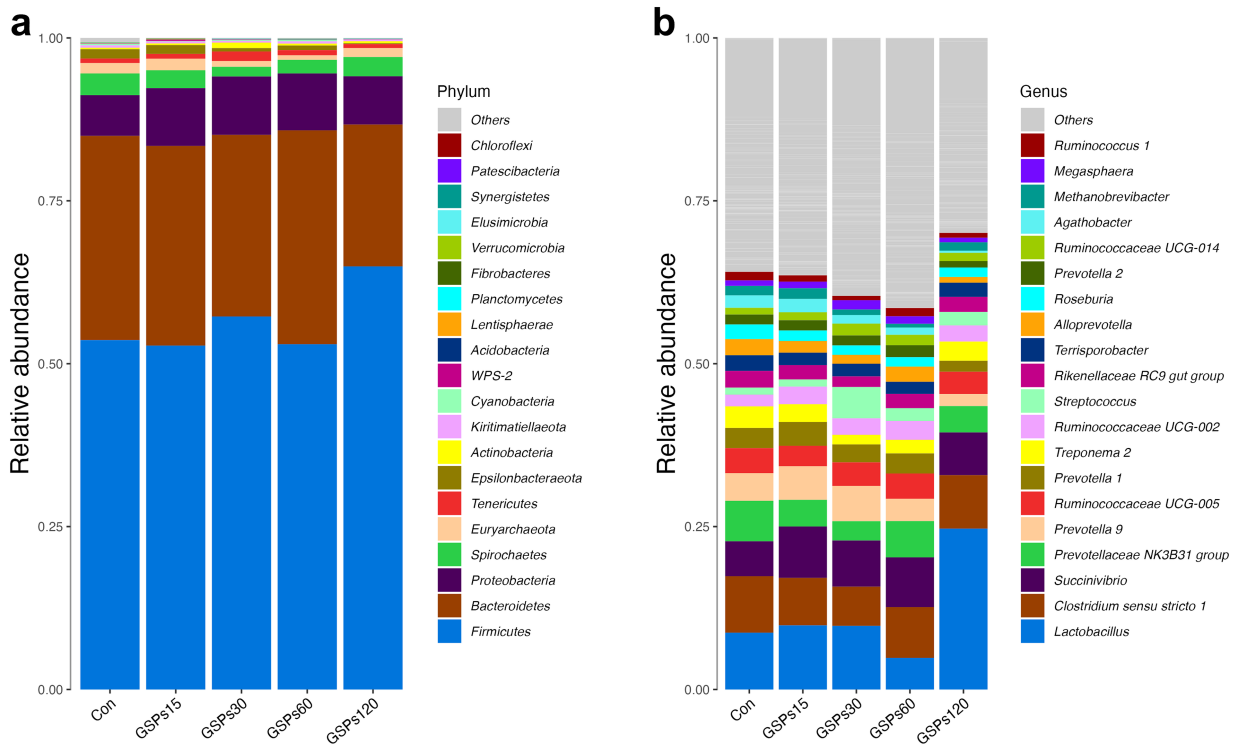

FIGURE 4
Bar graph shows the phylum (a) and genus (b) level composition of bacteria. Color coded bar plot shows the relative abundance of bacterial phyla and genus across the different samples. Con, control group; GSPs15, 15 mg/kg GSP group; GSPs30, 30 mg/kg GSP group; GSPs60, 60 mg/kg GSP group; GSPs120, 120 mg/kg GSP group (n = 6).

findings align with earlier reports indicating that dietary GSP supplementation can enhance serum antioxidant indices in finishing pigs through the activation of the Nrf2 signaling pathway (Feng et al., 2023).

The intestinal microbiota, which comprises all microorganisms residing in the digestive tract, is crucial for the normal functioning of digestive, immune, metabolic, and nervous systems through its balance and diversity (Álvarez et al., 2021). The microbial communities in different sections of the digestive tract exhibit significant differences in composition, whereas fecal microbiota provides a comprehensive reflection of the entire gut microbiome (Eckburg et al., 2005). Earlier research indicated that GSP significantly impacts the modulation of intestinal microbiota dysbiosis (Jin et al., 2018; Seo et al., 2017; Tao et al., 2019). In this study, PCoA analysis revealed distinct microbial community structures and compositions in the group receiving 120 mg/kg GSP compared to the other groups. This result aligns with earlier studies conducted on both mice and finishing pigs (Choy et al., 2014; Sheng et al., 2020). This change may reflect competitive displacement among microbial populations under GSP treatment, resulting in a new microbial equilibrium, which could affect nutrient absorption, immune response, and overall gut function (Biagi et al., 2016; Hertz et al., 2020).

Changes in the fecal microbiota have been shown in a previous study to be closely associated with intestinal health (Hopkins, 2001). In the present study, the phyla Firmicutes and Bacteroidetes were found to be the most predominant phyla in the fecal samples, which is consistent with a previous study in pigs (Verschuren et al., 2019). The bacteria of phylum Firmicutes can efficiently degrade plant fibers and other complex carbohydrates, producing short-chain fatty acid (Sun et al., 2022). In this study, we found that supplementation with GSP at 120 mg/kg significantly enhanced the abundance of the phylum Firmicutes, deepening our understanding of how dietary GSP can improve the bioavailability of nutrients. In animals, a major phylum present in the intestine is Bacteroidetes, which is involved in food digestion, nutrient absorption, and immune system regulation, but its overgrowth can lead to immune system imbalance (Ferolla et al., 2014; Pittayanon et al., 2019). In this study, we observed that GSP supplementation at 120 mg/kg reduced the ratio of the phylum Bacteroidetes in feces. This finding is consistent with earlier research indicating that plant polyphenols can inhibit Bacteroidetes growth, thereby affecting the host's energy metabolism in the intestine (Xue et al., 2016). Moreover, Firmicutes and Bacteroidetes are crucial members of the gut microbiota, and they may engage in resource competition (Ley et al., 2006). The substantial increase in members of Firmicutes such as *Lactobacillus* may occupy more ecological niches and nutrient resources, thereby restricting the growth and proliferation of Bacteroidetes (Chen M. L. et al., 2016; Chen S. et al., 2016; Wang et al., 2024).

The *Lactobacillus* genus is a group of Gram-positive bacteria that can regulate the intestinal environment by producing beneficial metabolic products such as lactic acid, maintaining the acid–base balance, and inhibiting the growth of harmful bacterial populations

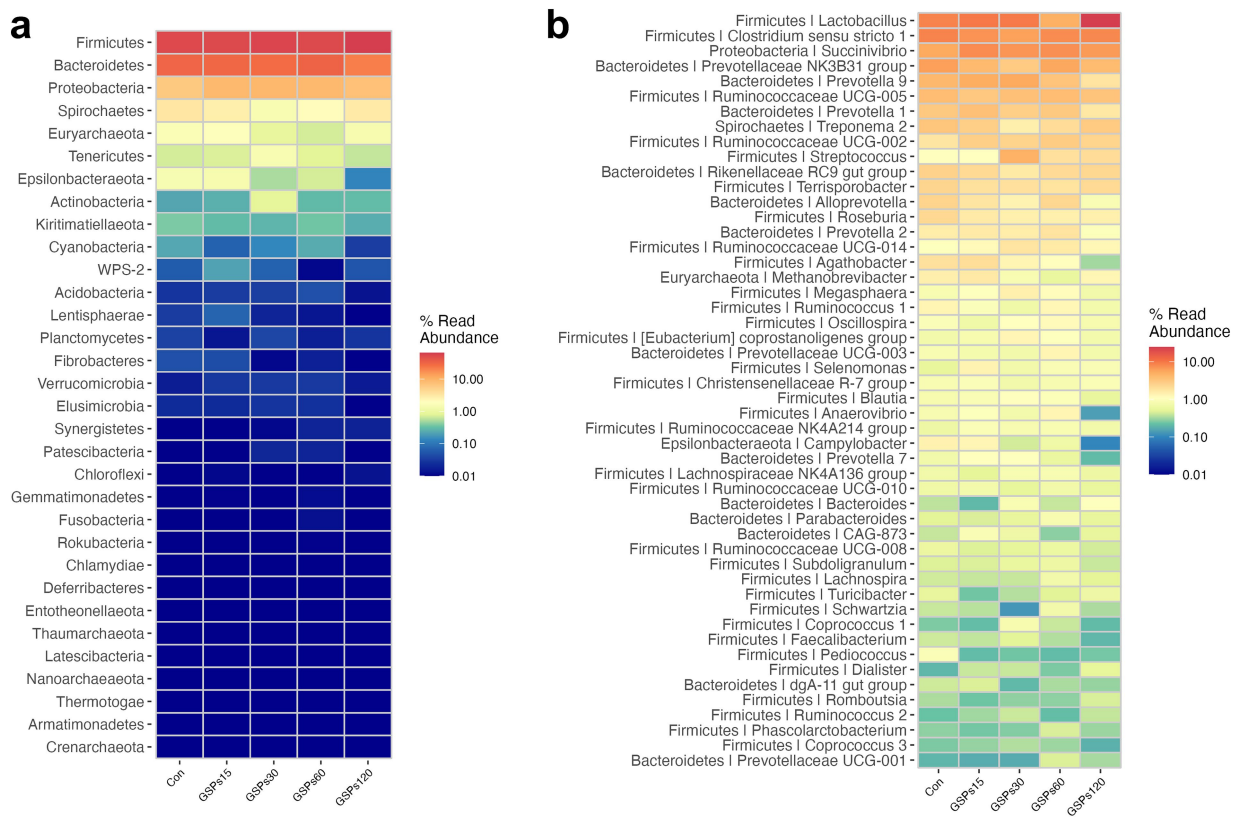

FIGURE 5
Heatmap distribution of OTUs at phylum (a) and genus (b) level. OTUs were arranged in rows and are clustered on the vertical axis. Samples are arranged vertically and are on the horizontal axis. Different colors indicate the relative abundance of taxons. Con, control group; GSPs15, 15 mg/kg GSP group; GSPs30, 30 mg/kg GSP group; GSPs60, 60 mg/kg GSP group; GSPs120, 120 mg/kg GSP group ($n = 6$).

(Dempsey and Corr, 2022). In this study, fecal samples from pigs receiving a diet supplemented with 120 mg/kg GSP showed a higher abundance of *Lactobacillus* compared to the CON group. This finding aligns with results from a previous study on another polyphenolic compound, resveratrol, which was shown to increase the levels of *Lactobacillus* in the gut, ultimately contributing to the regulation of bile acid metabolism (Chen M. L. et al., 2016; Chen S. et al., 2016). The *Prevotellaceae* is one of the major bacterial families in the large intestine of pigs, due to its ability to promote the production of short-chain fatty acids, is suggested to play an important role in intestinal metabolism (Amat et al., 2020; Zhang et al., 2021). Nevertheless, certain members of the *Prevotellaceae* family have been found to potentially exert negative effects on health by promoting inflammatory responses and contributing to disease progression. For instance, the mucin-degrading activity of the *Prevotellaceae NK3B31 group* may compromise intestinal epithelial integrity, fostering endotoxemia, inflammation, and insulin resistance (Hasain et al., 2021). Furthermore, previous research indicated that *Prevotella copri* (a member of *Alloprevotella*) exacerbates DSS-induced colitis in mice by downregulating ATF4 expression and altering the composition of intestinal microbiota (Wang and Cao, 2024). In the present study, GSP supplementation at 120 mg/kg decrease the genera abundances of the *Prevotellaceae NK3B31 group* and *Alloprevotella*. A previous study found that pigs with a low feed conversion ratio had higher abundances of taxa from the *Prevotellaceae* family in the ileum compared to those with a high feed conversion ratio (Quan et al., 2018). Consistently, the Spearman correlation analysis showed that the digestibility of DM was negatively correlated with the genus abundance of the *Prevotellaceae NK3B31 group*. Additionally, the abundance of *Alloprevotella* was found to be negatively correlated with both ADG and T-SOD concentration. Consequently, the observed dynamic changes in the intestinal microbiota community may partially account for the improvements in growth performance and nutrient digestibility noted in this study. Further studies, including fecal microbiota transplantation, are necessary to clarify the precise role and potential mechanisms underlying the biological events modulated by the intestinal microbiota.

5 Conclusion

In summary, dietary GSP supplementation not only increases the growth performance, but also improves the nutrient digestibility of growing pigs. The improved nutrient digestibility by GSP is likely linked to the enhancements in antioxidative capacity and improvement in the intestinal microbiota. Based on our findings, dietary supplementation of 30 and 60 mg/kg GSP may be optimal for growing pigs. This study may enhance the application of GSP in animal nutrition and the feed industry.

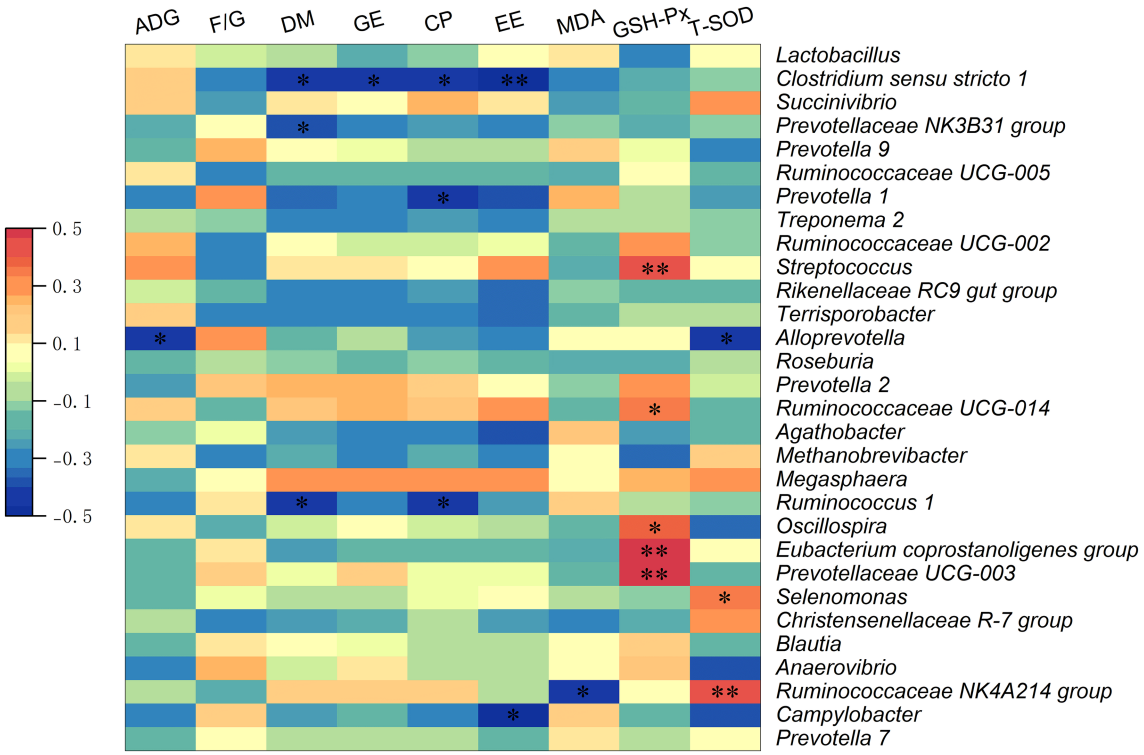

FIGURE 6
The Spearman correlation analysis of fecal microbial composition with growth performance, nutrient digestibility, and antioxidant capacity in growing pigs. Spearman correlation coefficients of ADG, *F/G*, nutrient digestibility (DM, GE, CP, and EE), serum MDA concentration, serum GSH-Px concentration, and serum T-SOD concentration with fecal microbiota at genus level, are displayed. The heatmap with red indicated a positive correlation, while blue represented a negative correlation. ADG, average daily gain; *F/G*, feed to gain ratio; DM, dry matter; GE, gross energy; CP, crude protein; EE, ether extract. $*p < 0.05$, $**p < 0.01$.

Data availability statement

The raw sequence data for the 16S rRNA presented in this study can be found in online repositories. The names of the repository/repositories and accession number(s) can be found at: NCBI, PRJNA1176302.

Ethics statement

The animal study was approved by Committee on Animal Care Advisory of Sichuan Agricultural University. The study was conducted in accordance with the local legislation and institutional requirements.

Author contributions

YZ: Data curation, Investigation, Software, Validation, Visualization, Writing – original draft. YLi: Investigation, Methodology, Resources, Software, Visualization, Writing – review & editing. BY: Software, Visualization, Writing – review & editing. ZH: Supervision, Visualization, Writing – review & editing. YLu: Software, Visualization, Writing – review & editing. PZ: Formal analysis, Supervision, Writing – review & editing. XM: Supervision, Visualization, Writing – review & editing. JY: Software, Supervision, Writing – review & editing. HT: Data curation, Investigation, Supervision, Validation, Writing – review & editing. JL: Supervision, Visualization, Writing – review & editing. HY: Software, Visualization, Writing – review & editing. JH: Conceptualization, Funding acquisition, Project administration, Resources, Supervision, Writing – review & editing.

Funding

The author(s) declare that financial support was received for the research, authorship, and/or publication of this article. This study was supported by the National Key R&D Program of China (2023YFD1301200) and the Porcine Innovation Team of Sichuan Province (SCCXTD-2024-8).

Acknowledgments

The support that Huifen Wang and Fali Wu provided throughout the animal testing and the gathering of samples is something for which we gratefully express our appreciation.

Conflict of interest

Author HT was employed by the company Wens Foodstuff Group Co., Ltd.

The remaining authors declare that the research was conducted in the absence of any commercial or financial relationships that could be construed as a potential conflict of interest.

Publisher's note

All claims expressed in this article are solely those of the authors and do not necessarily represent those of their affiliated organizations, or those of the publisher, the editors and the reviewers. Any product that may be evaluated in this article, or claim that may be made by its manufacturer, is not guaranteed or endorsed by the publisher.

Supplementary material

The Supplementary material for this article can be found online at: https://www.frontiersin.org/articles/10.3389/fmicb.2024.1501211/full#supplementary-material

References

Álvarez, J., Fernández Real, J. M., Guarner, F., Gueimonde, M., Rodríguez, J. M., Saenz de Pipaon, M., et al. (2021). Gut microbes and health. *Gastroenterol. Hepatol.* 44, 519–535. doi: 10.1016/j.gastre.2021.01.002

Amat, S., Lantz, H., Munyaka, P. M., and Willing, B. P. (2020). Prevotella in pigs: the positive and negative associations with production and health. *Microorganisms* 8:1584. doi: 10.3390/microorganisms8101584

AOAC (2007). Official method of analysis. *18th* Edn. Gaithersburg, MD, USA: AOAC International.

Assimakopoulos, S. F., Vagianos, C. E., Patsoukis, N., Georgiou, C., Nikolopoulou, V., and Scopa, C. D. (2004). Evidence for intestinal oxidative stress in obstructive jaundice-induced gut barrier dysfunction in rats. *Acta Physiol. Scand.* 180, 177–185. doi: 10.1046/j.0001-6772.2003.01229.x

Bhor, V. M., Raghuram, N., and Sivakami, S. (2004). Oxidative damage and altered antioxidant enzyme activities in the small intestine of streptozotocin-induced diabetic rats. *Int. J. Biochem. Cell Biol.* 36, 89–97. doi: 10.1016/s1357-2725(03)00142-0

Biagi, E., Franceschi, C., Rampelli, S., Severgnini, M., Ostan, R., Turroni, S., et al. (2016). Gut microbiota and extreme longevity. *Curr. Biol.* 26, 1480–1485. doi: 10.1016/j.cub.2016.04.016

Ceballos-Picot, I., Witko-Sarsat, V., Merad-Boudia, M., Nguyen, A. T., Thévenin, M., Jaudon, M. C., et al. (1996). Glutathione antioxidant system as a marker of oxidative stress in chronic renal failure. *Free Radic. Biol. Med.* 21, 845–853. doi: 10.1016/0891-5849(96)00233-x

Chedea, V. S., Braicu, C., and Socaciu, C. (2010). Antioxidant/prooxidant activity of a polyphenolic grape seed extract. *Food Chem.* 121, 132–139. doi: 10.1016/j.foodchem.2009.12.020

Chen, S., Cheng, H., Wyckoff, K. N., and He, Q. (2016). Linkages of Firmicutes and Bacteroidetes populations to methanogenic process performance. *J. Ind. Microbiol. Biotechnol.* 43, 771–781. doi: 10.1007/s10295-016-1760-8

Chen, M. L., Yi, L., Zhang, Y., Zhou, X., Ran, L., Yang, J., et al. (2016). Resveratrol attenuates trimethylamine-N-oxide (TMAO)-induced atherosclerosis by regulating TMAO synthesis and bile acid metabolism via remodeling of the gut microbiota. *MBio* 7, 2210–2215. doi: 10.1128/mBio.02210-15

China Feed Database. (2020). Tables of feed composition and nutritive values in China. Beijing, China: Institute of Feed Research, Chinese Academy of Agricultural Sciences.

Choy, Y. Y., Quifer-Rada, P., Holstege, D. M., Frese, S. A., Calvert, C. C., Mills, D. A., et al. (2014). Phenolic metabolites and substantial microbiome changes in pig feces by ingesting grape seed proanthocyanidins. *Food Funct.* 5, 2298–2308. doi: 10.1039/c4fo00325j

Dempsey, E., and Corr, S. C. (2022). Lactobacillus spp. for gastrointestinal health: current and future perspectives. *Front. Immunol.* 13:840245. doi: 10.3389/fimmu.2022.840245

Deng, C., Zhai, Y., Yang, X., Chen, Z., Li, Q., and Hao, R. (2023). Effects of grape seed procyanidins on antioxidant function, barrier function, microbial community, and metabolites of cecum in geese. *Poult. Sci.* 102:102878. doi: 10.1016/j.psj.2023.102878

Eckburg, P. B., Bik, E. M., Bernstein, C. N., Purdom, E., Dethlefsen, L., Sargent, M., et al. (2005). Diversity of the human intestinal microbial flora. *Science* 308, 1635–1638. doi: 10.1126/science.1110591

Fattman, C. L., Schaefer, L. M., and Oury, T. D. (2003). Extracellular superoxide dismutase in biology and medicine. *Free Radic. Biol. Med.* 35, 236–256. doi: 10.1016/s0891-5849(03)00275-2

Feng, Y., Chen, X., Chen, D., He, J., Zheng, P., Luo, Y., et al. (2023). Dietary grape seed proanthocyanidin extract supplementation improves antioxidant capacity and lipid metabolism in finishing pigs. *Anim. Biotechnol.* 34, 1–11. doi: 10.1080/10495398.2023.2252012

Ferolla, S., Armiliato, G., Couto, C., and Ferrari, T. (2014). The role of intestinal bacteria overgrowth in obesity-related non-alcoholic fatty liver disease. *Nutrients* 6, 5583–5599. doi: 10.3390/nu6125583

Fiesel, A., Gessner, D. K., Most, E., and Eder, K. (2014). Effects of dietary polyphenol-rich plant products from grape or hop on pro-inflammatory gene expression in the intestine, nutrient digestibility and faecal microbiota of weaned pigs. *BMC Vet. Res.* 10:196. doi: 10.1186/s12917-014-0196-5

Goh, T. W., Kim, H. J., Moon, K., and Kim, Y. Y. (2023). Effects of beta-glucan with vitamin E supplementation on the growth performance, blood profiles, immune response, pork quality, pork flavor, and economic benefit in growing and finishing pigs. *Anim Biosci* 36, 929–942. doi: 10.5713/ab.22.0433

Guo, L., Yang, Z.-Y., Tang, R.-C., and Yuan, H.-B. (2020). Grape seed proanthocyanidins: novel coloring, flame-retardant, and antibacterial agents for silk. *ACS Sustain. Chem. Eng.* 8, 5966–5974. doi: 10.1021/acssuschemeng.0c00367

Hao, Y., Xing, M., and Gu, X. (2021). Research progress on oxidative stress and its nutritional regulation strategies in pigs. *Animals* 11:1384. doi: 10.3390/ani11051384

Hasain, Z., Raja Ali, R. A., Abdul Razak, S., Azizan, K. A., El-Omar, E., Razalli, N. H., et al. (2021). Gut microbiota signature among asian post-gestational diabetes women linked to macronutrient intakes and metabolic phenotypes. *Front. Microbiol.* 12:680622. doi: 10.3389/fmicb.2021.680622

Hertz, F. B., Budding, A. E., van der Lugt-Degen, M., Savelkoul, P. H., Løbner-Olesen, A., and Frimodt-Møller, N. (2020). Effects of antibiotics on the intestinal microbiota of mice. *Antibiotics* 9:191. doi: 10.3390/antibiotics9040191

Hopkins, M. J. (2001). Age and disease related changes in intestinal bacterial populations assessed by cell culture, 16S rRNA abundance, and community cellular fatty acid profiles. *Gut* 48, 198–205. doi: 10.1136/gut.48.2.198

Ignea, C., Dorobanțu, C. M., Mintoff, C. P., Branza-Nichita, N., Ladomery, M. R., Kefalas, P., et al. (2013). Modulation of the antioxidant/pro-oxidant balance, cytotoxicity and antiviral actions of grape seed extracts. *Food Chem.* 141, 3967–3976. doi: 10.1016/j.foodchem.2013.06.094

Jin, G., Asou, Y., Ishiyama, K., Okawa, A., Kanno, T., and Niwano, Y. (2018). Proanthocyanidin-rich grape seed extract modulates intestinal microbiota in ovariectomized mice. *J. Food Sci.* 83, 1149–1152. doi: 10.1111/1750-3841.14098

John, L. J., Fromm, M., and Schulzke, J.-D. (2011). Epithelial barriers in intestinal inflammation. *Antioxid. Redox Signal.* 15, 1255–1270. doi: 10.1089/ars.2011.3892

Ley, R. E., Turnbaugh, P. J., Klein, S., and Gordon, J. I. (2006). Microbial ecology: human gut microbes associated with obesity. *Nature* 444, 1022–1023. doi: 10.1038/4441022a

Li, Y., He, G., Chen, D., Yu, B., Yu, J., Zheng, P., et al. (2021). Supplementing daidzein in diets improves the reproductive performance, endocrine hormones and antioxidant capacity of multiparous sows. *Anim Nutr.* 7, 1052–1060. doi: 10.1016/j.aninu.2021.09.002

Liu, Y., Li, Y., Yu, M., Tian, Z., Deng, J., Ma, X., et al. (2023). Magnolol supplementation alters serum parameters, immune homeostasis, amino acid profiles, and gene expression of amino acid transporters in growing pigs. *Int. J. Mol. Sci.* 24:13952. doi: 10.3390/ijms241813952

Ma, J., Fan, X., Zhang, W., Zhou, G., Yin, F., Zhao, Z., et al. (2023). Grape seed extract as a feed additive improves the growth performance, ruminal fermentation and immunity of weaned beef calves. *Animals* 13:1876. doi: 10.3390/ani13111876

Marnett, L. J. (1999). Lipid peroxidation—DNA damage by malondialdehyde. *Mutat Res* 424, 83–95. doi: 10.1016/s0027-5107(99)00010-x

Meng, Q., Guo, T., Li, G., Sun, S., He, S., Cheng, B., et al. (2018). Dietary resveratrol improves antioxidant status of sows and piglets and regulates antioxidant gene expression in placenta by Keap 1-Nrf2 pathway and Sirt1. *J Anim Sci Biotechnol.* 9:34. doi: 10.1186/s40104-018-0248-y

National Standard. (2009). National Standard of the People's republic of China animal feeding stuffs-determination of ash insoluble in hydrochloric acid. Beijing, China: Standardization Administration of China.

Novais, A. K., Deschene, K., Martel-Kennes, Y., Roy, C., Laforest, J. P., Lessard, M., et al. (2021). Weaning differentially affects mitochondrial function, oxidative stress,

inflammation and apoptosis in normal and low birth weight piglets. *PLoS One* 16:e0247188. doi: 10.1371/journal.pone.0247188

Pabst, O. (2012). New concepts in the generation and functions of IgA. *Nat. Rev. Immunol.* 12, 821–832. doi: 10.1038/nri3322

Park, J. C., Lee, S. H., Hong, J. K., Cho, J. H., Kim, I. H., and Park, S. K. (2014). Effect of dietary supplementation of procyanidin on growth performance and immune response in pigs. *Asian Australas. J. Anim. Sci.* 27, 131–139. doi: 10.5713/ajas.2013.13359

Pittayanon, R., Lau, J. T., Yuan, Y., Leontiadis, G. I., Tse, F., Surette, M., et al. (2019). Gut microbiota in patients with irritable bowel syndrome—a systematic review. *Gastroenterology* 157, 97–108. doi: 10.1053/j.gastro.2019.03.049

Quan, J., Cai, G., Ye, J., Yang, M., Ding, R., Wang, X., et al. (2018). A global comparison of the microbiome compositions of three gut locations in commercial pigs with extreme feed conversion ratios. *Sci. Rep.* 8:4536. doi: 10.1038/s41598-018-22692-0

Rodríguez, P., García, V., Guerra, H., and Verardo, V. (2019). Grape seeds proanthocyanidins: an overview of in vivo bioactivity in animal models. *Nutrients* 11:2435. doi: 10.3390/nu11102435

Seo, K.-H., Kim, D.-H., Jeong, D., Yokoyama, W., and Kim, H. (2017). Chardonnay grape seed flour supplemented diets alter intestinal microbiota in diet-induced obese mice. *J. Food Biochem.* 41:2396. doi: 10.1111/jfbc.12396

Sheng, K., Zhang, G., Sun, M., He, S., Kong, X., Wang, J., et al. (2020). Grape seed proanthocyanidin extract ameliorates dextran sulfate sodium-induced colitis through intestinal barrier improvement, oxidative stress reduction, and inflammatory cytokines and gut microbiota modulation. *Food Funct.* 11, 7817–7829. doi: 10.1039/d0fo01418d

Spranger, I., Sun, B., Mateus, A. M., Freitas, V. D., and Ricardo-da-Silva, J. M. (2008). Chemical characterization and antioxidant activities of oligomeric and polymeric procyanidin fractions from grape seeds. *Food Chem.* 108, 519–532. doi: 10.1016/j.foodchem.2007.11.004

Sun, Y., Zhang, S., Nie, Q., He, H., Tan, H., Geng, F., et al. (2022). Gut firmicutes: relationship with dietary fiber and role in host homeostasis. *Crit. Rev. Food Sci. Nutr.* 63, 12073–12088. doi: 10.1080/10408398.2022.2098249

Tao, W., Zhang, Y., Shen, X., Cao, Y., Shi, J., Ye, X., et al. (2019). Rethinking the mechanism of the health benefits of proanthocyanidins: absorption, metabolism, and interaction with gut microbiota. *Compreh Rev Food Sci Food Saf.* 18, 971–985. doi: 10.1111/1541-4337.12444

Tong, H., Song, X., Sun, X., Sun, G., and Du, F. (2011). Immunomodulatory and antitumor activities of grape seed proanthocyanidins. *J. Agric. Food Chem.* 59, 11543–11547. doi: 10.1021/jf203170k

Tyagi, A., Raina, K., Gangar, S., Kaur, M., Agarwal, R., and Agarwal, C. (2013). Differential effect of grape seed extract against human non-small-cell lung cancer cells: the role of reactive oxygen species and apoptosis induction. *Nutr. Cancer* 65, 44–53. doi: 10.1080/01635581.2013.785003

Verschuren, L. M. G., Schokker, D., Bergsma, R., Jansman, A. J. M., Molist, F., and Calus, M. P. L. (2019). Prediction of nutrient digestibility in grower-finisher pigs based on faecal microbiota composition. *J. Anim. Breed. Genet.* 137, 23–35. doi: 10.1111/jbg.12433

Wang, X., and Cao, H. (2024). P090 *Prevotella copri* promotes colitis in mice by reducing expression of ATF4 and disturbing the gut microbiota. *J. Crohns Colitis* 18:i368. doi: 10.1093/ecco-jcc/jjad212.0220

Wang, S., Mu, L., Yu, C., He, Y., Hu, X., Jiao, Y., et al. (2024). Microbial collaborations and conflicts: unraveling interactions in the gut ecosystem. *Gut Microbes* 16:2296603. doi: 10.1080/19490976.2023.2296603

Xiang, Q., Wu, X., Pan, Y., Wang, L., Cui, C., Guo, Y., et al. (2020). Early-life intervention using fecal microbiota combined with probiotics promotes gut microbiota maturation, regulates immune system development, and alleviates weaning stress in piglets. *Int. J. Mol. Sci.* 21:503. doi: 10.3390/ijms21020503

Xu, M., Niu, Q., Hu, Y., Feng, G., Wang, H., and Li, S. (2019). Proanthocyanidins antagonize arsenic-induced oxidative damage and promote arsenic methylation through activation of the Nrf2 signaling pathway. *Oxidative Med. Cell. Longev.* 2019, 1–19. doi: 10.1155/2019/8549035

Xue, B., Xie, J., Huang, J., Chen, L., Gao, L., Ou, S., et al. (2016). Plant polyphenols alter a pathway of energy metabolism by inhibiting fecal Bacteroidetes and Firmicutes in vitro. *Food Funct.* 7, 1501–1507. doi: 10.1039/c5fo01438g

Yang, C., Song, G., and Lim, W. (2020). Effects of mycotoxin-contaminated feed on farm animals. *J. Hazard. Mater.* 389:122087. doi: 10.1016/j.jhazmat.2020.122087

Zhai, S.-W., Lu, J.-J., and Chen, X.-H. (2016). Effects of dietary grape seed proanthocyanidins on growth performance, some serum biochemical parameters and body composition of tilapia (*Oreochromis niloticus*) fingerlings. *Ital. J. Anim. Sci.* 13:3357. doi: 10.4081/ijas.2014.3357

Zhang, Y., Yin, C., Schroyen, M., Everaert, N., Ma, T., and Zhang, H. (2021). Effects of the inclusion of fermented mulberry leaves and branches in the gestational diet on the performance and gut microbiota of sows and their offspring. *Microorganisms* 9:604. doi: 10.3390/microorganisms9030604

Zhao, Y., Flowers, W. L., Saraiva, A., Yeum, K. J., and Kim, S. W. (2013). Effect of social ranks and gestation housing systems on oxidative stress status, reproductive performance, and immune status of sows. *J. Anim. Sci.* 91, 5848–5858. doi: 10.2527/jas.2013-6388

Zhu, C., Yang, J., Nie, X., Wu, Q., Wang, L., and Jiang, Z. (2022). Influences of dietary vitamin E, selenium-enriched yeast, and soy isoflavone supplementation on growth performance, antioxidant capacity, carcass traits, meat quality and gut microbiota in finishing pigs. *Antioxidants* 11:510. doi: 10.3390/antiox11081510

frontiers | Frontiers in Microbiology

TYPE Review
PUBLISHED 29 January 2025
DOI 10.3389/fmicb.2025.1442282

OPEN ACCESS

EDITED BY
Abbas Yadegar,
Shahid Beheshti University of Medical Sciences, Iran

REVIEWED BY
Sardar Sindhu,
Dasman Diabetes Institute, Kuwait
Arun Karnwal,
Graphic Era University, India

*CORRESPONDENCE
Ma Jie
majie2023@gxu.edu.cn

RECEIVED 01 June 2024
ACCEPTED 13 January 2025
PUBLISHED 29 January 2025

CITATION
Zheng W, Liu M, Lv X, He C, Yin J and Ma J (2025) AhR governs lipid metabolism: the role of gut microbiota.
Front. Microbiol. 16:1442282.
doi: 10.3389/fmicb.2025.1442282

AhR governs lipid metabolism: the role of gut microbiota

Wanru Zheng[1], Mengkuan Liu[1], Xinyu Lv[1], Cuimei He[1], Jie Yin[2] and Jie Ma[1]*

[1]College of Animal Science and Technology, Guangxi University, Nanning, China, [2]College of Animal Science and Technology, Hunan Agricultural University, Changsha, China

The Aryl Hydrocarbon Receptor (AhR) is widely present in mammalian bodies, showing high affinity for various exogenous substances such as polycyclic aromatic hydrocarbons (PAHs) and coumarin. Under physiological conditions, AhR mainly participates in regulating the body's immune response, cell proliferation, and apoptosis among a series of processes. Recent studies have revealed a close connection between AhR and lipid metabolism. The gut microbiota plays a significant role in regulating host lipid metabolism. Growing evidence suggests an inseparable link between gut microbiota and AhR signaling. This review summarizes the relationship between AhR and lipid metabolism disorders, as well as the interaction between gut microbiota and AhR, exploring how this interaction modulates host lipid metabolism.

KEYWORDS

aryl hydrocarbon receptor, gut microbiota, lipid metabolism, inflammation, metabolic disease

Introduction

The aryl hydrocarbon receptor (AhR) is a ligand-dependent transcription factor that plays a crucial role in the regulatory network of the interaction between gut microbiota and the host (Hornedo-Ortega et al., 2018). Evidence suggested that AhR plays an important role in regulating metabolites involved in many biochemical pathways affecting biosynthesis and metabolism of fatty acids, bile acids, gut microbiome products, antioxidants, choline derivatives, and uremic toxins, with a central role in metabolism and signaling between multiple organs and across multiple scales (Granados et al., 2022). It was initially identified as a receptor that binds to environmental pollutant dioxins, primarily involved in detoxification and metabolic processes of dioxins and their analogs. Recent research has shown that the functions of AhR were much broader than previously understood. Further studies have shown that activating AhR influenced the differentiation, proliferation, and apoptosis of fat cells, regulating fat production (Kwack and Lee, 2000). Importantly, AhR sensed the ligands from diet, gut microbiota and host metabolites to regulate the host's physiological functions by triggering a series of signal transduction processes. For example, Cruciferous vegetables such as broccoli, cauliflower, and cabbage can be converted into AhR ligand precursors, indole-3-carbinol (I3C) and indole-3-acetonitrile (I3ACN), through enzymatic breakdown (Ito et al., 2007). Under the action of gastric acid, these precursors further transform into high-affinity AhR ligands such as 3,3′-diindolylmethane (DIM) and indole [3,2-b] carbazole (ICZ) (Bjeldanes et al., 1991). I3C and its condensation products have potential effects in treating inflammatory bowel diseases by modulating the differentiation and function of T cells (Treg cells) through AhR activation, while reducing the number of helper T cells (Th cells) to alleviate intestinal inflammation (Rouse et al., 2013). Additionally, the plant-derived compound resveratrol can inhibit AhR activity by blocking the binding of AhR with its ligands, potentially reversing the imbalance of Th17/Treg cells in patients with autoimmune diseases

and showing therapeutic potential for AhR-mediated diseases (Guo et al., 2019). *In vitro* experiments have shown that the flavonoid compound genistein can activate AhR through negative regulation of estrogen receptor alpha (ERα), promoting the expression of downstream target genes CYP1A1 and CYP1B1 (Gong F. et al., 2016; Gong P. et al., 2016). Plant extracts of the flavonoid compound cardamonin (CDN) can act as an exogenous ligand for AhR and play a crucial regulatory role in alleviating intestinal inflammation (Wang et al., 2018). Certain metabolites produced by gut microbiota such as tryptamine, indole, and their derivatives can also function as AhR ligands, inducing the production of IL-22 by intestinal immune cells and participating in gut homeostasis (Zindl et al., 2022). However, the AhR signaling mechanism by which gut microbiota regulate host lipid metabolism is unclear. Lipid metabolism disruption leads to a range of health issues such as obesity, hyperlipidemia (Li J. et al., 2016; Li M. et al., 2016), and cardiovascular diseases (Lee et al., 2005). Therefore, a thorough investigation into the mechanism by which gut microbiota modulates host lipid metabolism via AhR is beneficial for providing new insights and strategies for the prevention and treatment of related diseases.

AhR structure

The structure of AHR determines its biological function. (Figure 1).AhR is a transcription factor whose activation relies on ligands, which is member of the basic Helix–Loop–Helix (bHLH)-Per-ARNT-Sim (PAS) family (Fukunaga et al., 1995) and its protein encoded by the AhR gene consists of 848 amino acids (Itoh et al., 1998). The structure of AhR is divided into three segments: the N-terminal, DNA-binding domain, and C-terminal (Hankinson, 1995). The AhR protein consists of three domains: bHLH, PAS, and TAD (Trans activation domain). The bHLH domain located at the N-terminus facilitates AhR binding to the promoter region of target genes and protein dimerization (Murre et al., 1989). The PAS domain is divided into PAS-A and PAS-B2, with PAS-A binding to the AhR nuclear translocator (arnt) and PAS-B binding to AhR ligands (Fukunaga et al., 1995), mediates protein dimerization. What's more, the TAD at the C terminus is involved in protecting relevant coactivator factors. It comprises three subdomains, with the first two subdomains are enriched in acidic residues and glutamine, while the third subdomain is enriched in serine, threonine, and proline (S/T/P) (Lin et al., 2022).

The BHLH domain is located at the N terminus, initiates AhR binding and mediating protein dimerization, the PAS domain is the binding site for ARNT and AhR ligands, and the TAD at the C terminus, involved in transcription activation, containing three subdomains, the first rich in acidic residues, the second rich in glutamine, and the third rich in serine, threonine, and proline.

AhR expression

AhR exists in the form of a cytoplasmic protein complex composed of HSP90, p32, and XAP-2 within the cytoplasm of cells (Zhu et al., 2021), translocates to the nucleus upon activation by agonists and binds to aryl hydrocarbon receptor nuclear translocator (ARNT) or hypoxia-inducible factor 1β (HIF-1β), which interacts with xenobiotic response elements (XREs) to control the expression of key genes (Bahman et al., 2024). AhR is present in various tissues and cells of vertebrates, such as the intestines, liver, spleen, lymph nodes, and is expressed in various types of cells in the body, including immune cells, epithelial cells, endothelial cells, and stromal cells (Stockinger et al., 2014). Among these, immune cells are one of the main sites of AhR gene expression, especially macrophages, dendritic cells, and T lymphocytes (Trikha and Lee, 2020), which play an important role in immune responses and inflammatory reactions. Li et al. discovered that the AhR signal plays a significant regulatory role in the expression of CD117 on the surface of ILC3 (type 3 innate lymphoid cells), and in patients with Crohn's disease (CD), attenuation of the AhR signal can lead to the transformation of ILC3 into ILC1, thereby increasing inflammation in the terminal ileum (Li J. et al., 2016; Li M. et al., 2016). Climaco-Arvizu et al. reported that AhR could regulate the differentiation of IBD intestinal macrophages. Loss of the AhR gene enhances inflammatory M1 polarization of macrophages, weakens anti-inflammatory M2 polarization, and affects the production and secretion of inflammatory factors, thereby regulating inflammation development (Climaco-Arvizu et al., 2016). In addition to immune cells, epithelial cells and endothelial cells are also important sites of AhR gene expression (Major et al., 2023; Juan et al., 2006). Then researchers found that endothelial cells have higher levels of AhR expression compared to immune cells and epithelial cells through immunofluorescence detection techniques (Major et al., 2023). Further studies showed that AhR was expressed in many types of lung cells, and the cells with high expression mainly included lung endothelial cells and alveolar cells, affecting lung barrier function (Pang et al., 2017).

Gut microbiota regulates lipid metabolism by AhR signal

Increasing evidence suggested that AhR played a crucial role in regulating lipid metabolism, with the gut microbiota influencing AhR activity through its metabolites such as lipopolysaccharide (LPS),

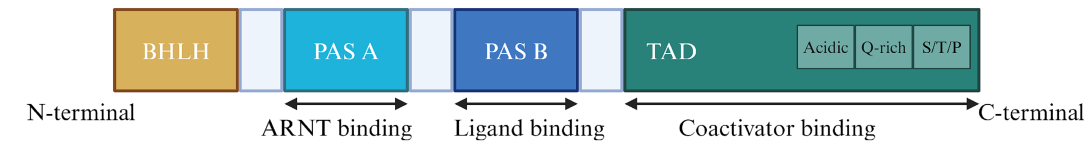

FIGURE 1
The functional domain of the AhR.

amino acid derivative, short-chain fatty acids (SCFAS) and bile acids (BAS) or direct interactions, thereby modulating the host's physiological processes (Figure 2). This article will explore the potential mechanisms by which the gut microbiota affects host lipid metabolism via the AhR signaling pathway, focusing on the gut microbiota itself and its metabolites influencing AhR activity.

AhR activation reduces IL-6 secretion by inhibiting the NF-κB pathway induced by LPS, IL-6 activates stat3 and inhibits the transcription and expression of zinc transporter SLC39A5, AhR enhances IL-10 levels by upregulating Src-STAT3 signaling triggered by LPS, alleviating lipid metabolism disorders. SCFAs exacerbates lipid peroxidation by inhibiting HDACS and increasing the expression of CYP1A1. SCFAs increase the AhR expression in CD4 T cells by activating STAT3 and mTOR signaling pathways after binding to the GPR41 and then promoted the production of IL-22; amino acids also promote IL-22 production after being metabolized by microorganisms into AhR ligands, and the increase of IL-22 improves hyperglycemia. BAs bind to TGR5 to increase AHR expression and promote transcription of ACOX 1 and CPT 1 A by triggering CAMP-ERK pathway and inhibit NLRP3 activity by triggering CAMP-PKA pathway, while AHR also inhibit activation of NLRP3, thus inhibiting hepatic steatosis.

LPS and AhR

LPS is a complex sugar-lipid-protein compound and a major component of bacterial endotoxins found widely in the outer walls of Gram-negative bacteria. Inside the host, LPS is recognized by the immune system as a pathogen-associated molecular pattern (PAMP), triggering an inflammatory response, and classical signaling involves the Toll-like receptor 4 (TLR4)(Facchini et al., 2020), which is a protein associated with the immune system and inflammatory responses, mainly expressed in lymphocytes, macrophages, endothelial cells, and cardiomyocytes (Biemmi et al., 2020), playing a crucial role in the host's immune system. Activation of TLR4 triggers MyD88-and TRIF-dependent signaling pathways (Sun et al., 2019). It recruits myeloid differentiation factor 88 (MyD88) and activates MyD88-dependent NF-κB signaling pathway, inducing the production of inflammatory factors (Wang B. et al., 2023; Wang Y. et al., 2023). AhR was expressed in peritoneal macrophages stimulated by LPS, being induced by TLR signaling. In the LPS signaling pathway, AhR can negatively regulate it by interacting with Stat1. In macrophages, the aryl hydrocarbon receptor (AhR) is activated, forming a complex with the transcription factors STAT1 and NF-kB, inhibiting NF-kB-mediated downstream factor IL-6 transcription, resulting in suppressed IL-6 expression, thus alleviating LPS-induced inflammatory response (Kimura et al., 2009). IL-6, as a pro-inflammatory factor, whose down-regulation inhibited hepatocyte adipogenesis and reduced macrophage inflammatory response. Blocking IL-6 signaling reduced the occurrence of NAFLD (Park et al., 2023) and inhibited obesity-related ventricular arrhythmias (Aromolaran et al., 2024). Moreover, IL-6 activated stat3, increased stat3 phosphorylation, and inhibited the transcription and expression of zinc transporter SLC39A5, thereby increasing glucagon secretion

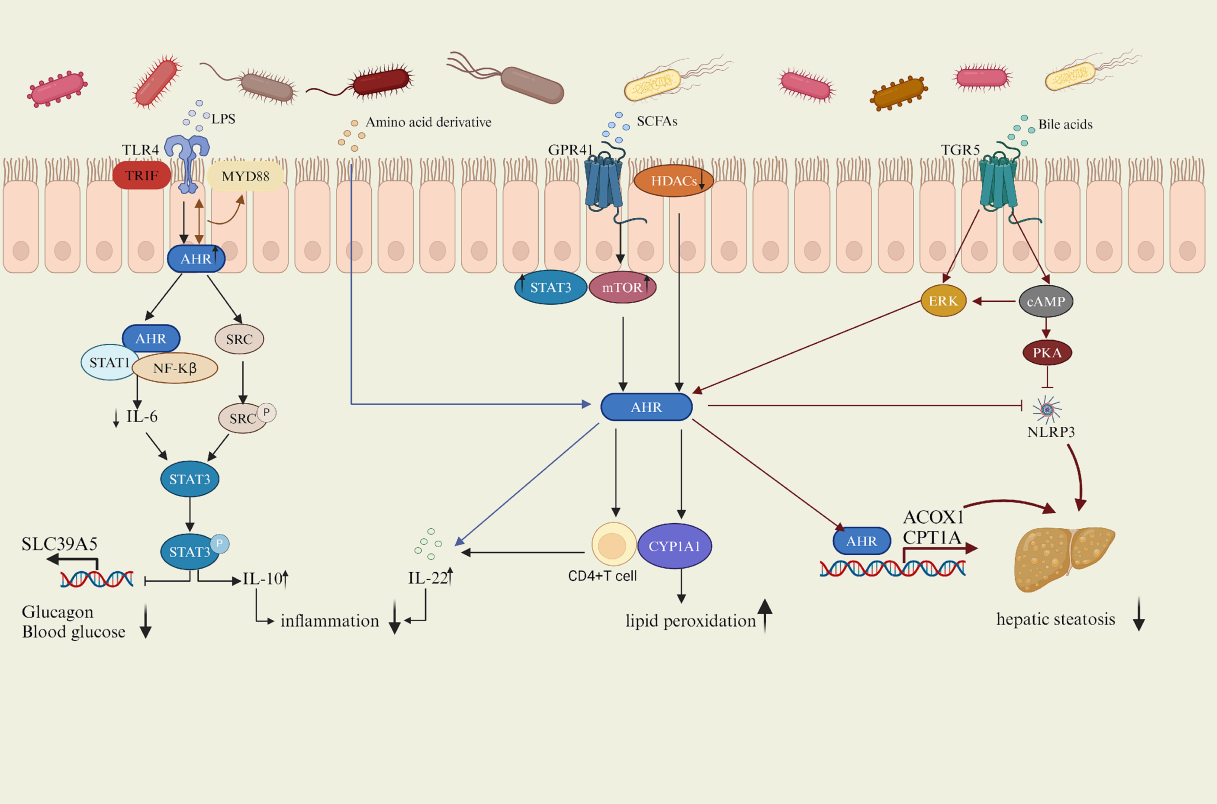

FIGURE 2
Mechanism of AhR regulation of lipid metabolism.

and the risk of T2D (Chen et al., 2023). Furthermore, LPS also triggered the AhR-mediated activation of the Src-STAT3 signaling pathway (Zhu et al., 2018). AhR in the cytoplasm upregulates the tyrosine phosphorylation of Src kinase (Src). Src, as a non-receptor tyrosine kinase, participated in various cellular signaling transduction processes, significantly affecting cell growth, proliferation, and differentiation (Brown and Cooper, 1996), catalyzing the phosphorylation of STAT3 (signal transducer and activator of transcription3) and leading to the activation of STAT3. Then STAT3 translocated to the nucleus and regulated the transcriptional expression of relevant genes. Src-STAT3 signaling pathway further promotes the secretion of IL-10 through AhR mediation, collectively inhibiting the inflammatory phenotype of macrophages. IL-10, an anti-inflammatory cytokine, suppresses the production and release of various inflammatory mediators, thereby attenuating the metabolic inflammation (Zhu et al., 2018). Adipose tissue-derived stem cells (ADSCs) promoted the expression of IL-10 to ameliorate hyperglycemia and insulin resistance and prevented T2D (Zhang et al., 2017). Overexpression of IL-10 had also been shown to restore intestinal repair after HFD feeding, normalizing barrier repair in HFD-treated mice (Hill et al., 2023). These studies indicated that the expression level of IL-10 is closely related to lipid metabolism. Interestingly, AhR was also shown to have an interaction with TLR4 and together regulate the downstream factor MyD88 (Zhang et al., 2023). These results indicate an inhibitory effect on the LPS-induced inflammatory response by enhancing the activation of AhR, suggesting that AhR agonists such as related ligands or probiotics can be used in clinical application to mitigate the inflammatory effects of LPS. For example, the AhR endogenous ligand indole-3-lactic acid (ILA) significantly attenuated NF-κB activation in macrophages (Calzetta et al., 2022) and *Bacillus amyloliquefaciens* alleviated LPS-induced intestinal inflammation through the AhR/STAT3 pathway (Wang et al., 2024).

SCFAs and AhR

Short-chain fatty acids (SCFAS) are metabolites generated by intestinal flora through biotransformation, mainly including acetic acid, propionic acid and butyric acid (He et al., 2020), in which Bacteroides mainly produce acetic acid and propionic acid, while Firmicutes mainly produce butyric acid (Macfarlane and Macfarlane, 2003). After SCFAS are uptaken by the intestine, it undergoes a series of transformation processes in the liver, mainly producing acetyl-CoA and propionyl-CoA, which participate in several biological metabolic pathways, such as glycogen synthesis, gluconeogenesis process and cholesterol synthesis, and then affect the host lipid metabolism (den Besten et al., 2013). SCFAs are reported to enhance gene expression mediated by the aromatic hydrocarbon receptor (AhR) and significantly increase the expression of AhR response genes such as Cytochrome P450 1A1 (CYP1A1) by inhibiting the activity of histone deacetylases (HDACs) (Jin et al., 2017). Interestingly, overexpression of CYP1A1 exacerbated lipid peroxidation in the NAFLD model (Huang et al., 2018). Moreover, butyrate also increased the AhR expression in CD4 T cells by activating the STAT3 and the mammalian target of rapamycin (mTOR) signaling pathways after binding to the G-protein-coupled receptor 41 (GPR41) and then promoted the production of IL-22 (Yang et al., 2020). IL-22 plays an important role in lipid metabolism, as it improves insulin sensitivity, protects the intestinal mucosal barrier, reduces endotoxemia and chronic inflammation, IL-22 receptor-deficient and high-fat-fed mice are prone to metabolic disorders, while administration of exogenous IL-22 to obese mice reversed the induced symptoms like hyperglycemia and insulin resistance (Wang et al., 2014).

BAs and AhR

Bile acids are vital signaling molecules synthesized from cholesterol in the liver, with the classic pathway of their synthesis triggered by cholesterol 7α-hydroxylase (CYP7A1) catalyzing cholesterol 7α-site hydroxylation (Ahmad and Haeusler, 2019). The host often promotes the utilization of bile acids through enterohepatic circulation, approximately 95% of primary bile acids are reabsorbed at the terminal ileum and return to the liver via the portal vein; a small portion of primary bile acids are catalyzed by BAs salt hydrolase (BSH) enzymes from gut microbiota into free BAs, which undergo conversion into secondary bile acids through pathways like dehydrogenation and dehydroxylation under the influence of intestinal flora (Hsu and Schnabl, 2023). Microorganisms expressing BSH are primarily members of the Firmicutes phylum (Jones et al., 2008), disturb the gut ecology, while in IBD, BSH-producing Firmicutes were reduced (Ramos and Papadakis, 2019), impeding the conversion of PBAs to SBAs and thereby affecting bile acid metabolism. Intraepithelial lymphocytes (IELs) play a protective role in IBD models (Panda et al., 2023), Furthermore, AhR regulated the development, proliferation, and function of intraepithelial lymphocytes (IELs) (Li et al., 2011), which may be beneficial for gut microbial balance and Maintenance of firmicutes diversity in IBD, thus enhancing secondary bile acid generation. SBAs inhibited the expression of pro-inflammatory genes by activating the membrane receptor TGR5 (Duboc et al., 2013), suggesting a potential synergistic effect between bile acids and AhR in suppressing inflammatory responses. TGR5 activation on ciliated and non-ciliated bile ducts triggered downstream signaling pathways such as expression of cAMP, AKT, and extracellular signal-regulated kinase (ERK) (Guo et al., 2016). Meanwhile TGR5 as a membrane-bound receptor played a significant role in glucose metabolism (Hui et al., 2020), lipid metabolism (Arab et al., 2017), and anti-inflammatory immune regulation (Chiang, 2013). For example, TGR5 suppressed the activation of the NLRP3 inflammasome by activating intracellular signaling pathways, particularly the cAMP-PKA axis (Tian et al., 1999). NLRP3 inflammasome, a crucial innate immune molecule, promotes the release of pro-inflammatory factors and exacerbates inflammatory responses when activated. Studies on TGR5−/− mouse models show that genetic deficiency leads to overactive NLRP3 inflammasomes, resulting in elevated pro-inflammatory factors and enhanced M1 polarization of macrophages in adipose tissue (Shi et al., 2021), exacerbating inflammation. While the inhibition of NLRP3 inflammasome activity reduced liver inflammation and fibrosis and improved NAFLD (Shen Q. et al., 2023; Shen X. et al., 2023). As a negative regulator of NLRP3 inflammasomes, AhR inhibited the activation of NLRP3 inflammasomes, the reason is that AhR bound to its endogenous ligand and inhibited NF-κB transcription, leading to reduced NLRP3 transcription (Huai et al., 2014; Qiao et al., 2022). Furthermore, TGR5 activated the ERK to induce phosphorylation of dynamin-related protein 1 (Drp1) in mitochondria dynamics. Activation of the ERK pathway can induce phosphorylation of Drp1

(Prieto et al., 2016), leading to mitochondrial fission, increasing the rate of fatty acid beta-oxidation while reducing fat accumulation. Additionally, cAMP is also involved in ERK signal transduction (Enserink et al., 2002). In cilia-related liver disorders such as autosomal dominant and autosomal recessive polycystic kidney diseases, cAMP levels are elevated and TGR5 is overexpressed in cholangiocytes but not localized on cilia. In ciliary cholangiocytes, TGR 5 agonists reduced cAMP levels and cell proliferation, but ERK signaling was activated, and the cAMP levels also affected the phosphorylation of ERK (Masyuk et al., 2013). The activation of ERK promoted AHR expression, then AHR directly binded to the promoter regions of the key fatty acid oxidation enzymes ACOX 1 and CPT1A to transcribe and activate their expression and then achieved normal fatty acid oxidation function, thus inhibiting hepatic steatosis (Han et al., 2021). Interestingly the upregulation of ERK signaling can inhibit AhR expression (Jiang et al., 2021), suggesting that activation of ERK pathway can inhibit AhR signaling and thus affect lipid metabolism.

Amino acids (AAs) and AhR

Most amino acids are absorbed in the small intestine, while those not absorbed enter the colon to participate in microbial metabolism processes, leading to the production of various metabolites such as ammonia, amines, short-chain fatty acids, branched-chain fatty acids, hydrogen sulfide, organic acids, and phenols (Abdallah et al., 2020; Ma and Ma, 2019). Studies indicate that branched-chain amino acids and aromatic amino acids play crucial roles in lipid metabolism disorders associated with obesity, insulin resistance, diabetes, and fatty liver (Ejtahed et al., 2020). And aromatic amino acids mainly include phenylalanine, tyrosine, and tryptophan, which activate the AhR to induce downstream pathway alterations (Yang et al., 2019). The ability of gut microbes to metabolize tryptophan is reduced, which lowering the activation of AhR to promote metabolic disease (Natividad et al., 2018), suggesting that AhR may regulate lipid metabolism through the gut microbiota. Tryptophan is a crucial source of endogenous AhR ligand precursors (Liu et al., 2021) and its metabolites such as kynurenine and the photoproduct 6-formylindolo [3,2-b] carbazole (FICZ), can bind to the aryl hydrocarbon receptor (AhR) in the intestine, thereby regulating the function and differentiation of intestinal immune cells (Gutiérrez-Vázquez and Quintana, 2018). Kynurenine promoted the differentiation of CD4+ naïve T cells into anti-inflammatory Treg cells (Mezrich et al., 2010), while FICZ, as a high-affinity ligand for AhR, activated the AhR signaling pathway at extremely low concentrations (Rannug and Fritsche, 2006), upregulating the expression of the cytochrome P450 family 1.

(CYP1) family of genes. Further CYP1A1 rapidly degraded FICZ, forming a negative feedback regulatory mechanism to ensure a low level of FICZ in the gastrointestinal tract (Wei et al., 2000). However, FICZ also induced the differentiation of Th17 cells and the expression of the inflammatory factor IL-17, which inhibited the differentiation of Treg cells (Quintana et al., 2008). Studies have shown that gut microbiota metabolized tryptophan into indole and its derivatives, thereby participating in the regulation of AhR signaling. For instance, tryptophan was metabolized by *Lactobacillus reuteri* to indole-3-aldehyde (Zelante et al., 2013). In mouse models, this substance can activate AhR and induce the production of IL-22, which plays a crucial role in maintaining intestinal mucosal immune homeostasis. Additionally, tryptophan metabolites from other commensal microbiota, such as indole-3-acetic acid, indole-3-aldehyde, tryptamine, and 3-methylindole (Shen et al., 2022; Dang et al., 2023), also exhibit AhR agonist activity, suggesting a potentially significant role in intestinal immune regulation. The microbial community in the gut generates AhR agonists during tryptophan metabolism, supporting the growth and development of ILC3 in the intestine. AhR is an essential transcription factor for ILC3 (Li J. et al., 2016; Li M. et al., 2016), ILC3 is a critical member of the intestinal mucosal immune system, and the dysfunction of ILC3s may lead to inflammatory diseases in intestinal mucosal tissues (Cording et al., 2018). What's more, ILC3 protected the body from damage by the symbiotic microbiome through producing key anti-inflammatory factors, such as IL-22 and IL-17A (Shen Q. et al., 2023; Shen X. et al., 2023), to prevent inflammation in adipose tissue.

AhR and lipid metabolism disorder

AhR plays a crucial role in numerous biological processes, including immune responses, cell proliferation and differentiation, as well as maintaining homeostasis (Wang et al., 2022). However, an increasing number of studies indicates that AhR plays an important role in lipid metabolism, causing lipid metabolic diseases such as obesity (Kerley-Hamilton et al., 2012), non-alcoholic fatty liver disease (NAFLD) (Moyer et al., 2017), and type 2 diabetes (T2D) (Wang et al., 2011). The expression of lipid metabolism-related phenotypes in these disease models can be promoted or inhibited by adjusting AhR levels. (Table 1) Therefore, it is necessary to study the effect of AhR on lipid metabolism in detail in order to use it as a potential therapeutic target for lipid metabolism diseases.

AhR and obesity

With the improvement of living standards, obesity is becoming more common and prevalent worldwide. Obesity refers to the excessive accumulation of fat in the body, mainly caused by the excessive accumulation of triglycerides in the body (Twig et al., 2020). Typically characterized by exceeding the normal weight range and an increase in body fat percentage, obesity is associated with various chronic diseases and health issues, severely affecting the quality of life (Piché et al., 2020). Therefore, finding effective methods to address obesity is crucial. Obesity affected the diversity of the gut microbiota, with a decrease in the abundance of Bacteroidetes and increased proportion of Firmicutes in obese individuals, suggesting a possible role in regulating obesity by remodeling gut microbial community structure (Ley et al., 2005). Studies have shown that the activation of AhR induced obesity (Kerley-Hamilton et al., 2012), It may be because the aryl hydrocarbon receptor repressor (AhRR) was significantly down-regulated in obese populations, while AhR and CYP1B1 are significantly upregulated, indicating that AhRR may regulate obesity by inhibiting AhR expression through the AhR-CYP1B1 axis (Shahin et al., 2020). AhR deficiency significantly reduced weight gain and adiposity, increasing the protein and mRNA expression of fibroblast growth factor 21 (FGF21), which activates thermogenesis in brown adipose tissue (BAT) and gWAT, thus increasing metabolic rate and energy expenditure, preventing obesity induced by a high-fat diet (Girer et al., 2019), making it a potential target for obesity treatment.

TABLE 1 Effect of AhR expression level on phenotype related to lipid metabolic diseases.

Disease	Model	AhR level	phenotypes	Reference
Obesity	Mouse	Inhibit	WAT ↓ Cyp1a1 ↓ PPARγ↓ Foxo1 ↓ Scd1 ↓ Spp1 ↓ CYP4A ↓ FGF21 ↓ FADS1 ↓ ELOVL5 ↓ IL-6 ↓ STAT3 ↓	Moyer et al. (2017), Xu et al. (2015), Huang et al. (2022)
	Human	Elevate	Cyp1b1 ↑ Leptin ↑ TC ↑ TG ↑ LDL-C ↑ Ghrelin ↓ Scd1 ↓ PPARγ2 ↓ ACC2 ↓ CPT1a ↓	Shahin et al. (2020)
NAFLD	Mouse	Inhibit	ALT ↓ AST ↓ TG ↓ TC ↓ Cyp1a1 ↓ TNF-a ↓	Xia et al. (2019)
	HepG2	Inhibit	MDA ↓ ROS ↓ SOD ↑	Xia et al. (2019)
T2D	Mouse	Inhibit	PPARα ↓ Aco ↓ Cpt1b ↓ Pepck ↓ G6pase ↓ Hepaticglycon↑ pAKT(Ser473)↑ Cyp1a1 ↓ Cyp1b1 ↓	Wang et al. (2011), Xia et al. (2019), Jaeger et al. (2017)
	Mouse	Elevate	pAKT ↓ pNFκB ↑ ICAM ↓ INOS ↓ FMO3 ↓ IL-10 ↑ IL-22 ↑ TG ↓ ALT ↑ GLP-1 ↑	Liu et al. (2020), Lin et al. (2019), Natividad et al. (2018)

Studies have shown that Kynurenine caused obesity by activating AHR (Moyer et al., 2016), while obesity and hepatic steatosis were prevented by inhibiting AhR, the AhR antagonist naphthoflavone (aNF) prevented and reversed obesity in high-fat diet mice by inhibiting AhR and related genes in its network, such as CYP1B1 and stearoyl-CoA desaturase-1 (SCD1) (Moyer et al., 2017; Xu et al., 2015). CYP1B1 is

a member of the cytochrome P450 superfamily that is involved in metabolizing endogenous compounds including steroid hormones and lipids, which regulate metabolism, accumulation, and distribution in adipose tissue. The expression of CYP1B1 influenced the development of obesity, in CYP1B1-null mice, the expression level of SCD1 was reduced, which inhibited obesity and thus affected lipid metabolism (Li et al., 2014). Further research found that SCD1 is a delta-9 fatty acid desaturase that catalyzes the synthesis of monounsaturated fatty acids. Similarly, SCD1-deficient mice reduced lipid synthesis and enhanced insulin sensitivity, promoting the suppression of obesity (Flowers and Ntambi, 2008). In obese patients, tryptophan was preferentially catabolized through the kynurenine pathway (KP), leading to an excessive increase in the concentration of kynurenine (Kyn) in the blood, which activated AhR and then transcribed STAT3 expression to enhance the secretion of IL-6 (Huang et al., 2022), which maintained the proliferation rates of obese adipose tissue (Ackermann et al., 2024). In contrast, knockdown of AhR from adipocytes abolished the effects of Kyn and prevented obesity.

AhR and NAFLD

NAFLD refers to the pathological condition where the liver accumulates fat without excessive alcohol consumption. NAFLD is the most common chronic liver disease (Zhou et al., 2020) and a significant component of metabolic syndrome (Haas et al., 2016), which included obesity, insulin resistance, hypertension, hypertriglyceridemia, and low high-density lipoprotein cholesterolemia (Chen et al., 2012). The spectrum of NAFLD ranges from simple steatosis (fatty liver) to non-alcoholic steatohepatitis (NASH), fibrosis, and cirrhosis (Schuster et al., 2018). Activation of the AhR has been shown to affect lipid metabolism in the liver, including synthesis and oxidation of fatty acids. Abnormal fat accumulation in the liver is a primary feature, and AhR activation can induce lipid deposition, potentially directly impacting the pathogenesis of NAFLD (Podechard et al., 2009). It has been observed that the activation of AhR signaling pathway indirectly induced the accumulation of lipid droplets in rat hepatocytes (Neuschäfer-Rube et al., 2015). The AhR-CYP1A1 signaling pathway was activated to cause intracellular lipid droplet accumulation in Hepatitis C virus (HCV) (Ohashi et al., 2018). As an exogenous ligand for the AhR, the Sulforaphane (SFN) can regulated the intestinal microflora of high-fat diet mice to prevent NAFLD by activating the AhR/SREBP-1C pathway, reduced the protein levels of indole-3-acetic acid (IAA), sterol regulatory element-binding protein-1c (SREBP-1C), acetyl-CoA carboxylase 1 (ACC1), and fatty acid synthase (FAS), And then regulates hepatic lipid metabolism, And to prevent NAFLD (Xu et al., 2021). Further studies showed that AhR promoted the absorption of fatty acids by activating its transcriptional target CD36.(Lee et al., 2010). Overexpression of the AhR in the liver significantly upregulates the expression of the fatty acid translocase (FAT) CD36 in mouse liver cells, promoting the uptake of fatty acids by liver cells (Yao et al., 2016), which exacerbated lipid deposition in the liver, leading to liver damage and promoting the development of NAFLD. AhR ligand 3-methylcholanthrene (3MC) also significantly increased the expression level of fatty acid translocase in liver by activating AhR, inducing hepatic steatosis (Kawano et al., 2010). Estrogen deficiency is one of the main causes of obesity and NAFLD (Zhu et al., 2020). However, the administration of endogenous agonists of AhR such as cinnabarinic acid (CA) down-regulated CD36 and reduced the uptake of free fatty acids in hepatocytes, thus achieving the inhibition of hepatic steatosis and liver injury (Patil et al., 2022). Importantly, CYP1A1 is an estrogen-metabolizing enzyme, and increased activity of CYP1A1 leads to estrogen deficiency (Niwa et al., 2015), for example, Benzo[a]pyrene (Bap) promoted the transcription and overexpression of CYP1A1 by activating the AhR pathway, inhibiting estrogen's protective effect on the liver, significantly increasing the risk of NAFLD (Mumtaz et al., 2022). In addition, alpha-naphthoflavone, as an AhR inhibitor, alleviated NAFLD by inhibiting the AhR-CYP1A1 pathway (Xia et al., 2019). The AhR-CYP1A1 axis regulates lipid peroxidation by influencing the level of reactive oxygen species (ROS) and superoxide dismutase (SOD) (Huang et al., 2018). When the expression of AhR increases, the CYP1A1 also increases to enhance ROS (Cui et al., 2024) while excess ROS will lead to the production of lipid peroxides such as malondialdehyde (MDA), which may exacerbate oxidative stress and mitochondrial damage (Wang B. et al., 2023; Wang Y. et al., 2023) and promote the production of NAFLD (Zhao et al., 2023).

AhR and T2D

T2D is the most common type of diabetes globally, accounting for over 90% of all diabetes cases. Unlike type 1 diabetes, T2D is characterized by insulin resistance and/or dysfunction of pancreatic β-cells, leading to sustained high blood sugar levels and the former is due to autoimmune destruction of insulin-producing cells (ElSayed et al., 2023). Abnormal expression of AhR will result in imbalanced glucose and lipid metabolism, indicating a crucial role of AhR in regulating these processes in the body (Biljes et al., 2015). Thus, AhR may be a key factor in the development of diabetes. The development of T2D is associated with a state of chronic low-grade inflammation (Gong F. et al., 2016; Gong P. et al., 2016). In high sugar-induced insulin resistance and diabetes complications, AhR is crucial for maintaining ILC3, promoting the development and maturation of ILC3, and stimulating the secretion of IL-22 by ILC3 to inhibit inflammation levels, thereby preserving intestinal homeostasis (Artis and Spits, 2015; Kobayashi et al., 2014). IL-22 released by ILC3 cells protected pancreatic islet beta cells from inflammation and glucotoxicity, potentially reversing the damage caused by hyperglycemia to pancreatic islet beta cells, thus improving insulin sensitivity (Abadpour et al., 2018). Furthermore, AhR ligands enhanced intestinal defense mechanisms, reduced bacterial translocation and systemic inflammation, effectively reversing glucose intolerance and insulin resistance induced by diabetes (Liu et al., 2020). The indirubin, an AhR agonist, induced the secretion of IL-10 and IL-22 by activating AhR to prevent high-fat diet-induced insulin resistance in mice model (Lin et al., 2019). Other AhR agonists, such as indoles, have been shown to effectively stimulate the secretion of glucagon-like peptide-1 (GLP-1), thus improving insulin resistance and alleviate symptoms of T2D (Natividad et al., 2018). Further studies have found that tryptophan, as a ligand of AHR, was metabolized by gut microbiota into 5-hydroxyindole-3-acetic acid (5-HIAA) promoting the ubiquitin–proteasome degradation of Suv39h1 by activating AhR, thereby stimulating TSC2 expression and inhibiting the activation of mTORC1 signaling, which would

promote insulin signaling, improve glucose intolerance and reduce the risk of T2D (Du et al., 2024). However, it has also been shown that lack of AhR improved insulin sensitivity and glucose tolerance (Wang et al., 2011) by increasing energy expenditure and ameliorating high-fat diet-induced insulin resistance in mice (Jaeger et al., 2017). Although these results are inconsistent, the important role of AhR cannot be ignored. Thus, further investigation and confirmation are needed on how AhR specifically affects glucose metabolism and T2D.

Limitations and future direction

Increasing evidences demonstrate that AhR signaling is associated with lipid metabolism, and although some significant progress has been gained about AhR regulating lipid metabolism, translating these findings into clinical treatment and preventive strategies still faces many challenges. The gut microbiome is highly diverse, containing thousands of different microbial species. There are complex interrelationships among these microorganisms, including symbiosis, competition and antagonism. Even though certain microorganisms have been found to be associated with AHR activation and lipid metabolism changes, the role of these microorganisms may be altered by the influence of other microorganisms in the context of the entire microbial community. AHR is a pleiotropic transcription factor, in addition to regulating the genes involved in lipid metabolism. It is also involved in many other biological processes, such as immune response, cell proliferation, and differentiation. AHR can regulate the expression of numerous genes that may have different functions in different cell types and physiological conditions. Therefore, it is difficult to distinguish between the direct and indirect effects of AHR on lipid metabolism and how these effects are synergized in complex physiological and pathological processes.

At present, relevant studies mainly focus on animal models and cell experiments, such as mice, rats and liver cell lines (Zhao et al., 2022). While these studies provide us with valuable experimental evidence, there are certain physiological and metabolic differences between animal models and humans, so these results may not fully reflect the real situation in the human body. In addition, different research teams use different experimental conditions and methods, resulting in a certain diversity of research results, which makes it difficult to interpret and apply these results. Some studies have shown that AhR is protective against diet-induced metabolic syndrome (Wada et al., 2016), while others are negative (Korecka et al., 2016). The AhR signaling pathway involves multiple molecular and cellular processes, so the experimental design needs to be highly precise and complex to accurately simulate what is really happening *in vivo*. However, these complex interactions may not be fully captured by the current experimental methods, the specific molecular mechanisms and signaling pathways still require further intensive investigation.

Author contributions

WZ: Writing – original draft. ML: Writing – review & editing. XL: Writing – review & editing. CH: Writing – review & editing. JY: Writing – review & editing. JM: Writing – review & editing.

Funding

The author(s) declare that no financial support was received for the research, authorship, and/or publication of this article.

Conflict of interest

The authors declare that the research was conducted in the absence of any commercial or financial relationships that could be construed as a potential conflict of interest.

Publisher's note

References

Abadpour, S., Halvorsen, B., Sahraoui, A., Korsgren, O., Aukrust, P., and Scholz, H. (2018). Interleukin-22 reverses human islet dysfunction and apoptosis triggered by hyperglycemia and LIGHT. *J. Mol. Endocrinol.* 60, 171–183. doi: 10.1530/JME-17-0182

Abdallah, A., Elemba, E., Zhong, Q., and Sun, Z. (2020). Gastrointestinal interaction between dietary amino acids and gut microbiota: with special emphasis on host nutrition. *Curr. Protein Pept. Sci.* 21, 785–798. doi: 10.2174/1389203721666200212095503

Ackermann, J., Arndt, L., Fröba, J., Lindhorst, A., Glaß, M., Kirstein, M., et al. (2024). IL-6 signaling drives self-renewal and alternative activation of adipose tissue macrophages. *Front Immunol.* 15:1201439. Published 2024 Feb 28. doi: 10.3389/fimmu.2024.1201439

Ahmad, T. R., and Haeusler, R. A. (2019). Bile acids in glucose metabolism and insulin signalling - mechanisms and research needs. *Nat. Rev. Endocrinol.* 15, 701–712. doi: 10.1038/s41574-019-0266-7

Arab, J. P., Karpen, S. J., Dawson, P. A., Arrese, M., and Trauner, M. (2017). Bile acids and nonalcoholic fatty liver disease: molecular insights and therapeutic perspectives. *Hepatology* 65, 350–362. doi: 10.1002/hep.28709

Aromolaran, K. A., Corbin, A., and Aromolaran, A. S. (2024). Obesity arrhythmias: role of IL-6 trans-signaling. *Int. J. Mol. Sci.* 25:8407. doi: 10.3390/ijms25158407

Artis, D., and Spits, H. (2015). The biology of innate lymphoid cells. *Nature* 517, 293–301. doi: 10.1038/nature14189

Bahman, F., Choudhry, K., Al-Rashed, F., Al-Mulla, F., Sindhu, S., and Ahmad, R. (2024). Aryl hydrocarbon receptor: current perspectives on key signaling partners and immunoregulatory role in inflammatory diseases. *Front. Immunol.* 15:1421346. doi: 10.3389/fimmu.2024.1421346

Biemmi, V., Milano, G., Ciullo, A., Cervio, E., Burrello, J., Dei Cas, M., et al. (2020). Inflammatory extracellular vesicles prompt heart dysfunction via TRL4-dependent NF-κB activation. *Theranostics* 10, 2773–2790. doi: 10.7150/thno.39072

Biljes, D., Hammerschmidt-Kamper, C., Kadow, S., Diel, P., Weigt, C., Burkart, V., et al. (2015). Impaired glucose and lipid metabolism in ageing aryl hydrocarbon receptor deficient mice. *Excli J.* 14, 1153–1163. doi: 10.17179/excli2015-638

Bjeldanes, L. F., Kim, J. Y., Grose, K. R., Bartholomew, J. C., and Bradfield, C. A. (1991). Aromatic hydrocarbon responsiveness-receptor agonists generated from indole-3-carbinol in vitro and in vivo: comparisons with 2,3,7,8-tetrachlorodibenzo-p-dioxin. *Proc. Natl. Acad. Sci. USA* 88, 9543–9547. doi: 10.1073/pnas.88.21.9543

Brown, M. T., and Cooper, J. A. (1996). Regulation, substrates and functions of src. *Biochim. Biophys. Acta* 1287, 121–149. doi: 10.1016/0304-419X(96)00003-0

Calzetta, L., Pistocchini, E., Cito, G., Ritondo, B. L., Verri, S., and Rogliani, P. (2022). Inflammatory and contractile profile in LPS-challenged equine isolated bronchi: evidence for IL-6 as a potential target against AhR in equine asthma. *Pulm. Pharmacol. Ther.* 73-74:102125. doi: 10.1016/j.pupt.2022.102125

Chen, W., Cui, W., Wu, J., Zheng, W., Sun, X., Zhang, J., et al. (2023). Blocking IL-6 signaling improves glucose tolerance via SLC39A5-mediated suppression of glucagon secretion. *Metabolism* 146:155641. doi: 10.1016/j.metabol.2023.155641

Chen, L. Y., Qiao, Q. H., Zhang, S. C., Chen, Y. H., Chao, G. Q., and Fang, L. Z. (2012). Metabolic syndrome and gallstone disease. *World J. Gastroenterol.* 18, 4215–4220. doi: 10.3748/wjg.v18.i31.4215

Chiang, J. Y. (2013). Bile acid metabolism and signaling. *Compr. Physiol.* 3, 1191–1212. doi: 10.1002/cphy.c120023

Climaco-Arvizu, S., Domínguez-Acosta, O., Cabañas-Cortés, M. A., Rodríguez-Sosa, M., Gonzalez, F. J., Vega, L., et al. (2016). Aryl hydrocarbon receptor influences nitric oxide and arginine production and alters M1/M2 macrophage polarization. *Life Sci.* 155, 76–84. doi: 10.1016/j.lfs.2016.05.001

Cording, S., Medvedovic, J., Lécuyer, E., Aychek, T., Déjardin, F., and Eberl, G. (2018). Mouse models for the study of fate and function of innate lymphoid cells. *Eur. J. Immunol.* 48, 1271–1280. doi: 10.1002/eji.201747388

Cui, J., Chen, W., Zhang, D., Lu, M., Huang, Z., and Yi, B. (2024). Metformin attenuates PM2.5-induced oxidative stress by inhibiting the AhR/CYP1A1 pathway in proximal renal tubular epithelial cells. *Toxicol Mech. Methods* 34, 1022–1034. doi: 10.1080/15376516.2024.2378296

Dang, G., Wen, X., Zhong, R., Wu, W., Tang, S., Li, C., et al. (2023). Pectin modulates intestinal immunity in a pig model via regulating the gut microbiota-derived tryptophan metabolite-AhR-IL22 pathway. *J. Anim. Sci. Biotechnol.* 14:38. doi: 10.1186/s40104-023-00838-z

den Besten, G., Lange, K., Havinga, R., van Dijk, T. H., Gerding, A., van Eunen, K., et al. (2013). Gut-derived short-chain fatty acids are vividly assimilated into host carbohydrates and lipids. *Am. J. Physiol. Gastrointest. Liver Physiol.* 305, G900–G910. doi: 10.1152/ajpgi.00265.2013

Du, W., Jiang, S., Yin, S., Wang, R., Zhang, C., Yin, B. C., et al. (2024). The microbiota-dependent tryptophan metabolite alleviates high-fat diet-induced insulin resistance through the hepatic AhR/TSC2/mTORC1 axis. *Proc. Natl. Acad. Sci. USA* 121:e2400385121. doi: 10.1073/pnas.2400385121

Duboc, H., Rajca, S., Rainteau, D., Benarous, D., Maubert, M. A., Quervain, E., et al. (2013). Connecting dysbiosis, bile-acid dysmetabolism and gut inflammation in inflammatory bowel diseases. *Gut* 62, 531–539. doi: 10.1136/gutjnl-2012-302578

Ejtahed, H. S., Angoorani, P., Soroush, A. R., Hasani-Ranjbar, S., Siadat, S. D., and Larijani, B. (2020). Gut microbiota-derived metabolites in obesity: a systematic review. *Biosci. Microbiota Food Health* 39, 65–76. doi: 10.12938/bmfh.2019-026

ElSayed, N. A., Aleppo, G., and Aroda, V. R. (2023). 2. Classification and diagnosis of diabetes: standards of Care in Diabetes. *Diabetes Care* 46, S19–S40. doi: 10.2337/dc23-S002

Enserink, J. M., Christensen, A. E., de Rooij, J., van Triest, M., Schwede, F., Genieser, H. G., et al. (2002). A novel Epac-specific cAMP analogue demonstrates independent regulation of Rap1 and ERK. *Nat. Cell Biol.* 4, 901–906. doi: 10.1038/ncb874

Facchini, F. A., di, D., Barresi, S., Luraghi, A., Minotti, A., Granucci, F., et al. (2020). Effect of chemical modulation of toll-like receptor 4 in an animal model of ulcerative colitis. *Eur. J. Clin. Pharmacol.* 76, 409–418. doi: 10.1007/s00228-019-02799-7

Flowers, M. T., and Ntambi, J. M. (2008). Role of stearoyl-coenzyme a desaturase in regulating lipid metabolism. *Curr. Opin. Lipidol.* 19, 248–256. doi: 10.1097/MOL.0b013e3282f9b54d

Fukunaga, B. N., Probst, M. R., Reisz-Porszasz, S., and Hankinson, O. (1995). Identification of functional domains of the aryl hydrocarbon receptor. *J. Biol. Chem.* 270, 29270–29278. doi: 10.1074/jbc.270.49.29270

Girer, N. G., Carter, D., Bhattarai, N., Mustafa, M., Denner, L., Porter, C., et al. (2019). Inducible loss of the aryl hydrocarbon receptor activates Perigonadal white fat respiration and Brown fat thermogenesis via fibroblast growth factor 21. *Int. J. Mol. Sci.* 20:950. doi: 10.3390/ijms20040950

Gong, P., Madak-Erdogan, Z., Flaws, J. A., Shapiro, D. J., Katzenellenbogen, J. A., and Katzenellenbogen, B. S. (2016). Estrogen receptor-α and aryl hydrocarbon receptor involvement in the actions of botanical estrogens in target cells. *Mol. Cell. Endocrinol.* 437, 190–200. doi: 10.1016/j.mce.2016.08.025

Gong, F., Wu, J., Zhou, P., Zhang, M., Liu, J., Liu, Y., et al. (2016). Interleukin-22 might act as a double-edged sword in type 2 diabetes and coronary artery disease. *Mediat. Inflamm.* 2016, 8254797–8254712. doi: 10.1155/2016/8254797

Granados, J. C., Falah, K., Koo, I., Morgan, E. W., Perdew, G. H., Patterson, A. D., et al. (2022). AhR is a master regulator of diverse pathways in endogenous metabolism. *Sci. Rep.* 12:16625. doi: 10.1038/s41598-022-20572-2

Guo, C., Chen, W. D., and Wang, Y. D. (2016). TGR5, not only a metabolic regulator. *Front. Physiol.* 7:646. doi: 10.3389/fphys.2016.00646

Guo, N. H., Fu, X., Zi, F. M., Song, Y., Wang, S., and Cheng, J. (2019). The potential therapeutic benefit of resveratrol on Th17/Treg imbalance in immune thrombocytopenic purpura. *Int. Immunopharmacol.* 73, 181–192. doi: 10.1016/j.intimp.2019.04.061

Gutiérrez-Vázquez, C., and Quintana, F. J. (2018). Regulation of the immune response by the aryl hydrocarbon receptor. *Immunity* 48, 19–33. doi: 10.1016/j.immuni.2017.12.012

Haas, J. T., Francque, S., and Staels, B. (2016). Pathophysiology and mechanisms of nonalcoholic fatty liver disease. *Annu. Rev. Physiol.* 78, 181–205. doi: 10.1146/annurev-physiol-021115-105331

Han, Q., Chen, H., Wang, L., An, Y., Hu, X., Zhao, Y., et al. (2021). Systemic deficiency of GHR in pigs leads to hepatic steatosis via negative regulation of AHR signaling. *Int. J. Biol. Sci.* 17, 4108–4121. doi: 10.7150/ijbs.64894

Hankinson, O. (1995). The aryl hydrocarbon receptor complex. *Annu. Rev. Pharmacol. Toxicol.* 35, 307–340. doi: 10.1146/annurev.pa.35.040195.001515

He, J., Zhang, P., Shen, L., Niu, L., Tan, Y., Chen, L., et al. (2020). Short-chain fatty acids and their association with Signalling pathways in inflammation, glucose and lipid metabolism. *Int. J. Mol. Sci.* 21:6356. doi: 10.3390/ijms21176356

Hill, A. A., Kim, M., Zegarra-Ruiz, D. F., Chang, L. C., Norwood, K., Assié, A., et al. (2023). Acute high-fat diet impairs macrophage-supported intestinal damage resolution. *JCI Insight* 8:e164489. doi: 10.1172/jci.insight.164489

Hornedo-Ortega, R., Da Costa, G., Cerezo, A. B., Troncoso, A. M., Richard, T., and Garcia-Parrilla, M. C. (2018). In vitro effects of serotonin, melatonin, and other related indole compounds on amyloid-β kinetics and neuroprotection. *Mol. Nutr. Food Res.* 62:383. doi: 10.1002/mnfr.201700383

Hsu, C. L., and Schnabl, B. (2023). The gut-liver axis and gut microbiota in health and liver disease. *Nat. Rev. Microbiol.* 21, 719–733. doi: 10.1038/s41579-023-00904-3

Huai, W., Zhao, R., Song, H., Zhao, J., Zhang, L., Zhang, L., et al. (2014). Aryl hydrocarbon receptor negatively regulates NLRP3 inflammasome activity by inhibiting NLRP3 transcription. *Nat. Commun.* 5:4738. doi: 10.1038/ncomms5738

Huang, B., Bao, J., Cao, Y. R., Gao, H. F., and Jin, Y. (2018). Cytochrome P450 1A1 (CYP1A1) catalyzes lipid peroxidation of oleic acid-induced HepG2 cells. *Biochemistry* 83, 595–602. doi: 10.1134/S0006297918050127

Huang, T., Song, J., Gao, J., Cheng, J., Xie, H., Zhang, L., et al. (2022). Adipocyte-derived kynurenine promotes obesity and insulin resistance by activating the AhR/STAT3/IL-6 signaling. *Nat. Commun.* 13:3489. doi: 10.1038/s41467-022-31126-5

Hui, S., Huang, L., Wang, X., Zhu, X., Zhou, M., Chen, M., et al. (2020). Capsaicin improves glucose homeostasis by enhancing glucagon-like peptide-1 secretion through the regulation of bile acid metabolism via the remodeling of the gut microbiota in male mice. *FASEB J.* 34, 8558–8573. doi: 10.1096/fj.201902618RR

Ito, S., Chen, C., Satoh, J., Yim, S., and Gonzalez, F. J. (2007). Dietary phytochemicals regulate whole-body CYP1A1 expression through an arylhydrocarbon receptor nuclear translocator-dependent system in gut. *J. Clin. Invest.* 117, 1940–1950. doi: 10.1172/JCI31647

Itoh, A., Miyabayashi, T., Ohno, M., and Sakano, S. (1998). Cloning and expressions of three mammalian homologues of Drosophila slit suggest possible roles for slit in the formation and maintenance of the nervous system. *Brain Res. Mol. Brain Res.* 62, 175–186. doi: 10.1016/S0169-328X(98)00224-1

Jaeger, C., Xu, C., Sun, M., Krager, S., and Tischkau, S. A. (2017). Aryl hydrocarbon receptor-deficient mice are protected from high fat diet-induced changes in metabolic rhythms. *Chronobiol. Int.* 34, 318–336. doi: 10.1080/07420528.2016.1256298

Jiang, Y., Xiao, H., Sun, L., Zhang, Y., Liu, S., and Luo, B. (2021). LMP2A suppresses the role of AhR pathway through ERK signal pathway in EBV-associated gastric cancer. *Virus Res.* 297:198399. doi: 10.1016/j.virusres.2021.198399

Jin, U. H., Cheng, Y., Park, H., Davidson, L. A., Callaway, E. S., Chapkin, R. S., et al. (2017). Short chain fatty acids enhance aryl hydrocarbon (ah) responsiveness in mouse Colonocytes and Caco-2 human Colon Cancer cells. *Sci. Rep.* 7:10163. doi: 10.1038/s41598-017-10824-x

Jones, B. V., Begley, M., Hill, C., Gahan, C. G., and Marchesi, J. R. (2008). Functional and comparative metagenomic analysis of bile salt hydrolase activity in the human gut microbiome. *Proc. Natl. Acad. Sci. USA* 105, 13580–13585. doi: 10.1073/pnas.0804437105

Juan, S. H., Lee, J. L., Ho, P. Y., Lee, Y. H., and Lee, W. S. (2006). Antiproliferative and antiangiogenic effects of 3-methylcholanthrene, an aryl-hydrocarbon receptor agonist, in human umbilical vascular endothelial cells. *Eur. J. Pharmacol.* 530, 1–8. doi: 10.1016/j.ejphar.2005.11.023

Kawano, Y., Nishiumi, S., Tanaka, S., Nobutani, K., Miki, A., Yano, Y., et al. (2010). Activation of the aryl hydrocarbon receptor induces hepatic steatosis via the upregulation of fatty acid transport. *Arch. Biochem. Biophys.* 504, 221–227. doi: 10.1016/j.abb.2010.09.001

Kerley-Hamilton, J. S., Trask, H. W., and Ridley, C. J. (2012). Obesity is mediated by differential aryl hydrocarbon receptor signaling in mice fed a Western diet. *Environ. Health Perspect.* 120, 1252–1259. doi: 10.1289/ehp.1205003

Kimura, A., Naka, T., Nakahama, T., Chinen, I., Masuda, K., Nohara, K., et al. (2009). Aryl hydrocarbon receptor in combination with Stat1 regulates LPS-induced inflammatory responses. *J. Exp. Med.* 206, 2027–2035. doi: 10.1084/jem.20090560

Kobayashi, T., Okada, M., Ito, S., Kobayashi, D., Ishida, K., Kojima, A., et al. (2014). Assessment of interleukin-6 receptor inhibition therapy on periodontal condition in

patients with rheumatoid arthritis and chronic periodontitis. *J. Periodontol.* 85, 57–67. doi: 10.1902/jop.2013.120696

Korecka, A., Dona, A., Lahiri, S., Tett, A. J., al-Asmakh, M., Braniste, V., et al. (2016). Bidirectional communication between the aryl hydrocarbon receptor (AhR) and the microbiome tunes host metabolism. *NPJ Biofilms Microb.* 2:16014. doi: 10.1038/npjbiofilms.2016.14

Kwack, S. J., and Lee, B. M. (2000). Correlation between DNA or protein adducts and benzo[a]pyrene diol epoxide I-triglyceride adduct detected in vitro and in vivo. *Carcinogenesis* 21, 629–632. doi: 10.1093/carcin/21.4.629

Lee, D. H., Folsom, A. R., and Jacobs, D. R. (2005). Iron, zinc, and alcohol consumption and mortality from cardiovascular diseases: the Iowa Women's health study. *Am. J. Clin. Nutr.* 81, 787–791. doi: 10.1093/ajcn/81.4.787

Lee, J. H., Wada, T., Febbraio, M., He, J., Matsubara, T., Lee, M. J., et al. (2010). A novel role for the dioxin receptor in fatty acid metabolism and hepatic steatosis. *Gastroenterology* 139, 653–663. doi: 10.1053/j.gastro.2010.03.033

Ley, R. E., Bäckhed, F., Turnbaugh, P., Lozupone, C. A., Knight, R. D., and Gordon, J. I. (2005). Obesity alters gut microbial ecology. *Proc. Natl. Acad. Sci. USA* 102, 11070–11075. doi: 10.1073/pnas.0504978102

Li, J., Doty, A., and Glover, S. C. (2016). Aryl hydrocarbon receptor signaling involves in the human intestinal ILC3/ILC1 conversion in the inflamed terminal ileum of Crohn's disease patients. *Inflamm Cell Signal.* 3:e1404. doi: 10.14800/ics.1404

Li, Y., Innocentin, S., Withers, D. R., Roberts, N. A., Gallagher, A. R., Grigorieva, E. F., et al. (2011). Exogenous stimuli maintain intraepithelial lymphocytes via aryl hydrocarbon receptor activation. *Cell* 147, 629–640. doi: 10.1016/j.cell.2011.09.025

Li, F., Jiang, C., Larsen, M. C., Bushkofsky, J., Krausz, K. W., Wang, T., et al. (2014). Lipidomics reveals a link between CYP1B1 and SCD1 in promoting obesity. *J. Proteome Res.* 13, 2679–2687. doi: 10.1021/pr500145n

Li, M., Shu, X., Xu, H., Zhang, C., Yang, L., Zhang, L., et al. (2016). Integrative analysis of metabolome and gut microbiota in diet-induced hyperlipidemic rats treated with berberine compounds. *J. Transl. Med.* 14:237. doi: 10.1186/s12967-016-0987-5

Lin, L., Dai, Y., and Xia, Y. (2022). An overview of aryl hydrocarbon receptor ligands in the last two decades (2002-2022): a medicinal chemistry perspective. *Eur. J. Med. Chem.* 244:114845. doi: 10.1016/j.ejmech.2022.114845

Lin, Y. H., Luck, H., Khan, S., Schneeberger, P. H. H., Tsai, S., Clemente-Casares, X., et al. (2019). Aryl hydrocarbon receptor agonist indigo protects against obesity-related insulin resistance through modulation of intestinal and metabolic tissue immunity. *Int. J. Obes.* 43, 2407–2421. doi: 10.1038/s41366-019-0340-1

Liu, W. C., Chen, P. H., and Chen, L. W. (2020). Supplementation of endogenous AhR ligands reverses insulin resistance and associated inflammation in an insulin-dependent diabetic mouse model. *J. Nutr. Biochem.* 83:108384. doi: 10.1016/j.jnutbio.2020.108384

Liu, J. R., Miao, H., Deng, D. Q., Vaziri, N. D., Li, P., and Zhao, Y. Y. (2021). Gut microbiota-derived tryptophan metabolism mediates renal fibrosis by aryl hydrocarbon receptor signaling activation. *Cell. Mol. Life Sci.* 78, 909–922. doi: 10.1007/s00018-020-03645-1

Ma, N., and Ma, X. (2019). Dietary amino acids and the gut-microbiome-immune Axis: physiological metabolism and therapeutic prospects. *Compr. Rev. Food Sci. Food Saf.* 18, 221–242. doi: 10.1111/1541-4337.12401

Macfarlane, S., and Macfarlane, G. T. (2003). Regulation of short-chain fatty acid production. *Proc. Nutr. Soc.* 62, 67–72. doi: 10.1079/PNS2002207

Major, J., Crotta, S., Finsterbusch, K., Chakravarty, P., Shah, K., Frederico, B., et al. (2023). Endothelial AhR activity prevents lung barrier disruption in viral infection. *Nature* 621, 813–820. doi: 10.1038/s41586-023-06287-y

Masyuk, A. I., Huang, B. Q., Radtke, B. N., Gajdos, G. B., Splinter, P. L., Masyuk, T. V., et al. (2013). Ciliary subcellular localization of TGR5 determines the cholangiocyte functional response to bile acid signaling. *Am. J. Physiol. Gastrointest. Liver Physiol.* 304, G1013–G1024. doi: 10.1152/ajpgi.00383.2012

Mezrich, J. D., Fechner, J. H., Zhang, X., Johnson, B. P., Burlingham, W. J., and Bradfield, C. A. (2010). An interaction between kynurenine and the aryl hydrocarbon receptor can generate regulatory T cells. *J. Immunol.* 185, 3190–3198. doi: 10.4049/jimmunol.0903670

Moyer, B. J., Rojas, I. Y., Kerley-Hamilton, J. S., Hazlett, H. F., Nemani, K. V., Trask, H. W., et al. (2016). Inhibition of the aryl hydrocarbon receptor prevents Western diet-induced obesity. Model for AHR activation by kynurenine via oxidized-LDL, TLR2/4, TGFβ, and IDO1. *Toxicol. Appl. Pharmacol.* 300, 13–24. doi: 10.1016/j.taap.2016.03.011

Moyer, B. J., Rojas, I. Y., Kerley-Hamilton, J. S., Nemani, K. V., Trask, H. W., Ringelberg, C. S., et al. (2017). Obesity and fatty liver are prevented by inhibition of the aryl hydrocarbon receptor in both female and male mice. *Nutr. Res.* 44, 38–50. doi: 10.1016/j.nutres.2017.06.002

Mumtaz, H., Hameed, M., Sangah, A. B., Zubair, A., and Hasan, M. (2022). Association between smoking and non-alcoholic fatty liver disease in Southeast Asia. *Front. Public Health* 10:1008878. doi: 10.3389/fpubh.2022.1008878

Murre, C., McCaw, P. S., and Baltimore, D. (1989). A new DNA binding and dimerization motif in immunoglobulin enhancer binding, daughterless, MyoD, and myc proteins. *Cell* 56, 777–783. doi: 10.1016/0092-8674(89)90682-X

Natividad, J. M., Agus, A., Planchais, J., Lamas, B., Jarry, A. C., Martin, R., et al. (2018). Impaired aryl hydrocarbon receptor ligand production by the gut microbiota is a key factor in metabolic syndrome. *Cell Metab.* 28, 737–749.e4. doi: 10.1016/j.cmet.2018.07.001

Neuschäfer-Rube, F., Schraplau, A., Schewe, B., Lieske, S., Krützfeldt, J. M., Ringel, S., et al. (2015). Arylhydrocarbon receptor-dependent mIndy (Slc13a5) induction as possible contributor to benzo[a]pyrene-induced lipid accumulation in hepatocytes. *Toxicology* 337, 1–9. doi: 10.1016/j.tox.2015.08.007

Niwa, T., Murayama, N., Imagawa, Y., and Yamazaki, H. (2015). Regioselective hydroxylation of steroid hormones by human cytochromes P450. *Drug Metab. Rev.* 47, 89–110. doi: 10.3109/03602532.2015.1011658

Ohashi, H., Nishioka, K., Nakajima, S., Kim, S., Suzuki, R., Aizaki, H., et al. (2018). The aryl hydrocarbon receptor-cytochrome P450 1A1 pathway controls lipid accumulation and enhances the permissiveness for hepatitis C virus assembly. *J. Biol. Chem.* 293, 19559–19571. doi: 10.1074/jbc.RA118.005033

Panda, S. K., Peng, V., Sudan, R., Ulezko Antonova, A., di Luccia, B., Ohara, T. E., et al. (2023). Repression of the aryl-hydrocarbon receptor prevents oxidative stress and ferroptosis of intestinal intraepithelial lymphocytes. *Immunity* 56, 797–812.e4. doi: 10.1016/j.immuni.2023.01.023

Pang, L. P., Li, Y., Zou, Q. Y., Zhou, C., Lei, W., Zheng, J., et al. (2017). ITE inhibits growth of human pulmonary artery endothelial cells. *Exp. Lung Res.* 43, 283–292. doi: 10.1080/01902148.2017.1367868

Park, J., Zhao, Y., Zhang, F., Zhang, S., Kwong, A. C., Zhang, Y., et al. (2023). IL-6/STAT3 axis dictates the PNPLA3-mediated susceptibility to non-alcoholic fatty liver disease. *J. Hepatol.* 78, 45–56. doi: 10.1016/j.jhep.2022.08.022

Patil, N. Y., Rus, I., Downing, E., Mandala, A., Friedman, J. E., and Joshi, A. D. (2022). Cinnabarinic acid provides Hepatoprotection against nonalcoholic fatty liver disease. *J. Pharmacol. Exp. Ther.* 383, 32–43. doi: 10.1124/jpet.122.001301

Piché, M. E., Tchernof, A., and Després, J. P. (2020). Obesity phenotypes, diabetes, and cardiovascular diseases. *Circ. Res.* 126, 1477–1500. doi: 10.1161/CIRCRESAHA.120.316101

Podechard, N., Le Ferrec, E., Rebillard, A., Fardel, O., and Lecureur, V. (2009). NPC1 repression contributes to lipid accumulation in human macrophages exposed to environmental aryl hydrocarbons. *Cardiovasc. Res.* 82, 361–370. doi: 10.1093/cvr/cvp007

Prieto, J., León, M., Ponsoda, X., Sendra, R., Bort, R., Ferrer-Lorente, R., et al. (2016). Early ERK1/2 activation promotes DRP1-dependent mitochondrial fission necessary for cell reprogramming. *Nat. Commun.* 7:11124. doi: 10.1038/ncomms11124

Qiao, P., Zhang, C., Yu, J., Shao, S., Zhang, J., Fang, H., et al. (2022). Quinolinic acid, a tryptophan metabolite of the skin microbiota, negatively regulates NLRP3 Inflammasome through AhR in psoriasis. *J. Invest. Dermatol.* 142, 2184–2193.e6. doi: 10.1016/j.jid.2022.01.010

Quintana, F. J., Basso, A. S., Iglesias, A. H., Korn, T., Farez, M. F., Bettelli, E., et al. (2008). Control of T(reg) and T(H)17 cell differentiation by the aryl hydrocarbon receptor. *Nature* 453, 65–71. doi: 10.1038/nature06880

Ramos, G. P., and Papadakis, K. A. (2019). Mechanisms of disease: inflammatory bowel diseases. *Mayo Clin. Proc.* 94, 155–165. doi: 10.1016/j.mayocp.2018.09.013

Rannug, A., and Fritsche, E. (2006). The aryl hydrocarbon receptor and light. *Biol. Chem.* 387, 1149–1157. doi: 10.1515/BC.2006.143

Rouse, M., Singh, N. P., Nagarkatti, P. S., and Nagarkatti, M. (2013). Indoles mitigate the development of experimental autoimmune encephalomyelitis by induction of reciprocal differentiation of regulatory T cells and Th17 cells. *Br. J. Pharmacol.* 169, 1305–1321. doi: 10.1111/bph.12205

Schuster, S., Cabrera, D., Arrese, M., and Feldstein, A. E. (2018). Triggering and resolution of inflammation in NASH. *Nat. Rev. Gastroenterol. Hepatol.* 15, 349–364. doi: 10.1038/s41575-018-0009-6

Shahin, N. N., Abd-Elwahab, G. T., Tawfiq, A. A., and Abdelgawad, H. M. (2020). Potential role of aryl hydrocarbon receptor signaling in childhood obesity. *Biochim. Biophys. Acta Mol. Cell Biol. Lipids* 1865:158714. doi: 10.1016/j.bbalip.2020.158714

Shen, Q., Chen, Y., Shi, J., Pei, C., Chen, S., Huang, S., et al. (2023). Asperuloside alleviates lipid accumulation and inflammation in HFD-induced NAFLD via AMPK signaling pathway and NLRP3 inflammasome. *Eur. J. Pharmacol.* 942:175504. doi: 10.1016/j.ejphar.2023.175504

Shen, X., Gao, X., Luo, Y., Xu, Q., Fan, Y., Hong, S., et al. (2023). Cxxc finger protein 1 maintains homeostasis and function of intestinal group 3 innate lymphoid cells with aging. *Nat. Aging* 3, 965–981. doi: 10.1038/s43587-023-00453-7

Shen, J., Yang, L., You, K., Chen, T., Su, Z., Cui, Z., et al. (2022). Indole-3-acetic acid alters intestinal microbiota and alleviates ankylosing spondylitis in mice. *Front. Immunol.* 13:762580. doi: 10.3389/fimmu.2022.762580

Shi, Y., Su, W., Zhang, L., Shi, C., Zhou, J., Wang, P., et al. (2021). TGR5 regulates macrophage inflammation in nonalcoholic Steatohepatitis by modulating NLRP3 Inflammasome activation. *Front. Immunol.* 11:609060. doi: 10.3389/fimmu.2020.609060

Stockinger, B., Di Meglio, P., Gialitakis, M., and Duarte, J. H. (2014). The aryl hydrocarbon receptor: multitasking in the immune system. *Annu. Rev. Immunol.* 32, 403–432. doi: 10.1146/annurev-immunol-032713-120245

Sun, L., Liu, W., and Zhang, L. J. (2019). The role of toll-like receptors in skin host defense, psoriasis, and atopic dermatitis. *J Immunol Res* 2019, 1–13. doi: 10.1155/2019/1824624

Tian, Y., Ke, S., Denison, M. S., Rabson, A. B., and Gallo, M. A. (1999). Ah receptor and NF-kappaB interactions, a potential mechanism for dioxin toxicity. *J. Biol. Chem.* 274, 510–515. doi: 10.1074/jbc.274.1.510

Trikha, P., and Lee, D. A. (2020). The role of AhR in transcriptional regulation of immune cell development and function. *Biochim. Biophys. Acta Rev. Cancer* 1873:188335. doi: 10.1016/j.bbcan.2019.188335

Twig, G., Zucker, I., Afek, A., Cukierman-Yaffe, T., Bendor, C. D., Derazne, E., et al. (2020). Adolescent obesity and early-onset type 2 diabetes. *Diabetes Care* 43, 1487–1495. doi: 10.2337/dc19-1988

Wada, T., Sunaga, H., Miyata, K., Shirasaki, H., Uchiyama, Y., and Shimba, S. (2016). Aryl hydrocarbon receptor plays protective roles against high fat diet (HFD)-induced hepatic steatosis and the subsequent lipotoxicity via direct transcriptional regulation of Socs3 gene expression. *J. Biol. Chem.* 291, 7004–7016. doi: 10.1074/jbc.M115.693655

Wang, W. L., Kasamatsu, J., Joshita, S., Gilfillan, S., di Luccia, B., Panda, S. K., et al. (2022). The aryl hydrocarbon receptor instructs the immunomodulatory profile of a subset of Clec4a4+ eosinophils unique to the small intestine. *Proc. Natl. Acad. Sci. USA* 119:e2204557119. doi: 10.1073/pnas.2204557119

Wang, K., Lv, Q., Miao, Y. M., Qiao, S. M., Dai, Y., and Wei, Z. F. (2018). Cardamonin, a natural flavone, alleviates inflammatory bowel disease by the inhibition of NLRP3 inflammasome activation via an AhR/Nrf2/NQO1 pathway. *Biochem. Pharmacol.* 155, 494–509. doi: 10.1016/j.bcp.2018.07.039

Wang, X., Ota, N., Manzanillo, P., Kates, L., Zavala-Solorio, J., Eidenschenk, C., et al. (2014). Interleukin-22 alleviates metabolic disorders and restores mucosal immunity in diabetes. *Nature* 514, 237–241. doi: 10.1038/nature13564

Wang, Y., Sadike, D., Huang, B., Li, P., Wu, Q., Jiang, N., et al. (2023). Regulatory T cells alleviate myelin loss and cognitive dysfunction by regulating neuroinflammation and microglial pyroptosis via TLR4/MyD88/NF-κB pathway in LPC-induced demyelination. *J. Neuroinflammation* 20:41. doi: 10.1186/s12974-023-02721-0

Wang, B., Wang, Y., Zhang, J., Hu, C., Jiang, J., Li, Y., et al. (2023). ROS-induced lipid peroxidation modulates cell death outcome: mechanisms behind apoptosis, autophagy, and ferroptosis. *Arch. Toxicol.* 97, 1439–1451. doi: 10.1007/s00204-023-03476-6

Wang, Q., Wang, F., Zhou, Y., Li, X., Xu, S., Jin, Q., et al. (2024). *Bacillus amyloliquefaciens* SC06 relieving intestinal inflammation by modulating intestinal stem cells proliferation and differentiation via AhR/STAT3 pathway in LPS-challenged piglets. *J. Agric. Food Chem.* 72, 6096–6109. doi: 10.1021/acs.jafc.3c05956

Wang, C., Xu, C. X., Krager, S. L., Bottum, K. M., Liao, D. F., and Tischkau, S. A. (2011). Aryl hydrocarbon receptor deficiency enhances insulin sensitivity and reduces PPAR-α pathway activity in mice. *Environ. Health Perspect.* 119, 1739–1744. doi: 10.1289/ehp.1103593

Wei, Y. D., Bergander, L., Rannug, U., and Rannug, A. (2000). Regulation of CYP1A1 transcription via the metabolism of the tryptophan-derived 6-formylindolo [3,2-b] carbazole. *Arch. Biochem. Biophys.* 383, 99–107. doi: 10.1006/abbi.2000.2037

Xia, H., Zhu, X., Zhang, X., Jiang, H., Li, B., Wang, Z., et al. (2019). Alpha-naphthoflavone attenuates non-alcoholic fatty liver disease in oleic acid-treated HepG2 hepatocytes and in high fat diet-fed mice. *Biomed. Pharmacother.* 118:109287. doi: 10.1016/j.biopha.2019.109287

Xu, X., Sun, S., Liang, L., Lou, C., He, Q., Ran, M., et al. (2021). Role of the aryl hydrocarbon receptor and gut microbiota-derived metabolites Indole-3-acetic acid in Sulforaphane alleviates hepatic steatosis in mice. *Front. Nutr.* 8:756565. doi: 10.3389/fnut.2021.756565

Xu, C. X., Wang, C., Zhang, Z. M., Jaeger, C. D., Krager, S. L., Bottum, K. M., et al. (2015). Aryl hydrocarbon receptor deficiency protects mice from diet-induced adiposity and metabolic disorders through increased energy expenditure. *Int. J. Obes.* 39, 1300–1309. doi: 10.1038/ijo.2015.63

Yang, F., Li, J., Deng, H., Wang, Y., Lei, C., Wang, Q., et al. (2019). GSTZ1-1 deficiency activates NRF2/IGF1R Axis in HCC via accumulation of Oncometabolite Succinylacetone. *EMBO J.* 38:e101964. doi: 10.15252/embj.2019101964

Yang, W., Yu, T., Huang, X., Bilotta, A. J., Xu, L., Lu, Y., et al. (2020). Intestinal microbiota-derived short-chain fatty acids regulation of immune cell IL-22 production and gut immunity. *Nat. Commun.* 11:4457. doi: 10.1038/s41467-020-18262-6

Yao, L., Wang, C., Zhang, X., Peng, L., Liu, W., Zhang, X., et al. (2016). Hyperhomocysteinemia activates the aryl hydrocarbon receptor/CD36 pathway to promote hepatic steatosis in mice. *Hepatology* 64, 92–105. doi: 10.1002/hep.28518

Zelante, T., Iannitti, R. G., Cunha, C., de Luca, A., Giovannini, G., Pieraccini, G., et al. (2013). Tryptophan catabolites from microbiota engage aryl hydrocarbon receptor and balance mucosal reactivity via interleukin-22. *Immunity* 39, 372–385. doi: 10.1016/j.immuni.2013.08.003

Zhang, L., Cheng, D., Zhang, J., Tang, H., Li, F., Peng, Y., et al. (2023). Role of macrophage AhR/TLR4/STAT3 signaling axis in the colitis induced by non-canonical AhR ligand aflatoxin B1. *J. Hazard. Mater.* 452:131262. doi: 10.1016/j.jhazmat.2023.131262

Zhang, J., Deng, Z., Jin, L., Yang, C., Liu, J., Song, H., et al. (2017). Spleen-derived anti-inflammatory cytokine IL-10 stimulated by adipose tissue-derived stem cells protects against type 2 diabetes. *Stem Cells Dev.* 26, 1749–1758. doi: 10.1089/scd.2017.0119

Zhao, W., Guo, M., Feng, J., Gu, Z., Zhao, J., Zhang, H., et al. (2022). *Myristica fragrans* extract regulates gut microbes and metabolites to attenuate hepatic inflammation and lipid metabolism disorders via the AhR-FAS and NF-κB signaling pathways in mice with non-alcoholic fatty liver disease. *Nutrients* 14:1699. doi: 10.3390/nu14091699

Zhao, Y., Zhou, Y., Wang, D., Huang, Z., Xiao, X., Zheng, Q., et al. (2023). Mitochondrial dysfunction in metabolic dysfunction fatty liver disease (MAFLD). *Int. J. Mol. Sci.* 24:17514. doi: 10.3390/ijms242417514

Zhou, J., Zhou, F., Wang, W., Zhang, X. J., Ji, Y. X., Zhang, P., et al. (2020). Epidemiological features of NAFLD from 1999 to 2018 in China. *Hepatology* 71, 1851–1864. doi: 10.1002/hep.31150

Zhu, J., Luo, L., Tian, L., Yin, S., Ma, X., Cheng, S., et al. (2018). Aryl hydrocarbon receptor promotes IL-10 expression in inflammatory macrophages through Src-STAT3 signaling pathway. *Front. Immunol.* 9:2033. doi: 10.3389/fimmu.2018.02033

Zhu, Q., Ma, Y., and Liang, J. (2021). AhR mediates the aflatoxin B1 toxicity associated with hepatocellular carcinoma. *Signal Transduct. Target. Ther.* 6:432. doi: 10.1038/s41392-021-00713-1

Zhu, X. Y., Xia, H. G., Wang, Z. H., Li, B., Jiang, H. Y., Li, D. L., et al. (2020). In vitro and in vivo approaches for identifying the role of aryl hydrocarbon receptor in the development of nonalcoholic fatty liver disease. *Toxicol. Lett.* 319, 85–94. doi: 10.1016/j.toxlet.2019.10.010

Zindl, C. L., Witte, S. J., Laufer, V. A., Gao, M., Yue, Z., Janowski, K. M., et al. (2022). A nonredundant role for T cell-derived interleukin 22 in antibacterial defense of colonic crypts. *Immunity* 55, 494–511.e11. doi: 10.1016/j.immuni.2022.02.003

frontiers | Frontiers in Microbiology

TYPE Original Research
PUBLISHED 01 April 2025
DOI 10.3389/fmicb.2025.1494994

OPEN ACCESS

EDITED BY
Jie Yin,
Hunan Agricultural University, China

REVIEWED BY
Cihua Zheng,
The Second Affiliated Hospital of Nanchang University, China
Ana Paula De Souza,
State University of Campinas, Brazil

*CORRESPONDENCE
Ana Flávia Marçal Pessoa
anabiorq@usp.br

RECEIVED 24 September 2024
ACCEPTED 28 February 2025
PUBLISHED 01 April 2025

CITATION
Freitas JA, Nehmi Filho V, Santamarina AB, Murata GM, Franco LAM, Fonseca JV, Martins RC, Souza GA, Benicio G, Sabbag IM, de Souza EA, Otoch JP and Pessoa AFM (2025) Nutraceutical supplement slim reshaped colon histomorphology and reduces *Mucispirillum schaedleri* in obese mice.
Front. Microbiol. 16:1494994.
doi: 10.3389/fmicb.2025.1494994

Nutraceutical supplement slim reshaped colon histomorphology and reduces *Mucispirillum schaedleri* in obese mice

Jessica Alves Freitas[1,2], Victor Nehmi Filho[1,2], Aline Boveto Santamarina[1,2], Gilson Masahiro Murata[3], Lucas Augusto Moyses Franco[4], Joyce Vanessa Fonseca[5], Roberta Cristina Martins[4], Gabriele Alves Souza[6], Gabriela Benicio[6], Isabella Mirandez Sabbag[6], Esther Alves de Souza[1,2], José Pinhata Otoch[1,2,7] and Ana Flávia Marçal Pessoa[1,4,8]*

[1]Laboratório de Produtos e Derivados Naturais, Laboratório de Investigação Médica-26 (LIM-26), Departamento de Cirurgia, Faculdade de Medicina da Universidade de São Paulo, São Paulo, SP, Brazil, [2]Pesquisa e Desenvolvimento Efeom Nutrição S/A, São Paulo, SP, Brazil, [3]Universidade de São Paulo Faculdade de Medicina da Universidade de São Paulo, Departamento de Clínica Médica, Laboratório de Nefrologia (LIM-29), São Paulo, SP, Brazil, [4]Universidade de São Paulo Instituto de Medicina Tropical de São Paulo, Departamento de Doenças Infecciosas e Parasitárias, Laboratório de Parasitologia Médica (LIM-46), São Paulo, SP, Brazil, [5]Universidade de São Paulo Instituto de Medicina Tropical de São Paulo, Departamento de Doenças Infecciosas e Parasitárias, Laboratório de Investigação Médica em Protozoologia, Bacteriologia e Resistência Antimicrobiana (LIM-49), São Paulo, SP, Brazil, [6]Universidade de São Paulo Faculdade de Medicina da Universidade de São Paulo, Departamento de Patologia, Laboratório de Neurociência (LIM-01), São Paulo, SP, Brazil, [7]Hospital Universitário da Universidade de São Paulo, Faculdade de Medicina da Universidade de São Paulo, São Paulo, SP, Brazil, [8]Instituto Botânio, São Paulo, Brazil

Introduction: Bioactive compounds and whole foods have emerged as promising interventions to address gut microbiota dysbiosis linked to obesity. Compounds such as berberine and coenzyme Q10 are well-recognized for their roles in managing metabolic syndrome and exerting antioxidant effects, while beet pulp, rich in fiber and antioxidants, enhances gut health through additional prebiotic benefits.

Methods: This study evaluated the effects of a nutraceutical supplement, Slim, on the modulation of gut microbiota in obese mice induced by a high-fat diet.

Results: Our results demonstrated that Slim supplementation significantly improved lipid metabolism, reshaped colon histomorphology, and decreased levels of *Mucispirillum schaedleri*, which were correlated with VLDL-c and triglycerides.

Discussion: We suggest these effects are driven by a duplibiotic effect, resulting from the synergistic action of the bioactive compounds.

KEYWORDS

nutraceutical, prebiotic, beet pulp, coenzyme q10, berberine, obesity, gut microbiota

1 Introduction

Supplements derived from natural compounds with therapeutic potential have garnered attention for their beneficial effects on various health conditions (Rahman et al., 2021; Guan et al., 2024). Obesity and overweight represent global public health challenges, being major risk factors for the development of metabolic syndrome, which includes disorders such as insulin resistance,

high blood pressure, dyslipidemia, chronic low-grade inflammation, and the gastrointestinal tract histomorphology (Grundy, 2004; Kern et al., 2018; Leocádio et al., 2020; Freitas et al., 2024). Gut health, mediated by the integrity of the intestinal function and the balance of the microbiota, plays a crucial role in the regulation of immune system and energy metabolism, being essential for the maintenance of homeostasis in overweight or obese individuals (Abenavoli et al., 2019; Miron, 2019). The colon contains crucial structures that play an essential role in fostering a harmonious relationship between microbiota and its host. Lieberkühn crypts supporting cell regeneration and the secretion of enzymes, guarantee the functionality of the intestinal mucosa, crucial for the defense against pathogens (Ma et al., 2018). In parallel, Peyer's patches monitor antigens and regulate the local immune response, preventing chronic inflammation that is commonly associated with obesity, thus promoting a balanced and healthy intestinal environment (Jung et al., 2010; Leocádio et al., 2020).

Gut microbiota has been widely studied due to its influence on host metabolism, particularly in obesity and overweight conditions (Esposito et al., 2003; Nehmi-Filho et al., 2023a). In obese individuals, the microbial composition is often altered, with a decrease in bacterial diversity and a predominance of microbial groups associated fat accumulation (John and Mullin, 2016; Saad et al., 2016). This can lead to increased intestinal permeability, favoring the translocation of bacterial endotoxins, such as lipopolysaccharide, which contribute to metabolic syndrome rises (Festi et al., 2014; Wang et al., 2024).

Bioactive compounds like FOS (Fructooligosaccharides), GOS (Galactooligosaccharides), yeast *β*-glucans, and silymarin in their formulation stand out, widely studied and recognized for their innumerous benefits from the gut microbiota and good consumers acceptance (Nehmi et al., 2021; Santamarina et al., 2022). Diversifying new nutrients and bioactive compounds is essential to maintaining and promoting biodiversity in the intestinal microbiota and thus preventing or improving diseases and symptoms related to obesity. Berberine (*Phellodendron amurense* Rupr., Rutaceae) stands out for its anti-inflammatory, hypoglycemic, and intestinal microbiota modulation properties, being especially useful in controlling type 2 diabetes and obesity (Habtemariam, 2020; Zhang et al., 2021). Coenzyme Q10 is an endogenous antioxidant compound with the role and its ability to improve mitochondrial function, contributing to the reduction of oxidative stress (Neergheen et al., 2017; Sifuentes-Franco et al., 2022). Beet or beetroot (*Beta vulgaris* L., Amaranthaceae) pulp is rich in insoluble fiber and bioactive compounds, such as nitrates, which can to improve intestinal health (Usmani et al., 2022; Adekolurejo et al., 2023). Combining these elements may result in a synergistic effect that helps prevent the emergence of metabolic diseases and alterations in the morphology and microbiota of the colon. This study aimed to evaluate the effects after 4 weeks of Slim supplementation on intestinal health and metabolic parameters, focusing on colon histomorphology and microbiota composition in obese mice induced by a high-fat diet.

2 Materials and methods

2.1 Supplement composition

The following elements constitute the supplement formulation (Patent: BR1020200161563) developed and tested in the present study: selenium (Se) 1.5%; FOS (Fructooligosaccharides) 30.10%; GOS (Galactooligosaccharides) 12.00% and 1,3/1,6- (β-glycosidic linkages) β-glucans from yeast (*Saccharomyces. cerevisiae*) 18% (Biorigin, Lençois Paulista, São Paulo, Brazil); chromium (Cr) 0.7%; beet pulp (*Beta vulgaris* L.) powder 30.10%; coenzyme Q10 1.5% and berberine (*Phellodendron amurense* Rupr.) extract 6.00%. Dietary reference values for the minerals described in this study were determined following guidance previously provided by the European Food Safety Authority (European Food Safety Authority, 2017). FOS (Sabater-Molina et al., 2009), GOS (Torres et al., 2010), yeast β-glucans (José Pereira, 2015; Andrade et al., 2016), beet pulp (ANVISA, 2018), coenzyme Q10 (Overvad et al., 1999; ANVISA, 2018) and berberine (Zamani et al., 2022) were determined based on previous studies considering the animal's body area, determined by the equation: human equivalent dose (mg/kg) = animal does (mg/kg) × 12.33 (Jacob et al., 2022). Filtered mineral water in 2% carboxymethyl cellulose solution was used as an emulsifier for the formula components.

2.2 Ethics committee approval

This study was approved by the Research Ethics Committee of the University of São Paulo, São Paulo, Brazil, under approval numbers 1185/2018 and 1519/2020. All experiments were conducted in accordance with the guidelines of the National Institutes of Health.

2.3 Animal model and oral supplementation

Eight-week-old male C57BL/6 N mice were kept in an air-conditioned room at (24 ± 2) °C and subjected to a 12-h light/12-h dark cycle. These mice were subsequently separated into two groups: control and obese. The control group was fed an AIN-93 non-fat diet (NFD) of 4.1 kcal/g and was composed of 9% fat, 67% carbohydrate, and 15% protein. The High-Fat Group (HFD) consumed an AIN-93-based high-fat and high-sugar diet that contained 6.1 kcal/g and was composed of 25% fat, 49% carbohydrate, and 20% protein (Reeves et al., 1993; Prag Soluções *Biosciences*, Jaú, São Paulo, Brazil). Mice were fed these diets for 14 weeks and received chow and water *ad libitum*. In the 10th week, mice were divided into the following groups: NFD vehicle (n = 8), HFD vehicle (n = 7), and HFD_Slim supplemented (n = 8). NFD vehicle and HFD vehicle groups received 2% carboxymethyl cellulose (Vehicle) in mineral water. While HFD_Slim group received full supplementation. The groups were supplemented with 300 µL of the vehicle (NFD and HFD) and supplemented (HFD_Slim) diarily by gavage for 4 weeks (28 consecutive days). After 4 weeks of supplementation, mice were euthanized with an intraperitoneal injection of ketamine (100 mg/kg body weight) and xylazine (5 mg/kg body weight) (Figure 1).

2.4 Food intake, body mass, intraperitoneal glucose tolerance test (ipGTT), biochemistry parameters and cytokines

The food intake was measured during the 4 weeks supplementation. The groups body mass was measured weekly

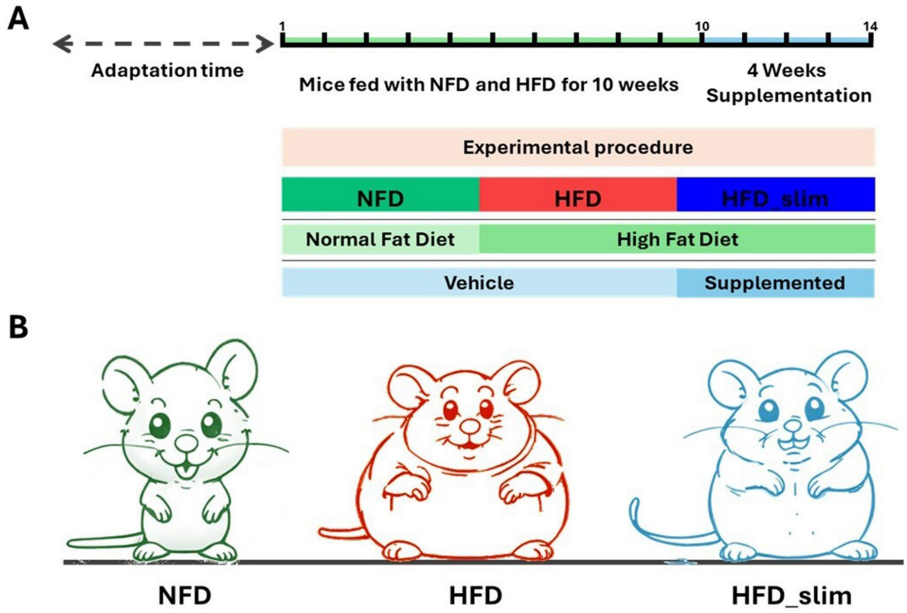

FIGURE 1
Schematic sketch of the experimental procedure and supplementation time. **(A)** Experimental schedule. **(B)** Experimental groups: NFD, Non-Fat Diet; HFD, High Fat Diet; HFD_Slim, High Fat Diet Slim.

throughout the 14-week experimental period. We realizing the ipGTT, in the third week of supplementation after 6-h fasting period. Subsequently, each mouse received an intraperitoneal injection of a 10% glucose solution at a dose of 1.0 g/kg of body weight. Blood samples were then collected from the tail at time points 0, 30, 60, and 90 min, and blood glucose levels were measured using an Accu-Chek Active glucometer (Roche, Mannheim, Germany). Blood sample was collected during the euthanasia to serum analysis of cholesterol, triglycerides, aspartate aminotransferase (AST), alanine aminotransferase (ALT), gamma-glutamyl transferase (gamma-GT) and urea in the plasma were measured with a commercially available kit (Bioclin, Belo Horizonte, MG, Brazil). The low-density lipoprotein cholesterol (LDL-c) and very-low-density lipoprotein cholesterol (VLDL-c) levels were calculated according to Friedewald et al. (1972). The cytokines Interleucin-6 (IL-6) and Interleucin-10 (IL-10) levels in the colon of the mice were determined by enzyme-linked immunosorbent assays (ELISAs) according to the manufacturer's instructions (R&D Systems, Inc., Shanghai, China).

2.5 Staining and histological analysis

The colon was removed, fixed in 4% formaldehyde for 24 h at room temperature, and processed as described by Pessoa et al. (2016). The 3-μm-thick sections of the colon were placed on glass slides and stained with Hematoxylin and Eosin (H&E) for histomorphology analysis. The slides were scanned using the Panoramic Scan scanner (3DHistech, Budapest, Hungary) analyzed using Slide Viewer software (3DHistech, Budapest, Hungary), and photographed at 200X and 400X magnifications.

2.6 Gut microbiota analysis

2.6.1 Stool specimen collection and extraction

Stool samples were collected from the intestinal mucosa and stored in sterile tubes at −80°C until DNA extraction. Genetic material was acquired by DNA extraction. Approximately 250 mg of stool was sampled using the DNeasy PowerSoil kit (Qiagen, Hilden, Germany) following the manufacturer's recommendations. The extracted DNA was stored at −20°C until sequencing library preparation.

2.6.2 Sequencing library preparation

The fecal microbial component of mice was assessed based on partial 16S rDNA and 16S rRNA (V4 region) sequences amplified using a bacterial primer set 515F/806R for each DNA sample (Caporaso et al., 2011). DNA was quantified on the Qubit® 4.0 equipment using the dsDNA HS Assay kit (Thermo Fisher Scientific, Waltham, Massachusetts, USA). Microbiota characterization was performed by amplification of the bacterial 16S ribosomal V4 region. Using the Q5 High-Fidelity 2x Master Mix kit (New W England Biolabs, Ipswich, Massachusetts, USA), the primer sequences F515 (5′-CACGGTCGKCGGCGCCATT-3′), R806 (5′-GGACTACHVGGG TWTCTAAT-3′) and 50 ng of DNA, the bacterial DNA from the mice microbiota were amplified (Caporaso et al., 2011). Samples were purified with AMPure XP (Beckman Coulter, Brea, California, USA) and washed repeatedly with 70% ethanol. The success of the reaction was determined by the appearance of a positive band of 350 bp amplified on a 1.25% agarose gel. Library was quantified and created after measuring the concentration, using the Qubit® 4.0 equipment and the dsDNA HS Assay kit. The model was performed by the Ion Chef System (Thermo Fisher Scientific, Waltham, Massachusetts, USA),

using the Ion 510™ & Ion 520™ & Ion 530™ Chef kit and library pool at 48pM. Sequencing was performed by an Ion S5 system, using the Ion S5 Sequencing kit and the Ion 520 Chip, according to the manufacturer's instructions (Thermo Fisher Scientific, Waltham, Massachusetts, USA).

2.6.3 16S rRNA gene data analysis

16S rRNA gene data, as well as diversity estimates, were processed and analyzed with Quantitative Insights Into Microbial Ecology (QIIME 2) software, version 2020.11 (Bolyen et al., 2019). Demultiplexed sequence data were filtered with DADA2 (using the q2-dada2 plugin) applying the default parameters: 200 bp length and an average Phred quality score ≥ 30, to generate amplicon sequence variants (ASVs) (Callahan et al., 2016). The phylogenetic tree was constructed by inserting the sequences into the Greengenes 13_8 reference tree, using the q2-fragment-insertion plugin, which employs the phylogenetic positioning insertion method enabled by SATé (SEPP) (Mirarab et al., 2011; Janssen et al., 2018). Alpha diversity metrics (Pielou evenness, Shannon, Simpson, and Chao1 indices, and Faith's phylogenetic diversity) and beta diversity metrics (Jaccard distance, Bray–Curtis dissimilarity, Weighted_unifrac, and Unweighted_unifrac) were calculated using Q2-diversity after samples were rarefied to 27.745 sequences per sample (Faith, 1992). Principal Coordinate Analysis (PCoA) plot for each beta diversity metric was created using EM-peror (Vázquez-Baeza et al., 2013). ASVs were taxonomically assigned using the Q2 feature classifier (Bokulich et al., 2018) naive Bayesian classifier was applied against Greengenes 13_8 reference sequences with 99% OTUs (Operational Taxonomic Units) (Mandal et al., 2015).

2.7 Statistical analysis

Data were classified as parametric or nonparametric based on the Shapiro-Wilks test. When parametric, data were expressed as mean ± standard deviation (SD), when nonparametric, data were classified as median and interquartile range. For parametric data, comparisons were performed using the t-test with or without Welch's correction. The Mann–Whitney test was applied when data were nonparametric. The NFD and HFD_Slim groups were compared with the HFD group. Comparisons between groups were performed using two-way analysis of variance (two-way ANOVA). Pearson correlation coefficients were calculated for the correlation between microbiota parameters and intestinal mucosa morphological structures. R^2 values greater than 0.7 and less than −0.7 were considered strong correlations. The composition of the microbiological organization of the intestinal mucosa was briefly inferred through different levels of taxonomy, of which we can mention: phylum, genus, and species. For α-diversity, the correction of all p-values was performed by the Benjamini-Hochberg procedure. We compared groups (β-diversity) by permutation-based multivariate analysis of variance (PERMANOVA) using Bray–Curtis dissimilarity, Weighted_unifrac, Unweighted, and Jaccard and tested the homogeneity of variations between the composition of microbiota communities by PERMDISP (Permutational Analysis of Multivariate Dispersions). For all analyses, significance was determined as $p < 0.05$. Analyses were performed using STATA® 14.0 (Stata Corp. LCC, College Station, TX, USA) and GraphPad Prism 9.0 (GraphPad Software, La Jolla, CA, USA) software.

3 Results

3.1 Slim nutraceutical effects on body mass, biochemistry parameters, and colon cytokine analysis after 4 weeks of supplementation

We observed a significant difference in body weight gain between the Normal Fat Diet (NFD) and High Fat Diet (HFD) groups during the 14 weeks of the experimental protocol (Supplementary Figures S1A,B). However, when we compared the groups at baseline (T0—week 10) and at the end of the supplementation period (T4—week 14), we did not find any differences (Table 1). While we present statistical differences in the data, we do not attribute the weight loss to the supplementation. This is because by the eighth week of the high-fat diet—before the supplementation began—statistical differences in weight between the groups were already observed (see Supplementary Figures S1A,B). The ipGTT and fasting glucose analyses showed statistically significant differences between the NFD group and the HFD groups. There was no statistically significant difference when comparing the HFD group with the Slim HFD group (Supplementary Figure S2A).

The NFD group showed lower of cholesterol, HDL-cholesterol and LDL-cholesterol level when compared with the HFD and HFD_Slim. VLDL-cholesterol, triglycerides, AST, gamma-GT and urea levels did not differ between the NFD and HFD groups. We observed lower ALT level in NFD group when compared with HFD and HFD_Slim (Table 1).

We did not find significant differences between the HFD and HFD_Slim groups in the parameters of cholesterol, HDL-cholesterol, LDL-cholesterol, AST, ALT, gamma-GT and urea. We observed VLDL-cholesterol ($p = 0.050$) and triglycerides ($p > 0.001$) lower level in HFD_Slim group when compared with NFD and HFD ($p < 0.05$; $p > 0.001$, respectively) groups (Table 1).

We evaluated the levels of the colon cytokines IL-6 and IL-10 and calculated the IL-6/IL-10 ratio in the colon of the different groups after 4 weeks of supplementation. The levels of the IL-6 cytokine did not differ significantly between the groups. However, the IL-10 cytokine levels were significantly higher in the NFD group compared to the HFD and HFD_Slim groups. Additionally, the IL-6/IL-10 ratio was elevated in the HFD and HFD_Slim groups compared to the NFD group (see Supplementary Figures S2D–F).

3.2 Slim nutraceutical reshaped colon histomorphology in obese mice after 4 weeks of supplementation

The colon histomorphology was evaluated by the external muscular layer (Supplementary Figure S3A) and the mucosal layer (Supplementary Figure S3B) which did not differ between the groups. Morphohistology of the large intestine (colon) was characterized using hematoxylin and eosin (H&E) staining to evaluate morphology, the number of goblet cells, Lieberkühn crypts, and the Auerbach plexus, as shown in Figure 2A. Remarkably, Goblet cells (Figure 2B) and Lieberkühn crypts (Figure 2C) number per linear millimeter was higher in HFD_Slim mice when compared to HFD animals, $p < 0.05$ and $p < 0.01$, respectively. The ratio between the number of Goblet cells and Lieberkühn crypts (Figure 2D) did not present significant differences between the groups. We also evaluated the Auerbach plexuses, both in

TABLE 1 Presentation of body mass data and biochemical parameters of Control and High Fat Diet groups after 4 weeks of supplementation.

Body mass in gram (g)			
	Time of supplementation		
	Before (T0)[a]	After (T4)[b]	*p* value
NFD	29.33 ± 0.98	30.56 ± 1.72	–
HFD	40.66 ± 3.70	42.54 ± 3.39	–
HFD_Slim	35.67 ± 2.87	35.71 ± 3.30	–

Biochemical data						
Parameters	NFD	HFD	HFD_Slim	NFD vs. HFD	NFD vs. HFD_Slim	HFD vs. HFD_Slim
	Mean ± SD	Mean ± SD	Mean ± SD	*p* value	*p* value	*p* value
Cholesterol (mg/dL)	137.90 ± 33.52	210.90 ± 16.52	196.30 ± 26.10	<0.001	<0.001	–
HDL-c (mg/dL)	61.00 ± 12.66	88.88 ± 6.01	77.38 ± 10.89	<0.001	<0.05	–
LDL-c (mg/dL)	54.13 ± 21.75	99.00 ± 13.44	98.13 ± 20.37	<0.001	<0.001	–
VLDL-c (mg/dL)	22.63 ± 1.76	22.88 ± 1.12	20.88 ± 1.24	–	0.050	<0.05
Triglycerides (mg/dL)	114.50 ± 8.31	113.00 ± 3.10	104.00 ± 5.75	–	<0.01	<0.05
Aspartate Transaminase – AST (U/L)	12.38 ± 5.73	12.38 ± 4.56	12.63 ± 3.54	–	–	–
Alanine Transaminase – ALT (U/L)	1.71 ± 1.38	11.88 ± 5.91	11.00 ± 30.38	<0.001	<0.001	–
Gamma-GT (U/L)	1.50 ± 1.06	2.37 ± 1.50	1.25 ± 0.88	–	–	–
Urea (mg/dL)	42.13 ± 7.69	38.50 ± 6.90	33.25 ± 7.70	–	–	–

[a]T0 = weight in gram (g) at week 10 before supplementation.
[b]T4 = weight in gram (g) at week 14 after supplementation.

quantity, height, and width per linear mm. We did not observe significant differences in Auerbach plexuses quantity and height between the groups (Figure 2F). However, we observed that the Auerbach plexus width was significantly greater in the HFD_Slim group than in the HFD group ($p < 0.05$; Figure 2G). Scatter plot to show the Auerbach plexus can be seen in Figure 2H. Morphohistological analysis of Peyer's patches in the large intestine (colon) was also performed using H&E staining, as presented in Figure 3A. We evaluated the Peyer's patches in terms of quantity, height, and width per linear mm, as shown in Figures 3B–D. Interestingly, Peyer's patches were significantly larger in the HFD_Slim group in quantity, height, and width, when compared to the HFD group, with $p < 0.5$ in all parameters. Scatter plot to show the Peyer's patches can be seen in Figure 3E.

3.3 Slim nutraceutical recover correlations in gut microbiota after 4 weeks of supplementation

We evaluated the obese mice gut microbiota profile (phylum, genus, species, and α-diversity) Pearson correlation with plasma lipid profile and colon histomorphology (goblet cells and Lieberkühn crypts). We observed a significant positively correlation between the VLDL-c and triglycerides and the *Mucispirillum schaedleri*, since phylum (*Deferribacteres*) and Genus (*Mucispirillum*), and *AF12* genus was correlation with plasmatic VLDL-c with the HFD group. However, after 4 weeks of the Slim supplementation this correlation was not observed in Slim_HFD group, like in NFD group.

Lieberkühn crypts and Goblet cells in the NFD group shown statistical correlated positively concomitantly with the phylum *Proteobacteria* (phylum), the genera *Adlercreutzia, Parabacteroides, Leuconostoc, Anaerofustis, Robinsoniella, P. [Clostridium],* and *Sutterella* (genera), and *Leuconostoc mesenteroides, Streptococcus luteciae, Clostridium symbiosum* and *Robinsoniella peoriensis* (species), and negatively correlated with α-diversity chao1, observed_features, and faith_pd. In the HFD group, we observed a positive correlation between Lieberkühn crypts and Goblet cells and the *Parabacteroides* and *Bilophila* genera. Goblet cells were also positively correlated with *Leuconostoc*. Interestingly, we did not observe significance correlations in the HFD_Slim group (Figure 4A). Sankey diagram showed flow and connections between phylum, genus, and species relative abundance in the gut microbiota groups in the groups (Figure 4B). We can observed the efficiency of Slim supplementation increasing the abundance of species in HFD_Slim group when compared with the other groups (Figure 4B). Main observations in the HFD_Slim group was able to decrease the gut microbiota abundance of Cyanobacteria and Deferribacteres phyla, *Oscillospira*, P. *[Prevotella]*, *Alistipes*, *Bilophila*, *AF12*, *Coprococcus*, *Adlercreutzia*, *Dehalobacterium* and *Mucispirillum* genera; and *Alistipes finegoldii and Mucispirillum schaedleri* species. However, Slim HFD increased Proteobacteria phylum, *Parabacteroides, Sutterella*, *Anaerofustis*, *Robinsoniella*, P. *[Clostridium]*genera, and *Clostridium symbiosum* and *Robinsoniella peoriensis* species when compared to the HFD group (Figure 4B).

3.4 Slim nutraceutical modulates alpha and beta diversity in obese mice after 4 weeks of supplementation

We observed significant differences in alpha diversity indexes (α) between the HFD and HFD_Slim groups. Specifically, Chao1 ($p < 0.0001$), Observed_Features ($p < 0.0001$), Faith's phylogenetic diversity ($p < 0.0001$), and Shannon entropy ($p < 0.01$) were all notably

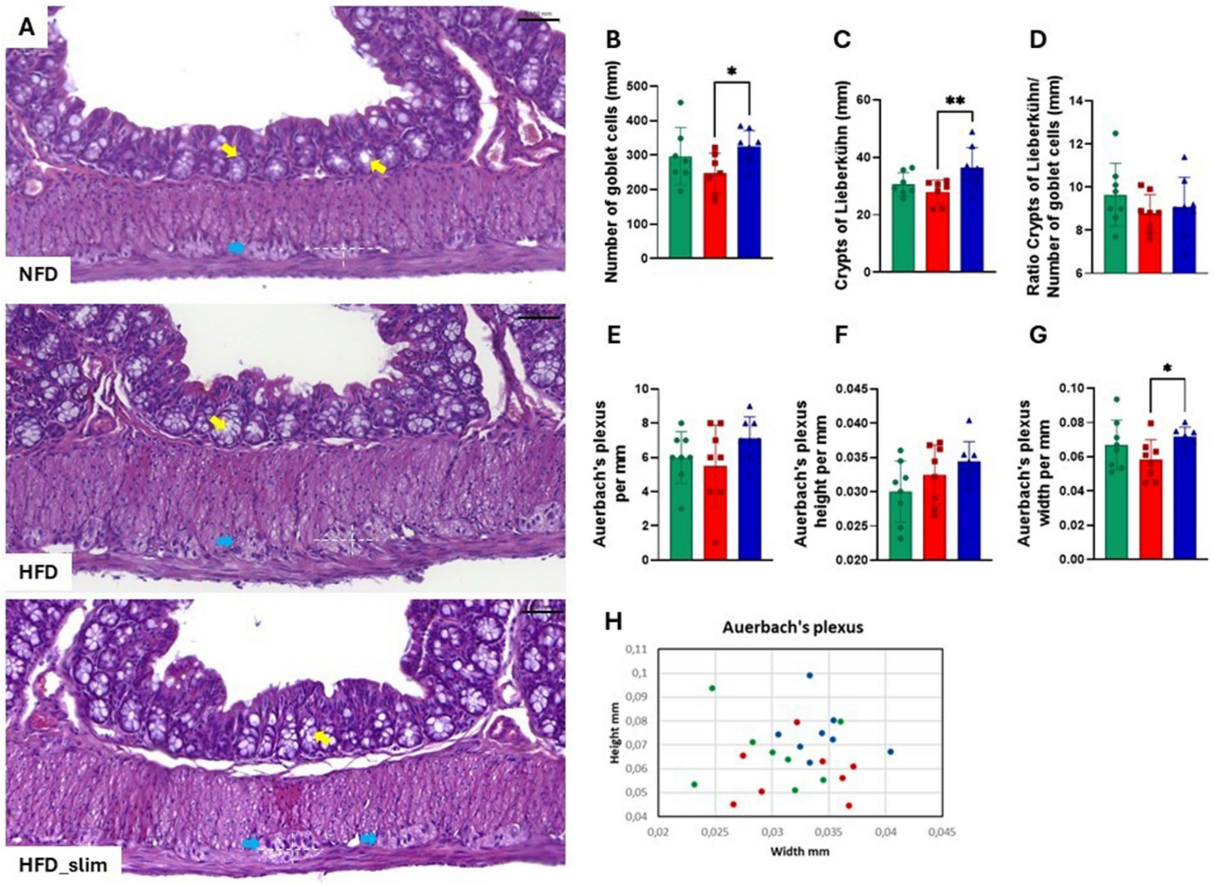

FIGURE 2
Assessment of histomorphological changes in the colon of control and high-fat diet groups after 4 weeks of supplementation. The H&E in stain shows **(A)** representative histological images of the colon. The graphics show **(B)** number of Goblet cells; **(C)** crypts of Lieberkühn; **(D)** ratio between the number of Goblet cells and crypts of Lieberkühn; **(E)** Auerbach plexus; **(F)** Auerbach plexus height **(G)** Auerbach plexus width **(H)** Scatter plot representing the Auerbach plexus. Scale bar = 0.050 mm, 200X magnifications. Statistical analyses were performed using the student's t-test or Kruskal-Wallis test. Data are represented as mean ± SD. n = 7–8 animals per group. Differences were calculated about the HFD group. *$p < 0.05$; **$p < 0.01$. NFD, Non-Fat Diet; HFD, High Fat Diet; HFD_Slim, High Fat Diet Slim; mm, millimeters. Goblet cells, yellow arrows; Auerbach plexus, blue arrows; Dashed white, Auerbach plexus area.

lower in the HFD_Slim group when compared with HFD. The analysis showed no differences between the groups regarding the Pielou Evenness and Simpson parameters (Figure 5A).

β diversity comparisons were evaluated using various methods: Bray–Curtis dissimilarity analysis, which considers abundances but not phylogenetic relationships; Unweighted UniFrac and Weighted UniFrac, which incorporate phylogenetic information; and the Jaccard index, which ignores exact abundances and focuses solely on presence/absence values. These analyses were visualized through Principal Coordinate Analysis (PCoA) plots, which indicated whether the samples clustered according to their bacterial composition (Figure 5B). Comparisons of β-diversity indicated significant differences in the composition of the mouse microbiota between the groups evaluated, as shown in Figure 5B. The differences that were found are established at the phylogenetic level. PERMANOVA indicated significant differences in β-diversity [Bray-curtis: HFD versus NFD $p < 0.046$ and HFD versus HFD_Slim ($p < 0.002$); Jaccard: HFD versus NFD $p < 0.001$ and HFD versus HFD_Slim ($p < 0.001$); Weighted_unifrac: HFD versus NFD $p < 0.272$ and HFD versus HFD_Slim ($p < 0.075$); Unweighted_unifrac: HFD versus NFD $p < 0.001$ and HFD versus HFD_Slim ($p < 0.001$) (Figure 5B)]. PERMDISP did not show significant differences in beta diversity [Bray-Curtis: HFD versus NFD $p < 0.915$ and HFD versus HFD_Slim ($p < 0.796$); Jaccard: HFD versus NFD $p < 0.811$ and HFD versus HFD_Slim ($p < 0.072$); Weighted_unifrac: HFD versus NFD $p < 0.519$ and HFD versus HFD_Slim ($p < 0.462$); Unweighted_unifrac: HFD versus NFD $p < 1.000$ and HFD versus HFD_Slim ($p < 0.732$) (Figure 5B)]. ANOSIM did not show significant differences in beta diversity [Bray-Curtis: HFD versus NFD $p < 0.046$ and HFD versus HFD_Slim ($p < 0.002$); Jaccard: HFD versus NFD $p < 0.001$ and HFD versus HFD_Slim ($p < 0.001$); Weighted_unifrac: HFD versus NFD $p < 0.208$ and HFD versus HFD_Slim ($p < 0.033$); Unweighted_unifrac: HFD versus NFD $p < 0.002$ and HFD versus HFD_Slim ($p < 0.001$) (Figure 5B)].

3.5 Slim nutraceutical influences gut microbiota in obese mice after 4 weeks of supplementation

Relative abundance of the gut microbiota phyla (Figure 6A). After 4 weeks of supplementation, we observed the abundance decrease

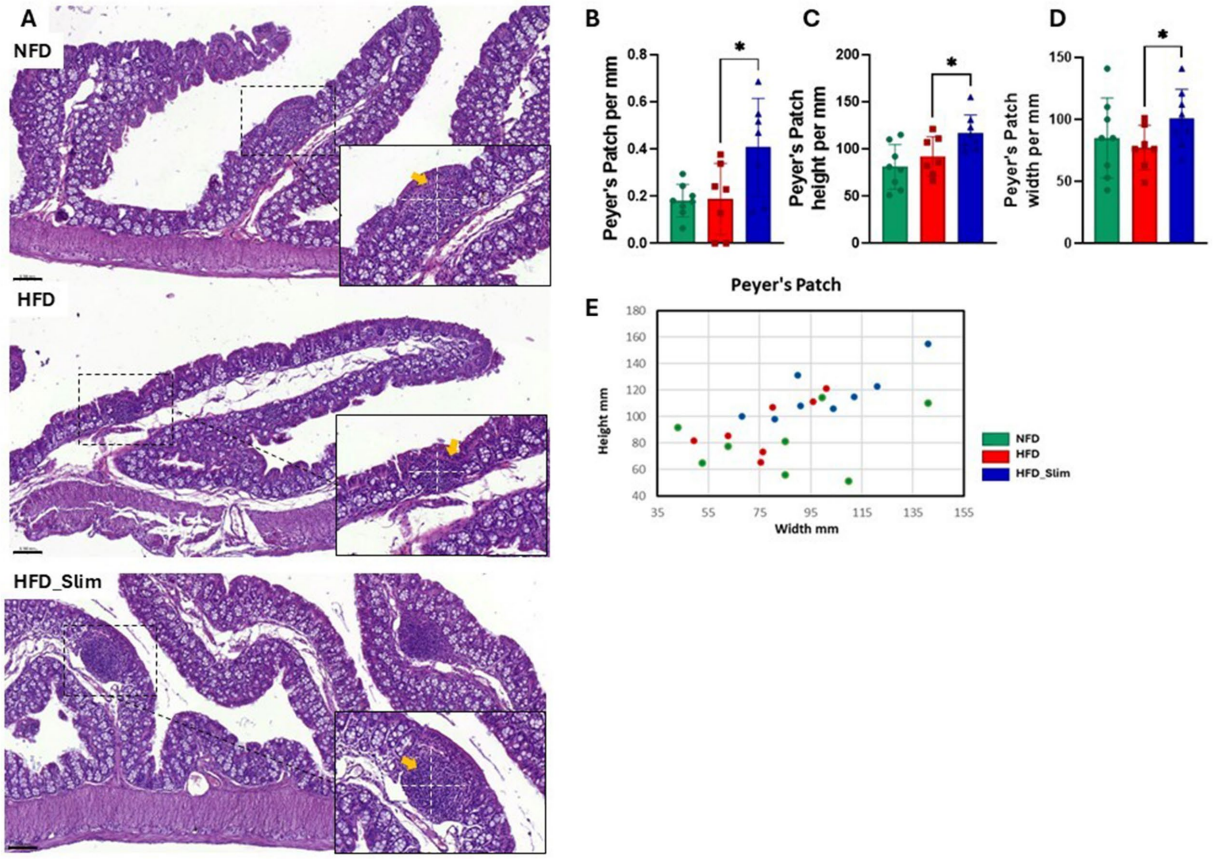

FIGURE 3
Peyer's patches histomorphometry in the colon of Control and High-Fat Diet groups after 4 weeks of supplementation. The H&E in stain shows **(A)** representative histological images of the colon. The graphics show **(B)** Peyer's patches; **(C)** Peyer's patches height; **(D)** Peyer's patches width; **(E)** Scatter plot representing Peyer's patches. Scale bar = 0.050 mm, 200X and 400X magnifications. Statistical analyses were performed using the student's t-test or Kruskal-Wallis test. Data are represented as mean ± SD. n = 7–8 animals per group. Differences were calculated about the HFD group. *$p < 0.05$; NFD, Non-Fat Diet; HFD, High Fat Diet; HFD_Slim, High Fat Diet Slim; Dashed white, Peyer's patches area.

Cyanobacteria ($p < 0.001$) and Deferribacteres ($p < 0.05$), and increased in the Proteobacteria ($p < 0.05$) in in the gut microbiota composition of the HFD_Slim when compared to the HFD group (Figure 6B). Tenericutes ($p < 0.05$) abundance was increase in NFD group when compared to the HFD group (Figure 6B).

Relative abundance of the gut microbiota genera (Figure 7A). We observed abundance decrease in *Oscillospira* ($p < 0.05$), *Lactobacillus* ($p < 0.05$), *Bilophila* ($p < 0.05$), *Desulfovibrio* ($p < 0.05$), R. *Ruminococcus* ($p < 0.05$), *Leuconostoc* ($p < 0.05$), and abundance increase in *Anaerovorax* ($p < 0.05$) in NFD group when compared with the HFD group (Figure 7B). After 4 weeks of the Slim supplementation was able to decrease *Oscillospira* ($p < 0.001$), P. *[Prevotella]* ($p < 0.01$), *Alistipes* ($p < 0.05$), *Bilophila* ($p < 0.01$), *AF12* ($p < 0.001$), *Coprococcus* ($p < 0.001$), *Adlercreutzia* ($p < 0.01$), *Dehalobacterium* ($p < 0.01$), *Mucispirillum* ($p < 0.001$) and increase *Parabacteroides* ($p < 0.05$), *Sutterella* ($p < 0.001$), *Anaerofustis* ($p < 0.05$), *Robinsoniella* ($p < 0.01$), P. *[Clostridium]* ($p < 0.05$) gut microbiota abundance when compared with the HFD group (Figure 7B).

LEfSe is an algorithm for high-dimensional biomarker discovery that identifies genomic features, such as genes, pathways, or taxa, characterizing differences between multiple biological conditions or classes (Figure 8). LEfSe analysis was used to identify the primary phylotypes responsible for the differences between the groups. This analysis helped to discern significantly and biologically distinct features, considering the importance of these effects and allowing for the identification of differentially abundant features (Segata et al., 2011). Linear discriminant analysis (LDA), combined with effect size measures (LEfSe) and derived cladogram, shows the significantly abundant bacterial taxa belonging to the NFD, HFD, and HFD_Slim groups (Figures 8A,B). The HFD_Slim supplementation was able to rise the *Eubacterium; Akkermansia; Clostridium; Enterococcus; Robinsoniella; Sutterella; Anaerofustis;* and *Clostridium* genera, and Erysipelotrichaceae family. The *Prevotella; Turicibacter; Coprococcus; Jeotgalicoccus; Clostridium; Anaerovorax* genera were observed in the composition of the relative abundance of the microbiota of the NFD group while the *Oscillospira; Ruminococcus; Allosprirae; Bilophila; AF12; Mucispirillum; Dehalobacterium; Leuconostoc* genera were observed in the composition of the relative abundance of the microbiota of the HFD group (Figure 8B). The HFD_Slim group showed *Mucispirillum schaedleri* ($p < 0.05$), *Alistipes finegoldii* ($p < 0.05$) abundance decreased, and *Clostridium symbiosum* ($p < 0.05$), and *Robinsoniella peoriensis* ($p < 0.05$) abundance decreased when compared to the HFD group (Figure 8C). *Leuconostoc*

10.3389/fmicb.2025.1494994

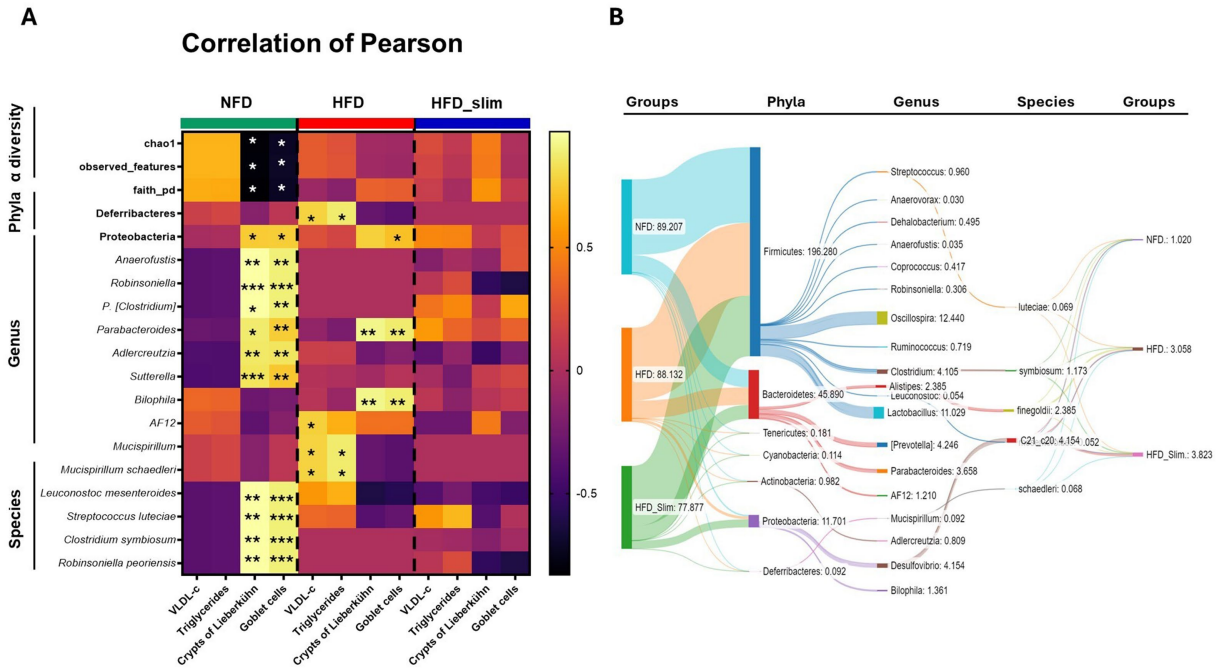

FIGURE 4
Person correlation analysis between α-diversity, phyla, genera, species, colon histomorphology, VLDL cholesterol and triglycerides of Control and High-Fat Diet groups after 4 weeks of supplementation. **(A)** Heatmap (correlation matrix) Pearson correlation coefficient (R) between the relative abundance (%) of bacteria α-diversity, phyla, genera, species, colon histomorphology, VLDL cholesterol and triglycerides of supplemented mice after 4 weeks. **(B)** Sankey diagram showing the relationship between phylum, genus, and species of bacteria from the intestinal mucosa of NFD, HFD, and HFD_Slim mice. *$p < 0.05$; **$p < 0.01$; ***$p < 0.001$. NFD, Non-Fat Diet; HFD, High Fat Diet; HFD_Sim, High Fat Diet Slim.

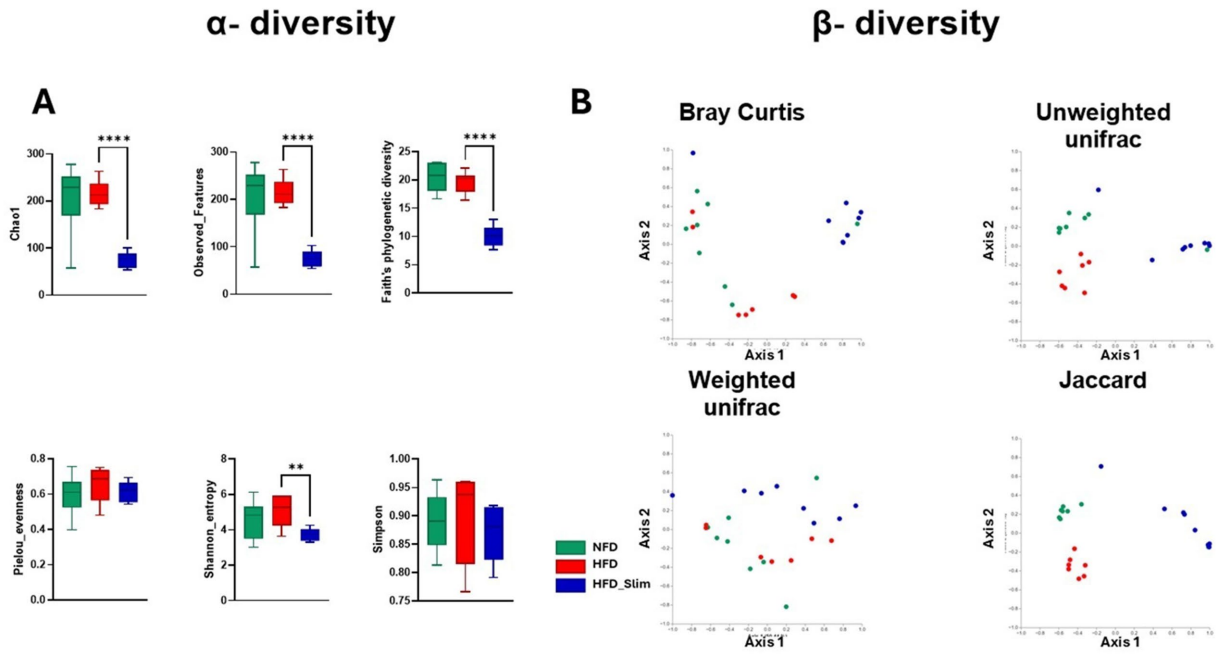

FIGURE 5
Alpha diversity (α) and beta diversity (β) in the gut microbiota in the Control and High-Fat Diet groups after 4 weeks of supplementation. **(A)** Alpha diversity (α) index. Chao1, Observed_Featured, Faith_pd, Pielou_evenness, Shannon_entropy and Simpson. **(B)** Beta diversity (β) index. Bray-Curtis, Jaccard, Unweighted_unifrac, Weighted_unifrac. Statistical analyses were represented by Student's t-test or Kruskal-Wallis. Data are represented as mean ± SD. $n = 7–8$ animals per group. Differences were calculated relative to the HFD group. **$p < 0.01$ and ****$p < 0.0001$. NFD, Non-Fat Diet; HFD, High Fat Diet; HFD_Slim, High Fat Diet Slim.

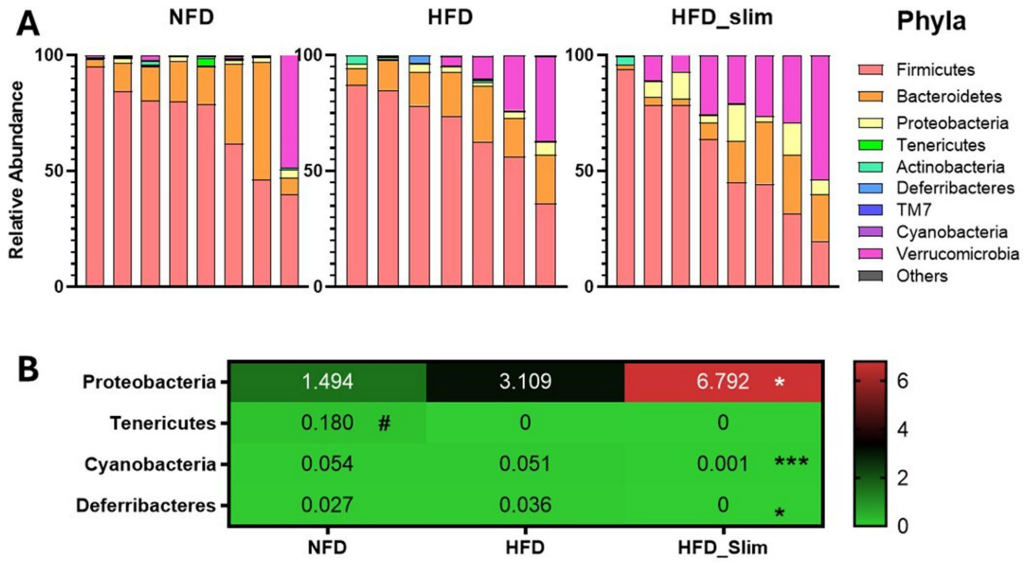

FIGURE 6
Composition of relative abundance of gut microbiota phyla in the Control and High-Fat Diet groups after 4 weeks of supplementation. **(A)** Relative abundance of phyla. **(B)** Heat map of relative abundance of phyla with statistical differences. Data were represented as mean ± SD. n = 7–8 animals per group. (#) Means the difference between NFD and HFD. (*) Means the difference between HFD and HFD_Slim. #$p < 0.01$; *$p < 0.0,5$, **$p < 0.01$, and ***$p < 0.001$. NFD, Non-Fat Diet; HFD, High Fat Diet; HFD_Slim, High Fat Diet Slim.

mesenteroides ($p < 0.05$), *Streptococcus luteciae* ($p < 0.05$) and *Desulfovibrio C21_c20* ($p < 0.05$) genera showed abundance decreased in NFD group compared to HFD group (Figure 8C).

4 Discussion

Bioactive compounds have shown potential as effective interventions to restore intestinal microbiota balance in obesity-related dysbiosis. The growing trend of using plant- and food-derived nutraceuticals as a complementary approach to treating health conditions reflects a shift toward more natural solutions (Rajapakse and Gantenbein, 2024). Our recent studies, both preclinical and clinical, have shown promising results in improving parameters related to obesity and overweight, especially through modulations in the intestinal microbiota with the use of nutraceutical compositions containing prebiotics, minerals, β-glucans and silymarin (Nehmi et al., 2021; Santamarina et al., 2022, 2024; Nehmi-Filho et al., 2023a, 2023b). In order to propose a nutraceutical formulation with a new diversity of active ingredients, we evaluated an innovative formulation named Slim, containing beet pulp, coenzyme Q10, berberine, prebiotics (fructooligosaccharides and galactooligosaccharides), minerals (selenium and chromium), and yeast β-glucans (from *Saccharomyces cerevisiae*), on the lipid profile, colon histomorphology shape, and in the gut microbiota in a high-fat diet obese mice.

The Slim supplement was formulated based on its components' functions and their synergistic effects. Berberine, a plant alkaloid from *Berberis vulgaris* Rupr., is recognized for a bioactive improvement metabolic syndrome like insulin sensitive, and anti-inflammatory effect on gut microbiota (Cheng et al., 2009; Habtemariam, 2020; Zhang et al., 2021). Beet pulp powder, rich in fiber and antioxidant compounds, like betaine, not only promotes intestinal health but also exerts prebiotic effects, encouraging the growth of beneficial bacteria (Prandi et al., 2018; Adekolurejo et al., 2023). Coenzyme Q10, a powerful antioxidant, protects against oxidative stress and improves mitochondrial function, crucial factors for metabolic.

One of our key objectives was to propose a formulation to achieve weight loss or reduce weight gain in obese mice model. While we observed this outcome in our previous studies (Nehmi et al., 2021), we did not see the same effect with the Slim supplement (see Supplementary Figure 1). However, we did note a reduction in plasma levels of VLDL cholesterol, triglycerides, and HDL cholesterol (Table 1), which supports our preclinical findings in the same high-fat diet-induced obesity model (see our first and second papers).

In our investigation of the Slim nutraceutical effects on lipid metabolism, we decided to assess the histomorphology of the colon. This choice is based on the understanding that prebiotic nutraceuticals influence not only the intestinal microbiota but also the host microenvironment (Santamarina et al., 2022). It is known that large intestine (colon) histomorphology and microbiota of the mice fed a high-fat diet significantly differ when compared with mice fed with normal-calorie diet (Paresque et al., 2013; John and Mullin, 2016; Nehmi-Filho et al., 2023a).

Goblet cells play a vital role in the production and secretion of mucus in the intestine. This mucus is crucial for maintaining the integrity of the intestinal barrier (Yang and Yu, 2021). It forms a hydrophobic barrier in the intestinal mucosa that reduces fat absorption (Lichtenberger, 1995) while enhancing nutrient uptake and supporting metabolic homeostasis. Our results showed that obese mice receiving Slim supplementation exhibited a significant increase in both Goblet cells and Lieberkühn crypts compared to those on a high-fat diet (HFD) (Figures 2B,C). This increase may explain the observed reduction in plasma VLDL-c and triglycerides in Slim HFD (Table 1).

We observed a positive Pearson correlation between the Parabacteroides and Bilophila genera with Goblet cells and Lieberkühn crypts in the high-fat diet (HFD) group (Figure 4A).

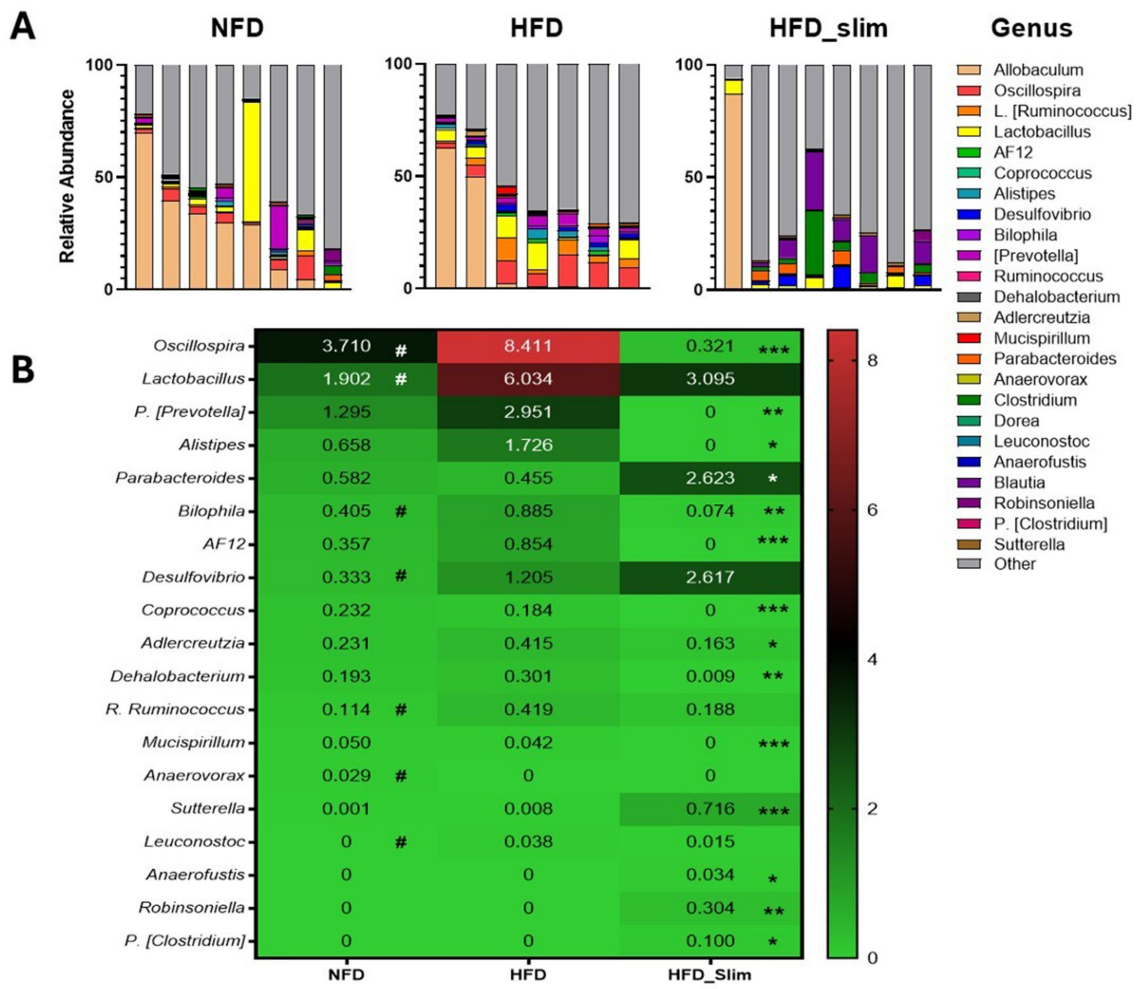

FIGURE 7
Composition of gut microbiota genera in the Control and High-Fat Diet groups after 4 weeks of supplementation. **(A)** Relative abundance of genera. **(B)** Heat map of relative abundance of genera with statistical differences. Data were represented as mean ± SD. n = 7–8 animals per group. (#) Means the difference between NFD and HFD. (*) Means the difference between HFD and HFD_Slim. #$p < 0.01$; *$p < 0.0,5$, **$p < 0.01$, and ***$p < 0.001$. NFD, Non-Fat Diet; HFD, High Fat Diet; HFD_Slim, High Fat Diet Slim; NFD, Non-Fat Diet; HFD, High Fat Diet; HFD_Slim, High Fat Diet Slim.

Parabacteroides is associated with the fermentation of complex polysaccharides and producing short-chain fatty acids (SCFAs), such as propionate (Medawar et al., 2021). *Bilophila* spp., a sulfate-reducing bacteria (SRB) seems to reduce butyrate-producing bacteria level (Ye et al., 2018). We observed a decreased and increased abundance in these genera, respectively, in the HFD group and an inverse result in the NFD and Slim HFD group after 4 weeks (Figure 4A). *Mucispirillum schaedleri*, a marker of a high-fat diet, showed a positive Pearson correlation with VLDL cholesterol and triglyceride levels, even as in the *Mucispirillum* genus in the HFD group, but we did not observe this phenotype in the NFD and HFD_Slim groups (Figure 4A). These results suggest a recovery of histomorphology and modulation of gut microbiota, supporting the known interrelation between the gut microbiota and the host microenvironment.

Obesity and high-fat diets can negatively impact gut-associated lymphoid tissue (GALT), including Peyer's patches (Jung et al., 2010; Leocádio et al., 2020). These factors contribute to chronic inflammation, reduced motility, and dysfunction of the enteric nervous system (ENS) (McMenamin et al., 2018; Miron, 2019), which may result in constipation and bacterial overgrowth. Peyer's patches are crucial for mucosal immune responses, while Auerbach's plexus is a network within the ENS that is essential for intestinal motility (Sharkey and Mawe, 2023). After 4 weeks of Slim supplementation, both Peyer's patches (Figure 3B) and Auerbach's plexus (Figure 2E) showed significant expansion. One noteworthy observation was that the anti-inflammatory effects of the components in the Slim formulation did not appear to impact the intestinal microenvironment, including histomorphology and microbiota. Although the Slim formulation contains anti-inflammatory characteristics, the analysis of the cytokines IL-6 and IL-10 in the colon of the treated groups showed no significant changes due to the supplement (Supplementary Figures S2D–F).

Lower alpha diversity is often associated with intestinal dysbiosis (Sharma et al., 2023), which may contribute to the development and persistence of obesity. However, in certain contexts, a reduction in alpha diversity can indicate a healthier state and a lower risk of complications and infections (The Human Microbiome Project Consortium, 2012; Baud et al., 2023). On the other hand, some studies suggest that increased alpha diversity might be linked to adverse

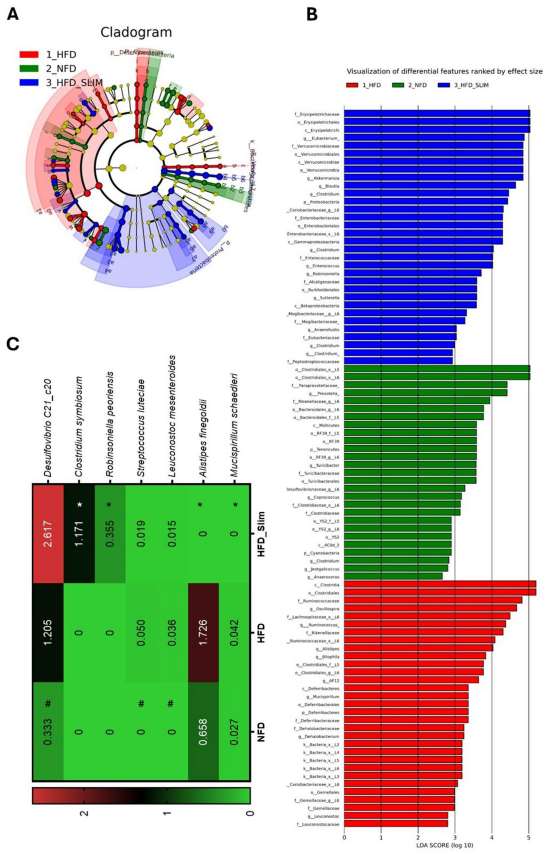

FIGURE 8
Differentially enriched bacterial taxons by LEfSe in gut microbiota of the Control and High-Fat Diet groups after 4 weeks of supplementation. **(A)** Cladogram of significant changes across taxonomic levels. The root of the cladogram represents the bacteria domain. Node size represents taxon abundance. The most abundant enriched taxon among the NFD (blue), HFD (green), and HFD_Slim (red) groups. **(B)** Graphical representation of the most abundant bacterial feature. Only taxon meeting an LDA significance threshold >2 is shown. **(C)** Heat map of the relative abundance of species with statistical differences. Data were represented as mean ± SD. n = 7–8 animals per group. Differences were calculated relative to the HFD group. #$p < 0.01$ – significant difference between NFD and HFD; *$p < 0.05$, **$p < 0.01$, and ***$p < 0.001$ – significant difference between HFD_Slim and HFD. NFD, Non-Fat Diet; HFD, High Fat Diet; HFD_Slim, High Fat Diet Slim.

outcomes (Kupritz et al., 2021). In contrast, beta diversity plays a critical role in understanding regional diversity, as it measures the similarity or dissimilarity between pairs of microbiomes (Su, 2021). We obtained some intriguing results with the Slim supplement (Figure 5B), which contradicted our earlier studies that utilized a different type of polyphenol (Nehmi-Filho et al., 2023a; Nehmi-Filho et al., 2024). In the HFD_Slim group, we observed a decrease in alpha diversity (diversity within each group) and an increase in beta diversity (diversity between groups) (Figures 5A,B). This indicates that the nutraceutical was able to modulate diversity when compared to the different groups evaluated.

Proteobacteria phylum is thought to play a key role in preparing the gut for intestinal mucosalization by strictly anaerobic bacteria necessary for healthy gut function by consuming oxygen and reducing the redox potential in the gut environment (Moon et al., 2018). The Proteobacteria abundance augmented (Figure 4A) indicates that the positive effects observed on gut diversity, histomorphology, and lipid metabolism, along with the reduction of the phyla Cyanobacteria and Deferribacteres after Slim supplementation, may be linked to the potential duplibiotic effect from the supplement (Figure 4A). This effect is believed to arise from the polyphenols in Beet pulp and Berberine (Habtemariam, 2020), which may exert an antimicrobial action to control and inhibit the growth of pathogenic bacteria while also having a prebiotic effect that stimulates the growth of beneficial, commensal bacteria (Wang et al., 2023; Rodríguez-Daza et al., 2021). Furthermore, polyphenols can alleviate metabolic diseases, increase mucus production, and promote the secretion of antimicrobial peptides (Rodríguez-Daza et al., 2021). Although the duplibiotic effect should not be mitigated, we believe the results obtained were due to the combination of active ingredients rather than any single isolated compound. This conclusion is supported by the fact that the suggested quantities of components, such as FOS and GOS, were below those recommended in the literature (Sabater-Molina et al., 2009; Tonon et al., 2021).

The Slim supplement shows its prebiotic effect in increasing the abundance of important genera that bring benefits in improving conditions associated with the obesity-induced model (Figure 7A). *Desulfovibrio* is a potent generator of acetic acid, which showed significant anti-NAFLD (Non-alcoholic fatty liver disease) effects in HFD-fed mice (Hong et al., 2021). *Sutterela* shows the ability to adhere to intestinal epithelial cells, indicating that they may have an immunomodulatory role (Hiippala et al., 2016). *Parabacteroides* is associated with the fermentation of complex polysaccharides and producing short-chain fatty acids (SCFAs), such as propionate (Medawar et al., 2021; Figure 7B). *Akkermancy,* a genus that plays a role in the renewal and production of mucin, can also influence the differentiation of Paneth and Goblet cells in the small intestine (Schneeberger et al., 2015; Kim et al., 2021). In our experiment, we observed an increase in these cell types in the colon, suggesting that *Akkermancy* may modulate their development (Figure 8B). The antibiotic effect of the Slim formulation was evident in the reduction of the genera *Bilophila* (Ye et al., 2018) and *Mucispirillum* (Herp et al., 2021). These genera are responsible for lowering the levels of butyrate-producing bacteria (BPB) and for degrading mucin, respectively (Figure 7B). The Slim supplement was able to influence some bacterium species that bring benefits in obese mice model increasing *Desulfovibrio C21-C20*, *Clostridium symbiosum* (Luo et al., 2023), and reducing *Mucispirillum schaedleri* (Loy et al., 2017), *Alistipes finegoldii* (Parker et al., 2020; Figure 8C) that seems involved in homeostasis breakdown in obese-gut microbiota.

5 Conclusion

In conclusion, the findings of our study support the potential of Slim as a nutraceutical intervention for obesity-related dysbiosis, enhancing gut health and mitigating some of the metabolic disruptions caused by high-fat diets. Although our findings are promising, we acknowledge several limitations in this study. First, it was not possible to assess the individual effects of beet pulp, coenzyme Q10, and berberine. Second, we were unable to measure short-chain fatty acids in the fecal samples of the experimental groups. While our sample size was adequate, a larger sample size would enhance the

robustness of the study and increase confidence in the reproducibility of our results. Additionally, a more in-depth evaluation of the intestinal barrier is needed to better understand its function. Future studies in both animal and human models will be essential to address these important questions.

Data availability statement

The datasets presented in this study can be found in online repositories. The names of the repository/repositories and accession number(s) can be found at: https://www.ncbi.nlm.nih.gov/genbank/, PRJNA941000.

Ethics statement

The animal study was approved by Research Ethics Committee of the University of São Paulo, São Paulo, Brazil. The study was conducted in accordance with the local legislation and institutional requirements.

Author contributions

JAF: Writing – original draft, Data curation, Formal analysis, Investigation. VN: Funding acquisition, Resources, Writing – review & editing. AS: Conceptualization, Supervision, Validation, Writing – original draft. GM: Data curation, Methodology, Writing – review & editing. LF: Data curation, Software, Writing – review & editing. JVF: Data curation, Methodology, Writing – review & editing. RM: Formal analysis, Software, Writing – review & editing. GS: Methodology, Validation, Writing – review & editing. GB: Investigation, Methodology, Writing – review & editing. IS: Investigation, Methodology, Writing – review & editing. ES: Validation, Visualization, Writing – review & editing. JO: Writing – review & editing, Resources, Supervision. AP: Conceptualization, Supervision, Writing – original draft, Project administration, Visualization.

Funding

The author(s) declare financial support was received for the research and/or publication of this article. This study was funded by Efeom Nutrição S.A. It was partially funded by the Coordenação de Aperfeiçoamento de Pessoal de Nível Superior, Brasil (CAPES), Finance Code 001, with a PNPD fellowship from the Graduate Program in Anesthesiology, Surgical Sciences, and Perioperative Medicine at FMUSP. LF was supported by FAPESP 18/14389- 0.

Acknowledgments

The authors would like to thank Márcia Alves and the LIM-26 and LIM-29 teams for their support and technical assistance. AP thanks CAPES (Finance Code 001) by the PNPD fellow from the Graduate Program in Anesthesiology, Surgical Sciences, and Perioperative Medicine, FMUSP. The authors Acknowledge the ChatGPT (version ChatGPT-4, model GPT-4-turbo, source OpenAI) for the support on English language improvement for clarity and Playground (version Playground v3, model PGv2.5P, source PlaygroundAI) for mice image creation used in Figure 1.

Conflict of interest

VN and JO are part of the Company Efeom Nutrition S.A as partners who may benefit in some way from revenues or financial losses with the publication of this manuscript, now or in the future. JAF, AS, ES, and AP received salaries from Efeom Nutrition S.A. VN, JO, and AP hold patents related to the content of the manuscript.

The remaining authors declare that the research was conducted in the absence of any commercial or financial relationships that could be construed as a potential conflict of interest.

Publisher's note

Supplementary material

The Supplementary material for this article can be found online at: https://www.frontiersin.org/articles/10.3389/fmicb.2025.1494994/full#supplementary-material

References

Abenavoli, L., Scarpellini, E., Colica, C., Boccuto, L., Salehi, B., Sharifi-Rad, J., et al. (2019). Gut microbiota and obesity: a role for probiotics. *Nutrients* 11:2690. doi: 10.3390/nu11112690

Adekolurejo, O. O., McDermott, K., Greathead, H. M. R., Miller, H. M., Mackie, A. R., and Boesch, C. (2023). Effect of red-beetroot-supplemented diet on gut microbiota composition and metabolite profile of weaned pigs—a pilot study. *Animals* 13:2196. doi: 10.3390/ani13132196

Andrade, E., Lima, A., Nunes, I., Orlando, D., Gondim, P., Zangeronimo, M., et al. (2016). Exercise and Beta-glucan consumption (*Saccharomyces cerevisiae*) improve the metabolic profile and reduce the Atherogenic index in type 2 diabetic rats (HFD/STZ). *Nutrients* 8:792. doi: 10.3390/nu8120792

ANVISA (2018). INSTRUÇÃO NORMATIVA - IN Nº 28, DE 26 DE JULHO DE 2018. Ministério da Saúde - MS, 1–48. Available online at: https://antigo.anvisa.gov.br/documents/10181/3898888/IN_28_2018_COMP.pdf/db9c7460-ae66-4f78-8576-dfd019bc9fa1

Baud, A., Hillion, K.-H., Plainvert, C., Tessier, V., Tazi, A., Mandelbrot, L., et al. (2023). Microbial diversity in the vaginal microbiota and its link to pregnancy outcomes. *Sci. Rep.* 13:9061. doi: 10.1038/s41598-023-36126-z

Bokulich, N. A., Kaehler, B. D., Rideout, J. R., Dillon, M., Bolyen, E., Knight, R., et al. (2018). Optimizing taxonomic classification of marker-gene amplicon sequences with QIIME 2's q2-feature-classifier plugin. *Microbiome* 6:90. doi: 10.1186/s40168-018-0470-z

Bolyen, E., Rideout, J. R., Dillon, M. R., Bokulich, N. A., Abnet, C. C., Al-Ghalith, G. A., et al. (2019). Reproducible, interactive, scalable and extensible microbiome data science using QIIME 2. *Nat. Biotechnol.* 37, 852–857. doi: 10.1038/s41587-019-0209-9

Callahan, B. J., McMurdie, P. J., Rosen, M. J., Han, A. W., Johnson, A. J. A., and Holmes, S. P. (2016). DADA2: high-resolution sample inference from Illumina amplicon data. *Nat. Methods* 13, 581–583. doi: 10.1038/nmeth.3869

Caporaso, J. G., Lauber, C. L., Walters, W. A., Berg-Lyons, D., Lozupone, C. A., Turnbaugh, P. J., et al. (2011). Global patterns of 16S rRNA diversity at a depth of millions of sequences per sample. *Proc. Natl. Acad. Sci. U. S. A.* 108, 4516–4522. doi: 10.1073/pnas.1000080107

Cheng, Z.-F., Zhang, Y.-Q., and Liu, F.-C. (2009). Berberine against gastrointestinal peptides elevation and mucous secretion in hyperthyroid diarrheic rats. *Regul. Pept.* 155, 145–149. doi: 10.1016/j.regpep.2008.12.008

Esposito, K., Pontillo, A., Giugliano, F., Giugliano, G., Marfella, R., Nicoletti, G., et al. (2003). Association of low Interleukin-10 levels with the metabolic syndrome in obese women. *J. Clin. Endocrinol. Metabol.* 88, 1055–1058. doi: 10.1210/jc.2002-021437

European Food Safety Authority (2017). Dietary reference values for nutrients summary report. *EFS3*:14. doi: 10.2903/sp.efsa.2017.e15121

Faith, D. P. (1992). Conservation evaluation and phylogenetic diversity. *Biol. Conserv.* 61, 1–10. doi: 10.1016/0006-3207(92)91201-3

Festi, D., Schiumerini, R., Eusebi, L. H., Marasco, G., Taddia, M., and Colecchia, A. (2014). Gut microbiota and metabolic syndrome. *WJG* 20, 16079–16094. doi: 10.3748/wjg.v20.i43.16079

Freitas, J. A., Santamarina, A. B., and Fl, A. (2024). Silymarin: a natural compound for obesity management. *Obesities* 4, 292–313. doi: 10.3390/obesities4030024

Friedewald, W. T., Levy, R. I., and Fredrickson, D. S. (1972). Estimation of the concentration of low-density lipoprotein cholesteroiln plasma, without use of the preparative ultra centrifuge. *Clin Chem* 18, 499–502.

Grundy, S. M. (2004). Obesity, metabolic syndrome, and cardiovascular disease. *J. Clin. Endocrinol. Metabol.* 89, 2595–2600. doi: 10.1210/jc.2004-0372

Guan, Y., Tang, G., Li, L., Shu, J., Zhao, Y., Huang, L., et al. (2024). Herbal medicine and gut microbiota: exploring untapped therapeutic potential in neurodegenerative disease management. *Arch. Pharm. Res.* 47, 146–164. doi: 10.1007/s12272-023-01484-9

Habtemariam, S. (2020). Berberine pharmacology and the gut microbiota: a hidden therapeutic link. *Pharmacol. Res.* 155:104722. doi: 10.1016/j.phrs.2020.104722

Herp, S., Durai Raj, A. C., Salvado Silva, M., Woelfel, S., and Stecher, B. (2021). The human symbiont *Mucispirillum schaedleri*: causality in health and disease. *Med. Microbiol. Immunol.* 210, 173–179. doi: 10.1007/s00430-021-00702-9

Hiippala, K., Kainulainen, V., Kalliomäki, M., Arkkila, P., and Satokari, R. (2016). Mucosal prevalence and interactions with the epithelium indicate commensalism of Sutterella spp. *Front. Microbiol.* 7:1706. doi: 10.3389/fmicb.2016.01706

Hong, Y., Sheng, L., Zhong, J., Tao, X., Zhu, W., Ma, J., et al. (2021). *Desulfovibrio vulgaris*, a potent acetic acid-producing bacterium, attenuates nonalcoholic fatty liver disease in mice. *Gut Microbes* 13, 1–20. doi: 10.1080/19490976.2021.1930874

Jacob, S., Nair, A. B., and Morsy, M. A. (2022). Dose conversion between animals and humans: a practical solution. *IJPER* 56, 600–607. doi: 10.5530/ijper.56.3.108

Janssen, S., McDonald, D., Gonzalez, A., Navas-Molina, J. A., Jiang, L., Xu, Z. Z., et al. (2018). Phylogenetic placement of exact amplicon sequences improves associations with clinical. *Information* 3:e00021-18. doi: 10.1128/mSystems.00021-18

John, G. K., and Mullin, G. E. (2016). The gut microbiome and obesity. *Curr. Oncol. Rep.* 18:45. doi: 10.1007/s11912-016-0528-7

José Pereira, L. (2015). Efectos metabólicos de los β-glucanos (*Saccharomyces cerevisiae*) a. *Nutricion Hospitalaria* 256–264. doi: 10.3305/nh.2015.32.1.9013

Jung, C., Hugot, J.-P., and Barreau, F. (2010). Peyer's patches: the immune sensors of the intestine. *Int. J. Inflamm.* 2010, 1–12. doi: 10.4061/2010/823710

Kern, L., Mittenbühler, M., Vesting, A., Ostermann, A., Wunderlich, C., and Wunderlich, F. (2018). Obesity-induced TNFα and IL-6 signaling: the missing link between obesity and inflammation—driven liver and colorectal cancers. *Cancers* 11:24. doi: 10.3390/cancers11010024

Kim, S., Shin, Y.-C., Kim, T.-Y., Kim, Y., Lee, Y.-S., Lee, S.-H., et al. (2021). Mucin degrader Akkermansia muciniphila accelerates intestinal stem cell-mediated epithelial development. *Gut Microbes* 13, 1–20. doi: 10.1080/19490976.2021.1892441

Kupritz, J., Angelova, A., Nutman, T. B., and Gazzinelli-Guimaraes, P. H. (2021). Helminth-induced human gastrointestinal Dysbiosis: a systematic review and Meta-analysis reveals insights into altered taxon diversity and microbial gradient collapse. *MBio* 12:e0289021. doi: 10.1128/mBio.02890-21

Leocádio, P. C. L., Oriá, R. B., Crespo-Lopez, M. E., and Alvarez-Leite, J. I. (2020). Obesity: more than an inflammatory, an infectious disease? *Front. Immunol.* 10:3092. doi: 10.3389/fimmu.2019.03092

Lichtenberger, L. M. (1995). The hydrophobic barrier properties of gastrointestinal mucus. *Annu. Rev. Physiol.* 57, 565–583. doi: 10.1146/annurev.ph.57.030195.003025

Loy, A., Pfann, C., Steinberger, M., Hanson, B., Herp, S., Brugiroux, S., et al. (2017). Lifestyle and horizontal gene transfer-mediated evolution of *Mucispirillum schaedleri*, a core member of the murine gut microbiota. *mSystems* 2:e00171-16. doi: 10.1128/mSystems.00171-16

Luo, X., Tao, F., Tan, C., Xu, C.-Y., Zheng, Z.-H., Pang, Q., et al. (2023). Enhanced glucose homeostasis *via* Clostridium *symbiosum-mediated* glucagon-like peptide 1 inhibition of hepatic gluconeogenesis in mid-intestinal bypass surgery. *World J. Gastroenterol.* 29, 5471–5482. doi: 10.3748/wjg.v29.i39.5471

Ma, N., Guo, P., Zhang, J., He, T., Kim, S. W., Zhang, G., et al. (2018). Nutrients mediate intestinal bacteria–mucosal immune crosstalk. *Front. Immunol.* 9:5. doi: 10.3389/fimmu.2018.00005

Mandal, S., Van Treuren, W., White, R. A., Eggesbø, M., Knight, R., and Peddada, S. D. (2015). Analysis of composition of microbiomes: a novel method for studying microbial composition. *Microbial Ecol. Health Dis.* 26, 1–7. doi: 10.3402/mehd.v26.27663

McMenamin, C. A., Clyburn, C., and Browning, K. N. (2018). High-fat diet during the perinatal period induces loss of myenteric nitrergic neurons and increases enteric glial density, prior to the development of obesity. *Neuroscience* 393, 369–380. doi: 10.1016/j.neuroscience.2018.09.033

Medawar, E., Haange, S.-B., Rolle-Kampczyk, U., Engelmann, B., Dietrich, A., Thieleking, R., et al. (2021). Gut microbiota link dietary fiber intake and short-chain fatty acid metabolism with eating behavior. *Transl Psychiatry* 11:500. doi: 10.1038/s41398-021-01620-3

Mirarab, S., Nguyen, N., and Warnow, T. (2011). "SEPP: SATé-enabled phylogenetic placement" in Biocomputing 2012 Pac Symp Biocomput (Kohala Coast, Hawaii, USA: World Scientific), 247–258.

Miron, I. (2019). Gastrointestinal motility disorders in obesity. *Acta Endo* 15, 497–504. doi: 10.4183/aeb.2019.497

Moon, C. D., Young, W., Maclean, P. H., Cookson, A. L., and Bermingham, E. N. (2018). Metagenomic insights into the roles of *Proteobacteria* in the gastrointestinal microbiomes of healthy dogs and cats. *MicrobiologyOpen* 7:e00677. doi: 10.1002/mbo3.677

Neergheen, V., Chalasani, A., Wainwright, L., Yubero, D., Montero, R., Artuch, R., et al. (2017). Coenzyme Q_{10} in the treatment of mitochondrial disease. *J. Inborn Errors Metabolism Screening* 5:232640981770777. doi: 10.1177/2326409817707771

Nehmi, V. A., Murata, G. M., Moraes, R. C. M., Lima, G. C. A., De Miranda, D. A., Radloff, K., et al. (2021). A novel supplement with yeast β-glucan, prebiotic, minerals and *Silybum marianum* synergistically modulates metabolic and inflammatory pathways and improves steatosis in obese mice. *J. Integr. Med.* 19, 439–450. doi: 10.1016/j.joim.2021.05.002

Nehmi-Filho, V., De Freitas, J. A., Franco, L. A., Martins, R. C., Turri, J. A. O., Santamarina, A. B., et al. (2024). Modulation of the gut microbiome and Firmicutes phylum reduction by a nutraceutical blend in the obesity mouse model and overweight humans: a DOUBLE-BLIND clinical trial. *Food Sci. Nutr.* 12, 2436–2454. doi: 10.1002/fsn3.3927

Nehmi-Filho, V., Freitas, J. A., Augusto Moysés Franco, L., Vanessa Da Silva Fonseca, J., Cristina Ruedas Martins, R., Boveto Santamarina, A., et al. (2023a). Novel nutraceutical (silymarin, yeast β-glucan, prebiotics, and minerals) shifts gut microbiota and restores large intestine histology of diet-induced metabolic syndrome mice. *J. Funct. Foods* 107:105671. doi: 10.1016/j.jff.2023.105671

Nehmi-Filho, V., Santamarina, A. B., de Freitas, J. A., Trarbach, E. B., de Oliveira, D. R., Palace-Berl, F., et al. (2023b). Novel nutraceutical supplements with yeast β-glucan, prebiotics, minerals, and *Silybum marianum* (silymarin) ameliorate obesity-related metabolic and clinical parameters: a double-blind randomized trial. *Front. Endocrinol.* 13:1089938. doi: 10.3389/fendo.2022.1089938

Overvad, K., Diamant, B., Holm, L., Hùlmer, G., Mortensen, S., and Stender, S. (1999). Review coenzyme Q10 in health and disease. *Eur. J. Clin. Nutr.* 53, 764–770. doi: 10.1038/sj.ejcn.1600880

Paresque, R., Nascimento, M., and Queiroz, B. N. (2013). Gastrointestinal morphological alterations in obese rats kept under hypercaloric diets. *IJGM* 2013, 479–488. doi: 10.2147/IJGM.S35482

Parker, B. J., Wearsch, P. A., Veloo, A. C. M., and Rodriguez-Palacios, A. (2020). The genus Alistipes: gut Bacteria with emerging implications to inflammation, Cancer, and mental health. *Front. Immunol.* 11:906. doi: 10.3389/fimmu.2020.00906

Pessoa, A. F. M., Florim, J. C., Rodrigues, H. G., Andrade-Oliveira, V., Teixeira, S. A., Vitzel, K. F., et al. (2016). Oral administration of antioxidants improves skin wound healing in diabetic mice: antioxidants improve diabetic wound healing. *Wound Rep. Reg.* 24, 981–993. doi: 10.1111/wrr.12486

Prandi, B., Baldassarre, S., Babbar, N., Bancalari, E., Vandezande, P., Hermans, D., et al. (2018). Pectin oligosaccharides from sugar beet pulp: molecular characterization and potential prebiotic activity. *Food Funct.* 9, 1557–1569. doi: 10.1039/C7FO01182B

Rahman, M. H., Bajgai, J., Fadriquela, A., Sharma, S., Trinh, T. T., Akter, R., et al. (2021). Therapeutic potential of natural products in treating neurodegenerative disorders and their future prospects and challenges. *Molecules* 26:5327. doi: 10.3390/molecules26175327

Rajapakse, T., and Gantenbein, A. R. (2024). "Nutraceuticals in migraine" in *Handb. Clin. Neurol.* (Elsevier), 957–958.

Reeves, P. G., Nielsen, F. H., and Fahey, G. C. (1993). AIN-93 purified diets for laboratory rodents: final report of the American Institute of Nutrition ad hoc Writing Committee on the reformulation of the AIN-76A rodent diet. *J. Nutr.* 123, 1939–1951. doi: 10.1093/jn/123.11.1939

Rodríguez-Daza, M. C., Pulido-Mateos, E. C., Lupien-Meilleur, J., Guyonnet, D., Desjardins, Y., and Roy, D. (2021). Polyphenol-mediated gut microbiota modulation: toward prebiotics and further. *Front. Nutr.* 8:689456. doi: 10.3389/fnut.2021.689456

Saad, M. J. A., Santos, A., and Prada, P. O. (2016). Linking gut microbiota and inflammation to obesity and insulin resistance. *Physiology* 31, 283–293. doi: 10.1152/physiol.00041.2015

Sabater-Molina, M., Larqué, E., Torrella, F., and Zamora, S. (2009). Dietary fructooligosaccharides and potential benefits on health. *J. Physiol. Biochem.* 65, 315–328. doi: 10.1007/BF03180584

Santamarina, A. B., De Freitas, J. A., Franco, L. A. M., Nehmi-Filho, V., Fonseca, J. V., Martins, R. C., et al. (2024). Nutraceutical blends predict enhanced health via microbiota reshaping improving cytokines and life quality: a Brazilian double-blind randomized trial. *Sci. Rep.* 14:11127. doi: 10.1038/s41598-024-61909-3

Santamarina, A. B., Moraes, R. C. M., Nehmi Filho, V., Murata, G. M., de Freitas, J. A., de Miranda, D. A., et al. (2022). The symbiotic effect of a new nutraceutical with yeast β-glucan, prebiotics, minerals, and *Silybum marianum* (Silymarin) for recovering metabolic homeostasis via Pgc-1α, Il-6, and Il-10 gene expression in a Type-2 diabetes obesity model. *Antioxidants* 11:447. doi: 10.3390/antiox11030447

Schneeberger, M., Everard, A., Gómez-Valadés, A. G., Matamoros, S., Ramírez, S., Delzenne, N. M., et al. (2015). *Akkermansia muciniphila* inversely correlates with the onset of inflammation, altered adipose tissue metabolism and metabolic disorders during obesity in mice. *Sci. Rep.* 5:16643. doi: 10.1038/srep16643

Segata, N., Izard, J., Waldron, L., Gevers, D., Miropolsky, L., Garrett, W. S., et al. (2011). Metagenomic biomarker discovery and explanation. *Genome Biol.* 12:R60. doi: 10.1186/gb-2011-12-6-r60

Sharkey, K. A., and Mawe, G. M. (2023). The enteric nervous system. *Physiol. Rev.* 103, 1487–1564. doi: 10.1152/physrev.00018.2022

Sharma, M., Dhaliwal, M., Tyagi, R., Goyal, T., Sharma, S., and Rawat, A. (2023). Microbiome and its Dysbiosis in inborn errors of immunity. *Pathogens* 12:518. doi: 10.3390/pathogens12040518

Sifuentes-Franco, S., Sánchez-Macías, D. C., Carrillo-Ibarra, S., Rivera-Valdés, J. J., Zuñiga, L. Y., and Sánchez-López, V. A. (2022). Antioxidant and anti-inflammatory effects of coenzyme Q10 supplementation on infectious diseases. *Healthcare* 10:487. doi: 10.3390/healthcare10030487

Su, X. (2021). Elucidating the Beta-diversity of the microbiome: from global alignment to local alignment. *mSystems* 6, 1–5. doi: 10.1128/msystems.00363-21

The Human Microbiome Project Consortium (2012). Structure, function and diversity of the healthy human microbiome. *Nature* 486, 207–214. doi: 10.1038/nature11234

Tonon, K. M., Tomé, T. M., Mosquera, E. M. B., Perina, N. P., and Lazarini, T. (2021). The effect of infant formulas with 4 or 8 g/L GOS/FOS on growth, gastrointestinal symptoms, and behavioral patterns: a prospective cohort study. *Global Pediatr. Health* 8:2333794X211044115. doi: 10.1177/2333794X211044115

Torres, D. P. M., Gonçalves, M. D. P. F., Teixeira, J. A., and Rodrigues, L. R. (2010). Galacto-oligosaccharides: production, properties, applications, and significance as prebiotics. *Comp. Rev. Food Sci. Food Safe* 9, 438–454. doi: 10.1111/j.1541-4337.2010.00119.x

Usmani, Z., Sharma, M., Diwan, D., Tripathi, M., Whale, E., Jayakody, L. N., et al. (2022). Valorization of sugar beet pulp to value-added products: a review. *Bioresour. Technol.* 346:126580. doi: 10.1016/j.biortech.2021.126580

Vázquez-Baeza, Y., Pirrung, M., Gonzalez, A., and Knight, R. (2013). EMPeror: a tool for visualizing high-throughput microbial community data. *GigaSci* 2:16. doi: 10.1186/2047-217X-2-16

Wang, Y., Do, T., Marshall, L. J., and Boesch, C. (2023). Effect of two-week red beetroot juice consumption on modulation of gut microbiota in healthy human volunteers – a pilot study. *Food Chem.* 406:134989. doi: 10.1016/j.foodchem.2022.134989

Wang, K., Lai, W., Min, T., Wei, J., Bai, Y., Cao, H., et al. (2024). The effect of enteric-derived lipopolysaccharides on obesity. *IJMS* 25:4305. doi: 10.3390/ijms25084305

Yang, S., and Yu, M. (2021). Role of goblet cells in intestinal barrier and mucosal immunity. *JIR.* 14, 3171–3183. doi: 10.2147/JIR.S318327

Ye, Z., Zhang, N., Wu, C., Zhang, X., Wang, Q., Huang, X., et al. (2018). A metagenomic study of the gut microbiome in Behcet's disease. *Microbiome* 6:135. doi: 10.1186/s40168-018-0520-6

Zamani, M., Zarei, M., Nikbaf-Shandiz, M., Hosseini, S., Shiraseb, F., and Asbaghi, O. (2022). The effects of berberine supplementation on cardiovascular risk factors in adults: a systematic review and dose-response meta-analysis. *Front. Nutr.* 9:1013055. doi: 10.3389/fnut.2022.1013055

Zhang, L., Wu, X., Yang, R., Chen, F., Liao, Y., Zhu, Z., et al. (2021). Effects of Berberine on the gastrointestinal microbiota. *Front. Cell. Infect. Microbiol.* 10:588517. doi: 10.3389/fcimb.2020.588517

Frontiers in Microbiology

Explores the habitable world and the potential of microbial life

The largest and most cited microbiology journal which advances our understanding of the role microbes play in addressing global challenges such as healthcare, food security, and climate change.

Discover the latest Research Topics

See more →

Frontiers

Avenue du Tribunal-Fédéral 34
1005 Lausanne, Switzerland
frontiersin.org

Contact us

+41 (0)21 510 17 00
frontiersin.org/about/contact